University of Southampton

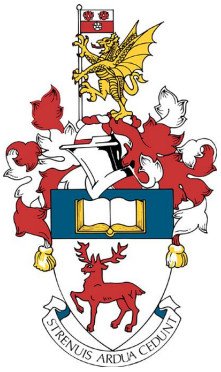

FACULTY OF MEDICINE

Cancer Sciences

Development of On-Target Hexamerisation for Effective Antibody Immunotherapy

Volume 1 of 1

by

Joshua Michael Sopp

Doctor of Philosophy

March, 2020

University of Southampton

Abstract

Faculty of Medicine

Cancer Sciences

Doctor of Philosophy

Development of On-Target Hexamerisation For Effective Antibody Immunotherapy

Joshua Michael Sopp

Monoclonal antibodies represent one of the fastest growing sectors of human therapeutics used in the treatment of cancer and autoimmune diseases. The majority of monoclonal antibodies approved for use in cancer elicit a therapeutic response via Fc-mediated effector functions. Antibodies have been shown to have natural Fc:Fc interactions that help to mediate these effector functions. Specifically, when the Fc-molecules are arranged hexamerically at the target cell surface this leads to the optimal activation of complement-dependent cytotoxicity.

Herein is described a novel antibody engineering approach based around the tailpiece of the naturally multimeric IgM. Fusion of the C-terminal 'tailpiece' sequence of IgM promoted stable hexamerisation of hIgG1 in solution. Mutation of the penultimate cysteine residue of the tailpiece to serine (C575S) ablated covalent hexamer formation. However, hIgG1 C575S tailpiece mutants retained the potential to self-associate into reversible, non-covalent hexamers after concentration in solution. These hIgG1 IgM tailpiece C575S fusion antibodies could be expressed and purified with standard hIgG protocols, without any loss of yield or additional quality control processes, whereas the native hIgG1 tailpiece required additional purification steps to isolate a single species and delivered lower yields.

First, constructs were assessed in the context of CD20 specificity. Anti-CD20 hIgG tailpiece hexamers demonstrated enhanced C1q affinity and complement-dependent cytotoxicity *in vitro*, but exhibited reduced depletion of target cells in whole blood assays, lacked *in vivo* efficacy, and demonstrated a significantly faster clearance rate than wild-type hIgG1. The hIgG1 IgM tailpiece C575S also had an enhanced ability to recruit C1q and elicit complement-dependent cytotoxicity, in the absence of enhanced C1q affinity. Additionally, there was no compromise to FcγR-mediated effector functions, with whole blood depletion comparable to wild-type hIgG1. *In vivo* efficacy, safety, and half-life were also comparable to wild-type hIgG1, with enhanced depletion in the lymph node for some anti-CD20 antibodies. Hence, the hIgG1 IgM tailpiece C575S represents a more suitable *in vivo* format.

The same technology was also applied to anti-CD40 monoclonal antibodies, which rely on effective receptor clustering for agonistic activity, and so were proposed to benefit from hexamerisation. In B cell stimulation assays *in vitro*, hexameric hIgG1, hIgG2, and hIgG4 demonstrated potent CD40 agonism, however, only the hIgG4 tailpiece C575S showed enhanced agonism compared to the inactive hIgG4 wild-type. In contrast, the hIgG1 tailpiece C575S did not exhibit more agonism and all hIgG2 formats were equivalently active. Further analysis of the hIgG4 anti-CD40 antibodies *in vivo* showed the native tailpiece hexamer was inactive, whereas the tailpiece C575S promoted CD40 agonism and humoral responses, in an FcγR-independent manner.

These results are in-line with the proposed activity of IgG on-target hexamer formation. Therefore, the IgG IgM tailpiece C575S represents a novel format for promoting on-target antibody hexamerisation for enhanced complement-dependent cytotoxicity or agonistic activities.

Contents

List of Figures

List of Tables

Declaration of Authorship

I, Joshua Sopp, declare that this thesis titled, Development of on-target hexamerisation for effective antibody immunotherapy, and the work presented in it are my own. I confirm that:

1. This work was done wholly or mainly while in candidature for a research degree at this University;
2. Where any part of this thesis has previously been submitted for a degree or any other qualification at this University or any other institution, this has been clearly stated;
3. Where I have consulted the published work of others, this is always clearly attributed;
4. Where I have quoted from the work of others, the source is always given. With the exception of such quotations, this thesis is entirely my own work;
5. I have acknowledged all main sources of help;
6. Where the thesis is based on work done by myself jointly with others, I have made clear exactly what was done by others and what I have contributed myself;
7. None of this work has been published before submission.

Signed:

_____

Date:

_____

Acknowledgements

I would like to start by thanking Prof Mark Cragg for his constant guidance and support throughout my PhD, and Prof Steven Beers and Prof Martin Glennie for their input in lab meetings, without who this work would not have come together as it did. A big thank you to Dr David Humphreys and Dr Shirley Peters for their guidance and exciting ideas over the course of my project, although maybe the idea of one too many constructs! Also to Dr Shirley Peters and Dr Tania Rowley for their guidance in the lab work at UCB, and for making me feel welcome during my time there.

Furthermore, I would like to thank all my colleagues in the Cragg lab group, particularly Michael Marshall, Robert Oldham, Kirstie Cleary, Matthew Carter, Thomas Murray, and Kerry Cox, for all their help and guidance with my lab work. All members of the antibody and vaccine group and the preclinical unit are deserving of a thank you for their excellent and patient training, assistance, and for being fantastic people to work with. Finally I would like to thank my collaborators UCB and the BBSRC for funding this project.

Personally, I would like to thank Lauren for supporting me and putting up with me being a student again for the last four years! Of course a special thanks goes to my family who have supported and encouraged me all these years throughout my studies, even if they don't really understand what I have been doing. I am sure they will be happy in the knowledge that I am finally done!

Abbreviations

ADC	Antibody-drug conjugate
ADCC	Antibody-dependent cellular cytotoxicity
ADCP	Antibody-dependent cellular phagocytosis
ADCR	Antibody-dependent cytokine release
AFM	Atomic form microscopy
A:I	Activator to inhibitory ratio
AID	Activation induced cytidine deaminase
α-chain	IgA heavy chain
αtp	IgA tail-piece
APC	Antigen presentation cell
AU	Absorbance Units
AUC	Analytical ultracentrifugation
BCR	B cell receptor
BSA	Bovine serum albumin
CBP	Carboxypeptidase B
CD	Cluster of differentiation
CDC	Complement-dependent cytotoxicity
CDR	Complementary determining region
CFSE	Carboxyflourescin succinimidyl ester
CH	Constant heavy chain domain
CHO	Chinese hamster ovary
CL	Constant light chain domain
CLL	Chronic lymphocytic leukaemia
CNV	Copy number variation
CO_2	Carbon dioxide
CPM	Count per minute
CRD	Cysteine rich domain
cRPMI	Complmete Roswell Park Memorial Institute medium

CTI	Cytotoxicity index
CTL	Cytotoxic T lymphocyte
CTLA4	Cytotoxic T-lymphocyte-associated protein 4
D	Diversity
DAMP	Damage associated molecule pattern
DC	Dendritic cell
DCD	Direct cell death
DC-SIGN	Dendritic Cell-Specific Intercellular adhesion molecule-3-Grabbing Non-integrin
δ-chain	IgD heavy chain
E.coli	Escherichia coli
EGFR	Epidermal growth factor receptor
ELISA	Enzyme-linked immunosorbent assay
EM	Electron Microscopy
ϵ-chain	IgE heavy chain
ER	Endoplasmic reticulum
F(ab)	Fragment antigen binding
Fc	Fragment crystallisable
FcαR	Fc alpha receptor
FcϵR	Fc epsilon receptor
FcγR	Fc gamma receptor
FcμR	Fc mu receptor
FcRγ	Common Fc gamma chain
FcRn	Neonatal Fc receptor
FCS	Foetal calf serim
fDC	Follicular dendritic cell
FSC	Forward scatter
γ-chain	IgG heavy chain
GITR	Glucocorticoid-induced TNFR receptor-related protein
GPI	Glycosylphosphatidylinositol
HAGG	Heat aggregated IgG
HC	Heavy Ig chain
HMWS	High molecular weight species
HPLC	High performance liquid chromatography
HRP	Horse radish peroxidase
HSC	Haematopoeitic stem cell
IFN-γ	Inteferon gamma

Ig	Immunoglobulin
IL	Interlukin
i.p.	Intraperitoneal
ITAM	Immunoreceptor tyrosine-based activatory motif
ITIM	Immunoreceptor tyrosine-based inhibitory motif
ITP	Immune thrombocytopenic purpura
i.v.	Intravenous
IVC	Individually ventilated cages
IVIG	Intravenous immunoglobulin
J	Joining
K_A	Affinity constant
κ-chain	Kappa light chain
KIR	Killer inhibitory receptor
LAL	Limulous amoebocyte lysate
λ-chain	Lambda light chain
LC	Light Ig chain
LMWS	Low molecular weight species
LPS	Lipopolysaccharide
mAb	Monoclonal antibody
MAC	Membrane attack complex
MALS	Multi-angle light scattering
MAPK	Mitogenactivated protein kinases
MASP	MBP-associated serine protease
MBP	Mannan binding protein
M-CSF	Macrophage colony-stimulating factor
MHC	Major histocompatability complex
MID	*Moraxella catarrhalis* outer membrane protein
MR	Mannose receptor
MSD	Mesoscale Discovery
μ-chain	IgM heavy chain
μtp	IgM tail-piece
MW	Molecular weight
NF-κB	Nuclear factor κ B
NHL	Non-Hodgkin's lymphoma
NK	Natural killer
ORR	Overall response rate

PAMP	Pattern associated molecular patterns
PBMC	Peripheral blood mononuclear cells
PBS	Phosphate buffered saline
PCR	Polymerase chain reaction
PD1	Programmed cell death protein 1
PI	Propidium iodide
PI3K	Phosphoinositide 3-kinase
PIP2	Phosphatidylinositol 4,5-bisphosphate
PLCγ	Phospholipase C γ
PNGase F	Peptide-*N*-glycosidase F
RPMI	Roswell Park Memorial Institute medium
PRR	Pattern recognition receptor
RTX	Rituximab
SDM	Site-directed mutagenesis
SDS-PAGE	Sodium dodecyl sulfate polyacrylamide gel electrophoresis
SEC	Size exclusion chromatography
sIg	Surface bound immunoglobin
SSC	Side scatter
TAE	Tris-acetate-EDTA
TAM	Tumour associated macrophages
TCR	T cell receptor
Tg	Transgenic
T_h	T helper
TLR	Toll-like receptor
TNFR	Tumour necrosis factor receptor
TRAF	TNF receptor associated factor
TRAIL	TNF-related apoptosis-inducing ligand
T_{reg}	T regulatory
UV	Ultraviolet
V	Variable
VEGF	Vascular endothelial growth factor
VH	Variable heavy chain domain
VL	Variable light chain domain
WT	Wild-type

Chapter 1

Literature review

1.1 Immune system

The human immune system is continuously being exposed to a large range of pathogens, such as microbes, viruses, and parasites, or altered self, such as diseased or cancerous cells. To counteract such potentially harmful threats and maintain health, the human immune system possesses a vast array of defence mechanisms at its disposal. These can be divided into two broad categories - innate and adaptive immunity.

1.1.1 Innate immune system

Innate immunity is provided by a network of cells and effectors molecules that are present from birth; it provides a broadly acting and immediate defence against pathogens. The innate immune system is the human body's first line of defence against environmental threats, with the aim of intercepting and neutralising foreign material [1], or in cases where neutralisation is not possible, aims to control the infection whilst the adaptive immune system develops a more specific response [2]. The innate immune system is pre-programmed to have a broad specificity, typically responding to the recognition of pathogenic motifs and invariant molecules [2] via a response that is not significantly altered upon repeated challenge [3]. These molecules are typically expressed on pathogenic surfaces or damaged host cells, and referred to as pathogen or damage associated molecular patterns (P/DAMPS). The innate immune system then recognises P/DAMPS by germline encoded pattern recognition receptors (PRRs) [4], which take the form of cell membrane bound protein, such as Toll like receptors (TLRs) [5], or soluble protein, such as C1q [2, 6].

The innate immune system utilises a number of different cell types, including myeloid cells and

natural killer (NK) cells [2]. Within the myeloid lineage of innate effector cells there are neutrophils, monocytes, macrophages, and dendritic cells (DCs). Neutrophils have a major role in the innate response, acting as a first line of defence against pathogens that have breached the physical barriers of the body (skin or mucosa) [7]. At the site of infection, neutrophils can act to phagocytose material, release cytotoxic granules, and secrete pro-inflammatory cytokines [8]. Monocytes are released from the bone marrow into the systemic circulation where they have the ability to phagocytose pathogens and secrete pro-inflammatory cytokines [9]. In addition to circulatory surveillance, monocytes have the capacity to extravasate out of the blood into tissues at the site of inflammation. When in tissues, monocytes can then differentiate into other myeloid effector cells, including macrophages and DCs [10]. Macrophages are tissue resident cells that are specialised phagocytes with heterogenous polarisation states determined by a complex milieu of stimulation, able to engulf large numbers of targets via a wide spectrum of PRRs [3]. DCs are another highly heterogenous myeloid cell population [11]. A crucial function of DCs is to phagocytose and present antigens to the adaptive immune system and to provide activation [12]. Monocytes, macrophages, DCs, and B cells are all referred to as professional antigen presenting cells (APCs) [3]. APCs phagocytose antigenic particles, such as bacteria and opsonised cells, processing them before displaying on the cell surface bound to class II major histocompatability complex (MHC-II) [13]. This allows for cross presentation to T cells and subsequent activation of the adaptive immune system.

NK cells are a lymphocyte population with PRRs expressed on their cell surface called killer inhibitory receptors (KIR) [14]. These receptors bind to 'self' receptors, such as class-I major histocompatabiltiy complex (MHC-I) on host cells. When engaged these receptors prevent the killing of host cells [15]. Therefore, any cell not displaying such 'self' receptors, such as non-host pathogens or infected host cells with downregulated MHC-I, are unable to bind KIRs on the NK cells and are targeted for destruction [16]. NK cells induce cellular lysis by releasing lytic granules containing perforins and granzymes [17] as well as delivering inflammatory responses through the secretion of cytokines.

The complement system is an example of an innate immune process utilising soluble protein as a PRR. The recognition of PAMPs by complement proteins induces a proteolytic cascade ultimately resulting in cellular or bacterial lysis, and recruitment of further immune cells [2, 6]. There are a variety of different PRRs that are recognised by the complement system, including, bacteria, viruses, and antibody immune complexes on opsonised targets [6, 18].

1.1.2 Adaptive immune system

Whereas the innate immune response is provided quickly (within minutes to hours), the adaptive immune response takes time to adapt after initial exposure and develop a highly specific response, through a period of selection before responding to the threat [3, 19]. In addition to eliciting a specific immune response to a particular antigen, the adaptive immune system also displays the key property of immunological memory [19]. The memory response enables the adaptive immune system to launch a counter-attack far more rapidly and with a greater magnitude in the event of a repeated challenge [20]. The cell types that mediate the adaptive immune response are T and B lymphocytes and have the capacity to detect and eliminate a vast repertoire of self and non-self antigens. In humans these cells are generated from haematopoietic stem cells (HSC) that mature either in the thymus (T cells) or bone marrow (B cells). Such lymphocytes express antigen specific receptors capable of recognising any potential molecular target. Activation of these antigen specific receptors results in expansion of the specific cells expressing reactivity to the given antigen and delivery of an effector response to eliminate the threat (see below) and the production of an immunological memory [19].

1.1.3 T cells

Naïve T cells migrate out of the bone marrow and develop in the thymus. During development, the cells generate a T cell receptor (TCR) specific for a single MHC-peptide complex. The TCR is composed of two polypeptide chains, an α and a β chain, both composed of a constant and variable domain [21]. A single α and a single β chain are complexed as a heterodimer, bound by a disulphide bond, to produce the TCR. Each TCR is associated with cluster of differentiation (CD) 3 and a homodimeric ζ chain, which mediate the intracellular signalling of the receptor [22]. Each individual cell generates an antigen specific TCR from random recombination of a diverse set of gene segments [3]. These gene segments are known as variable (V), diversity (D), and joining (J) segments [23]. The TCRα locus contains V and J gene segments, and the TCRβ locus contains V, D, and J segments. These gene loci undergo VDJ recombination to generate a unique antigen specificity, which allow the T cell pool to be capable of recognising almost any potential target [24].

Following TCR generation, T cells undergo a process called thymic selection. Here, self-antigens are presented to naïve T cells as peptides displayed on MHC molecules. Any TCR that has high affintiy for self-antigens are edited by TCR mutation or deleted. This process of negative selection prevents T cells specific for self antigens from being released into the periphery attacking the host

[25]. Non-functional T cells with TCR that do not bind MHC molecules are also deleted during thymic selection [26].

Following selection, T cells are released from the thymus as naïve T cells [27]. In the periphery a TCR can interact with MHC molecules complexed with a foreign peptide antigen [3]. Binding of the TCR to its cognate antigenic peptide presented by an MHC molecule results in an intracellular signalling cascade and activation of transcription factors and changes to gene expression [28]. However, this interaction is insufficient to fully activate naïve T cells and a concurrent co-stimulatory signal is required through engagement with molecules such as CD28, 4-1BB (CD137), or OX40 (CD134) on the T cell surface [29–31].

T cells can differentiate into a variety of subsets, such as $CD4^+$, $CD8^+$, and regulatory T cells (T_{regs}). Differentiation into either $CD4^+$ or $CD8^+$ T cells is determined by the ability of the TCR to bind with either MHC-II or MHC-I, respectively. MHC-I molecules are expressed on all nucleated cells and present cytosolic peptides of 8-15 amino acids in length to CD8 TCRs, and MHC-II molecules are expressed on APCs and complex with peptides of 11-30 amino acids to CD4 TCRs. $CD4^+$ cells are referred to as T helper (T_h) cells and can differentiate into a variety of lineages, dependent on their exposure to different cytokines [32]. This further differentiation enables $CD4^+$ T cells to provide both immunostimulatory (T_h1) or immunosuppressive (T_h2) immunological responses [3]. $CD8^+$ T cells, or cytotoxic T lymphocytes (CTL), recognise their peptide antigen in complex with MHC-I. Upon activation CTLs release perforin and granzymes to lyse the target cell, in addition to secretion of pro-inflammatory cytokines [33]. Regulatory T cells (T_{regs}) have a critical role in immune regulation. Generally T_{regs} down-regulate immune response to non-pathogenic antigens, such as gut flora, but are also involved in regulating chronically inflamed environments through release of immunosupressive cytokines [34]. In addition to the important immunological functions of $CD4^+$ and $CD8^+$ effector T cells, both subsets contain cells that are long-lived, known as memory T cells. These cells cache immunological memory for a specific antigen which allows for a rapid proliferation and higher magnitude response to a repeat challenge [35].

1.1.4 B cells

Humoral immunity is orchestrated by B cells. B cells develop in the bone marrow from HSCs (Figure 1.3). Similar to T cells, B cells also have a surface expressed receptor with unique specificity to an antigenic determinant, called the B cell receptor (BCR). The BCR is a complex of two signalling chains, CD79a and CD79b, and a surface bound immunoglobulin (sIg). The sIg consists of two chains: heavy chain (HC) and light chain (LC). Two identical HC and two identical LC, bound by

intermolecular disulphide bonds form a Y-shaped molecule that make an immunoglobulin (Ig) (Ig structure discussed in detail later). Igs are capable of recognising an extensive array of molecular targets with high degrees of specificity and affinity, essentially labelling their targets for detection and/or destruction by the innate immune system or blocking them from interacting with host receptors. The molecular target of an antibody is known as an antigen. The antigen contains a specific sequence of amino acids or tertiary/quaternary protein structure that is recognised and bound by the antibody, called the epitope. When antigen is bound to the sIg, the BCR is activated and the complexed CD79 heterodimer transduces a signal via intracellular immunoreceptor tyrosine activation motifs (ITAMs) to activate the B cell [36].

Initially the BCR will be either the IgM or IgD isotype (Ig isotypes discussed in detail later). Like the TCR, the specificity of the BCR is generated through the process of VDJ recombination [37] that has the potential to generate antigen binding to approximately 5×10^{13} different molecular epitopes [38]. The VDJ segments are present in the genome in multiple copies that differ in their nucleotide sequence. These differences give rise to the diversity of potential recognisable epitopes [37]. VDJ recombination occurs during B-cell development over a number of genetic reorganisation events (Figure 1.1). In the case of the HC, a random D segment is first joined to a random J segment in pre-pro-B cells. This is followed by the joining of the DJ segment with a V segment to produce a functional HC [39]. In addition to VDJ antigenic diversity, further variability is introduced at the joining sites between each segment produced by the random addition or deletion of nucleotide bases, occurring through DNA repair mechanisms [3]. This produces the pre-BCR, which is expressed and coupled with a surrogate LC. The final pre-BCR is trafficked to the cell surface of large pre-B-cell and starts signalling to promote proliferation and differentiation into small-pre-B cells (assuming correct folding and expression). The LC then undergoes a similar process of recombination to the HC, with the exception that there is no D segment and only VJ recombination [40]. The mature HC and LC are then expressed and complex to form a heterodimer, which is trafficked to the cell surface as sIg to form the BCR on the immature B cell. Following mature BCR expression B cells undergo negative selection and subsequent elimination (clonal deletion) in the bone marrow if the BCR expressed is self-reactive and binds to self antigens [3]. If the BCR does not interact with self-antigen, the B-cell will migrate to the spleen to differentiate into mature follicular or marginal B cells. Here the B cell requires the BCR to be stimulated through antigenic interaction in order to survive (clonal selection). Strong BCR signalling induces maturation to follicular lineages whereas weaker signals result in marginal zone B cells [35]. Follicular B cells circulate between secondary lymphoid organs where detection of their cognate antigen stimulates activation and migration to the border of the T zone and interact with T cells through CD40-CD40L to induce germinal centre formation [41].

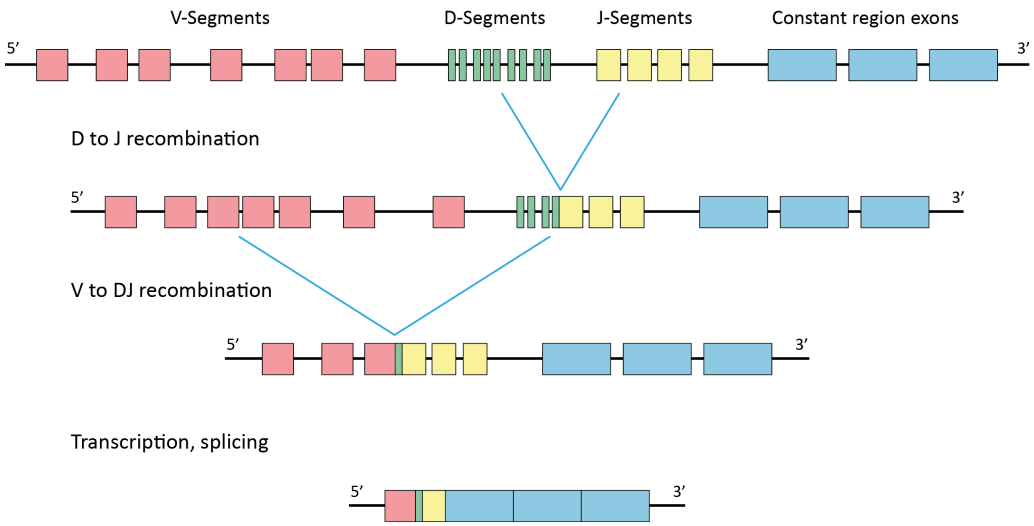

Figure 1.1: Schematic diagram of HC VDJ recombination.
VDJ recombination occurs in the bone marrow during B cell development to produce the HC nucleotide sequence.

Germinal centres are formed of dark and light zones that aid in B cell differentiation. In the dark zone of germinal centres B cells undergo rapid proliferation and somatic hypermutation [42]. During the process of somatic hypermutation, further mutations are introduced randomly into the variable domain of the BCR through double strand DNA breaks and error prone repair mechanisms involving the enzyme activation induced cytidine deaminase (AID) [43]. Competition between mutated B cell clones expressing mutated BCR in the face of limiting antigen allows selection of higher affinity clones that will out-compete low affinity clones for antigen binding. Low affinity clones will not be selected and undergo apoptosis, whereas high affinity clones will progress to the light zone [44]. After B cells leave the dark zone, they can re-enter to undergo further somatic hypermutation, producing even higher affinity clones [45].

In the light zone B cells can also undergo a process of somatic class switching from IgM/D to IgA, IgD, IgE, or IgG [41] which is promoted by CD40 and/or TLR stimulation, in addition to cytokines from T_h cells upon specific antigen stimulation [46]. The process of class switching involves irreversible genetic rearrangement of VDJ relocation to the constant region encoding another Ig class (Figure 1.2) [42, 43, 46]. The light zone also has follicular dendritic cells (fDCs) that provide pro-survival signals to B cells and retain unprocessed antigens as long term deposits.

B cells subsequently differentiate into either plasma cells or memory B cells [38] (Figure 1.3). Plasma cells are specialised at expressing and secreting high titres of antibodies to effectively neutralise and/or flag targets for destruction, with specificity towards the antigen that promoted activation of the original B cell. Plasma cells can secrete antibody at a rate of 2000 molecules per second [3] and are either short-lived, only surviving for the duration of the infection, or long-lived, residing in the bone marrow, maintaining circulating levels of antibody for years [47]. Alternatively, memory B cells proliferate rapidly upon rechallenge with their cognate antigen resulting

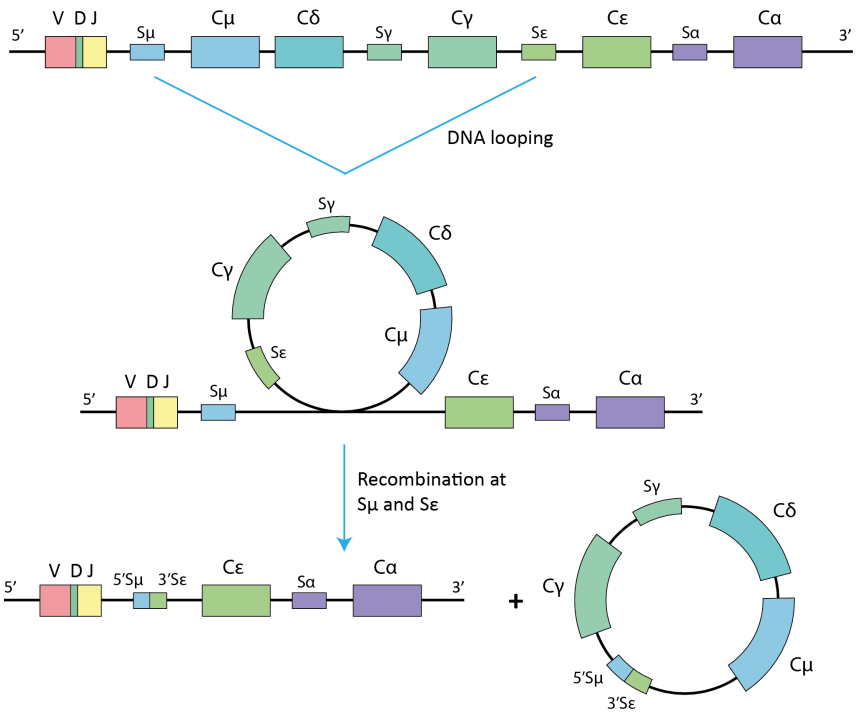

Figure 1.2: Schematic diagram of Ig class switching from Cμ to Cϵ.
Somatic class switching occurs after clonal selection through the process of DNA looping in response to activation and T_h cell stimulation.

in higher levels of antibody production, more rapidly than during a primary response [48]. This principal underpins almost all successful vaccines used to date.

B cells provide protection against a wide array of pathogens through the production and secretion of highly effective antibodies, a component of which is encoded by the isotype. Each antibody isotype impart specialised roles in humoural immunity, thus yielding comprehensive protection from environmental threats which will be discussed in further detail below.

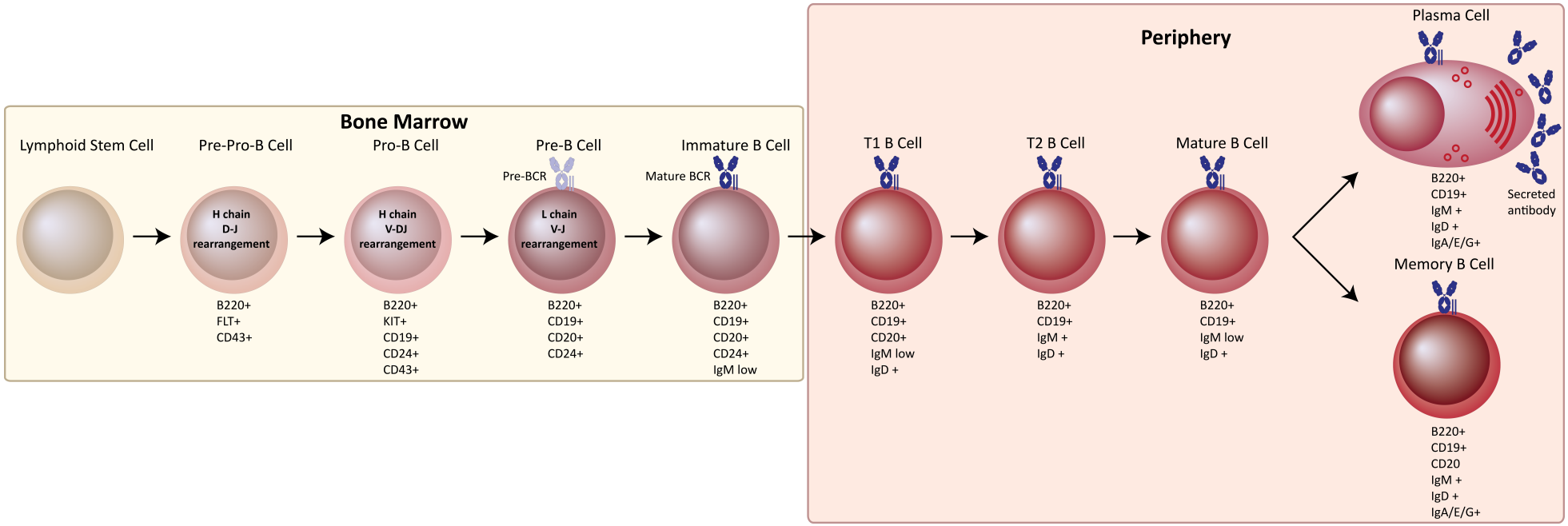

Figure 1.3: The development of B cells and their respective cellular markers.
The development of B cells in the bone marrow and periphery which undergo rounds of developmental and selection stages to yield highly specific non-self BCR to produce potent immunity and a memory response. Adapted from [49]

1.2 Antibodies

Antibodies are glycoproteins secreted by plasma cells generated in response to environmental threats as detailed above. The main function of secreted antibodies is to serve as effectors of the humoral branch of the adaptive immune system, binding their cognate antigen for neutralisation and/or destruction by elements of the innate immune system [50]. Due to the specific and effective nature of antibodies in the humoral immune response, antibodies have been exploited therapeutically. The induction of anti-pathogen antibodies via vaccinations [51], and the passive transfer from immunocompetent patients to an immunocompromised patient have both been successful therapeutically [52]. More recently recombinantly produced monoclonal antibodies (mAb) have been utilised, approved, and employed for use in the treatment of cancer [53] and autoimmune diseases, such as rheumatoid arthritis [54].

1.2.1 Antibody structure

Antibodies are tetrameric glycoproteins, composed of two different polypeptide chains, a HC and a LC. The HC folds into either four or five Ig domains, depending on the isotype, with a molecular weight between 50 - 80 kDa. The LC folds into two Ig domains with a molecular weight of $\sim$25 kDa [50]. The amino terminus of the HC and the LC is referred to as the variable domain, named the VH in the heavy chain and the VL in the light chain. The sequence of the V-domain differs between antibodies and determines the epitope specificity. The bulk of the variability is contained in three hypervariable polypeptide loops. These are responsible for interacting with the specific epitope and are known as the complementary determining regions (CDRs). Each of the VL and VH donates three CDRs to the antigen binding interface, with CDR3 being the most diverse.

The other domains are known as the constant domains, named CH in the HC and the CL in the LC. The sequences of the constant domains are conserved between the HC and LC classes that make up the antibody isotypes. The HC denotes the isotype of the antibody and is composed of either a α, δ, ϵ, γ, or μ-chain. The LC can be either a κ-chain or a λ-chain. One HC and one LC are bound together by disulphide bonds and other non-covalent interactions, such as salt bridges, hydrogen bonding, and hydrophobic interactions, to form a HC-LC heterodimer. Two identical HC-LC heterodimers are then linked together by further disulphide bonds and non-covalent interactions to form the $(\text{HC-LC})_2$, composing the four polypeptide chain antibody structure. The resulting antibody is bivalent with two identical binding arms (Figure 1.4).

Igs are bi-functional molecules, able to bind both antigen and immune effector molecules or re-

ceptors, which is achieved through spatial separation of the two functional functions. Antigen binding and specificity derives from the fragment antigen binding (F(ab)) domain, and the fragment crystallisable (Fc) domain (Figure 1.4) is responsible for recruitment of the immune system. The Fc domain is crucial for eliciting the cytotoxic mechanisms of antibodies and interacts with a range of immune effectors such as the serum molecule C1q, the first component of the complement system, and cell surface expressed Fc receptors (discussed later). When antibodies are digested with the protease papain two functionally distinct domains are produced, a F(ab) fragment and an Fc fragment [55]. Incubation with the protease pepsin results in the digestion of the Fc portion to leave the F(ab')$_2$ fragment, that retains antigen bivalency but removes the Fc and its associated functions of the full length IgG [56] (digestions shown in Figure 1.4).

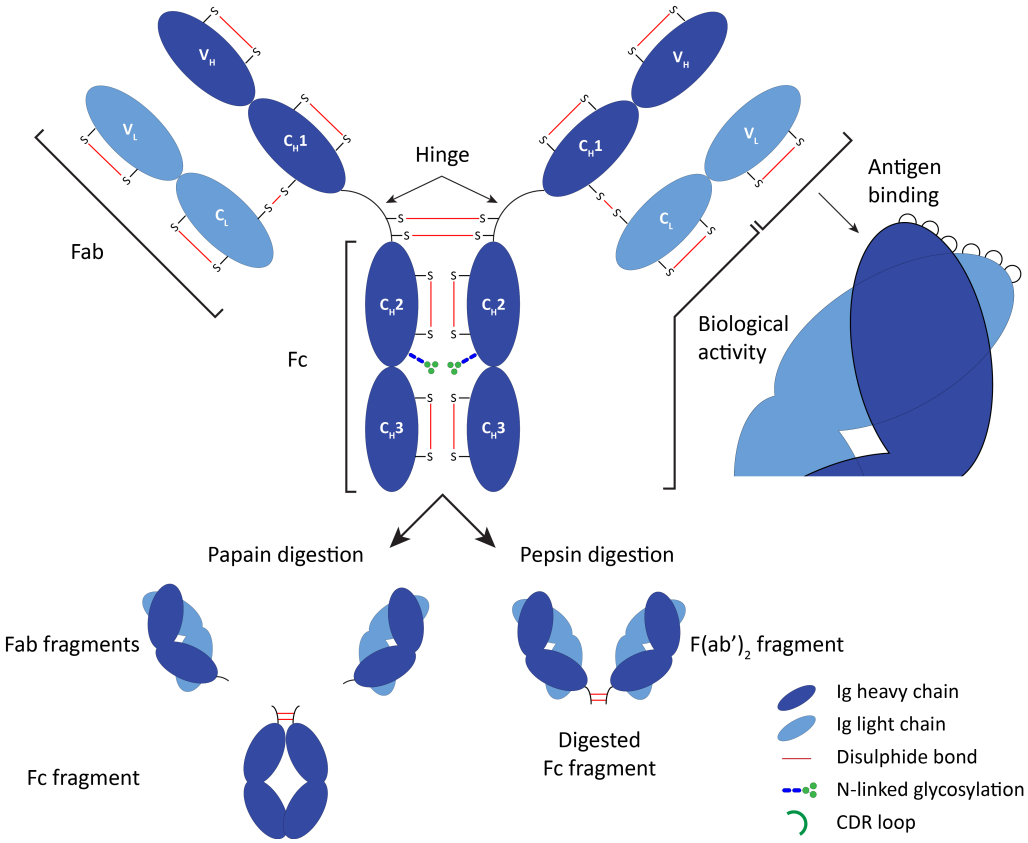

Figure 1.4: Schematic diagram of IgG structure.
IgG is a glycoprotein of approximately 150 kDa with a single N-linked glycosylation site in the Fc region. IgG's are composed of six Ig domains, four heavy chain domains (dark blue) and two light chain domains (light blue) stabilised by disulphide bonds. The flexible hinge region is located between CH1 and CH2 domains. The VL and VH combine to form the antigen binding region and contain the CDR loops (green). The three constant domains of the heavy chain confer the biological activity of the molecule. The two C-terminal constant domains (CH2 and CH3) of IgG1 compose the Fc portion of the antibody. Digestion with pepsin produced individual F(ab) fragments, which display monovalent binding properties and the Fc fragment. Digestion with papain removes the Fc region to leave F(ab')$_2$ fragments that retain bivalent binding properties.

1.2.2 Antibody isotypes

In humans, antibodies are split into five classes of antibodies, named IgA, IgM, IgE, IgD, and IgG, distinguished by their class-specific structure and biological functions encoded by their differing HC. The structure differs slightly between antibody isotypes. In the case of IgD, IgG, and IgA the two F(ab) arms are linked by a hinge region composed of a disordered peptide linker that permits F(ab) arm flexibility. The length and composition of each of the peptide hinge regions varies between the isotypes IgA, IgD, and IgG. In the case of IgM and IgE an additional constant domain constitutes the hinge (Figure 1.5,A). Each of the isotypes IgA, IgG, IgE, and IgM bind to exclusive Fc receptors; FcαR, FcγR, FcϵR, and FcμR, respectively. Each isotype also has a specific pattern of glycosylation that aids in stabilising the structure of the antibody, in addition to facilitating its functional binding to effector molecules such as C1q and Fc receptors. The oligomeric state of the antibody isotypes is also important to their function. IgA, IgG, IgD, and IgE are produced and secreted as monomers, whereas IgM and secretory IgA are active in oligomeric species of pentamers

and dimers, respectively [50] (Figure 1.5,B).

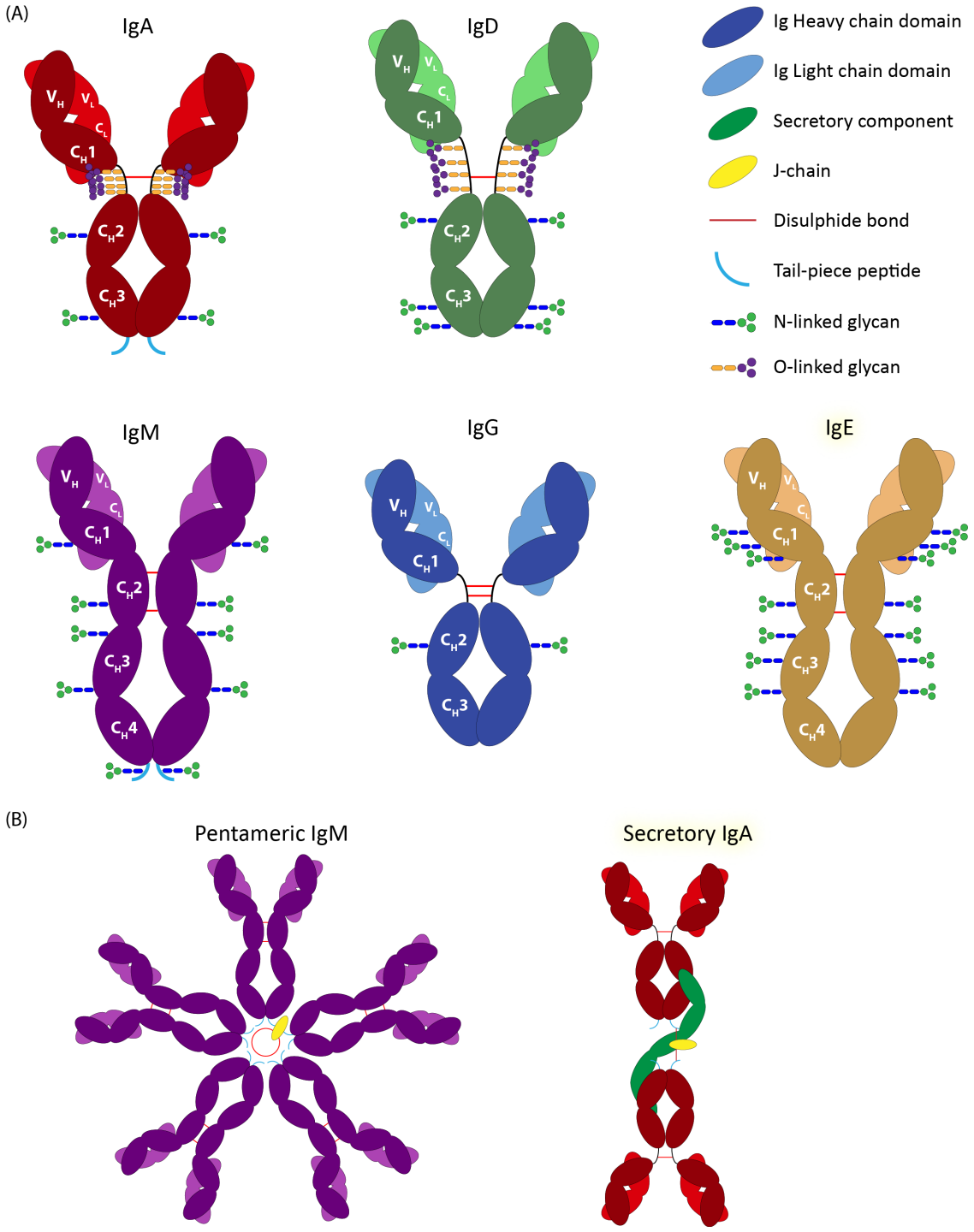

Figure 1.5: Structures of human Ig isotypes.
(A) The structure of the five human Ig isotypes: IgA, IgD, IgM, IgG, and IgE. Each monomer contains two heavy chains and two light chains bound by disulphide bonds. Antigen binding is facilitated by the variable domains, VL and VH, of the heavy and light chains. Each of IgA, IgD, and IgG have three constant domains, whereas IgM and IgE have an additional constant domain and a shorter hinge region (B) IgM and IgA exist secreted as pentamers and dimers respectively through interaction with the J-chain. Secretory IgA also interacts with the secretory component. Heavy chains are shown in dark colours and light chains shown in light colours.

1.2.2.1 IgA

IgA is the most abundantly produced Ig isotype and the predominant Ig class in external secretions, such as saliva, but only accounts for 10-14% of total serum Ig [57]. In the serum IgA is largely present in its monomeric form, but polymeric structures are also observed. Externally secreted IgA is known as secretory IgA, which consists of two IgA molecules each containing an 18 amino acid extension at the C-terminus, named the IgA or α tailpiece (αtp: PTHVNVSVVMAEVDGTCY) [58], a J-chain, and a polypeptide called the secretory component. The conserved cysteine present at the penultimate position of the αtp of one IgA monomer forms a disulphide linkage with the J-chain, which then forms a disulphide bond with the αtp of an adjacent IgA monomer [59]. The secretory component is derived from the poly-Ig receptor. The poly-Ig receptor interacts with the J-chain of IgA dimers or IgM pentamers, and transports the antibodies across membranes into mucosal secretions, where the receptor is enzymatically cleaved to become the secretory component [60]. In the protease-rich mucosal environment the secretory component also extends the half-life of the antibody. The mucosal environment is the main entry site for pathogens such as bacteria and viruses. IgA opsonises such pathogens to prevent attachment to mucosal surfaces and serves an import defence mechanism [50].

In contrast to secretory IgA, serum IgA is present as a monomer and is able to engage with the FcαR present on a number of myeloid derived cells such as granulocytes and macrophages. There are two subclasses of IgA produced, IgA1 and IgA2. The two IgA heavy chains differ by 22 amino acid residues, predominalty due to a 13 amino acid deletion to the hinge region of IgA2. The extended hinge of IgA1 also contains several O-linked glycosylation sites [61]. The lack of this extended region makes IgA2 more resistant to protease degradation [57].

1.2.2.2 IgM

IgM accounts for 5 – 10% of total serum Ig. IgM is primarily secreted as a pentamer (95%) in association with the J-chain, but in low-levels or absence of a J-chain it can self-associate to be secreted in a hexameric format (5%) [62]. The C-terminus of the CH4 domain contains an additional 18 amino acid peptide, named the IgM or μ tailpiece (μtp: PTLYNVSLVMSDTAGTCY). The μtp shares 60% sequence homology to the αtp and also contains a conserved cysteine residue (C575) at the penultimate residue [63, 64] and a glycosylation site occupied predominantly by high mannose glycans [65, 66]. The oligomeric pentamers and hexamers are stabilised by disulphide bonds linking cysteines in neighbouring CH3 domains and μtp peptides [67]. The glycosylation of the μtp has also been suggested to be involved in stabilising these structures and J-chain incorporation in

IgM pentamers [68].

Through partial reduction of disulphide bonds and analytical ultracentrifugation (AUC) sedimentation analysis this cysteine has been determined to be involved in intermolecular disulphide bond formation between monomer sub-units within the polymeric IgM complexes [69]. Two of the penultimate cysteines in the μtp's of two IgM monomers are bound by disulphide bonds to the J-chain and the others to neighbouring μtp cysteines (Figure 1.5,B). The Fc domains of the IgM polymer are arranged towards the centre of the complex, and the antigen binding sites to the periphery. Due to the presence of the J-chain, IgM can also bind to poly-Ig receptors and be secreted into mucosal secretions. Although it is not as abundant as IgA, IgM still plays an important role in combating pathogens in mucosal secretions [70].

The 180 kDa monomeric IgM can also be expressed as a membrane bound antibody at the B cell surface. IgM is the first BCR to be displayed on immature B cells, with the role of detecting antigen. When expressed as a surface bound receptor there is an addition to the C-terminal tailpiece of a short cytoplasmic tail containing a conserved lysine (K), valine (V), lysine (K) motif, which is required for membrane integration [71]. IgM is the first isotype of antibody to be produced in the humoral immune response. IgM antibodies typically have low monovalent affinity, but due to their high valency are efficient at binding antigens with high avidity to opsonise and neutralise a target.

1.2.2.3 IgE

Although IgE exists in the serum in the lowest concentration of any antibody isotype (around 0.05% or 0.3 μg/ml of total Ig), it exhibits potent biological activity. IgE binds to its high affinity FcϵR, expressed on eosinophils, basophils, mast cells, and Langerhans cells in the absence of any antigen [72]. Cross-linking of the receptor bound IgE by an antigen induces rapid degranulation in these cell types, giving rise to allergic manifestations, releasing mediators such as histamine, serotonin, lipid mediators (prostaglandin, leukotrienes), proteases, chemokines, and cytokines. IgE mediates the immediate hypersensitive reactions in allergic reaction, such as asthma or hay fever, and is responsible for the symptoms of anaphylactic shock [73]. This antibody class is also involved in the response to parasitic infections, such as helminths [74].

1.2.2.4 IgD

IgD constitutes around 0.2% of total serum Ig, circulating in the serum at 30 μg/ml. Together with IgM, IgD is the major membrane bound Ig expressed by mature B cells, containing either a transmembrane domain or a glycosylphosphatidylinositol (GPI) anchor [75]. It has a long hinge region, consisting of 64 amino acid residues with multiple O-linked glycosylation sites, which gives rise to a distinctive 'T-shape' [76]. This distinctly long hinge region has recently been suggested to impart responsiveness to polyvalent but not monovalent antigens [77]. Currently its role in the immune system is unclear and no discrete biological function of the antibody has been identified. IgD is however bound in a non-immune manner, not involving the normal antigen binding site, by an outer membrane protein (MID) of the *Moraxella catarrhalis* microbe. The binding of MID to the IgD B-cell receptor causes activation of B-lymphocytes [78].

1.2.2.5 IgG

IgG is the most abundant antibody isotype found in serum, making up around 80% of total serum Ig. IgG antibodies have a molecular weight around of $\sim$150 kDa, a single N-linked glycosylation site at Asn297, and in general have high affinity for their antigens. They are typically efficient at recruiting and engaging immune effector cells, fixing complement, and causing direct effects through F(ab) binding, although this varies with subclass. There are four human IgG (hIgG) subclasses in humans that have been characterised by differences in the heavy γ chain, so-called IgG1, IgG2, IgG3, and IgG4 based on their relative concentration in serum (in decreasing order) [79]. The germ-line genes that encode each γ-chain share 90 - 95% homology in their amino acids sequences (Figure 1.6,A) [80]. The structural differences observed between subclasses are localised largely to the hinge region, which differ in size and number of inter-chain disulphide bonds. The functional differences are largely restricted to amino acid differences in the upper CH2 domain which implicate their interactions with receptors of the immune system (properties of IgG subclasses detailed in Figure 1.6,B) [80]. The IgG subclasses interact with the 5 activating receptors (FcγR) expressed in humans, FcγRI (CD64), FcγRIIa (CD32a), FcγRIIc (CD32c), FcγRIIIa (CD16a), and FcγRIIIb (CD16b), as well as one inhibitory receptor, FcγRIIb (CD32b). This interaction occurs via their Fc domain with varying affinities. In addition to the FcγRs, IgG binds to the neonatal Fc receptor (FcRn) on various cells types, including epithelial cells [81]. IgG has also been reported to bind various other surface expressed receptors, such as the C-type lectin receptor DC-SIGN [82], although conflicting evidence has recently been reported that query this observation [83].

(A)

```
Isotype                                                                                                  Amino Acid #
                                                CH1
hIgG1  ASTKGPSVFPLAPSSKSTSGGTAALGCLVKDYFPEPVTVSWNSGALTSGVHTFPAVLQSS  60
hIgG2  ASTKGPSVFPLAPCSRSTSESTAALGCLVKDYFPEPVTVSWNSGALTSGVHTFPAVLQSS  60
hIgG4  ASTKGPSVFPLAPCSRSTSESTAALGCLVKDYFPEPVTVSWNSGALTSGVHTFPAVLQSS  60
       ************:*:***::******************************************
                                                Hinge
hIgG1  GLYSLSSVVTVPSSSLGTQTYICNVNHKPSNTKVDKKVEPKSCDKTHTCPPCPAPELLGG  120
hIgG2  GLYSLSSVVTVPSSNFGTQTYTCNVDHKPSNTKVDKTVERKCCV---ECPPCPAPPV-AG  116
hIgG4  GLYSLSSVVTVPSSSLGTKTYTCNVDHKPSNTKVDKRVESKYGP---PCPSCPAPEFLGG  117
       ***************::**:**:***:**********:**:*:::::::**:****::::*
                                                CH2
hIgG1  PSVFLFPPKPKDTLMISRTPEVTCVVVDVSHEDPEVKFNWYVDGVEVHNAKTKPREEQYN  180
hIgG2  PSVFLFPPKPKDTLMISRTPEVTCVVVDVSHEDPEVQFNWYVDGVEVHNAKTKPREEQFN  176
hIgG4  PSVFLFPPKPKDTLMISRTPEVTCVVVDVSQEDPEVQFNWYVDGVEVHNAKTKPREEQFN  177
       ********************************:******:**********************:*

hIgG1  STYRVVSVLTVLHQDWLNGKEYKCKVSNKALPAPIEKTISKAKGQPREPQVYTLPPSRDE  240
hIgG2  STFRVVSVLTVVHQDWLNGKEYKCKVSNKGLPAPIEKTISKTKGQPREPQVYTLPPSREE  236
hIgG4  STYRVVSVLTVLHQDWLNGKEYKCKVSNKGLPSSIEKTISKAKGQPREPQVYTLPPSQEE  237
       **:*********:******************:**::********:****************::*
                                                CH3
hIgG1  LTKNQVSLTCLVKGFYPSDIAVEWESNGQPENNYKTTPPVLDSDGSFFLYSKLTVDKSRW  300
hIgG2  MTKNQVSLTCLVKGFYPSDISVEWESNGQPENNYKTTPPMLDSDGSFFLYSKLTVDKSRW  296
hIgG4  MTKNQVSLTCLVKGFYPSDIAVEWESNGQPENNYKTTPPVLDSDGSFFLYSRLTVDKSRW  297
       :*********************:******************:************:*********

hIgG1  QQGNVFSCSVMHEALHNHYTQKSLSLSPGK  330
hIgG2  QQGNVFSCSVMHEALHNHYTQKSLSLSPGK  326
hIgG4  QEGNVFSCSVMHEALHNHYTQKSLSLSLGK  327
       *:****************************:**
```

(B)

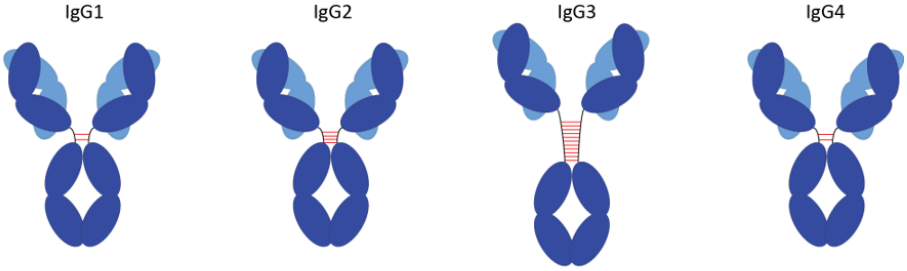

	IgG1	IgG2	IgG3	IgG4
Average Mr	146	146	170	146
Hinge Length (AA)	15	12	62	12
Disulpide bonds in hinge	2	4	11	2
Half-life (days)	21	21	7	21
Placenta transfer	++++	++	++++	+++
Serum levels (mg/ml)	6.98	3.8	0.51	0.56
Relative Abundance (%)	60	32	4	4

Figure 1.6: Sequence and structural differences of hIgG subtypes.
(A) Sequence alignment of human hIgG1, hIgG2, and hIgG4 HCs, covering the CH1, hinge, CH2, and CH3 regions. Amino acid homology is indicated by a * and amino acid differences are indicated by : (B) Structural differences in IgG arise from the molecular weight, hinge length (number of amino acids), and number of hinge disulphide bonds. The isotypes also exhibit differences in their properties such as half-life and placental transfer. The half-life of IgGs is relatively long with the exception of IgG3. The serum levels and relative abundance in the serum varies across subtypes.

IgG1 and IgG3 are the most pro-inflammatory subclasses, and are generated in response to soluble protein and surface antigens [80]. These two IgG subclasses have the strongest affinities of all subclasses to the FcγRs [84]. IgG1 is the most commonly produced subclass and have a half-life similar to IgG2 and IgG4 subclasses. IgG3 possesses an extended hinge region with 11 interchain disulphide bonds which, due to high proteolytic degradation, is partly responsible for its short

serum half-life compared to other IgG subclasses (Figure 1.6) [85]. Notably, IgG3 also has an Arg at position 435, whereas other IgG subclasses have a His residue at this position. The R435 effects interactions with the neonatal Fc receptor (FcRn), and is outcompeted by other IgG subclasses for binding. This has been suggested to reduce the half-life of IgG3, as a R435H mutation gives IgG3 a half-life comparable to IgG1 [86].

IgG2 is thought to be produced to target bacterial carbohydrate antigens [87] and has a much weaker affinity for most FcγRs, with particular regards to FcγRI compared to IgG1 and IgG3 [84]. The presence of additional Cys residues in the upper hinge gives rise to IgG2 isoforms with differences in their disulphide bond configurations, these are named IgG2-A, -B, and –A/B [88]. It is thought that the different isoforms of IgG2 have different structures and functions, and *in vivo* is speculated to interconvert, so its net activity is considered to be dependent on the distribution of IgG2 isoforms [89, 90].

IgG4 is mostly associated with a response to chronic or repeated antigens [91]. IgG4 displays weak interactions with all FcγRs except for FcγRI [84]. In contrast to other IgG subclasses, IgG4 is known to undergo the process of F(ab)-arm exchange, resulting in a bispecific, monovalent antibody form. F(ab)-arm exchange involves the shuffling of HC-LC dimers between different IgG4 molecules to produce an antibody with specificity for two separate antigens (Figure 1.7). The process is enhanced by reducing conditions driven by a combination of labile disulphides in the hinge [92] and weak non-covalent CH3:CH3 interactions compared to other IgG antibody classes [93, 94]. Mutation of S228P (P being the amino acid in IgG1 and IgG2) in the hinge region reduces F(ab) flexibility, inhibiting the formation of intra-chain disulphide bonds in the hinge, and stabilises IgG4 molecules from F(ab) arm exchange [95].

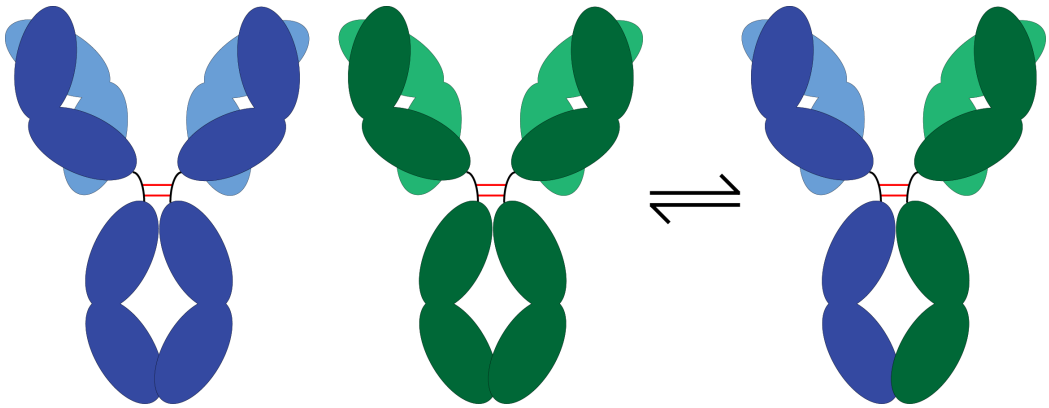

Figure 1.7: F(ab)-arm exchange of IgG4
The HC-LC dimers of IgG4 undergo reduction of the disulphide bonds linking the two dimers of a monospecific IgG4 and subsequent shuffling of the HC-LC dimers with another IgG4 molecule to produce a full IgG4 containing two different antigen binding specificities (indicated by blue and green colours)

1.2.3 Antibody glycosylation

All antibody isotypes have distinct glycosylation profiles, that differ in terms of number of glycosylation sites and composition of sugars (Figure 1.5,A). The glycans are covalently bound to either the amide nitrogen of asparagine (N) or oxygen atoms in serine or threonine residues, named N-linked and O-linked, respectively. The processing of O-linked glycans occurs in the golgi, where a single sugar is added at a time catalysed by specific enzymes [96]. Conversely, the addition of N-linked glycans occurs co-translationally in the endoplasmic reticulum. A 14 carbohydrate precursor, Glu3Man9GlcNac2, is transferred to the amide group of an Asn residue within an Asn-X-Ser/Thr motif (where X is any amino acid except proline) of the nascent polypeptide during translation [97, 98]. The N-linked glycan is then processed by glycosylases and glycosyltransferases downstream in the endoplasmic reticulum (ER) and golgi to produce the mature glycan [99].

The antibody isotypes and subclasses display considerable diversity in the location and abundance of conserved glycan sites [100]. Between these glycan sites there is also differentially processed glycosylation profiles that can include complex, hybrid, or oligomannose carbohydrate chains depending on accessibility by processing enzymes. In general, germ line glycosylation sites are only present on the constant domains of HC and there are no conserved glycosylation sites on LC. However, during the process of somatic hypermutation additional glycosylation sites can be randomly inserted into either chain. It has been estimated that 15 - 25% of IgG in the serum contains N-glycosylation sites in the F(ab) region, which can have significant implications on stability, half-life, and functional characteristics [101]. The presence of glycosylation on antibodies has been demonstrated to be important for their immunological functions [100]. In IgG, for example, the N-linked glycan at Asn297 of the C_H2 domain is required to maintain structural stability of the Fc though glycan-glycan interactions and is important for subsequent interactions with effector molecules and receptors, such as FcγRs [102].

1.3 Fc gamma receptors

Humans possess the genes to express six different Fcγ receptors: FcγRI (CD64), FcγRIIa (CD32a), FcγRIIb (CD32b), FcγRIIc (CD32c), FcγRIIIa (CD16a), FcγRIIIb (CD16b). The structures and expression pattern of these receptors are shown in Figure 1.8. FcγRs are members of the Ig receptor superfamily. Structurally they are composed of multiple extracellular Ig domains, three in the case of FcγRI and two in all other FcγRs, that are able to bind to the Fc of antibodies, albeit with differing affinities [103]. Intracellularly, the FcγR's differ in their signalling domains and are grouped into either activatory or inhibitory receptors. The activatory receptors induce an intra-

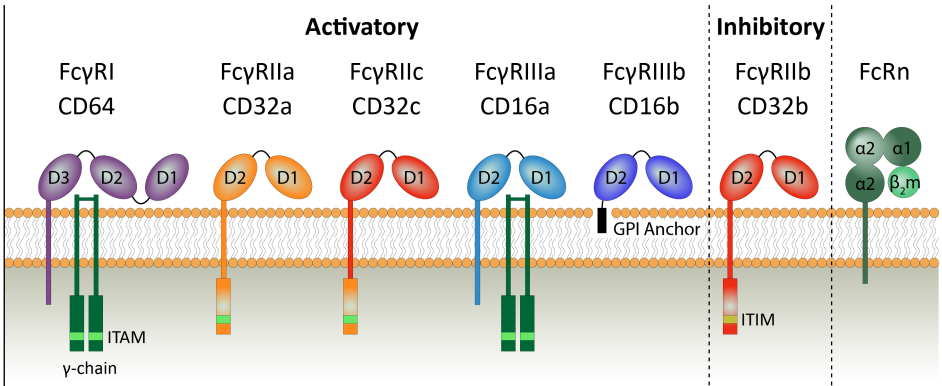

Cell Type	Cell Frequency						
B cell	-	-	+/-	-	-	+	-
T cell	-	-	-	-	-	-	-
Monocyte	+	+	-	+	-	+	+
Macrophage	+	+	-	+	-	+	+
Neutrophil	-	+	-	-	+	+	+
NK-cell	-	-	+/-	+	-	-	-
Dendritic cell	+	+	-	-	-	-	+
Eosinophil	+	-	-	-	+	-	-
Basophil	-	+	-	-	+/-	+	-

Figure 1.8: Structure and expression pattern of human Fcγ receptors.
The FcγR's expressed in humans consist of two or three extracellular Ig domains, a transmembrane region (or lipid anchor), and an intracellular domain. The extracellular domains bind to the Fc of IgGs. The intracellular domains either contains an integrated signalling domain or an associated signalling domain (γ-chain). The signal provoked depends on the FcγR where activatory receptors have an ITAM and inhibitory receptors contain an ITIM. The expression patterns of human FcγRs varies across cell types. Some cell types express several FcγRs (such as neutrophils), while other express only one FcγR (such as B cells). + indicates expression is detectable, - indicates expression is not detectable, and +/- indicates the expression differs between cells or the receptor is only expressed in a subset of humans (such as FcγRIIc). Figure adapted from [112].

cellular signal via immunoreceptor tyrosine-based activation motifs (ITAM). The cytoplasmic domains of FcγRIIa and FcγRIIc contains an integrated ITAM [104]. However, FcγRs I and IIIa lack an ITAM in their intracellular domain, and instead are associated with the common γ chain (FcRγ). This contains a cytoplasmic ITAM which is required for receptor function and stable surface expression of FcγRI and IIIa [105, 106]. The only inhibitory receptor, FcγRIIb, contains an integrated intracellular immunoreceptor tyrosine-based inhibitory motif (ITIM) in its cytoplasmic tail [104]. The remaining FcγR, FcγRIIIb, does not have a transmembrane or cytoplasmic region, but instead is anchored to the cell surface via a GPI anchor [107, 108] and is incapable of transducing a signal directly [105]. Many immune cells co-express multiple FcγRs, including activatory and inhibitory receptors, that act as a threshold to determine cellular activation [109]. Macrophages for example express a variety of activating FcγRs (FcγRI, FcγRIIA, and FcγRIIIA) and the inhibitory FcγRIIb [110], where FcγRIIb is thought to have a role in regulating the cells pro-inflammatory response [111]. In contrast, B cells and NK cells typically express only one FcγR, FcγRIIb and FcγRIIIa respectively.

1.3.1 FcγRI

Human FcγRI is considered to be the high affinity receptor for IgG, and the only receptor to have three extracellular domains. Critically it is the only FcγR capable of binding to monomeric IgG1, 3, and 4 with a K_A in the range of 3.6 - 6.5 x10^7 M^{-1}, but does not bind to monomeric IgG2 [84]. The crystal structure for FcγRI in complex with IgG1 Fc has been previously been solved and provided an understanding into the high affinity interaction between these two proteins. Human IgG1 was demonstrated to bind an interface between the second and third Ig domains of the receptor. Further analysis revealed a hydrophobic pocket only present within FcγRI which interacts with L235 of the IgG1 Fc, and is suggested to contribute to the high affinity binding observed [113]. The importance of this residue was later highlighted with mutagenesis studies, whereby altering L235 reduced receptor affinity for IgG1 [114].

FcγRI is expressed on activated granulocytes, most myeloid populations, and dendritic cells [115]. Due to its high affinity, the receptor is thought to bind monomeric IgG in the serum which can be displaced by immune complexes (ICs) to mediated cellular effector functions [116]. Evidence has suggested that the preference of the receptor for ICs over monomeric IgG is dictated by cytokines, where the presence of local IL-3 was found to enhance IC engagement by FcγRI This mechanism has been proposed to be driven by altering receptor mobility and/or clustering [117]. After activation the receptor induces an intracellular signalling pathway that is mediated by the associated common γ chain.

1.3.2 FcγRIIa

Human FcγRIIa is able to bind to all human isotypes, with a maximum affinity for IgG1 (3.5 - 5.2 x10^7 M^{-1})[84] and lower affinities for all other subclasses. The receptor is expressed on monocytes, macrophages and neutrophils [103]. In humans several of the FcγRs have polymorphisms that impart functional differences in the binding of IgG and subsequent FcγR activation. FcγRIIa has a polymorphism present at position 131 of the amino acid sequence, which encodes either a histidine (H131) or arginine (R131) [118]. The H131 polymorphism is associated with an increased binding affinity for IgG2 [119].

FcγRIIa is a single chain receptor and contains an integrated ITAM motif in its cytoplasmic domain which imparts the receptors activatory signalling and subsequent effector functionality, such as phagocytosis. The signalling of CD32a is thought to be reliant on efficient receptor dimerisation. Mutating the residues at the proposed dimerisation interface of CD32a did not interfere with antibody binding, but did reduce ITAM phosphorylation and subsequent signalling [120].

Activation of FcγRIIa has been demonstrated to contribute to the phagocytic potential of neutrophils [84], which has been confirmed with additional studies by reducing neutrophil-mediated phagocytosis with the use of anti-FcγRIIa blocking antibodies [120], and increasing macrophage-mediated phagocytosis by enhancing antibody affinity for CD32a [121]. Together these studies provide strong evidence that FcγRIIa is important in facilitating phagocytosis of mAb opsonised cells.

1.3.3 FcγRIIb

FcγRIIb is the sole inhibitory FcγR, expressed on B cells, macrophages and neutrophils [103]. FcγRIIB has the lowest affinity out of all FcγRs for IgG1, 2 and 3 with K_A of 1.2, 0.2, and 1.7 x10^5 M^{-1}, respectively. However, its affinity for IgG4 is comparable with the other low affinity receptors, with a K_A of 2.0 x10^5 M^{-1} [84]. Through its inhibitory action, the receptor plays an important role in regulating immune responses through a broad range of functions. In the context of B cells, where FcγRIIb is the only FcγR typically expressed, it has been suggested to provide negative feedback on B cell activation [122] and the production of antibodies, thereby reducing the risk of autoimmunity [103]. It is also expressed on the surface of macrophages and neutrophils alongside several other activatory FcγRs. Here it is believed that the inhibitory receptor tightly regulates the pro-inflammatory responses of these cells. This was demonstrated using FcγRIIb deficient mice that display enhanced macrophage activity, in addition to increased susceptibility to collagen-induced arthritis [111]. The receptor also has an important role in follicular dendritic cells, where it traps ICs with associated antigen in the germinal centre to aid B cell development [123].

1.3.4 FcγRIIc

Human FcγRIIc has arisen from an unequal crossover event between FcγIIa and FcγRIIb during the evolution of the low affinity FcγR gene locus, resulting in a receptor that contains the extracellular domain of FcγRIIb and the intracellular domains of FcγRIIa [124]. As a consequence of acquiring the extracellular domain of FcγRIIb, the binding affinity for IgGs between these two receptors is identical. The coding region for FcγRIIc can contain a stop codon in the third exon of the gene to produce a null FcγRIIc allele. The presence of two copies of the null FcγRIIc allele results in the lack of transcription and expression [125]. The majority of the population do not express FcγRIIc, with 80% of the European population homozygous for the stop-codon [126]. Initially, FcγRIIc expression was believed to be restricted to NK cells [125], but was more recently reported

on the surface of B cells [82]. However, recent studies indicate the effector activity of FcγRIIc$^+$ individuals displayed no improvement in antibody-dependent cellular cytotoxicity (ADCC) [127]. This is in contrast to earlier studies that suggested ADCC was facilitated by certain isoforms of FcγRIIc [128]. Taken together these results could suggest that FcγRIIc is capable of inducing ADCC, but its contribution to Fc-mediated effector functions in physiological conditions is unclear.

1.3.5 FcγRIIIa

FcγRIIIa is the second activatory FcγR that transduces signals via an associated common γ chain and is expressed on NK-cells, macrophages and monocytes [103]. The receptor has varying affinities for IgG, that is dependent on the polymorphism present, but demonstrates the highest affinity for IgG1 and IgG3, with K_A of 12-20 and 77-98 x10^5 M^{-1}, respectively. The receptors affinity for IgG2 and IgG4 are lower, observing K_A of 0.3-0.7 and 2.0-2.5 x10^5 M^{-1}, respectively [84]. FcγRIIIa also exhibits a polymorphism that affects the binding properties to all four IgG subclasses. Position 158 can either contain a valine (V158) or phenylalanine (F158) [129]. Individuals with the V158 polymorphism demonstrate an increased affinity for IgG [130] that is associated with greater response to antibody therapy in tumour bearing patients [131].

Activation of the receptor on NK cells promotes potent cytotoxicity via ADCC, demonstrated by potent anti-tumour activity of anti-CD20 immunotherapy [132]. FcγRIIIa is also suggested to have an important role in antibody-dependent cellular phagocytosis (ADCP), evidenced by efficient phagocytosis induced by a fibroblast cell line (lacking all FcγR) transfected with FcγRIIIa [133]. In agreement with this data is further evidence of the receptors role in phagocytosis whereby blocking FcγRIIIA on human monocyte-derived macrophages (MDMs) significantly decreases phagocytosis of rituximab (RTX) opsonised target cells [134]. Taken together, these reports indicate FcγRIIIa to be important in the antibody-mediated cell killing process.

1.3.6 FcγRIIIb

The extracellular domain of FcγRIIIb is structurally similar to FcγRIIIa, with the difference being that FcγRIIIb is membrane bound by a GPI-linked anchor. The expression of CD16b has been demonstrated to be limited to the surface of neutrophils [103] and basophils [135], and intracellularly on eosinophils [136]. FcγRIIIb has low affinities for IgG1 and 3 with K_A values < 20 x 10^5 M^{-1}, and undetectable binding to IgG2 and 4 [84]. Polymorphisms have also been detected in genes encoding FcγRIIIb, with two different allelic variants, NA1 and NA2, that differ at four amino acids [137]. The mutations observed in these polymorphisms affects N-linked glycosylation of the

receptor and binding affinity for IgG1 and IgG3 [138].

Even though the receptor is expressed on the surface of immune cells, there is limited data on the function or signalling of the receptor. FcγRIIIb has no inherent signalling capabilities, but studies have suggested that the receptor can functionally signal through association with FcγRIIa [139], complement receptor 3 [140], or accessory signalling molecules in lipid rafts [141]. Studies into the function of FcγRIIIb have given competing conclusions. In several studies, FcγRIIIb has been demonstrated to aid in the clearance of ICs in the absence of neutrophil activation [142], and that the NA1 allele has been shown to exhibit higher IgG1 and IgG3 affinity and have an increased capacity for neutrophil-mediated phagocytosis [138]. However, other reports have provided evidence that that IgG may bind FcγRIIIb and not induce any functional signalling. Instead the receptor sequesters antibody and acts as a decoy receptor, reducing activation by competing with FcγRIIa. In support of this suggestion, blocking of FcγRIIIb significantly enhances FcγRIIA-mediated ADCC by neutrophils [143]. Therefore, studies have suggested that FcγRIIIb does have functional consequences, but its role in Fc-mediated effector functions are still uncertain.

1.3.7 FcRn

IgGs are also bound by FcRn. After its initial discovery in neonatal rats [144], this receptor was shown to be expressed on the surface of numerous cell types in humans, such as epithelial cells [81], monocytes, macrophages, DCs [145], and neutrophils [146]. FcRn is more structurally related to MHC proteins than FcγR, composed of three alpha domains and an associated β2-microglobulin molecule (Figure 1.8) [147]. It binds to a region spanning the CH2-CH3 interface of the Fc of antibodies [148]. All IgG subclasses, except IgG3, bind to FcRn with comparable affinity in acidic environments, which explains the long serum half-life of IgG compared to other Ig classes [149].

The roles of FcRn include transporting IgG from mother to foetus during pregnancy as a form of passive immunity [150], and ensuring the long serum half-life of IgGs through protection from serum proteases. After endocytosis from the extracellular fluid, IgG is transported into endosomes with a slightly acidic environment. FcRn binds to IgG in a pH-dependent manner and only binds IgG below pH 6.5, when key histidine residues in the CH2-CH3 binding interface become protonated. In the acidic endosomes FcRn binds IgG molecules and prevents intracellular lysosomal degradation by triggering FcRn-mediated translocation back to the cell surface. At the cell surface, the neutral pH allows release of the IgG back into the extracellular fluid [151]. In experimental models involving mice lacking FcRn, IgG half-life is demonstrated to be significantly reduced [152]. Aside from its role in transporting and recycling IgG, FcRn has also been reported to

transport IgG-antigen complexes thus facilitating antigen presentation and subsequent immune activation [153].

As discussed above human FcγRs display differential binding properties for IgG subclasses. Bruhns *et al* have analysed the binding potential of all IgG subclasses for the human FcγRs, which are capable of binding to monomeric and aggregated IgG, albeit with much lower affinity to monomeric IgG. Aggregated IgG1 and IgG3 display the highest affinity for all FcγRs, whereas IgG2 and IgG4 display low to undetectable affinity for most FcγRs (Table 1.1) [84]. FcγR's bind at the interface between the hinge region and CH2 domains of Fc [154] typically in an immune complex or an opsonised cell to impart some of the effector functions of antibodies, such as ADCC [155] and ADCP [156].

	IgG1	**IgG2**	**IgG3**	**IgG4**
FcγRI	650.0	*n.m*	610.0	340.0
FcγRIIa H131	52.0	4.5	8.9	1.7
FcγRIIa R131	35.0	1.0	9.1	2.1
FcγRIIb/c	1.2	0.2	1.7	2.0
FcγRIIIa V158	11.7	0.3	77.0	2.0
FcγRIIIa F158	20.0	0.7	98.0	2.5
FcγRIIIb NA1	2.0	*n.m*	11.1	*n.m*
FcγRIIIb NA2	2.2	*n.m*	9.1	*n.m*

Table 1.1: FcγR binding affinities of hIgG subclasses.
Affinity constants (K_A; x 10^5 M^{-1}) determined by surface plasmon resonance. IgG1 and IgG3 have the highest binding affinities to all FcγR, whereas IgG2 and IgG4 display the lowest binding affinities. *n.m* = non-measurable (Table modified from [84])

1.4 Antibody effector functions

Antibodies achieve their desired functional responses through a variety of different mechanisms, either during an infection or when passively transferred in the case of antibody therapeutics (discussed later). These are summarised in Figure 1.9. Antibodies can elicit such responses directly or indirectly. Indirect immune responses come in the form of Fc mediated effector mechanisms through interfacing with key elements of the immune system, including complement and immune effector cells. These effector mechanisms are; ADCC, ADCP, and complement-dependent cytotoxicity (CDC). Direct effects are F(ab) mediated and can occur, for example, through the induction of direct cell death (DCD), whereby after target binding an intracellular signal is provoked leading to apoptosis or other forms of cell death.

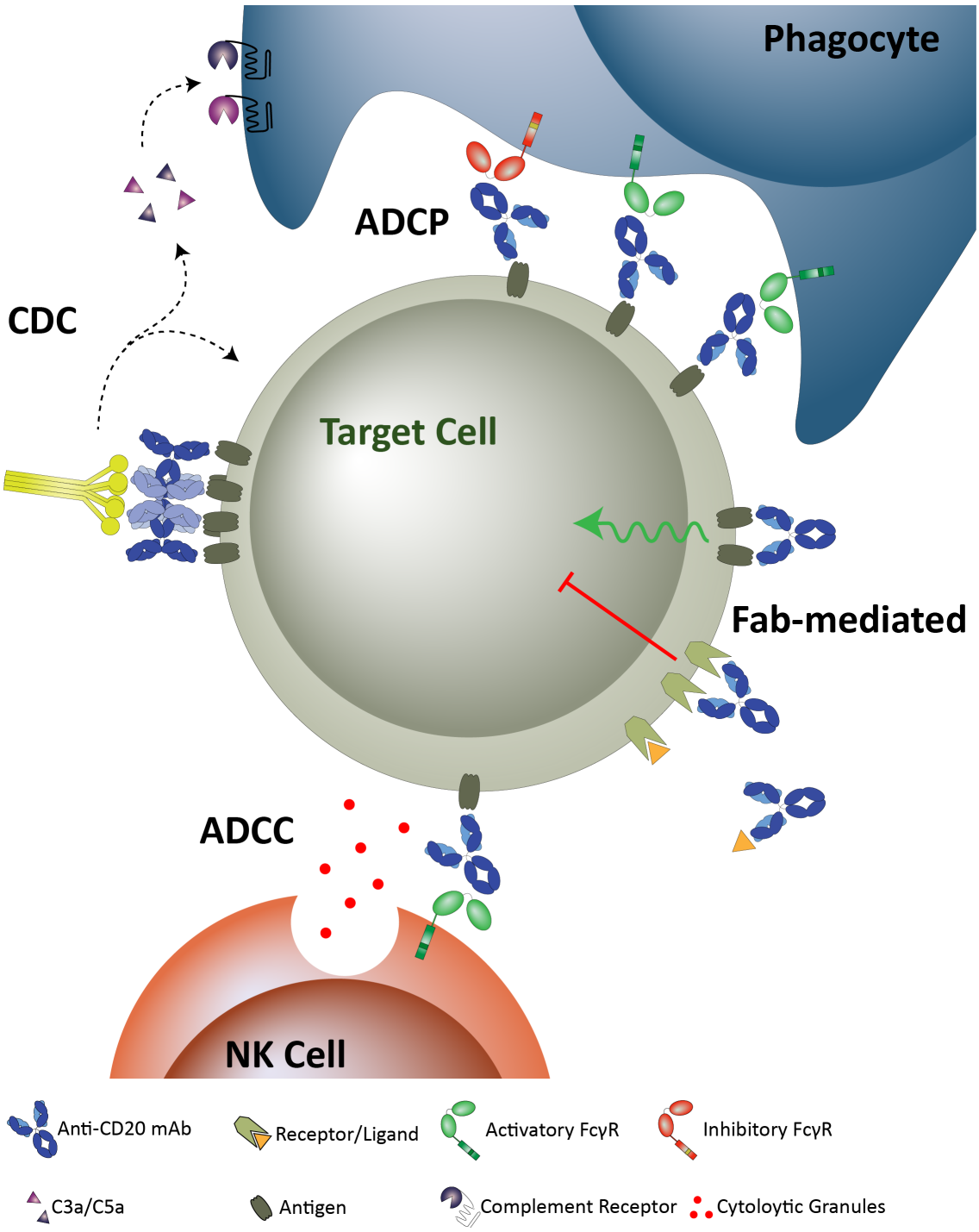

Figure 1.9: Effector functions of IgG.
IgG antibodies elicit a range of effector functions towards a target cell. ADCP (top-right) is initiated by antibodies binding to their target cells and engaging FcγRs on phagocytes, such as macrophages. Antibodies provoke several direct effects after target binding (centre-right), such as inducing a cell death signal or blocking ligand binding. CDC (centre-left) is initiated after C1q recruitment and activation, resulting in a cascade of protein interactions resulting in cell lysis. ADCC (bottom-centre) involves natural killer cell activation by IgG-opsonised cells to induce the release of cytotoxic granules and cell death.

1.4.1 F(ab)-mediated effects

Some IgGs bind to their cognate target and initiate a F(ab)-mediated response independent of the Fc-region and in the absence of Fc-mediated effectors. Such antibodies either have agonis-

tic or antagonistic properties (Figure 1.9). The characteristics of these antibodies are commonly exploited in therapeutic mAb of different classes. Antagonistic antibodies bind to their target receptors to block receptor ligand interaction, as in the case with neutralising antibodies against HIV or influenza, or prevent a signal from an endogenous ligand or otherwise activated receptor, as in the case with certain therapeutic mAb. An example of the latter are anti-epidermal growth factor receptor (EGFR) mAb, such as cetuximab, which bind with high affinities to this key growth receptor to block its phosphorylation and activation, thus preventing unwanted proliferation in cancer cells [157]. Therapeutic antibodies that can bind and neutralise soluble ligands to prevent them from engaging and activating their receptor include those targeted to vascular endothelial growth factor (VEGF) [158].

Agonistic antibodies in contrast bind to their surface target receptor to induce a signal, typically in the absence of the receptor's ligand. These can include antibodies directed against death receptors on the cell surface, such as TNF-related apoptosis-inducing ligand (TRAIL) receptor, whereby agonism promotes a strong apoptotic signal [159], or in the case of some anti-CD20 mAbs binding to the target antigen can promote a signal to initiate a non-apoptotic type of cell death [160, 161]. Alternatively a whole series of antibodies directed to members of the tumour necrosis factor receptor (TNFR) super-family such as CD40, OX40 and 4-1BB have been shown to agonise their respective targets [162].

1.4.2 Antibody-dependent cellular cytotoxicity

In contrast to F(ab)-mediated effects, which are dependent on target specificity, the Fc is capable of recruiting elements of the immune system, such as FcγR-bearing cells or the complement system, after cell opsonisation. One of the FcγR-mediated mechanisms of antibody-mediated cell clearance is ADCC (Figure 1.9). This mechanism involves the direct killing of an antibody opsonised target by FcγR bearing immune cells. ADCC is thought to be primarily mediated by NK cells, but can also be used by monocytes, macrophages, and neutrophils [163–165]. ADCC is initiated after sufficient Fc density on the target cell surface results in binding to certain activatory FcγRs on the immune cell surface. In the case of NK cells the receptor is predominantly FcγRIIIa. After receptor clustering the FcγRIIIa ITAM is phosphorylated by Src family kinases, which triggers Syk activation and initiation of an intracellular signalling cascade that stimulates degranulation of lytic vesicles, stored within the NK cell. These lytic vesicles contain a diverse range of cell-death mediators including perforin, a membrane-disrupting protein, and granzymes, a family of serine proteases, that are released via exocytosis into the extracellular space [17]. Perforin was originally thought to form pores in the cell membrane to allow the granzymes to enter the cell to initiate apoptosis

through the cleavage of caspases [166], although this likely represents an oversimplification.

1.4.3 Antibody-dependent cellular phagocytosis

Another FcγR-mediated mechanism able to remove antibody opsonised cells is ADCP (Figure 1.9). This mechansism of action is mainly produced by macrophages, but neutrophils and monocytes also have the ability to phagocytose target cells [167]. Macrophages are present in almost all tissues with the capability of phagocytosing diseased and dying cells as well as pathogens. They also have the capacity to engulf antibody opsonised target cells, such as tumour cells, following engagement and activation of their FcγR. The cross-linking of FcγRs by multiple Fcs from the opsonised target cell is required for a stable interaction with the macrophage [168]. As above, the intracellular ITAM is a substrate for phosphorylation by Src family kinases and served to elicit a downstream signalling cascade. Initiation of phagocytosis also induces a downstream signalling cascade involving soluble proteins in the cytosol and membrane lipids [169]. A transient increase in phosphatidylinositol-4,5-bisphosphate (PIP2) followed by a sharp decrease in the pseudopods of the phagocytic cup facilitates actin disassembly [170]. The subsequent actin remodelling allows for the membrane to extend around the opsonised target to form a membrane-bound vacuole, called the phagosome [169].

The phagosome subsequently enters a maturation process by fusing with early and late endosomes, and lysosomes, forming the phagolysosome [171]. The phagolysosome contains an array of digestive enzymes and hydrolases, and antimicrobial peptides, that react with proteins, membrane and carbohydrates of phagocytosed target cells to mediate their destruction [169]. It is also a highly oxidative environment as a result of NOX2 oxidase and inducible nitrous oxide synthase producing reactive oxygen and nitrogen species, respectively [172, 173]. Protons are pumped into the vacuole by vacuolar-ATPase and greatly accumulate due to a reduced passive proton permeability of the phagolysosome, making it a highly acidic environment (pH 4.5-5) [174]. Combined, these mechanisms and mediators have the ability to destroy the phagocytosed target within the phagolysosome.

Macrophages are often defined based on their anatomical location, such as different tissue resident macrophages, and functional state [175]. These states impact the activity of the macrophages. Influence from the environment skews macrophage phenotype in continuum between two highly polarised states [176]. Classically activated macrophages (M1) are classed as pro-inflammatory and have roles in the defence against invading pathogens and anti-tumour immunity. Differentiation into M1 macrophages is stimulated by the presence of IFN-γ and lipopolysaccharide (LPS)

[177]. Conversely, M2 macrophages have anti-inflammatory functions and regulate wound healing. Anti-inflammatory cytokines, such as IL-4 and IL-13, skew macrophages into this direction [177]. Typically, M1 macrophages have higher phagocytic activity than M2 skewed macrophages. There is also an additional subset of macrophages that are found in close proximity or within tumours, called tumour-associated macrophages (TAMS). TAMS inflitrate tumour masses in response to selected cytokines released by tumour cells [178, 179]. TAMS have pro-tumourigenic properties and aid in angiogenesis and metastasis [180, 181], and have been associated with poor prognosis [182].

1.4.4 Complement-dependent cytotoxicity

After engaging their target antigen, antibodies can activate the complement pathway and induce CDC. The classical complement cascade involves the cleavage of a series of serum proteins and zymogens that generate target cell destruction and inflammatory signals. In the majority of cases antibodies activate the classical complement pathway. After antigen opsonisation, the Fc regions cluster at the cell surface to provide a binding platform for the first component in the classical complement cascade, C1q (Figure 1.10). C1q exists as a 460 kDa multimeric protein complex formed from six heterotrimeric polypeptide chains, composed of C1qa, C1qb, and C1qc [183]. C1q is predominantly expressed by macrophages, but can also be produced by immature dendritic cells and mast cells [184]. The polypeptide chains contain a collagen-like region forming a helix structure and carboxyl-terminal head groups that combine into a six-headed complex [185]. The globular domains of the C1q complex are responsible for the ligand binding properties, whereas the helical region is responsible for associating with the serine proteases C1r and C1s. The globular heads have the capacity to bind to a broad range of antigens and are not limited to Fc domains, these include bacterial surfaces, viral surfaces, apoptotic cells, amyloid proteins, and prion proteins [186–190].

Although various ligands are recognisable by C1q, the predominant ligands are IgG and IgM. C1q binds to these antibodies in their upper Fc regions. In the case of IgG C1q recognises an area in the upper CH2 and hinge region, whereas in IgM the CH3 region is bound. Each of the six globular head groups has the capacity to bind the Fc of one antibody, but the binding of several is required for complement activation through an avidity driven process [191]. The binding between C1q and IgG has been determined to be driven by ionic interactions, where modifications of charged residues in the globular head group blocks C1q binding [192, 193]. In addition, there is a calcium ion at the apex of the globular head group that has been implicated in ligand binding. Sequestering the ion with EDTA decreases C1q's interaction with its ligand [194]. The interaction between C1q and

monomeric IgG has been demonstrated to be in the millimolar range. Such a low affinity is thought to avoid the binding of C1q and antibody in solution, thereby preventing unwanted non-target activation of the complement pathway and potentially damaging immune activation [6, 195, 196]. It has recently been shown to be critical that IgG's cluster and organise into hexamers through specific, non-covalent interactions after antigen binding to initiate the complement cascade [197]. This process of antibody 'on-target' hexamerisation is though to provide a cluster of Fcs to aid in the avidity driven C1q binding by allowing several C1q head groups to bind adjacent IgG to induce the complement cascade.

The process of antibody 'on-target' hexamerisation to antigens embedded in a lipid bilayer has been delineated with the use of atomic force microspcopy (AFM) analysis. In these studies it was described that, following surface-antigen binding of a monomeric IgG molecule there is recruitment of further IgG molecules via either diffusion-driven lateral collisions or from solution. The subsequent binding of C1q was most stable in the presence of higher order oligomers, such as IgG hexamers. Furthermore, assessment of CDC induction indicated that intermediates along the hexamerisation pathway such as monomeric, dimeric and trimeric IgG clusters exhibit weak complement activity [198]. This is consistent with earlier cryo-EM analysis that indicated the formation of IgG-C1 complexes requires the binding of four to six C1q headpieces binding to adjacent Fc in an IgG hexamer [199]. In addition to the IgG hexamer being an optimum binding platform for C1q, such cryo-EM studies have hypothesised that C1q is activated by compaction of the globular heads which induces sufficient conformation change required to activate C1r and C1s. This process can only occur after binding at least four antigen-bound IgG Fcs [199].

The binding between IgM and C1q is thought to be much stronger than IgG. As previously described IgM is naturally occurring as an Ig multimer and displays potent CDC activity [6]. However, in order to avoid spontaneous C1q binding and complement activation in solution, IgM undergoes a conformation change to allow C1q binding following antigen binding [200]. Recent work by Hiramoto *et al* has suggested that both hexameric IgM and pentameric IgM adopt similar hexagonal symmetry to bind C1q, whereby the J-chain spaces the IgM molecules of pentameric IgM [201]. This work consolidates the hypothesis of the requirement for IgG on-target hexamerisation in the recruitment of C1q, and also that C1q recognises molecular structures for activation that are steriosimilar between hexameric IgG, pentameric IgM and hexameric IgM.

In the serum, C1q is complexed with C1r and C1s serine proteases; two copies of the C1r and C1s are associated with one C1q. Binding of C1q to surface bound ligand results in a conformational change leading to the autocatalytic cleavage of the C1r protease. C1r is then able to cleave and activate C1s [202], which in turn cleaves and activates the serum proteins C4 (into C4a and C4b)

and C2 (into C2a and C2b). The C4b cleavage product contains a reactive thioester to facilitate cell membrane deposition in the immediate vicinity of C1q [203]. Surface bound C4b then binds to C2a, an active serine protease [204], to form the surface-bound C3 convertase (C4b2a) (Figure 1.10) [203]. Formation of the C3 convertase results in cleavage of C3 into C3a and C3b. C3b also contains a thioester bond to enable covalent deposition onto the cell surface [205]. The C3 convertase is able to cleave a large number of C3 molecules. This pathway amplification results in large numbers of surface bound C3b molecules that has additional cell killing benefits by acting as an opsonin. Surface bound C3b can be bound by complement receptors on phagocytic cells [206, 207]. C3b is also able to bind the C3 convertase to form the C5 convertase (C4bC2aC3b) to continue the complement cascade (Figure 1.10) [208]. The C3b in the C5 convertase binds to C5 to trigger C2a-mediated cleavage of C5 to produce C5a and C5b [209] to trigger the final stages of the complement cascade. Soluble C3a and C5a can act as potent anaphylatoxins to recruit and activate immune effector cells by binding to surface-bound complement receptors on immune cells, such as macrophages, thereby increasing local inflammation [210–212].

C5b binds to C6, which in turn binds C7 which undergoes a conformational change allowing it to be inserted into the cell membrane [213]. This complex then binds C8, which undergoes a similar conformational change to be inserted into the cell membrane. Finally, C8 recruits 10-15 copies of the final complement protein, C9. C9 polymerises at the cell surface and is inserted into the cell membrane [214] to form the membrane attack complex (MAC) (Figure 1.10), a pore 10 nm wide which disrupts membrane integrity. Insertion of the MAC allows calcium influx, subsequently resulting in mitochondrial poisoning and finally cell death [215]. For metabolically active nucleated cells, several MAC complexes are required to elicit successful lysis [216], and often this does not occur in the face of complement defence molecules.

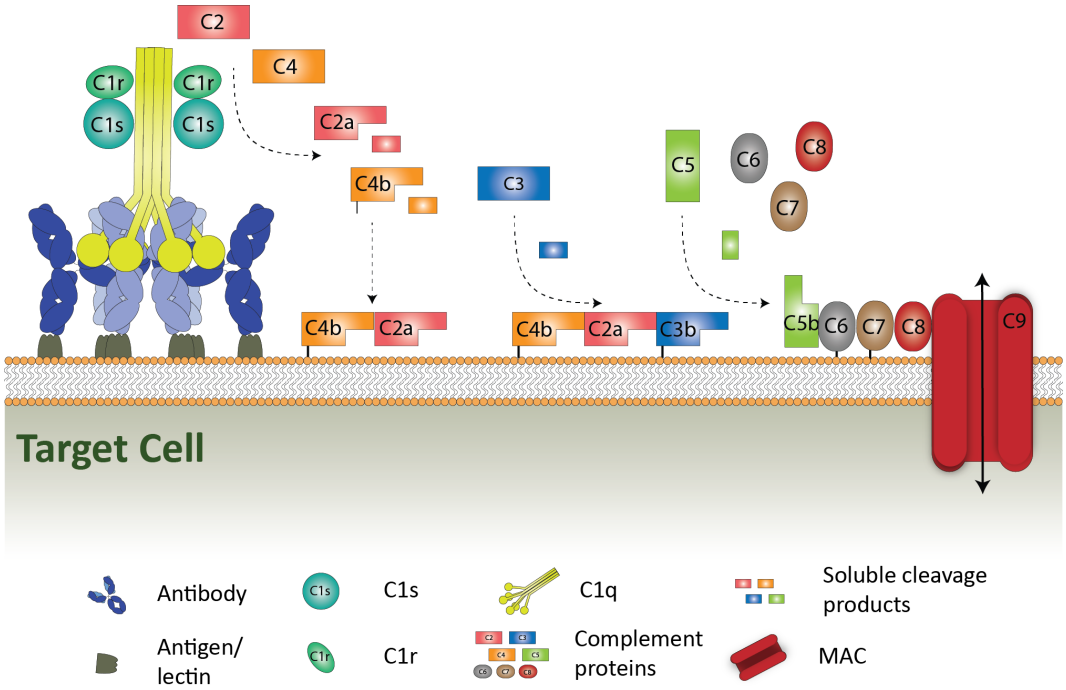

Figure 1.10: Activation of the classical complement cascade.
The classical cascade is initiated by the binding of an antibody and recruitment of C1q to the cell surface. The C1q associated proteases cleave complement proteins to instigate a cascade of enzymatic cleavage of further complement proteins, that results in formation of the MAC.

Antibodies predominantly activate the classical pathway of complement, however in the case of IgM the lectin pathway can also be activated due to the high-mannose content of this isotype [217]. Principally, the lectin pathway is largely activated in response to carbohydrate antigens on pathogens, in the absence of antibody binding (Figure 1.11). The lectin pathway is highly analogous to the classical pathway but is instead initiated by the mannan-binding protein (MBP) [218]. MBP has a similar structure and function to C1q, with six globular head groups composed of six heterotrimeric polypeptides that bind in a multivalent manner to specific sugar residues [219]. In serum, MBP is complexed with MBP associated serine proteases (MASPs), the functional equivalents to C1r and C1s [220], which cleave C4 and C2 to generate the C3 convertase. The resulting cascade is identical to the classical cascade [221].

Finally, complement-mediated killing can also be activated by the alternative pathway (Figure 1.11). This pathway relies on spontaneous cleavage of C3 facilitated by water molecules to bind to Factor B [222], which is cleaved by Factor D to generate the fluid phase C3 convertase (C3(H_2O)Bb). The fluid phase C3 convertase can cleave serum C3 to generate C3b, which becomes deposited on the surface of nearby cells [223, 224], similar to the C3 convertase in the classical and lectin pathways. C3b can then bind to surface bound C3bBb to generate the C5 convertase C3b2Bb [225] to trigger MAC formation in a similar fashion to the classical pathway.

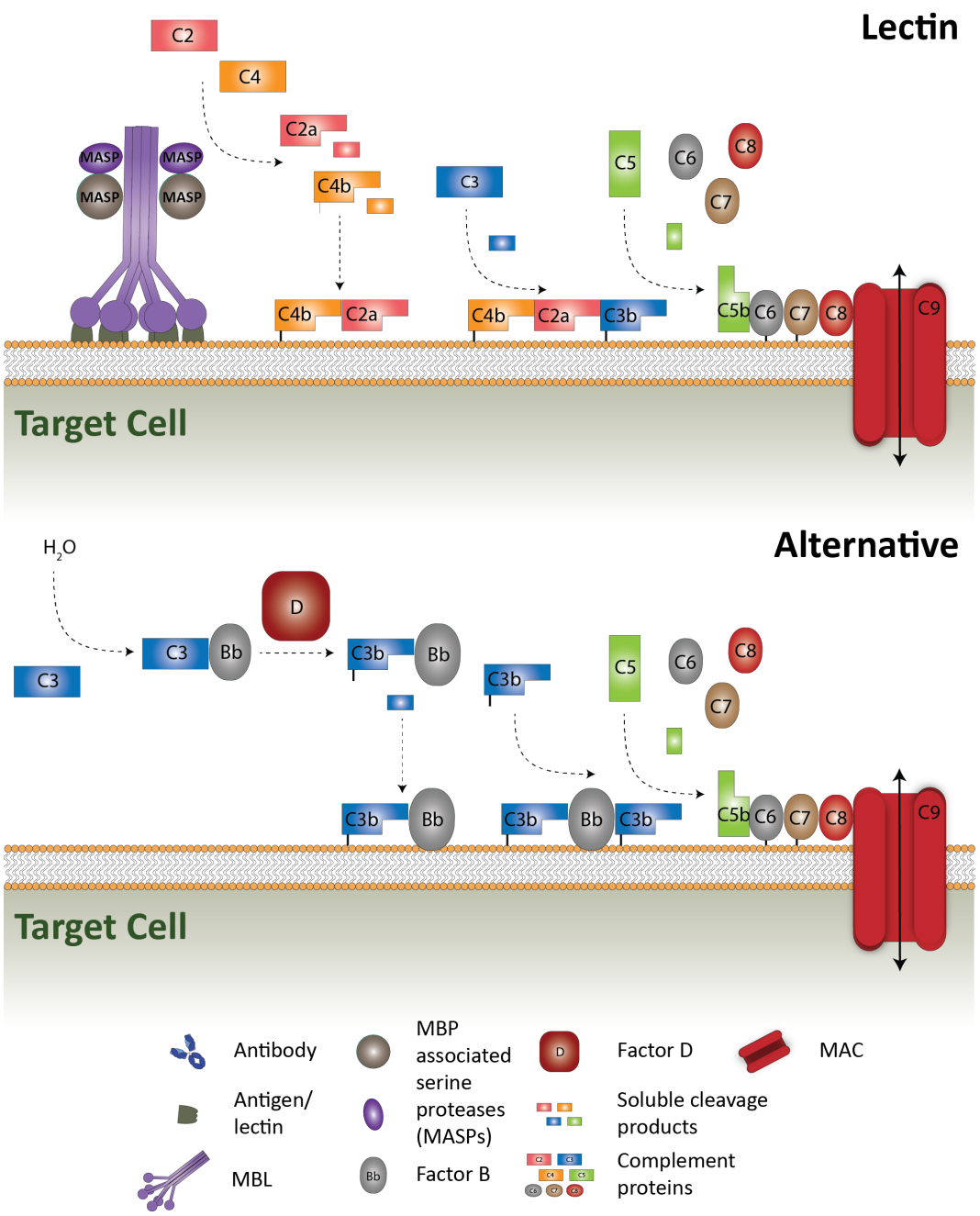

Figure 1.11: Activation of the lectin and alternative complement cascades.
The lectin pathway involves the binding of MBL to carbohydrate targets that results in activation of associated MASPs to cleave complement proteins, C4 and C2, similar to the classical pathway. This begins a cascade of steps resulting in formation of the MAC at the cell surface. The alternative pathway starts with spontaneous cleavage and activation of C3 in solution initiated by complement factors B and D. The activated C3 can form a C5 convertase, ending in formation of the MAC.

Host cells contain various complement defence molecules to limit unwanted activation of the complement system, for example, spontaneous activation by the alternative pathway on healthy host cells. Several of these complement defence molecules are expressed anchored to the cell surface by GPI anchors which include CD55 and CD59. CD55, or decay accelerating factor, promotes decay of the C3 and C5 convertases by inducing dissociation of C2a or Bb from the relevant classical and alternative complexes, respectively [226, 227]. CD59 by contrast prevents C5b-C8 catalysed polymerisation and insertion of C9 into the MAC and so inhibits pore formation in the

cell membrane, thereby retaining membrane integrity [228, 229].

1.5 Monoclonal antibodies in therapy

As well as a humoral response against infections, antibodies can be used passively as therapeutics. They achieve a therapeutic response in several different ways as summarised in Figure 1.9. Antibodies are now routinely used as therapeutics against various autoimmune diseases and cancer. As a result extensive research is currently being undertaken to further develop and generate mAbs as therapeutics. Historically the generation of mAbs involved *in vivo* immunisation of mice with a specific non-self antigen, peptide fragment of the antigen, or cells expressing the antigen. This invokes an immune response and subsequent antibody production by the host. Repeated immunisation boosts the immune response to elicit a higher yield of antigen specific cells. The subsequently produced antibodies in the serum will be a heterogenous mix known as a polyclonal antibody response. For many therapeutic purposes a single antibody species is desired. So-called mAb are monospecific, uniform and typically high affinity preparations that can be studied and utilised more effectively. The purification of a mAb from a polyclonal serum of antibodies is not readily possible, and so in 1975 Georges Köhler and Cesar Milstein developed a technique known as hybridoma technology. This involved the fusion of an immunised antibody-producing B-cell with a myeloma cell (a cancerous plasma cell) to generate a hybridoma. The hybridoma has the immortal growth properties of the myeloma cell and the antibody-producing properties of the B-cell [230]. Each hybridoma clone is formed from a single B cell and so will produce a single antibody species recognising one molecular epitope [231]. Rounds of subcloning are required to isolate single hybridoma clones, eventually resulting in a stable cell line continuously producing the single desired mAb [232].

After the development of hybridoma technology in 1975 there was scope to produce mAb on an industrial scale. The first FDA approved mAb was muromonab (OKT3) in 1986, which was designed to prevent organ rejection in transplant patients who had become resistant to steroids [233]. However, muromonab is a murine IgG2a antibody which gives rise to a host anti-mouse immune response in humans after administration. The antibody will be recognised as foreign and studies have demonstrated that 40 – 80% of patients will develop anti-muromonab antibodies [234]. The resulting anti-drug antibodies result in clearance from the circulation, limiting their therapeutic potential. To overcome the immunogenicity of murine mAb, a genetic engineering approach was developed to produce a chimeric antibody where the murine VH and VL domains are fused onto the human heavy and light chain scaffolds. Immunogenicity can be reduced further by minimising

the amount of murine framework in the form of a humanised mAb, whereby the CDRs of the murine antibody are engrafted onto the human HC and LC. To completely remove anti-mouse immunogenicity, other approaches have been developed, such as the use of humanised mice. Here, utilisation of genetically modified mice carrying human Ig heavy and light chain V, D, and J genes instead of the natural mouse genes allows the production of fully human CDRs with mouse constant regions following immunisation. The mAb produced in these mice can be subsequently cloned into expression vectors with human Fc regions to produce fully human antibodies [235, 236].

Once the hybridoma has been isolated, mAb production is simple, efficient and reproducible. However, epitope and affinity selection is not as easily dictated using *in vivo* methodologies and hybridoma isolation can be a slow process with low throughput [237]. Therefore, an alternative method for generating antigen-specific antibodies has been developed involving bacteriophage peptide libraries in a process known as phage display. These approaches vary but typically libraries are created through amplification of heavy and light chain mRNA from B cells and random combination into a single chain by a molecular linker [238]. The resulting antibodies are expressed at the surface of bacteriophages as short-chain fragment variable (scFv) molecules fused to the pIII minor capsid protein. The phages undergo multiple rounds of antigen guided screening to select those displaying the highest specificity and affinity. The plasmids encoding the high affinity chains are isolated from the bacteriophage and the variable domains fused onto a human antibody framework to produce a functional mAb [239]. The affinity of the resulting mAb can be further enriched by undergoing error-prone site-directed mutagenesis (SDM) of the CDRs, in a process known as affinity maturation [240]. Affinity maturation allows for the binding affinity to be optimised and selected to tailor the mAb application [241].

Phage display enables high throughput and faster mAb discovery at the early stages of selection, as a large number of potential V-regions can be tested simultaneously and the phage library is sufficient for multiple screenings against different antigens. The method is also cheap and once the library has been created can be stored indefinitely. However, the potential V-regions generated are limited to the size of the library, and subsequent mAb production in mammalian cell lines can be more challenging and less efficient compared to a hybridoma. One of the advantages and disadvantages of this approach is that it is not guided by selections *in vivo* – i.e. on the one hand, all possible combinations in the library exist and can be assessed for binding to a target, with no issues of self-reactive clones being deleted; but on the other the combined V regions have not been readily assessed for immunogenicity, self-reactivity and or stability *in vivo*. Therefore, although the use of phage-display has many advantages over hybridoma technology, currently there are more mAbs in clinical use and trials that have been derived from *in vivo* methods than

phage display technologies [237].

Once mAbs have been generated by any of the methods detailed above the DNA can be sequenced and synthesised into a relevant expression vector to be produced recombinantly using established expression systems. Mammalian host cells possess the prerequisite translation and folding machinery, and the ability to process relevant post-translational modifications, such as glycosylation, in order to generate a biologically active recombinant protein. Production of recombinant mAb is undertaken by transfection of DNA containing the genes for transcription into mammalian host cell lines. The most common mammalian host cell lines used in recombinant mAb expression are chinese hamster ovary (CHO), NS0, Sp2/0, HEK293, and Per.C6 [242]. However, the preferred choice for recombinant protein expression is CHO cell lines. These cells are the workhorses of industrially expressed proteins, with 70% expressed in them [243]. CHO cells were used as a host cell line in the first FDA approved protein biopharmaceutical, tissue plasminogen activator in 1984, and the first oncology-approved mAb, Rituxan (rituximab; RTX) in 1997 [244]. Currently, CHO, NS0, and Sp2/0 are the only cell lines used to express mAbs approved for human therapy [245].

1.5.1 Current therapeutic monoclonal antibodies

MAbs and their related products currently represent one of the fastest growing sectors in the pharmaceutical industry with over 70 clinically approved as of July 2019 [246]. In 2017 the global antibody therapeutics market was valued at $95.5 billion and is expected to exceed $100 billion by 2020 [247]. Their target specificity, repertoire of potentially available epitopes, and potency makes them attractive therapeutics. Since the approval of RTX there has been continuing approval of anti-cancer mAb and currently 29 are approved for use, targeting multiple molecular antigens against a number of different cancer indications (Table 1.2). As a result of their strong effector functions (FcγR-mediated, CDC, and F(ab)-mediated) and long half-life, IgGs are the most common Ig utilised in mAb therapy, and more specifically, the IgG1 sub-class [246].

Although IgG1 is the main subclass of IgG exploited in antibody therapeutics there are approved antibody therapeutics on other IgG backbones. As of July 2019 there was nine approved human or humanized IgG2 antibodies and 13 approved human or humanized IgG4 mAb, for a number of indications including autoimmune conditions and cancer indications. There are currently no approved IgG3 mAb due to production difficulties and short half-life associated with the extended hinge region. In addition to the natural IgG scaffold there are several approved antibody-drug conjugates (ADC), two bispecific mAb, one approved tandem scFV, one glycoengineered mAb,

and one pegylated mAb. [246].

In addition to IgG other antibody isotypes have been considered as potential therapeutic candidates, such as IgM. IgM is highly efficient at activating complement, attributed to its favourable interaction with C1q [197] (with IgM hexamers being more efficient than IgM pentamers present within serum [248]), as detailed earlier. However, IgM as therapeutics have displayed a lack of efficacy in pre-clinical investigations and clinical trials, in addition to a difficult and costly manufacturing process, resulting in its withdrawal as a therapeutic candidate [249]. Irrespective of isotype, therapeutic antibodies can be broadly split into direct targeting and immunomodulatory mAb, depending on their mechanism of action.

mAb name	Brand name	Format	Target	Indication	FDA approval	EU approval
Polatuzumab vedotin	Polivy	Humanized IgG1, ADC	CD79b	Diffuce large B cell lymphoma	2019	*In review*
Moxetumomab pasudotox	Lumoxiti	Murine IgG1 dsFv immunotoxin	CD22	Hairy cell leukemia	2018	*NA*
Cemiplimab	Libtayo	Human mAb	PD-1	Cutaneous squamous cell carcinoma	2018	2019
Durvalumab	IMFINZI	Human IgG1	PD-L1	Bladder cancer	2017	2018
Gemtuzumab ozogamicin	Mylotarg	Humanized IgG4, ADC	CD33	Acute myeloid leukemia	2017	2018
Avelumab	Bavencio	Human IgG1	PD-L1	Merkel cell carcinoma	2017	2017
Inotuzumab ozogamicin	BESPONA	Humanized IgG4, ADC	CD22	Acute lymphoblastic leukemia	2016	2017
Atezolizumab	Tencentriq	Humanised IgG1	PD-L1	Bladder Cancer	2016	207
Olaratumab	Lartruvo	Human IgG1	PDGFRα	Soft tissue sarcoma	2016	2016
Daratumumab	Darzalex	Human IgG1	CD38	Multiple myeloma	2015	2016
Elotuzumab	Empliciti	Humanised IgG1	SLAMF7	Multiple meloma	2015	2015
Dinutuximab	Unituxin	Chimeric IgG1	GD2	Neuroblastoma	2015	2015
Nivolumab	Opdivo	Human IgG4	PD1	Melanoma, non-small cell lung cancer	2014	72015
Blinatumomab	Blincyto	Murine bispecific tandem scFv	CD19, CD3	Acute lymphoblastic leukaemia	2014	2015
Pembrolizumab	Keytruda	Humanised IgG4	PD1	Melanoma	2014	2015
Ramucirumab	Cyramza	Human IgG1	VEGFR2	Gastric cancer	2014	2014
Obinutuzumab	Gazyva	Humanised IgG1; Glycoengineered	CD20	Chronic lymphocytic leukaemia	2013	2014
Ado-trastuzumab emtansine	Kadcyla	Humanised IgG1, ADC	Her2	Breast cacner	2013	1013
Pertuzumab	Perjeta	Humanised IgG1	Her2	Breast cancer	2012	2013
Brentuximab vedotin	Adcetris	Chimeric IgG1, ADC	CD30	Hodgkin lymphoma, systemic anaplastic large cell lymphoma	2011	2012
Ipilimumab	Yervoy	Human IgG1	CTLA-4	Metastatic melanoma	2011	2011
Ofatumumab	Arzerra	Human IgG1	CD20	Chronic lymphocytic leukaemia	2009	2010
Panitumumab	Vectibix	Human IgG2	EGFR	Colorectal cancer	2006	2007
Bevacizumab	Avastin	Humanised IgG1	VEGF	Colorectal cancer	2004	2005
Cetuzimab	Erbitux	Chimeric IgG1	EGFR	Colorectal cancer	2004	2005
Tositumomab-I131*	Bexxar	Murine IgG2a	CD20	Non-Hodgkin lymphoma	2003	N/A
Ibritumomab tiuxetan	Zevalin	Murine IgG1	CD20	Non-Hodgkin lymphoma	2002	2004
Trastuzumab	Herceptin	Humanised IgG1	Her2	Breast cancer	1998	2000
Rituximab	MabThera, Rituxan	Chimeric IgG1	CD20	Non-Hodgkin lymphoma	1997	1998

Table 1.2: Current approved mAbs for use in cancer therapy.
*Tositumomab was approved for use in a radiolabelled form (I131) but was discontinued in 2014. Table adapted from http://www.antibodysociety.org/news/approved-antibodies/. Information correct in September 2019.

1.5.2 Direct targeting monoclonal antibodies

Direct targeting mAb elicit their therapeutic response via the classical antibody effector functions ADCC, ADCP, CDC, and DCD as explained previously, and potentially by blocking signals through binding to receptors directly on the target cell. The majority of approved mAbs in the treatment of cancer are currently direct targeting mAb, many of which utilise the Fc portion of the antibody to engage the immune system to destroy the cancerous cells, as detailed below. However, signal/receptor blockade is also an important mechanism. The anti-Her2 antibody, trastuzumab, is an example of a therapeutic mAb that targets the aberrantly expressed tumour antigen receptor Her2, blocking its activation. Normally Her2 provides proliferative and survival signals to the cancer cell and so trastuzumab leads to reduced tumour growth whilst also enabling destruction through Fc-mediated mechanisms [250]. Whilst trastuzumab binds a receptor to block a signal, bevacizumab binds and sequesters the signalling ligand VEGF-A to prevent angiogenesis [158]. In contrast, mapatumumab is an example of a mAb that targets the TRAIL receptor to induce a cell death signal [251]. Perhaps the best example of a direct targeting mAb is RTX, directed against the pan B cell molecule CD20 to delete B cells through Fc-mediated effector functions.

1.5.2.1 CD20 as a therapeutic target

Since its discovery in 1980, CD20 was the first B cell specific antigen to be identified [252–254] and has become a well recognised B-cell specific marker [255]. Despite this the physiological function of CD20 has remained unclear and the natural ligand for CD20 is currently unknown or not present. As a result, functional data has been mainly inferred from antibody engagement studies. In the absence of any structural data, sequence analysis and enzymatic digestion have predicted CD20 to be composed of four membrane spanning domains and two extracellular loops, and it is now known to be a non-glycosylated member of the membrane-spanning 4-A family [256, 257]. Co-precipitation studies have shown that human CD20 is a membrane-bound protein, existing as a homo-tetramer, a common structural feature of ion channels, indicating a possible function of CD20 in the regulation of calcium flux. This was evidenced by experiments using cell lines transfected with CD20 which demonstrated increased ionic conductance that was eliminated in the presence of a calcium chelator [258]. However, further investigations have suggested that CD20 is not involved in regulating calcium flux directly, but rather it modulates calcium signalling arising from the BCR. This was demonstrated in the context of Ramos B cells lacking the BCR, where engagement of CD20 did not promote calcium flux [259]. This is consistent with other experiments that suggest CD20 is physically associated with the BCR [259, 260].

Further analysis into the physiological function of CD20 using knock-out mice has had limited success. In 1998, a CD20 deficient mouse was described which had no observable defects in B cell maturation, proliferation, or Ig production [261]. This general lack of phenotype was confirmed in an independent CD20 knock-out mouse strain, although in this latter study there was reduced calcium influx detected following BCR cross-linking [262]. Further reports of this observation were described in a CD20 deficient patient. B cell lines generated from this patient demonstrated impaired BCR signalling and overall a reduced antibody response to vaccination with T-independent antigens was observed, which was confirmed using CD20 deficient mice *in vivo* [263]. Conversely, CD20 deficient mice were subsequently demonstrated to have reduced levels of neutralising antibodies to T-dependent adeno-associated virus [264]. Therefore, the evidence gathered from these studies suggests that CD20 plays a subtle and indirect role in BCR signalling in humoral immunity.

Since the discovery of CD20 and subsequent lack of functional understanding, the focus of CD20 biology has shifted to its application as a B cell specific target for antibody therapy. CD20 is expressed on the majority of B cell malignancies, in addition to being a useful therapeutic tool in the treatment of autoimmune conditions involving B cells, such as rheumatoid arthritis. In both of these cases therapeutic efficacy and improved symptoms are observed with the depletion of B cells. Additionally, the lack of CD20 expression on HSCs or plasma cells allows the protection of bone marrow resident plasma cells to provide normal serum Ig titres, thereby maintaining a degree of humoral immunity following anti-CD20 therapy [265]. Anti-CD20 antibodies are classed as direct targeting antibodies and several have been approved for use in humans (Table 1.2). They have been classified into two groups based on their ability to redistribute CD20 into detergent-insoluble lipid rafts in the plasma membrane [266]. In addition, there are clear differences in their interaction with CD20. Experiments using radiolabelled F(ab')$_2$ indicated a difference in the binding stoichiometry between type I and type II mAb with twice as many type I antibodies binding as type II, which was interpreted as two type I molecules binding to each CD20 tetramer, and only one type II antibody [132, 267, 268]. Subsequent comparison of the obinutuzumab and RTX F(ab) crystal structures complexed with cyclical CD20 peptide indicated that the type II obinutuzumab binds in a tilted orientation in relation to RTX [267, 269]. Taken together, these observations support the observation that type II reagents bind in a 1:1 ratio of mAb to CD20 tetramer and the tilted binding angle prevents another mAb binding the same tetramer (Figure 1.12).

After cell opsonisation, anti-CD20 mAb are capable of inducing ADCC, ADCP, CDC, and DCD (Figure 1.13). A further difference between the two types of anti-CD20 mAb is present in the effector functionalities observed. Type I antibodies, such as RTX, have been comprehensively demonstrated to bind CD20 and trigger reorganisation of CD20 into lipid rafts [266]. This CD20 clustering

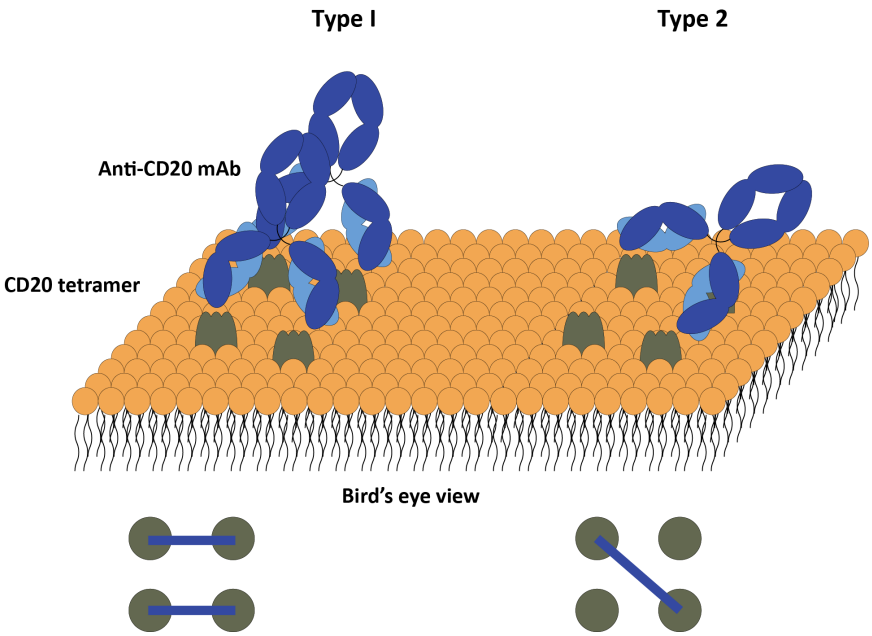

Figure 1.12: Proposed binding stoichiometry of type I vs type II anti-CD20 mAb.
Type I anti-CD20 mAb are known to bind at twice the level of type-II mAb; this figure highlights the proposed binding stoichiometry for this observation. Figure adapted from [270].

is thought to enable type I antibodies to exhibit higher levels of complement activation as compared to type II antibodies due to a more favourable Fc distribution for recruiting C1q [268], now known to be a result of hexamerisation [271]. Additionally, the degree of internalisation has been demonstrated to be higher with type I mAb due to the more efficient receptor clustering, which is further augmented through an FcγR-mediated process [272], specifically being facilitated by binding to FcγRIIb via a cis interaction on target cells [273]. This process of internalisation reduces the mAb effector functions, and therefore depletion efficiency, and is an influential characteristic of anti-CD20 resistance. Conversely, type II antibodies do not cluster CD20 and do not elicit potent CDC. However, type II display far less CD20:mAb internalisation after binding [253] and so retain Fc effector functions. Type II antibodies also exhibit a stronger DCD response. The specific binding conformation of type II antibodies is thought to elicit a non-apoptotic form of programmed cell death, activated through actin cytoskeleton remodelling, resulting in homotypic adhesion [274] and lysosomal membrane permeabilization [275].

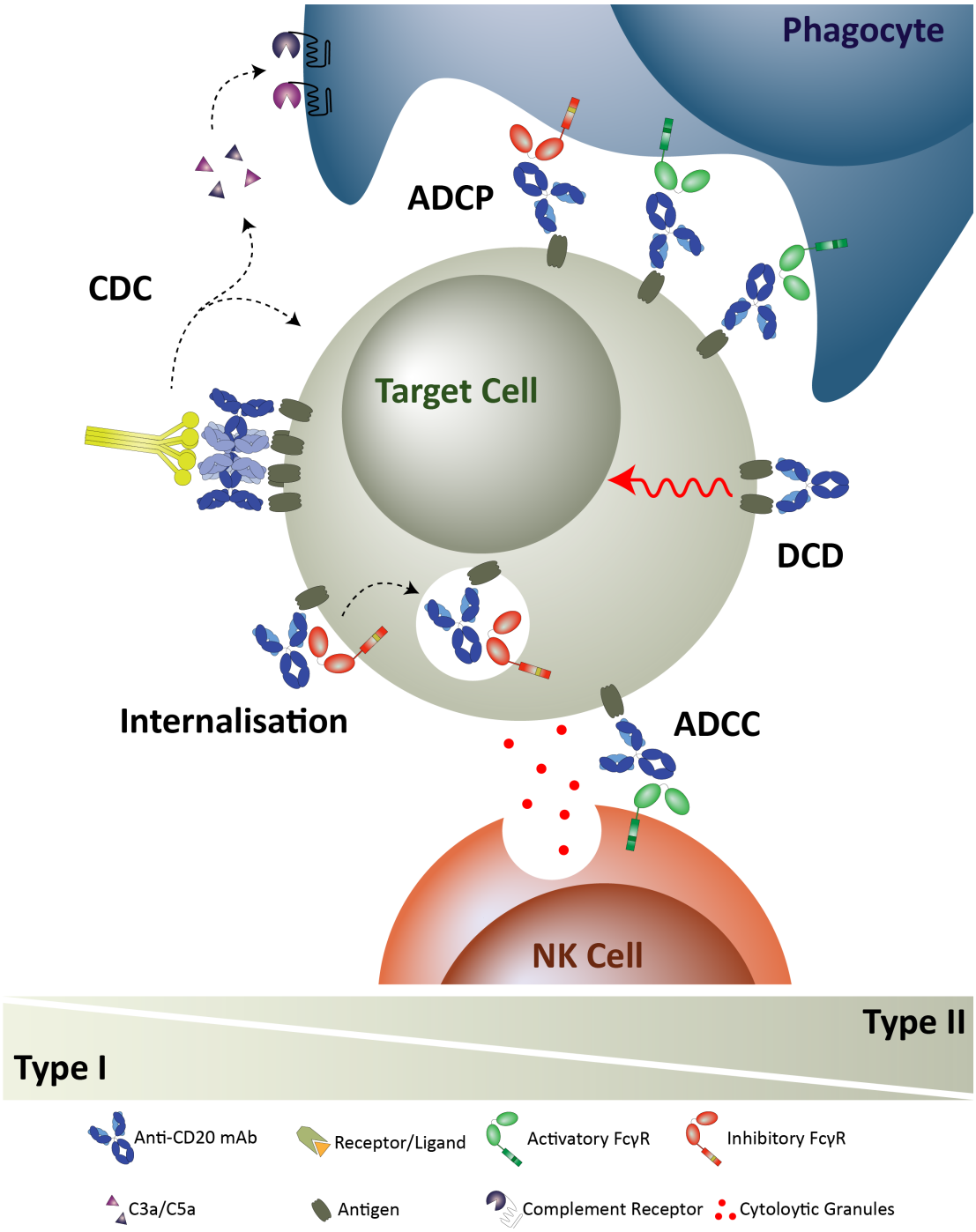

Figure 1.13: Potential mechanisms of action of B cell depleting anti-CD20 mAb.
CD20 mAbs have the potential to engage the three main Fc-mediated effector functions: CDC, ADCP, ADCC. In addition these mAb can induce DCD independent of engagement with FcγR. There are distinct characteristics in the effector function more readily activated depending on the type of CD20 mAb. Type I mAb are more effective in CDC, but more readily cluster CD20 and internalise. In contrast, type II mAb elicit a DCD to a greater propensity. Figure adapted from [276].

The first mAb aproved for the treatment of cancer was the anti-CD20 antibody, RTX. RTX is a chimeric IgG1 containing murine variable regions and human constant regions with potent B-cell depleting activities *in vivo* [277]. RTX is approved for the treatment of chronic lymphocytic leukaemia (CLL) and non-Hodgkin's lymphoma (NHL), and considered a front-line therapy in combination with chemotherapy [278]. More recently, other therapeutic CD20 antibodies have been developed and approved for similar indications. These include ofatumumab, a fully-human IgG1

that has a different binding epitope to RTX, in closer proximity to the membrane [269] and exhibits greater complement activity [279]. Another more recent anti-CD20 mAb to be approved in 2013 for first-line treatment of CLL is obinutuzumab [280]. This CD20 antibody is a type II glycoengeineered (detailed later) mAb exhibiting increased affinity for FcγRIIIa, and demonstrated to have superior ADCC and ADCP activity than RTX *in vitro* and increased B-cell depletion *in vivo* [281–283].

1.5.3 Immunomodulatory monoclonal antibodies

In addition to direct targeting antibodies, immunomodulatory antibodies are now in development in a bid to revolutionise cancer immunotherapy. By binding to receptors on immune cells, not directly on cancer cells, immunomodulatory antibodies attempt to boost immune function to destroy cancer. Immunomodulatory antibodies are grouped into two categories dependent on their biological activity, antagonistic checkpoint blockers and agonistic immunostimulatory antibodies. Examples of checkpoint receptors targeted by antagonistic antibodies include cytotoxic T-lymphocyte associated antigen 4 (CTLA4) and programmed cell death protein 1 (PD1) [284]. These antibodies work by blocking a suppressive signal in immune cells, that can be upregulated in the tumour environment. Recent clinical success with improved response rates and survival outcomes with antagonistic antibodies across a range of solid tumours, such as lung cancers and melanoma, have been described [285–288]. For example, in March 2011, an anti-CTLA-4 mAb (Ipilimumab; fully human IgG1) was approved by the FDA after demonstrating prolonged survival in patients with advanced melanoma in phase III clinical trials [285, 289, 290]. Although less developed than immune checkpoint mAb, immunostimulatory mAb have shown great potential as future cancer therapeutics in pre-clinical studies [291, 292]. However, the use of potent immnostimulatory antibodes comes with considerable safety risk, this was most notably observed with the TeGenero TGN1412 anti-CD28 superagonist that induced a near fatal cytokine storm in their first-in-man study [293]. Nonetheless, there are a number of immunostimulatory mAb in clinical developement targeting co-stimulatory targets, such as 4-1BB (CD137), OX40 (CD134), glucocorticoid-induced tumor necrosis factor receptor-related protein (GITR), and CD40 [162].

1.5.3.1 CD40 as a therapeutic target

CD40 is a 48 kDa transmembrane glycoprotein and a member of the TNFR superfamily [294], first identified in 1985 on normal and malignant B cells and human urinary bladder carcinomas [295]. The TNFR superfamily are type-I transmembrane proteins that adopt an elongated structure and

contain characteristic cysteine-rich domains (CRDs). There are 22 cysteine residues in the extracellular domains that are conserved between the TNFR superfamily [294] and act to stabilise the protein through a disulphide scaffold [296]. The ligands of TNFRs are type-II transmembrane proteins that are active as non-covalent trimers [297] in both membrane-bound and soluble forms [298]. The CD40 ligand (CD40L or CD154) is primarily expressed on activated $CD4^+$ T cells under inflammatory conditions [299].

CD40 is expressed on the surface of APCs including DC cells, B cells, and monocytes, in addition to many non-immune cells [291, 300, 301]. CD40 activation exerts profound effects on APCs, mediating a broad spectrum of systemic and inflammatory immune responses [302]. The interaction of CD40 with the trimeric CD40L induces receptor trimerisation that results in intracellular signalling facilitated by adapter molecules, involving the recruitment of TNFR-associated factors (TRAFs) to the cytoplasmic domain of CD40 [303]. The recruitment of TRAFs results in the activation of the canonical and non-canonical nuclear factor κ B (NF-κB) signalling pathways. In addition, CD40 stimulation fosters further downstream kinase activation to assemble a multicomponent signalling complex [304] that transduces to a number of well characterised signalling pathways, involving mitogenactivated protein kinases (MAPKs), phosphoinositide 3-kinase (PI3K), as well as phospholipase C γ (PLCγ) [303, 305, 306].

CD40 stimulation is considered to be important in the licensing of DC cells [307] which drives $CD8^+$ T cell priming and memory differentiation, a requirement for the induction of adaptive immunity [308–310]. DC cells present an exogenous antigenic peptide to $CD4^+$ T cells via MHC-II complexes in concert with co-stimulatory molecules. The resulting activated $CD4^+$ T cells express CD40L which signals back to DCs through CD40:CD40L interactions, resulting in DC licensing. CD40 licensed DC cells have been demonstrated to upregulate co-stimulatory receptors, such as CD70 [308, 309, 311], and promote antigen cross-presentation of exogenous antigens onto MHC-I molecules at the DC surface [312]. This resulting presentation of antigen to $CD8^+$ T cells, alongside critical CD27 signalling via CD70 from licensed DC cells, facilitates $CD8^+$ T cell priming, and thus an adaptive immune response [308–310]. Additionally, CD40 stimulation in the context of B cells has been shown to promote T cell-dependent humoral responses, germinal centre formation, isotype switching, somatic hypermutation, differentiation, and proliferation [294, 305, 313–315].

This important functional role of CD40L has made CD40 an attractive target for immunostimulatory mAb. Firstly, in tumour cells expressing the CD40 receptor, such as $CD40^+$ B cell malignancies, antagonistic anti-CD40 reagents can be therapeutic by blocking CD40/CD40L interactions, thereby preventing proliferative signals deriving from CD40 [316]. In such cases there is also the potential

for direct immunocytotoxicity and tumour deletion via Fc-mediated mechanisms (Figure 1.14,A). Direct tumour lysis also provides a source of tumour-associated antigens that can be recognised and presented by CD40 activated DCs to T cells to further boost the response [307].

Agonistic CD40 mAb have been demonstrated to generate anti-tumour responses through multiple mechanisms (Figure 1.14) [307]. It has been proposed that anti-CD40 mAb could be used to substitute for normal APC activation induced by CD40L. Stimulation of DCs by anti-CD40 mAb increases the expression of CD70 [90] and the secretion of pro-inflammatory cytokines associated with cross-priming tumour-specific CTLs (Figure 1.14,B) [317, 318] to induce $CD8^+$ T cell priming as discussed above [308–310], independent of $CD4^+$ T cell help. CTLs have been demonstrated to be an important immune cell involved in CD40-mediated anti-tumour activity. Studies involving mice depleted of $CD4^+$ T cells have shown that CD40-activated DCs can overcome tolerance to restore antigen-specific CTLs [319–321]. Conversely, depletion of $CD8^+$ T cells abrogates anti-tumour immunity [317]. Preclinical work in syngeneic mouse models has suggested that one of the most potent effects of anti-CD40 mAb in the treatment of cancer relates to their ability to licence DCs to directly activate anti-tumour CTLs, bypassing the requirement for $CD4^+$ T cell help [317, 322, 323]. Such models using rat anti-mouse CD40 antibodies have been shown to achieve an 80 - 100% survival rate and a memory response upon re-challenge in a T cell-dependent manner [322, 324]. These studies have highlighted the central role of CTL-mediated tumour control during CD40 immunotherapy for certain cancer models. However, in pancreatic cancer therapeutic efficacy was linked to activation of myeloid cells [325, 326].

Further to the activation of the adaptive immune system described, the innate system can also be utilised in CD40 mAb therapy. Stimulation of CD40 on macrophages has also been proposed to induce macrophage-dependent cytotoxicity to directly destroy cancerous cells. This involves the increased production of TNF-α, nitric oxide, and TRAIL by these cells (Figure 1.14,C) [294, 325, 327–329]. Such mechanisms do not require CD40 expression in the tumours themselves, and therefore have the potential to be efficacious towards a wide-range of cancers.

Lastly, Stimulation of B cells by anti-CD40 mAb has been shown to enhance antigen presentation and proliferation (Figure 1.14,D) [307], and increase the levels of IgM and IgG in the serum [330], suggesting anti-CD40 mAb also promote Ig class switching and maturation into plasma cells.

Crucial studies have been undertaken to address the role of isotype in anti-CD40 mAb immunotherapy, which have highlighted the importance of the inhibitory FcγRIIb [331, 332]. These experiments have shown that FcγRIIb on neighbouring cells is required to cross-link the Fc, which in turn clusters the receptor to provide efficient CD40 stimulation, mimicking the effect of the endogenous multimeric ligand. Therefore, isotypes with high or preferential engagement with FcγRIIb,

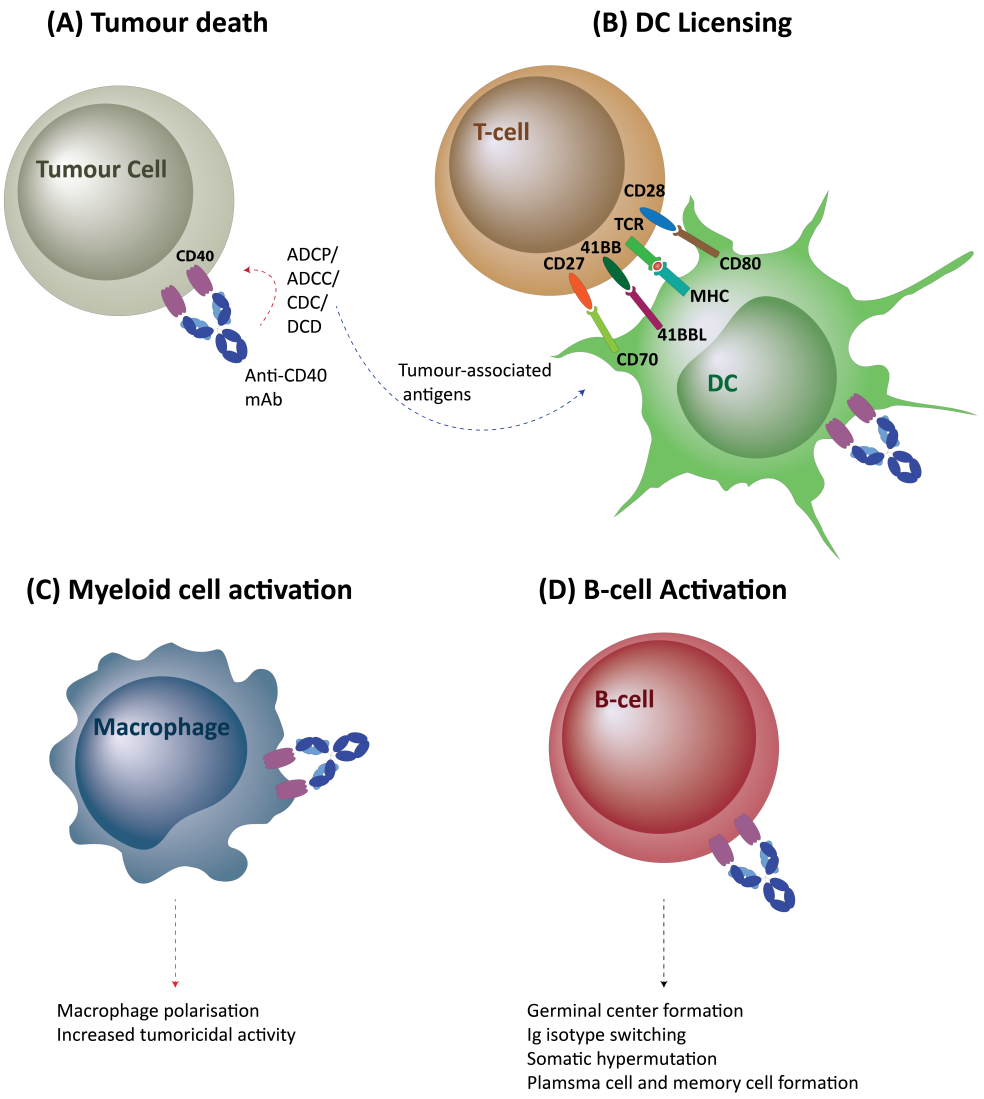

Figure 1.14: Potential mechanisms of action of agonistic anti-CD40 mAb.
(A) Depending on the isotype, anti-CD40 mAb have the capacity to induce a direct cytotoxic effect on $CD40^+$ tumour cells via ADCC, ADCP, CDC, or PCD. Additionally, tumour associated antigens released from lysed cells have the potential to cross-prime APC and be presented to T cells (B) CD40 agonism licences DCs to increase their ability to process and present tumour associated antigens to CTLs (C) Agonistic CD40 activation of myeloid cells can promote tumouricidal myeloid cells in the absence of T cell responses (D) Agonism of CD40 expressed on B cells induces germinal centre formation, isotype switching, somatic hypermutation, differentiation, and proliferation. Figure adapted from [307].

such as mouse IgG1 are efficacious whereas the mouse IgG2a, which has a high activatory:inhibitory (A:I) ratio and predominantly associates with activatory FcγR are ineffective [333]. In humans, the isotype choice is more complex. Human IgG1 also engages preferentially with activatory FcγRs leading to Fc-mediated effector functions. Therefore, the two mechanisms (FcγRIIb-mediated receptor clustering and activation versus activatory FcγR-mediated deletion) would be in conflict with one another, i.e. $CD40^+$ APCs may be deleted instead of activated, alongside tumour. More recently, studies have demonstrated that human anti-CD40 mAbs can elicit efficient receptor agonism through FcγR-independent mechanisms, which are dependent upon the hinge region of human IgG2 [90] and binding epitope [334]. Together, these studies illustrate the influence of different isotypes on the agonistic mechanisms that are achieved, which should be carefully considered depending on the effector mechanism with anti-CD40 therapy.

Human anti-CD40 mAb have also been investigated in early human clinical trials, these include agonistic antibodies, such as CP-870,893 (CP) [335, 336] and ChiLob 7/4 [337], and antagonistic antibodies, such as lucatumumab [316], towards a range of lymphoid and solid tumours, as monotherapies and in combination with other reagents. Clinical trials using anti-CD40 mAb in single agent studies and in combination with chemotherapy have shown initial promise, however, there are outstanding questions surrounding doses, schedule, formulation, and administration route. Although extensive effort has been undertaken to develop a clinically relevant CD40 agonist, approval has been limited by concerns with the associated dose-limiting toxicities. CD40 mAb have been demonstrated to induce cytokine release syndrome [338], autoimmune reactions [338], tumour angiogenesis [339], and thromboembolic syndromes (due to CD40 expression on platelets) [340, 341]. The most promising results have been produced with the use of CP, a fully human IgG2 anti-CD40 mAb in the treatment of pancreatic cancer [325]. However, the dose-limited toxicities and the lack of observed therapeutic response in clinical trials with agonistic CD40-mAb has stunted further clinical development. More recently, the fully human IgG2 anti-CD40 mAb, CDX-1140 (Celldex), has demonstrated positive preclinical results for CD40 agonism and low cytokine production in studies using human whole blood [342], and is currently in phase I clinical studies to assess safety [343]. An alternative to the development of novel anti-CD40 mAbs that exhibit lower toxicity is through Fc engineering of existing mAb.

1.6 Fc engineering

Although the number of conditions that can be treated with mAb is increasing, so too are the number of patients that don't respond or become resistant to antibody therapy and so more efficacious treatments are becoming vital. Critical for future progression in mAb therapeutics is the need for better understanding of their mechanisms of action and development of new or improved antibodies in order to deliver safer and more effective therapies. The majority of existing mAb utilised in the clinic elicit a therapeutic response via Fc mediated mechanisms through an interface with key elements of the immune system, including complement and FcγR-bearing effector cells. The focus of recent improvement to mAb technology has been to augment potency by modifying the Fc region responsible for recruitment with the immune effector functions. Conversely, engineering an antibody to become more potent can result in a less tolerated drug product, with greater side-effects and dose-limiting toxicity. Therefore, a careful balance between efficacy and toxicity must be reached.

Fc engineering approaches focus on silencing or augmenting Fc-mediated effector functions. The

regions within the Fc and amino acids involved in interaction with immune effectors such as C1q and FcγR have been mapped and multiple mutations that influence effector functions have been identified [344]. The simplest means to silence antibody effector functions is to remove the Fc to produce small antibody formats, such as F(ab')$_2$, F(ab), or scFV, but these generally exhibit short serum half-lives [345]. Removal of the N-linked glycosylation site in the CH2, either by enzymatic methods or mutation of Asn297, has been demonstrated to significantly decrease IgG1 effector functions by reducing binding to C1q and FcγR [346]. Alternatively, amino acids mutations made to the hinge region of IgG1 to reduce flexibility and length have been demonstrated to have profound negative effects on CDC and ADCC [347].

In the case of the majority of currently approved anti-cancer mAbs, Fc functions are required to eliminate the target cell, therefore improving effector mechanisms is a desirable feature. ADCP has been demonstrated to be enhanced by mutations that increase Fc affinity for FcγRIIa, required for phagocytosis by macrophages. This is exemplified by a single G236A mutation that enhances the affinity to FcγRIIa but not FcγRIIb to mediate enhanced macrophage-dependent phagocytosis of antibody opsonised target cells [121]. Conversely, mutations that increase affinity for FcγRIIIa, such as the double mutant S239D-I332E, display higher levels of ADCC *in vitro* [348]. Finally, by increasing IgG1 Fc affinity for C1q the level of CDC can be enhanced relative to wild-type (WT) IgG1. This has been demonstrated by SDM of K326 and E333 at the C1q binding region of the CH3 [349].

In contrast to Fc mutations that enhance affinity for the activating FcγR, there are circumstances whereby enhanced affinity for the inhibitory FcγRIIb has beneficial activities. As previously mentioned, CD40 agonism in the context of human IgG1 required cross-linking with FcγRIIb in a trans configuration. Mutagenesis studies in which the V11 (G237D/P238D/H268D/P271G/A330R) [350] or SELF (S267E/L328F) [351] mutations have been utilised which demonstrated enhanced binding to FcγRIIb, significantly enhancing the anti-tumour immunity observed with CP-870,893 *in-vivo* [352]

In addition to the important role of the amino acids in the FcγR and C1q binding sites, the glycan composition of the N-linked glycosylated Asn297 is known to play important regulatory functions to the activity of antibodies. Depending on the sugars present antibody glycoslation is thought to have either pro- or anti-inflammatory properties. Sialyated antibodies are regarded as anti-inflammatory and important for the therapeutic effect of intravenous immunoglobulin (IVIG) [353]. Moreover, the fucosylation status has been demonstrated to have significant effects on IgG function. Fucosylated IgG has been reported to be detrimental in the binding to FcγRs and C1q, resulting in reduced CDC, ADCC, and ADCP activity [102, 354, 355]. Alternatively, afucosylated

antibodies have been shown to have increased binding to FcγRIIIa with a subsequent enhancement in ADCC [346]. As such the glycan can be modified to manipulate the effector properties of therapeutic antibodies, for example using a FUT8(-/-) CHO cell line to express defucosylated antibodies [356] which has been exploited in the anti-CD20 mAb obinutuzumab.

In addition to improving cell killing mechanisms, the induction of antibody-dependent cytokine release (ADCR) has been recently studied as an Fc-engineering approach [357]. ADCR influences the tumour microenvironment and therapeutic outcome via antibody interaction with FcγRs. Antibodies have been recognised to influence macrophage polarisation to limit tissue damage within disease microenvironments. The activation of FcγRI on macrophages induces the secretion of IL-10. This anti-inflammatory cytokine converts pro-inflammatory macrophages into anti-inflammatory macrophages [358]. Recent reports have demonstrated that a co-culture of macrophages with cetuximab opsonised cancer cells stimulates the production of IL-10 [359]. One strategy to minimise the potentially detrimental effects of ADCR on anti-inflammatory macrophage polarisation has been to mutate residues on the Fc of IgG1 to reduce binding to FcγRI without affecting binding to FcγRIIa and FcγRIIIa. In order to achieve this, firstly IgG1 was mutated to contain E233P/L243V/L235A mutations and G236 deleted to render the antibody Fc silent in terms of ADCC and CDC. In order to restore binding to FcγRIIa/FcγRIIIa and Fc-mediated effector functions either S239D/K326A/E333A or K326A/I332E/E333A mutations were introduced. The result was an Fc-engineered IgG1 which demonstrated macrophage-mediated ADCP, but silenced macrophage IL-10 secretion [357].

Knowledge of the properties of antibody isotypes and IgG subclasses has enabled the potential use of cross-subclass and cross-isotype engineering. IgG1 and IgG3 are known to be capable of inducing efficient CDC, ADCC, and ADCP responses. Effective complement activation is hugely variable between subclasses, and is activated in a decreasing fashion as follows IgG3 > IgG1 > IgG2 >IgG4. For example, the lack of complement activity with IgG4 has been attributed to residue Ser331 which is responsible for low binding to C1q [360], but IgG4 has been demonstrated to induce ADCP [357]. By combining the known properties of IgG sub-classes novel antibodies can be designed with more desirable effector and therapeutic functions. Natsume *et al* have reported that a chimeric IgG1/IgG3 constant domain displayed enhanced effector functions. Specifically a variant containing the CH1 and hinge of IgG1, and the CH2 and CH3 from IgG3 displayed complement activating activity far superior to IgG1 and IgG3 parental mAb [361].

These chimeras are not limited to IgG isotypes. In terms of cross-isotype antibodies, an IgG1 with the IgA1 CH3 and a chimeric IgG1:IgA1 CH2, named IgGA, have been designed [362]. IgA antibodies have previously been shown to mediate potent ADCC [363] and ADCP [364] effector functions,

and recently have been demonstrated to be effective anti-cancer agents *in vivo* [365]. However, due to the short serum half-life compared to IgG [149] and its inability to interact with complement [366, 367] there is currently little clinical activity in the application of IgA therapeutics [62]. The use of cross-isotype engineering in this case produced a molecule with enhanced ADCC, ADCP, and CDC activities through interactions with both FcγRs, FcαRs, and C1q [362]. In addition to these modifications designed to manipulate binding to different effector molecules, another approach has been to enhance therapeutic efficiency of IgG by promoting IgG multimers/hexamers [197, 368, 369].

1.6.1 IgG hexamers

As previously discussed IgA and IgM are secreted in polymeric formats attributed in part to the 18 amino acid tailpiece at the C-terminal of each antibody. The tailpieces between IgA and IgM differ by seven amino acids, sharing 60% sequence homology, but both have a conserved N-linked glycosylation site and a cysteine residue at the penultimate residue [59]. IgM is secreted in either a pentameric or hexameric format partly due to the formation of disulphide bonds between neighbouring tailpiece cysteines [69].

Using molecular engineering, the 18 amino acid μtp has been fused to the C-terminus of IgG molecules resulting in hexameric IgG complexes (IgG μtp), driven by the intermolecular disulphide bond forming abilities of the cysteine residue [368, 369]. These hexameric IgG molecules exhibits enhanced complement effector function *in vitro* [369], that could be translated to a more efficacious therapeutic agent *in vivo*. However, *in vivo* there are several potentially severe side effects to consider with the intravenous administration of a hexameric IgG molecule, such as the non-specific activation of the complement system. In the case of the pentameric or hexameric IgM, antigen binding is a requirement for complement activation due to induction of a conformational change in the Fc domain [370]. Further experimental evidence detailed the differences in the exposure of C1q binding sites in the Fc region with and without the presence of an antigen, by measuring the change in accessibility of the IgM J-chain located at the Fc core of the pentameric IgM [67]. When in complex with an antigen the J-chain becomes exposed. This suggests an antigen-dependent conformational change, which has been postulated to be important in the display of C1q binding sites [371]. This mechanism, therefore, acts as a level of control in the prevention of IgM pentamer activating complement when not complexed with antigen.

IgG, however, does not have the same level of regulation, but relies on low-affinity, high avidity interactions with complement to prevent undesirable immune activation. Individual IgG's contain

two C1q binding sites, with each HC containing one. In solution monomeric IgG has low affinity to C1q, as a result cannot activate complement (Kd 10^{-4} M) [196]. However, when in complex with their antigen the affinity of IgG for C1q is much tighter (Kd 10^{-8} M) and complement activation is higher [372]. The multimeric Fc arrangement of a hexameric IgG molecule may enhance the avidity for C1q and FcγRs without the requirement for antigen. This would lead to an uncontrolled immune activation resulting in the release of anaphylatoxins and upregulation of cytokines, potentially leading to unwanted negative side-effects such as cytokine storms and anaphylaxis.

IgG is naturally secreted in a monomeric format, but it has long been speculated that such efficient antigen-driven CDC activity of IgG is achieved through the formation of hexameric ring structures through Fc-Fc interactions [372]. Crystallographic studies have provided crucial evidence that has eluded to the ability of IgG to form ordered, hexameric ring structures [373, 374]. In the solved crystal structure of the human anti-HIV-1 gp120 antibody (protein data bank entry 1HZH) the Fc regions are arranged in a hexameric ring in the crystal packing, with interactions at the CH2:CH3 interface [374] (Figure 1.15). Such a hexamer would give six accessible C1q binding sites at the surface, each IgG providing one, while the other six direct away from the hexamer surface. It was observed that Lys322, a critical residue in the C1q binding site, was still accessible for C1q binding and suggested a favourable interaction between the six-headed globular protein and the six Fc binding sites in the hexamer [374]. This led to speculation that these Fc:Fc interactions could be important in the activation of complement.

Recent evidence has suggested that upon target binding the antibody Fc domains cluster into ordered hexamers through specific, non-covalent interactions forming a high avidity binding platform for C1q, reminiscent of polyvalent IgM structures. Mutagenesis of the IgG1 Fc region with the triple mutant RGY (E345R, E430G, S440Y) in the CH3 domain of IgG1 enables the formation of hexamers at low concentrations in solution, which translates to superior cell killing by CDC when compared to a WT IgG1 mAb. At the cell surface, these hexamers recruit C1q to initiate the complement cascade, suggested to be a result of increased avidity of the C1q interaction with the hexameric Fc organisation [197].

Additional mutagenesis studies into the hexamerisation enhancing mutations has determined that only one of the mutants is required for CDC killing comparable to the triple RGY mutant. The mutations E345R, E345K, or E430G alone still elicit a significantly higher level of killing when compared to their WT counterparts. Structural analysis led to the proposition that the side-chain of the E345 residue is pointed out towards G358 of the neighbouring CH3 to hinder interactions. Furthermore, the E430 residue forms a salt-bridge which acts to stabilise the CH2:CH3 domain conformation of IgG molecules to restrict Fc flexibility. Together these residues restrain Fc:Fc in-

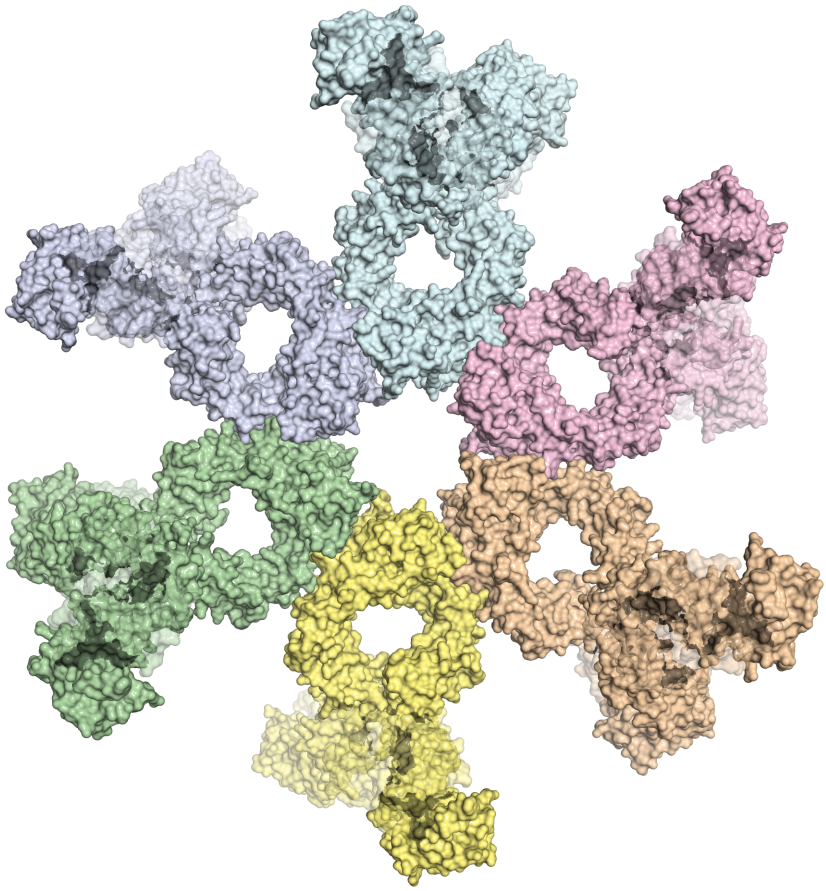

Figure 1.15: Crystal packing arrangement of hIgG1.
In the crystal structure of IgG1 the arrangement of monomers is observed as a hexameric ring structure with interactions in the C_H2 and C_H3 domains of neighbouring Fc's. The heavy chains are shown in solid colours and light chains shown in transparent colours. Structure source: PDB entry 1HZH [374]. Image created using PyMol by Chris Orr.

teractions and inhibit optimal CDC activity [271]. Biophysical characterisation of these single mutants revealed at low concentrations the mAbs are monomers, and the formation of a hexamer is only possible when high concentrations are achieved (100 mg/ml). This led to the proposal that this mutant IgG1 has enhanced clustering at the cell surface through Fc:Fc interactions that increase CDC via increased C1q binding [375]. Being monomeric in solution also has the added benefit of reducing unwanted side effects, and when subjected to normal human serum at concentrations up to 100 μg/ml, non-specific complement activation was undetectable [271].

Further analysis delineated the improved CDC to be due to an increased activation of the classical pathway leading to more potent cell death induction. Hexamerisation enhanced mutant IgG1 (IgG1 with single E345R or S440Y mutations, or both) elicited a higher level of cell killing as a direct result of more rapid recruitment of CDC components to the cell surface. The entire cytotoxic process is complete in under two minutes with RTX hexamerisation enhanced mutant (E430G) compared to over 8 minutes with WT RTX [215]. Subsequent experimentation has revealed that hexamerisation enhanced mAb with the E430G mutation have an increased population of higher

order IgG complexes after antigen binding, but such mutations were restricted to cluster of a maximum of six IgG moelcules (IgG hexamers) [198]. Therefore, the formation of IgG hexamers after target binding indicates a potentially favourable stoichiometry for the recruitment of C1q, and by enhancing these interactions CDC killing efficiency can be augmented. However, in the case of high density or pre-clustered antigen, antibody-induced clustering may be less important for enhancing CDC. Conversely, this technology could be applied to low-density antigens with limited or no self-clustering lateral membrane diffusion as an efficient method for enhancing complement-mediated target killing.

These mAb bearing the E430G or E345K mutation were initially characterised on targets bearing CD20 or CD38 antigens [197, 271]. More recent reports have applied these mutations to mAb targeting a range of immunologically relevant antigens, focussed on target destruction by CDC. In addition to these antigens, E430G enhanced CDC has been observed in mAb targeting EGFR for therapy of solid tumour [376], CD37 for therapy against B cell malignancies [377], and even a gonococcal lipooligosaccharide epitope for the treatment of multidrug-resistant *Neisseria gonorrhoeae* bacterial infections [378]. Aside from direct targeting antibodies this application has also been applied to immunomodulatory receptors such as members of the TNFR superfamily, where clustering induces agonism. Zhang *et al* have demonstrated that targeting the co-stimulatory molecule OX40 with hexamerisation enhanced mAb leads to more efficient agonism of the target cell [379, 380]. Similarly, the use of a mixture of non-competing anti-DR5 mAb with hexamerisation enhancing mutations has been reported to induce increased cytotoxicity of multiple myeloma tumour cells [381], and is currently in clinical development.

The absence of IgG hexamers in WT IgG could be an intrinsic level of control, required to dial-down IgG potency. However, this level of control is not required in therapeutic mAbs, where a high level of cellular killing is desirable. This understanding of Fc engineering could be harnessed by pre-existing and next generation mAb technologies, thereby shifting the current paradigm of therapeutic research from identifying new cellular targets to enhancing mAbs as a more efficacious tools by exploiting their ability to self-assemble into ordered complexes following efficient antigen binding.

1.6.2 IgG Fc hexamers

In addition to the use of IgG hexamers, there is current interest in the development of IgG Fc hexamers. The activation of Fc receptors and complement by immune complexes is predicted to be a common pathogenic trigger in autoimmune diseases. The blockade of such innate immune path-

ways is an attractive therapeutic target. Recent studies have focussed on the use of Fc multimer, including hexamers, as an IVIG biomimetic. IVIG is pooled human IgG, that when used at high-doses, alleviates the symptoms of autoimmune conditions such as immune thrombocytic purpura (ITP), Guillain-Barré syndrome, and chronic idiopathic demyelinating polyneuropathy [382, 383]. These conditions are thought to be mediated by pathogenic autoantibodies that induce tissue destruction through FcγR bearing effector cells and the complement cascade [384, 385]. Currently, the mechanism of action of IVIG is proposed to be via blockade of FcγR [386], scavenging and depletion of complement proteins [387], and saturation of FcRn [388]. The blockade of FcγR induced by IVIG is supported by human trials involving the infusion of Fc-only IVIG that was effective in the treatment of ITP [389] and the observed reduction in the phagocytic potential of patients macrophages infused with IVIG [390]. FcγR blockade is thought to be mediated by low levels of non-monomeric Ig, such as dimers, present before infusion and those formed by anti-idiotype networks after infusion [391]. IVIG for human administration is typically composed of >90% monomer/dimer and <0.5% higher order aggregate. Depending on formulation the proportion of dimer is between 3-16% [392, 393]. Therefore, the use of high avidity Fc multimers has been postulated to have the potential to treat such autoimmune conditions more effectively.

The use of recombinant IgG1 Fc fused to the μtp (Fc μtp) produces stable Fc hexamers which have been demonstrated to recapitulate the anti-inflammatory activity of IVIG *in vitro* and *in vivo* [394–401]. Such studies have demonstrated that Fc μtp hexamers can bind with high avidity to FcγR to limit autoantibody pathogenesis *in vitro* where Fc μtp hexamers efficiently inhibit FcγR-mediated phagocytosis [401] and act to sequester C1q and consume C4 without further activation of terminal complement proteins (C3, C5) [400, 401]. In addition, *in vivo* murine models have suggested that treatment with Fc μtp hexamer provides therapeutic benefits to ITP [401] and the suppression of inflammatory arthritis [400], with the use of 10-100 fold lower doses as compared to IVIG. One current potential mechanism of action is that administration of Fc μtp hexamer results in altering FcγR density, and the triggering of FcγR internalisation and degradation [399], thereby preventing autoimmune antibody-mediated tissue destruction through FcγR effector mechanisms.

However, such Fc hexamer complexes observe short *in vivo* half-lives, in both mice and cynomolgus monkeys [399], even though the complex binds to FcRn at high affinity [400]. In addition, there are several safety concerns when using Fc hexamers, highlighted by the potentially high levels of pro-inflammatory cytokines released in human whole blood assays, postulated to be induced by FcγRIIa activation on platelets and FcγRIIIb activation on neutrophils [401]. Overall, the use of IgG and Fc hexamers have proven to be a potentially useful tool in antibody engineering and future therapeutics, albeit requiring further development to increase half-life and overcome

any unwanted cytokine toxicity.

1.7 Aims and hypothesis

It has recently been demonstrated that hIgG1 activates complement optimally when arranged as ordered hexamers after target binding. In addition, several techniques have been described that serve to hexamerise IgG, such as fusion of μtp and Fc mutagenesis (e.g. EGY). This current research will focus on expanding the current understanding of the utility of antibody hexamerisation in direct targeting and immunomodulatory mAb using IgG hexamers and hexamerisation enhanced IgG based around the μtp. The hypothesis was that IgG hexamers and hexamerisation enhanced IgG would display augmented CDC and agonistic activity. Hexamerisaiton enhanced IgG were produced by addition of the μtp with a Cys-Ser mutation at position 575 (C575S). This allows for the mAb to be monomeric in solution but have a higher propensity for the Fcs to cluster at the cell surface, through enhanced attraction between the μtps. The exploration of this novel antibody technology was implemented and validated using molecular biology, protein engineering, immunoassays, and *in vivo* models.

The specific aims for this project were as follows:

1. Generate Fc-engineered mAbs in the format of an IgG hexamer and a hexamerisation enhanced mutant IgG (Figure 1.16).
    (a) Generate IgG hexamers through engraftment of the 18 amino acid μtp at the C-terminus.
    (b) Use SDM to replace the cysteine at position 575 of the μtp to a serine (C575S) to produce monomeric IgG with a hexamerisation enhancement.
    (c) Express and purify as above in the context of direct targeting and immunomodulatory mAb.
    (d) Characterise the IgG hexamers and hexamerisation enhanced IgG for purity, size, antigen binding, and hexamerisation enhancement.
2. Assess the direct targeting mAb *in vitro* and *in vivo* for cell killing enhancement and therapeutic potential:
    (a) Use *In vitro* techniques to examine IgG hexamers and hexamerisation enhanced IgG for enhanced cell killing in assays for anti-CD20-mediated CDC, ADCC, ADCP, CDC, and whole blood B-cell depletion.
    (b) Use *In vivo* models to investigate IgG hexamers and hexamerisation enhanced IgG for half-life and B-cell depleting activity in murine models.
3. Investigate the molecular requirements for hexamerisation enhanced IgG.

(a) Use SDM, deglycosylation and isotype switching to decrease C1q affinity and CDC activity to determine if increasing IgG clustering can overcome low C1q affinity

(b) Use SDM to introduce new mutations in the Fc and μtp to further enhance hexamerisation efficiency and CDC activity.

4. Examine the agonistic activity of IgG hexamers and hexamerisation enhanced IgG *in vitro* and *in vivo*.

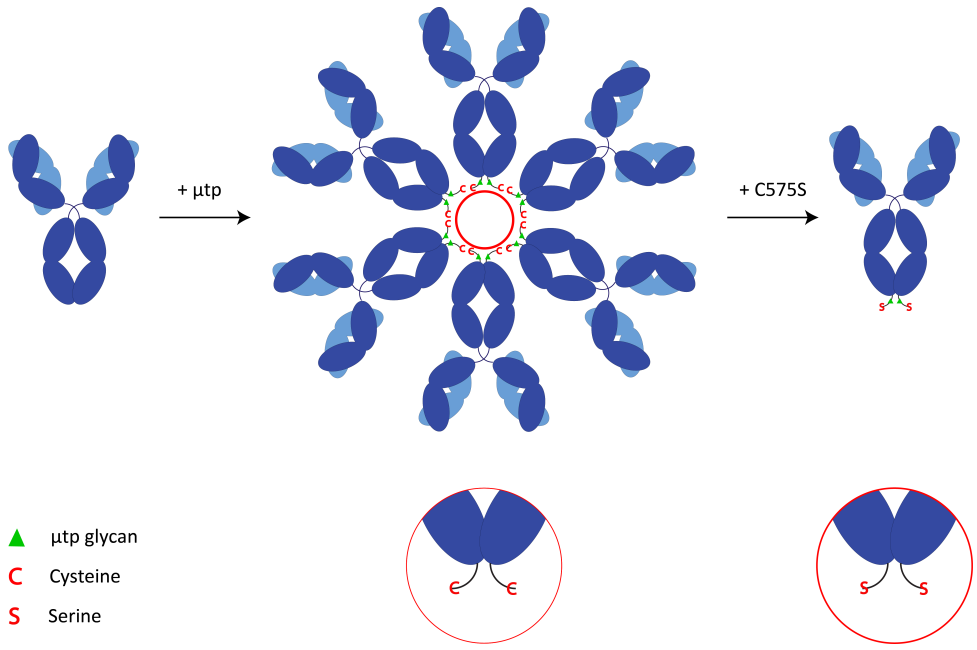

Figure 1.16: Schematic of proposed Fc-engineered hIgG.
Addition of the μtp was used to produce IgG hexamers. SDM of Cys575 of the μtp to Ser was used to remove the disulphide bond and produce a monomeric form with a hexamerisation enhancement.

Chapter 2

Methods and Materials

2.1 Cell culture

2.1.1 Cell thawing

Cells were removed from liquid nitrogen and immediately placed on ice. Cells were rapidly thawed in a water bath set at 37^{o}C. After thawing, the cells were transferred to a 50 ml falcon tube and diluted to 50 ml in pre-warmed media. The cells were then centrifuged at 300 x g for 5 minutes and the supernatant poured off. The pelleted cells were then resuspended again in 50 ml of media and centrifuged for a further 5 minutes at 300 x g. Pelleted cells were then resuspended to 1 x 10^6 cells/ml and incubated at 37^{o}C, 5% CO_2.

2.1.2 Cell line maintenance

Burkitts lymphoma cell lines (Ramos and Raji) were cultured in suspension in complete (c)RPMI (Rowsell park memorial institute [RPMI] 1640 media [ThermoFisher] supplemented with 2 mM L-glutamine [ThermoFisher], 1 mM pyruvate [ThermoFisher], and 10% foetal calf serum [FCS] [ThermoFisher]). Jurkat NF-κB-GFP cells stably transfected with CD40 (generated by Dr C Chan) were cultured in suspension in R10 media (cRPMI with 2 mM 2-Mercaptoethanol (Sigma)) supplemented with 1 μg/ml puromycin (Sigma). CHO cells stably transfected with human Fcγ receptors (generated by Dr R Oldham) were cultured in cRPMI supplemented with 0.5 mg/ml Geneticin (ThermoFisher). CHO cells were cultured as adherent cells and when sub-cultured were gently scraped to remove adherent cells from culture flasks. All cell lines were maintained in culture at 37^{o}C, 5% CO_2, incubated in a New Brunswick Galaxy 170R incubator. Cell lines were sub-cultured

every 2-4 days, to maintain a density of 0.2 – 2 x 10^6 cells/ml. The CHO-SXE [402] cell line was cultured in suspension in CD-CHO media (ThermoFisher), supplemented with 2 mM Glutamax (ThermoFisher). Cells were maintained at 37^{o}C, 5% CO_2, shaking at 140 rpm in a 1SF1-X Shaker incubator (Kuhner). CHO-SXE cells were sub-cultured every 3-4 days, to maintain a density of 0.2 – 4 x 10^6 cells/ml.

2.1.3 Ethics

Ethical approval for the use of clinical samples was obtained by the Southampton University Hospital's NHS Trust from the Southampton and South West Hampshire Research Ethics Committee. Informed consent was given in accordance with ethics committee approvals under the Declaration of Helsinki. Anonymized leukocyte cones used in this study were released from the Southampton General Hospital National Blood Service following ethical approval.

2.1.4 Peripheral blood mononuclear cells isolation

Peripheral blood mononuclear cells (PBMCs) were isolated from leukocyte cones. During plateletpheresis, platelets are separated from red blood cells, white blood cells, and the serum which are collected as waste products into leukocyte cones. These were acquired from Southampton General Hospital NHS blood service and emptied into a 50 ml falcon tube, and diluted 1 in 5 with PBS, 2 mM EDTA, 10% FCS. 25 ml of blood was carefully layered on top of 12.5 ml Lymphoprep (Axid Shield). The blood was then centrifuged at 800 x g for 10 minutes, in a covered centrifuge with the brake set to the lowest setting. The interphase layer containing the peripheral blood mononuclear cells (PBMCs) was collected using a Pasteur pipette and washed three times in PBS, 2mM EDTA by centrifugation at 400 x g for 5 minutes. After washing PBMCs were resuspended in cRPMI with or without FCS supplementation.

2.1.5 Determination of cell concentration

Concentration of mammalian cells in suspension was determined using either a Coulter counter z1 particle counter (Beckman Coulter) or a Vi-CELL XR Cell Counter and viability analyser (Beckman Coulter). For the Coulter counter z1 a 20 μl cell suspension was diluted in 10 ml Isoton II diluent (Beckman Coulter), with the addition of 2 drops of Zap-OGLOBIN II Lytic agent (Beckman Coulter) to lyse red blood cells in blood samples. The concentration of cells was determined using the particle counter. For the Vi-Cell XR Cell counter, 500 μl of cell suspension was loaded into the

sampler to assess cell density and viability.

2.1.6 Determination of cell viability

To determine cell viability, 200 μl of cell suspension was stained with 1 drop of 10 μg/ml propidium iodide (PI; Sigma) and analysed by flow cytometry. Cell viability was calculated by observing cells negative for PI staining. Alternatively, cell viability was determined using the Vi-Cell XR Cell counter and viability analyser, as above.

2.2 Molecular biology techniques

2.2.1 DNA digestion

DNA digestion reactions were prepared containing 5 μg DNA, 1 μl of each of the appropriate restriction enzymes, 5 μl 10 x buffer (NEB), and dH_2O to a total volume of 50 μl. For heavy chain digests, backbone and V-region restriction enzymes HindIII (NEB) and XhoI (NEB) were added to the mixture simultaneously and incubated for 2 hours at 37^{o}C. For the backbone and V-region light chain digests the restriction enzymes HindIII (NEB) and BsiWI (NEB) were added sequentially; first HindIII was added and incubated for 2 hours at 37^{o}C before BsiWI was then added and incubated for a further 2 hours at 55^{o}C. Samples were then assessed by DNA Gel Electrophoresis.

2.2.2 DNA gel electrophoresis

1% agarose gel was prepared by dissolving 1 g Agarose (Sigma) per 100 ml Tris-acetate-EDTA (TAE) (40 mM Tris, 20 mM acetic acid, 1 mM EDTA) buffer. To visualise DNA under ultraviolet light, 0.5 μg/ml ethidium bromide was added. DNA was mixed with loading dye (15% Ficoll (Sigma), Orange G (Sigma) dissolved in PBS) prior to loading. DNA samples and 2-log ladder (NEB) to determine fragment size were loaded onto the gel. The gel was run at 80 V for 60 minutes and DNA was subsequently visualised on a UV transilluminator at 356 nm (UVP).

2.2.3 DNA gel extraction

DNA was extracted from 1% agarose DNA electrophoresis gels using QIAquick Gel Extraction Kit (Qiagen) using manufacturer's instructions. DNA extraction involved excising the DNA fragment

from the agarose gel using a sharp, clean scalpel. The gel slice was dissolved in a 3 x volume of buffer QG to 1 x volume of gel and incubating at 50^{o}C for 10 minutes. Once dissolved, 1 x volume of 100% isopropanol was added and the sample transferred to a QIAquick spin column in a 2 ml collection tube. The DNA was bound to the column by centrifugation for 1 minute at 15,000 g. The high salt content of the QG buffer allows the DNA to bind to the silica membrane of the spin column. The resulting flow-through was discarded and the column washed with a further 500 μl of QG buffer by centrifugation for 1 minute at 15,000 g. The column was then further washed with 750 μl of Buffer PE by centrifugation for 1 minute at 15,000 g, and centrifuged for a further 1 minute to remove any residual wash buffer. To elute the bound DNA, the QIAquick column was transferred to a clean 1.5 ml microcentrifuge tube and 50 μl dH$_2$O added to the resin. The column was left to stand for 1 minute at room temperature prior to centrifugation for 1 minute at 15,000 g. The low salt content of the dH$_2$O allows elution from the spin column. Extracted DNA was quantified by absorbance at 260 nm on a Nanodrop 1000 (ThermoFisher).

2.2.4 DNA ligation

In order to combine the digested V-region DNA with the appropriate backbone vector DNA, the two fragments were ligated together using the Quick Ligation Kit (NEB). Vector DNA (50 ng) was combined with a 3-fold molar excess of insert DNA, with 10 μl of 2X Quick Ligation buffer, 1μl Quick T4 DNA Ligase, and dH$_2$0 to a final volume of 20 μl. The mixture was briefly centrifuged and incubated at room temperature (25^{o}C) for 5 minutes. Once ligation had occurred the DNA was transformed (Section 2.2.6) into *E. coli* and colonies miniprepped (Section 2.2.7) for sequencing.

2.2.5 Site-directed mutagenesis

Oligonucleotide primers were designed and synthesised to contain the desired mutation, flanked by unmodified nucleotide sequence. Primers were designed by the QuikChange Primer design tool (http://www.genomics.agilent.com/primerDesignProgram.jsp) according to the guideline that each set of primers should be 25 – 45 bases in length (with the mutation in the middle with 10 – 15 bases either side), have a melting temperature (Tm) $\geq$78^{o}C, and a minimum GC content of 40%. The primer sequences used for mutagenesis reactions are detailed in Table 2.1. Mutations were introduced using the QuikChange Lightning SDM Kit (Agilent). Site-directed mutagenesis (SDM) reactions were prepared containing 50-100 ng DNA, 5 μl 10x reaction buffer, 1 μl of each primer (at 10 μM), 0.75 μl QuikSolution, 1 μl enzyme mix, and dH$_2$0 to a total volume of 50 μl. The reaction was placed in a thermocycler for the reaction cycles detailed in Table 2.2. Briefly 1

μl Dpn I restriction enzyme (10 units) was added, and the mixture incubated at 37^{o}C for 1 hour to digest the methylated and hemimethylated parental dsDNA. The mutated DNA was transformed into *E. coli* and colonies miniprepped for sequencing.

Mutation(s)	Forward Oligo (5' - 3')	Reverse Oligo (5' - 3')
IgG1		
R355Q	CTGCCCCCATCCCAGGATGAGCTGACC	GGTCAGCTCATCCTGGGATGGGGGCAG
P331S	CAAAGCCCTCCCAGCCAGCATCGAGAAAACCATC	GATGGTTTTCTCGATGCTGGCTGGGAGGGCTTTG
IgG4		
Q355R	CTGCCCCCATCCCGGGAGGAGATGACC	GGTCATCTCCTCCCGGGATGGGGGCAG
μtp		
V564D	CCGACCCTGTATAACGACAGCCTGGTGATG	CATCACCAGGCTGTCGTTATACAGGGTCGG
V564L	CCGACCCTGTATAACTTGAGCCTGGTGATG	CATCACCAGGCTCAAGTTATACAGGGTCGG
S565T	ACCCTGTATAACGTGACCCTGGTGATGAGC	GCTCATCACCAGGGTCACGTTATACAGGGT
C575S	CGATACCGCGGGCACCAGCTATTGATGAGAATT	AATTCTATCAATAGCTGGTGCCCGCGGTATCG
S575C	CGATACCGCGGGCACCTGCTATTGATGAGAATTG	CAATTCTATCAATAGCAGGTGCCCGCGGTATCG

Table 2.1: Primer sequences used for SDM manipulations
Desired mutations and corresponding forward and reverse oligo's used, grouped by isotype or μtp.

Segment	# of cycles	Temperature (^{o}C)	Time (seconds)
1	1	95	120
2	18	95	20
		60	10
		68	180
3	1	68	300

Table 2.2: Thermocycler reaction used in SDM manipulations.
Temperatures and times calculated by following Agilent QuikChange Lightning Site-Directed Mutagenesis Kit manufacturer's instructions.

2.2.6 DNA transformation

XL-10 Ultracompetent Blue E.coli bacteria (Agilent) were thawed from -80^{o}C on ice. To 40 μl of cells, 2 μl of DNA was added and incubated at 4^{o}C for 10 minutes. The bacteria/DNA mixture was heat-shocked at 42^{o}C for 45 seconds, before cooling to 4^{o}C for 5 minutes. Cells were recovered by addition of 200 μl SOC media (ThermoFisher) and incubated at 37^{o}C for 60 minutes, shaking at 225 rpm. Agar plates were prepared and inoculated with 25 μg/ml Kanamycin (Sigma). 200 μl of bacterial cells were transferred to Agar plates and incubated at 37^{o}C overnight. Plates were checked for bacterial colonies the following day.

2.2.7 Small scale plasmid DNA purification (Miniprep)

5 ml sterile L-Broth supplemented with 25 μg/ml Kanamycin was inoculated with a single colony of transformed *E. coli* and incubated at 37^{o}C for 16 hours, shaking at 225 RPM. The culture was centrifuged for 10 minutes at 400 x g to pellet the bacteria. Plasmid DNA was isolated using the Plasmid Miniprep Kit (Qiagen) following manufacturer's instructions. Pelleted bacterial cells were resuspended in 250 μl buffer P1 (resuspension buffer supplemented with RNase) and transferred to a clean 1.5 ml microcentrifuge tube. 250 μl of buffer P2 (lysis buffer) was subsequently added, followed by 350 μl buffer N3 (neutralisation buffer), and mixed thoroughly before centrifugation at 15,000 x g for 10 minutes. The supernatant was applied to a QIAprep spin column in a 2 ml collection tube, and centrifuged for 1 minute at 15,000 x g to bind DNA to the column. The flow-through was discarded and the column washed with 750 μl buffer PE (wash buffer) by centrifugation at 15,000 x g for 1 minute. The column was centrifuged for a further 2 minutes at 15,000 x g to remove residual residue. The QIAprep spin column was placed in a clean 1.5 ml microcentrifuge tube and 50 μl sterile dH_2O added to the column. The column was left to stand for 1 minute a room temperature before centrifugation at 15,000 x g for 1 minute to elute the DNA. Eluted DNA was collected and stored at -20^{o}C.

2.2.8 Large scale plasmid DNA purification (Gigaprep)

500 ml sterile L-Broth supplemented with 25 μg/ml Kanamycin was inoculated with a single colony of transformed E. coli and incubated at 37^{o}C for 16 hours, shaking at 225 RPM. The culture was centrifuged for 10 minutes at 500 x g to pellet the bacteria. DNA was isolated using Plasmid Giga Plus Prep Kit (Qiagen) following manufacturer's instructions. The harvested bacterial pellet was resuspended in 100 ml buffer P1 (resuspension buffer, supplemented with RNase), and lysed

with 100 ml of buffer P2 (lysis buffer). 100 ml of buffer S3 (neutralisation buffer) was added and transferred to a QIAfilter cartridge attached to vacuum-safe 45 mm neck glass bottle. A vacuum was applied until all liquid had been drawn through and 100 ml buffer BB (binding buffer) added to the flow-through. Filtered lysate was transferred to a QIAGEN plasmid plus spin column attached to vacuum pump. The lysate was drawn through the column to bind the DNA. The column was washed with 80 ml buffer ETR (endotoxin removal), and 50 ml buffer PE (wash buffer). The column was centrifuged at 5,000 x g for 10 minutes to remove residual residue. To elute the DNA 2 ml sterile dH_20 was added to the column under stile conditions and incubated for 10 minutes at room temperature and centrifuged at 5000 x g for 5 minutes. Eluted DNA was collected under sterile conditions, quantified using absorbance at 260 nm and stored at -20^{o}C.

2.2.9 DNA sequencing

DNA sequencing reactions were prepared by mixing 300–500 ng of DNA, 1 μl sequencing buffer, 1 μl Big Dye v5.0, 1 μl primer (10 μM), and 3.5 μl dH_20. The primers used for sequencing are detailed in Table 2.3. The reaction was placed in a thermocycler for the reaction cycle detailed in Table 2.4. The resulting PCR mix was then sent for sequencing in-house at UCB.

Primer Sequence	Primer Location
GCTGACAGACTAACAGACTGTTCC	CMV promoter forward
GGCTGATTAATGATCAATGAATTC	SV40 PolyA reverse
AGCGGCGTGCACACCTTCC	CH1 forward
GCCTGAGTTCCACGACACC	CH1 reverse
TTCCCCCCAAAACCCAAGGAC	CH2 forward
CCACCACCACGCATGTGACC	CH2 reverse
AACCAGGTCAGCCTGACCTGCC	CH3 forward
TCTTGTAGTTGTTCTCCGGC	CH3 reverse

Table 2.3: Primers used for DNA sequencing of full-length IgG1 heavy and light chain at UCB.
Detailed are the primer sequences in addition to the location and direction of sequence read.

Segment	# of cycles	Temperature (^{o}C)	Time (seconds)
1	1	96	30
2	38	96	10
		50	5
		60	240

Table 2.4: Thermocycler reaction used for in-house sequencing at UCB.

2.3 Protein techniques

2.3.1 Antibody expression

To express mAb, CHO-SXE cells were transfected with plasmids containing the desired antibody genes by either electroporation or lipofection. For cell electroporation, CHO-SXE cells were centrifuged at 300 x g for 10 minutes. The resulting pellet was resuspended in 20 ml ice-cold sterile Earls Balanced Salt solution (Lonza), transferred to a sterile Falcon tube and centrifuged for a further 10 minutes at 300 g. Cells were resuspended again in ice-cold sterile Earls Balanced Salt solution to 2 x 10^8 cells/ml. 400 μg/ml of DNA (200 μg/ml each of heavy and light chain) was mixed with the cells for electroporation. 800 μl cell/DNA mixture was transferred to a GenePulser/MicroPulser Electroporation Cuvette (BioRad). The cuvettes were then placed in a Gene Pulser ShockPod Cuvette Chamber (BioRad) and subjected to the following electrical parameters: 1 ms at 9.6 amps, 10 ms at 0 amps, 40 ms at 3.2 amps. After electroporation cells were transferred to PROCHO5 media with 0.1% Pluronic, without L-Gln or HT (Lonza) enriched with 2 mM GlutaMAX and 1 in 500 Antibiotic-Antimycotic (Gibco), in Erlenmeyer flasks (Corning). Transfected cell cultures were incubated in a Kuhner Shaker incubator set at 37^{o}C, 5% CO_2, 140 RPM. After 24 hours, 2.8% total volume ActiCHO Feed A CD (GE Lifesciences), 0.4% total volume ActiCHO Feed B CD (GE Lifesciences), and 0.7 mM Sodium Butyrate (Sigma) were added, and the temperature dropped to 32^{o}C for a further 13 days culture. After 14 days of culture, antibody-containing supernatant was harvested by centrifugation for 30 minutes at 2,500 g, 4^{o}C. The supernatant was collected and filtered through a Vacuum filter 500 ml unit Stericup (0.2 μm pore size; MerckMillipore), and stored at 4^{o}C for up to 1 month prior to purification.

For CHO lipofection, CHO-SXE cells were transfected using the Expifectamine CHO Transfection Kit (ThermoFisher). On the day of transfection, CHO-SXE cells were resuspended to 1 x 10^6 viable cells/ml in ExpiCHO Expression Media (ThermoFisher). The high titre protocol was followed and 100 ml expression culture used to express mAb. For IgG expressions 40 μg of HC, 60 μg of LC were used for each 100 ml transfection. Plasmid DNA and 320 μl Expifectamine CHO reagent were diluted in 7.7 ml of OptiPro medium (ThermoFisher) incubated for 5 minutes at room temperature. The mixture was then slowly transferred to the cells and incubated at 37^{o}C, 8% CO_2. After 20 hours, 600 μl Expifectamine CHO Enhancer and 24 ml ExpiCHO Feed were added to the cells. CHO-SXE cells were then transferred to an incubator at 32^{o}C, 5% CO_2. After 10 days of culture antibody was harvested by centrifugation for 30 minutes at 2,500 g, 4^{o}C. The supernatant was collected and filtered through Vacuum filter 250 ml unit Stericup (0.2 μm pore size; MerckMillipore), and stored at 4^{o}C for up to 1 month prior to purification.

2.3.2 Estimation of protein yield

In order to estimate the protein yield from the expression of each mAb, 100 μl of expression supernatant was loaded onto a 1 ml HiTrap Protein G column (GE LifeSciences) attached to a High performance liquid chromatography (HPLC) Infinity System (Agilent). Bound antibody was washed with 20 mM $NaPO_4$, 50 mM NaCl pH 7.4, and eluted with 50 mM Glycine pH 2.7. The eluted protein absorbance at 280 nm was measured and area under the peak calculated. Protein yield was calculated using a standard curve calculated from the elution profile of an IgG standard at different concentrations.

2.3.3 Antibody purification

Expressed mAb were purified using liquid chromatography either using an ÄKTAXpress or ÄKTA-Pure system (GE LifeSciences). For ÄKTAXpress purifications, prior to sample loading a 5 ml HiTrap MabSelect Sure affinity column (GE LifeSciences), and either 26/60 Superdex 200 or 16/60 Superdex 200 gel filtration columns (GE LifeSciences) were decontaminated by incubation with 0.1 M NaOH for 1 hour. The purification system and columns were subsequently equilibrated with PBS pH 7.4. To reduce risk of endotoxin in the end product, sterile buffers were used. The process used for purification was a successive 2-column method whereby both columns were connected to the ÄKTAXpress in series. Expression supernatant was loaded onto the HiTrap MabSelect Sure column at a flow-rate of 5 ml/min and unbound protein washed with 5 column volumes of PBS pH 7.4. Bound protein was eluted with 0.1 M sodium citrate (VWR) pH 3.4 for 5 column volumes and effluent above the threshold of 100 mAU was collected. Up to 10 ml for the 16/60 column or 20 ml for the 26/60 column was stored in an internal loop. Collected protein was subsequently loaded onto the Superdex 200 column and eluted with PBS pH 7.4. Gel filtration columns were run at a flow-rate of 1.2 ml/min for the 16/60 column and 2.6 ml/min for the 26/60 column. Effluent was collected in 2 ml fractions.

For ÄKTAPure purifications, the system and columns were decontaminated and equilibrated as detailed above. Clarified supernatant was then loaded onto the HiTrap MabSelect Sure column at a flow-rate of 1.5 ml/min and unbound protein washed with 5 column volumes of PBS pH 7.4 at aflow-rate of 5 ml/min. Bound protein was eluted at 5 ml/min with 0.1 M sodium citrate (VWR) pH 3.4 in 1 ml fractions into 96-deep-well plates. The low pH buffer 1 ml fractions were neutralised with 1 ml PBS and 130 μl 2M Tris-HCL pH 8, pre-loaded into the plates. Alternatively, protein samples eluted from the HiTrap MabSelect Sure column were concentrated to 5 ml and loaded onto a 16/60 Superdex 200 column. Protein was eluted at 1.2 ml/min in PBS, into 96 deep-well

plates in 1 ml fractions. Fractions containing protein were analysed and based on a purity >95% when analysed by HPLC or 98% when analysed by UPLC.

2.3.4 Protein concentration analysis

The concentration of protein samples was determined with a NanoDrop spectrophotometer (ThermoFisher) by measuring the absorbance at 280 nm. The NanoDrop was blanked with appropriate buffer prior to 2 μl of sample being added to the nanodrop stage and recording the absorbance. Final concentration was calculated after adjusting for the extinction coefficient using the following equation:

$$Concentration = \frac{Absorbance\ (A280)}{Ext.\ Coeff \times Path\ Length}$$

2.3.5 Size exclusion-high performance liquid chromatography

To analyse the purity of purified mAb analytical size exclusion-high performance liquid chromatography (SE-HPLC) was used. Protein samples were diluted to 1 mg/ml and 50-200 μl transferred to HPLC vials. 20 μg was loaded onto a TSKgel G3000SWxl gel filtration column (Tosoh Bioscience) attached to a HPLC Infinity System (Aglient). Protein was eluted over 17 minutes with a 0.2 M phosphate buffer pH 7 (0.25 M Na_2HPO_4; Sigma, 0.23 M NaH_2PO_4, Sigma). The absorbance at 280 nm was analysed to give absorbance units (AU) to produce a chromatography trace. Peak integration was then to measure the area under each peak which could be used to caclulate the purity of the antibody peak.

2.3.6 Size exclusion-ultra performance liquid chromatography

Another approach used to assess the purity of purified mAb was analytical size exclusion-ultra performance liquid chromatography (SE-UPLC). Protein samples were diluted to 1 mg/ml and 40 μl transferred to UPLC vials. 2 μg was loaded onto a TSKgel G3000SWxl gel filtration column (Tosoh Bioscience) attached to a Aquity UPLC System (Waters). Protein was eluted over 10 minutes with a 0.2 M phosphate buffer pH 7 (0.25 M Na_2HPO_4; Sigma, 0.23 M NaH_2PO_4, Sigma). The absorbance at 280 nm was analysed to give absorbance units (AU) to produce a chromatography trace. Peak integration was then to measure the area under each peak which could be used to caclulate the purity of the antibody peak.

2.3.7 Size exclusion chromatography-multi angle light scattering

To determine the molecular weight of mAb oligomers and monomers size exclusion chromatography-multi angle light scattering (SEC-MALS) was used. 50 μg of protein was loaded onto a Superdex 200 Increase 10/30 GL column (GE LifeSciences) attached to an Infinity LC system (Agilent). The sample was run through the SEC column and successively through a Viscotek SEC-MALS 20 multi angle light scattering detector (Malvern) attached in series. MALS data was analysed by the OmniSEC software (Malvern).

2.3.8 Sodium dodecyl sulphate-polyacrylamide gel electrophoresis

To assess protein purity of antibody monomers, sodium dodecyl sulphate-polyacrylamide gel electrophoresis (SDS-PAGE) using NuPAGE 4-12% Bis-Tris gels (Invitrogen) was performed. 2 μg of protein was prepared for loading onto the gel with NuPAGE LDS sample buffer (4X), 10 nM N-ethylmaleimide (NEM) (ThermoFisher) (non-reduced) or 10% NuPAGE sample reducing agent (Invitrogen), and made up to 16 μl with water. Prepared samples were boiled at 95^{o}C and all 16 μl loaded into a well. The gel was run in NuPAGE MES running buffer (Invitrogen) at 200 V for 35 minutes. The samples were run alongside SeeBlue Pre-stained molecular weight (MW) marker (Invitrogen) to determine molecular weight.

To measure the purity of high molecular weight antibody oligomers SDS-PAGE using NuPAGE Novex 3-8% Tris-Acetate Protein Gels (Invitrogen) were used. Sample was prepared as described above but Novex Tris-Glycine SDS Sample Buffer (2X) used. The sample was run in NuPAGE Tris-Acetate SDS Running Buffer (Invitrogen) at 150 V for 70 minutes. The samples were run alongside NativeMark MW Marker (Invitrogen) or HiMark MW marker (Invitrogen).

Gels were stained with InstantBlue protein stain (Expedeon) for 30 minutes on a shaking platform at room temperature. Gels were transferred to water to destain until residual stain had been removed. The destained gel was imaged using an ImageQuant LAS 400 imaging system (GE LifeSciences).

2.3.9 Western blot

In order to assess the presence of hIgG in mouse serum a western blot was used. Firstly, serum protein concentration was determined colourimetrically using the Bradford assay. 250 μl of 1:5 diluted Bradford reagent was added to 5 μl of serum and the intensity of the sample was mea-

sured at 570 nm in an Epoch plate reader (Biotek). Protein concentration was calculated using a BSA standard curve. SDS-Page was run by loading 20 μg of protein in serum samples under reducing conditions as described in Section 2.3.8. Subsequently protein was transferred onto a nitrocellulose blotting membrane using the iBlot 2 Dry Blotting system (Invitrogen), following the manufacturers protocol. The blot was then washed in Tris-buffered saline (TBS) (10 nM Tris pH 7.6, 150 nM NaCl) with 0.05% Tween-20 (TBS-T). The membrane was blocked in 5% BSA TBS-T for 60 minutes. The HRP conjugated F(ab')$_2$ goat anti-human (Fc specific) (JacksonImmunoResearch) detection antibody was added at a dilution of 1:10,000 and incubated overnight at 4^{o}C on rollers. The following day the membrane was washed with 5% BSA TBS-T 3 times for 5 minutes. ECL Western Blot Substrate (Pierce) was used to detect HRP activity and imaged using the Chemi Doc-it Imaging system (UVP) and the VisionWorks LS software (UVP).

2.3.10 Endotoxin analysis

To measure endotoxin (LPS) levels in purified protein samples the endotoxin assay from Charles River was used. Protein samples were diluted 1 in 10 in endotoxin free dH$_2$O. 25 μl of diluted sample was pipetted into all four channels of the Endosafe-PTS cartridge using a sensitivity of either 0.1 EU/ml or 0.5 EU/ml (Charles River). The loaded cartridge was inserted into the Endosafe-PTS cartridge reader (Charles River) for the endotoxin assay. Endosafe-PTS uses limulus amebocyte lysate (LAL), an aqueous extract of blood cells from the horseshoe crab which reacts with LPS, a bacterial endotoxin from the membrane of gram-negative bacteria. Any endotoxin present in the sample will react with the LAL in the cartridge, resulting in a colour change that is detected and quantified by the reader. This is used to calculate the amount of endotoxin present per mg of protein. Samples of >2 EU/mg were taken forward for subsequent *in vitro* and *in vivo* assays.

2.3.11 Endotoxin removal

In order to remove endotoxin the Proteus NoEndo endotoxin removal kit was used (Generon). The size of the spin column was dependent on the volume of the sample. The Proteus NoEndo spin columns were first equilibrated with PBS by centrifugation at 500 x g for 3 minutes. The sample was filtered through a 1.2 μm syringe filter and loaded onto the spin column. Endotoxin was removed by centrifugation at 100 x g for 30 minutes. The eluted sample collected in the collection tube was then re-examined for endotoxin using the LAL assay (Charles River) to confirm endotoxin removal.

2.3.12 Protein concentration

Antibody samples were concentrated using Amicon Ultra 15 ml, 4 ml, or 0.5 ml centrifugal filters (EMD Millipore), with 10-30 kDa molecular weight cut-offs. Samples were centrifuged at 3,200 x g until the desired protein concentration was reached.

2.3.13 Protein deglycosylation

In order to cleave all N-linked glycans, 50 μg antibody was incubated with 5 units of PNGase F (Promega) diluted in PBS, at 37^{o}C for 18 hours. Conversely, to specifically cleave the heavy-chain antibody N-linked glycans 50 μg antibody was incubated with 1 μl of ENDO-S (NEB) diluted in PBS at 37^{o}C for 1 hour. Removal of glycans was analysed by SDS-PAGE and observed as a reduction in molecular weight of the IgG HC, and by mass spectrometry (Section 2.3.14)

2.3.14 Mass spectrometry glycan analysis

In order to analyse the glycan profile of antibody constructs mass spectrometry was used, performed by Ben Holmes at UCB. Antibody samples were reduced using DTT under guanadine denaturing conditions. Samples were then alkylated using 2-iodoactamide to cap free cysteines and enzymatically digested with trypsin. Digested peptides were injected onto a liquid chromatography-electrospray ionization-mass spectrometer (LC-ESI-MS). Peptides were chromatographically separated through reverse-phase before entering the mass spec where they were separated and detected by their mass to charge ratio (m/z). Peptides were identified by searching against a known sequence of possible fragments and glycans identified. The percentage of each glycan species was calculated using peak intensities.

2.3.15 Carboxypeptidase B cleavage capacity of C-terminal μtp fused to IgG1

To determine if a μtp peptide fused to the C-terminus of the IgG1 was still susceptible to endopeptidase cleavage relevant antibodies were treated with carboxypeptidase B (CPB). Full-length IgG1 μp C575S constructs were incubated with 1 unit of CPB, purified from human pancreas (Sigma), and incubated for 56 hours at room temperature. Cleavage of μtp C575S was analysed by SDS-PAGE and observed by a reduction in molecular weight of the IgG HC.

2.3.16 Negative stain electron microscopy

Electron microscopy grids coated with a continuous carbon film were glow-discharged. A single drop of mAb solution (10 μg/ml diluted in PBS and filtered at 22 μm), 2 drops of dH_2O and a drop of 2% uranyl acetate solution were applied separately on a microscope cover slip. The EM grid (dull side down) was then carefully applied to the drop of mAb for 60 seconds before being carefully dabbed dry on filter paper, followed by application to the first drop of water to wash and immediately removed and dabbed dry. The cover grid was then washed in the second drop of water for 30 seconds before being dabbed dry. After washing the grid was stained with the 2% uranyl acetate solution for 40 seconds. the majority of the stain was removed by careful dabbing on filter paper and left to dry and then stored for later use. Electron microscope images were acquired using a Hitachi HT7700 Transmission Electron Microscope at 80,000x magnification. Images were processed using Adobe Photoshop.

2.4 Flow cytometry

For extracellular flow cytometry of cell surface proteins or detection of human IgG at the cell surface, 1 x 10^5 cells or 100 μl of cell suspension was transferred to a FACS tube. Cells were incubated with fluorescently labelled antibodies for 30 minutes at 4^oC or 15 minutes at room temperature, in the dark. In-house antibodies were used at a final concentration of 10 μg/ml and commercial antibodies were used at their recommended concentrations. Labelled cells were washed twice with 1-3 ml FACS wash (PBS, 1% BSA (Europa Bioproducts), 0.01% sodium azide (Sigma) at 400 x g for 5 minutes. Samples were analysed using a FACS Calibre or Canto (Becton Dickinson) and data analysis performed using FCS Express software 3 (DE Novo software). A list of fluorescently labelled antibodies used for flow cytometry are detailed in Table 2.5.

2.5 *In vitro* experiments

2.5.1 Human serum collection

40-50 ml of fresh peripheral blood was collected from a healthy volunteer in glass tubes, in the absence of any anti-clotting agents, by a qualified physician or phlebotomist. Blood was allowed to clot at room temperature for 30-60 minutes with a wooden applicator present. Clotted blood

Antigen	Clone	Isotype	Fluorophore	Source	Ref
Anti-mouse					
CD19	1D3	Rat IgG2a	PE	In-house	[403]
CD45R (B220)	RA3-6B2	Rat IgG2a	APC	e-Bioscience	[404]
CD23	B3B4	Rat IgG2a	PE	e-Bioscience	[405]
CD8	53-6.7	Rat IgG2a	APC	e-bioscience	[406]
Anti-human					
CD45	HI30	Mouse IgG1	APC	BD Biosciences	[407]
CD19	HIB19	Mouse IgG1	PE	BD Biosciences	[408]
CD3	UCHT1	Mouse IgG1	FITC	BD Biosciences	[409]
IgG	SB2H2	Mouse IgG1	FITC	In-house	-
IgG	Polyclonal	Goat	PE	JacksonImmunoresearch	-
CD16	3G8	F(ab')$_2$ mIgG1	APC	In-house	[410]
CD32	AT10	F(ab')$_2$ mIgG1	FITC	In-house	[125]
CD64	10.1	F(ab')$_2$ mIgG1	FITC	In-house	[411]
C1q	Polyclonal	Rabbit	FITC	Abcam	[412]
Irrelevant mouse	WR17	F(ab')$_2$ mIgG2a	FITC	In-house	-
Miscellaneous					
SIINFEKL		MHC-II	PE	In-house	-

Table 2.5: Reagents used to stain cell surface antigens for extracellular flow cytometry.
– = No reference available.

was centrifuged at 900 g, 4^{o}C for 20 minutes to separate cells from serum. Serum was carefully pipetted off into 1-2 ml aliquots in glass vials and frozen at -80^{o}C for storage. Glassware was sterilised using 10 g/L Virkon (Day-Impex).

2.5.2 Complement-dependent cytotoxicity assay

In a 96-well flat bottomed plate, 5 x 10^4 target cells were opsonised with antibody at room temperature for 15 minutes at the desired antibody concentration. Human serum was thawed from -80^{o}C in a 37^{o}C water bath and serum added to each well to give a final concentration of 20%. The plate was incubated at 37^{o}C, 5% CO_2 for 30 minutes, and then transferred to ice. The samples were transferred to FACS tubes with 10 μg/ml PI and analysed on a FACS Calibre. Dead cells were observed as PI positive.

2.5.3 C1q cell binding

Ramos cells were centrifuged at 300 x g for 5 minutes and resuspended in cRPMI at 2 x 10^6 cells/ml. Resuspended Ramos cells were opsonised with antibody at the desired concentration in a 96 well flat-bottomed plate for 15 minutes at room temperature or 30 minutes at 4^{o}C. Human purified C1q was added to opsonised Ramos cells at 2 μg/ml and incubated at 37^{o}C for 10 minutes. The cell:antibody:C1q mixture was transferred to FACS tubes and washed twice by addition of 3 ml FACS wash and centrifugation at 300 x g for 5 minutes. After the final wash cells were

resuspended in 200 μl FACS wash and stained with FITC-Anti-C1q (Abcam) for 15 minutes at room temperature or 30 minutes at 4^{o}C. Stained cells were washed twice by addition of 3 ml FACS wash and centrifugation at 300 x g for 5 minutes. After the final wash cells were resuspended in 200 μl FACS wash and analysed using a FACS Calibur, gating on the viable cell population using scatter properties and C1q-bound cells were observed as FITC positive.

2.5.4 Enzyme-linked immunosorbant assay

The concentration of analyte binding in solution was assessed using multiple variants of enzyme-linked immunosorbant assays (ELISA). 96-well MaxiSorp plates (NUNC) were coated with the appropriate protein at the required concentration in coating buffer (0.015 M Na_2CO_3, 0.035 M $NaHCO_3$), and serially diluted across the plate to give final volumes of 100 μl per well. The plates were coated at 37^{o}C for 1 hour, followed by 4^{o}C overnight, or at 37^{o}C for 2 hours. Plates were then incubated with 150 μl 1% BSA PBS for 1 hour at room temperature or overnight at 4^{o}C. After washing the plates 3 times, 2 μg/ml in 100 μl protein or serum was added to each well, and incubated at 37^{o}C for 90 minutes or room temperature for 2 hours. After washing 3 more times with PBS 0.05% Tween20, the horseradish peroxidase (HRP) conjugated detection antibody was added at the desired dilution, diluted in 1% BSA PBS. 100 μl loaded into each well and incubated at 37^{o}C for 90 minutes or room temperature for 2 hours. Plates were washed 5 times in PBS, 0.05% tween20 and 100 μl of substrate was added (o-Phenylnediamine dyhydrochloride tablet (Sigma) dissolved in 24.7 ml citrate (stock: 0.02 M BDH succinate salt; Fisher-Scientific), 25.3 ml Na_2PO_4 (Stock: 0.2 M Na_2PO_4; Fisher-Scientific), 50 ml dH2O, and 40 μl hydrogen peroxide 30% (MerckMillipore)). After sufficient development (indicated by colour change), 50 μl H_2SO_4 (VWR) was added to each well. Absorbance was measured at 450 nm on an Epoch plate reader (Biotek). Analysis was performed using Microsoft Excel, linear regression was used to calculate the unknown values from the linear range of the plotted standard curve. The details of each specific ELISA are defined below.

C1q ELISA

To asses the binding affinity of C1q to generated mAb an ELISA was used. 96-well MaxiSorp plates (NUNC) were coated with the appropriate mAb was added at serial dilutions from 1 μg/ml. Following coating and blocking, 2 μg/ml of human purified C1q was added and incubated for 2 hours at room temperature. In the case of the C1q ELISA a primary rabbit anti-C1q antibody (Abcam) at a 1:2000 dilution was added next and incubated, followed by the HRP conjugated donkey anti-rabbit IgG (Sigma) detection antibody was added at a dilution of 1:20,000.

Human IgG1 ELISA

In order to determine the concentration of human IgG1 in the circulation of mice after administration the serum or plasma was analysed using a human IgG1 ELISA. 96-well MaxiSorp plates (NUNC) were coated with goat anti-human (gamma chain specific) (Sigma-Aldrich) at serial dilutions from 100 μg/ml. Following coating and blocking, serum or plasma samples were added to the plate at an initial dilution of 1:100 or matched controls at a starting concentration of 1 μg/ml and serially diluted across the plate, and incubated at 37^{o}C for 90 minutes. Following incubation the HRP conjugated F(ab')$_2$ goat anti-human (Fc specific) (JacksonImmunoresearch) detection antibody was added at a dilution of 1:10,000.

Anti-OVA antibody ELISA

To assess the concentration of anti-OVA antibody produced after administration of OVA and anti-CD40 mAb an ELISA was utilised. 96-well MaxiSorp plates (NUNC) were coated with OVA (Sigma) at 100 μg/ml. Following coating and blocking, serum or plasma samples were added to the plate at an initial dilution of 1:100 or a standard mouse anti-OVA antibody (KB4) at a starting concentration of 1 μg/ml and serially diluted across the plate, and incubated at 37^{o}C for 90 minutes. Following incubation the HRP conjugated rabbit anti-mouse IgG (Sigma) detection antibody was added at a dilution of 1:2000.

2.5.5 Solution C4 activation ELISA

Complement activation in human serum was determined by measuring C4d levels. Antibody constructs at 100 μg/ml were incubated in normal human serum and incubated at 37^{o}C for 1 hour. C4d levels in the stimulated serum were measured by ELISA (MicroVue EIA Kits, Quidel) according to the manufacturer's protocol and compared with serum alone.

2.5.6 Direct cell death assay

In a 96-well flat bottomed plate, 5 x 10^4 target cells were opsonised with antibody at the desired concentration. The plate was incubated at 37^{o}C, 5% CO_2 for 24 hours. Cell death was observed by incubating with 18 μg/ml PI and 10 μg/ml Annexin-V-FITC in binding buffer (100 mM Hepes pH 7.4, 1.4 M NaCl, 0.25 mM $CaCl_2$) for 15 minutes at room temperature. The plate was transferred to ice, and samples transferred to FACS tubes to be analysed on a FACS Calibre. Dead cells were observed as double positive for PI and annexin-V-FITC positive.

2.5.7 Antibody-dependent cellular cytotoxicity assay

Target cells were washed and resuspended to 1 x 10^7 cells/ml in PBS (Severn Biotech). The cell suspension was labelled with 10 μg/ml Calcein AM (Life Technologies) at 37^{o}C for 30 minutes with periodic inversion. Labelled cells were washed 3 times with PBS, 10% FCS. After washing the cells were resuspended to 1.6 x 10^6 cells/ml in cRPMI. 8 x 10^4 cells target cells were opsonised with antibody at the desired concentration in a 96-well round bottomed plate at 4^{o}C for 30 minutes. PBMCs isolated from leukocyte cones were resuspended to 4 x 10^7 cells/ml in cRPMI. 4 x 10^6 PBMC effector cells (50:1 effector cell to target ratio) or lysis buffer (4% Triton X-100) were added to the opsonised cells. The plate was briefly pulsed at 200 x g and incubated at 37^{o}C for 4 hours. The plate was centrifuged at 200 x g for 5 minutes and 80 μl of supernatant carefully transferred to a 96-well flat-bottomed white-walled plate. The plate was read using Varioskan Flash plate reader (Calcein AM: Excitation 495 nm, emission 515 nm). The data was then presented as a percentage of maximum lysis:

$$\%\, Max\ Lysis = \frac{Test\ RFU - Background\ RFU}{Max\ Lysis\ RFU - Background\ RFU} \times 100$$

Where RFU = relative fluorescence units, Test RFU = targets + antibody + effector, background RFU = targets + effector.

2.5.8 Human-monocyte-derived-macrophage derivation and polarisation

PBMCs isolated from leukocyte cones as above were resuspended to a density of 1 x 10^7 cells/ml in cRPMI (without FCS) supplemented with 1% human AB serum. 2 x 10^6 cells were plated into each well of a 6-well plate and incubated for 2 hours at 37^{o}C, 5% CO_2 to allow cells (predominately monocytes) to adhere. The majority of the adherent cells will be monocytes. The media was drawn off and cells washed one or two times with 1 ml PBS. 2 ml of cRPMI media was added to each well and incubated overnight at 37^{o}C, 5% CO_2. 200ng of human macrophage colony-stimulating factor (M-CSF) (Sigma) was added to each well to drive differentiation of monocytes into monocyte-derived-macrophages (MDM). Every 2 days media was replenished by drawing off 850 μl media and replacing with 1 ml of fresh cRPMI (with FCS) including 100ng of human M-CSF. 48 hours prior to use, macrophage polarisation reagent was added. For 'M0' unactivated macrophages media was replenished as normal. For 'M1' activated macrophages media was replenished and 200 ng PAM 3CSK4 (Invivogen) added to each well. For 'M2' activated macrophages media was replenished and 80 ng IL4 (Sigma) and 16 ng IL13 (Sigma) added to each well. 24 hours prior to use, media was replenished as before and 100 ng PAM 3CSK4 added to 'M1' wells or 40

ng IL4 and 8 ng IL13 added to 'M2' wells. MDM's were used 7 – 9 days after monocyte isolation.

2.5.9 Antibody-dependent cellular phagocytosis assay

MDM were generated as above. To isolate them for ADCP assay, media was replaced with 1 ml ice cold PBS and incubated for 10 minutes on ice. Cells were gently scraped off the bottom of the wells with a cell scraper and transferred to 20 ml sterilin tubes. Cells were washed once in PBS and resuspended to 1 x 10^6 cells/ml in cRPMI, and plated into 96 well flat-bottomed plates at 1 x 10^5 cells/well. MDMs were incubated at 37^{o}C, 5% CO_2 for at least two hours to allow cells to adhere to the bottom of the plate. Target cells were washed and resuspended in cRPMI (no FCS) to 2 x 10^7 cells/ml. Target cells were labelled with 5 μm CFSE (ThermoFisher) for 15 minutes at room temperature in the dark. An equal volume of FCS was added, incubated for one minute, and washed twice with cRPMI. Target cells were resuspended to a density of 2 x 10^6 cells/ml in cRPMI and opsonised with antibody at 4^{o}C for 30 minutes, in the dark. Cells were washed once in cRPMI and resuspended to 2.5 x 10^6 cells/ml. 2.5 x 10^5 target cells were added to the MDMs and co-cultured at 37^{o}C, 5% CO_2 for one hour. The final target cell to effector cell ratio was 5:1. MDMs were stained for CD16 (FcγRIII) using 3G8 F(ab')$_2$ as detailed in Table 2.4 and incubated for 15 minutes at room temperature in the dark. The media was then removed, 130 μl ice cold FACs wash added, and the plate incubated on ice for 10 minutes. MDMs were harvested and transferred to FACS tubes. Samples were analysed on a FACs Calibre with phagocytosed target cells observed as double positive for CD16 and CFSE. Phagocytosis was calculated as a phagocytic index, using WT mAb as a phagocytic index of 1, with the following equation:

$$Phagocytic\,index = \frac{\%\,double\,positive\,macrophages\,of\,test\,sample}{\%\,double\,positive\,macrophaes\,of\,WT\,sample}$$

2.5.10 Internalisation assay

In order to examine the internalisation potential of μtp mAb, 1 x 10^5 Ramos cells were opsonised with mAb at 10 μg/ml in a 96-well flat-bottomed plate. Opsonised cells were incubated for up to 24 hours at 37^{o}C. At various time-points over 24 hours (O, 2, 6, and 24 hours), cells were removed from the wells and washed twice by centrifugation at 300 x g for 5 minutes in 3 ml of FACs wash. Following washing, cells were stained with anti-human-Fc-FITC (SB2H2) and washed again. Bound antibody was measured by monitoring the fluorescent intensity of FITC positive cells by flow cytometry using a FACs Calibre. Antibody internalisation was calculated as a percentage decrease of MFI from time 0.

2.5.11 Surface plasmon resonance

Surface plasmon resonance (SPR) was carried out to assess the binding affinities of mAb using a Biacore T100 system (GE Healthcare). A Series S Sensor CM5 chip (GE healthcare) was primed and normalised with BIA Normalising solution (GE Healthcare). The normalised chip dextran was activated with a 1:1 mixture of EDC (0.4 M 1-ethyl-3-(3-dimethylaminopropyl)-carbodiimide) and NHS (0.1 M N-hydroxysuccinimide) (Amine Coupling kit; GE Healthcare) for 10 minutes. The mAb ligand was prepared by dilution to 25 μg/ml in Acetate pH5 (GE Healthcare) and approximately 2000 response units (RU) were immobilised to the CM5 sensor chip flow cells via amine chemistry. Ethanolamine (Amine Coupling kit; GE Healthcare) was used to deactivate excess dextran groups on the chip flow cells. Recombinantly produced FcγRs (I, IIA, IIB, IIIA, IIIB) (R&D Systems) were prepared in HBS-EP (GE Healthcare) at 0.16 - 100 nM (FcγRI) or 1.6 - 1000 nM (FcγRIIa, IIb, IIIa, IIIb). Kinetic analysis was performed according to the following parameters: sample on/off times 300 seconds at a flow rate of 30 μl/min with 30 seconds regeneration with 30 μl/min 10 mM Glycine pH2.0. FcγRs were flowed through all cells simultaneously. A blank reference cell was also used to be subtracted from antibody containing flow cells. Kinetic analysis and steady state affinity calculation were performed using Biacore Evaluation software (GE Healthcare).

2.5.12 FcγR cell binding analysis

To assess the binding efficiency of human IgG μtp constructs to cell surface expressed FcγR, CHO cells stably expressing human FcγR were used. The adherent cells were harvested with 2 mM EDTA, PBS for 10 minutes at room temperature before being washed at 300 x g for 5 minutes. Cells were resuspended to 1 x 10^6 cells/ml in cRPMI. To a FACs tube, 1 x 10^5 cells were added and incubated with 10 μg/ml mAb and incubated for 30 minutes at 4^{o}C. Cells were then washed twice by addition of 3 ml FACS wash and centrifugation at 300 x g for 5 minutes and resuspended in 200 μl FACS wash. Antibodies bound to FcγRs were detected by staining with anti-human-Fc-FITC (SB2H2) and expression of FcγRs was detected using 10.1 (FcγRIa), AT10 (FcγRII), and 3G8 (FcγRIII), MC106A5 was used as an isotype control. Bound antibody and FcγR expression were analysed on a FACs Calibre, gating on the viable cell population using scatter properties and bound IgG labels were observed as FITC positive.

2.5.13 FcRn binding analysis

To assess the binding affinity of μtp antibodies to FcRn, a FcRn affinity column (Roche Custom Biotech) with a 5 cm bed height was utilised, connected to a HPLC Infinity System (Aglient). Antibodies were buffer exchanged into 20 mM MES-HCL pH 5.5, 140 mM NaCl and adjusted to 1 mg/ml. The antibody was then loaded onto the column and washed with 5 column volumes of 80% 20 mM MES-HCL pH 5.5, 140 mM NaCl and 20% 20 mM Tris-HCL pH 8.8, 140 mM NaCl to give a pH 6.0 buffer. The bound antibody was eluted with a pH gradient over 30 column volumes by increasing the percentage of 20 mM Tris-HCL pH 8.8 up to 100%. FcRn affinity was calculated by peak integration and comparison of retention time, a larger retention time indicating that a higher pH is required for dissociation.

2.5.14 Stimulation of Jurkat NF-κB-GFP cell line expressing CD40

To assess the ability of mAb constructs to elicit CD40 agonism, a GFP reporter cell line was utilised. In this assay Jurkat NF-κB-GFP cells expressing CD40 were stimulated with various anti-CD40 mAb, activation of CD40 could be assessed by increased GFP expression. In a 96-well round-bottomed plate 1x10^5 Jurkat cells NF-κB-GFP reporter cells were stimulated with CD40 mAb at the desired concentrations. Stimulated cells were incubated for 6 hours at 37^{o}C before being washed by centrifugation at 300 x g for 5 mins and resuspended in 100 μl FACS wash. Stimulated cells were analysed for expression of GFP by flow cytometry using a FACS Canto, gating on the viable cell population using scatter properties and expression of GFP indicated CD40-mediated NK-κB activation.

2.6 Whole-blood B cell depletion assay

Fresh peripheral blood was collected from healthy volunteers in heparin coated tubes by a qualified physician or phlebotomist. The blood was incubated with mAb at the desired concentration at 37^{o}C, 5% CO_2 for 24 hours in 96-well U-bottomed plates. Blood was mixed by pipetting up and down before being stained for CD45, CD19, and CD3 using the antibodies reported in Table 2.5. 300 μl red blood cell lysis solution (BD Biosciences) was added and incubated for 10 minutes at room temperature, to lyse red blood cells and fix the cells for analysis. Samples were analysed using a FACS Canto II (BD Biosciences). B cell depletion was calculated by analysing the ratio of T cells to B cells after gating on the CD45 positive lymphocyte population, termed cytotoxicity index (CTI). Samples without antibody were set as 0% killing and used as a baseline.

$$CTI = 100 - \frac{100}{\%CD19^{+} \div \%CD3^{+}} \times \frac{\%CD19^{+}\ Control}{\%CD3^{+}\ Control}$$

2.7 IFN-γ measurement

Fresh peripheral human blood was stimulated with mAb as described above for the whole blood assay and human plasma was collected by centrifuging human blood at 500 x g for 10 minutes. Plasma was carefully pipetted off and storing at -80^{o}C. V-PLEX human IFN-γ plate (Mesoscale Discovery) was used to measure IFN-γ concentrations in stimulated blood samples. The IFN-γ cytokine analysis was completed according to manufacturer's instructions. The plate was read with a MESO SECTOR S 600 (Mesoscale Discovery) plate reader and the data analysed using the Discovery Workbench software (Mesoscale Discovery).

2.8 Mouse B cell assays

2.8.1 Mouse B cell isolation

Spleens were harvested from relevant transgenic mice after culling. The spleens were dissociated using a 70 μm cell strainer, resuspended in 20 ml of PBS and centrifuged at 300 x g for 5 minutes. The collected pellet was resuspended to 1 x 10^{8} cells/ml and B cells were isolated using StemCell EasySep kit according to manufacturer's instructions. Isolated cells were resuspended to 1 x 10^{6} cells/ml in R10 media.

2.8.2 B cell homotypic adhesion

Isolated B cells were stimulated with anti-CD40 mAb constructs at the desired concentration at 37^{o}C, 5% CO_2. After 48 hours the cells were observed for cell clustering using an Olympus CKX41 microscope at 4x objective.

2.8.3 B cell activation

Isolated B cells were stimulated with anti-CD40 mAb constructs at the desired concentrations at 37^{o}C, 5% CO_2. After the 48 hours the cells were stained for CD23 expression, using the antibodies reported in Table 2.5, for 15 minutes at room temperature or 30 minutes at 4^{o}C. Cells were then

washed twice by centrifugation at 300 x g for 5 minutes and resuspended in FACs wash. Cells were analysed by flow cytometry using a FACS Canto-II.

2.8.4 B cell proliferation

Isolated B cells were stimulated with anti-CD40 mAb constructs at the desired concentration at 37^{o}C, 5% CO_2. After 96 hours, 50 μl of R10 media supplemented with 1 μl of tritiated thymidine (^{3}H) was added to each well and incubated for 18 hours at 37^{o}C. After 18 hours the cells were harvested onto a unifilter plate using a vacuum pump. The plate was then washed with dH_2O 10 times by repeated dispensing into the wells, followed by drawing up through the unifilter plate with the vacuum pump. Plates were then dried at 37^{o}C for 2 hours. The bottom of the plate was sealed and 40 μl of scintillation fluid was added to each well, followed by sealing of the top of the plate. To measure the levels of ^{3}H incorporation the radiation was monitored using a scintillation β-counter (Topcount NXTHTS; Perkin Elmer) that quantifies the radioactivity of DNA recovered from the cells. The level of radioactivity emitted is used to determine the extent of cell division, which is displayed as count per minute (CPM).

2.9 *In vivo* experiments

2.9.1 Animals

Balb/C WT, Balb/C human (h)CD20Tg [413], C57 BL/6, C57 BL/6 hCD20Tg, C57 BL/6 hCD40Tg [414], C57 BL/6 FcγR1234KO/hCD40Tg, and OTI TCR Tg BL/6 [415] were bred and maintained in-house. hCD20Tg mice were a kind gift of Dr Mark Schlomchick; hCD40Tg mice were a kind gift of Prof Randolph Noelle; FcγR1234KO mice were a kind gift of Dr Sjef Verbeek; OTI TCR Tg mice were a kind gift of Dr. Matthias Merkenschlager. FcγR1234KO/hCD40Tg mice were produced by inter-breeding FcγR1234KO and hCD40Tg mice. Animals used throughout these experiments were maintained in conventional barrier facilities or individually ventilated cages (IVC). All procedures were carried out in accordance with Home Office regulations. All procedures carried out were approved by the local ethics committee and performed in accordance to the Animals (Scientific Procedures) Acts 1986 and Home Office licences PPL P4D9C89EA and PIL IF72AF73E.

2.9.2 B cell depletion (adoptive transfer)

To assess mAb-induced B cell depletion of low levels of hCD20Tg target cells an adoptive transfer model was used. Spleens were collected from human hCD20Tg BL/6 mice and BL/6 WT mice after culling. Each spleen was dissociated separately using a 70 μm cell strainer, washed with PBS and resuspended to 2 x 10^7 cells/ml. The hCD20Tg splenocytes were stained with 5 μM CFSE (ThermoFisher) and the WT splenocytes stained with 0.5 μM CFSE to give splenocytes labelled with high and low levels of CFSE, respectively. After addition of the CFSE, the splenocytes were incubated for 15 minutes at room temperature in the dark to label, and quenched with an equivalent volume of sterile FCS for one minute. Cells were washed twice and re-suspended to 2.5 x 10^6 cells/ml. The CFSE high and low splenocytes were mixed in a 1:1 ratio. The staining and ratio were checked by flow cytometry after staining for mouse B220 using the antibody detailed in Table 2.5. Once the 1:1 ratio of hCD20Tg and WT splenocytes was confirmed, the cell mixture was administered into mice by intravenous (i.v.) injection of 5 x 10^6 cells/mice. After 24 hours 25 μg of sterile filtered mAb was administered by intraperitoneal (i.p.) injection. A further 24 hours later, blood was collected from each mouse by tail tipping and the mice culled to collect spleens. Each spleen was dissociated using a cell strainer as above, washed, and re-suspended in 5 ml of PBS. Cell suspensions were stained for B220 and analysed by flow cytometry on a FACS Calibre. B cell depletion was calculated using the ratio of hCD20Tg (CFSE high) to BL/6 WT (CFSE low) cells remaining, compared to the ratio observed after administering an isotype control.

2.9.3 B cell depletion (systemic)

To asses mAb-induced B cell depletion in the systemic circulation, hCD20Tg mice were used. One day prior to the commencement of the experimental cohorts, hCD20Tg mice were pre-bled by tail tipping to obtain base-line B cell levels in the periphery. 20 μl of blood into 10 μl of heparin and stained for B220 x CD19, followed by flow cytometry (see below). On the day of the experiment (day 0) of sterile-filtered mAb was administered by i.v. injection. Subsequent tail-bleeds were performed on days 1, 2, and 7. On day 8, a further dose was administered by i.p. injection, and tail bleeds taken on days 9 and 13. On day 15, mice were sacrificed by terminal bleed and other samples collected for analysis. Mice were dissected to collect spleen and inguinal lymph nodes for flow cytometry analysis. Spleens and lymph nodes were prepared by dissociating cells using a cell strainer, washed, and re-suspended in 5 ml of PBS for spleen and 2 ml PBS for lymph nodes. Cell suspensions were stained for B220 and CD19 and analysed using FACS Calibre. B cell numbers were calculated as the percentage of B cells present in the lymphocyte gate.

2.9.4 Antibody clearance *in vivo*

To assess antibody clearance over time, 100 μg sterile filtered mAb was administered to BL/6 WT mice by i.v. injection, and serum samples obtained by tail tipping as before on days 1, 2, 7, 9, 13, and 15. Serum was isolated as detailed in Section 2.9.6 and antibody concentration in the serum was determined by ELISA as detailed in Section 2.5.4.

2.9.5 OTI adoptive transfer

To assess antigen-specific T cell response, OTI TCR Tg mice were used. OTI TCR Tg BL/6 mice were sacrificed and spleens harvested, dissociated using a 70 μm cell strainer, resuspended in 20 ml of PBS and centrifuged at 300 x g for 5 minutes. The pellet was resuspended and 100 μl stained with anti-mouse CD8-APC and SIINFEKL tetramer-PE for 15 minutes at room temperature. Cells were then washed and analysed by flow cytometry to calculate the percentage of $CD8^+SIINFEKL^+$ T cells. Using the cell count and percentage of $CD8^+SIINFEKL^+$ T cells the cells were diluted and $1x10^5$ $CD8^+SIINFEKL^+$ T cells were administered to hCD40Tg or hCD40Tg/FcgR1234 KO Bl/6 mice by i.v. injection. The following day 30 μg of mAb and 100 μg ovalbumin (Sigma) were co-administered by i.v. administration. Blood samples were taken by tail tipping on subsequent days to monitor $CD8^+SIINFEKL^+$ T cells in the periphery. Blood samples were stained with CD8-APC and SIINFEKL tetramer-PE for 15 minutes at room temperature and red blood cells lysed with 1 ml red blood cell lysis buffer (BioRad). After centrifuging at 300 x g twice cell suspensions were analysed by FACS Canto. $SIINFEKL^+$ T cells were calculated as the percentage of total CD8 T cells.

2.9.6 Mouse serum and plasma collection

Serum was collected by tail tipping by taking approximately 20 μl of blood into a 0.5 ml microfuge tube and allowing clotting to occur at 4^oC for 1 hour. Clotted blood was centrifuged at 5,000 x g for 10 minutes with serum collected and stored at -20^oC until required. Plasma was collected by taking approximately 20 μl of blood into 10 μl heparin and centrifuging at 2,500 x g for 10 minutes to remove cellular material. Plasma was collected and stored at -20^oC until required.

2.10 Statistics

Statistical analysis was performed using GraphPad Prism. Statistical significance between >2 groups was assessed by using a multiple comparison one way ANOVA test (*$p \leq 0.05$, **$p \leq 0.01$, ***$p \leq 0.001$,

****$p \leq 0.0001$).

Chapter 3

Generation of hexamerisation-enhanced Fc-engineered human IgG

3.1 Chapter introduction

Antibodies have become a crucial component of the effective treatments of many diseases, including cancer, due to the highly specific and efficacious nature of these molecules. Presently, the vast majority of clinically approved antibodies are unmodified hIgG1, hIgG2, or hIgG4 formats, and research has been focussed on expanding the repertoire of therapeutic antibodies by identifying new target specificities. Although this approach may yield further therapeutic antibodies, there is also an opportunity to expand upon this success by enhancing the reagents we already have through Fc-engineering [121, 344, 348, 349]. By modifying the properties of the Fc domain there is scope to fine-tune and augment the effector functions elicited by antibodies. Harnessing and manipulating the properties of different hIgG sub-classes through such an approach will allow characteristics to be selected that either enhance or restrict important effector functions [361, 416, 417].

Diebolder *et al* have recently reported that the complement cascade is favourably activated when Fc's cluster and form ordered hexamers at the cell surface, and that this probably can be enhanced with a single Fc mutation in the hIgG HC, such as E430G [197]. By altering the interaction between neighbouring Fc molecules and the components of the immune system more desirable therapeutic properties can be designed. In addition to the use of antibodies in their native format, there has been an increasing interest in the design of novel antibody derivatives as potential therapeutics, such as Fc-multimer formats that lack Fab domains [395, 396, 399, 401]. These formats have been reported to have enhanced binding to low-affinity Fc receptors and offer a unique approach

to potential treatment of autoimmune diseases .

As hIgG is the main antibody class exploited in antibody therapeutics, research has mainly focussed on manipulating the pre-existing hIgG backbone. However, Smith *et al* explored the potential for inter-class engineering using fragments from IgA and IgM [368]. The C-terminal tailpiece of IgA and IgM offers the potential to produce multimeric hIgG structures when fused to the C-terminus [368, 369]. Those authors showed that hIgG containing the tailpiece from IgM (μtp) spontaneously form oligomeric hIgG in solution through covalent disulphide bonds, exhibiting a MW similar to IgM. However, hIgG hexamers might not be ideal for use as therapeutics due to potentially short half-lives and toxicities. Therefore, with the use of genetic engineering a mutated form of the μtp was utilised, whereby the cysteine (C575) involved in intermolecular disulphide bonds was mutated to a serine residue (C575S). Fusion of μtp C575S to the C-terminus of human hIgG was predicted to be expressed in a monomeric format, but retain non-covalent μtp:μtp interactions. These interactions would only occur when hIgG1 μtp C575S molecules were in close proximity, such as at a target cell surface after antigen binding. Herein, such mAb will be termed hexamerisation enhanced hIgG or hIgG on-target hexamers. To test this hypothesis, full-length hIgG molecules were engineered with the WT μtp and a mutated μtp (C575S). These antibodies were expressed using a modified CHO-S cell line and characterised extensively.

3.2 Generation of hIgG constructs for expression

In order to generate Fc-engineered antibodies capable of hexamerisation, a series of constructs were first produced using molecular biology techniques. The hexameric hIgG construct was designed through the fusion of the 18 amino acid peptide found at the C-terminus of the IgM HC, denoted the μtp [67] (Figure 3.1,A), to the C-terminus of the hIgG HC (Figure 3.1,B). The μtp contains a cysteine at position 575 (Cys575 of full-length IgM: Eu numbering - www.imgt.org) which forms inter-tailpiece disulphide bonds. Accordingly, backbone vectors for the κ LC, hIgG WT HC, and hIgG μtp HC were ordered for synthesis from DNA 2.0 (now ATUM) with spacer DNA acting as a surrogate V-region, ultimately producing DNA vectors encoding the amino acid sequences of the κ LC (Appendix Figure A1), hIgG1 constructs (Appendix Figure A2), hIgG2 constructs (Appendix Figure A3), and hIgG4 constructs (Appendix Figure A4). The backbone heavy and light chains were engineered to contain HindIII/XhoI and HindIII/BsiWI restriction sites respectively. These restriction sites flank the V-region insert to allow for genetic manipulation. Heavy and light chain V-regions were also ordered for synthesis from DNA 2.0 in standard vectors engineered with the same restriction sites as their backbone hIgG HC and κ LC counterparts. To produce the μtp

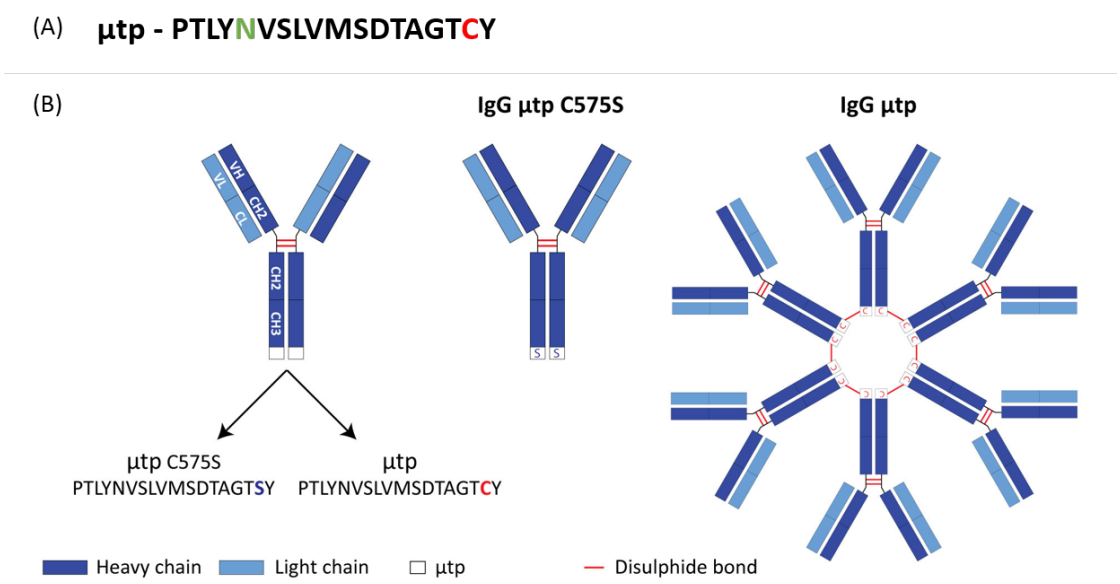

Figure 3.1: Design of μtp fusion mAb.
(A) Sequence of μtp, denoting the N-linked glycosylation site in green and cysteine residue in red (B) Schematic showing the structure of μtp fusion constructs: hIgG μtp hexamer and hIgG μtp C575S monomer.

monomer, the cysteine of the μtp (C575) was mutated to a serine residue (C575S) by site-directed mutagenesis (Figure 3.2,A). This residue change prevents the formation of the disulphide bonds between neighbouring μtp. The objective was to produce DNA plasmids encoding: WT hIgG, pre-formed hIgG hexamers (μtp), and hexamerisation enhanced hIgG monomers (μtp C575S).

Fab specificity was dictated depending on the V-region sub-cloned into each vector. Full-length antibody constructs with the desired V-regions, both heavy and light chain, were generated by digestion using the appropriate restriction enzymes, and DNA isolated through agarose gel extraction of the relevant DNA bands (Figure 3.2,B-C). The aim of the digestion and gel extraction was to linearize the backbone vectors and generate V-region fragments that could be ligated together to produce the desired full-length constructs. Backbone vectors and V-region inserts were successfully constructed for all human hIgG isotypes attempted (hIgG1, 2, and 4) and V-regions in the desired formats. For hIgG WT HC constructs the DNA was encoded as genomic DNA (gDNA) in the pMgh expression vector (Figure 3.2,D). For hIgG μtp the DNA was encoded as complementary DNA (cDNA) in the pNAFH expression vector (Figure 3.2,E). The same expression vector was used for mAb HC containing the μtp C575S modification, encoded as cDNA. The corresponding LC was produced on the κ LC backbone (Figure 3.2,F). Vectors were successfully constructed for all required HC and LC formats and antigen specificities, summarised in Table 3.1. Expression vectors also contained a kanamycin resistance gene, for efficient bacterial cloning, and the human cytomegalovirus intermediate/early (hCMVie) promoter.

For the current study V-regions targeting CD20 or CD40 were chosen. The V-regions from RTX

and BHH2 were selected to bind human CD20, whereas V regions from ChiLOB7/4 and 21.4.1 (CP) were selected to bind to human CD40. V-regions from Herceptin which binds to human Her2, and from a mAb called 1151, which recognises a *Clostridium difficile* (C. *diff*) exotoxin, where chosen as negative control that would lack antigen binding in the assays to be used.

The resulting DNA from the cloning above was amplified using a maxiprep or gigaprep to produce sufficient material for subsequent electroporation or lipofection required for antibody production. There was a requirement for 1 mg of HC and LC DNA for a 500 ml CHO cell expression culture using the electroporation technique or 40 μg HC and 60 μg LC for a 100 ml CHO expression culture using the lipofection technique. Prior to transfection the DNA was sequenced, covering the full HC and LC regions to verify the sequence was correct.

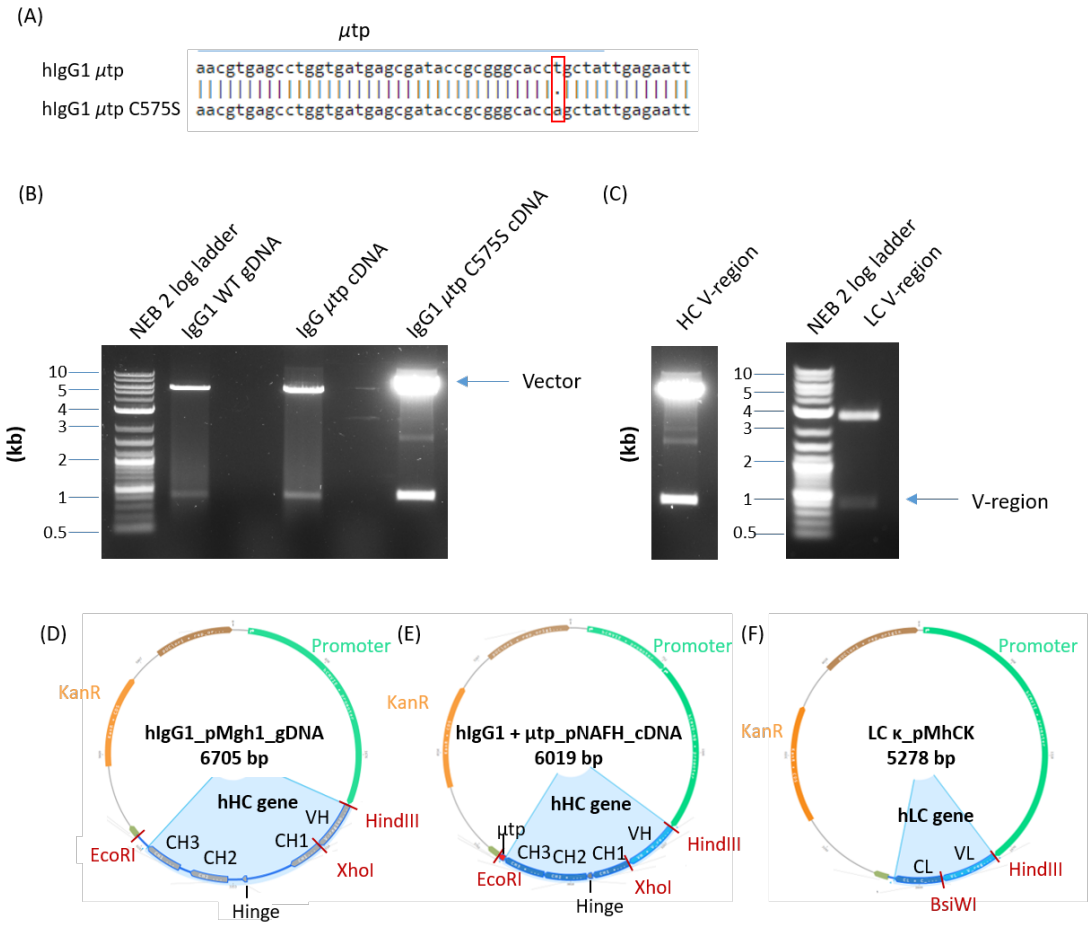

Figure 3.2: SDM and sub-cloning to produce DNA constructs.
The μtp DNA was mutated to replace the cysteine residue (C575) through SDM and DNA digested to produce linear backbone and V-region DNA for ligation (A) DNA sequences of μtp and mutated μtp C575S fused to the hIgG1 C-terminus (B/C) Representative agarose gels depicting the digestion of DNA vectors to produce (B) linear HC hIgG1 backbone formats and (C) linear HC V regions and LC V regions (of RTX). DNA vector backbones and V-region bands were extracted from the gel. Plasmid design incorporating (A) hIgG1 WT (B) hIgG1 μtp fusion mAb and (C) human κ light chain (hLC).

Gene	V-region	Vector	Mutation
IgG1 HC			
hIgG1 WT	RTX, BHH2, Herceptin, ChiLOB7/4, 1151	pMhIgG1*	-
hIgG1 μtp	RTX, BHH2, Herceptin, ChiLOB7/4, 1151	pNAFH hIgG1*	-
hIgG1 μtp CS	RTX, BHH2, Herceptin, ChiLOB7/4, 1151	pNAFH hIgG1*	C575S
IgG2 HC			
hIgG2 WT	RTX, ChiLOB7/4, 21.4.1	pMhg2*	-
hIgG2 μtp	RTX, ChiLOB7/4, 21.4.1	pMhg2*	-
hIgG2 μtp CS	RTX, ChiLOB7/4, 21.4.1	pMhg2*	C575S
IgG4 HC			
hIgG4 WT	RTX, ChiLOB7/4, 21.4.1	pMhg4*	-
hIgG4 μtp	RTX, ChiLOB7/4, 21.4.1	pNAFH hIgG4*	-
hIgG4 μtp CS	RTX, ChiLOB7/4, 21.4.1	pNAFH hIgG4*	C575S
LC			
κ	RTX, BHH2, Herceptin, ChiLOB7/4, 21.4.1, 1151	pMhCk*	-

Table 3.1: List of DNA backbone vectors generated by molecular biology techniques containing desired antibody constructs.
* Proprietary UCB Vectors; - = no mutation.

3.3 Analysis of the expression of antibody constructs

The corresponding heavy and light chain antibody DNA vectors were transiently transfected into CHO-SXE cells following electroporation or lipofection. CHO-SXE cells have been engineered to express X-box binding protein (XBP-1S), involved in protein secretion, and endoplasmic reticulum oxidoreductase (ERO1-Lα), involved in disulphide bond formation, for increased transient gene expression [402]. Cells were cultured to allow mAb expression and subsequently harvested with the yield estimated by loading 100 μl of culture supernatant onto a 1 ml HiTrap Protein G column. Protein G can bind hIgG antibodies from within the supernatant and so when captured and eluted the area under the curve can be integrated and used to estimated yield from a standard curve of hIgG1 eluted at pre-defined concentrations (Figure 3.3,A). The estimated yields obtained from each culture are detailed in Table 3.2. The results suggested that fusion of the μtp C575S or μtp to hIgG1 did not significantly impact expression, although there was a trend for higher yield with μtp C575S and a trend for lower yield with cells expressing μtp constructs (Figure 3.3,B). Results for hIgG2 constructs suggested there was lower expression of μtp C575S and μtp formats, but no significant differences observed (Figure 3.3,C). Finally, hIgG4 μtp C575S and μtp formats demonstrated a small decrease in protein expression compared to canonical hIgG4, but again no significant difference was seen (Figure 3.3,D). This analysis of protein expression has limitations, namely that not all expression runs between WT, μtp C575S, and μtp were assessed side-by-side, i.e. samples were not cultured simultaneously, and different batches and passages of CHO-SXE cells were used. Therefore, these analyses should only be taken as a general trend of expression and firm conclusions regarding the impact of μtp fusion on mAb expression efficiency should not be made from the data. Although overall there were no statistically significant changes in the

mAb expression when either the μtp C575S or μtp are fused to hIgG and expressed in CHO-SXE cells, this required confirmation following purification of the desired mAb products.

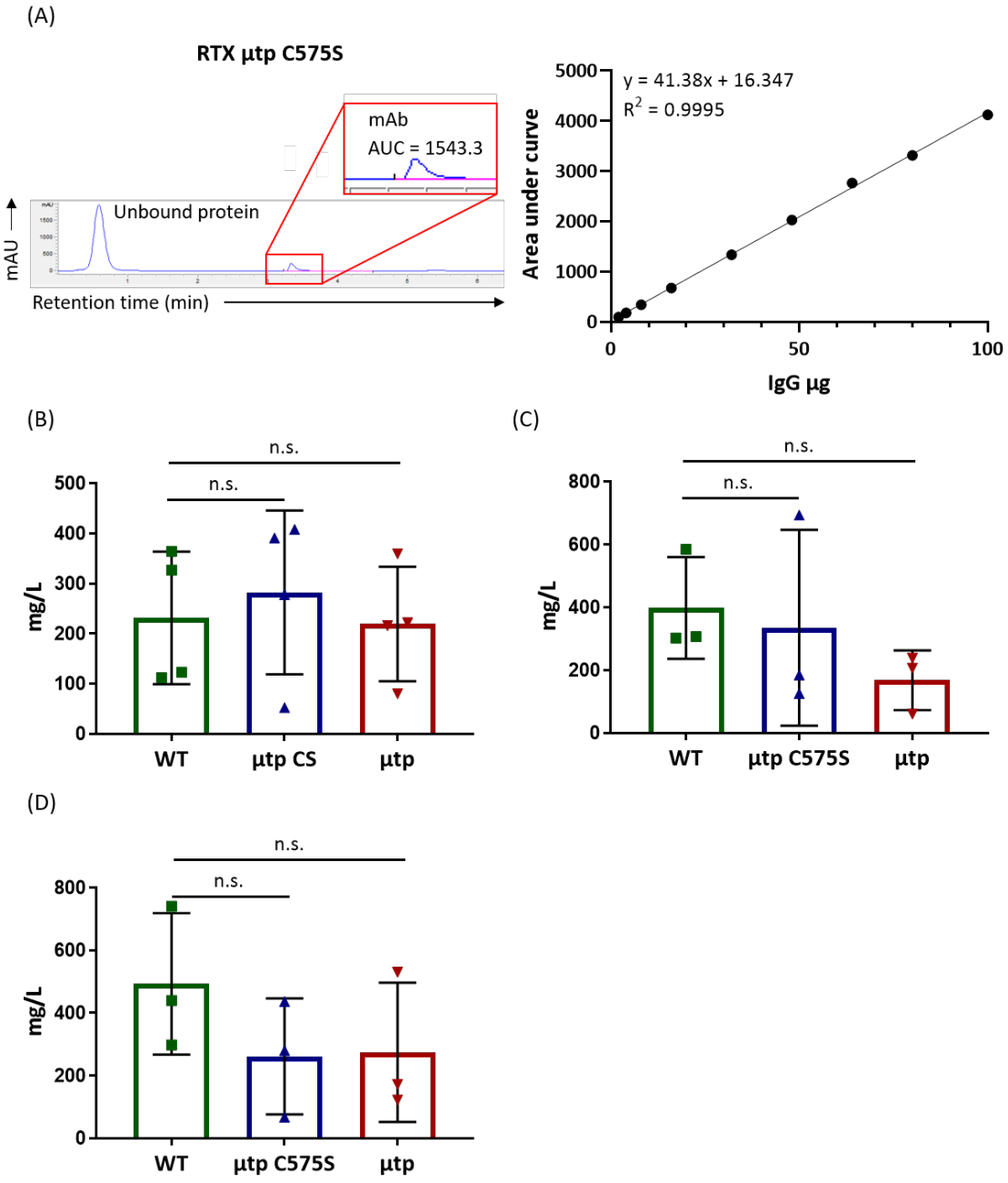

Figure 3.3: Expression yield analysis of μtp fusion constructs.
CHO cells were transfected with WT, μtp, or μtp C575S constructs and expression cultures were harvested 10 - 14 days later. The supernatant was assessed for concentrations using protein G affinity chromatography (A) After harvesting each expression culture, 100 μl of supernatant was loaded onto a protein G column and the area under the curve produced by the mAb effluent (left) was compared with a standard curve of known mAb eluted off the column (right). The μg of mAb calculated by the standard curve is then calculated as mg/L depending on expression volume. Each V-region in WT, μtp, and μtp C575S formats expressed as either (B) hIgG1 (N=4) (C) hIgG2 (N=3) or (D) hIgG4 (N=3) isotype was examined. Data plotted is mean and SEM of independent expressions performed at different times. Statistical significance calculated using one-way ANOVA analysis.

Isotype	Format	Mutations	Titre (mg/L)	Volume (L)	Yield (mg)
RTX					
hIgG1	WT	-	360	0.45	163.9
hIgG1	μtp	-	220	0.45	99.9
hIgG1	μtp	C575S	410	0.45	183.7
hIgG2	WT	-	307	0.1	30.7
hIgG2	μtp	-	206	0.1	20.6
hIgG2	μtp	C575S	694	0.1	69.4
hIgG4	WT	-	741	0.1	74.1
hIgG4	μtp	-	530	0.1	53.0
hIgG4	μtp	C575S	437	0.1	43.7
BHH2					
hIgG1	WT	-	326	0.45	147.1
hIgG1	μtp	-	60	0.45	30.8
hIgG1	μtp	C575S	380	0.45	172.3
Herceptin					
hIgG1	WT	-	123	0.45	55.5
hIgG1	μtp	-	220	0.45	97.2
hIgG1	μtp	C575S	280	0.45	125.1
ChiLOB7/4					
hIgG1	WT	-	98	0.1	9.8
hIgG1	μtp	-	250	0.1	25
hIgG1	μtp	C575S	395	0.1	39.5
hIgG2	WT	-	218	0.1	21.8
hIgG2	μtp	-	238	0.1	23.8
hIgG2	μtp	C575S	185	0.1	18.5
hIgG4	WT	-	298	0.1	29.8
hIgG4	μtp	-	172	0.1	17.2
hIgG4	μtp	C575S	280	0.1	28.0
21.4.1 (CP)					
hIgG2	WT	-	302	0.1	30.2
hIgG2	μtp	-	60	0.1	6.0
hIgG2	μtp	C575S	126	0.1	12.6
hIgG4	WT	-	163	0.1	16.3
hIgG4	μtp	-	132	0.1	13.2
hIgG4	μtp	C575S	68	0.1	6.8
1151					
hIgG1	WT	-	112	0.45	50.6
hIgG1	μtp	-	80	0.45	36.0
hIgG1	μtp	C575S	290	0.45	128.7

Table 3.2: Expressions yields from electroporation of hIgG construct plasmids into CHO-SXE cells.
Aproximate yield from representative expression cultures of various constructs calculated by the protein G assay described in Figure 3.3. The elution profile was compared to an hIgG standard to calculate titre (mg/L) of hIgG present in the culture supernatant. Titre was used to estimate the total yield from the expression volume (Yield (mg) = Titre (mg/L) x Volume (L)).

3.4 Antibody purification

Purification of WT hIgG constructs from the expression supernatant was performed by MabSelect SuRe affinity chromatography. MabSelect Sure resin is coupled with a protein A ligand that binds with selective hydrophobic interactions to the Fc regions between CH2 and CH3 domains of hIgG in the culture supernatant. Following hIgG binding, any unbound protein from the supernatant

is washed away and discarded. Low pH buffers weaken the hydrophobic interactions between protein A and hIgG, allowing the bound protein to be eluted which can be collected in fractions. The low pH buffer, however, can result in hIgG aggregation. In order to negate this possibility, the hIgG is eluted into a high pH buffer to neutralise the effluent [418]. The fractions were analysed by analytical SE-HPLC or SE-UPLC and pooled based on the presence of the species of interest, with priority for minimal contaminants or unwanted mAb species. Affinity chromatography was followed by either SEC (if purity was below 95% by HPLC or 98% by UPLC) or a buffer exchange step (if purity was above 95% by HPLC or 98% by UPLC) (Figure 3.4,A). The hIgG μtp C575S mAb were purified in the same way with an initial affinity chromatography step (MabSelect Sure), followed by either SEC or a buffer exchange step depending on purity of the pooled affinity column effluent (Figure 3.4,B). The chromatography traces for μtp C575S hIgG1 constructs indicated the resolution of a single protein peak after SEC or buffer exchange, comparable with the retention time of the WT hIgG1 counterpart (Figure 3.4,B). Purification of the hIgG μtp construct was first performed by MabSelect SuRe affinity chromatography before (Figure 3.4,C). However, due to the presence of a low molecular weight species (LMWS) and a high molecular weight species (HMWS) in the effluent after analysis of fractions by SE-HPLC or SE-UPLC (Figure 3.4,C), a second chromatography step (SEC) was required to produce pure HMWS (Figure 3.4,C). All final mAb products were buffer exchanged into PBS pH 7.4 for storage until required.

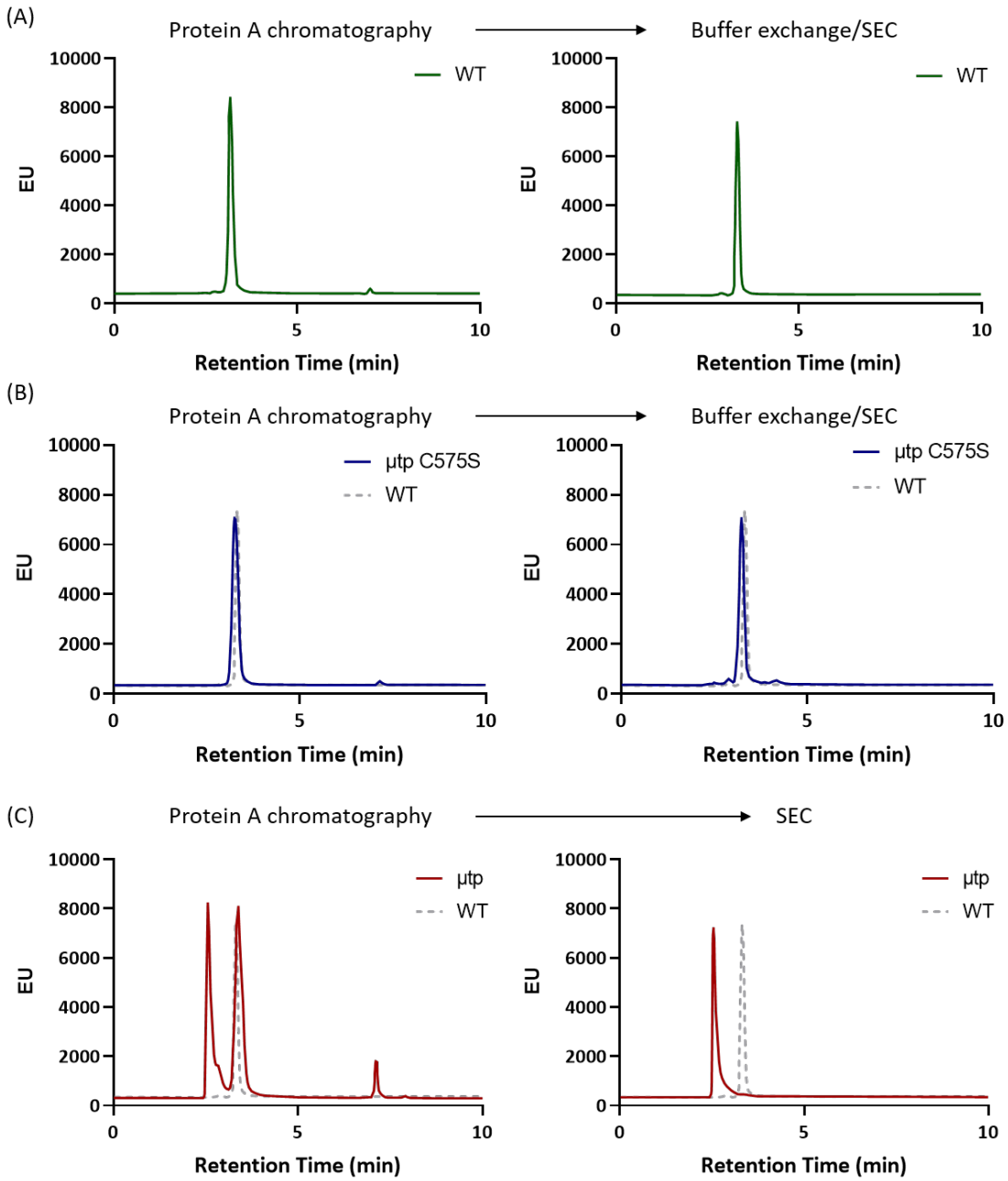

Figure 3.4: Elution profiles of the RTX hIgG μtp fusion constructs.
Recombinant hIgG μtp mAb were purified using either protein A chromatography followed by buffer exchange or by preparative SEC (depending on purity after protein A elution) (A) Schematic of purification protocol used for hIgG WT constructs (top), and representative SE-UPLC trace post protein A elution (bottom-left) and post buffer exchange or SEC elution (bottom-right) (B) Schematic of purification protocol used for hIgG μtp C575S constructs (top), and representative SE-UPLC trace post protein A elution (bottom-left) and trace post buffer exchange or SEC elution (bottom-right) overlaid with hIgG1 WT (dotted grey) (C) Schematic of purification protocol used for hIgG μtp constructs (top), and representative SE-UPLC trace post protein A elution (bottom-left) and trace post buffer exchange or SEC elution (bottom-right) overlaid with hIgG1 WT (dotted grey).

Analysis of the purification yield between hIgG constructs demonstrated a general trend that fusion of the μtp C575S to either hIgG1, 2, or 4 isotypes did not significantly impact purification yield (Figure 3.5, A-C). In fact, the final yield of hIgG1 and hIgG2 μtp C575S mAb observed a moderate increase compared to the WT hIgG. In contrast, the purification yield analysis of hIgG4 μtp C575S suggested there was a decrease in final yield. Purification analysis of the final yields of the target

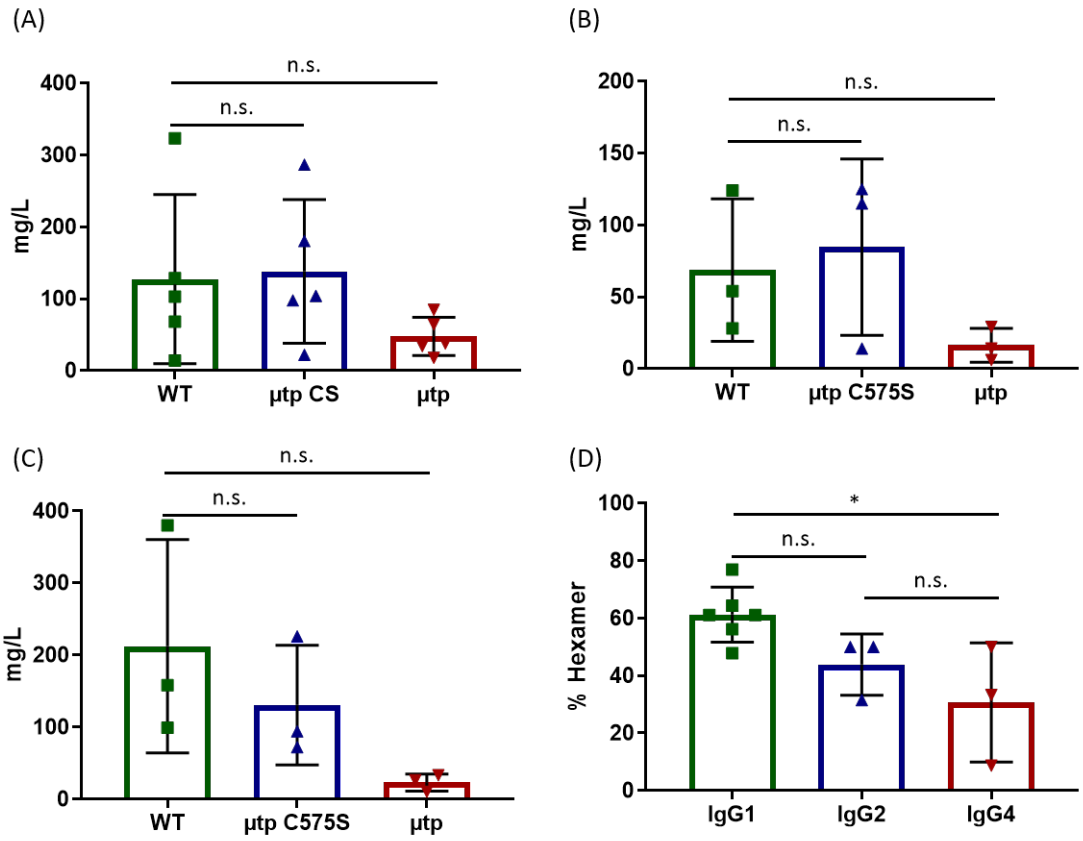

Figure 3.5: Final yield analysis of purified μtp fusion constructs.
Recombinant hIgG mAb were purified using either protein A chromatography followed by buffer exchange or by preparative SEC (depending on purity after protein A elution) and the yield of the final pure product (Final Yield (mg/L) = Yield (mg)/Volume (L)) calculated for (A) hIgG1 (N=5) (B) hIgG2 (N=3) and (C) hIgG4 (N=3) constructs after the buffer exchange or SEC step (D) Comparison of the % of hexamer purified from hIgG μtp expressions calculated as a % of hIgG μtp HMWS compared to hIgG μtp LMWS in the protein A effluent (N=3). Data plotted is mean and SEM of independent expressions. Statistical analysis was calculated using one-way ANOVA.

HMWS of hIgG1, 2, and 4 μtp indicated that there was a general trend that μtp fusion and purification of hIgG hexamers does impact the final yield, although again no statistically significant differences were observed (Figure 3.5,A-C).

The apparently lower yield observed with μtp hexamers could be accounted for by the presence of both a monomeric (LMWS) and hexameric (HMWS) species in the affinity chromatography effluent, where the HMWS comprised between 30-70% of the product. The percentage of HMWS present appeared to be influenced by the isotype and analysis revealed that the percentage of yield that was comprised of the HMWS demonstrated a hierarchy such that hIgG1>hIgG2>hIgG4 (Figure 3.5,D), being significant between hIgG1 and hIgG4 μtp constructs. However, as detailed above this current analysis has limitations as purifications were not performed side-by-side, with the same column, or using the same AKTA purification system. In addition, there were also added limitations with human judgement and consistency regarding to pooling of purification fractions.

3.5 Antibody quality control

Quality control of all purified mAb constructs was performed by assessing purity with analytical SE-HPLC or SE-ULPC, SDS-PAGE, measuring endotoxin levels, and analysing target antigen binding. Purification and pooling of the hIgG1 WT constructs achieved high levels of purity (>99%) when analysed by SEC (Figure 3.4,A). The SDS-PAGE results (Figure 3.6,A) using 4-12% Bis-Tris gels also revealed high levels of purity with no visible breakdown products in either both non-reduced or reduced conditions, and all protein bands were observed at the expected size when compared to the protein ladder. Treatment with PNGase F was used to remove the glycans present on the Fc of the antibodies. This allows for the size of the full-length hIgG and HC's of reduced samples to be analysed by SDS-PAGE without the interference of the potentially heterogeneous glycan profile associated with mAbs [419]. When deglycosylated the HC band reduced in size slightly, indicating the loss of the N-linked glycosylation at position N297. This suggests the expressed antibodies were post-translationally modified with glycan as expected, which is important for antibody structure and function of hIgG [100].

The hIgG1 μtp C575S constructs also had high purity (>99%) when analysed by SEC (Figure 3.4,B), and no visible impurities observed by SDS-PAGE analysis (Figure 3.6,A). In addition to glycosylation of the Fc at N297, the μtp also has its own N-linked glycosylated site which increased the potential heterogeneity. As with the WT, when the μtp C575S mAb was deglycosylated with PNGase there was decrease in size of the HC as expected from a removal of glycans. When treated with reducing agent, the glycosylated HC form was separated into multiple species on the gel, which was resolved to a single species under deglycosylating conditions. This is indicative of alternative glycan processing of one or more of the glycans, not observed with the WT HC the. Presumably, these differences can be attributed to post-translational modification of the μtp glycan.

The calculated purity of the pooled hIgG1 μtp HMWS by SEC (>93%) was lower when compared with the material produced from the monomeric constructs. This drop in purity was associated with the presence of small levels of hIgG μtp monomer after pooling (Figure 3.4,C). A 3-8% Tris-Acetate gel was used to access the purity of the HMWS by SDS-PAGE (Figure 3.6,B). The composition of this gel allows for the separation of a higher molecular weight range. The gel showed the HMWS in its non-reduced form is present in multiple species with protein bands corresponding to molecular weights of 150 kDa and upwards. There are visible bands on the gel that correspond with $\sim$150 (monomer), $\sim$300 (dimer), and $\sim$450 (trimer) kDa, and a further four major bands. These bands are larger than the MW marker used and therefore the molecular weight cannot be estimated accurately by this method, however, the increasing trend would suggest that they are multiples of 150 kDa and therefore further species of hIgG multimer. The LMWS fraction of the

hIgG1 μtp purification exhibited a molecular weight of 150 kDa, akin to the smallest species observed in the HMWS sample, indicating these species are antibody monomers. When reduced, the HMWS and LMWS samples displayed bands consistent with sizes for HC and LC, similar to monomeric hIgG1. Under reducing conditions, the glycosylated HMWS sample HC was observed as multiple species, which was consolidated to a single species when deglycosylated, similar to the hIgG1 μtp C575S HC. This indicated that the glycosylation of the μtp is still present and the sugar composition is in multiple forms, consistent with SDS-PAGE analyses of the μtp C575S.

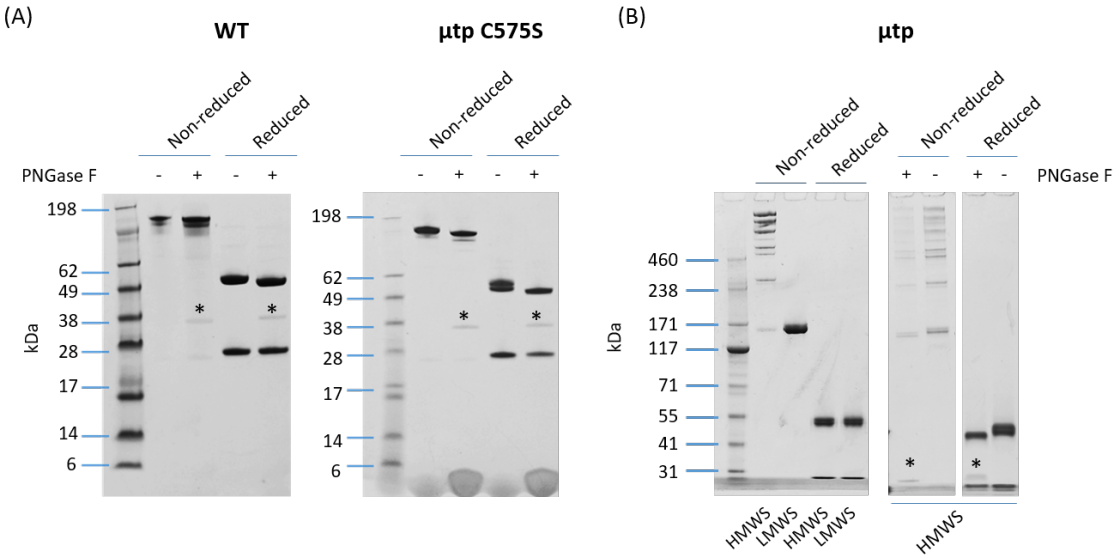

Figure 3.6: SDS-PAGE purity anlaysis of RTX hIgG μtp constructs.
Recombinant hIgG µtp mAb were assessed for purity using SDS-PAGE analysis. Non-reduced samples were prepared with the addition of 10 nM NEM to prevent disulphide shuffling and reduced samples were prepared by the addition of 10% NuPAGE sample reducing agent to the loading buffer. Deglycosylated samples were prepared by treatment with PNGase F. (A) Representative 4-12% Bis-Tris SDS-PAGE analysis following purification of hIgG1 WT (left) and hIgG1 μtp C575S (right). The molecular weight marker used was the SeeBlue Protein Standard (B) Representative 3-8% Tris-acetate SDS-PAGE used to assess protein purity. SDS-PAGE gels show hIgG µtp HMWS and LMWS (left) and deglycosylated HMWS (right). The molecular weight marker used was the HiMark Pre-stained Protein Standard. The band present between the heavy and light chain represents the PNGase F (36 kDa) indicated on gel images by *.

To determine if the spread of bands observed in the SDS-PAGE analysis of RTX hIgG1 μtp C575S was a result of glycan heterogeneity glycan analysis was conducted. The species of glycans present on the CH2 and μtp glycans of RTX hIgG1 μtp C575S was analysed separately using mass spectrometry techniques (performed at UCB). The results demonstrated that WT and μtp C575S hIgG1 CH2 glycan sites were highly glycosylated and had similar levels of complex-nonfucosylated glycans. The hIgG1 μtp C575S had a higher proportion of high mannose glycans and a lower proportion of complex-fucosylted glycans (Figure 3.7,A). The μtp C575S glycan site (N563) was $\sim$50% glycosylated, with the glycan present being predominantly complex-fucosylated. There was also small levels of complex-nonfucosylated, high mannose, and deamidated sites (Figure 3.7,B). These data again supported that the band heterogeneity related to differential glycosylation of the CH2 and μtp.

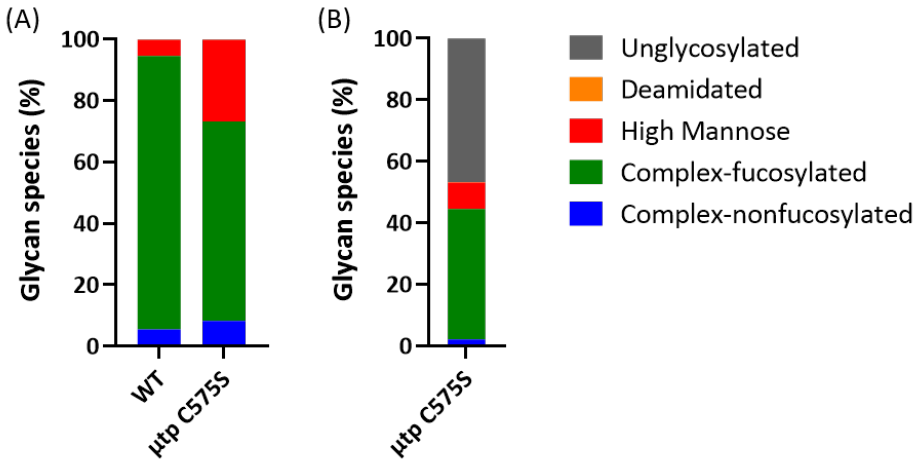

Figure 3.7: Glycan profiling of RTX hIgG1 μtp C575S.
Glycan analysis was undertaken using mass spectrometry techniques of RTX hIgG1 constructs. A range of glycoprofiles was detected which have been grouped into four main glycan species: demaidated, high mannose, complex-fucosylated, complex-nonfucosylated. The glycan species present were analysed on the (A) CH2 N297 and (B) μtp N563 glycan sites.

The potential contamination with the bacterial endotoxin, LPS, was calculated as endotoxin units (EU) per mg of protein (EU/mg). A threshold of 2 EU/mg was set as being low enough so as not to interfere with *in vitro* assays and to be safe for *in vivo* use. All expressed protein was calculated to be below this threshold using the LAL assay from Charles River. The yield of pure protein obtained, purity, and endotoxin levels of the purified antibodies was therefore deemed sufficient for subsequent characterisation, including *in vitro* and *in vivo* investigations. The summary of the produced material is detailed in Table 3.3.

Isotype	Format	Mutations	MW (kDa)*	Concentration (mg/ml)	Yield (mg)	Purity (%)	Eu/mg
RTX							
hIgG1	WT	-	145.00	5.2	145.6	100.0	0.35
hIgG1	μtp	-	893.04	2.4	22.8	96.7	0.71
hIgG1	μtp	C575S	148.80	4.3	129.0	99.7	<1.00
hIgG2	WT	-	144.59	0.7	2.8	98.7	0.14
hIgG2	μtp	-	890.52	0.2	0.6	97.3	0.79
hIgG2	μtp	C575S	148.39	0.3	1.4	95.8	0.33
hIgG4	WT	-	144.63	2.2	9.9	99.6	0.45
hIgG4	μtp	-	890.76	0.4	2.6	99.9	0.75
hIgG4	μtp	C575S	148.43	2.4	7.2	98.8	0.04
BHH2							
hIgG1	WT	-	146.34	0.9	30.6	100.0	<0.5
hIgG1	μtp	-	900.96	3.8	38.0	97.4	0.56
hIgG1	μtp	C575S	150.12	4.3	120.4	100.0	0.21
Herceptin							
hIgG1	WT	-	145.34	3.5	58.0	99.4	0.29
hIgG1	μtp	-	895.08	0.9	8.0	97.6	<1.87
hIgG1	μtp	C575S	149.14	0.5	10.0	100.0	<2.00
ChiLOB7/4							
hIgG1	WT	-	146.33	0.9	1.4	97.8	0.38
hIgG1	μtp	-	900.96	1.6	4.5	100.0	0.02
hIgG1	μtp	C575S	150.13	1.6	14.6	100.0	1.26
hIgG2	WT	-	145.92	1.8	5.4	97.7	2.10
hIgG2	μtp	-	898.50	1.0	2.9	100.0	0.03
hIgG2	μtp	C575S	149.75	3.0	12.5	100.0	0.24
hIgG4	WT	-	146.02	5.4	38.0	97.7	1.80
hIgG4	μtp	-	899.10	0.4	1.0	93.5	0.030
hIgG4	μtp	C575S	149.81	2.9	22.6	99.0	1.00
21.4.1 (CP)							
hIgG2	WT	-	154.84	1.5	12.1	100.0	2.50
hIgG2	μtp	-	953.66	0.5	1.4	96.1	0.04
hIgG2	μtp	C575S	158.94	3.4	11.5	93.4	0.04
hIgG4	WT	-	155.24	1.9	15.8	97.0	0.40
hIgG4	μtp	-	954.26	1.4	3.3	100.0	0.13
hIgG4	μtp	C575S	159.04	1.1	9.4	100.0	0.50
1151							
hIgG1	WT	-	144.62	2.9	46.4	99.7	0.02
hIgG1	μtp	-	890.76	1.7	17.0	95.6	0.87
hIgG1	μtp	C575S	148.46	2.9	81.2	99.8	0.46

Table 3.3: Results of purifications from expression supernatants of hIgG constructs.
The concentration of purified protein was calculated using a nanodrop. Final yield was calculated based on the volume of mAb. Purity was calculated by analytical SEC. Endotoxin levels (EU/mg) were calculated by LAL assay from Charles River. * = Expected MW

3.5.1 Antibody conformation and molecular weight analysis

Electron microscopy (EM) was used to visualise the antibody formats and determine their native valency. Antibodies bound to EM grids were stained with 2% uranyl acetate and observed at 80,000x magnification using EM. As expected, analysis of hIgG1 WT at 80,000x magnification demonstrated that this construct was in a monomeric form, displaying a trimeric protein structure, composed of 2 F(ab) domains and an Fc (Figure 3.8,A). Visualisation of an hIgG1 μtp molecule

revealed that this molecule was in a hexameric form in solution. At 80,000x magnification individual molecules could be observed as hIgG1 multimers. These were characterised by Fc:Fc interactions visible at the centre of the structure and F(ab) domains protruding from the Fc ring of the hIgG1 μtp hexamer (Figure 3.8,B).

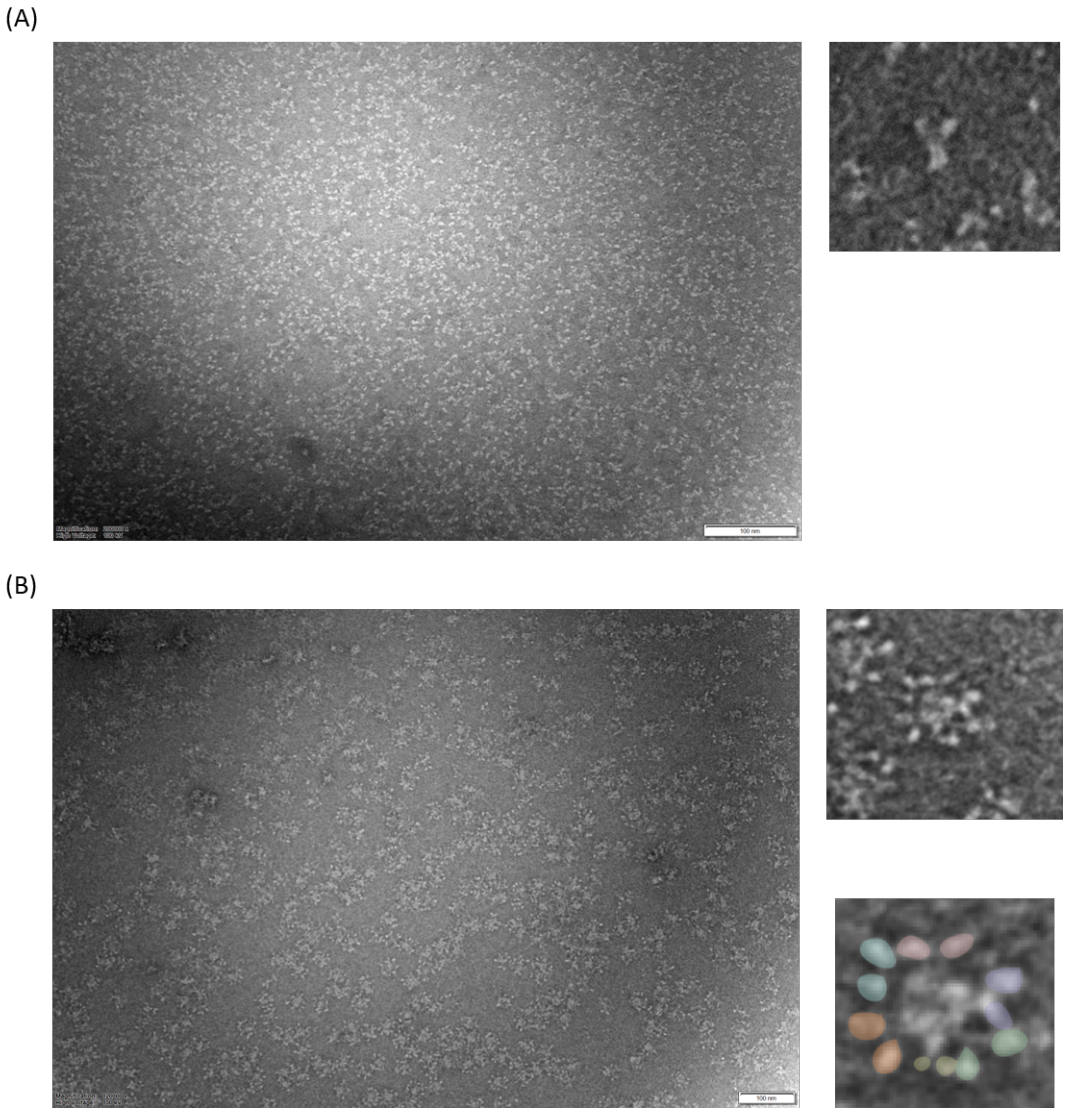

Figure 3.8: Negative-stain EM analysis of RTX hIgG1 μtp hexamer.
mAb were applied to glow discharged electron microscopy grids and stained with 2% uranyl acetate solution. Electron microscope images were acquired using a Hitachi HT7700 Transmission Electron Microscope at 80,000x magnification and images were processed using Adobe Photoshop (A) hIgG1 WT at 80,000x magnification (left) and a single hIgG1 monomer digitally magnified post image capture (right) (B) hIgG1 μtp at 80,00 x magnification (left), a single hIgG1 hexamer digitally magnified (middle), and digitally magnified hIgG1 hexamer with the F(ab) highlighted (right)

In order to determine the size of the mAb formats in solution, samples were analysed using analytical SEC-MALS. It had been predicted that the hIgG μtp C575S would be a monomeric hIgG species, whereas the hIgG μtp would produce stable hIgG hexamers. This was based on evidence that IgM forms hexamers through interactions via its tailpiece, in the absence of the J-chain, and previous characterisation of an hIgG1 Fc μtp construct which construct forms 600 kDa complexes (concordant with a hexameric-Fc format) when analysed by SEC-MALS (personal communication

– Dr. S. Peters). SEC-MALS can be used to determine the unknown molecular weight of a sample by measuring the scatter of light from a laser source from a sample of known concentration. The radius of the molecule in solution is related to the light scatter, which can be used to calculate MW based on calibration using the scatter of a sample of known MW, in this case BSA. The results of the SEC-MALS analysis calculated Herceptin hIgG1 WT to be 148.75 kDa and the monomeric Herceptin hIgG1 μtp C575S to be slightly larger at 153.94 kDa. The MW of the hIgG1 μtp C575S corresponds with a monomeric species and closely compares with the 149.14 kDa theoretical molecular weight calculated by the amino acid sequence, in the absence of glycosylation. The 5.19 kDa difference between the WT and μtp C575S likely represents the μtp peptide at the C-terminus, alongside its N-linked glycosylation. The molecular weight of the high molecular weight species obtained from the purification of the Herceptin hIgG1 μtp construct was calculated to be 870.67 kDa. This molecular weight corresponds with a hexameric hIgG1 species and compares with the 895.05 kDa that is predicted from the amino acid sequence.

3.5.2 Antigen binding efficiency

To confirm the generated proteins were capable of binding their cognate antigen targets, each expressed mAb was assessed using a cellular binding assay. The $CD20^{+}/CD40^{+}$ Ramos cell line was used for anti-CD20 and anti-CD40 constructs. Ramos cells were selected due to a lack of FcγRIIb expression to reduce the risk of FcγRIIb cross-linking and non-specific FcγRIIb binding by the Fc. Binding was assessed by indirect flow-cytometry using a secondary anti-human Fc-FITC labelled antibody (clone SB2H2) to detect mAb binding at the cell surface. Live Ramos cells were gated based on their forward and side scatter properties (Figure 3.9,A) and the binding determined by a positive FITC signal on this population. The results indicated that RTX hIgG1 with the addition of the μtp C575S or μtp (i.e. in the monomer or hexamer form, respectively) retained antigen binding through their V-region interactions (Figure 3.9,B). The antigen binding of the RTX hIgG1 μtp C575S monomeric construct was comparable to the WT construct when determined by flow cytometry. In the case of the hIgG1 μtp hexamer there was an observable drop in secondary antibody FITC signal compared with RTX hIgG1 WT.

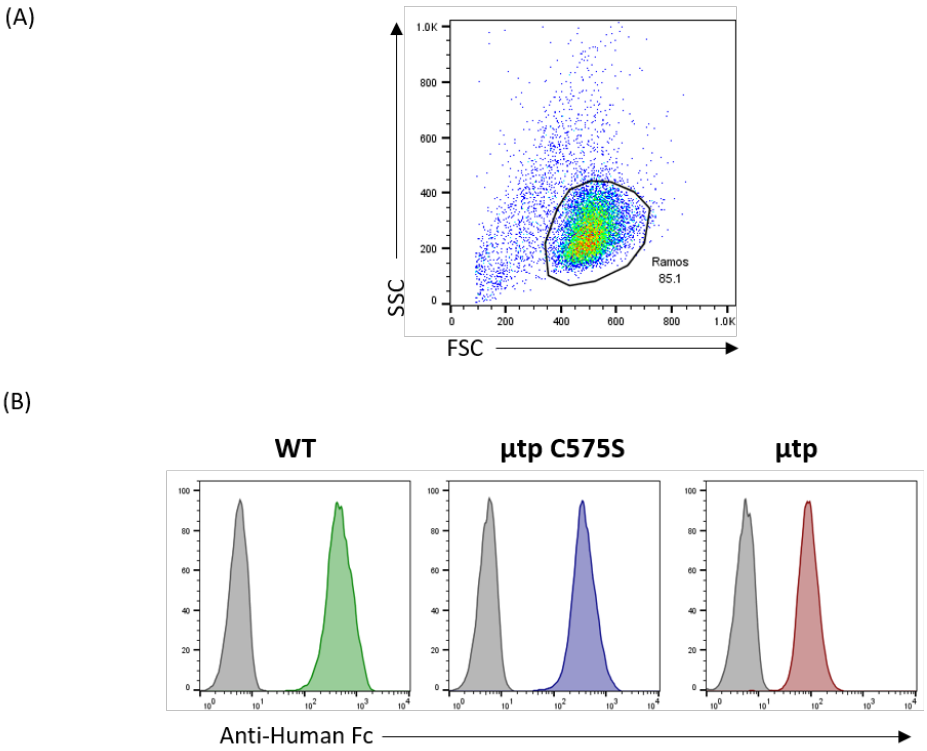

Figure 3.9: Binding profiles of RTX μp fusion mAb constructs to Ramos cells.
1 x 10^5 Ramos cells were opsonised with purified isotype control or anti-CD20 antibody constructs and stained with a secondary anti-human Fc (SB2H2) FITC labelled antibody to assess CD20 binding capacity (A) Gating strategy of Ramos cells after opsonisation with primary anti-CD20 antibody or isotype control and labelling with secondary anti-human Fc-FITC labelled antibody (B) Ramos cells opsonised with construct matched Herceptin isotype control (solid grey) or RTX antibodies (red line) were assessed and FITC signal displayed as a histogram.

The binding of hIgG2 and hIgG4 anti-CD20 and anti-CD40 mAb were also found not to be impacted by the addition of the μtp C575S, and demonstrated comparable binding to WT (Figure 3.10,A-B). There was a non-statistically significant decrease with hIgG4 μtp C575S compared to hIgG4 WT mAb (Figure 3.10,C). Conversely, μtp hexamers displayed decreased MFI in the context of hIgG1, 2, and 4 isotypes. hIgG1 μtp hexamers had a geomean MFI of 2.6-fold lower than hIgG1 WT (Figure 3.10,A), hIgG2 μtp hexamers displayed a 2.3-fold decrease compared to hIgG2 WT (Figure 3.10,B), and hIgG4 μtp hexamers had a 2.8-fold decrease in MFI compared to hIgG4 WT (Figure 3.10,C). Overall, these results demonstrated that hIgG μtp C575S on-target hexamers and μtp hexamers retain their ability to bind to their target antigen.

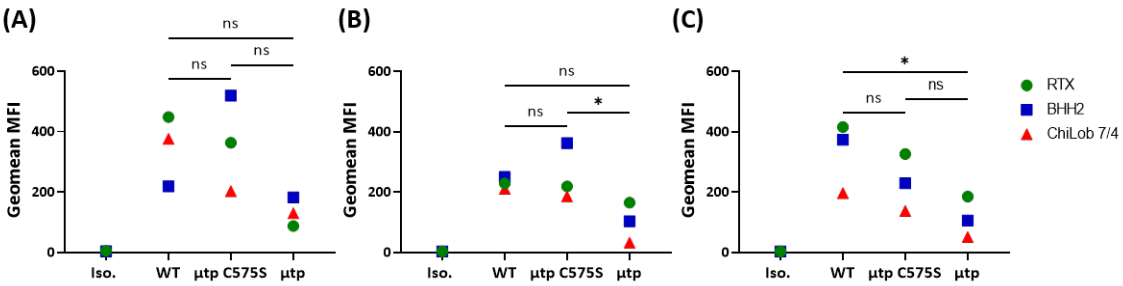

Figure 3.10: Geomean MFI of the CD20 and CD40 binding of RTX μp fusion mAb constructs to Ramos cells.
1 x 10^5 Ramos cells were opsonised with purified isotype control, anti-CD20, or anti-CD40 antibody constructs and stained with a secondary anti-human Fc (SB2H2) FITC labelled antibody to assess CD20 binding capacity. Antigen binding was analysed for (A) hIgG1 (N=3), (B) hIgG2 (N=3), and (C) hIgG4 (N=3). Data shown is mean and SD of independent experiments. Statistical analysis was calculated using one-way ANOVA.

3.6 Chapter discussion

Recently, specific clustering of hIgG Fcs at the target cell surface has been demonstrated to be important in the efficient activation of complement [197, 271, 375, 376]. Herein, stable multimeric hIgG molecules and monomeric hIgG with a predicted propensity to multimerise through addition of a mutated form of the μtp were designed (Figure 3.1). Fc-engineered recombinant antibodies were generated through molecular biology techniques in three different formats: hIgG WT, hIgG μtp, hIgG and μtp C575S; in the context of three human isotypes: 1, 2, 4; with six different V-regions: RTX, BHH2, Herceptin, ChiLOB 7/4, 21.4.1, and 1151; targeting four different molecular antigens: CD20, Her2, CD40, and *C. diff* toxoid B (Table 3.1). Expression of these constructs was performed in CHO-SXE cells, which were subsequently purified using standard chromatography techniques. It is important to note that the hIgG4 constructs produced were cloned into UCB hIgG4 vectors which has S228P incorporated. The S228P mutation is used to improve stability for hIgG4 antibodies by abolishing the heterogeneity of inter-HC disulphide bonds in the hinge region. Such a mutation prevents hIgG4 F(ab)-arm exchange [420]. The resulting mAbs underwent careful assessment and quality control to determine yield, aggregation, purity, endotoxin contamination, MW, valency and antigen binding.

In this study a CHO cell line, CHO-SXE, was employed as an expression platform. As described previously, CHO cells are one of the most common and preferred host cells in which mAbs are industrially produced [242]. CHO-SXE cells have been specifically engineered at UCB to produce higher titres of antibodies, without impacting product quality [402]. In the current study, the estimated expression titre differed greatly between each antibody format and V-region expressed (Table 3.2). Titre may be impacted by cell viability, cell concentration, DNA concentration, DNA quality, and the voltage passed across cells during electroporation. The antibodies in this study were expressed at different times, with DNA transfected into cells from different passages and/or

levels of cell cycle synchronicity, therefore a direct comparison between expression titres cannot be accurately made. For a more robust comparison, expression runs could be repeated and constructs expressed side-by-side using the same batch of CHO-SXE cells. These caveats notwithstanding, analysis revealed higher titres for WT and μtp C575S constructs over μtp constructs, a trend which was apparent across hIgG1 and hIgG2 isotypes, although no statistical significance was observed. hIgG4 isotype constructs demonstrated a decrease in expression titre for both μtp C575S and μtp constructs. This observation was potentially a result of the fusion of the μtp peptide making the construct express less efficiently or the mAb less stable, and more prone to aggregation. Nonetheless, all constructs were produced in sufficient amounts to facilitate initial characterisation, as well as *in vitro*, and *in vivo* experimentation. As the expression of the monomeric hIgG1 μtp C575S was comparable to the hIgG1 WT across multiple V-regions and the purification process was unaltered, it can be assumed that the production could be scaled-up efficiently for industrial manufacturing.

Purification of all constructs was achieved through a 1 or 2 column method; MabSelect SuRe affinity chromatography followed by buffer exchange or Superdex 200 gel filtration chromatography (Figure 3.4), depending on purity of the effluent from the affinity chromatography column. The yield after purification varied between V-regions, isotypes, and formats (Figure 3.3). There was some loss of material when pooling the purified fraction from WT and μtp C575S formats due to the requirement for strict MW exclusions. Monomers were strictly pooled to achieve the high levels of purity required, excluding all dimer or high MW aggregate impurities. As a result all constructs had a purity >95%. This was in contrast to purification of hIgG1 μtp hexamers where there was a general observation that the final yield was consistently lower for this format. The low recovery observed from the hIgG1 μtp oligomer can be attributed to loss of material in the monomeric fraction. Due to the requirement for a highly pure oligomeric HMWS some fractions were excluded from pooling due to contamination with the LMWS fractions as purified by the Superdex 200. The Superdex 200 column has the capacity to resolve MW proteins in the range of 10 kDa to 500 kDa. Although this column has an ideal range and resolution to purify hIgG monomers from dimers and aggregate, it does not have the required range to effectively separate the high quantity of LMWS. Furthermore, due to the sometimes large proportion of monomer in the purifications (up to 70%) there was some overlap in the resolution of the two species. In order to obtain the required yield of the HMWS a slight reduction in purity was accepted from all μtp constructs and as a result μtp constructs had a purity of >93% (Table 3.3). It is important to note that in this context impurity purely relates to the monomeric LMWS of the desired mAb, as opposed to any undersired protein breakdown species or other contaminants.

Analysis of the final yield revealed that hIgG4 μtp hexamers exhibited the lowest percentage of

hexamer compared with monomer in the effluent. This is followed by hIgG2, with hIgG1 μtp having the highest percentage of HMWS (presumed covalent hexamer). There are multiple differences in the amino acid sequence of the constant domains between hIgG1, 2 and 4 (Figure 1.6). There are 27 differences between hIgG1 and hIgG2, 27 differences between hIgG1 and hIgG4, and 26 differences between hIgG2 and hIgG4. These amino acid differences are known to correspond with the Fc-dependent mechanisms of action of these isotypes such as binding to C1q and FcγR. One example is P331 in the hIgG1 amino acid sequence. Mutation of proline to serine at position 331 (P331S) decreases affinity for FcγRIIa, IIb, and IIIA [344] and C1q [421]. Serine is the native amino acid residue at position 331 in the hIgG4 amino acid sequence, an isotype known to display weak FcγR binding affinity [84] and C1q affinity [360, 422, 423]. Vice versa, the S331P mutation in hIgG4 increases its CDC activity [360]. It could therefore be speculated that the inherent differences in the core constant domain or hinge regions that make each isotype different could contribute to differences in the Fc:Fc attractions and repulsions that contribute to the formation of stable hIgG hexamers when the μtp is present, in the same way amino acid differences impact FcγR and C1q affinity.

The purity assessment by SDS-PAGE and analytical SEC indicated a high level of purity for all constructs (Figures 3.4, 3.6). A single, pure peak was observed on the SEC traces for all monomeric constructs, and a small contamination observed with hexameric products corresponded with the presence of hIgG1 μtp monomers. SDS-PAGE of the hIgG1 μtp C575S protein indicated the presence of two distinct species of heavy chain. There was also a broader peak present in the SE-UPLC trace, compared to hIgG1 WT, which would agree with the presence of two similarly-sized species. These bands were consolidated when deglycosylated, indicating that the multiple species corresponded to multiple glycoforms of the μtp N-linked glycan. This was confirmed with glycan analysis that showed $\sim$50% of μtp C575S peptides were unglycosylated, which would have a smaller MW. Therefore, the bands observed on the SDS-PAGE gel most likely correspond to hIgG1 μtp C575S molecules that are either glycosylated or unglycosylated.

In order to overcome the limitations of the 4-12% Bis-Tris gel routinely used for monomeric hIgG1 analysis, several gel compositions were evaluated to analyse the multimeric hIgG1 in its native and denatured form. The optimal gel was determined to be a 3-8% Tris-Acetate gel under denaturing conditions. The laddering visible on the gel under non-reducing conditions suggests that not all of the hIgG1 multimers present in solution were covalently bound by a disulphide bond at the μtp cysteine. When the hIgG1 μtp oligomer was reduced there were two species of heavy chain, similar to the μtp monomer. The two heavy chain species of hIgG1 μtp were consolidated when the antibody was deglycosylated and analysed by reducing SDS-PAGE. This suggests that the two species represent differing glycoforms of the μtp glycan, as only one species is present within

hIgG1 WT monomers. As with the hIgG1 μtp C575S N563 glycan, it is likely that the μtp glycan is also alternatively glycosylated and the two species observed are either glycosylated or unglycosylated μtp. Glycan analysis will need to be undertaken on hIgG1 μtp hexamers to confirm this. In the context of the hIgG1 μtp hexamer it could be presumed that prior to post-translational modification, the oligomeric state of the μtp constructs would cause alternative glycan processing of the μtp N-linked glycan, as with polymeric IgM [424]. The resulting differences in glycosylation may prevent the formation of covalent disulphide bonds between neighbouring C575 residues, due to a physical constraint, either by size, charge, or hydrophobicity. This would lead to the multiple species observed on the SDS-PAGE gel stemming from a single species in solution.

Antibodies are glycoproteins and generally have complex N-linked oligosacharrides (Figure 3.11,A). These are generated from Glu3Man9GlcNac2 precursors (Figure 3.11,B) that are processed along the exocytic pathway [99]. However, in some instances glycans are not processed and remain in the high-mannose state of Man6-9GlcNac2 (Figure 3.11,D) [425]. Folding, assembly, and olgomerisation can affect maturation of glycans passing through the Golgi apparatus. IgM polymerisation is thought to take place in the ER [426, 427] prior to Golgi processing. Polymeric and monomeric IgM have been observed to contain differentially processed glycans, mainly at the μtp Asn563 N-linked glycosylation site. In its pentameric or hexameric form, the μtp Asn563 is composed of a high mannose glycan structure, while mature complex glycans are found at the other four glycosylation sites [428]. In its monomeric form it is thought the N-linked sugar at Asn563 undergoes Golgi mediated processing to form complex carbohydrates. When oligomerised the Asn563 N-linked glycan is buried within the hIgG1 complexes making it inaccessible to processing in the Golgi [425]. In addition, the Asn563 glycan moiety is important for the formation of polymers of the correct size. Mutation of this residue to alanine results in large aggregates when analysed by SDS-PAGE and sucrose gradients [429].

It has previously been reported that a range of glycan profiles are observed occupying the Asn563 glycosylation site in recombinantly expressed IgM pentamers and hexamers. These include oligomannose (Figure 3.11,D), hybrid (Figure 3.11,E), and complex glycans (including sialylated glycans) (Figure 3.11,C) [424]. However, other reports have indicated that Asn563 exclusively possesses oligomannose glycans, Man6GlcNac2, Man7GlcNac2, or Man8GlcNac2 [65, 66, 430]. In addition, site-occupancy analysis of Asn563 glycosylation in recombinant IgM hexamers indicated that only 60% of N-linked glycosylation sites are occupied on the μtp [424], whereas human serum IgM is considered to have full occupancy at Asn563, exclusively filled with oligomannose structures [431]. The N-glycosylation site occupancy of recombinant glycoproteins expressed in CHO cells has been shown to be altered by conditions in which cells were cultured, such as temperature, and the presence of ions, such as manganese [432]. Alternative glycan processing between com-

plex and oligomannose N-linked glycosylation of the μtp would result in a difference in molecular weights between 0.4 – 1.2 kDa depending on the processing status (Figure (3.11). Therefore, the differences in glycan composition or occupancy observed in this study could be caused by glycan processing and culture conditions. This may explain the MW disparity between the HC bands observed on SDS-PAGE with constructs containing the μtp.

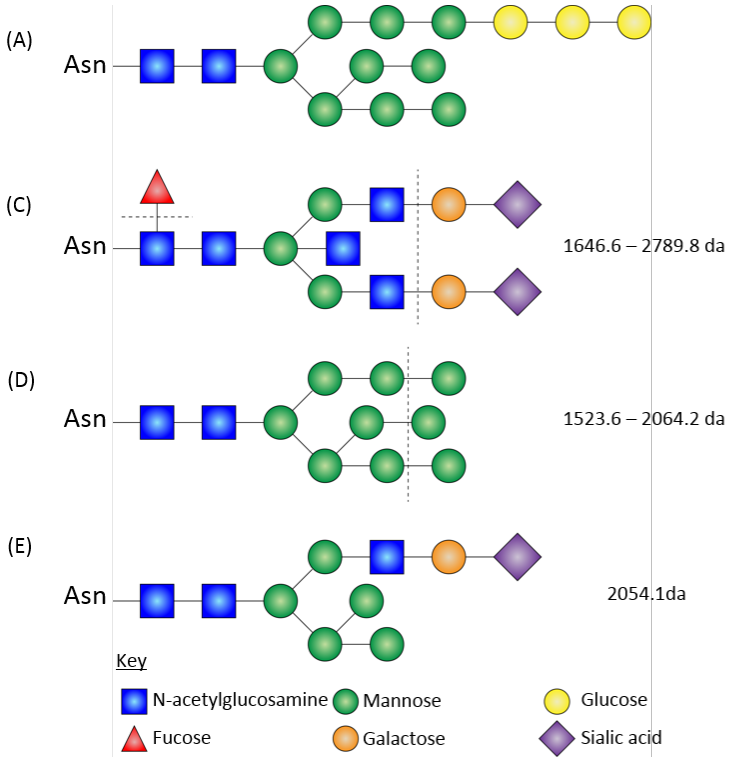

(B)

Sugar	Mw (da)
N-acetylglucosamine	221.2
Mannose	180.2
Glucose	180.2
Fucose	164.2
Galactose	180.2
Sialic acid	309.3

Figure 3.11: Possible N-linked glycosylation structures of hIgG μtp fusion or IgM at Asn563.
IgM Asn573 glycosylation is processed from glycan precursors (A) into a complex N-linked glycan (C), an oligomannose N-linked glycan (D) or a hybrid glycan (E). The dashed lines indicate potential different states of complex and oligomannose N-linked glycans. The theoretical molecular weight (MW) of complex, oligomannose, and hybrid glycans is indicated in daltons (Da) calculated from the MW of sugar residues in (B).

To gain further insight into the structure of the purified hIgG μtp HMWS negative stain EM was undertaken. Previous studies using cryo-EM and atomic force microscopy (AFM) have shown that IgM can be observed with a pentameric structure, with five pairs of Fab arms extending from the interior Fc ring [200, 433]. Additionally, electron microscopy images of an hIgG hexamer have been reported to show six antibody molecules arranged hexamerically [197]. The published images show six Fc regions at the centre of the complex, interacting through Fc:Fc contacts, and 12 F(ab) domains extending from this complex, available for antigen binding. The images obtained in the current study for hIgG1 μtp demonstrated similar characteristics (Figure 3.8).

In order to calculate the MW of the oligomeric species present in the purified μtp HMWS, SEC-MALS was used. MALS determines MW based on the average radius of complexes in a sample. If

the sample is heterogeneous it will calculate the average of all MW values [434]. In this case, the MW provided by the MALS detector was averaged across the potentially various HMWS eluted from the SEC column. The MW calculated by the MALS detector corresponded to a value of 870 kDa, the size comparable to an hIgG hexamer (monomeric size $\sim$150 kDa and hexameric size $\sim$900kDa). This result is consistent with the observation from EM and provides further confirmation that the HMWS purified is an hIgG hexamer.

After the initial quality control and characterisation of the various Fc-engineered constructs, the antigen binding of these antibody molecules was assessed. The addition of the μtp to the C-terminus of RTX hIgG1 did not prevent antigen binding in either format (Figure 3.9). These results were consistent with the other V-regions and isotypes (Figure 3.10). The decreased FITC signal for the hexamer constructs suggests that a limited number of Fc molecules in the complex can be detected by the secondary anti-Fc antibody in the multimer, perhaps as a result of steric hindrance of the multiple Fc or the orientation of the multimer at the cell surface. Nonetheless, addition of the μtp in either WT (hexamer) or C575S (monomer) formats does not prevent antigen binding of these mAb.

Having designed, produced, and characterised the various mAb formats, the following chapters set about to characterise the ability of these antibody formats to display augmented activity *in vitro* and *in vivo*.

Chapter 4

Characterisation of hexamerisation-enhanced μtp C575S anti-CD20 antibodies

4.1 Chapter introduction

Direct targeting antibodies elicit a therapeutic response through interaction and activation of immune effector mechanisms via their Fc domain, in addition to direct F(ab) mediated effects. Anti-CD20 mAb have been an effective tool for the treatment of B cell lymphomas and leukaemias, but not all patients are successfully treated or subsequently develop resistance [435, 436]. Therefore, new, more effective therapies are required. CD20 antibodies are separated into two groups based on their ability to elicit CD20 reorganisation into lipid rafts [268]. Type I CD20 mAb induce the efficient reorganisation of CD20 molecules into lipid rafts at the target cell surface. The resulting clustering of the associated antibody elicits powerful activation of complement-dependent cell killing [268]. Type II CD20 mAb weakly activate the complement system, due to a lack of CD20 reorganisation, but induce efficient DCD [274]. However, both mAb types have the ability to kill via FcγR-mediated mechanisms, such as ADCP and ADCC [283] .

Previous *in vivo* studies have shown mAb interaction with FcγRs are crucial for therapeutic efficacy of anti-CD20 mAb, with macrophages thought to be the primary effector cell responsible [253, 262]. With this knowledge, one obvious approach to improving the efficacy of these therapies is to promote target cell clearance by improving Fc:FcγR interactions. Reports have shown that these interactions can be enhanced with Fc mutagenesis [344] and glycoengineering of the

Fc glycan attached to Asn297 [346]. The presence of IgG N-linked glycosylation is necessary for binding to the FcγR [354, 437], and glycoengineering can alter the Fc-mediated effector functions of hIgG1 [346, 438]. For example, afucosylation of hIgG1 significantly improves the binding to FcγRIIIa, which translated to an improvement in ADCC *in vitro* [346] and superior B cell depletion *in vivo* [281] compared with non-glycoengineered CD20 antibodies. An afucosylated type II CD20 antibody, obinutizumab, has now been approved for treatment of previously untreated CLL by the FDA in 2013 [246], which has showed improved survival compared to the non-glycomodified type I RTX in a phase 3 clinical study, when treated in combination with a chemotherapeutic agent chlormabucil [439]. The success of bringing a glycomodified mAb to the clinic could indicate there is a bright future for the development and approval of Fc-engineered mAb.

Recently it has been reported that an IgG hexamer and a hexamerisation enhanced hIgG1 mutant may offer favourable improvements to anti-CD20 therapy [197, 271]. Mutagenesis of the hIgG1 Fc region with the triple mutant, E345R, E430G, S440Y (RGY), enables the formation of hexamers at low concentrations in solution. These hIgG1 hexamers exhibit superior cell killing by CDC through higher avidity for C1q [197]. This augmentation of CDC killing efficacy by a hexameric formation of hIgG1 indicates a potential stoichiometry more favourable to the activation of the immune system. This raises the question as to whether hIgG hexamers formats can also improve therapeutic efficacy.

Although there is convincing evidence that the complement system is optimally activated by hIgG1 hexamers, these studies do not address if other effectors of the immune system are more optimally activated by hIgG1 hexamers or if such hIgG1 hexamers provide improved *in vivo* efficacy. This chapter focuses on characterising the efficacy of anti-CD20 mAb in the context of hIgG1 hexamers and hexamerisation-enhanced hIgG1 monomers derived from the μtp fusion described in chapter 3. *In vitro* assays focused on the main mAb effector mechanisms CDC, ADCC, ADCP, and DCD, and *in vivo* investigations studied B cell depletion of the hexamerisation enhanced mutant hIgG1 were utilised.

4.2 Analysis of hIgG1 μtp C575S hexamerisation propensity

Addition of the μtp C575S to the C-terminus of hIgG1 was hypothesised to retain the potential to spontaneously multimerise through non-covalent interactions between neighbouring C-terminal μtp peptides when in close proximity. In order to test this hypothesis, hIgG1 WT and hIgG1 μtp C575S constructs of RTX were concentrated up to 20 mg/ml. Concentrations of 1, 5, 10, and 20 mg/ml were analysed by SE-UPLC in order to determine the presence of any HMWS present in

solution. The purified hIgG1 μtp hexamer species had previously been observed as a covalent hexamer species at concentrations as low as 1 mg/ml (Figure 4.1,A). The results from the SE-UPLC analysis showed that the hIgG1 WT did not have any inherent ability to form multimers in solution (Figure 4.1,B), even when forced into a high concentration environment (20 mg/ml). The hIgG1 μtp C575S demonstrated an intermediate phenotype, exhibiting and enhanced ability to form in-solution multimers, but only at higher concentrations, compared to hIgG1 WT (Figure 4.1). Hexamerisation of the hIgG1 μtp C575S construct was initially observed from 5 mg/ml (3.2%), where a multimeric peak was observed with a shorter retention time than the monomer peak. The percentage of hexamer then steadily increased with concentrations up to 20 mg/ml. At 20 mg/ml the percentage of concentration-induced hexamerisation reached 16.9%. This was also performed at higher concentrations with RTX and Herceptin hIgG1 μtp constructs and analysed by SE-HPLC. Here it was observed that a plateau of hexamerisation was reached at 50 mg/ml. At this concentration $\sim$40% of the material was observed in the multimer peak and was not increased when the concentration was further elevated to 70 mg/ml (Appendix Figure A5). Additionally, when the hIgG1 μtp C575S was diluted from the high concentrations, hexamerisation was reversed and the mAb were entirely monomeric at 1 mg/ml (Appendix Figure A5). This suggested that the multimeric species formed at high concentrations were through non-covalent interactions involving the μtp C575S. Having confirmed that the engineered anti-CD20 mAb bind to their antigen (Figure 3.9) and that hIgG1 μtp C575S is able to reversibly self-associate in solution, the on-target hexamerisation of the RTX and BHH2 hIgG1 μtp C575S constructs was assessed.

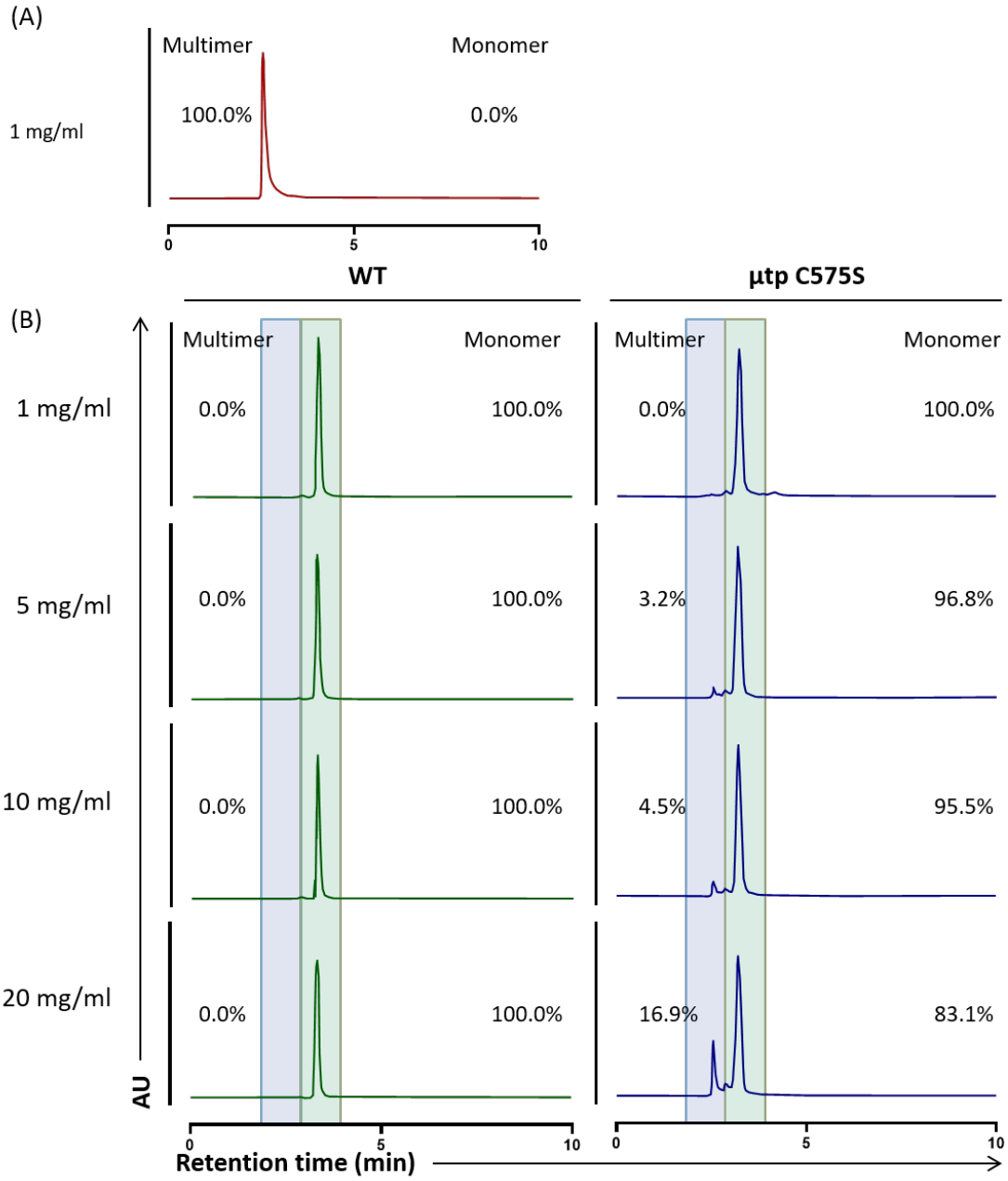

Figure 4.1: Hexamerisation enhancement of RTX hIgG1 μtp C575S mutant construct at increasing concentrations in solution.
RTX hIgG1 constructs were concentrated to the required concentrations and the percentage of monomeric and multimeric species was determined by SE-UPLC (A) Representative SE-UPLC trace of the preformed RTX hIgG1 μtp hexamer at 1 mg/ml (B) Representative SE-UPLC traces of RTX hIgG1 WT (left) and hIgG1 μtp C575S (right) at increasing concentrations from 1 mg/ml up to 20 mg/ml.

4.3 *In Vitro* effector functionality

4.3.1 CDC activity

Firstly, the binding of the hIgG1 WT, μtp C575S, and μtp to C1q was investigated to determine if this had been effected by the μtp peptide fusions. Wells of maxisorp plates were coated in

duplicate with antibodies at concentrations between 0.01 and 10 μg/ml. One plate was used to assess the amount of IgG bound to the plate, to ensure this was consistent between the three different constructs examined. The second plate was used to assess the binding of purified human C1q in an ELISA. The results for the RTX constructs showed that all three were similarly bound to the plate (Figure 4.2,A). In terms of C1q binding, the results suggested that the WT and μtp C575S had comparable binding to C1q in an ELISA. However, at the lower concentrations, the μtp hexamer demonstrated clearly increased binding to C1q (Figure 4.2,B), indicating that the covalent hIgG1 μtp hexamer had a higher avidity for C1q.

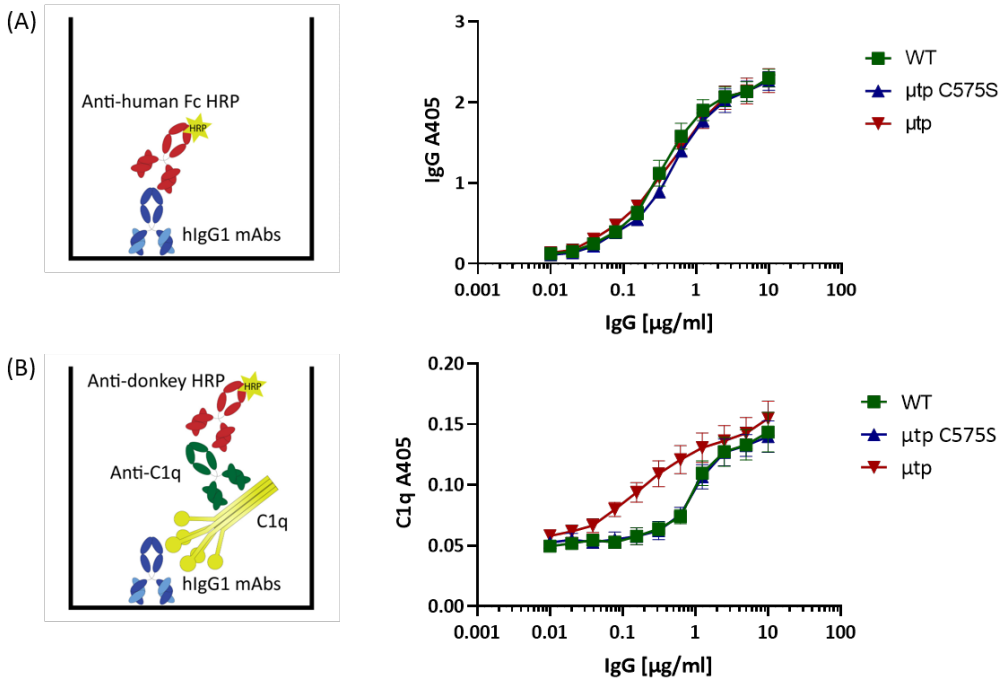

Figure 4.2: Binding of human C1q to RTX hIgG1 μtp fusions in an ELISA.
(A) ELISA plates were coated with RTX IgG at various concentrations and detected with an HRP-conjugated goat anti-human IgG to confirm similar levels of antibody was bound to the plate. Schematic of the experimental design shown on left. ELISA results shown on right (B) ELISA plates were coated with RTX IgG at various concentrations, followed by human C1q at 2 μg/ml. Bound C1q was detected with a goat anti-human C1q antibody followed by a peroxidase-conjugated anti-goat IgG-Fc antibody. Schematic of the experimental design shown on left. ELISA results shown on right. Data plotted is mean and SEM of duplicate results from independent experiments (N=6).

Next the hIgG1 hexamers (μtp) and hIgG1 on-target hexamers (μtp C575S) were assessed for their potential to activate complement in solution when exposed to serum, in a non-target-specific manner [271]. In order to address this, an ELISA measuring the levels of C4d, an anaphylatoxin and by-product of the classical complement pathway, was performed in target-free serum in the presence of various RTX constructs. Production of C4d would indicate that the complement pathway is being activated in the absence of target. The results show that the only construct that induced target-less C4d production was the RTX hIgG1 μtp hexamer (Figure 4.3). The hexameric hIgG1 μtp construct elicited a significantly higher production of C4d when compared to WT, μtp

C575S, and even the the heat aggregated hIgG (HAGG) positive control. Together, the C1q and C4d ELISA indicated that RTX hIgG1 μtp had the ability to bind C1q and activate the classical complement pathway in the absence of any target and demonstrated potential toxicities if used *in vivo*.

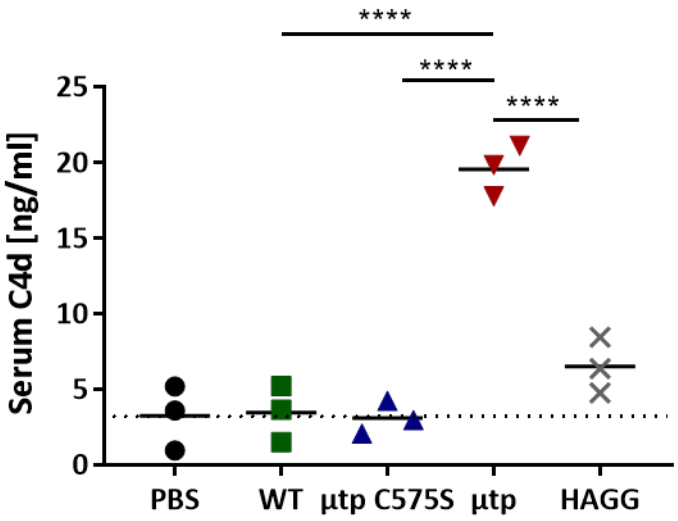

Figure 4.3: Activation of complement in solution by RTX hIgG1 μtp fusions.
Fluid-phase C4d was measured in human serum after 1 hour incubation with RTX hIgG1 μtp fusions or heat aggregated IgG (HAGG) at 100 μg/ml. Graphs show individual donor data (N=3). Statistical analysis was carried out by one-way ANOVA; **** = P<0.0001.

To assess the ability of the RTX hIgG1 μtp C575S construct to undergo on-target hexamerisation, a cell-based assay was performed to observe C1q recruitment to the target cell surface. As the μtp C575S was able to more effectively multimerse in solution than WT mAb, it was hypothesised that μtp C575S would recruit more C1q to the surface (due to enhanced clustering of the Fc into a hexameric stoichiometry). In order to investigate cell surface C1q recruitment, $CD20^{+}$ Ramos cells were opsonised with RTX hIgG1 WT, μtp C575S, or μtp mAb and the recruitment of C1q was analysed by flow cytometry (Figure 4.4,A). The results showed that the μtp C575S and μtp both recruited higher levels of C1q to the target cell surface than the WT hIgG1. At 10 μg/ml, RTX hIgG1 μtp C575S had an increase of 64 MFI and the RTX hIgG1 μtp had an increase of 79 MFI. This indicated that the μtp C575S behaves as a monomer when in solution but has a higher propensity to form hexamers when bound to its target antigen at the cell surface. This is consistent with the hypothesis of hexamerisation enhanced mAb and on-target hexamers.

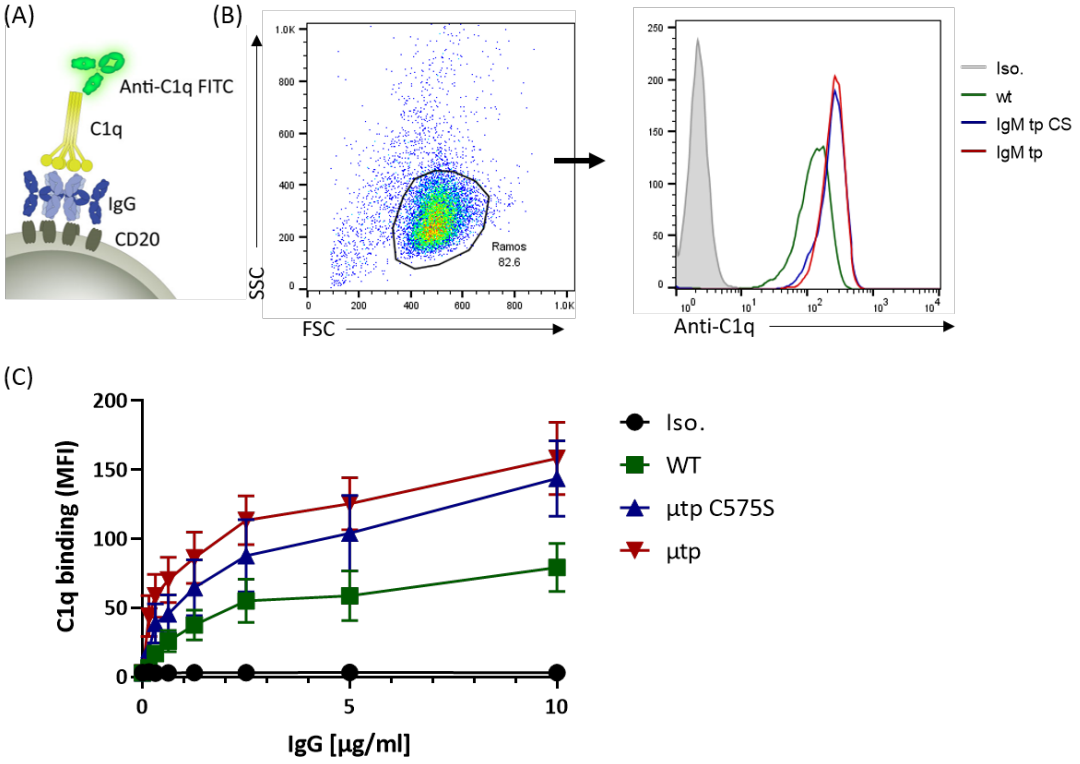

Figure 4.4: Recruitment of C1q by RTX hIgG1 μtp fusions to the cell surface.
$CD20^{+}$ Ramos cells were opsonised with antibody at various concentrations, followed by incubation with 2 μg/ml human C1q. Deposition of C1q was determined by incubation with a FITC-conjugated anti-C1q antibody and analysed by flow cytometry (A) Schematic diagram of assay design depicting antibody opsonised cells recruiting C1q, and secondary staining to detect C1q (B) Gating strategy of Ramos cells (left) and representative FITC signal displayed as a histogram (right) demonstrating differences in C1q recruitment to CD20 Ramos cells by hIgG1 μtp fusions at 10 μg/ml, measured by secondary staining with anti-C1q (FITC) antibody (C) MFI of C1q bound to cell surface over a concentration range of opsonised mAb; 1151 hIgG1 WT used as isotype control. Data plotted is mean and SEM from independent experiments (N=7).

Finally, the ability of RTX hIgG1 μtp formats to elicit CDC was determined. The CDC assay was performed using Ramos and Raji cell lines as target cells. In these assays, both cell lines were opsonised with a range of mAb concentrations and incubated with a final concentration of 20% human serum. Dying or dead cells were observed by positive PI staining when analysed by flow cytometry (Figure 4.5,A). Ramos cells exhibit high sensitivity to complement components due to a lack of complement defence molecules [268]. The results shown in Figure 4.5,B indicated that the RTX hIgG1 ability to elicit CDC could be greatly improved when present as a pre-formed hexamer (μtp) and also enhanced when in the hexamerisation enhanced μtp C575S format. When targeting Ramos cells all RTX formats achieved 100% cell killing at the highest concentration of mAb. However, the dose required to achieve this was very different between constructs. The RTX μtp hexamer reached 100% cell killing at 0.1 μg/ml a two-fold shift compared to the RTX μtp C575S and a seven-fold shift compared to RTX WT. The RTX μtp C575S reached 100% cell killing at 0.33 μg/ml, four-fold lower than RTX WT, which had 100% cell death at 1 μg/ml. When an asymmetric sigmoidal dose-response curve was interpolated (analysis completed on GraphPad Prism) EC50 values can be calculated, which were as follows: RTX WT 0.223 μg/ml, RTX μtp C575S

0.114 μg/ml, and RTX μtp hexamer 0.025 μg/ml.

RTX antibodies were also tested on Raji cells (Figure 4.5,B). This cell line has a lower sensitivity to CDC than Ramos cells, due to the expression of the complement defence molecules CD55 and CD59 [268]. This was confirmed by the fact that the WT RTX hIgG1 evoked only low levels of CDC, far less than seen with Ramos cells (Figure 4.12,B). In contrast, the RTX μtp hexamer reached 100% cell killing against Raji cells at 5 μg/ml. The maximum cell killing of RTX μtp C575S was observed at around 70%, at the highest concentration tested (10 μg/ml). The EC50 values for the Raji cell line were non-recordable, 5.000 μg/ml, and 0.355 μg/ml for RTX WT, μtp C575S, and μtp hexamer, respectively. These data clearly demonstrate the potential of the μtp technology to augment CDC.

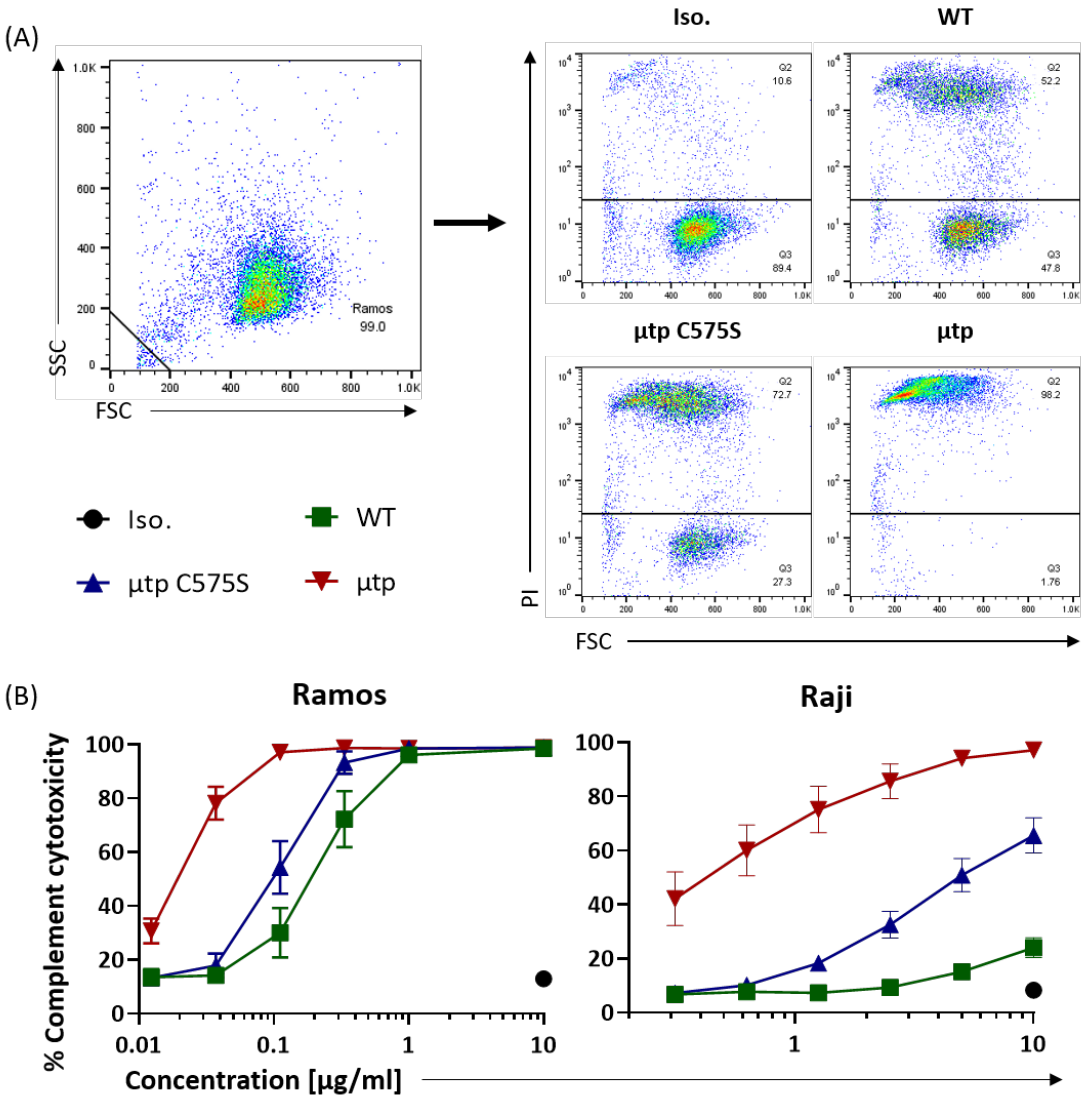

Figure 4.5: CDC activity of RTX hIgG1 μtp fusions.
Ramos or Raji target cells were opsonised with isotype control (1151 hIgG1) or RTX anti-CD20 antibodies prior to incubation with 20% NHS. Complement activity was detected by staining cells with PI. PI will only enter and fluoresce cells permeabilised by the MAC complex (A) Flow cytometry gating strategy of complement activation. Dead and dying cells gated (left) to find % PI positive cells (right). Representative FACS plots of $CD20^{+}$ Raji cells treated with isotype control or RTX μtp fusion mAb at 10 μg/ml. Complement cytotoxicity calculated as percentage of cells positive for PI in the FSC/SSC target cell gate cells (B) Percentage (%) cell cytotoxicity over a range of antibody concentrations for Ramos (left) and Raji (right) target cells. Data is plotted as mean and SEM of duplicate repeats from independent experiments of opsonised Ramos cells (N=6) and Raji (N=4).

In addition to RTX antibodies, a type II anti-CD20 mAb, BHH2, was also investigated in both μtp formats for C1q binding and complement activity as above. Analysis of C1q binding by ELISA demonstrated that, as with RTX μtp, the BHH2 μtp hexamer exhibited increased C1q binding compared to WT and μtp C575S in the plate-bound ELISA (Figure 4.6,B). The results also indicated a small increase in C1q binding by BHH2 μtp C575S over its WT counterpart, although analysis of the plate-bound IgG demonstrated the amount of IgG to be comparable (Figure 4.6,A).

The recruitment of C1q to Ramos cells suggested that the BHH2 hIgG1 WT constructs was very inefficient at C1q binding, as expected for a non-clustering type II mAb. The μtp C575S displayed a

modest increase when compared to the WT mAb, only exhibiting an increase of 17 MFI. However, the BHH2 hIgG1 μtp demonstrated greatly enhanced C1q recruitment (Figure 4.6,C). Therefore, as a preformed hexamer, BHH2 can overcome its inherent lack of C1q recruitment, whereas addition of the μtp C575S, although more active, is not enough to drive the efficient receptor clustering required to recruit C1q.

These mAb were also examined in CDC cell killing assays. The non-modified BHH2 exhibited a maximum cell killing of around 20% at the top concentration tested (Figure 4.6,D). In contrast, the BHH2 μtp hexamer demonstrated the capacity for 100% Ramos cell killing at 10 μg/ml, which is a concentration 100-fold higher than the RTX μtp hexamer. The BHH2 μtp C575S had an enhancement in CDC activity when compared to the BHH2 WT, with a maximum cell killing of around 40% at 10 μg/ml. The observed EC50 values against Ramos cells were around 0.062 μg/ml for BHH2 μtp hexamer and over 10 μg/ml for BHH2 μtp C575S. The EC50 value for BHH2 WT was not calculable over the concentration range investigated. When targeted against Raji cells (Figure 4.6,D) the BHH2 μtp hexamer again exhibited 100% cell killing at the top concentration tested. However, the BHH2 μtp C575S construct did not demonstrate any improvement in CDC activity over the BHH2 WT. The BHH2 μtp hexamer had a calculated EC50 value of around 0.642 μg/ml, whereas the other constructs had an non calculable EC50 values in the concentration range used.

The current results have provided clear evidence that μtp C575S on-target hexamers, and μtp hexamers offer an advantage in the binding of C1q and the activation of the classical complement pathway, leading to enhanced cell killing activity. However, it was not clear whether hIgG on-target hexamers and hIgG hexamers also augment FcγR and F(ab)-mediated effector functionality. In order to investigate these antibody-dependent cell-mediated killing mechanisms the μtp fusion mAb was assessed for FcγR binding, ADCC, ADCP, and DCD.

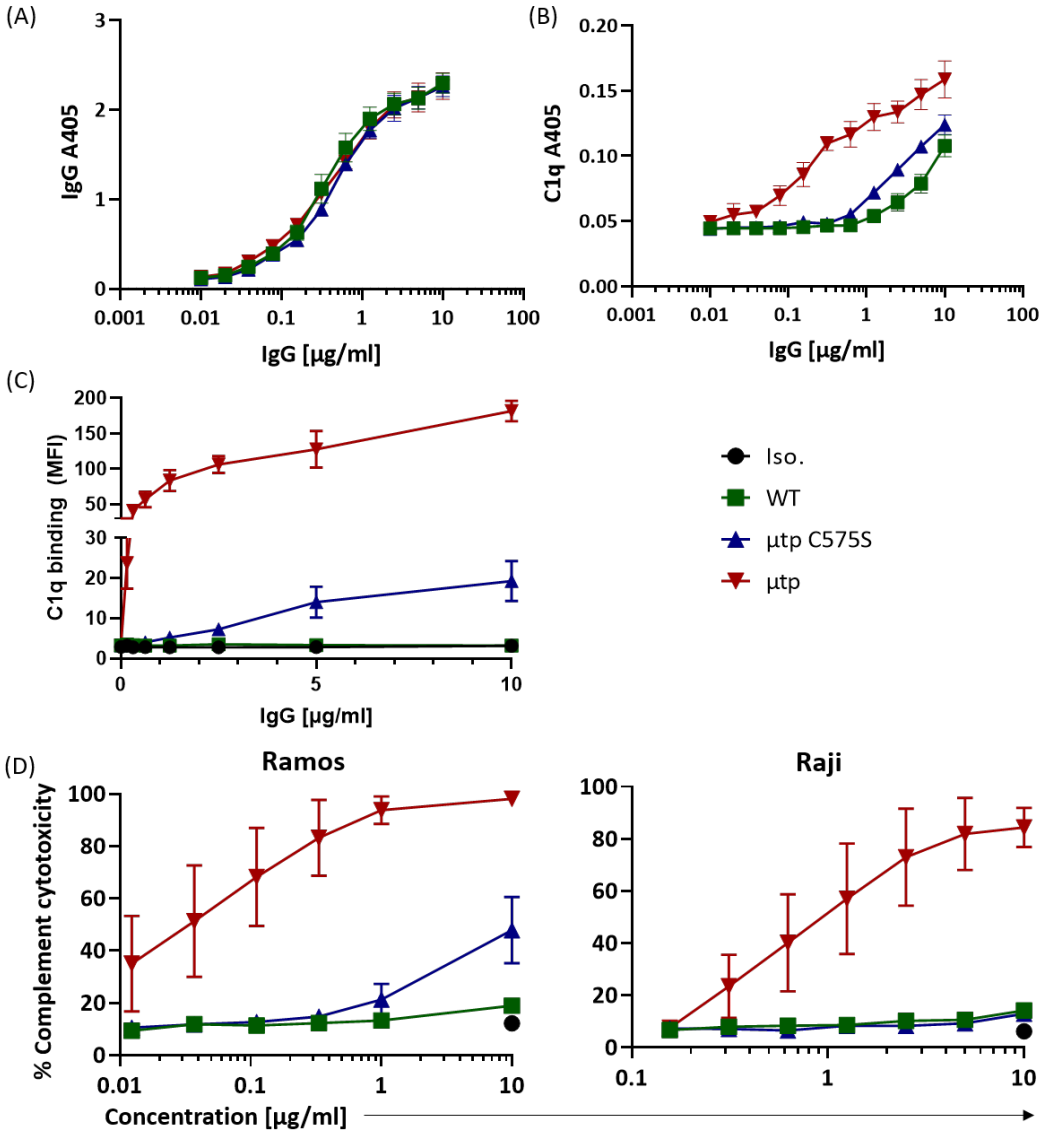

Figure 4.6: C1q binding, C1q cell recruitment, and CDC activity of BHH2 hIgG1 μtp fusions.
(A/B) ELISA plates were coated with BHH2 hIgG1 μtp constructs at various concentrations. Side-by-side, coated plates were measured for bound IgG (left) and C1q binding (right). To measure C1q binding, human C1q (2 μg/ml) was added and bound C1q was detected with a goat anti-human C1q antibody followed by a peroxidase-conjugated anti-goat IgG-Fc antibody. Data shows absorbance at A405 of bound C1q (N=3) (C) $CD20^+$ Ramos cells were opsonised with BHH2 hIgG1 μtp constructs at various concentrations followed by 2 μg/ml human C1q. Bound C1q was determined using an anti-C1q-FITC antibody and analysed by flow cytometry. Data shows MFI of anti-C1q-FITC antibody (N=3) (D) $CD20^+$ cells were opsonised with BHH2 hIgG1 μtp constructs and incubated with 20% NHS. Cellular lysis was determined by staining cells with PI and analysed by flow cytometry for PI positive cells. CDC activity of BHH2 hIgG1 μtp fusions measured using opsonised Ramos (left) and Raji (right) cell lines; data shows percentage (%) of cell cytotoxicity of independent experiments (N=3). 1151 hIgG1 was used as an isotype control. Data plotted is mean and SEM of multiple independent experiments.

4.3.2 FcγR binding

It was clear that hIgG1 μtp hexamers had enhanced binding to C1q, but what wasn't clear was whether hexameric hIgG1 was a more favourable conformation for FcγR binding. Therefore, the binding of μtp fusion mAb for human FcγR was assessed using surface plasmon resonance (SPR) and CHO cells expressing the different human FcγRs. Firstly, SPR was performed by immobilising

the various hIgG1 μtp fusion mAb to the flow cells of a Biacore sensor chip. Recombinant FcγRs were then passed over at various concentrations and binding was measured in response units (RU) to produce a sensogram (Figure 4.7), with a blank flow cell used for reference. The high affinity FcγRI was flowed over the sensor chip at concentrations ranging from 100 - 0.16 nM, and all other low affinity FcγR flowed over at concentrations ranging from 1000 - 1.6 nM. The sensograms were used to calculate KD using the steady-state affinity model.

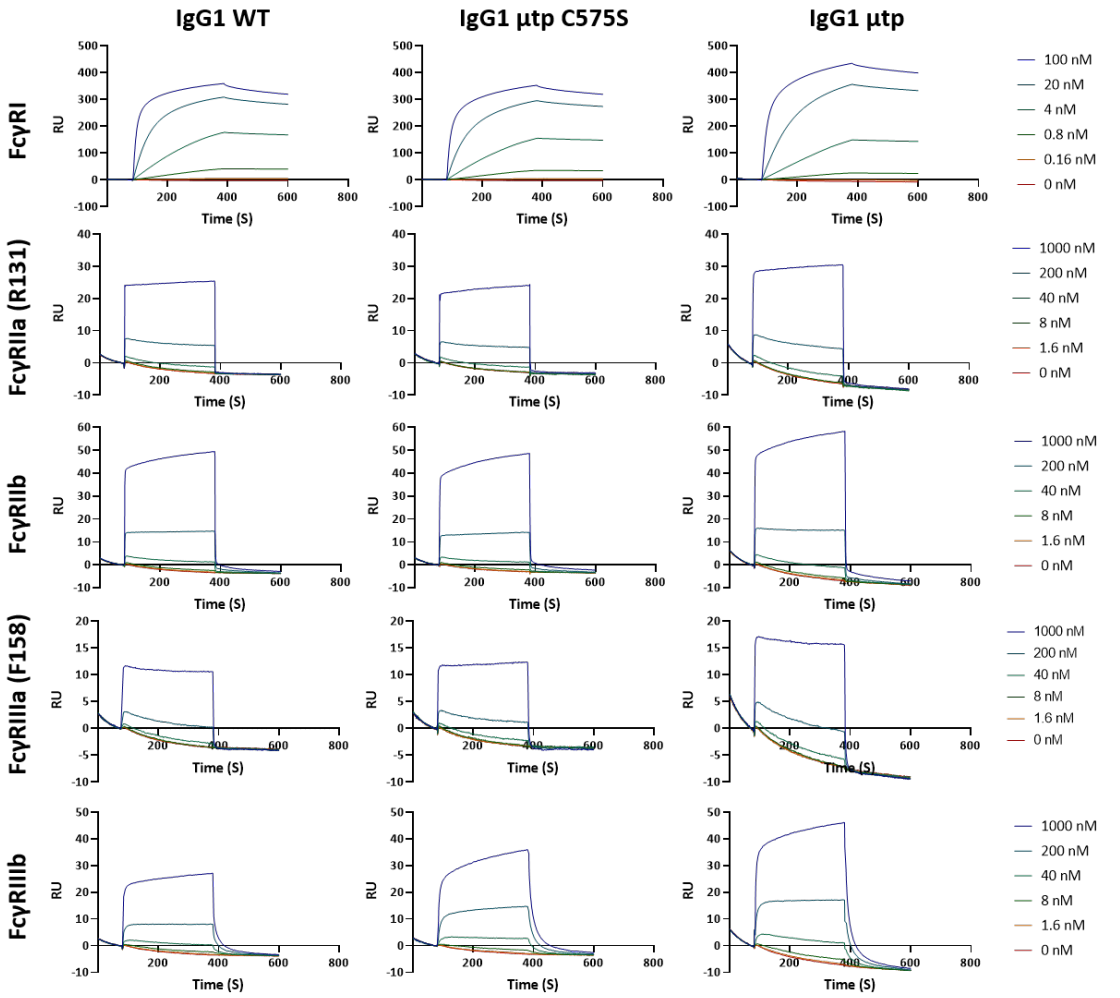

Figure 4.7: SPR analysis of RTX μtp fusion hIgG1 mAb binding human FcγR.
The SPR sensograms of RTX hIgG1 WT, μtp C575S, and μtp constructs were determined using SPR. Antibody was immobilised to a Biacore binding chip and recombinant FcγRs flowed over at several concentrations depending on the FcγR for 300 seconds on and 300 seconds off. Binding of FcγR to immobilised mAb is measured in response units (RU).

The calculated KD are summarised in Table 4.1. For hIgG1 WT, μtp C575S, and μtp the KD indicated that the binding to FcγRIIa, IIb, and III was largely unaffected by the presence of the WT or C575S μtp peptide. Although, the KD was slightly higher for hIgG1 μtp hexamer, they may simply reflect experimental variation. Overall, SPR analysis of FcγR binding affinities suggested that most low affinity FcγR do not have preferential binding for hexameric hIgG1 over monomeric hIgG1. In addition to SPR the binding of μtp fusion mAb for human FcγR was also assessed using CHO cells expressing the different human FcγR to determine any differences in cell surface binding.

	KD (nM)		
Receptor	**hIgG1 WT**	**hIgG1 μtp C575S**	**hIgG1 μtp**
FcγRI	4.36	5.33	7.53
FcγRIIa (R131)	935	1000	964
FcγRIIb	1360	1540	1470
FcγRIIIa (F158)	719	415	410
FcγRIIIb	1860	1680	1510

Table 4.1: Effect of RTX hIgG1 μtp fusions on binding affinity to human FcγR.
The affinities of RTX hIgG1 WT, μtp C575S, and μtp constructs were determined using SPR. Antibody was immonbilised to a Biacore binding chip and recombinant FcγRs flowed over at several concentrations depending on the FcγR. Affinities were calculated using a steady state affinity model.

CHO cells were incubated with mAb and bound mAb was detected by a fluorescently labelled secondary anti-human mAb before interrogation by flow cytometry. The cells were also examined for the level of FcγR expression which varied and should be taken into account with analysis of mAb binding efficiency (Figure 4.8,A). Although FcγRI, FcγRIIa R131, FcγR IIIb were all expressed at high levels, FcγRIIa H131 and both FcγRIIIa SNPs were poorly expressed.

The investigation of FcγR binding was performed with mAb fusions in the context of RTX V regions. The results shown in Figure 4.8,B-C indicated small levels of non-specific binding to untransfected CHO cells by WT and μtp C575S hIgG1, and significantly higher levels of non-specific binding with the μtp hexamer. Analysis of the binding to the high affinity FcγRI showed no significant differences between mAb formats. However, significant differences were observed with the low affinity FcγRs. In the case of FcγRIIa, the two well-characterised polymorphisms (H131 and R131) were investigated for mAb binding. The R131 polymorphism observed higher binding, most prevalent with the μtp hexamer in comparison to the H131. However, the level of expression of the FcγRIIa H131 SNP was lower than FcγRIIa R131 on the CHO cells examined. In the case of both FcγRIIa polymorphisms, the μtp hexamer demonstrated significantly increased binding over the WT and μtp C575S constructs. The highest binding to the low affinity FcγRs was observed with the μtp hexamer in the context of CHO cells expressing FcγRIIb, which was significantly higher than the monomeric mAb formats. In the context of FcγRIIIa V158 and F158, the binding was higher for FcγRIII F158, but the receptor expression was low for both the FcγRIIIa polymorphisms. Again, the hIgG1 μtp hexamer demonstrated significantly enhanced FcγR binding over the WT and μtp C575S constructs. Overall it was clearly observed that the μtp hexamer exhibited higher FcγR binding for all low affinity FcγR when compared to either WT or μtp C575S, suggesting that a pre-formed μtp hexamer has a higher avidity for FcγR. That the μtp C575S demonstrated comparable binding to the WT suggests that this construct acts as a monomeric mAb in regards to FcγR interactions in the absence of target binding. These results demonstrated potential avidity enhancement for hIgG1 μtp hexamers binding human FcγR. However, it was unclear whether an hIgG1 μtp hexamer or μtp C575S hexamerisation enhanced hIgG1 offered any advantage in the

activation of FcγR-mediated effector functions. In order to determine any potential enhancement given by these Fc-engineered antibodies, their ability to induce ADCC was next studied.

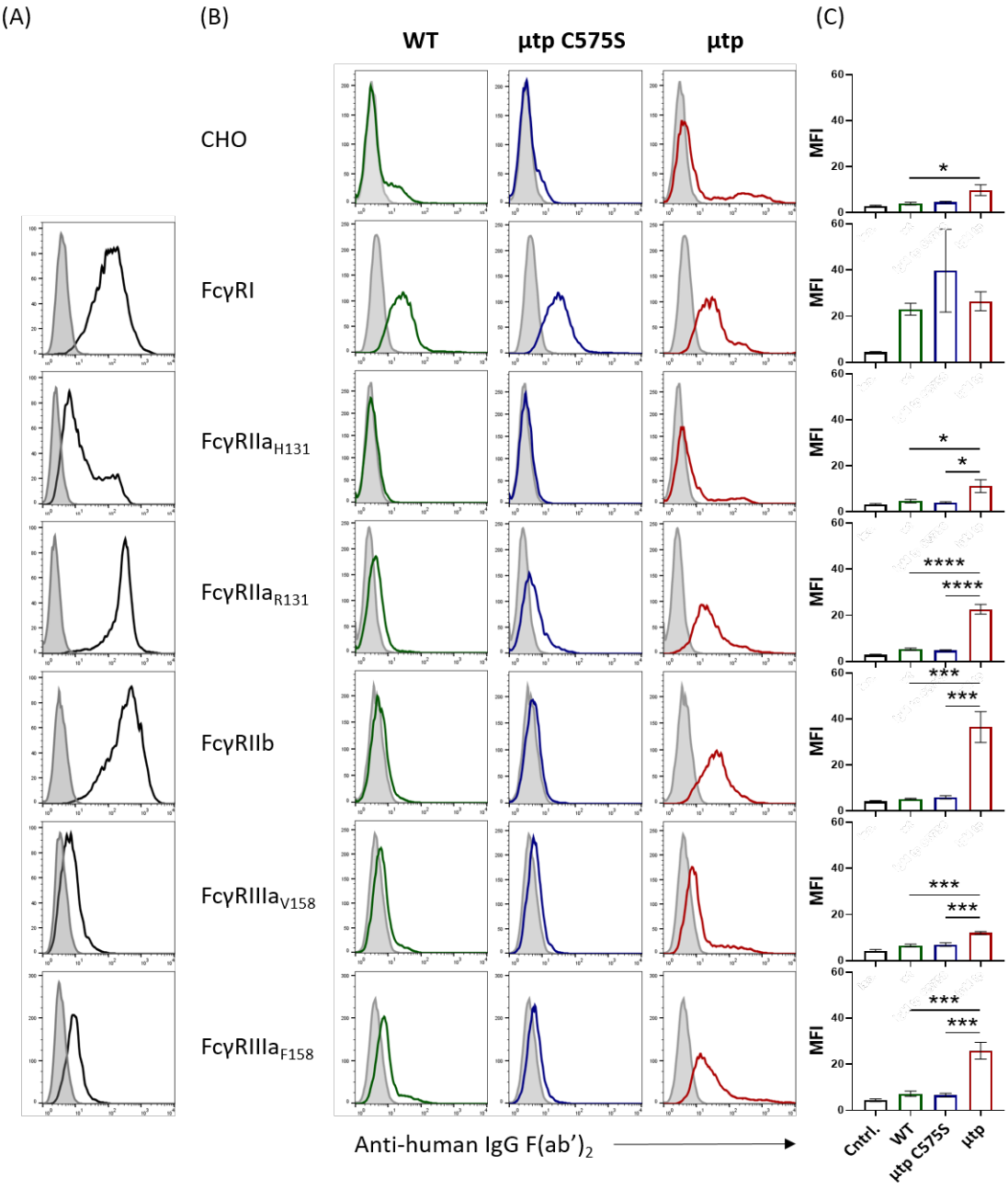

Figure 4.8: Effect of hIgG1 μtp fusions on binding capabilities to human FcγR.
hIgG1 μtp fusions were incubated with CHO cells expressing human FcγR. Bound mAb was detected by anti-human F(Ab')$_2$ (PE) and binding levels analysed by flow cytometry (A) Representative FcγR expression pattern of transfected CHO cells displayed as a histogram showing control (PBS; solid grey) and FcγR expression (black line) (B) Representative binding of hIgG1 μtp fusion mAb to CHO cells expressing human FcγR displayed as a histogram showing control (PBS; solid grey) and antibody binding (coloured lines) (C) MFI of binding profiles. Data shown is mean and SEM of four independent experiments (N=4). Statistics calculated using one-way-ANOVA test. * P ≤ 0.05; *** P ≤ 0.001; **** P ≤ 0.0001.

4.3.3 ADCC activity

The ADCC assay used was a fluorescent assay using calcein release as a read-out. Here target cells are labelled with calcein-AM and then opsonised and incubated with effector cells, in this case PBMCs. Lysed $CD20^{+}$ cells release the fluorescent calcein, initially observed as fluorescent units on a fluorimiter. These measurements are then converted to percentage of the maximum lysis (% max lysis), applying the detergent lysed cells as 100% and the labelled target cells in the absence of PBMC effector cells (background) as 0% (Figure 4.9,A).

A large concentration range of 0.0001 – 1 μg/ml of each mAb was used in an attempt to detect any subtle differences in efficacy. The RTX hexamer constructs demonstrated no observable enhancement in their ability to induce ADCC over the concentration range investigated (Figure 4.9,B). At the top concentration of 1 μg/ml the cellular cytotoxicity of all three RTX formats was around 30%. The ADCC activity of the RTX μtp C575S construct was observed at around 35%, but no significant increase was observed compared to the RTX WT. Over the remaining concentration range, below 1 μg/ml, the activity of the RTX μtp C575S constructs was comparable with the non-modified comparator. The assay was also reported with the type II BHH2 constructs.

The results with the BHH2 hexamer constructs shown in Figure 4.9,C also indicated that there was no improvement in ADCC with either the hIgG1 μtp hexamer or hIgG1 μtp C575S. The maximum cell cytotoxicity observed with all three BHH2 constructs was around 30% at the top concentration investigated. The cell death decreased at comparable rates over the concentration range down to 0.0001 μg/ml, where activity was recorded at about 5% cell cytotoxicity. These results indicated that the neither the type I or type II anti-CD20 mAb elicited any significant enhancement in ADCC activity in either of the μtp formats. However, the results do imply that a complex of multiple Fc's arranged at the target cell surface does not negatively impact the induction of a cellular cytotoxic response. Nonetheless, the second FcγR-mediated effector function, ADCP, was also assessed with the same μtp anti-CD20 mAb for any increase in their phagocytic potential.

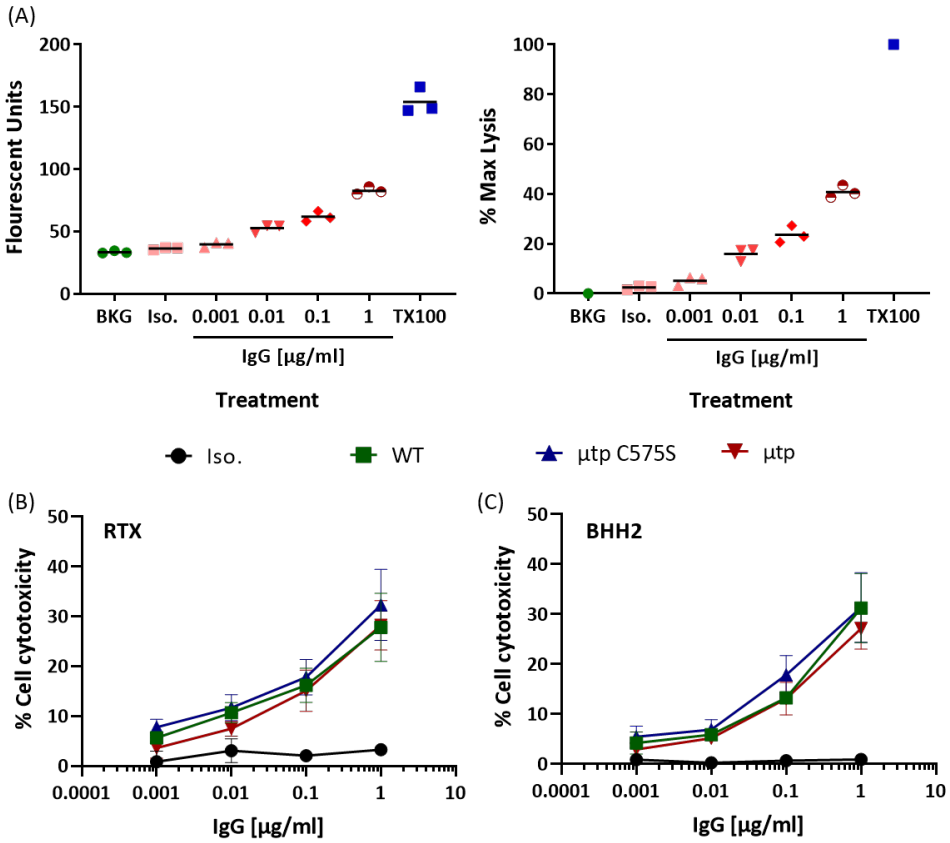

Figure 4.9: Effect of hexamerisation of anti-CD20 antibodies on ADCC activity.
Calcein labelled Ramos cells were opsonised with an isotype control (1151 hIgG1) or anti-CD20 hIgG1 mAb (WT or μtp fusions) over a concentration range and incubated with freshly purified human PBMCs as effector cells. Calcein release in cell supernatants was measured as a readout for ADCC. (A) Fluorescent readout and calculated % max lysis of RTX WT opsonised Ramos cells after effector cell lysis. (B/C) Cell cytotoxicity (% max cell lysis) of Ritux (B) and BHH2 (C) WT and μtp fusion hIgG1. Data plotted is the mean and standard deviation of triplicate repeats from 3 independent experiments (N=3).

4.3.4 ADCP activity

For the phagocytosis assay a concentration of 0.5 μg/ml was used based upon prior experience of the assay. B-CLL tumuor cells were used as target, after first labelling them with fluorescent CFSE. After culturing with MDMs the samples were stained with anti-FcγRIII-APC to identify the macrophages and assessed by flow cytometry. Phagocytosis of mAb opsonised CLL cells was assessed for double positive macrophages (FcγRIII-APC and CFSE labelled CLL cells) by flow cytometry (Figure 4.10,A-B). No enhancement in phagocytic activity at 0.5 μg/ml was seen with any μtp anti-CD20 mAb, with a mean of $\sim$20% phagocytosis observed for both, that was comparable to the RTX WT (Figure 4.10,C).

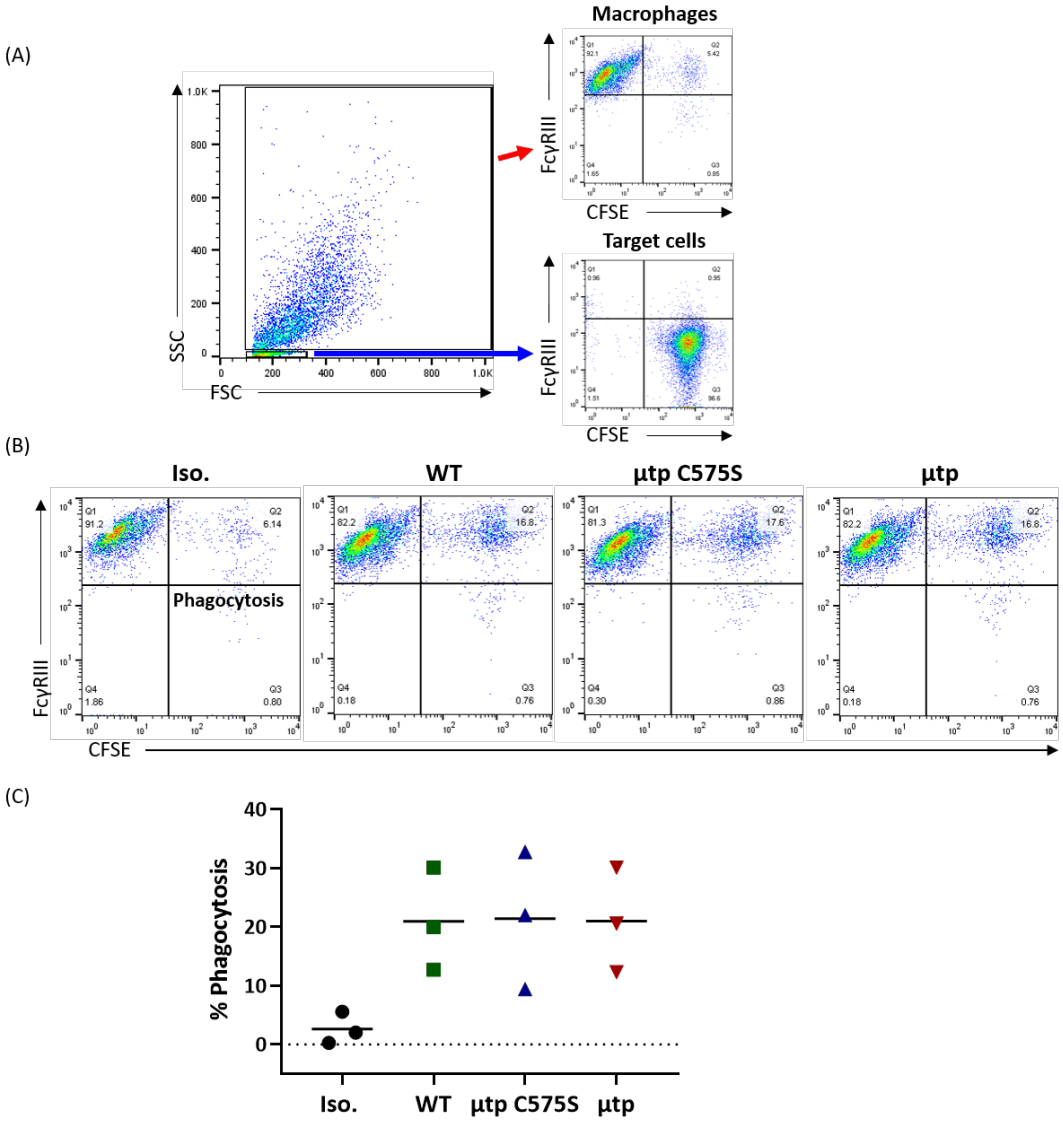

Figure 4.10: ADCP activity of RTX hIgG1 μtp fusions.
CFSE labelled human CLL patient PBMCs (target cells) were opsonised with 0.5 μg/ml isotype control (1151 hIgG1) or anti-CD20 antibodies (WT or µtp fusions) and co-cultured with human MDM. Phagocytosis was calculated by double positive staining for FcγRIII expression on macrophages and CFSE stained target cells by flow cytometry (A) Flow cytometry gating strategy to isolate FcγRIII positive macrophages and CFSE positive target CLL PBMCs. Representative FACS plots of RTX mAb at 0.5 μg/ml (B) Representative flow cytometry plots of opsonised CLL cells with RTX hIgG1 WT, μtp C575S, or μtp (C) Percentage (%) of macrophage phagocytosis. Data plotted is the mean of duplicate repeats from independent experiments (N=3).

For the remaining ADCP results the phagocytic index of each mAb was calculated using hIgG1 WT mAb as having a phagocytic index of one. The use of a phagocytic index negated some of the variability observed when using different human primary cells as target cells and different donors leading to the MDMs. Additionally, the polarisation state of the macrophages was subsequently manipulated to further examine any potential differences between the efficacies of these antibodies in the ADCP assay. The M0 state previously used represents unstimulated macrophages and displayed a basal level of phagocytosis. The M1 state is considered activated and should display an increased level of activation over the M0 state. Conversely, the M2 state is considered to be suppressed, resulting in a reduction in phagocytosis compared to M0. M1 and M2

polarised macrophages were therefore produced by incubating macrophages with Pam3SK4 or IL4/13, respectively. The differences in phagocytic activity with WT RTX hIgG1 between M0, M1, and M2 can be observed in Figure 4.11,A. However, the results from Figure 4.11,B indicated that the activation state of the macrophage did not impact the activity of the RTX hIgG1 μtp C575S constructs. The phagocytic index for RTX hIgG1 μtp C575S was not enhanced in the context of M0 or M1 macrophages and slightly increased in M2 macrophages in 2 out of 3 donors. The phagocytic index for RTX hIgG1 μtp did not increase in the context of M0, M1 or M2 polarised macrophages.

Similarly, no enhancement in phagocytic index of the BHH2 μtp C575S construct was observed over the BHH2 WT in M0 macrophages. The BHH2 μtp hexamer displayed a slight, but not significant, increase in phagocytic index with M0 macrophages (Figure 4.11,C). The BHH2 μtp hexamer and μtp C575S hexamerisation enhanced antibodies also demonstrated no change in ADCP over different macrophage polarisation states compared to the BHH2 WT construct (Figure 4.11,C). The phagocytic index of BHH2 hIgG1 μtp C575S was not altered from around 1, comparable with BHH2 hIgG1 WT, independent of macrophage polarisation. Similarly, BHH2 hIgG1 μtp hexamers did not demonstrate enhanced phagocytic potential for M0 and M1 macrophages, but did demonstrate a slightly increased phagocytic index in the context of M2 macrophages in 2 out of the 3 donors. Overall, these results indicated that hIgG1 hexamers do not offer any benefit to phagocytosis of target cells, irrespective of macrophage polarisation state. These results suggested that hIgG1 hexamers do not significantly augment FcγR-effector functionality, but have profound effects on CDC. Next, the impact of IgG hexamerisation was assessed for DCD, the Fc-independent effector function.

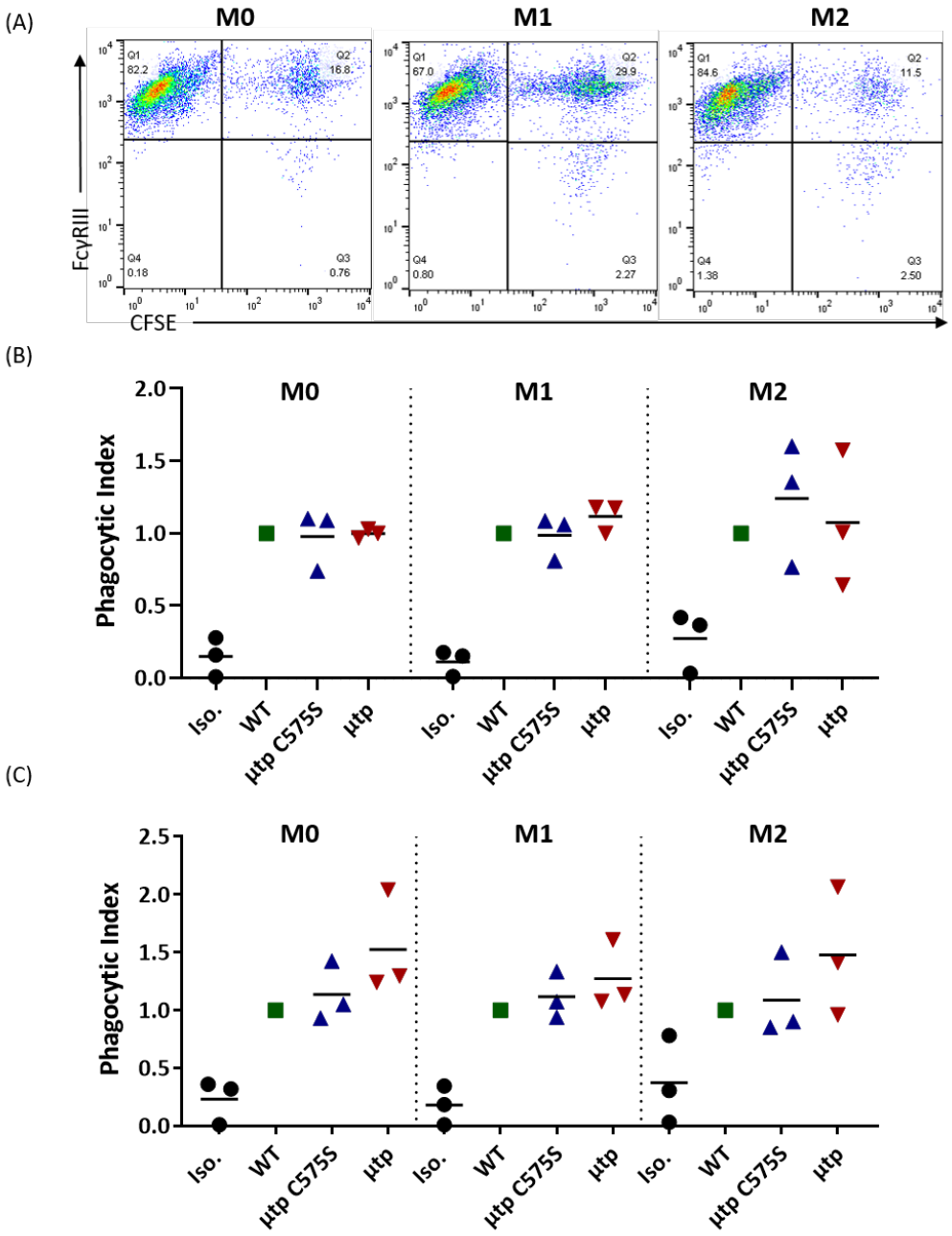

Figure 4.11: Effect of macrophage polarisation on the phagocytic activity of anti-CD20 μtp fusion mAb.
CFSE labelled human CLL patient PBMCs (target cells) were opsonised with 0.5 μg/ml isotype control (1151 hIgG1) or anti-CD20 antibodies (WT and μtp engineered) and co-cultured with human MDMs. Phagocytosis was calculated by double positive staining for FcγRIII expression on macrophages and CFSE stained target cells by flow cytometry (A) Representative flow cytometry plots of the phagocytic capacity of differentially polarised human MDMs M0 (left; no stimulation), M1 (middle; Pam3SK4 stimulation), and M2 (right; IL4/IL13 stimulation) and RTX hIgG1 WT opsonised CLL target cells (B/C) Phagocytic index of RTX (B) and BHH2 (C) hIgG1 μtp C575S and μtp mAb compared to their WT counterpart with macrophages skewed to M0, M1, and M2 phenotypes. Data plotted is the mean of duplicate repeats from 3 independent experiments (N=3).

4.3.5 DCD activity

The induction of direct cell death by anti-CD20 antibodies has previously been shown to differ between the type I and type II mAb. Type II anti-CD20 mAb typically generate a larger DCD re-

sponse resulting from induction of non-apoptotic cell death, thought to be related to the different binding conformations between type I and type II mAb [274, 275]. To investigate the effect of hexamerisation on the ability of anti-CD20 antibodies to induce DCD, Raji cells were incubated with the modified mAb in the absence of any immune effectors. Cell death was then measured by observing Annexin V and PI fluorescent positivity 24 hours later by flow cytometry (Figure 4.12,A). The results from Figure 4.12 shows that RTX WT did not induce efficient direct cell death of the target cells and exhibited only 20% cell death at the top concentration of 10 μg/ml. This activity was unaltered by the addition of the μtp C575S, which also demonstrated 20% cell death at 10 μg/ml. The RTX μtp hexamer, however, enhanced the extent of direct cell death compared to the non-modified RTX. The RTX μtp hexamer had higher induction of DCD compared to the RTX WT and RTX μtp C575S at 1 μg/ml and 10 μg/ml. At 0.01 μg/ml all three RTX constructs exhibited around 6% cell death similar to the isotype control.

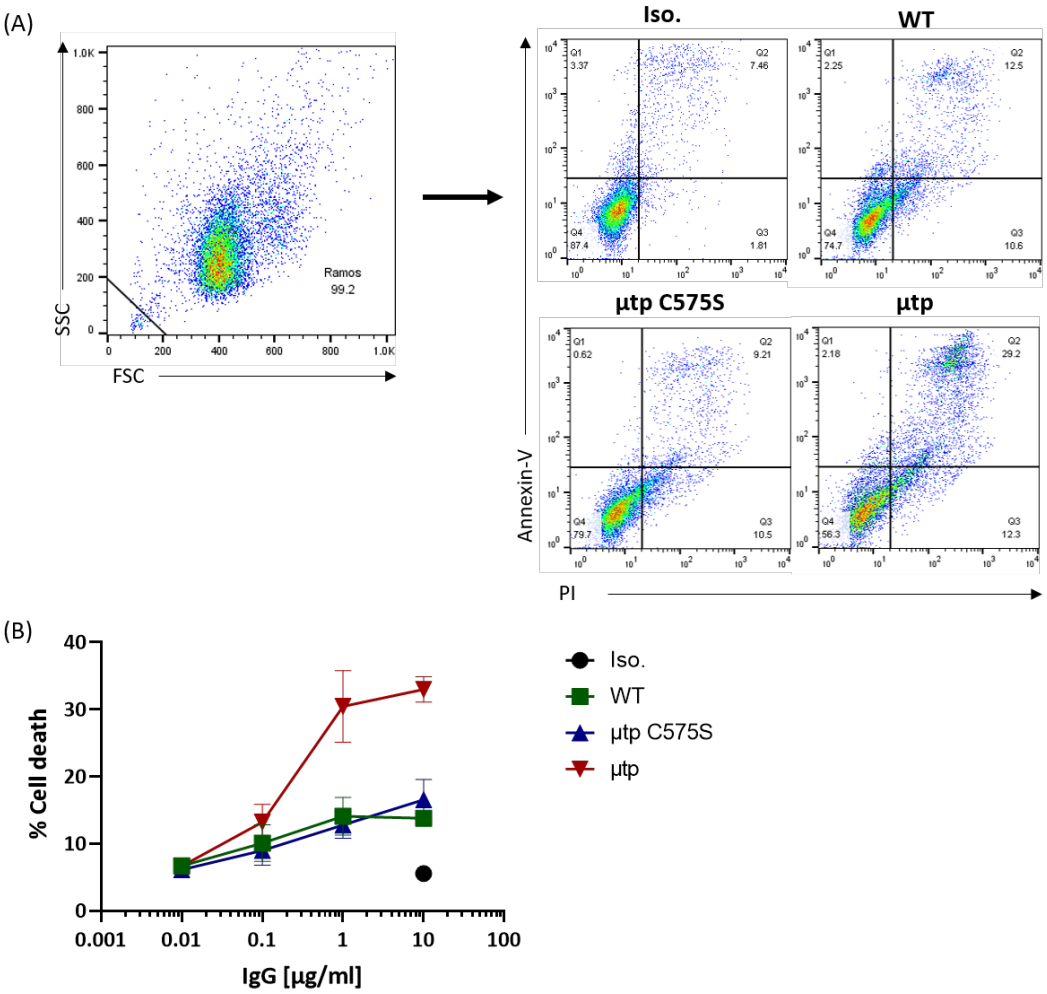

Figure 4.12: Effect of type I anti-CD20 RTX hIgG1 μtp fusions on DCD.
Raji target cells were opsonised with an isotype control (1151 hIgG1) or RTX antibodies (WT and μtp fusions) over a concentration range and incubated for 24 hours with 10 % FCS. DCD was observed via flow cytometry for annexin-V and PI positive target cells. (A) Flow cytometry gating strategy to calculate double positive cells in the FSC/SSC target cell gate (left) and representative flow cytometry plots of DCD (right) showing target cells opsonised with 10 μg/ml isotype control or RTX mAb (B) Cell cytotoxicity caused by DCD (% ANN V^+ PI^+) of RTX μtp fusions. Data plotted is the mean and standard deviation of triplicate repeats from independent experiments (N=3).

DCD was also investigated using BHH2 constructs which inherently induce a higher level of direct cytotoxicity (Figure 4.13,A). The BHH2 WT induced around 80% DCD at 1 μg/ml, which was not increased at 10 μg/ml (Figure 4.13,B). This demonstrated the differences between the direct cytotoxicity induced by type I and type II antibodies. However, the μtp hexamer and μtp C575S hexamerisation enhanced BHH2 antibodies displayed a decreased level of DCD compared to the BHH2 WT (Figure 4.13,B). Although DCD levels at 1 μg/ml were similar, they were both lower than BHH2 hIgG1 WT mAb. At 10 μg/ml the levels of DCD of the BHH2 μtp C575S and BHH2 μtp hexamer were decreased by around 10% and 20%, respectively. These results indicate that DCD induced by hexameric anti-CD20 mAb was affected, which can be positive or negative depending on the type of CD20 mAb.

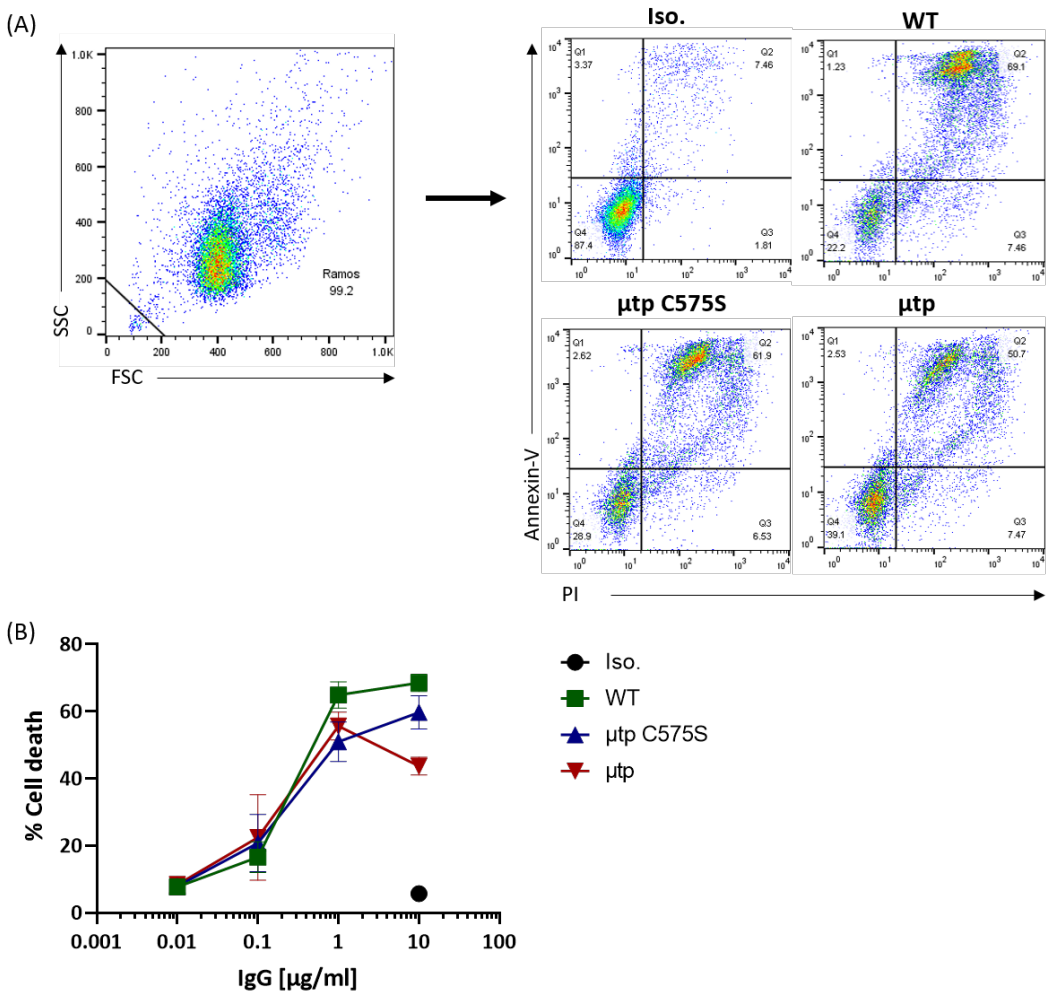

Figure 4.13: Effect of type II anti-CD20 BHH2 hIgG1 μtp fusions on DCD.
Raji target cells were opsonised with an isotype control (1151 hIgG1) or anti-CD20 antibodies (WT and μtp fusions) over a concentration range and incubated for 24 hours with 10% FCS. DCD was observed via flow cytometry for annexin-V and PI positive target cells. (A) Flow cytometry gating strategy to calculate double positive cells in the FSC/SSC target cell gate (left) and representative flow cytometry plots of DCD (right) showing target cells opsonised with 10 μg/ml isotype control and BHH2 mAb (B) Cell cytotoxicity caused by DCD (% ANN V^+ PI^+) of BHH2 μtp fusion mAb. Data plotted is the mean and standard deviation of triplicate repeats from independent experiments (N=3).

4.4 Antibody internalisation

One potential mechanism that could account for the lack of augmentation of FcγR-mediated effector mechanisms was the possibility of enhanced internalisation of hIgG1 μtp C575S on-target hexamer and μtp hexamers. In order to determine the level of internalisation of hIgG1 μtp constructs, Ramos cells were opsonised with mAb and monitored by a secondary-fluorescently labelled anti-human Fc antibody by flow cytometry (Figure 4.14,A). Lower levels of surface-bound antibody were inferred to represent a higher levels of antibody internalisation, which was calculated as a percentage of the initial binding level. The results showed that RTX hIgG1 WT had a maximum of $\sim$20% internalisation over 24 hours, a peak that was reached after 6 hours and remained constant (Figure 4.14,B). The RTX hIg1 μtp C575S construct exhibited higher levels of internalisation, after 6 hours incubation there was $\sim$60% of internalisation, which remained constant over the next 18 hours (Figure 4.14,B). Similarly, RTX hIgG1 μtp demonstrated similar levels of internalisation (Figure 4.14,B). Over the 24 hour incubation period there was $\sim$60% internalisation recorded, but this maximum was reached by 2 hours where there was $\sim$80% internalisation. The apparent decrease in internalisation from 2 hours to 24 hours could be due to antibody recycling to the cell surface.

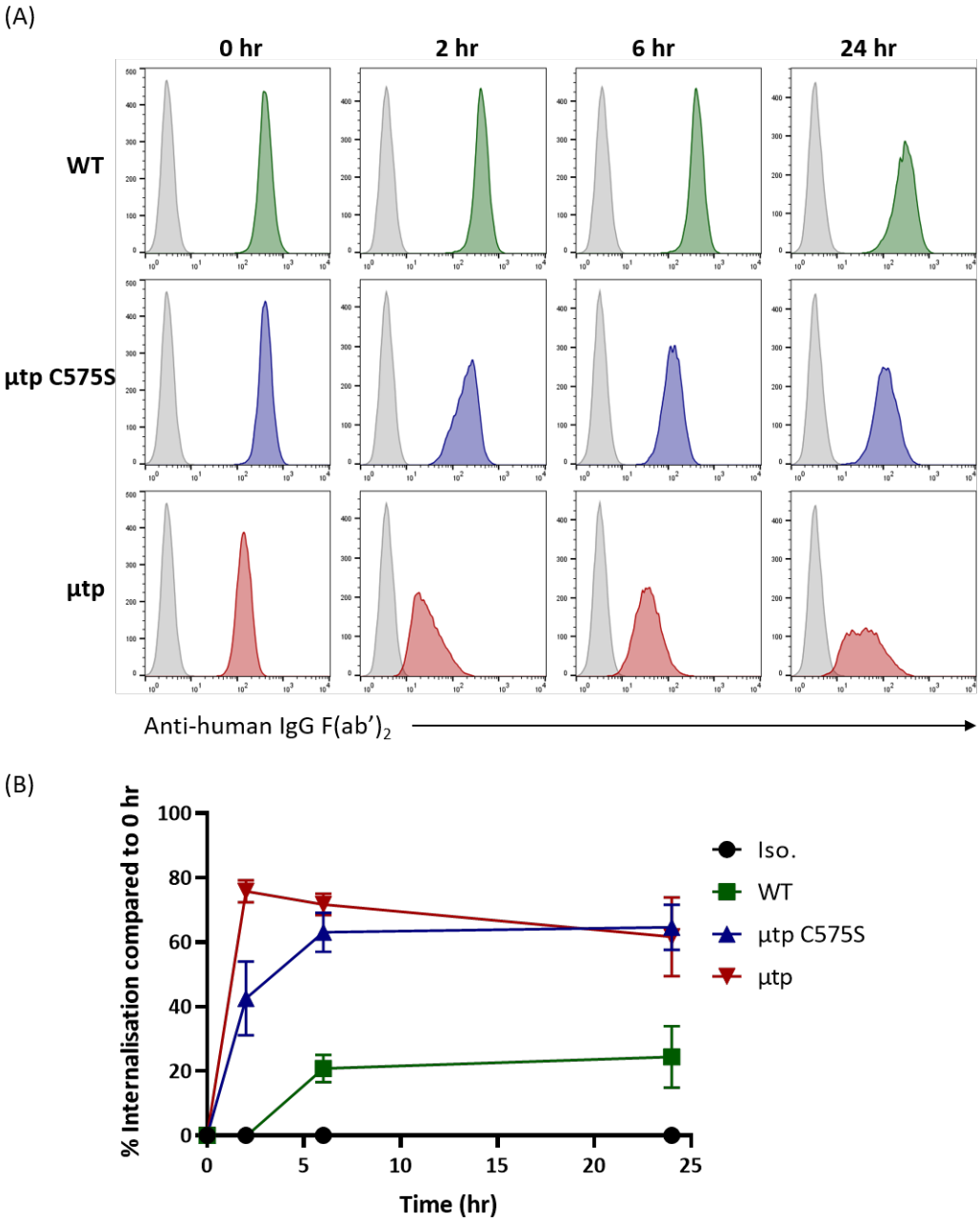

Figure 4.14: Effect of RTX hIgG1 μtp fusions on antibody internalisation.
1 x 10^5 Ramos cells were opsonised with hIgG1 isotype (1151) or RTX constructs and the bound antibody was monitored using an anti-human Fc (SB2H2) FITC labelled antibody at 0, 2, 6, and 24 hour by flow cytometry. Any decrease in bound antibody was calculated as internalisation compared to 0 hours (A) Representative flow cytometry histograms over time showing isotype control (solid grey) and RTX (coloured lines) opsonised cells (B) Percentage (%) internalisation compared to time 0. Data shown is mean and SD from independent experiments; N=3.

In addition to RTX reagents, the BHH2 hIgG1 μtp constructs were assessed for internalisation. Unlike the RTX hIgG1 μtp mAb there was no observable difference between the internalisation of the three constructs (Figure 4.15). The data showed that BHH2 hIgG1 WT was internalised to a maximum of ~40% after 6 hours (Figure 4.15,B). There was a similar trend of internalisation observed for BHH2 hIgG1 μtp C575S, with a maximum of ~40% after 6 hours (Figure 4.15,B). The BHH2 μtp hexamer was internalised slightly more slowly, and reached a maximum internalisation of ~40% after a 24 hour incubation period (Figure 4.15,B). Similar to the RTX hIgG1 μtp hexamer,

BHH2 hIgG1 WT and μtp C575S constructs demonstrated a decrease in internalisation from 6 hours ($\sim$40%) to 24 hours ($\sim$20%). The results indicated that internalisation may not be restricting ADCC and ADCP, as BHH2 hIgG1 μtp hexamers do not have a greater internalisation efficiency compared to BHH2 hIgG1 WT. The μtp constructs were next assessed for the efficiency of B cell depletion in a more physiologically relevant environment, where multiple effector mechanisms were present simultaneously.

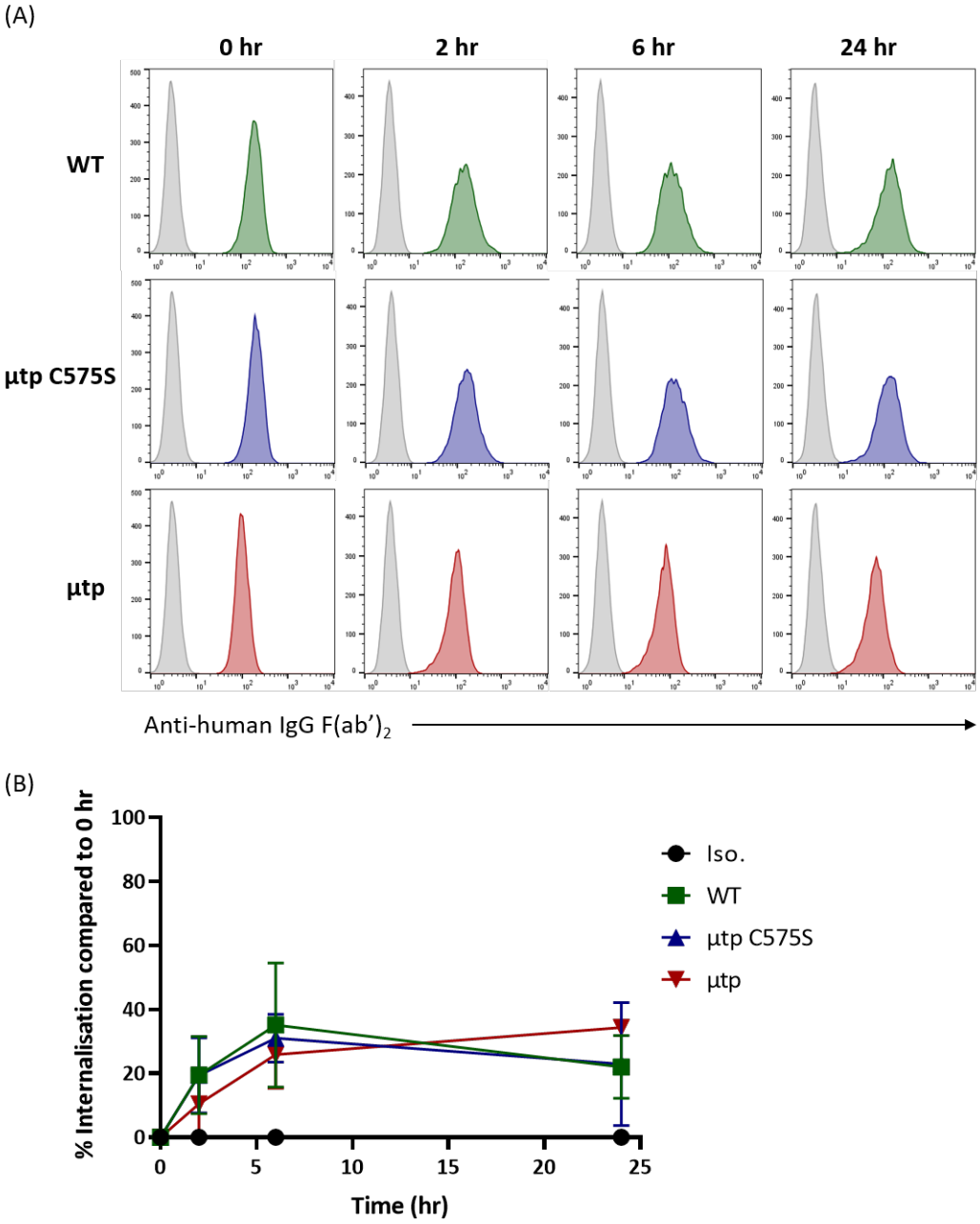

Figure 4.15: Effect of BHH2 hIgG1 μtp fusions on antibody internalisation.
1 x 10^5 Ramos cells were opsonised with hIgG1 isotype (1151) or BHH2 constructs and the bound antibody was monitored using an anti-human Fc (SB2H2) FITC labelled antibody at 0, 2, 6, and 24 hour by flow cytometry. Any decrease in bound antibody was calculated as internalisation compared to 0 hours (A) Representative flow cytometry histograms over time showing isotype control (solid grey) and RTX (coloured lines) opsonised cells (B) Percentage (%) internalisation compared to time 0. Data shown is mean and SD from independent experiments; N=3.

4.5 *Ex vivo* B cell depletion

The results from the above *in vitro* assays demonstrated that the hexameric and hexamerisation enhanced hIgG1 mAb had enhanced CDC activity and retained their FcγR-mediated effector functionality. However, it was unclear if this would lead to any improvement in target cell depletion in a more physiological relevant environment, for example where multiple effectors are available. Fresh peripheral whole blood containing B cells and immune effectors, such as complement and NK cells, was therefore used to investigate B cell depletion *ex vivo*. Human whole blood was treated with mAb and incubated for 24 hours, at which time the whole blood was analysed for B cell depletion by flow cytometry (Figure 4.16A). Initially a range of mAb concentrations were tested to determine an optimal concentration to assess mAb effects with the μtp formats. Addition of 1 μg/ml RTX hIgG1 WT demonstrated a moderate level of B cell depletion (Figure 4.16,B), and was used in subsequent assays to assess differences in activity between μtp fusion mAb. Results from the first donor indicated that there was no large difference in depletion effect of the different μtp formats compared to WT RTX. The experiment was then performed with a further series of donors using the pre-determined 1 μg/ml concentration.

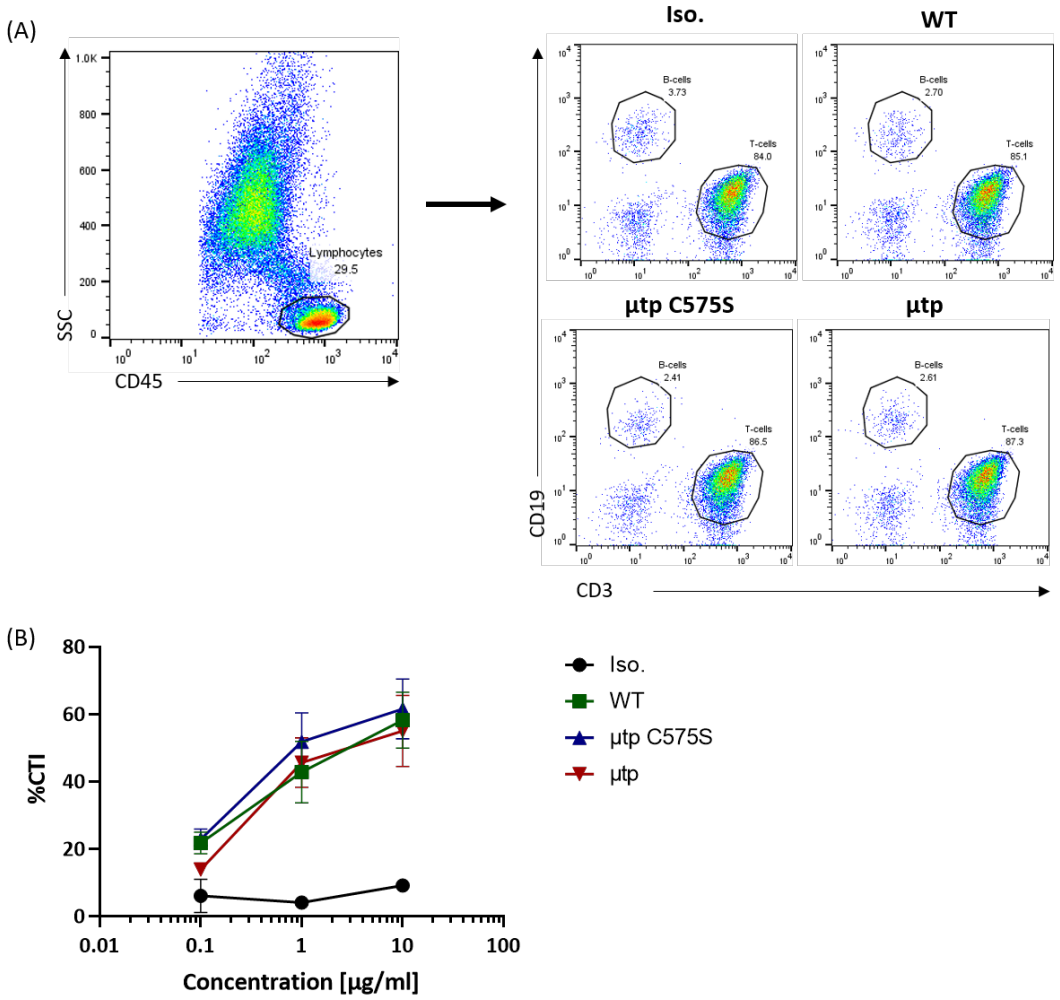

Figure 4.16: Whole blood assay was used to determine B cell depletion in human blood after incubation with RTX hIgG1 μtp fusions.
Fresh peripheral whole blood incubated with 1 μg/ml isotype control (1151 hIgG1) or hIgG1 RTX mAb. B cell depletion calculated using ratio between CD3 positive T-cells and CD19 positive B cells in CD45 positive lymphocyte population (A) Flow cytometry gating strategy to isolate CD45 positive lymphocyte population in CD45/SSC plot with a high CD45 threshold (left). T-cells and B cells isolated from CD45 positive population by CD3 (T-cells) and CD19 (B cells) with representative plots to demonstrate depletion of isotype control hIgG1 and RTX mAb treated whole blood at 1 μg/ml (right) (B) Cytotoxicity index (% CTI) is used as a readout for B cell depletion in RTX hIgG1 mAb treated whole blood over a concentration range between 0.1 μg/ml to 10 μg/ml. Data shown is mean and SD from triplicate wells from a single donor.

The results from the whole blood assay show that RTX WT had efficient B cell depleting activity in the assay (Figure 4.17). The B cell depletion of RTX hIgG1 μtp C575S showed a slight but not significant trend of decreased B cell depletion compared to hIgG1 WT. In contrast, RTX hIgG1 μtp hexamer demonstrated a significant decrease in B cell depletion compared to RTX WT and RTX μtp C575S. Similarly, BHH2 WT exhibited efficient B cell depleting activity in whole blood. Addition of μtp C575S demonstrated the same trend for decreased B cell depletion, whereas the BHH2 μtp hexamer also induced significantly less B cell depletion compared to the WT and μtp C575S BHH2 (Figure 4.17).

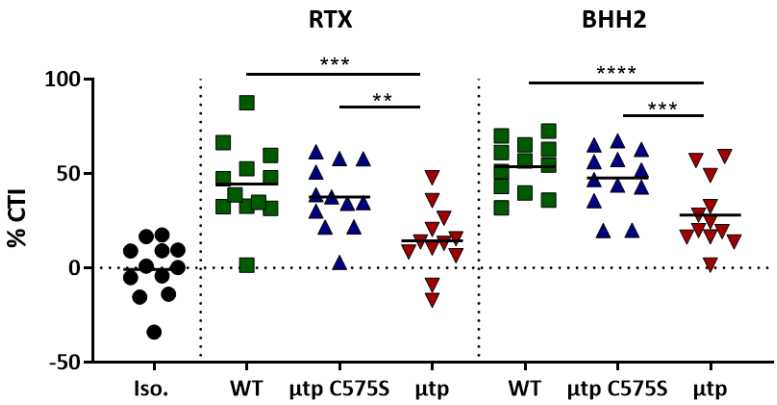

Figure 4.17: Effects of anti-CD20 hIgG1 μtp fusions on B cell depletion in whole human blood.
Fresh peripheral whole blood was incubated with 1 μg/ml isotype control (1151 hIgG1) or anti-CD20 antibody. B cell depletion calculated using ratio between CD3 positive T-cells and CD19 positive B cells in CD45 positive lymphocyte population. Cytotoxicity index (% CTI) was used as a readout for B cell depletion in RTX and BHH2 treated whole blood. Data plotted showing mean for individual donors treated with RTX mAb and BHH2 mAb (N=12). Statistics calculated using one-way-ANOVA test. ** P ≤ 0.01; *** P ≤ 0.001; **** P ≤ 0.0001.

The blood donors used had been previously genotyped (collaboration between University of Southampton and UCB Pharma [440]) which enabled investigation of the effects of different FcγR polymorphisms. Donors exhibiting either a VV, VF, or FF at residue 158 of the FcγRIIIa gene were selected, whilst attempting to keep other FcγR genotypes constant i.e. FcγRIIa were kept as HH where possible. FcγRIIIa genotypes were selected as there is a high presence of the receptor on NK cells and ADCC is one of the main effector functions observed in whole blood. The FcγRIIIa polymorphisms appeared to make little difference to either RTX or BHH2 induced B cell depletion. Each polymorphisms had comparable levels of B cell depletion for each mAb tested, but overall the F/F polymorphism exhibited the lowest levels of depletion, as expected (Figure 4.18) [131].

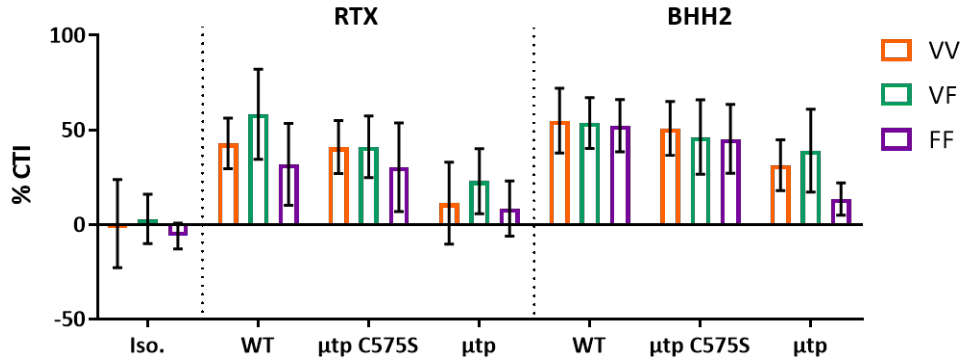

Figure 4.18: Effect of FcγRIIIa polymorphism on whole blood B cell depletion of anti-CD20 hIgG1 μtp fusions.
Fresh peripheral whole blood incubated with 1 μg/ml isotype control (1151 hIgG1) or anti-CD20 antibody. B cell depletion calculated using ratio between CD3 positive T-cells and CD19 positive B cells in CD45 positive lymphocyte population. Cytotoxicity index (% CTI) is used as a readout for B cell depletion in RTX and BHH2 treated whole blood. FcγRIIIa phenotypes indicated by colour – VV = red; VF = green; FF = blue. Data plotted showing mean for individual donors treated with RTX antibodies and BHH2 antibodies (N=12; FcγRIIIa VV/VF/FF n=4 each).

Coincident with analysis of the B cell depletion in whole blood, the cell supernatant was collected and the levels of IFN-γ was determined as a marker for pro-inflammatory signalling after treatment. The results mimicked the B cell depleting activities of each antibody. Interestingly, the BHH2 constructs promoted higher IFN-γ secretion than the RTX constructs, although the levels of B cell depletion are similar. Both the RTX and BHH2 mAb exhibited a similar trend in IFN-γ production, i.e. the WT CD20 mAb induced the highest levels of stimulation, followed similar levels with the μtp C575S constructs, and the μtp hexamers stimulated the lowest IFN-γ response. Both the RTX and BHH2 μtp hexamers had statistically significant lower IFN-γ responses compared to their μtp C575S monomer counterparts. The BHH2 μtp hexamer also demonstrated a statistically significant lower response compared to the BHH2 WT monomer (Figure 4.19). The different FcγRIIIa polymorphisms appeared to make little impact on the IFN-γ secretion, similar with the B cell depletion, and there was no correlation between that affinity of the FcγRIIIa genotype and levels of IFN-γ secretion when treated with either RTX or BHH2 hIgG1 constructs (Appendix Figure A6). These results indicated that there may be a potential disadvantage of the pre-formed hIgG1 μtp hexamer in mediating B cell depletion in the presence of multiple effectors. In order to confirm if this potential negative effect of μtp fusions was observed *in vivo*, B cell depletion was examined in relevant mouse models.

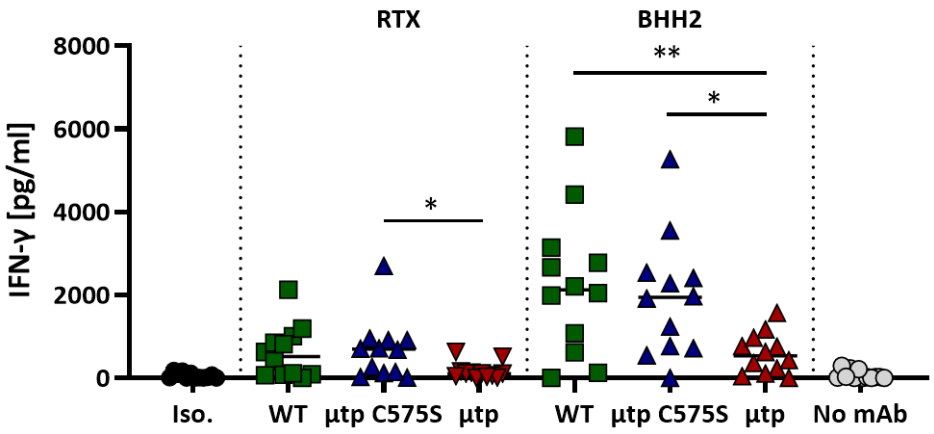

Figure 4.19: Effect on IFN-γ production in whole blood treated with anti-CD20 hIgG1 μtp fusions.
Fresh peripheral whole blood was incubated with 1 μg/ml isotype control (1151 hIgG1) or anti-CD20 antibody for 24 hours. Plasma was collected by centrifugation and MSD plate used to calculate IFN-γ production (pg/ml). Data plotted showing mean for individual donors treated with RTX antibodies and BHH2 antibodies (N=12). Statistics calculated using 1-way-ANOVA. * $P \leq 0.05$; ** $P \leq 0.01$.

4.6 *In vivo* efficacy

4.6.1 Analysis of μtp C575S and μtp FcRn interaction and *in vivo* clearance rates

Before investigating the activity of the anti-CD20 antibodies *in vivo*, the binding to FcRn and antibody half-life was assessed. FcRn binding was analysed using a HPLC column with immobilised FcRn and eluted over a pH gradient. The retention times suggested that FcRn binding of BHH2 hIgG1 μtp C575S was similar to that of BHH2 hIgG1 WT (Figure 4.20). The retention time of BHH2 hIgG1 μtp hexamer was increased when compared to the WT mAb. Therefore a higher pH was required to elute the protein, indicating the hexamer exhibited a higher binding avidity for FcRn (Figure 4.20).

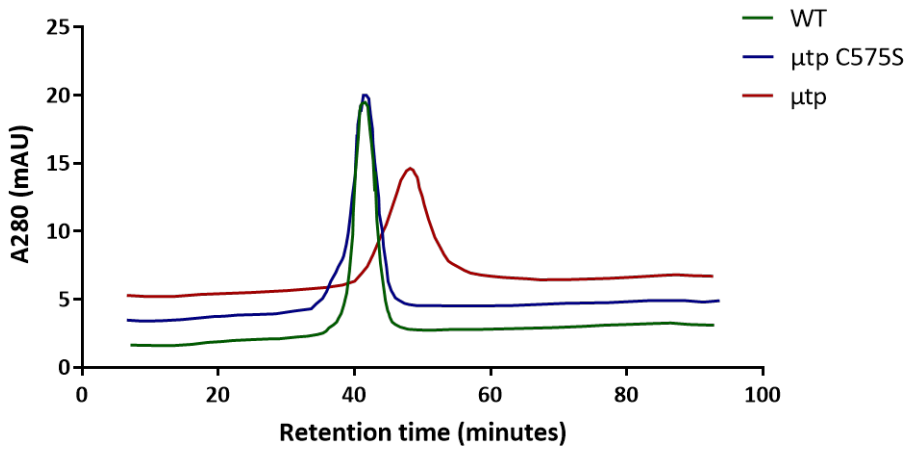

Figure 4.20: Binding of hIgG1 μtp fusions to FcRn.
hIgG1 µtp fusions (BHH2) were loaded onto an FcRn affinity column at 1 mg/ml, pH 5.5. The mAb were eluted using a pH gradient up to pH 8.8 and the effluent analysed by absorbance at A280 nm.

Non-target mediated antibody clearance was assessed in Balb/C WT mice by administering a single 100 μg i.v. dose per mouse and monitoring circulating mAb concentration in serum at successive time-points by ELISA. At the doses used no adverse effects were observed with any of the hIgG1 μtp formats. Analysis of IgG concentration in the serum has indicated that the half-life of μtp C575S was unaffected and cleared at a similar rate to WT mAb. Over the first 14 days there was detectable levels of both of the mAb (Figure 4.21). However, the μtp hexamer was rapidly cleared from the circulation (Figure 4.21). After 1 hour, the serum concentration of RTX hIgG1 μtp was half that of the monomeric mAb, and rapidly diminished over the first 24 hours. Over the following 7 days the hexamer was gradually cleared and was not detectable 14 days after administration. These results suggested that hIgG1 μtp hexamer format results in rapid clearance from the circulation, whereas an hIgG1 μtp C575S on-target hexamer observes similar mAb clearance rates to WT antibody. After it was determined that hIgG1 μtp C575S did not display any decrease

in circulating half-life *in vivo*, the constructs ability to deplete B cells was examined.

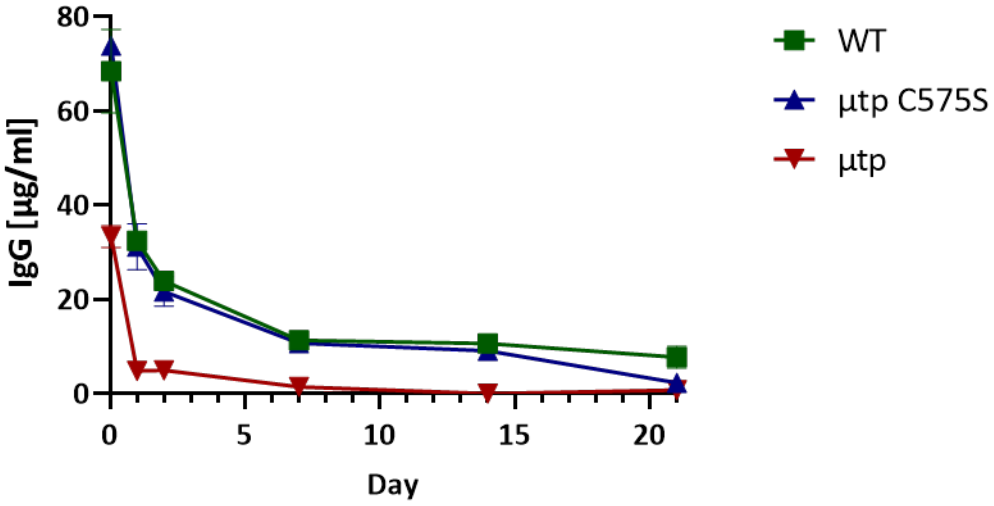

Figure 4.21: Clearance rates of RTX hIgG1 μtp fusions *in vivo* in Balb/C WT mice.
RTX mAb (100 μg) was administered on day 0 to Balb/C WT mice. Peripheral blood was collected by tail tipping at 2hr and days 1, 2, 7, 14, and 21. Serum was collected by centrifugation of the collected blood after clotting. Concentration of hhIgG1 (μg/ml) in mouse serum was calculated by ELISA. Data plotted to show mean and SEM. Results from a single experiment; N=3 mice per group.

4.6.2 B cell depletion *in vivo*: adoptive transfer

Previous results from the *in vitro* analysis demonstrated that the hIgG1 μtp C575S anti-CD20 mAb elicited enhanced CDC activity but no improvement in FcγR-mediated effector functions, in addition to an equivalent level of B cell depletion in an *ex vivo* whole blood model. The next step was to investigate the efficacy of hexamerisation-enhanced mAb in *in vivo* B cell depletion models. Firstly an adoptive transfer model was performed, where low levels of hCD20^{+} target cells were injected into WT recipient mice. Specifically the spleens from one hCD20Tg C57 Bl/6 and one WT C57 BL/6 mice were harvested. The splenocytes were stained with either high or low level of CFSE and 2.5 x 10^{6} cells adoptively transferred into WT C57 BL/6 recipient mice in a 1:1 ratio (Figure 4.22,A). In addition to low levels of target cells, only 25 μg of either RTX hIgG1 WT, RTX hIgG1 μtp C575S, RTX hIgG1 μtp, or isotype control μtp C575S was administered. After administration all animals were closely monitored for 15 minutes and had regular check-ups for the remainder of the day and the following morning. Under these conditions (low target cell numbers, 25 μg mAb) no adverse side-effects were observed. After 24 hours the mice were sacrificed and spleens collected to be analysed by flow cytometry for the ratio of hCD20Tg and wild-type CFSE labelled B cells (Figure 4.22,B-C). This ratio was used to calculate the efficiency of hCD20Tg B cell depletion.

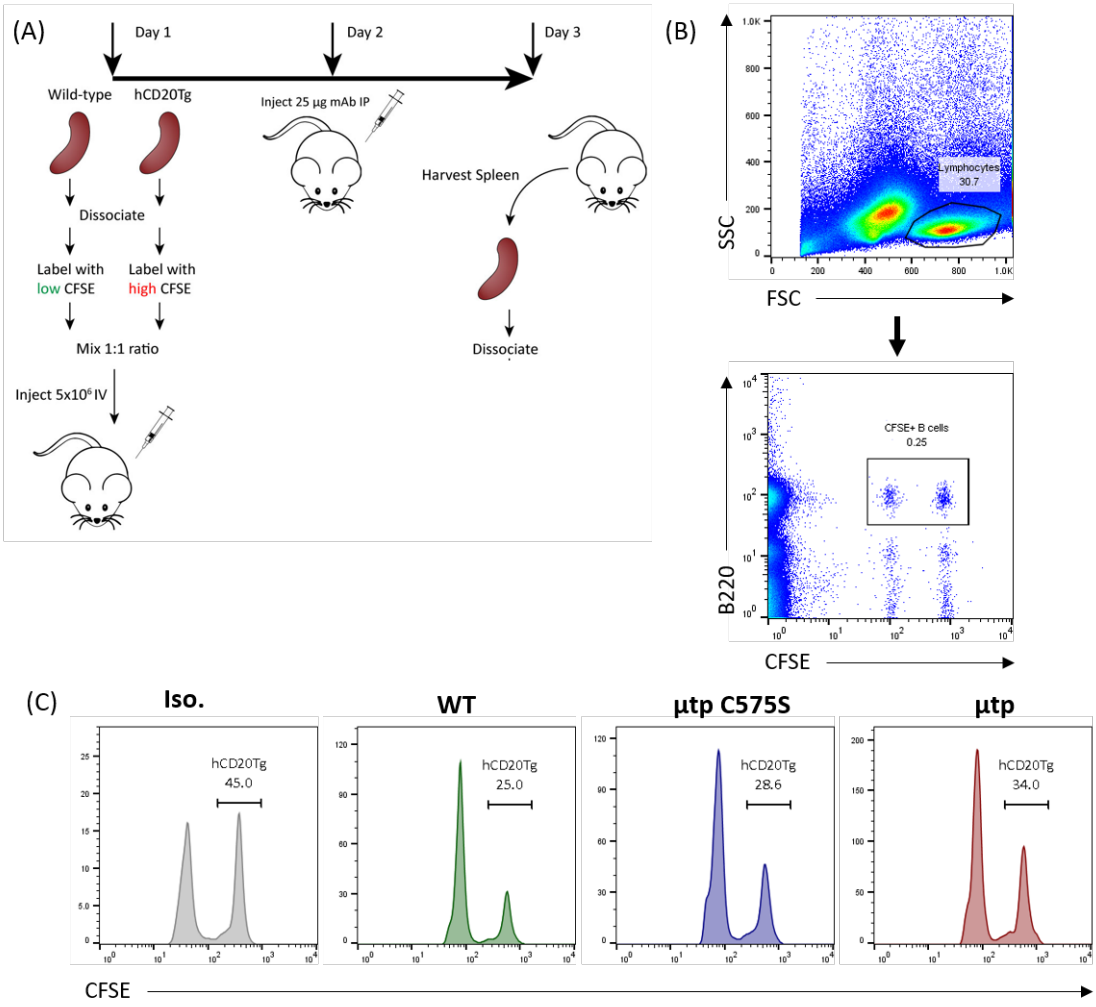

Figure 4.22: Experimental design of hIgG1 μtp fusions in adoptive transfer B cell depletion model.
(A) Experimental design of B cell depletion analysis in adoptive transfer model. A mix of CFSE high hCD20tg splenocytes and CFSE low WT splenocytes were adoptively transferred i.v. into WT C57 BL/6 mice and 24 hours later 25 μg of isotype control (1151 hIgG1), RTX WT, μtp C575S, or μtp was administered by i.p. injection. B cell depletion was calculated using a ratio of CFSE high to CFSE low B220 positive splenocytes. IgG concentration in the serum was also determined by collecting serum by tail tipping and a performing a human hIgG1 ELISA (B) FSC/SSC flow cytometry plot used to gate on lymphocyte population, and CFSE high and CFSE low adoptively transferred splenocytes determined by B220 positive lymphocytes (C) Representative histrograms demonstrating hCD20Tg B cell depletion in adoptive transfer model of RTX μtp fusions. Depletion of hCD20Tg B cell was calculated by a ratio between CFSE low (WT) cells and CFSE high (hCD20Tg) cells.

There was no advantage or disadvantage of the addition of the μtp C575S to RTX in regard to targeting and depleting B cells *in vivo* (Figure 4.23). The calculated depletion of the RTX WT and RTX μtp C575S was comparable at around 50%. However, there was significantly decreased B cell depletion when RTX hIgG1 μtp was administered, as evidenced by the high ratio of hCD20:WT B cells. Before culling, blood was taken by tail-tipping and serum collected by centrifugation. The serum IgG levels indicated that there was only a small variation in the concentration of IgG 24 hours post administration between the three formats (Figure 4.23,B).

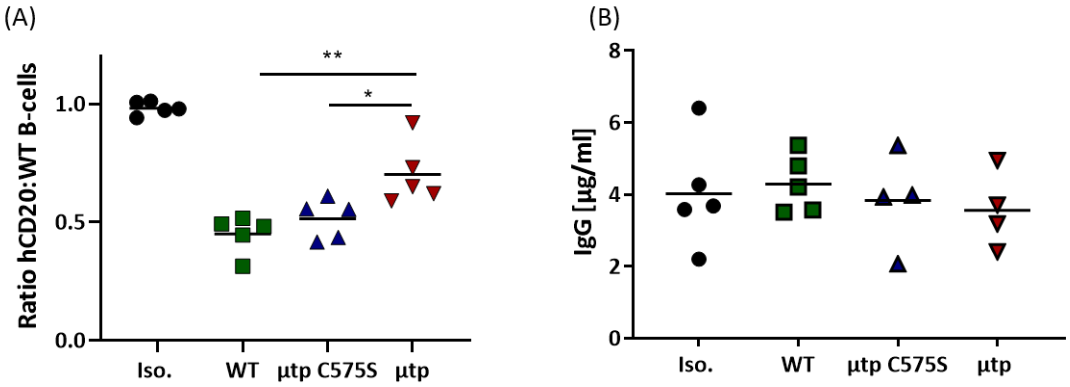

Figure 4.23: Effect of RTX hIgG1 μtp fusions in adoptive transfer B cell depletion model.
(A) A mix of CFSE high hCD20tg splenocytes and CFSE low WT splenocytes were adoptively transferred into C57 BL/6 WT mice and 24 hours later 25 μg of isotype control (1151 hIgG1), RTX hIgG1 WT, μtp C575S, or μtp mAb was administered by i.p. injection. B cell depletion was calculated using a ratio of CFSE high to CFSE low B220 positive splenocytes. IgG concentration was determined by collecting serum by tail tipping and performing a human hIgG1 ELISA (A) hCD20tg B cell depletion was calculated as a ratio of hCD20:WT B cells (B) Human hIgG1 concentration (μg/ml) in mouse serum. Data plotted displaying mean of N=5 mice per group from two experiments. Statistical analysis completed using one-way-ANOVA test. * $P \leq 0.05$; ** $P \leq 0.01$.

The BHH2 mAb were also investigated in the adoptive transfer model. In the context of BHH2 hIgG1 the WT and μtp C575S elicited potent B cell depletion, decreasing the ratio of hCD20:WT B cells to around 0.1 (Figure 4.28,A). However, the μtp hexamer demonstrated significantly lower B cell depletion and only decreased the ratio of hCD20:WT B cells to about 0.9 (Figure 4.28,A), indicating that *in vivo* the hexameric format was not an efficient B cell depleting mAb when compared to WT hIgG1 BHH2. Analysis of the concentration of mAb in the serum after 24 hours indicated that the μtp hexamer had the lowest residual concentration ($\sim$2 μg/ml), followed by μtp C575S ($\sim$5 μg/ml), and the WT mAb ($\sim$7 μg/ml) (Figure 4.24,B). Additionally, the ELISA results suggested that there were low levels of circulating isotype control ($\sim$4 μg/ml), a lower amount than the WT BHH2 (Figure 4.24,B), potentially reflecting small differences in injected dose.

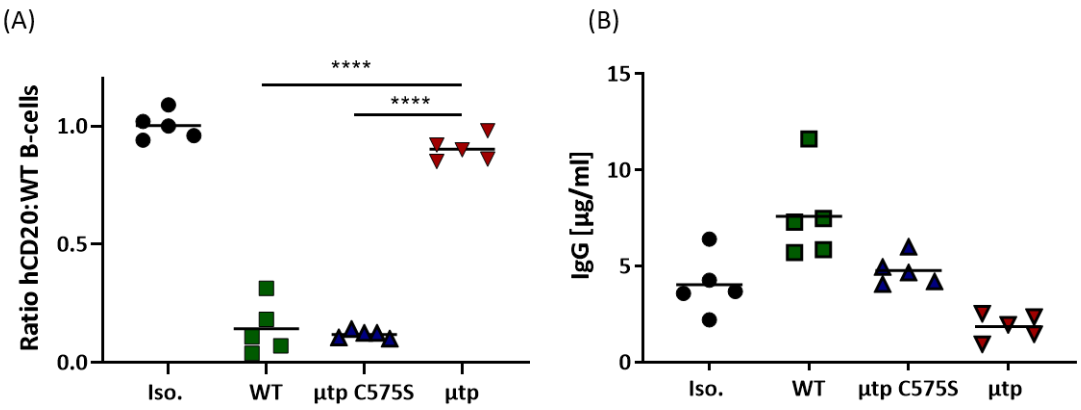

Figure 4.24: Effect of BHH2 hIgG1 μtp fusions in adoptive transfer B cell depletion model.
(A) A mix of CFSE high hCD20tg splenocytes and CFSE low WT splenocytes were adoptively transferred into C56 BL/6 WT mice and 24 hours later 25 μg of isotype control (1151 hIgG1), BHH2 hIgG1 WT, μtp C575S, or μtp mAb was administered by i.p. injection. B cell depletion was calculated using a ratio of CFSE high to CFSE low B220 positive splenocytes. IgG concentration was determined by collecting serum by tail tipping and performing a human hIgG1 ELISA (A) hCD20tg B cell depletion was calculated as a ratio of hCD20:WT B cells (B) Human hIgG1 concentration (μg/ml) in mouse serum. Data plotted displaying mean of n=5 mice per group from two experiments. Statistical analysis completed using one-way-ANOVA test. **** $P \leq 0.0001$.

4.6.3 Systemic B cell depletion

To investigate the safety and efficacy of the μtp technology in a system with high levels of target cells *in vivo*, B cell depletion in hCD20tg Balb C mice was assessed. 100 μg ($\sim$4 mg/kg) sterile filtered antibody was administered i.v. followed by 100μg by i.p. one week later. Blood samples were withdrawn at selected time-points to assess B cell depletion and circulating concentration of hIgG (Figure 4.25,A). Circulating levels of B cells were analysed by flow cytometry by staining for the B cell markers B220 and CD19. The percentage of B cells in the circulation was calculated from double positive B220/CD19 cells in the lymphocyte population (Figure 4.25,B-C). Percentage B cell depletion was calculated as the percentage of B cells compared to a base line reading one day prior to administration of the antibody.

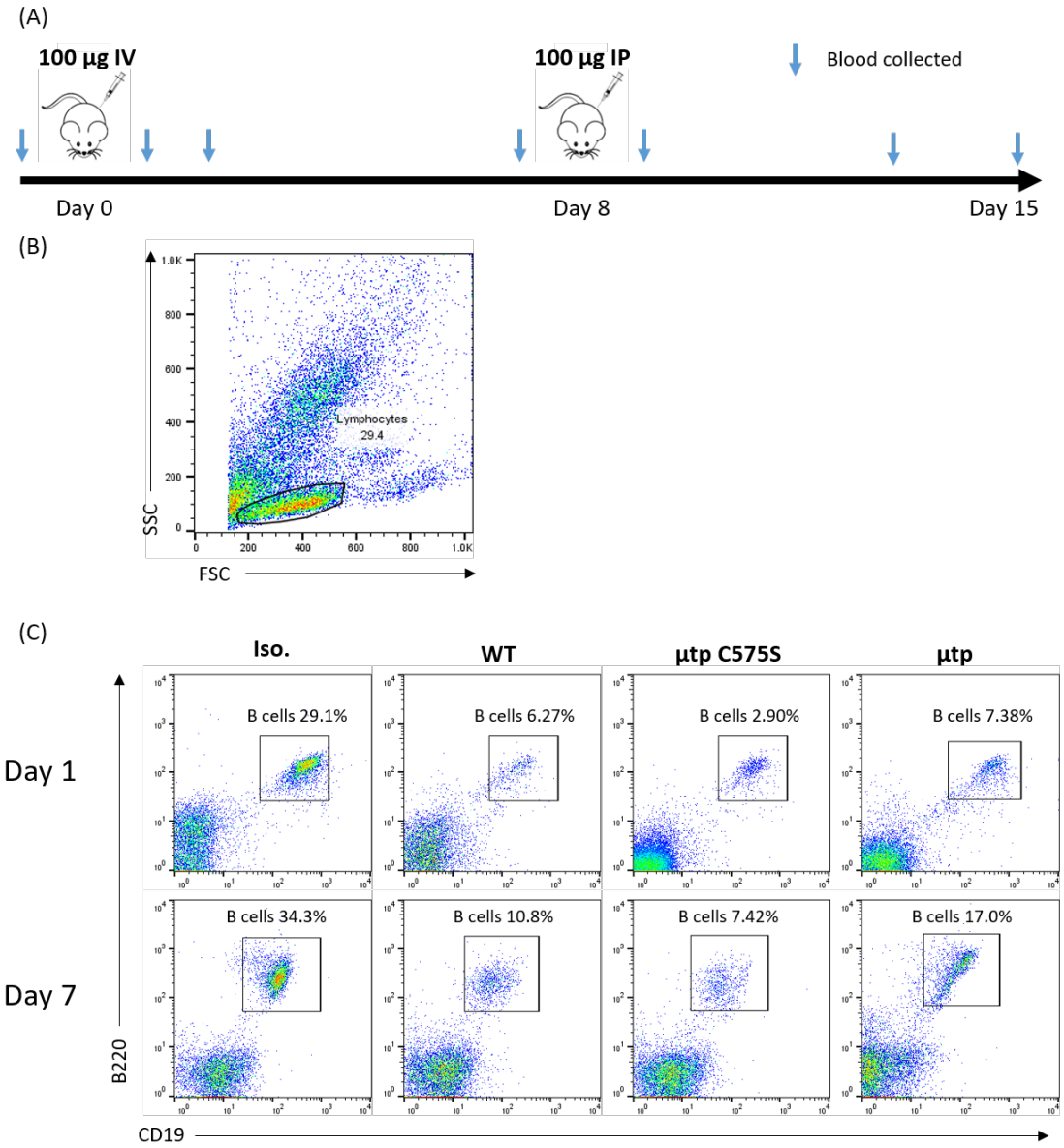

Figure 4.25: Experimental design of hIgG1 μtp fusion *in vivo* B cell depletion in hCD20Tg balb/C mice.
(A) Experimental design of *in vivo* B cell depletion in hCD20Tg Balb/C mice. Isotype control (1151 hIgG1; 100 μg) or RTX mAb (100 μg) administered on day 0 and day 8 to hCD20Tg Balb/C mice. Peripheral blood was collected by tail tipping prior to antibody administration and on days 1, 2, 7, 9, 13, and 15 to measure B-cell levels. 10,000 lymphocyte events recorded, and % B cells in lymphocyte population calculated. (B/C) Gating strategy to detect $B220^{+}CD19^{+}$ mouse B-cells in lymphocyte population (C) Representative FACs plots demonstrating B-cell depletion at days 1 and day 7 for RTX IgG1 μtp fusions.

Administration of the RTX μtp C575S and μtp was well tolerated in all hCD20tg mice, with no adverse effects being observed. The levels of B cells appeared to fluctuate between readings in the control mice, with a range between 60% and 100% of the levels before mAb administration (Figure 4.26,A). The results showed that administration of RTX WT resulted in efficient depletion of peripheral B cells by 48 hours to 20% of the level of circulating B cells seen before treatment. The analysis of peripheral blood on day 7 indicated that B cells had begun to be replenished in the mice. This depletion was sustained out to the day 15 time-point by the additional injection of a further 100 μg i.p. (Figure 4.26,A). The RTX μtp C575S elicited a similar response to RTX WT

and depleted around 80% of circulating B cells over 48 hours post administration (Figure 4.26,A). B cells did appear to recover marginally quicker after 7 days compared to WT, but depletion was sustained over the 15 days period, comparable to WT. The RTX μtp effectively depleted B cells over 24 hours, at a similar rate to the WT and μtp constructs. However, from 48 hours to 15 days the level of B cell recovered at a faster rate than compared to the monomeric counterparts, and had completely recovered to background levels by day 15 (Figure 4.26,A).

In addition to B cell depletion, the serum clearance of the antibody was assessed. The monomeric isotype control, RTX hIgG1 WT, and RTX hIgG1 μtp C575S exhibited a similar trend in mAb clearance over the 15 day period and indicated mAb clearance was not impacted by the addition of the μtp C575S (Figure 4.26,B). In contrast, the μtp hexamer was rapidly cleared from the circulation over the first 48 hours. After the second i.p. administration the IgG concentration was increased, similar to the monomeric WT and μtp C575S, and then cleared over 7 days up until day 15 (Figure 4.26,B).

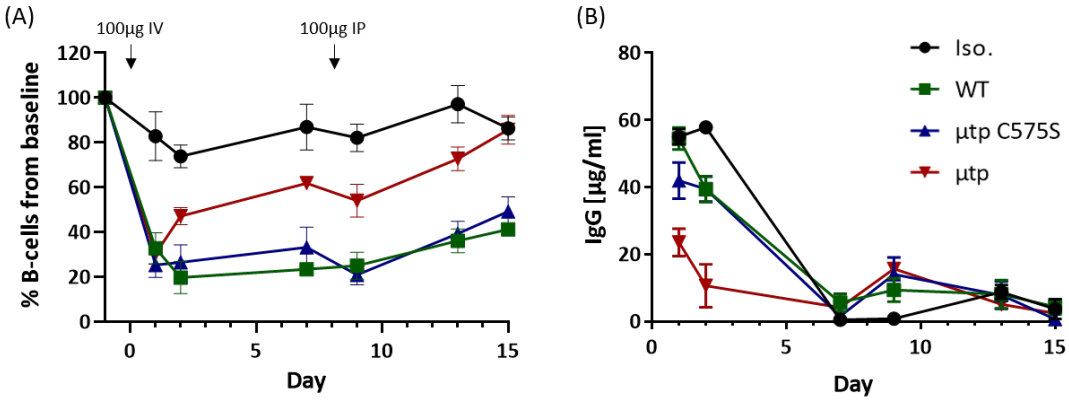

Figure 4.26: Effect of RTX hIgG1 μtp fusions on *in vivo* B cell depletion in hCD20Tg Balb/C mice.
Isotype control (1151 hIgG1; 100 μg) or RTX mAb (100 μg) were administered on day 0 and day 8 to hCD20Tg Balb/C mice. Peripheral blood was collected by tail tipping prior to antibody administration and on days 1, 2, 7, 9, 13, and 15 to measure B cell levels. Depletion analysed by flow cytometry through the calculation of the % B cells ($B220^{+}CD19^{+}$) in the lymphocyte population. (A) Changes in % B cells over the course of the experiment plotted as a mean and SEM of each group compared with B cell numbers prior to antibody administration (B) Plasma was collected at each time-point and used to determine circulating IgG concentration by ELISA. Data plotted is mean and SEM. Results from two experiments; N=5 mice per group.

After 15 days the animals were sacrificed, and B cell depletion was also determined in the inguinal lymph nodes and spleen. The RTX μtp C575S exhibited a similar percentage of B cells in the spleen compared to RTX WT at this time. The μtp hexamer demonstrated slightly lower B cell depletion in the spleen (Figure 4.27,B). Analysis of B cell depletion in the lymph nodes showed a significantly elevated level of B cell depletion with μtp C575S over WT and μtp at day 15 (Figure 4.27,D). Overall, initial *in vivo* investigations indicated that the RTX μtp C575S was comparable in terms of B cell depletion compared with non-modified RTX, whereas the μtp hexamer was less efficient than its monomeric counterparts.

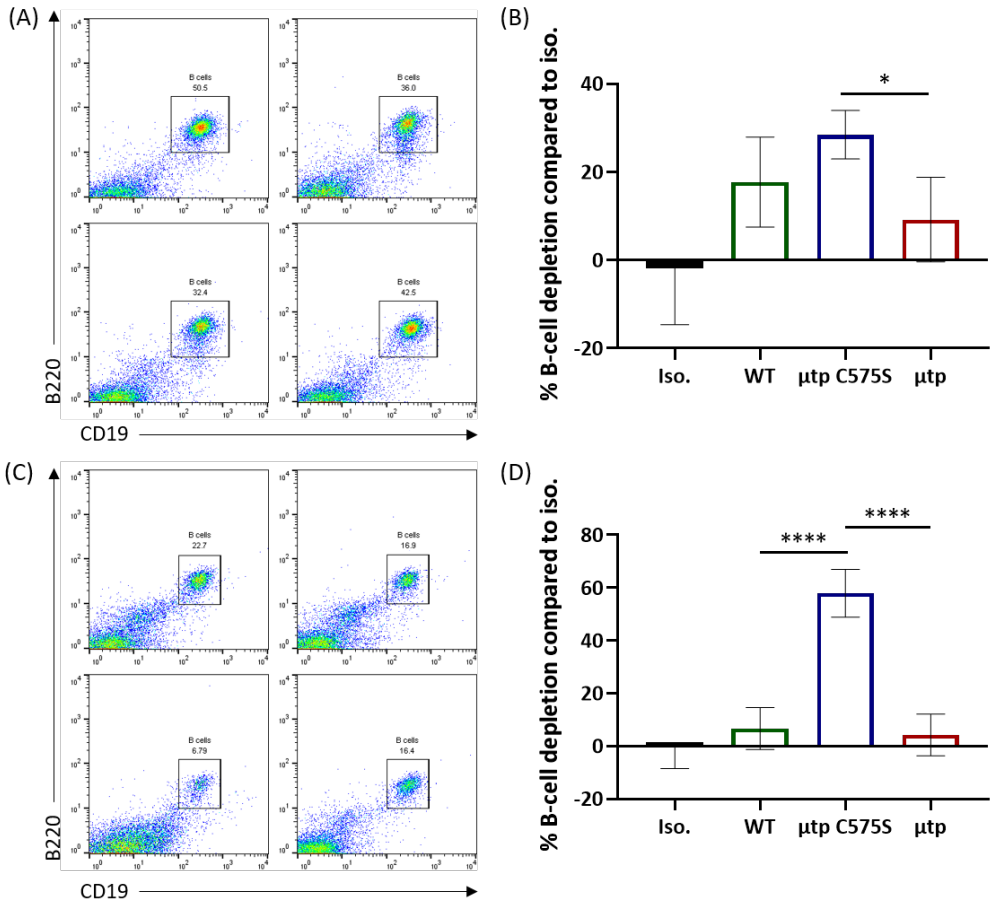

Figure 4.27: Effect of RTX hIgG1 μtp fusions on *in vivo* B cell depletion in spleen and lymph nodes.
Isotype control (1151 hIgG1; 100 μg) or RTX mAb (100 μg) were administered on day 0 and day 8 to hCD20Tg Balb/C mice. Mice were sacrificed in day 15 and spleen and lymph nodes were harvested. Depletion of B cells was analysed by flow cytometry through the calculation of the % B cells ($B220^{+}CD19^{+}$) in the lymphocyte population. (A) Representative flow cytometry plots of B cell depletion in the spleen in lymphocyte population (B) and percentage depletion of B cells compared to isotype control. (C) Representative flow cytometry plots of B cell depletion in the inguinal lymph node in lymphocyte population (D) and percentage depletion of B cells compared to isotype control. Data is showing mean and SEM. Results from two experiments; N=5 mice per group. Statistical analysis carried out by one-way ANOVA analysis. * $P \leq 0.05$; **** $P \leq 0.0001$.

Efficacy of B cell depletion was also assessed with the type II anti-CD20 reagent BHH2 in hCD20Tg Balb/C mice. Here, 10 μg of mAb was administered per mouse i.v., due to the more efficient B cell depleting activity of the type II mAb. Analysis of systemic depletion showed the BHH2 hIgG1 WT demonstrated more efficient B cell depletion than μtp formats, and rapidly depleted B cells over a 48 hour period to 10% circulating B cells. This depletion was sustained throughout the experiment. In the context of BHH2 hIgG1 μtp C575S construct, there was an observed depletion of around 60% of circulating B cells over a 48 hour period, $\sim$30% less than the WT. Additionally, the hexameric μtp only depleted 30-40% of circulating B cells over the same period. Between days 7 and 15 the circulating B cells in animals treated with the WT and μtp C575S mAb were restored at a similar rate up to around 40% on day 15. The μtp hexamer treated animals also recovered over the same period to a final circulating B cell level of 80-90% (Figure 4.28,A). Therefore, although initial depletion with the μtp C575S was slower, it reached the same level of B cell depletion as

the WT by day 7 and thereafter maintained B cell levels at a similar level. In contrast, the μtp construct only maximally reduced B cell levels to $\sim$60%.

The concentration of mAb in the serum was also monitored throughout the experiment (Figure 4.28,B). The systemic clearance of the BHH2 hIgG1 reagents was similar to that of the RTX reagents, albeit starting from lower levels due to the lower starting dose. BHH2 hIgG1 μtp C575S had comparable clearance compared to its WT counterpart. Consistently the BHH2 hIgG1 μtp was rapidly cleared over the first 24 hours with a serum concentration of 2 μg/ml versus 4-6 μg/ml for monomeric reagents. The BHH2 hexamer demonstrated a higher clearance rate than the WT BHH2 after both the initial i.v. administration and second i.p. administration. These results again infer that the mAb containing the μtp C575S fusion demonstrate monomeric WT hIgG1 behaviour *in vivo* in terms of systemic depletion and antibody half-life. Conversely, the preformed hIgG1 μtp hexamer was rapidly cleared and has stunted B cell depletion in the circulation and tissues.

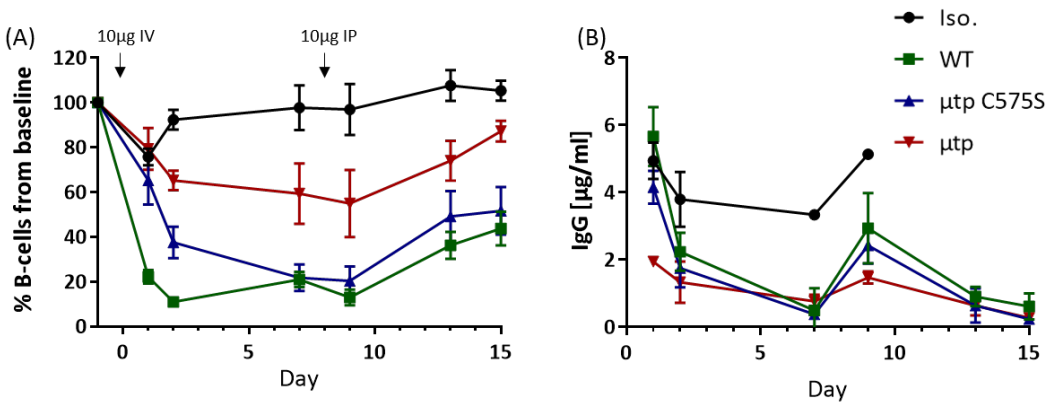

Figure 4.28: Effect of BHH2 hIgG1 μtp fusions on *in vivo* B cell depletion in hCD20Tg Balb/C mice.
Isotype control (1151 hIgG1; 10 μg) or BHH2 mAb (10 μg) were administered on day 0 and day 8 to hCD20Tg Balb/C mice. Peripheral blood was collected by tail tipping prior to antibody administration and on days 1, 2, 7, 9, 13, and 15 to measure B cell levels. Depletion analysed by flow cytometry through the calculation of the % B cells ($B220^{+}CD19^{+}$) in the lymphocyte population. (A) Changes in % B cells over the course of the experiment plotted as a mean and SEM of each group compared with B cell numbers prior to antibody administration (B) Plasma was collected at each time point and used to determine circulating IgG concentration by ELISA. Data plotted is mean and SEM. Results from two experiments; N=5 mice per group.

As with the RTX treated animals the final B cell depletion was calculated in the spleen and inguinal lymph nodes. In contrast to the RTX reagents, the only significant differences in B cell depletion was observed in the spleen. Here, the BHH2 hIgG1 WT had cleared and maintained a significantly higher depletion than the μtp C575S and the μtp hexamer (Figure 4.29,B). Administration of the μtp C575S resulted in $\sim$50% reduction in B cell depletion, whereas the μtp construct resulted in B cell numbers being comparable to the isotype control at day 15. This could indicate that B cells were not depleted in the spleen in this context or had recovered to normal B cell levels. Depletion of B cells in the lymph node was not significantly different, however the WT construct again appeared to have depleted a higher percentage than the μtp C575S and the μtp hexamer

(Figure 4.29,D). These results suggest that the use of a monomeric μtp C575S on-target hexamer may have beneficial properties *in vivo* when compared to IgG hexamers.

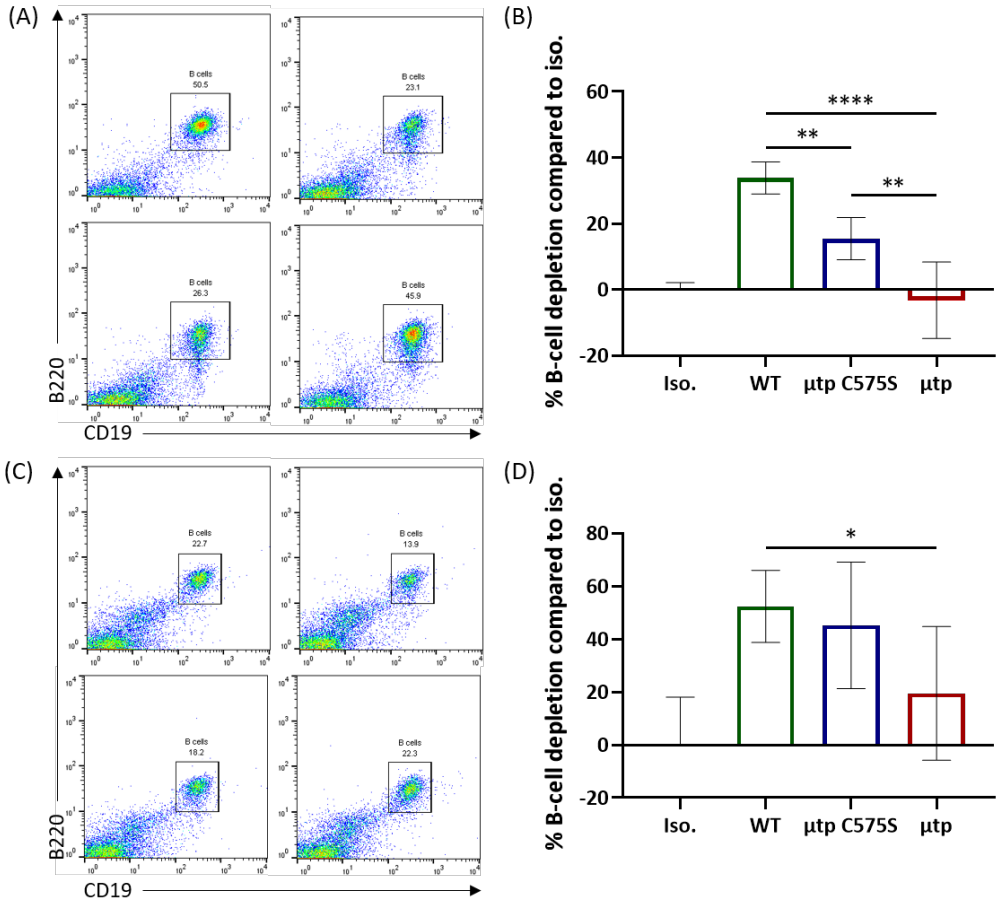

Figure 4.29: Effect of BHH2 hIgG1 μtp fusions on *in vivo* B cell depletion in spleen and lymph nodes.
Isotype control (1151 hIgG1; 10 μg) or BHH2 mAb (10 μg) were administered on day 0 and day 8 to hCD20Tg Balb/C mice. Mice were sacrificed in day 15 and spleen and lymph nodes were harvested. Depletion of B cells was analysed by flow cytometry through the calculation of the % B cells ($B220^{+}CD19^{+}$) in the lymphocyte population. (A) Representative flow cytometry plots of B cell depletion in the spleen in lymphocyte population (B) and percentage depletion of B cells compared to isotype control. (C) Representative flow cytometry plots of B cell depletion in the inguinal lymph node in lymphocyte population (D) and percentage depletion of B cells compared to isotype control. Data is showing mean and SEM. Results from two experiments; N=5 mice per group. Statistical analysis carried out by one-way ANOVA analysis. * $P \leq 0.05$; ** $P \leq 0.001$; **** $P \leq 0.0001$.

One further potential concern with the *in vivo* use of the μtp technology was that the μtp peptide could be cleaved from the hIgG1 after administration by endogenous serum peptidases. It has previously been documented that the C-terminal lysine of the hIgG1 HC is cleavable by endopeptidases, such as CPB [441]. This would therefore mean that the mAb would behave as a WT molecule and exhibit similar half-life and depleting activities. Clipping of the C-terminal lysine was therefore investigated *in vitro* and *in vivo*.

4.7 Endopeptidase clipping of C-terminal fused μtp C575S

To investigate as proof of concept if the C-terminal lysine was susceptible to cleavage by human CPB, the hIgG1 μtp C575S mAb was treated with purified enzyme *in vitro* and incubated for 56 hours. Analysis by SDS-PAGE revealed a decrease in MW of the μtp C575S construct to match the MW of WT hIgG1. The shift in MW was most clearly observed with the treated hIgG1 μtp C575S when compared with untreated hIgG1 μtp C575S and untreated hIgG1 WT molecules in their reduced form (Figure 4.30,A). These results indicated that the C-terminal lysine was accessible and cleavage results in loss of the μtp peptide at the C-terminus. The loss of the μtp also removed the heterogenity observed with the reduced hIgG1 μtp C575S HC's by SDS-PAGE, again suggesting that the differences in glycan processing are due to the presence of the μtp glycan. This provided evidence that the lysine was still accessible to cleavage by CPB. However, this experimental system was artificial and not likely to be replicated *(in vivo*). This experiment involved a long incubation period with the enzyme in PBS in the absence of any other potentially influencing factors (such as other serum components which would act as competitive substrates). Furthermore, CPB is only found at low levels (11.25 μg/L) in the serum of healthy individuals [442], reducing the possibility of cleavage. Therefore, a more physiological experiment was performed assessing the breakdown and cleavage of the μtp C575S construct following *in vivo* exposure.

Western blot was used to analyse the serum of mice previously exposed to the RTX hIgG1 μtp C575S construct, compared to non-cleaved hIgG1 WT and hIgG1 μtp C575S controls not administered to mice. Following SDS-PAGE under reducing conditions and blotting for human HC, all antibodies were detected and with the RTX hIgG1 μtp C575S mAb exhibiting a larger MW than RTX hIgG1 WT, suggesting that there was no or limited cleavage of the C-terminal peptide after 48 hours of exposure *in vivo* (Figure 4.30,B). The RTX hIgG1 μtp C575S detected by western blot appeared to be present in more than one species, indicated by multiple bands, and comparable with the non-cleaved hIgG1 μtp C575S control, suggesting that the μtp C575S was still present at the IgG C-terminus.

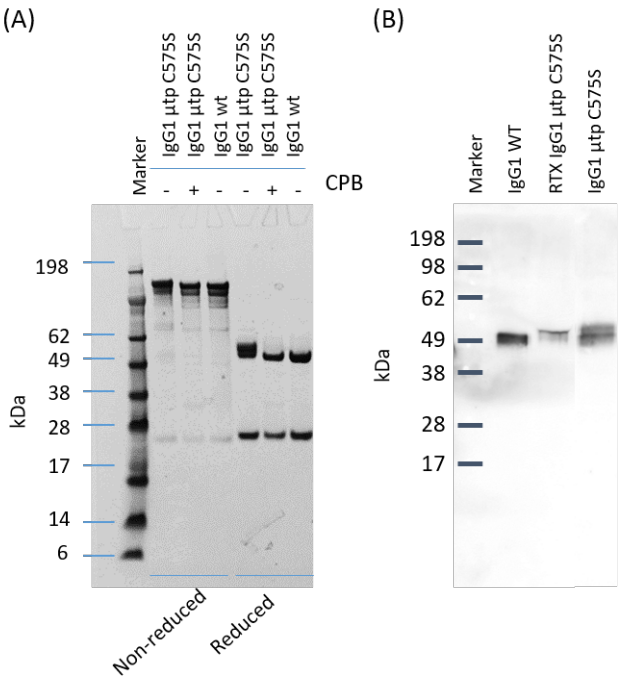

Figure 4.30: Stability of μtp C575S C-terminal fusion *in vitro* and *in vivo*.
(A) 50 µg of hIgG1 μtp C575S was incubated with 1 unit of CPB purified from human pancreas for 56 hours at room temperature. Proteins were analysed by SDS-PAGE gel and cleavage was determined by a shift in molecular weight. Reduced samples were prepared by the addition of DTT to the loading buffer. The molecular weight marker used was the SeeBlue Protein Standard (B) Serum collected 48 hrs post administration was analysed by western blot to detect the cleavage of μtp C575S whilst in the systemic circulation of mice. 2 µg of RTX hIgG1 μtp C575S was loaded onto the gel under reducing conditions for analysis, as calculated by serum concentration of IgG from ELISA results. IgG was detected using a HRP conjugated F(ab')$_2$ goat anti-human antibody.

4.8 Chapter discussion

After the initial quality control and characterisation of the μtp and μtp C575S mAb described in Chapter 3, the hypothesis that such constructs would elicit enhanced effector functionality as a result of preformed or on-target hexamerisation was investigated. Firstly, the hIgG1 μtp C575S was examined to determine if the hIgG1 had gained a propensity to multimerise when in close proximity. To replicate the high local concentration at the target cell surface, antibodies were concentrated to high levels up to 20 mg/ml and analysed for a shorter retention time by SE-UPLC, indicating a shift from a monomeric molecule to a multimer. Mutated μtp C575S at the C-terminus of the hIgG1 antibody enhanced the ability to form multimers in solution compared to WT hIgG1 antibodies (Figure 4.1). This activity was consistent for several constructs independent of V-region (e.g. RTX and Herceptin). At high concentrations the Fc-engineered antibodies spontaneously clustered into large, soluble multimer complexes. The resulting multimer complexes were reversible and returned to a monomeric state when diluted. The maximum multimerisation observed was around $\sim$40% when analysed by SE-HPLC at 50 mg/ml, indicating only a third of these antibodies formed complexes. However, this technique for assessing in-solution multimeri-

sation does have limitations. Firstly, the protein solution will be diluted through the column before assessment allowing complex disassembly which could affect the percentage of multimerisation detected. Secondly, the column used had a resolution limit of 500 kDa, therefore the multimer species cannot be precisely identified. This could be overcome by additional biophysical techniques, such as analytical ultrcentrifugation (AUC), which allows analysis of the solution without dilution or size limitation and provides a precise measurement of the molecular weight at high concentration.

The observed enhancement in C1q binding (Figure 4.2), C4 activation in solution (Figure 4.3) C1q recruitment to the target cell (Figure 4.4), and complement cytotoxicity (Figure 4.5) with preformed hIgG1 hexamers can be explained by the molecule possessing an increased avidity for the hexameric C1q [183]. The data here is in agreement with recent literature suggesting CDC is optimally activated by a hexameric Fc arrangement [197]. The results demonstrated a 5-fold increase in activity for the RTX μtp hexamer compared to the RTX WT when targeting Ramos cells, based on the calculated EC50 values. When Raji cells were used as a target very little CDC was evoked by the WT hIgG1 RTX mAb, such that an EC50 value was unrecordable over the concentration range, but significant CDC was observed with the μtp hexamer construct, allowing an EC50 to be calculated which indicates greatly enhanced CDC activity.

The data for C1q binding, C1q recruitment, and complement cytotoxicity of RTX hIgG1 μtp C575S demonstrated a monomeric mAb with hexamerisation enhancement as detailed in recent publications [197, 271]. This antibody construct displayed activity akin to an antibody monomer in solution, demonstrated by SE-UPLC at physiological conditions at 1 mg/ml, C1q binding in an ELISA format (Figure 4.2) and the lack of spontaneous C4 activation in human serum (Figure 4.3). However, when bound to an antigen at a cell surface, the RTX μtp C575S displayed activity more comparable to an antibody hexamer, exhibited as enhanced C1q recruitment (Figure 4.4) and a 2-fold enhancement in CDC activity over the WT mAb (Figure 4.5).

The enhanced complement activity observed with RTX μtp C575S was directly associated with enhanced C1q recruitment to the target cell surface. As previously mentioned this may be driven by enhanced Fc:Fc interactions which results in more hexamers at the cell surface. However, the CDC activity of the RTX μtp C575S does not match the level of the preformed RTX μtp hexamer. This suggests that the formation, stability, or number of Fc:Fc interactions that lead to hexamers is not optimal, and reduced compared with covalently linked pre-formed μtp hexamer. As described earlier in this chapter, when characterising the hexamerisation enhancement of these antibodies there was an upper limit of $\sim$40% hexamer formation in solution with hIgG1 μtp C575S. It can therefore be proposed that if the hexamerisation enhancement of these monomeric molecules

were to be optimised, the C1q recruitment and complement activation would be further enhanced to the level of an IgG hexamer.

The type II BHH2 antibodies also exhibited complement enhancement, although to a lesser extent (Figure 4.6). Data from the C1q binding ELISA indicated that there was an increase in C1q avidity with the μtp construct and potentially a small increase with the μtp C575S. There was also a modest enhancement in C1q recruitment and an improvement in the CDC activity when targeting the sensitive Ramos cell line, but not Raji cells except with the hIgG1 μtp format. An EC50 value of 10 μg/ml could be calculated for the Ramos cells, whereas the EC50 for the BHH2 hIgG1 WT was unable to be defined. These results indicated that addition of the μtp but not μtp C575S was sufficient to effectively overcome the low CDC activity inherent in type II mAb, even in the presence of complement defence molecules. Enhanced CDC activity was observed with BHH2 μtp hexamer against both Ramos and Raji cells with EC50 values of 0.062 μg/ml and 0.642 μg/ml, respectively. This ten-fold difference likely reflects the difference in complement defence molecules. The BHH2 μtp hexamer demonstrated an increase in C1q binding and CDC compared to WT hIgG1, but this was reduced when compared to the RTX μtp counterpart. This supports the type II nature of this antibody and indicated that even as a preformed hexamer the type II mAb was less active in terms of CDC. Overall the results particularly confirmed that CDC activity is greatly improved when hIgG1 is present as a hexamer, independent of the type of anti-CD20 antibody. Hexameric hIgG1 was shown to be able to overcome any inherent lack of complement activating ability, as with type II CD20 mAb, and endogenous complement defence (Raji cells) to initiate efficient complement cell killing. This is further evidence that complement is optimally activated when Fc are arranged hexamerically at the target cell surface. The hexamerisation enhanced μtp C575S constructs also demonstrated this, albeit to a lesser extent.

Type II antibodies bind to different epitopes in CD20 that type I mAb and potentially different CD20 complexes but they do not redistribute CD20 into lipid rafts to cluster mAb at the cell surface, a process thought to aid complement activation [268]. This clustering is thought to underpin the increased C1q deposition seen with type I CD20 reagents [132]. These results indicate that the attraction elicited by addition of the μtp C575S mutant was not strong enough to force efficient CD20 reorganisation or clustering of type II anti-CD20 antibodies at the cell surface, demonstrated by the reduced C1q recruitment and subsequent CDC activity.

Taken together, these results indicate a clear advantage of preformed μtp hexamers in the recruitment of C1q and induction of complement-mediated lysis. Additionally, there was evidence that addition of μtp C575S peptide to hIgG1 provides the ability of an anti-CD20 mAb to hexamerise after target cell binding, thereby recruiting more C1q and inducing CDC more efficiently, akin to

the preformed hexamer, albeit not as efficiently (Figure 4.31). This was more evident with the type I RTX than the type II BHH2, most likely a result of their underlying characteristics as detailed above.

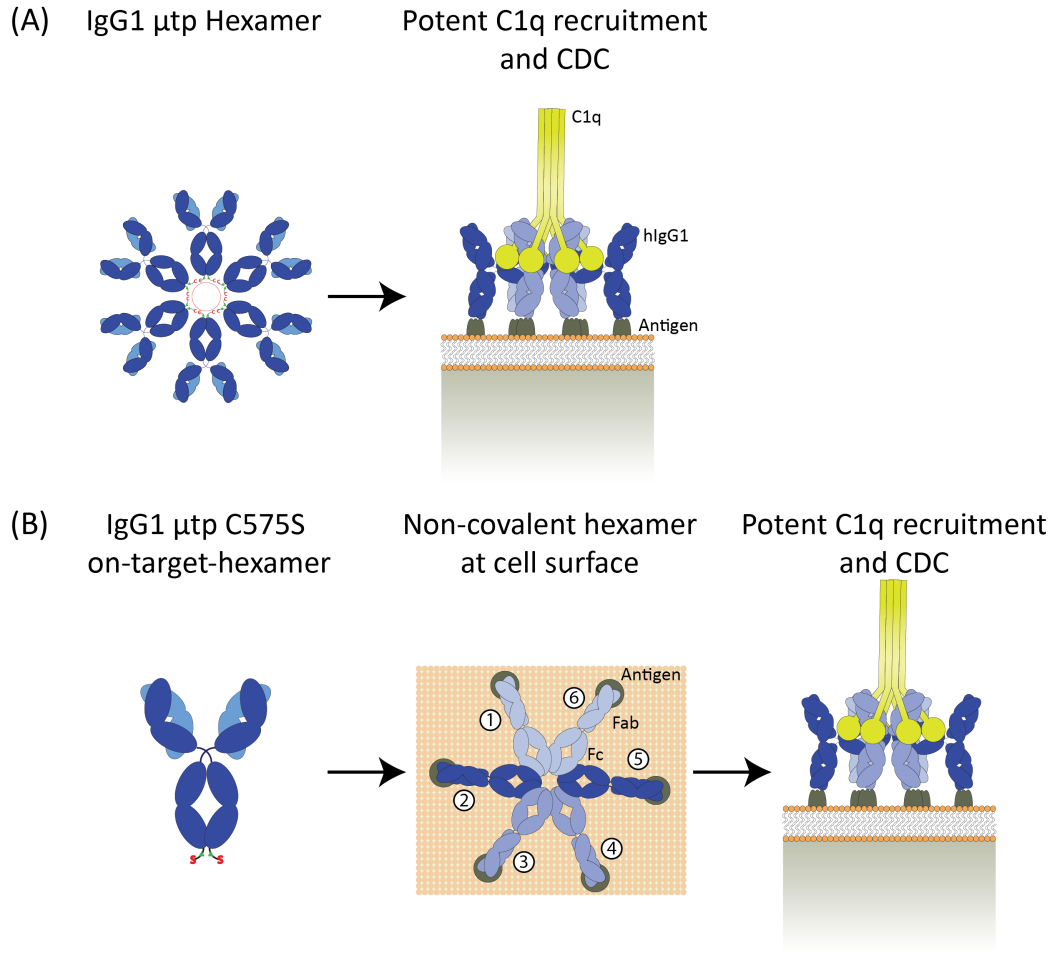

Figure 4.31: On-target hexamerisation and CDC enhancement by hIgG1 μtp technology.
(A)Fusion of the μtp to hIgG1 results in covalent IgG hexamers that demonstrate enhanced C1q recruitment and complement cytotoxicity (B) Fusion of the μtp C575S to hIgG1 results in a monomeric, hexamerisation enhanced IgG molecule that forms non-covalent hexamer structures at after antigen binding to result in enhanced C1q recruitment and complement cytotoxicity.

Results for the binding of hIgG1 μtp to FcγRs was inconsistent between SPR and CHO cells expressing FcγR. SPR analysis suggested that the FcγR bind with equivalent affinity to both hIgG1 μtp constructs as well as WT IgG1 (Table 4.1). The use of SPR to measure binding affinity may not be the most efficient method to compare hIgG1 monomers and hexamers. The immobilisation of antibody to the chip could result in an immune-complex like environment, with closely aligned Fc's, similar to that of the μtp hexamer and could be influenced by the same avidity interactions hypothesised to occur with the hexamer. By decreasing the number of units immobilised on the chip or immobilising the FcγR on the chip could help resolve this. Therefore, the examination of hIgG1 μtp mAb binding to FcγR expressed on CHO cells may be a more relevant assay. Here the results indicated that WT and μtp C575S RTX hIgG1 constructs had similar binding efficiencies to the FcγRs, whereas binding to FcγRs on CHO cells appeared to be significantly enhanced in

the context of the hIgG1 μtp hexamer (Figure 4.8). However, the detection antibody used was specific for the human Fc domain, and so for each hexameric μtp bound 6 Fc domains would be available, which may explain the greater binding. Alternatively, the greater observed binding may be explained by the higher avidity of the hexameric structure in a scenario where the affinity for FcγR is low and washing is performed during the flow cytometry. Here, antibody would be expected to be released, due to low affinity/high off-rate unless it is recaptured again. Such recapture would be more likely with the hexameric mAb (effectively 6 x higher concentration of Fc). When observing antigen binding in Chapter 3, the hIgG μtp hexamers had lower MFIs indicating potentially lower levels of binding or structural occlusion preventing multiple detection antibodies binding the Fc's of a hexameric complex. Therefore, the observed increase in MFI of IgG bound CHO cells may imply that there is enhanced FcγR binding with the hIgG1 μtp hexamer. Such behaviour would not necessarily be expected in SPR analysis where flow conditions are present and effective antigen concentration/localisation may be lower.

Even though the binding appeared to be enhanced with hIgG1 μtp hexamers, the lack of improvement in FcγR mediated effector functions suggests that a multimeric Fc does not optimally augment the engagement and activation of FcγR's on NK cells (Figure 4.9) or macrophages (Figure 4.11). This is perhaps not surprising as Fc:FcγR binding occurs at 1:1 stoichiometry [114, 443–445] (unlike C1q which is a 6:1 relationship with Fc). This indicates that the optimal interaction or activation of these receptors does not involve Fc multimers, unlike C1q molecules. Additionally, in the previous chapter, the CD20 binding for the hIgG1 μtp hexamers demonstrated a 2.6-fold lower signal than the WT, suggesting a constricted binding of secondary antibody to the Fc. This questions the availability of the hexameric Fc for FcγR binding and suggests that the binding ratio of antibody hexamer complex to FcγR was 1:1. In this scenario only one FcγR is bound and activated to initiate an immune response similar to a monomeric IgG, with the recruitment and activation of only one receptor per hexamer.

Alternatively, the lack of increased FcγR-mediated effector function could be explained if the hexameric (μ) and hexamerisation enhanced (μtp C575S) mAb caused more rapid internalisation of the target from the cell surface. However, only the RTX hIgG1 μtp constructs demonstrated any increase in internalisation. The BHH2 μtp C575S on-target hexamer and μtp hexamer did not internalise more efficiently than the WT hIgG1 construct, and also did not demonstrate enhanced FcγR-mediated effector functions. Therefore, internalisation of μtp constructs is likely not significantly restricting the augmentation of such effector mechanisms. The more efficient internalisation observed with RTX hIgG1 μtp C575S could be accounted for by the enhanced receptor clustering that is induced by this mAb. However, the same was not observed for the BHH2 μtp hexamer, which could indicate that even as a preformed hexamer, receptor clustering does not

occur with the type II reagent. Therefore, the internalisation induced by μtp constructs is likely to be antigen and epitope-dependent. To address this, further anti-CD20 antibodies and different antigens could be examined for their clustering and internalisation. As opposed to solely being a negative consequence any internalisation benefit found for these constructs could be exploited by ADCs to more efficiently deliver a toxic payload into the target cell. A similar strategy has recently been demonstrated with a bispecific ADC targeting Her2 and CD63. Her2 allows for the mAb to specifically target Her2$^+$ tumour cells and CD63 (lysosome-associated membrane glycoprotein 3) facilitates efficient internalisation and lysosomal transport to deliver the cytotoxic payload [446].

The multimerisation of anti-CD20 mAb was however able to influence DCD. The type-I and type-II anti-CD20 antibodies [268] elicit a cell death response through different mechanisms of action. Type-I mAb, such as RTX, redistributes CD20 into lipid rafts in the cell membrane where they can engage with a host of signalling proteins and enzymes associated with BCR signalling [270]. The increase in DCD with the RTX μtp hexamer (Figure 4.12) suggests that the hexameric aggregation of CD20 and mAb molecules at the cell surface after binding has a positive impact on inducing DCD with type I CD20 mAb. These results are in agreement with studies whereby cross-linking RTX with an anti-human IgG significantly increases DCD of Ramos cells [161].

The type II mAb, BHH2, binds to CD20 in a different conformation and binding ratio to RTX; only one type II mAb has been proposed to bind a CD20 tetramer, whereas two type I mAb bind a CD20 tetramer [268, 270]. This difference is thought to be related to the efficiency of type II mAb inducing cell death by evoking a programmed cell death pathway through actin cytoskeleton remodelling, resulting in subsequent homotypic adhesion [274] and lysosomal membrane permeabilisation [275], for which antibody bivalency is a pre-requisite [160]. The type II BHH2 antibody inherently induces a strong DCD signal without the requirement for further clustering of targeting antibodies at the cell surface (Figure 4.13), indicating the binding geometry is the driving force for anti-CD20 mAb induced DCD. The decrease in cell death with the type II BHH2 μtp hexamer (Figure 4.13) suggests that this optimal binding geometry was affected by mAb multimerisation and was detrimental to induction of a DCD signal with such μtp fusion mAb.

The whole blood B cell depletion assay allows for a more complete analysis of the potential effects of the various mAb formats in deleting target cells. Here, multiple effector mechanisms are simultaneously (and potentially competitively) available, enabling the net effect of CDC, NK cell-mediated ADCC, and DCD, to be assessed, in addition to the effects of other FcγR-bearing cells such as neutrophils [447]. A slight trend for reduction in B cell depletion for the hIgG1 μtp C575S, and a statistically significant reduction for μtp hexamer constructs was seen (Figure 4.17). Additionally, the presence of the hIgG1 μtp hexamers suppressed both IFN-γ secretion, when

compared to hIgG1 WT and μtp C575S mAb (Figures 4.17, 4.19). It has already been shown that BHH2 μtp hexamers do not more efficiently internalise compared to BHH2 WT. Therefore, the decrease in B cell depletion mediated by BHH2 μtp constructs cannot be accounted for by internalisation decreasing surface bound immune complexes available to recruit FcγR-bearing cells, such as NK cells. The only other effector function that has been demonstrated to be augmented by the preformed μtp hexamer and the μtp C575S constructs is complement. Together, these data suggest that over-activation of the complement system may have a detrimental effect on the efficacy of an B cell depletion in whole blood. This result was consistent across both types of anti-CD20 antibody.

The complement by-product C3b can opsonise cells during an immune response, including neighbouring cells not directly being targeted by the complement system [448]. A previous report has described a C3b-dependent down-regulation of NK cell binding to IgG immune complexes and cytotoxicity of RTX coated cells [449]. Furthermore, inactivation of complement *in vivo* has been demonstrated to improve mAb therapy [450]. NK cells are characterised by their cytotoxic activities and secretion of cytokines, such as IFN-γ and TNF-α, in response to target recognition through activation of FcγRIIIa [451–454]. These results may indicate that B cell depletion in the whole blood assay is dictated by FcγRIIIa$^+$ NK cells and recruitment leads to the production of an IFN-γ response. Therefore, it is possible the decrease in efficacy observed is caused by a reduction in NK-cell mediated cytotoxicity through complement over-activation and C3b-mediated blockade of FcγRIIIa.

FcγRIIIa has a polymorphism at position 158 that effects IgG binding to the receptor. The residue at this position is either a valine (V158) or phenylalanine (F158) [455], where the V158 polymorphism has an increased affinity for hIgG1 [130] as described earlier. NK cells expressing FcγRIIIa are considered to be important in the therapeutic effects of mAb through the efficient induction of ADCC. Administration of RTX to non-Hodgkin lymphoma patients who are homozygous for V158 have been reported to exhibit a superior response to therapy when compared with patients who carry the one or two copies of the F158 polymorphism [131, 456]. However, other studies have not confirmed this association and contradictory evidence suggests no such relationship exists; reviewed by Mellor et al [457]. In the whole blood B cell depletion assay performed here, the donors had been genotyped as part of another study [440] and individuals selected based on their FcγRIIIa polymorphism status (VV, VF, or FF for FcγRIIIa). The current data did not indicate any clear relationship between FcγRIIIa polymorphism and B cell depletion or IFN-γ production in the whole blood assay, albeit a relatively small number of donors for each genotype were assessed, reducing the power of any statistical analysis. There were no statistically significant difference was observed when using WT, μtp C575S, or μtp hexamer reagents between the three pheno-

types (Figures 4.18 and 4.19). Although donors expressing the F/F genotype did generally display the lowest overall B cell depletion when treated with RTX.

The safety of the Fc-engineered μtp C575S monomers *in vivo* was of an initial concern. The multimeric Fc arrangement of a hexameric μtp hIgG molecule has demonstrated enhanced binding to C1q and triggering of C4d without the requirement for antigen. The risk of non-specific immune activation and resulting anaphylactic shock was therefore deemed to be high with a hexameric hIgG and also possibly with the μtp C575S monomer. However, initial studies demonstrated that the hIgG1 μtp C575S monomer hIgG1 μtp hexamer were both safe for administration up to 100 μg per animal through i.p. and i.v. injection routes in the absence of target. However, it should be noted that mice typically display lower levels of complement activity that humans, so this may not give clear indication of potential toxicities.

Analysis of the μtp fusion mAb half-life indicated that μtp C575S constructs exhibited comparable binding to FcRn (Figure 4.20) and comparable clearance rate to their WT counterpart (Figure 4.21). This suggested that RTX hIgG1 μtp C575S hexamers are not formed non-specifically in the peripheral circulation. However, the hexameric μtp construct was rapidly cleared from the circulation, even though the molecule had enhanced FcRn binding. This is consistent with previous results that demonstrated hIgG1 Fc μtp hexamer had rapid serum clearance, even in the context of mutations that increased FcRn binding [399]. These observations seem paradoxical as binding to FcRn should extend mAb maintenance in the serum. Indeed, enhancing the affinity of hIgG1 for hFcRn using the YTE mutation [347] or hIgG1 for cynomolgus FcRn using T250Q/M428L mutations [458] should increase the circulating serum half-life of mAb. However, enhanced FcRn binding does not appear to correlate to increased serum half-life with μtp hexamers. This could be explained by the enhanced interaction at pH 7.4, the pH at which antibodies are released back into the serum after recycling [151]. Enhanced interaction at pH 7.4 may prevent release of the hIgG1 μtp hexamers into the circulation and contribute to the molecules clearance.

Previous studies have highlighted that soluble immune complexes are efficiently removed from the serum by liver endothelial and kupffer cells via interaction with FcγRs [459, 460]. This is reviewed further in [461] where it is documented that injection of immune complexes containing more than two IgGs are more abundantly removed from the circulation by the liver. The hexameric IgG is a large molecular complex with a MW of $\sim$900 kDa. Therefore, there was a high possibility that the hIgG1 μtp hexamer was binding to FcγR in the liver, resulting in removal from the circulation. Other factors could also contribute to rapid clearance. As stated in the previous chapter, IgM is produced and secreted with high mannose glycan structures. Accordingly, the IgG μtp hexamer could also be hypothesised to possess high oligomannose structures at its glycosy-

lation sites due to similar production and golgi processing of recombinantly expressed IgM. The presence of high mannose glycans on proteins results in more rapid elimination from the circulation of mammals [462, 463]. Clearance is mediated by the mannose receptor (MR), which is expressed on immune cells and endothelial cells [464], and occurs via endocytic and phagocytic routes [465]. Antibodies containing high mannose glycan structures have been previously shown to be cleared significantly faster than non-high mannose-containing antibodies in the circulation of mice [466] and humans [463]. It could therefore be suggested that an IgG μtp hexamer with oligomannose glycan structures will demonstrate enhanced mAb clearance through interaction with FcγR and MR. This could be assessed by performing glycan analysis of the IgG μtp hexamer.

Additionally, a recent study with hIgG Fc μtp hexamers has suggested that *in vivo* administration of hIgG hexamers in mice results in internalisation and downregulation of murine FcγR expression [399]. The study suggested that this process is mediated by Fc μtp hexamer binding which result in interalisation and degradation of the Fc μtp hexamer:FcγR complex, thereby removing the molecule from the circulation. This could also help account for the significant decrease in the molecules half-life. The expression and downregulation of FcγR *in vivo* after administration of the current μtp hexamers in future studies could be used to address if these constructs also result in this phenomenon.

Having established that both hIgG μtp constructs were able to be delivered safely, they were assessed in B cell depletion models; either adoptive transfer or systemic B cell depletion. Although not optimal, the hIgG1 is able to bind to all murine FcγRs and efficiently activate ADCC and ADCP [283, 467] so there was no issue with using hIgG1 in a murine system. Overall, the data suggests that there was no observable improvement in the efficacy at the doses tested. The RTX μtp C575S was proven to be safe with no immediate adverse reactions following administration of a low dose of 25 μg into a mouse with a low number of target cells in the adoptive transfer model. The results also indicated that after addition of the μtp C575S the molecule retained the functionality to deplete B cells, as expressed by a ratio of target to non-target cells that had accumulated in the spleen 48 hours post adoptive-transfer (Figure 4.23,A). Analysis of the serum IgG also indicated that the half-life in the presence of the target antigen had not been negatively affected by the μtp C575S (Figure 4.23,B).

The B cell depleting efficacy of μtp mAb were also investigated in the context of the type II BHH2 anti-CD20 reagent *in vivo*. Type II reagents such as BHH2 demonstrate highly efficient *in vivo* B cell depleting activity [468] which was observed in the current experiments with the monomeric WT and μtp C575S. The μtp hexamer depleted significantly less, which can be partly explained by the advanced clearance observed with quantification of serum IgG levels (Figure 4.24).

The indication of safety and B cell depleting activity in the adoptive transfer mouse model led to investigation in an *in vivo* model with a physiologically relevant number of target levels and administration of an increased antibody dose (100 μg). The use of the hCD20tg model allows for the measurement of the depletion and recovery of endogenous B cells to be measured over time in a physiologically relevant environment, such as systemic circulation, with extensive B cell presence in secondary lymph organs such as lymph nodes and spleen. The systemic clearance rate of antibodies was also monitored over the course of the experiment. In both *in vivo* assays the systemic B cell depleting activity and the clearance rate of the RTX and BHH2 hIgG1 μtp C575S was unaltered by the Fc-engineering approach (Figures 4.26, 4.28). In syngeneic mouse models there is compelling evidence to suggest that B cells are depleted by RTX predominantly by FcγR effector functions and complement activation is redundant [253]. This data is consistent with these results and with the results from the *in vitro* effector function assays, where no enhancement was observed with FcγR-mediated effector functions, only with CDC. As mentioned previously, adminsitration of Fc μtp hexamers resulted in internalisation and downregulation of FcγR in mice [399]. If this is the case with full-length hIgG μtp hexamers it could also help explain the decrease in B cell depletion, due to a lower availability of FcγR-bearing cells.

However, there did appear to be augmented B cell depletion with RTX hIgG1 μtp C575S in the lymph node, that was observed in 2 independent experiments. The greater B cell depletion in this environment could be due to a higher dependence on complement-mediated cellular lysis as opposed to recruitment of FcγR-bearing cells. This effect was not seen with the BHH2 construct, perhaps supporting the notion that complement is important for this effect, as BHH2 is much less efficient at CDC even as the μtp C575S construct. To address such a requirement for complement in the lymph nodes, the use of a C1q KO mouse model or complement inhibiting hIgG1 Fc mutations could be utilised in future studies.

The lack of any augmentation in B cell depleting activity *in vivo* in most compartments could have been attributed to cleavage of the μtp C575S peptide by serum enzymes. The current data indicates that the IgG C-terminal lysine appears to be susceptible cleavage when treated with CPB *in vitro*, despite the addition of the μtp (Figure 4.30). CPB is present at low levels in serum (11.25 μg/L) [442], and so may have limited effects under physiological conditions. However, other endoproteases such as, carboxypeptidase N, are present at higher levels and are also potentially involved in removal of C-terminal lysine residues [469]. This may lead to issues with stability when used *in vivo* in humans, whereby the μtp is removed in the serum, eliminating the hexamerisation enhancement. Cleavage of the μtp peptide by CPB *in vitro* provided further evidence that the differences in glycosylation between the two species observed on SDS-PAGE was due to glycans attached to the Asn563. However, when analysed in the serum 48 hours after adminis-

tration, there was indication that the μtp C575S was still present and not cleaved. This would suggest that *in vivo* the fusion peptide may not be cleaved within the first 48 hours. The caveat being that this was assessed in a mouse system where there would be murine carboxypeptidase enzymes present.

The current results therefore indicate that the hIgG1 μtp C575S is monomeric in solution, but upon CD20 binding the mAb induces efficient antigen reorganisation and Fc clustering thereby recruiting C1q and activating the classical complement pathway (Figure 4.31). Presently, no clear advantages (with the one potential exemption of lymph node depletion) have been observed in human B cell depletion models or *in vivo*, although the μtp C575S fusion mAb displayed similar pharmacokinetic properties to hIgG1 WT. The complement activity, FcγR-mediated effector functionality, and *in vivo* analysis of the current μtp C575S on-target hexamer and μtp hexamer constructs is summarised in Figure 4.32. Further exploration of the μtp C575S on-target hexamer for therapeutic applications would likely centre on understanding if the LN is a region that can be more effectively targeted in this way and also exploring other targets that may be more susceptible to complement killing, such as bacteria [378, 470].

In the context of the μtp hexamer, the data clearly indicate that this format has issues with spontaneous (non target-mediated) activation of complement and therefore potential toxicity as well as very short-half-life. Therefore, development in this context would have to be very careful and perhaps exploit the short-half-life to its benefit.

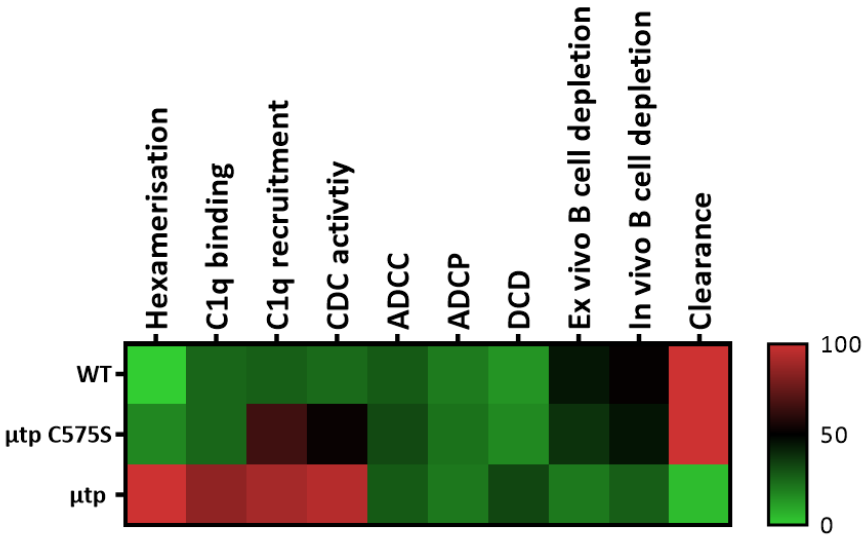

Figure 4.32: Summary of the *in vitro* and *in vivo* activity induced by anti-CD20 μtp fusion mAb.
The complement, FcγR-mediated, and B cell depleting activity of anti-CD20 mAb Fc-engineered with as either on-target hexamers (μtp C575S) or preformed hexamers (μtp) expressed as a percentage (%) of maximal activity

Chapter 5

Characterisation of hexamerisation-enhanced μtp C575S Fc-engineered and isotype switched anti-CD20 antibodies

5.1 Chapter introduction

In the previous chapter it was demonstrated that hIgG1 could be engineered to gain activity consistent with IgG on-target hexamerisation through fusion of the μtp C575S peptide. This was demonstrated by increased on-target C1q recruitment and complement-mediated cell death. This hexameric Fc arrangement is thought to have higher avidity interactions with the C1q molecule [197]. Following *in-vitro* characterisation it was demonstrated that the only effector function that was augmented with hIgG1 hexamers (μtp) and on-target hexamers (μtp C575S) was complement-mediated cell death. In addition to Fc clustering, there are several other features of the hIgG1 Fc that have been shown to play a part in the interaction between the Fc and C1q, including amino acid residues in the hinge and upper CH2 domain, and glycosylation in the CH2 domain. The amino acid contacts have been identified and previously reported in the literature, which include: E233, L234, L235, G236, G237 in the hinge [199] and E269, D270, E294, S298, Y300, K322, A327, P329, P331 in the CH2 domain [199, 344, 421]. These studies have also undertaken mutagenesis analysis that demonstrated mutating these residues results in decreasing or abolishing CDC activity compared to WT hIgG1. Two such examples of single mutants that render IgG1 unable to recruit C1q are P331S [421–423] and K332A [471].

In addition to amino acid binding contacts in the hIgG Fc, gylcosylation in the CH2 is also important and can be modified to provide both CDC-enhancing and -inhibiting activities [438, 472–474]. Complement enhancing glycoengineering was recently exemplified with the use of fully galactosylated RTX hIgG1. By enzymatic treatment, hIgG1 was fully galactosylated using recombinant β-1,4-galactosyltransferase in the presence of uridine diphosphate (UDP-) galactose, post production. Such glycan-modified mAb demonstrated an increase in C1q binding and CDC activity compared to degalactosylated RTX hIgG1 [438]. Conversely, deglycosylation of hIgG1, either by digestion with endoglycosidases or mutagenesis (N297A), results in abrogation of complement-mediated cell killing [472–474].

Although the main strategies for modulating CDC activity include the use of hIgG1 of Fc engineering and glycan engineering as detailed above, other hIgG isotypes, IgG2 and IgG4, represent alternatives as they have an inherently low ability to activate CDC [475, 476]. The current utilisation of hIgG2 and hIgG4 subclasses has typically been in the context of immunomodulatory mAb [477]. In such a setting the therapeutic action is centred around antigen binding and a lack of Fc-mediated effector function. This is desirable when the target is on the surface of tumour-specific cytotoxic T-cells, where depletion would result in a loss of therapeutic efficacy. For this reason, hIgG2 and hIgG4 have not been considered the isotype of choice for direct targeting antibodies and no current literature has focussed on augmenting their CDC activities. In contrast, hIgG3 naturally exhibits the most potent CDC activity of all the human subclasses [422]. However, there are currently no approved therapeutics utilising the hIgG3 sub-class, likely due to its relatively short half-life and bioprocessing issues associated with its long hinge [62].

This chapter focused on understanding the complement induction of C1q null, deglycosylated, and isotype switched RTX hIgG μtp C575S on-target hexamer and μtp hexamer, and if molecular engineering could be used to further boost μtp C575S on-target hexamerisation. As described above, complement activation is dependent on the critical residues in the CH2 and hinge regions, Fc glycosylation, and IgG isotype. However, all previous studies understanding C1q binding requirements have been performed using monomeric human IgG. Here, the μtp C575S was investigated in the context of C1q null binding mutants as well as the contribution of the μtp C575S glycan in order to gain an understanding of the requirements for hexameric hIgG in the context of complement activation. Additionally, hIgG isotypes 2 and 4 were produced in μtp formats to determine if hexamerisation could augment the CDC potential and further mutagenesis was undertaken in an effort to enhance hIgG μtp on-target hexamerisation.

5.2 Impact of C1q binding mutations on IgG1 μtp fusion mAb CDC efficacy

As previously stated, several amino acids have been identified to be crucial for C1q binding and subsequent lytic activation of the complement pathway. To investigate if such residues could reduce the activation of the complement pathway with μtp C575S on-target hexamers and μtp hexamers, the C1q null mutation P331S was incorporated into these constructs. P331S constructs were expressed and purified as previously described (Appendix Tables A1, A2) and examined for on-target hexamerisaiton using a C1q ELISA, a C1q recruitment assay, and a CDC assay as previously described. In the C1q binding ELISA, RTX hIgG1 P331S and RTX hIgG1 μtp C575S/P331S demonstrated a slight reduction in C1q binding, whereas a larger decrease in C1q binding was observed with RTX hIgG1 μtp P331S (Figure 5.1,A) with comparable levels of plate-bound IgG (Appendix Figure A7).

Consistent with a decrease in C1q binding, RTX hIgG1 P331S completely abolished C1q recruitment to Ramos cells. The RTX hIgG1 μtp C575S/P331S decreased C1q recruitment to the target cells surface, but C1q was still observed at comparable levels to RTX hIgG1 WT. In the context of the covalent hIgG1 μtp hexamer, P331S resulted in $\sim$50% reduction in C1q recruitment. This level of C1q recruitment was still greater than that of RTX hIgG1 WT (Figure 5.1,B).

As expected, due to not recruiting C1q to the target cell surface, the RTX hIgG1 P331S did not induce any complement-mediated cell killing. However, even though P331S is thought of as a complement 'null' mutant, there was still complement activity with the hIgG1 μtp C575S/P331S and μtp P331S hexamer (Figure 5.1,C), in keeping with their ability to retain C1q recruitment. RTX hIgG1 μtp C575S/P331S induced $\sim$50% of the cell lysis that is observed with RTX hIgG1 μtp C575S at 10 μg/ml. The RTX hIgG1 μtp P331S hexamer induced efficient complement cell killing against Raji cells at the top concentration, wherein only a 40% drop in activity was observed. However, the CDC activity did titrate at a faster rate than the RTX hIgG1 μtp hexamer and reached background killing levels at the lowest concentration.

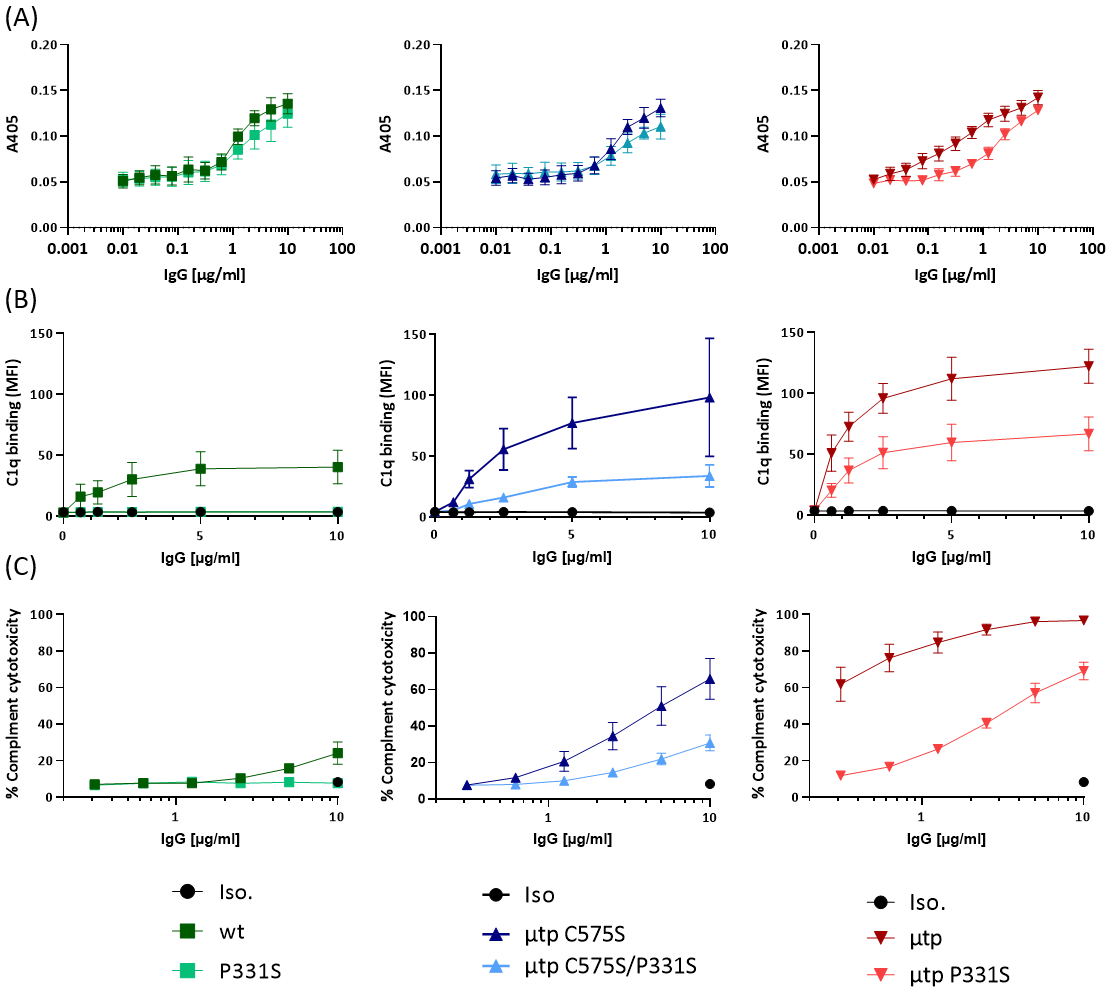

Figure 5.1: Effect of P331S mutation on RTX hIgG1 μtp fusion mAb-mediated complement activation.
(A) ELISA plates were coated with RTX hIgG1 constructs at various concentrations. Human C1q (2 μg/ml) was added and bound C1q was detected with a goat anti-human C1q antibody followed by a peroxidase-conjugated anti-goat IgG-Fc antibody. Data shows absorbance at A405 of bound C1q to WT (left), μtp C575S (middle), and μtp (right) mAb (N=3) (B) $CD20^{+}$ Ramos cells were opsonised with 1151 hIgG1 isotype control or RTX hIgG1 mAb at various concentrations followed by 2 μg/ml human C1q. Bound C1q was determined using an anti-C1q-FITC antibody and analysed by flow cytometry. Data shows MFI of anti-C1q-FITC antibody of WT (left), μtp C575S (middle), and μtp (right) opsonsied cells (N=3) (C) Raji cells were opsonised with 1151 hIgG1 isotype control or RTX hIgG1 constructs and incubated with 20% NHS. Cellular lysis was determined by staining cells with PI and analysed by flow cytometry for PI positive cells. Data shows percentage (%) of cell cytotoxicity of WT (left), μtp C575S (middle), and μtp (right) opsonised cells (N=3). Data plotted is mean and SEM of multiple independent experiments.

Mutagenesis of P331S in the context of a RTX hIgG1 μtp hexamer did not completely abolish C1q binding or CDC activity. These results indicated that other hIgG1 Fc residues must influence C1q binding and CDC. Next, an alternative C1q 'null' mutant, K322A, was examined to determine if the CDC could be further reduced or completely abolished with the covalent hIgG1 μtp hexamer format. The results detailed in Figure 5.2 suggested K322A was more efficient at inhibiting CDC. The RTX hIgG1 μtp K322A demonstrated reduced C1q binding in an ELISA, compared to WT and P331S μtp (Figure 5.2,A). Furthermore, the C1q recruitment assay results suggested that K322A completely prevented C1q recruitment to the cell surface (Figure 5.2,B). However, this molecule still demonstrated complement cell killing when targeting Raji cells (Figure 5.2,C). Overall, these results indicated that in the context of an IgG1 on-target hexamer and IgG1 covalent hexamer,

complement 'null' mutants can be overcome by both preformed and on-target μtp hexamers and the resulting higher avidity interactions. A second factor responsible for C1q binding and efficient CDC is the presence of the glycans within the Fc domains. The μtp also carries a glycosylation site which may influence these properties. Therefore, in the next series of experiments the importance of the glycans to C1q binding and CDC was assessed.

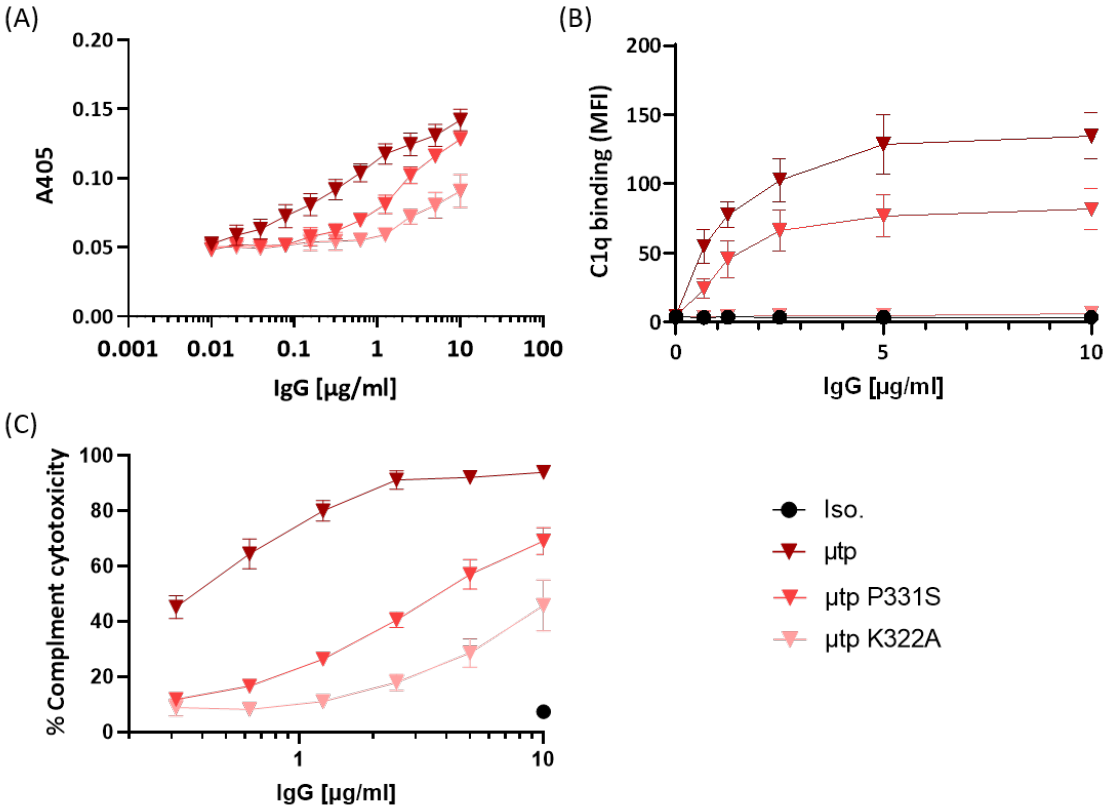

Figure 5.2: Comparison of P331S and K332A complement mutations on C1q binding and CDC activity of RTX hIgG1 μtp hexamers.
(A) ELISA plates were coated with RTX hIgG1 μtp constructs at various concentrations. Human C1q (2 μg/ml) was added and bound C1q was detected with a goat anti-human C1q antibody followed by a peroxidase-conjugated anti-goat IgG-Fc antibody. Data shows absorbance at A405 of bound C1q (N=3) (B) $CD20^+$ Ramos cells were opsonised with 1151 hIgG1 isotype control or RTX hIgG1 μtp constructs at various concentrations followed by 2 μg/ml human C1q. Bound C1q was determined using an anti-C1q-FITC antibody and analysed by flow cytometry. Data shows MFI of anti-C1q-FITC antibody (C) Raji cells were opsonised with 1151 hIgG1 isotype control or RTX hIgG1 μtp constructs and incubated with 20% NHS. Cellular lysis was determined by staining cells with PI and analysed by flow cytometry for PI positive cells. Data shows percentage (%) of cell cytotoxicity (N=3). Data plotted is mean and SEM of multiple independent experiments.

5.3 Impact of deglycosylation on IgG1 μtp C575S on-target hexamerisation

In order to determine the requirement for glycosylation of both the Fc N-linked glycan and the μtp glycan, RTX hIgG1 μtp C575S was deglycosylated with PNGase treatment. Deglycosylation was confirmed using SDS-PAGE (Figure 3.6) where a decrease in molecular weight was observed, indicating glycan cleavage, and mass spectrometry glycan analysis. The results showed that both the N297 (Figure 5.3,A) and N563 (Figure 5.3,B) glycans were deglycosylated. Treatment with PNGase F cleaves all N-linked glycans and deamidates the asparagine residue to an aspartic acid [478]. Therefore, the presence of a deamidated glycan site is indicative of PNGaseF deglycosylation.

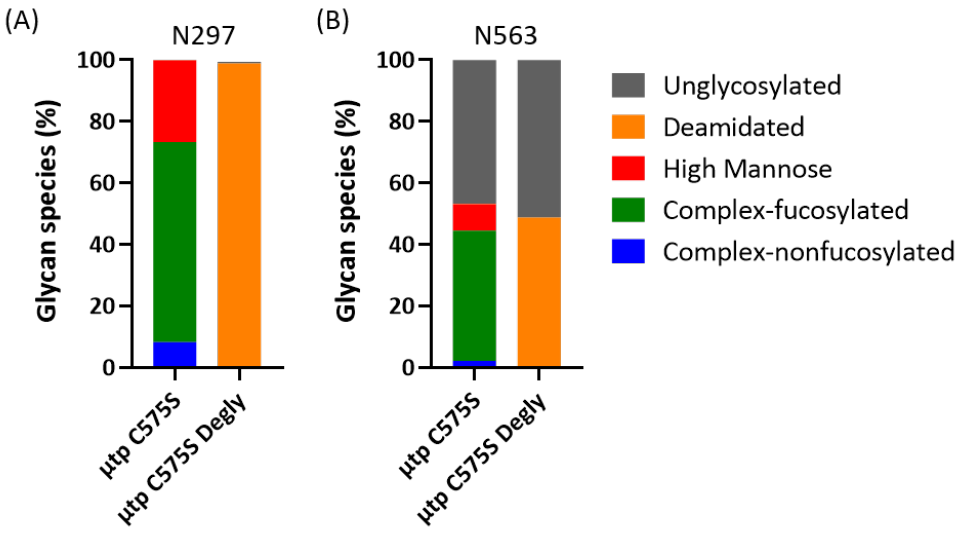

Figure 5.3: Glycan profiling of deglycosylated hIgG1 μtp C575S constructs.
Glycan analysis was undertaken using mass spectrometry techniques of deglycosylated RTX hIgG1 μtp C575S. A range of glycoprofiles were detected which have been grouped into four main glycan species: demaidated, high mannose, complex-fucosylated, complex-nonfucosylated. The glycan species present were analysed on the (A) CH2 N297 and (B) μtp N563 glycan sites.

Following confirmation of efficient deglycosylation with PNGase F treatment, the impact on on-target hexamerisation was investigated. Firstly, the hexamerisation propensity in solution was examined at concentrations up to 20 mg/ml using SE-UPLC. The results indicated that when deglycosylated there was no tendency to multimerise in solution at high concentrations (Figure 5.4). At 20 mg/ml there was no evidence of a multimeric species in solution, whereas the native glycolsylated RTX hIgG1 μtp C575S demonstrated 16.9% multimeric species at 20 mg/ml.

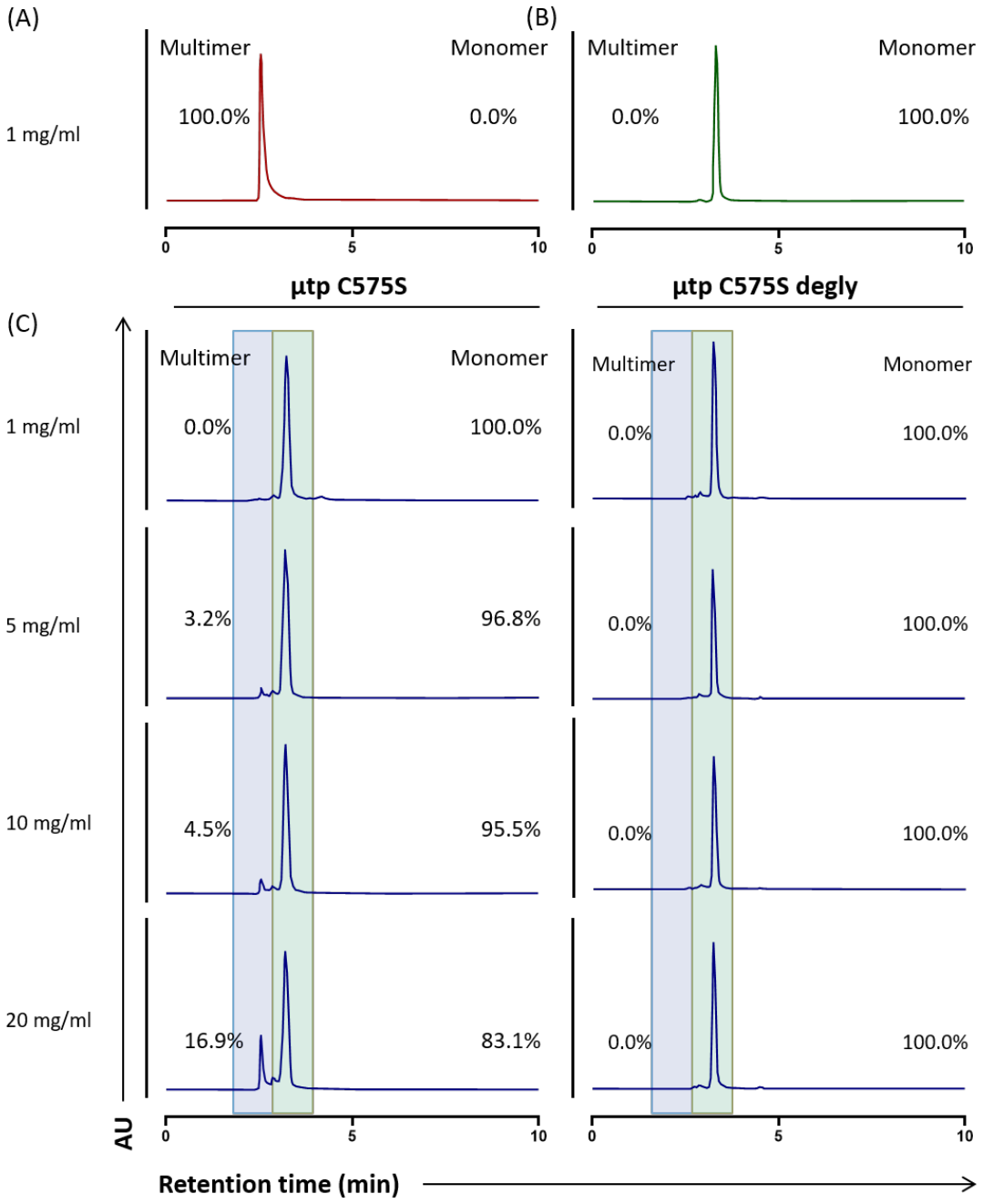

Figure 5.4: Effect of deglycosylation of RTX hIgG1 μtp C575S mAb on in-solution hexamerisation.
RTX hIgG1 μtp C575S mAb was concentrated up to 20 mg/ml and the percentage (%) of monomeric and multimeric species was determined by SE-UPLC (A) Representative SE-UPLC trace of the preformed hIgG1 μtp hexamer at 1 mg/ml (B) Representative SE-UPLC trace of the hIgG1 WT at 1 mg/ml (C) Representative traces of hIgG1 μtp C575S (left) and hIgG1 μtp C575S deglycosylated (right) at increasing concentrations from 1 mg/ml to 20 mg/ml.

In a C1q ELISA there was similar levels of plate-bound IgG (Appendix Figure A8) and a small decrease in C1q binding observed (Figure 5.5,A), but a complete absence of C1q recruitment (Figure 5.5,B), suggesting that glycosylation of the Fc and μtp C575S mAb is essential for physiological (cell-surface) C1q binding and recruitment. The results from the CDC assay using Raji cells as targets provided more evidence of the requirement of Fc and μtp glycans for on-target hexamerisation. There was no observed CDC activity for the deglycosylated RTX hIgG1 μtp C575S, whereas a maximum cytotoxicity for glycosylated RTX hIgG1 μtp C575S of $\sim$50% was observed (Figure

5.5,C), indicating that glycosylation was critical for complement activity.

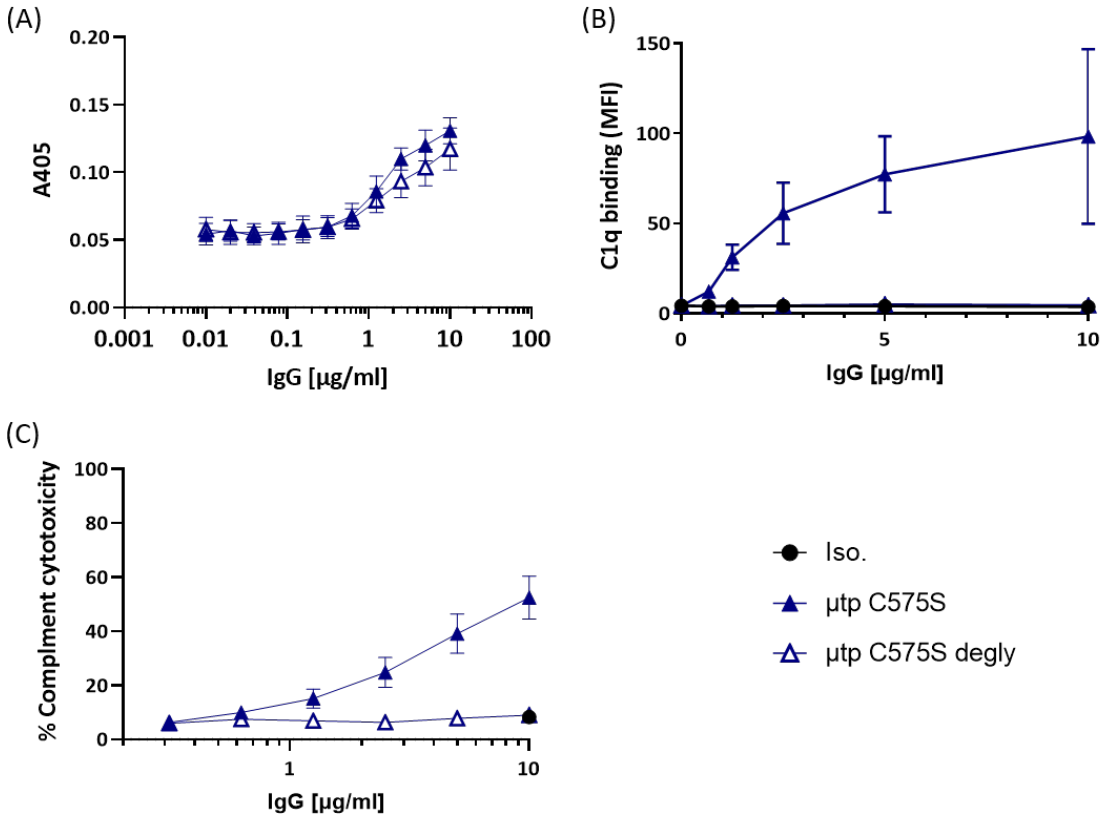

Figure 5.5: Effect of deglycosylation of RTX hIgG1 μtp C575S mAb on C1q binding and CDC activity.
(A) ELISA plates were coated with RTX hIgG1 μtp C575S at various concentrations. Human C1q (2 μg/ml) was added and bound C1q was detected with a goat anti-human C1q antibody followed by a peroxidase-conjugated anti-goat IgG-Fc antibody. Data shows absorbance at A405 of bound C1q (N=4) (B) $CD20^{+}$ Ramos cells were opsonised with 1151 hIgG1 isotype control or RTX hIgG1 μtp C575S at various concentrations followed by 2 μg/ml human C1q. Bound C1q was determined using an anti-C1q-FITC antibody and analysed by flow cytometry. Data shows MFI of anti-C1q-FITC antibody (N=6) (C) Raji cells were opsonised with 1151 hIgG1 isotype control or RTX hIgG1 μtp C575S and incubated with 20% NHS. Cellular lysis was determined by staining cells with PI and analysed by flow cytometry for PI positive cells. Data shows percentage (%) of cell cytotoxicity (N=6). Data plotted is mean and SEM of multiple independent experiments.

These results clearly indicated that the glycosylation of hIgG1 Fc and and μtp C575S is essential for the observed hexamerisation enhancement in-solution, as demonstrated by UPLC analysis (Figure 5.4) The lack of solution hexamerisation could explain why there is no C1q recruitment and CDC activity of the deglycosylated RTX hIgG1 μtp C575S. Together these results indicated that the glycosylation of the hIgG1 μtp C575S mAb is crucial for efficient on-target hexamerisation, C1q binding and CDC. However, this does not address whether the increased avidity of an hIgG μtp hexamer could still elicit complement activation (C1q binding and CDC) in an aglycosylated form. To examine this, the covalent RTX hIgG1 μtp hexamer was deglycosylated with PNGase treatment. Deglycosylation of RTX hIgG1 μtp demonstrated a decrease in C1q binding in a plate-bound ELISA format compared to glycosylated RTX hIgG1 μtp (Figure 5.6,A) with comparable levels of plate-bound IgG observed (Appendix Figure A9). However, the deglycosylated μtp hexamer was still able to recruit C1q to Ramos cells (Figure 5.6,B) and exhibited CDC against Raji cells (Figure 5.6,C).

These activities were significantly reduced compared to the native RTX hIgG1 μtp, however, the results indicated that deglycosylation does not completely inhibit complement mediated events and that these can be overcome to some extent with high avidity interactions, albeit with lower recruitment and cell killing compared with glycosylated hexamers.

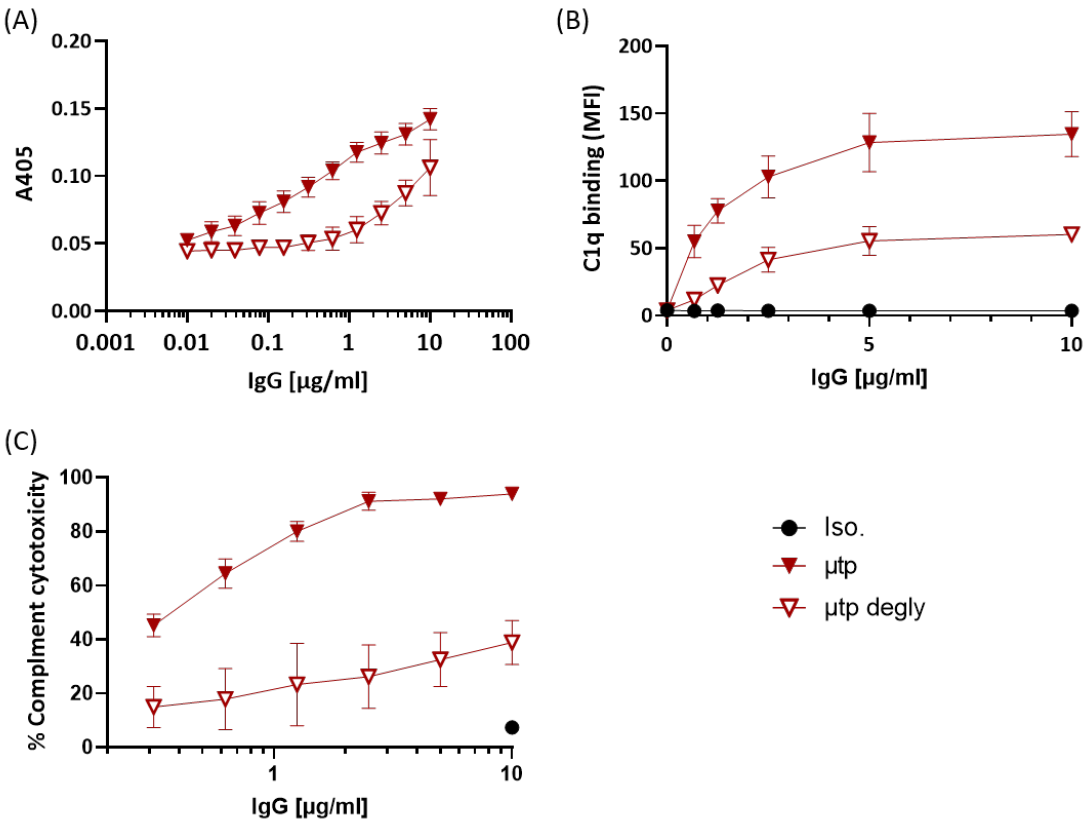

Figure 5.6: Effect of deglycosylation of RTX hIgG1 μtp hexamer on C1q binding and CDC activity.
(A) ELISA plates were coated with RTX hIgG1 μtp at various concentrations. Human C1q (2 μg/ml) was added and bound C1q was detected with a goat anti-human C1q antibody followed by a peroxidase-conjugated anti-goat IgG-Fc antibody. Data shows absorbance at A405 of bound C1q (N=3) (B) $CD20^{+}$ Ramos cells were opsonsised with 1151 hIgG1 isotype control or RTX hIgG1 μtp at various concentrations followed by 2 μg/ml human C1q. Bound C1q was determined using an anti-C1q-FITC antibody and analysed by flow cytometry. Data shows MFI of anti-C1q-FITC antibody (N=3) (C) Raji cells were opsonised with 1151 hIgG1 isotype control or RTX hIgG1 μtp and incubated with 20% NHS. Cellular lysis was determined by staining cells with PI and analysed by flow cytometry for PI positive cells. Data shows percentage (%) of cell cytotoxicity (N=3). Data plotted is mean and SEM of multiple independent experiments.

5.4 Impact of μtp glycosylation occupancy on IgG1 μtp C575S on-target hexamerisation

After demonstrating that the glycosylation state of the hIgG1 μtp C575S was important to its hexamerisation capabilities and CDC activity, it was hypothesised that this could be manipulated through molecular engineering. Here, the amino acids adjacent to the N-linked glycosylation site of the μtp C575S peptide sequence (Figure 5.7,A) were mutated to encourage a change in glycosylation processing during expression (work initially undertaken by Dr Michael Parkinson at UCB in

hIgG1 Fc μtp hexamer formats). There is evidence that the amino acids adjacent to N-linked glycosylation sites influence the occupancy, processing efficiency, and composition of the glycan moiety [479, 480]. Results published by Huang *et at* have suggested that aspartic acid or leucine at position *n*+1 decreases glycan occupancy and threonine at position *n*+2 increases glycan occupancy [480]. To investigate this theory the residues at position *n*+1 (valine-564) and *n*+2 (serine-565) adjacent to the N-linked glycan site on the μtp peptide were mutated. The selected mutagenesis reactions at *n*+1 were V564D or V564L, and at *n*+2 was S565T. These constructs were then expressed and purified as detailed in Chapter 3, the expression and purification yields of which are detailed in Appendix Tables A1, A2.

Glycan analysis was then undertaken using mass spectrometry techniques which enabled calculation of the glycan occupancy and the glycan species present. The results showed that the glycan occupancy of the CH2 N297 was unchanged with the RTX hIgG1 μtp C575S constructs, compared to RTX hIgG1 WT. The CH2 was ~100% occupied in all mAb formats (Figure 5.7,B). Analysis of the μtp C575S N563 demonstrated that hIgG1 μtp C575S had 54% occupancy, which was comparable to the hIgG1 μtp C575S/V546L mutant (50%). The hIgG1 μtp C575S/V564D had the lowest μtp occupancy (36%) and hIgG1 μtp C575S/S565T had the highest occupancy (96%) (Figure 5.7,C).

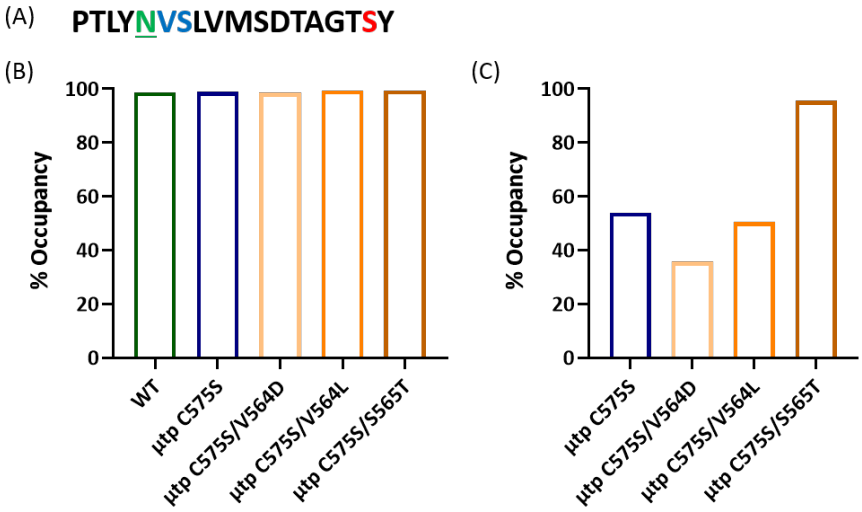

Figure 5.7: Glycan occupancy of hIgG1 μtp C575S constructs.
Glycan analysis was undertaken using mass spectrometry techniques of RTX hIgG1 μtp C575S constructs (A) Sequence of μtp, denoting the N-linked glycosylation site in green, cysteine residue in red, and V564/S565 amino acids in blue (B/C) The glycan occupancy of (B) the CH2 N297 and (C) μtp N563 glycans was calculated by analysis of the percentage (%) of unglycosylated molecules.

In addition to occupancy, the glycan species that was present was examined. The results for the CH2 N297 site showed that the hIgG1 μtp C575S had a higher percentage of high mannose species and a lower proportion of complex-fucosylated glycans. The other hIgG1 μtp C575S constructs (V564D, V564L, and S565T) had comparable CH2 glycosylation to the hIgG1 WT, with a slightly higher percentage of high mannose species and fewer complex-fucosylated glycans (Figure 5.8,A).

Analysis of the N563 glycan also demonstrated the hIgG1 μtp C575S had higher levels of high mannose compared to the other hIgG1 μtp C575S constructs. The hIgG1 μtp C575S/V564D, hIgG1 μtp C575S/V564L, and hIgG1 μtp C575S/V564L all had similar levels of complex-fucosylated glycans with low levels of high mannose, complex-nonfucosylated, and deamidated N-linked glycans. (Figure 5.8, B). These results suggested that the only major difference between the hIgG1 μtp C575S constructs was the percentage occupancy of N563 glycan sites. The impact of these differences on hexamerisation efficiency in solution and on-target hexamerisation enhancement was examined and compared.

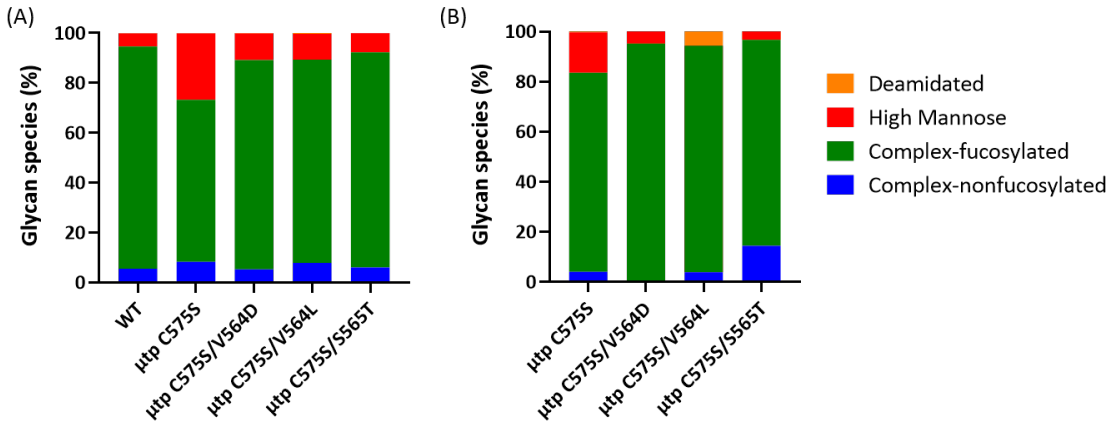

Figure 5.8: Glycan profiling of hIgG1 μtp C575S constructs.
Glycan analysis was undertaken using mass spectrometry techniques of RTX hIgG1 μtp C575S constructs. A range of glycoprofiles was detected which have been grouped into four main glycan species: demaidated, high mannose, complex-fucosylated, complex-nonfucosylated. The glycan species present were analysed on the (A) CH2 N297 and (B) μtp N563 glycan sites. Results shown are for glycan species only, excluding the non-occupied N-linked glycan sites.

The results demonstrated that the solution-based hexamerisation efficiency was significantly modified by mutagenesis of the amino acids surrounding the N-linked glycan site (Figure 5.9,B). The hIgG1 μtp C575S/V564D mutation ablated any hexamerisation, with no multimer species observed even at 20 mg/ml. In contrast, the hIgG1 μtp C575S/V564L had improved hexamerisation efficiency with 36.3% multimer present at 20 mg/ml (Figure 5.9,B), about twice that of the native hIgG1 μtp C575S. The hIgG1 μtp C575S/V564L construct also demonstrated greatly enhanced multimerisation at lower concentrations (27.8% at 5 mg/ml). The hIgG1 μtp C575S/S565T demonstrated a further enhancement for in-solution multimerisation efficiency at both the high and low concentrations (Figure 5.9,B). At 20 mg/ml there was 48.6% multimer species and 34.8% at 5 mg/ml. Importantly, there was no increase in multimers with any construct at the 1 mg/ml concentration.

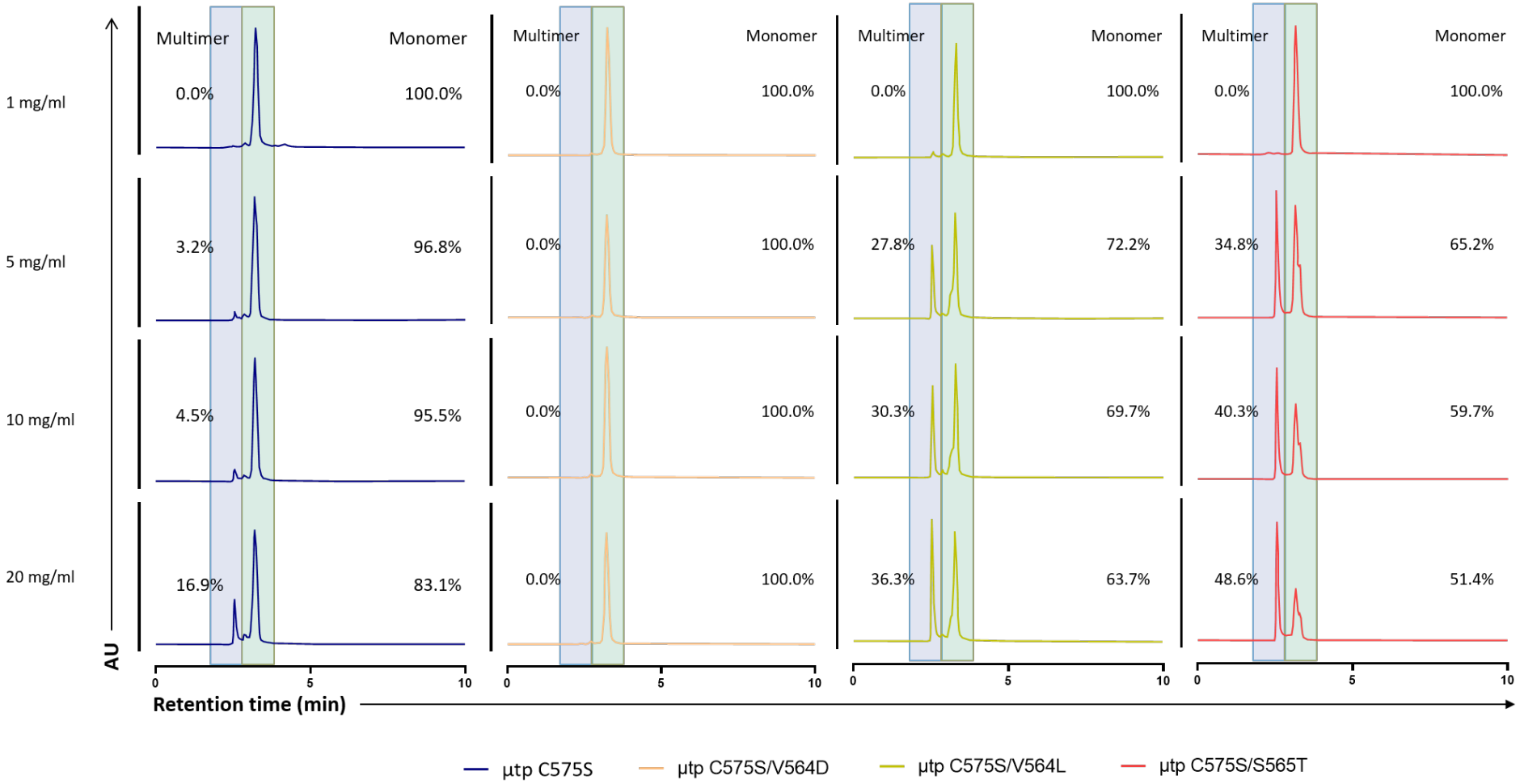

Figure 5.9: Solution multimerisation tendency of hIgG1 μtp C575S with additional μtp amino acid mutations.
RTX hIgG1 μtp C575S constructs were concentrated up to 20 mg/ml and the percentage (%) of monomeric and multimeric species was determined by SE-UPLC. Data is showing representative traces of RTX hIgG1 μtp C575S constructs at increasing concentrations from 1 mg/ml to 20 mg/ml.

After demonstrating that the glycan occupancy of the μtp C575S was modified by altering the amino acid residues surrounding the glycan attachment site and the there was an impact on the hexamerisation efficiency, the on-target hexamerisation and complement activity were then investigated. Analysis of the C1q binding in an ELISA demonstrated that none of the mutations or change in glycan profiles of the μtp C575S altered inherent binding to C1q. All of the constructs demonstrated comparable levels of plate-bound IgG (Appendix Figure A10) and C1q binding to the native hIgG1 μtp C575S format (Figure 5.10,A).

In contrast the C1q recruitment assay did demonstrate differences between the three mutated μtp C575S constructs. RTX hIgG1 μtp C575S/V564D form demonstrated a decrease in cell surface C1q recruitment compared to RTX hIgG1 μtp C575S (Figure 5.10,B), in-line with the observed ablation of in-solution hexamerisation. RTX hIgG1 μtp C575S/V564L recruited slightly more C1q than RTX hIgG1 μtp C575S at the top concentration of 10 μg/ml, but had comparable recruitment at lower concentrations (Figure 5.10,B). RTX hIgG1 μtp C575S/S565T had the highest level of C1q recruitment, greater than seen with native RTX hIgG1 μtp C575S (Figure 5.10,B). The enhanced C1q recruitment for the V564L and S565T were therefore correlated with the enhanced solution hexamerisation observed, and are in-line with an enhanced on-target hexamerisation of the mAb.

The CDC activity of the various RTX hIgG1 μtp C575S mutants were then explored. The V564D variant was completely abolished, whereby no observed cellular cytotoxicity over the isotype control was seen (Figure 5.10,C). The RTX hIgG1 μtp C575S/V564L demonstrated CDC activity that was equivalent to the RTX hIgG1 μtp C575S (Figure 5.10,C). Finally, the RTX hIgG1 μtp C575S/S565T mutant exhibited an enhancement in CDC activity over the RTX hIgG1 μtp C575S (Figure 5.10,C).

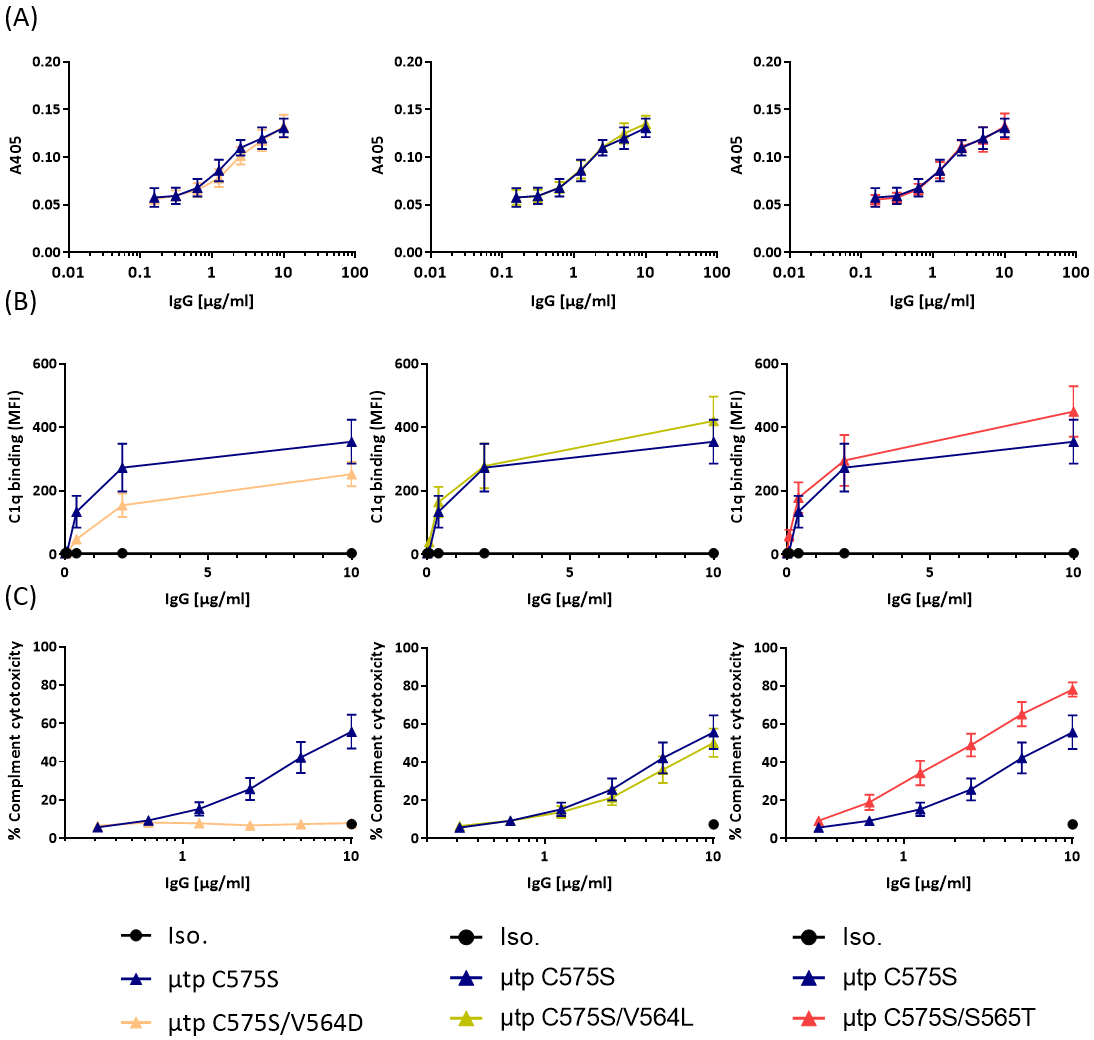

Figure 5.10: Effect of additional μtp mutations on RTX hIgG1 μtp C575S on-target hexamerisation.
(A) ELISA plates were coated with RTX hIgG1 μtp C575S constructs at various concentrations. Human C1q (2 μg/ml) was added and bound C1q was detected with a goat anti-human C1q antibody followed by a peroxidase-conjugated anti-goat IgG-Fc antibody. Data shows absorbance at A405 of bound C1q to V564D (left), V564L (middle), and S565T (right) μtp C575S mAb (N=4) (B) CD20$^+$ Ramos cells were opsonsised with 1151 hIgG1 isotype control or RTX hIgG1 μtp C575S constructs at various concentrations followed by 2 μg/ml human C1q. Bound C1q was determined using an anti-C1q-FITC antibody and analysed by flow cytometry. Data shows MFI of anti-C1q-FITC antibody of V564D (left), V564L (middle), and S565T (right) μtp C575S mAb opsonsied cells (N=6) (C) Raji cells were opsonised with 1151 hIgG1 isotype control or RTX hIgG1 μtp C575S constructs and incubated with 20% NHS. Cellular lysis was determined by staining cells with PI and analysed by flow cytometry for PI positive cells. Data shows percentage (%) of cell cytotoxicity of V564D (left), V564L (middle), and S565T (right) μtp C575S mAb opsonised cells (N=6). Data plotted is mean and SEM of multiple independent experiments.

To assess whether the CH2 and/or μtp glycan was important for C1q binding and CDC activity a second deglycosylation experiment was performed. The modified μtp C575S mAb were deglycosylated through treatment with either EndoS or PNGase. EndoS is an enzyme that specifically deglycosylates the IgG Fc at N297 [481], so it should leave the μtp glycan intact, whereas PNGase does not discriminate between glycan sites and will cleave all N-linked glycan [482]. After enzymatic treatment, the mAb were analysed by reducing SDS-PAGE to observe the deglycosylation of the HC. The SDS-PAGE results indicated that there was a difference in glycan profiles amongst the four different μtp C575S constructs (Figure 5.11). There were small differences in the migra-

tion rates and also in the spread of glycan heterogeneity (observed by the spread and number of different bands on the gel) that most likely represent glycan-occupied and non-occupied μtp C575S molecules (Figure 5.7,B). Treatment with EndoS appeared to reduce the size of the different hIgG1 μtp C575S, hIgG1 μtp C575S/V564D, and hIgG1 μtp C575S/S565T molecuels (Figure 5.11). Interestingly, there were still multiple bands observed on the gel following Endo-S treatment that would suggest the heterogeneity was caused by processing of the μtp C575S N-linked glycan, and not the Fc N-linked glycan. Endo-S treatment of the hIgG1 μtp C575S/V564L did not result in an obvious difference in the size of banding compared to the untreated mAb (Figure 5.11). Treatment with PNGase appeared to remove all glycan heterogeneity between the four hIgG1 μtp C575S constructs, evidenced by a single band after deglycosylation (Figure 5.11). The heterogeneity observed following treatment with Endo-S would indicate that the four hIgG1 μtp C575S mAb have different μtp N-linked glycosylation profiles and occupancy and is consistent with the glycan analysis.

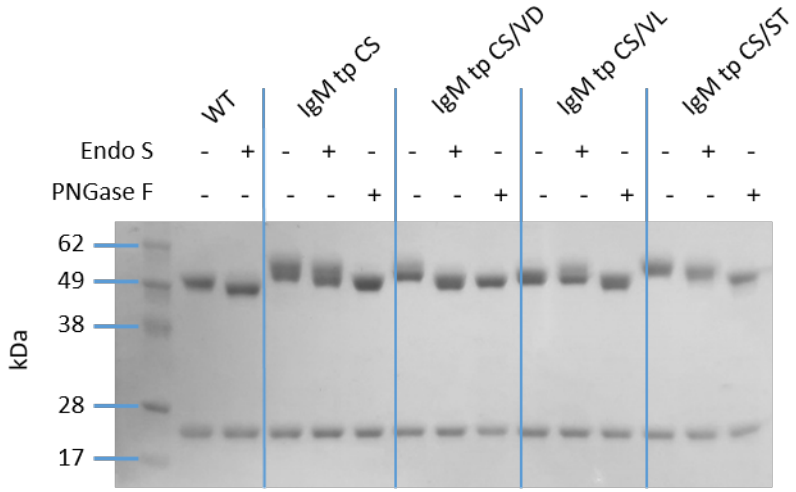

Figure 5.11: Deglycosylation of RTX hIgG1 μtp C575S constructs using EndoS and PNGase treatment
RTX hIgG1 μtp C575S constructs were assessed deglycosylation using a 4-12% Bis-Tris SDS-PAGE gel under reducing conditions. The molecular weight marker used was the SeeBlue Protein Standard.

These differently glycosylated hIgG1 μtp C575S constructs were then examined for their dependence on glycans for CDC activity by examining PNGase F treated RTX hIgG1 μtp C575S constructs in the relevant assay. Deglycosylation of RTX hIgG1 μtp C575S/V564D had no impact on the CDC activity due to the mAb possessing no CDC activity even when glycans were present (Figure 5.12,A). Deglycosylation of RTX hIgG1 μtp C575S/V564L and RTX hIgG1 μtp C575S/S565T resulted in a complete loss of complement-mediated Raji cell killing (Figure 5.12,B-C). These results indicate that glycosylation is also critical for the CDC activity of the glycan-modified μtp C575S mAb.

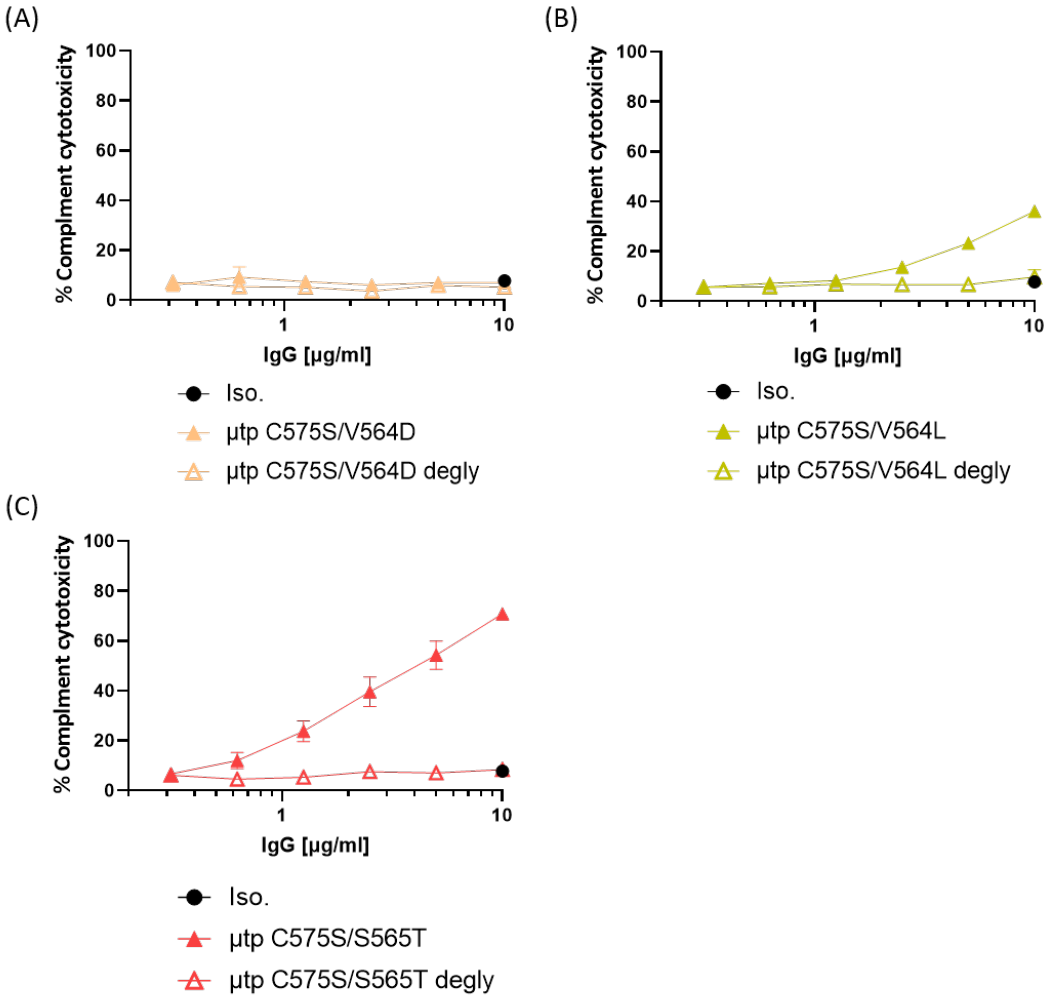

Figure 5.12: Effect of deglycosylation of RTX hIgG1 μtp C575S with additional μtp mutations on CDC activity. Raji cells were opsonised with 1151 hIgG1 isotype control or RTX hIgG1 μtp C575S constructs and incubated with 20% NHS. Cellular lysis was determined by staining cells with PI and analysed by flow cytometry for PI positive cells. Data shows percentage (%) of cell cytotoxicity of V564D (A), V564L (B), and S565T (C) μtp C575S mAb opsonised cells. Data plotted is mean and SEM of multiple independent experiments (N=3).

These results have clearly demonstrated that mutagenesis of residues surrounding the N-linked glycan site of the μtp can alter the glyan occupancy, which has impacts on C1q binding and CDC activity. The glycosylation profile of hIgG1 is also known to have a role in FcγR binding and ADCC activity [346]. In order to characterise the influence of the described μtp mutations on FcγR-mediated effector functions, the ADCC activity of these mAb was investigated. The results from the ADCC assay indicated that the cell cytotoxicity, elicited by NK cells through activation of FcγRIIIa, was not affected by the different μtp C575S mutations (Figure 5.13). All three mutations demonstrated comparable FcγR-mediated effector induction compared with RTX hIgG1 μtp C575S. Therefore, these μtp mutations demonstrate that on-target hexamerisation efficiency and complement activity of μtp C575S mAb can be modified independently of FcγR-mediated cell killing. Next it was assessed whether the μtp and μtp C575S technology could be applied to other hIgG isotypes.

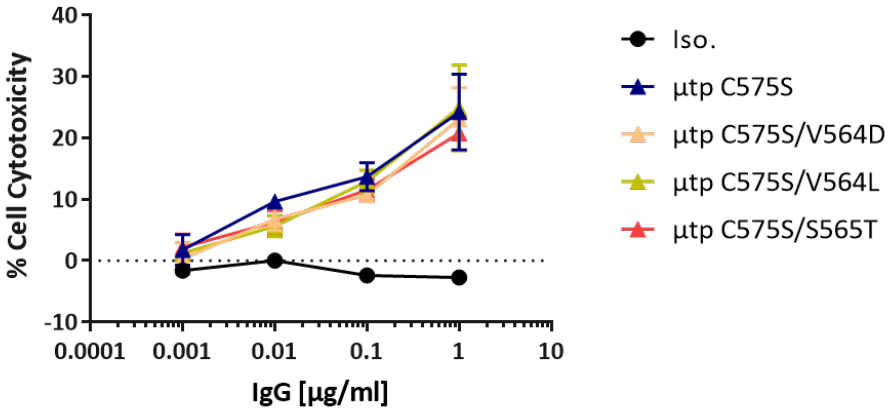

Figure 5.13: Effect of additional μtp mutations of RTX hIgG1 μtp C575S on ADCC efficacy.
Calcein labelled Ramos cells were opsonised with an isotype control (1151 hIgG1) or RTX hIgG1 μtp C575S mutants over a concentration range and incubated with freshly purified human PBMCs as effector cells. Calcein release in cell supernatants was measured as a readout for ADCC. Data shows cell cytotoxicity (% max cell lysis) and plotted as mean and SEM of independent experiments (N=3).

5.5 On-target hexamerisation of IgG2 μtp C575S

The hIgG2 isotype is known to naturally exhibit limited levels of CDC activity, unlike hIgG1 and hIgG3. It was therefore considered whether the μtp peptide technology could overcome this inherent lack of complement fixation by exploiting the higher avidity interactions displayed by IgG μtp hexamers and μtp C575S on-target hexamers. IgG2 μtp constructs were expressed and purified as previously described (Appendix Tables A1, A2), and characterised for enhanced hexamerisation propensity. The hexamerisation efficiency in solution of hIgG2 μtp C575S constructs was comparable to hIgG2 WT (Figure 5.14). The results indicated that both the hIgG2 WT and μtp C575S had no ability to hexamerise in solution when tested at concentrations up to 20 mg/ml.

After demonstrating that there was no solution-based hexamerisation enhancement, the on-target hexamerisation efficiency of hIgG2 μtp C575S was investigated. Again, there was similar levels of plate-bound hIgG2 (Appendix Figure A11), and the ELISA results suggested that the binding to C1q was not enhanced by the addition of the μtp C575S, when compared to WT. The results also indicated that the preformed covalent hIgG2 μtp hexamer did not have an enhanced binding to C1q in the ELISA (Figure 5.15,A). The C1q recruitment assay demonstrated a small improvement of C1q binding at the cell surface of RTX hIgG2 μtp C575S compared to WT but far fewer than would be seen with a WT hIgG1 comparator. Accordingly, the hIgG2 μtp hexamer demonstrated a small enhancement in C1q recruitment to the Ramos cell surface, compared to WT hIgG2 reagents (Figure 5.15,B). As with the C1q binding assay, the magnitude of effect was modest and lower than would be seen with WT hIgG1.

The complement cytotoxicity of the hIgG2 μtp fusion mAb was investigated using the more sen-

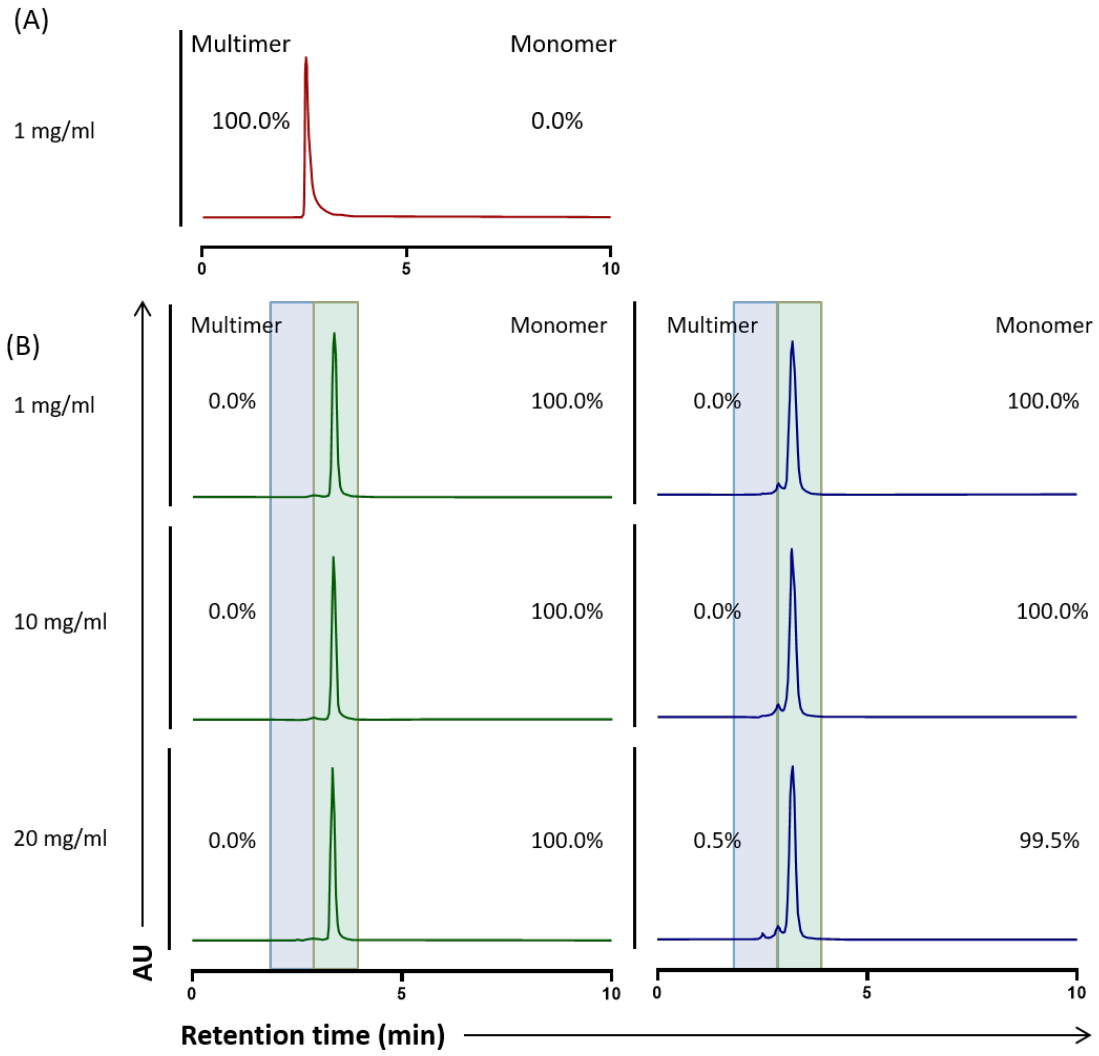

Figure 5.14: Solution multimerisation tendency of hIgG2 μtp C575S.
RTX hIgG2 μtp constructs was concentrated up to 20 mg/ml and the percentage (%) of monomeric and multimeric species was determined by SE-UPLC (A) Representative SE-UPLC trace of the preformed hIgG2 μtp hexamer at 1 mg/ml (B) Representative traces of hIgG2 WT (left) and hIgG2 μtp C575S (right) at increasing concentrations from 1 mg/ml to 20 mg/ml.

sitive Ramos cell line, due to the low CDC efficiency associated with hIgG2. Here it was observed that addition of the μtp C575S gave only a modest benefit to complement cytotoxicity over the inert hIgG2 WT. The maximum cytotoxicity observed was 30.6% at 10 μg/ml, whereas the WT had 16.7% and isotype control 14.0%. The μtp hexamer did have 100% cell killing at 10 μg/ml, but cell killing quickly decreased as the concentration of mAb decreased, reaching background levels by 0.1 μg/ml. The EC50 calculated for the RTX hIgG2 μtp hexamer was 1.073 μg/ml, 5-fold lower than RTX hIgG1 WT (Figure 5.15,C). This suggests that the μtp technology can indeed increase complement activation with a previously inert isotype but that it cannot efficiently overcome the low complement deposition and killing that is associated with hIgG2. Even in the form of a covalent hIgG2 hexamer the molecule still had relatively weak cell killing efficiency, especially compared to the hIgG1 μtp hexamer. Next, the ability of the μtp technology to augment hIgG4 capacity was assessed.

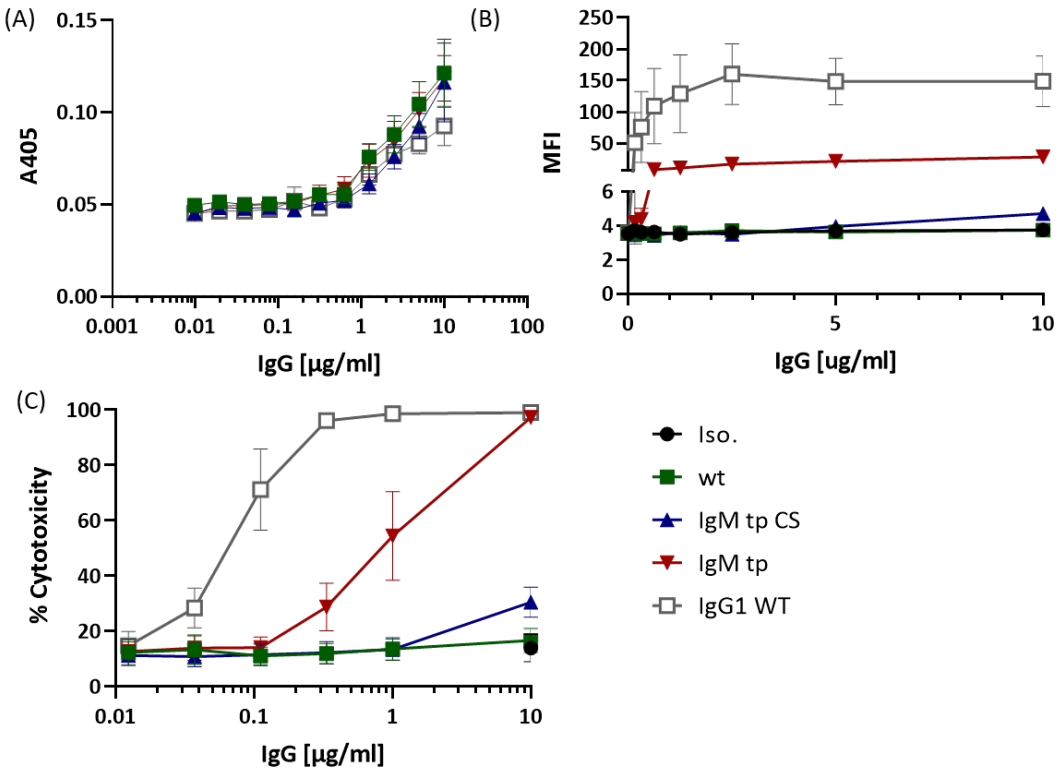

Figure 5.15: Analysis of on-target hexamerisation and complement activation by hIgG2 μtp fusion mAb.
(A) ELISA plates were coated with RTX hIgG2 μtp C575S constructs at various concentrations. Human C1q (2 μg/ml) was added and bound C1q was detected with a goat anti-human C1q antibody followed by a peroxidase-conjugated anti-goat IgG-Fc antibody. Data shows absorbance at A405 of bound C1q (N=3) (B) CD20$^+$ Ramos cells were opsonised with anti-OX40 hIgG2 isotype control or RTX hIgG2 μtp C575S constructs at various concentrations followed by 2 μg/ml human C1q. Bound C1q was determined using an anti-C1q-FITC antibody and analysed by flow cytometry. Data shows MFI of anti-C1q-FITC antibody (N=3) (C) Ramos cells were opsonised with anti-OX40 hIgG2 isotype control or RTX hIgG2 μtp C575S constructs and incubated with 20% NHS. Cellular lysis was determined by staining cells with PI and analysed by flow cytometry for PI positive cells. Data shows percentage (%) of cell cytotoxicity of (N=3). Data plotted is mean and SEM of multiple independent experiments.

5.6 On-target hexamerisation of IgG4 μtp C575S

Similar to the hIgG2 mAb, RTX hIgG4 μtp mAb fusions were produced (Appendix Tables A1, A2) in order to investigate the capacity to augment hIgG4 efficiency for hexamerisation and CDC activity. As previously described, hIgG4 are also known to induce low complement deposition and killing. First, the ability to exhibit hexamerisation in solution was examined. There was no hexamerisation at concentrations up to 20 mg/ml observed with either the WT or μtp C575S (Figure 5.16), indicating that hIgG4 WT and μtp C575S had no ability to hexamerise in solution.

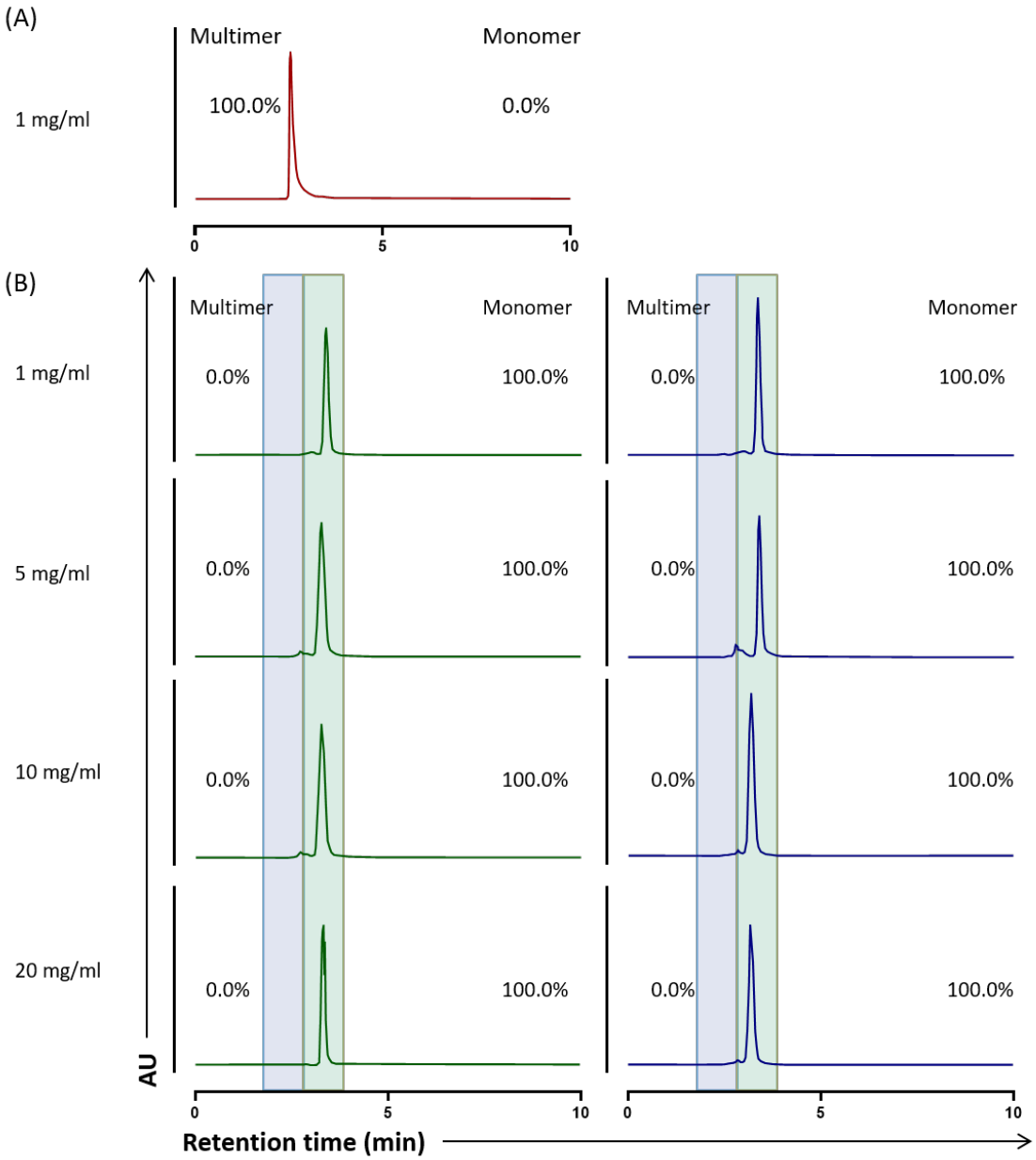

Figure 5.16: Solution multimerisation tendency of hIgG4 μtp C575S.
RTX hIgG4 μtp constructs were concentrated up to 20 mg/ml and the percentage (%) of monomeric and multimeric species was determined by SE-UPLC (A) Representative SE-UPLC trace of the preformed hIgG2 μtp hexamer at 1 mg/ml (B) Representative traces of hIgG4 WT (left) and hIgG4 μtp C575S (right) at increasing concentrations from 1 mg/ml to 20 mg/ml.

Next, the ability of hIgG4 μtp C575S to bind C1q was investigated. There was comparable levels of hIgG4 μtp constructs bound to the duplicate ELISA plate (Appendix Figure A12) For hIgG4 WT and hIgG4 μtp C575S the observed C1q binding was low. Even at the top concentrations examined there was only a small level of absorbance, indicating low amounts of C1q binding in the ELISA. The preformed hIgG4 μtp hexamer did demonstrate an increased binding of C1q, but only at the top concentrations, thereby indicating that higher avidity interactions can increase C1q binding in the context of hIgG4 (Figure 5.17,A).

The cell surface C1q recruitment assay demonstrated that hIgG4 μtp C575S did not have any C1q

recruitment activity, comparable to the hIgG4 WT. However, the hIgG4 μtp hexamer did show a modest increase in C1q recruitment to the Ramos cell surface (Figure 5.17,B), greater than that seen with the hIgG2 μtp hexamer (Figure 5.15), but still less than WT hIgG1 (Figure 4.5). In assays measuring CDC, the hIgG4 μtp hexamer demonstrated contrasting activities. The hIgG4 μtp C575S mAb had decreased CDC activity compared to hIgG4 WT, comparable to the background level. Conversely, the hIgG4 μtp hexamer had enhanced complement cell killing compared to hIgG4 WT (Figure 5.17,C). The EC50 of the hIgG4 μtp hexamer was 0.221 μg/ml, comparable to that of hIgG1 wt (0.223 μg/ml). These results indicated that a covalent hIgG4 hexamer had greatly enhanced CDC activity compared to hIgG4 WT. However, with the RTX hIgG4 μtp C575S on-target hexamer all complement-mediated cell killing activity was lost and no enhancement was observed.

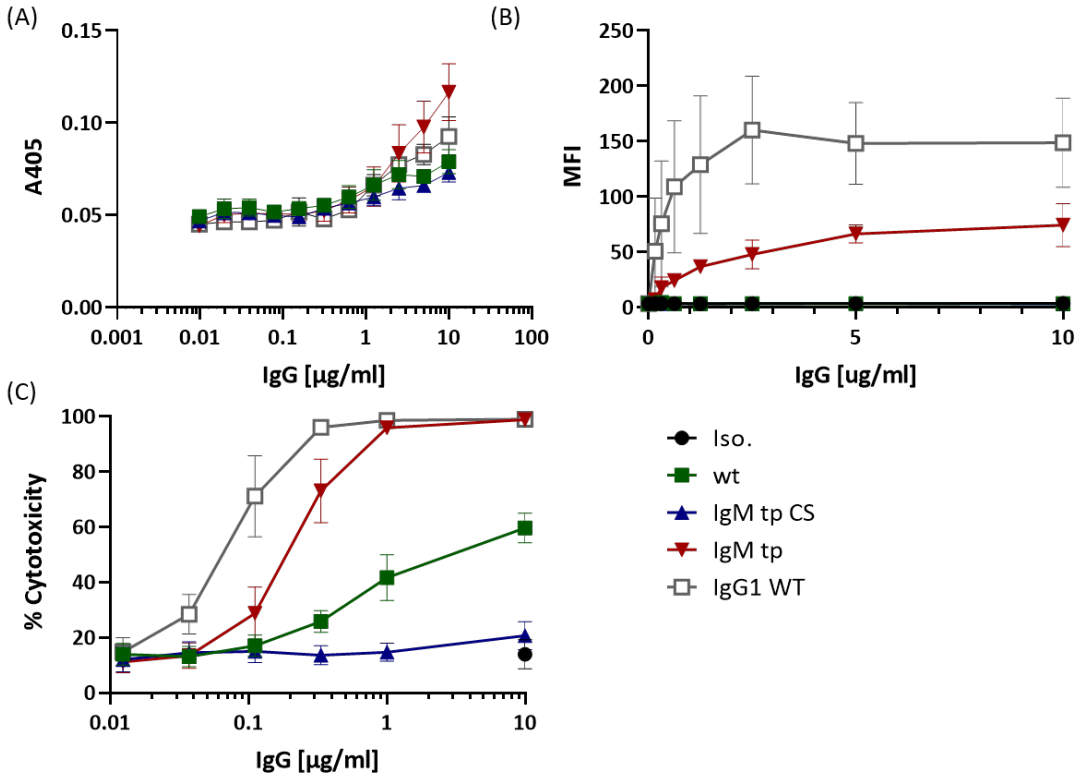

Figure 5.17: Analysis of on-target hexamerisation and complement activation by hIgG4 μtp fusion mAb.
(A) ELISA plates were coated with RTX hIgG4 μtp C575S constructs at various concentrations. Human C1q (2 μg/ml) was added and bound C1q was detected with a goat anti-human C1q antibody followed by a peroxidase-conjugated anti-goat IgG-Fc antibody. Data shows absorbance at A405 of bound C1q (N=3) (B) CD20^{+} Ramos cells were opsonsised with anti-OX40 hIgG4 isotype control or RTX hIgG4 μtp C575S constructs at various concentrations followed by 2 μg/ml human C1q. Bound C1q was determined using an anti-C1q-FITC antibody and analysed by flow cytometry. Data shows MFI of anti-C1q-FITC antibody (N=3) (C) Ramos cells were opsonised with anti-OX40 hIgG4 isotype control or RTX hIgG4 μtp C575S constructs and incubated with 20% NHS. Cellular lysis was determined by staining cells with PI and analysed by flow cytometry for PI positive cells. Data shows percentage (%) of cell cytotoxicity of (N=3). Data plotted is mean and SEM of multiple independent experiments.

5.7 Impact of Fc mutations on IgG μtp C575S CDC efficacy

The marked difference in effect of μtp C575S peptide in the hIgG1 and hIgG4 isotypes regarding hexamerisation, C1q binding, and CDC (increasing and decreasing, respectively) were of particular interest and led to questions regarding the underpinning molecular explanation. There are differences in the amino acid sequences between hIgG1 and hIgG4 that have been suggested to be important to key the characteristics of each isotype. A recent study has undertaken mutagenesis studies to determine the residues involved in FcγR interaction and effector functions, which has helped to understand the inherent activities of hIgG1 and hIgG4 [401]. In addition, previous work undertaken at UCB had identified a residue in the CH3 domain of hIgG1, R335, that was important in the hexamerisation efficiency of the hIgG1 Fc domain in the context of μtp C575S technology. Mutagenesis of the hIgG1 R355 for glutamine (the amino acid at the same position in hIgG4) led to a loss of in-solution hexamerisation efficiency of an Fc hexamer. Vice versa, the reverse mutation (hIgG4 Q355R/W417G) increased the hexamerisation efficiency in hIgG4 to that

observed with hIgG1 (personal communication - Dr S Peters). R355 is situated at the base of the hIgG1 Fc, in close proximity to the C-terminal lysine (Figure 5.18,A). Analysis of the surface charge in this region surrounding R355 indicates a positively charged region with a closed cleft, which is predicted to become negatively charged following *in-situ* mutagenesis to Q355, with an open cleft (Figure 5.18,B).

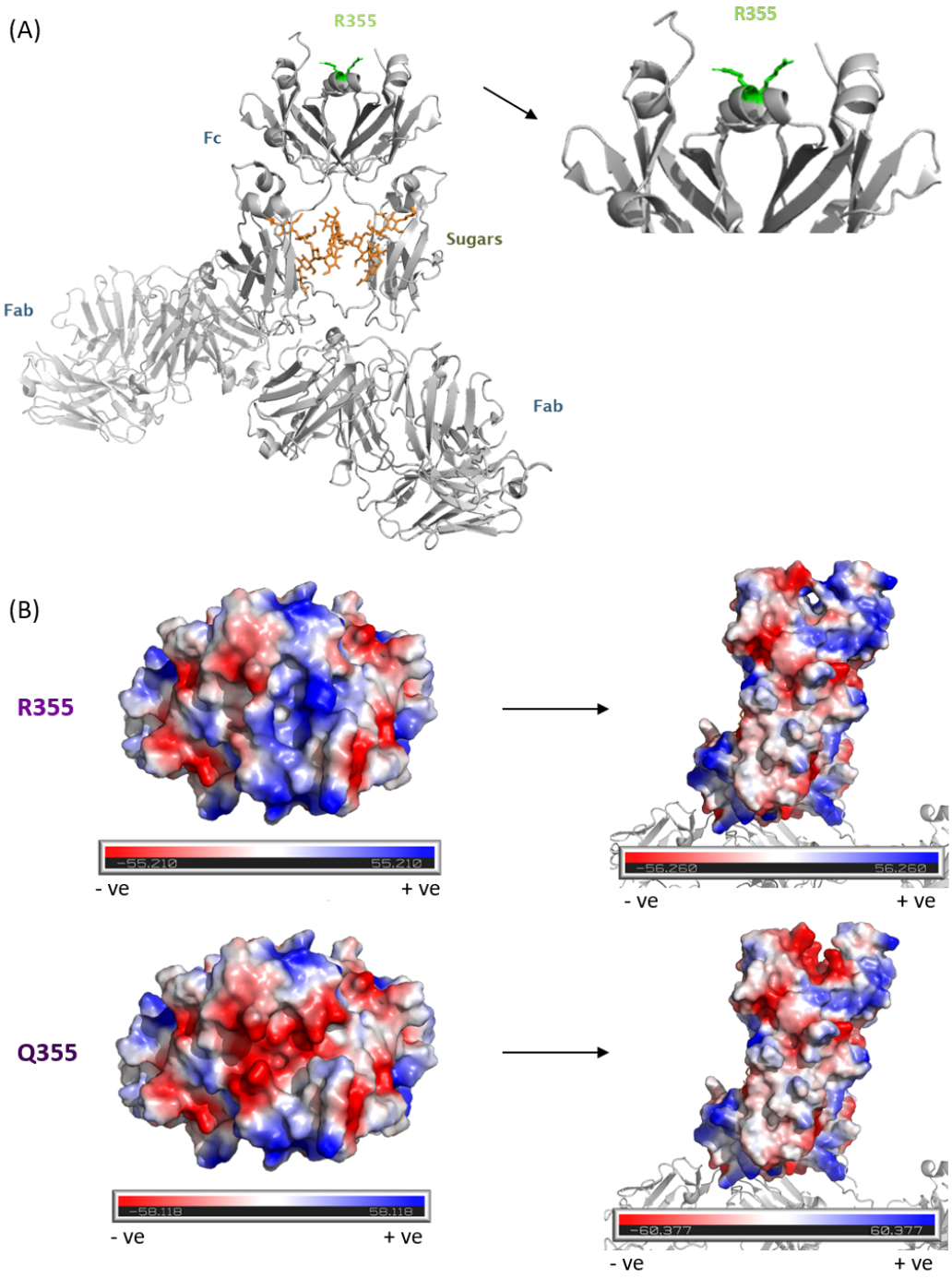

Figure 5.18: Structural analysis of hIgG1 R355.
(A) R355 is located at the base of the hIgG Fc in the CH3 domain. The heavy chain and light chain are shown in grey, N-linked glycosylation in orange, and R355 in green (B) Surface charge analysis of hIgG1 Fc with R355 (left) and Q355 (right). Positive charge shown as red, neutral charge as white, and negative charge as blue.

To investigate if this residue was also important in the hexamerisation enhancement of full-length

hIgG1, mutagenesis was performed on RTX hIgG1 μtp C575S and RTX hIgG4 μtp C575S to incorporate the R355Q and Q355R/W417G mutations, respectively. These constructs were produced and purified as previously described in Chapter 3 to yield RTX hIgG1 μtp C575S/R355Q and RTX hIgG4 μtp C575S/Q355R/W417G (Appendix Tables A1, A2). Subsequently it was noted during sequence analysis for further mutagenesis that there was an additional mutation introduced during mutagenesis (W417G) that was not noticed. This should be kept in consideration during the results herein, and the nomenclature will become as RTX hIgG4 μtp C575S/Q355R/W417G (or μtp CS/QR/WG).

The in-solution hexamerisation tendency was examined and the results suggested that the RTX hIgG1 μtp C575S/R355Q had lost this activity, and did not shift to a multimeric complex in solution at the top concentration of 20 mg/ml (Figure 5.19). Conversely, the RTX hIgG4 μtp C575S/Q355R/W417G gained the ability to undergo hexamerisation in solution as predicted. A multimer species was initially observed at 5 mg/ml, and increased to 18.4% multimer at 20 mg/ml (Figure 5.19). This level of hexamerisation was comparable with hIgG1 μtp C575S, where 16.9% was observed at 20 mg/ml.

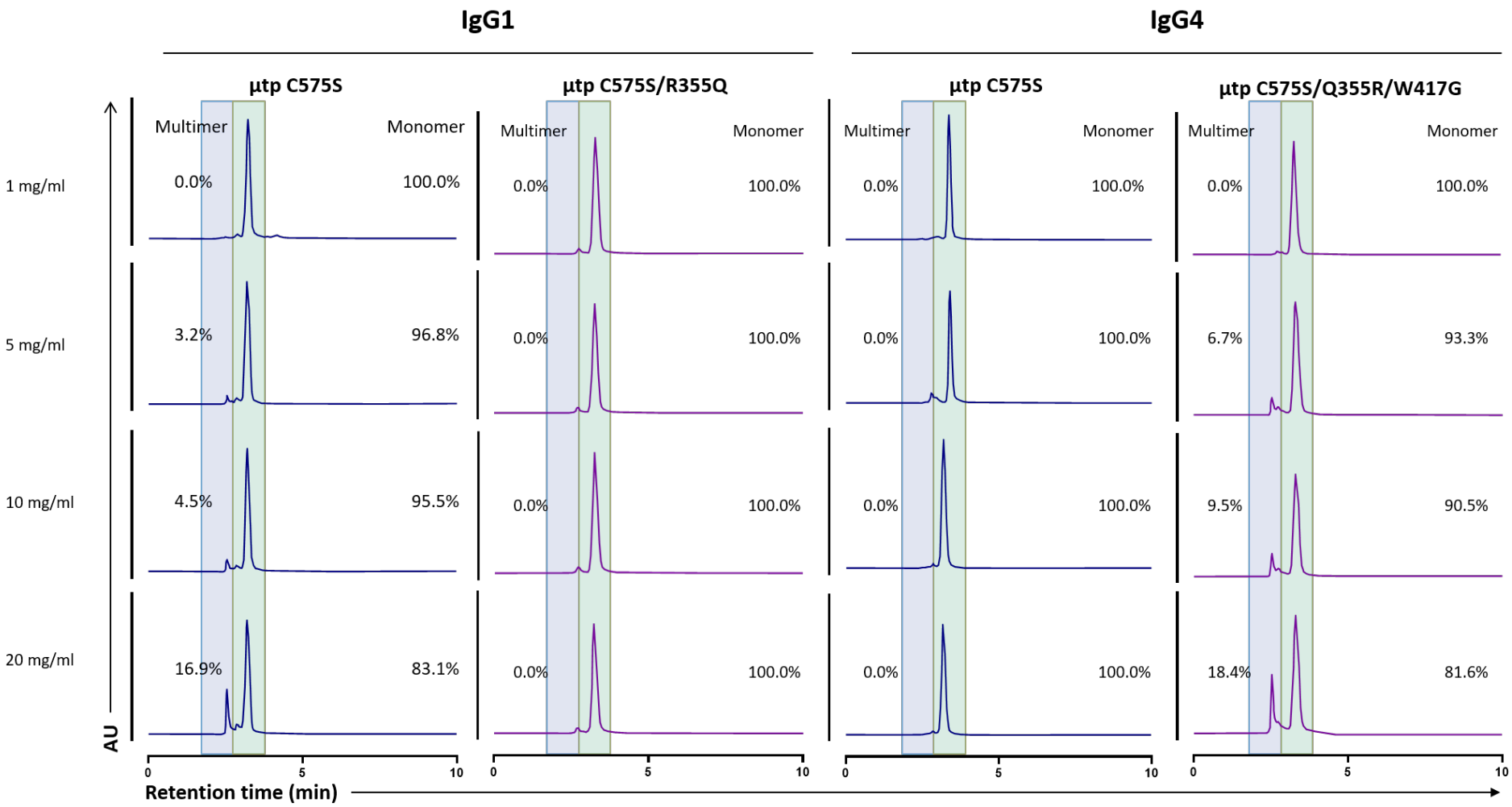

Figure 5.19: Additional CH3 amino acid mutations identified were analysed for the ability to self-associate in solution.
RTX hIgG μtp C575S constructs were concentrated up to 20 mg/ml and the percentage (%) of monomeric and multimeric species was determined by SE-UPLC. Data is showing representative traces of RTX for hIgG1 (left) and hIgG4 (right) μtp C575S constructs at increasing concentrations from 1 mg/ml to 20 mg/ml.

After the in-solution hexamerisation enhancement was investigated, the C1q binding activity was examined. The level of C1q binding in an ELISA for both the hIgG1 μtp C575S/R355Q and hIgG4 μtp C575S/Q355R/W417G was comparable with their μtp C575S isotype counterparts (Figure 5.20,A), with comparable levels of plate-bound mAb (Appendix Figure A13). In terms of cell surface recruitment, hIgG1 μtp C575S/R355Q had an increase in C1q recruitment compared with RTX hIgG1 μtp C575S and was more analogous to the hIgG1 μtp hexamer (Figure 5.20,B). This was unexpected as previous results had shown a decrease in the in-solution hexamerisation. The RTX hIgG4 μtp C575S/Q355R/W417G construct demonstrated greater C1q recruitment to Ramos cells, in this case to a greater extent than the hIgG4 μtp C575S and hIgG4 μtp hexamer (Figure 5.20,B). This increased activity over the hIgG4 μtp C575S is consistent with the enhancement observed to the solution-based hexamerisation, but is unexpected with regards to its activity exceeding that of the preformed hexamer.

The CDC activity against Ramos cells of RTX hIgG1 μtp C575S/R355Q showed a reduction in CDC activity compared with RTX hIgG1 μtp C575S (Figure 5.20,C). The calculated EC50 for RTX hIgG1 μtp C575S/R355Q in the current assay was 0.113 μg/ml, comparable to the EC50 of WT hIgG1 at 0.105 μg/ml. However, this activity was 2.6 fold lower than RTX hIgG1 μtp C575S (EC50: 0.043) and 5.7 fold lower than RTX hIgG1 μtp (EC50: 0.020). Conversely, RTX hIgG4 μtp C575S/Q355R/W417G had greatly enhanced CDC activity compared with RTX hIgG4 μtp C575S, which did not induce complement-mediated cell death (Figure 5.20,C). The results observed indicated that RTX hIgG4 μtp C575S/Q355R/W417G mutant induces higher levels of complement cytotoxicity than the hIgG4 WT and hIgG4 μtp hexamer. The calculated EC50 of the RTX hIgG4 μtp C575S/Q355R/W417G mutant construct was 0.113 μg/ml, 1.9 fold higher than RTX hIgG4 μtp (EC50: 0.218 μg/ml) and comparable with RTX hIgG1 WT (EC50: 0.105 μg/ml). These results are consistent with the RTX IgG4 μtp C575S/Q355R/W417G ability to self-associate in solution and recruit C1q at levels higher than its hexameric counterpart, whilst its C1q binding in an ELISA remained constant. Therefore, the current results are most consistent with an on-target hexamerisation enhancement with IgG4.

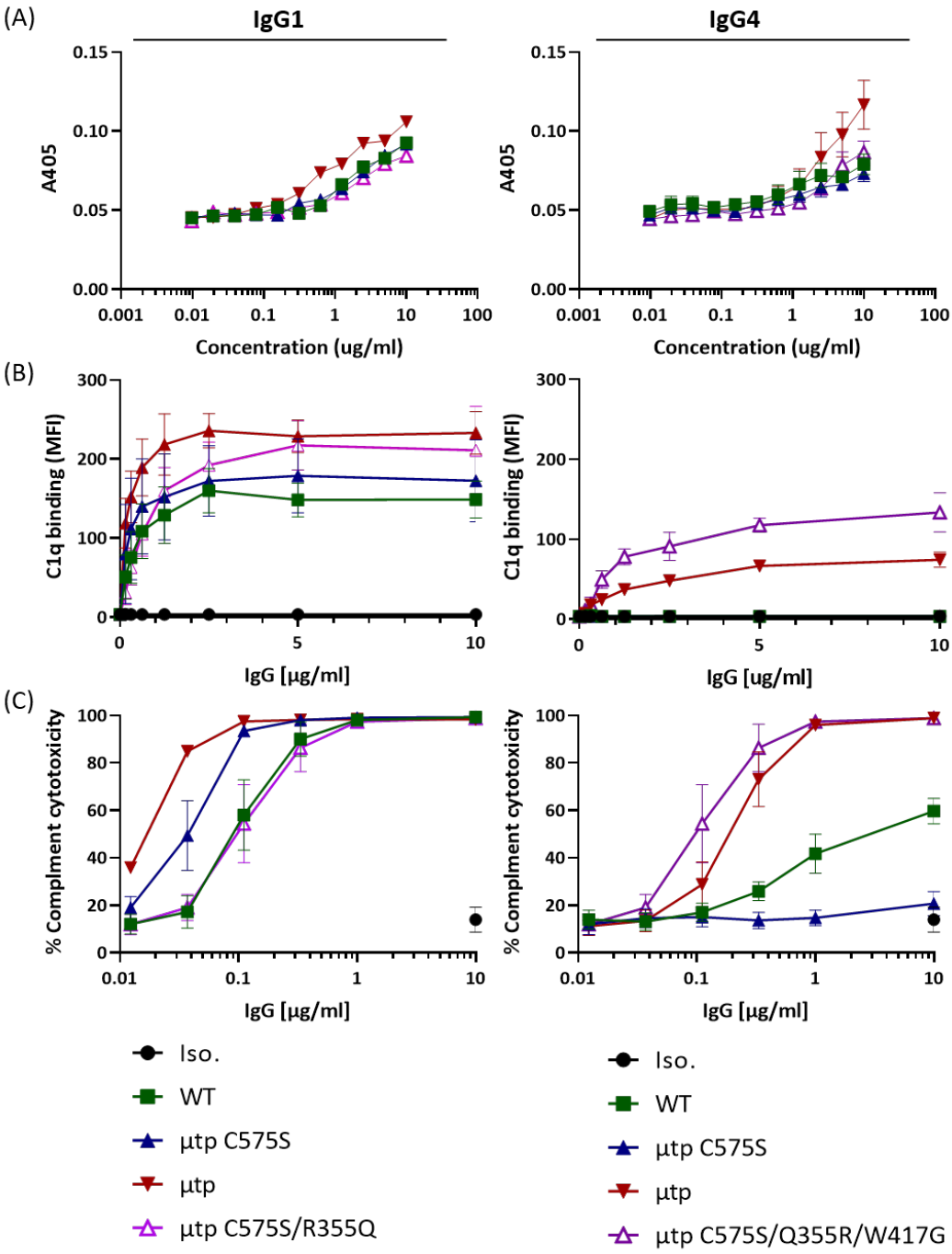

Figure 5.20: Analysis of complement activation by hIgG1 and hIgG4 μtp C575S with Fc mutations.
(A) ELISA plates were coated with RTX hIgG μtp constructs at various concentrations. Human C1q (2 μg/ml) was added and bound C1q was detected with a goat anti-human C1q antibody followed by a peroxidase-conjugated anti-goat IgG-Fc antibody. Data shows absorbance at A405 of bound C1q to hIgG1 (left) and hIgG4 (right) constructs (N=3) (B) $CD20^+$ Ramos cells were opsonsised with 1151 isotype controls or RTX hIgG constructs at various concentrations followed by 2 μg/ml human C1q. Bound C1q was determined using an anti-C1q-FITC antibody and analysed by flow cytometry. Data shows MFI of anti-C1q-FITC antibody for cells opsonised with hIgG1 (left) and hIgG4 (right) constructs (N=3) (C) Ramos cells were opsonised with RTX hIgG constructs and incubated with 20% NHS. Cellular lysis was determined by staining cells with PI and analysed by flow cytometry for PI positive cells. Data shows percentage (%) of cell cytotoxicity of cells opsonised with hIgG1 (left) and hIgG4 (right) constructs (N=4). Data plotted is mean and SEM of multiple independent experiments.

5.8 Chapter discussion

It is well-known that the induction of CDC requires critical residues in the Fc and the N297-linked glycan that enable efficient C1q recruitment [199, 346, 421]. These factors (C1q contact residues and glycosylation) were investigated in this chapter in order to ascertain their influence on CDC stimulated by hIgG1 μtp hexamers and μtp C575S on-target hexamers. As highlighted earlier in the chapter, two specific mutations used to inhibit complement activation are P331S and K322A. Mutagenesis of P331S in the μtp fusion mAb showed that this mutation does not completely inhibit the CDC activity of the hIgG1 μtp hexamer or hIgG1 μtp C575S on-target hexamer, although there was complete inhibition with the WT hIgG1, as predicted from the literature (Figure 5.1). As an alternative, the K322A mutation was utilised and demonstrated complete inhibition of C1q recruitment with the RTX μtp hexamer, but the construct could still induce CDC, albeit to a much lesser extent than the WT RTX μtp hexamer (Figure 5.2). Together, these results demonstrated that hexamerisation of hIgG1 is able to overcome low affinity C1q binding. Therefore these mutations (P331S and K322A), thought of as CDC null mutations, should be carefully considered depending on the mAb format. It should also be noted that the mechanism by which RTX hIgG1 μtp C575S/P331S displayed decreased complement cytotoxicity in the presence of these mutations was not formally investigated. For example, whether the observed loss of C1q recruitment and CDC was a result of a loss of hexamerisation efficiency or C1q affinity alone. This could be investigated by examining the in-solution hexamerisation propensity of this construct.

A more effective method of inhibiting CDC with hexamerisation enhanced mAb was through deglycosylation (Figure 5.5, 5.6). Glycans are important post-translational modifications that can influence stability, function, and receptor recognition [483–485]. Glycoproteins that are membrane bound or secreted are generally glycosylated to aid in the recognition of, and interaction with, ligands [486–488]. The composition of the N297 glycan site has previously been demonstrated to influence Fc-mediated effector functions. This has been exemplified by afucosylated hIgG1 that induce potent ADCC [346] and Fc-degalactosylation that has enhanced C1q binding and CDC activity [438]. Conversely, deglycosylation has been shown to inhibit all of the Fc-mediated effector functions (ADCC, ADCP, CDC) of IgG [472]. The CH2 sugars engage in carbohydrate to carbohydrate interactions that stabilise the Fc domain [473]. The stabilising effect is thought to contribute to the stability of the lower hinge region, where FcγR and C1q binding sites are present [355, 489]. Aglycosylation of the Fc, either by digestion with endoglycosidases or mutagenesis (N297A), results in a conformational change in the CH2 domain and subsequently reduces binding to FcγRs and C1q [102, 355, 473, 474].

In all cases of hIgG1 μtp C575S deglycosylation there was a complete loss of complement cytotox-

icity (Figures 5.5, 5.12). However, in the context of hIgG1 μtp hexamers there was not a complete inhibition of C1q recruitment or CDC (Figure 5.6). This could indicate that a high avidity interaction of an hIgG1 hexamer with C1q is strong enough to overcome the weak C1q affinity caused by Fc deglycosylation. Additionally, it could be suggested that the inhibition of CDC with deglycosylated hIgG1 μtp C575S mAb was a result of the loss of in-solution hexamerisation efficiency, and therefore hexamerisation enhancement (Figure 5.5). Therefore, glycosylation could be proposed to be essential for the Fc:Fc interactions between hIgG1 μtp C575S molecules. These results also suggest that for studies whereby a CDC silent mAb is essential, Fc deglycosylation are more effective than the P331S or K322A mutations. The caveat is that deglycosylation also renders IgG1 unable to find FcγRs, whereas Fc mutations can be introduced to selectively decrease C1q binding over FcγR binding, and vice versa [344, 421].

In addition to CH2 glycosylation within the Fc, the μtp C575S has a glycosylation site (N563). It was considered that the glycan occupancy of this site was also likely to impact the CDC activity. As described previously, glycosylation occurs after the OST enzyme recognises a Asn-X-Ser/Thr sequence for N-linked glycosylation on the nascent polypeptide chain during translocation into the ER [425, 490–492]. Studies have determined that not all N-glycosylated consensus regions are glycosylated during ER translocation [493–495]. A more recent study has investigated the optimum consensus sequence for efficient N-linked glycan occupancy. Here amino acids at position *n*+1 and *n*+2 were mutated and the results indicated that *n*+1 favours hydroxyl- or amide-containing residues and *n*+2 favours threonine over serine for more complete glycan occupancy [480].

In order to investigate these aspects on the glycosylation occupancy on the μtp C575S N-linked glycosylation site, residues of the consensus sequence were altered by mutagenesis. This was initially undertaken at UCB with hIgG1 Fc μtp C575S constructs which demonstrated these mutations influenced the hexamerisation propensity, and so were proposed to have a similar effect on full-length hIgG1 μtp C575S constructs. RTX hIgG1 μtp C575S mAb were engineered to contain either aspartic acid or leucine at position *n*+1 (V564) or the serine was exchanged for threonine at position *n*+2 (S565). Glycan analysis of these μtp C575S mutants showed that the V564D and V564L has slightly reduced levels of glycan occupancy, whereas S565T has substantially higher levels of occupancy. Importantly, these mutations did not alter the occupancy of the CH2 N297 glycan site (Figure 5.7), or substantially alter the glycan species present on either the CH2 or μtp glycan site (Figure 5.8). These results are in accordance with results published by Huang *et al* indicating that residues D or L at position *n*+1 should reduce glycosylation and T at position *n*+2 should increase glycan occupancy [480].

Altering glycan occupancy of the μtp C575S had clear impacts on the in-solution hexamerisation

efficiency of hIgG1 μtp C575S mAb and on-target hexamerisation (Figure 5.9 and 5.20) without impacting FcγR-mediated cell killing (Figure 5.13). The results suggested that the hexamerisation enhancement gained with the μtp C575S can be further increased, and in the case of the μtp C575S/S565T construct translated to augmented complement cytotoxicity (Figure 5.11). Additionally, there was a decrease in the solution-hexamerisation and CDC activity of the hIgG1 μtp C575S/V564D construct which corresponded to reduced cell surface C1q binding and negligible CDC. Glycan analysis suggested this construct had the lowest occupancy of the μtp N563 glycan. The hIgG1 μtp C575S/V564L construct demonstrated an enhancement in solution hexamerisation and C1q cell surface recruitment, but no CDC enhancement was observed. To probe the importance of the glycans, digestion of the N297 and N563 glycans was performed, rendering these mAb unable to induce CDC. Together with the glycan analysis it could be inferred that the occupancy of the μtp C575S glycan has profound effects on the hexamerisation enhancement and CDC activity, and that higher occupancy of the μtp glycan is the driving force for enhanced CDC activity. Therefore, it could be concluded that the presence of glycans on both the CH2 and μtp are essential for efficient complement-mediated cell death. Potentially, the CH2 glycans are involved in the canonical C1q interactions within the Fc, whereas the μtp C575S glycans drive the hexamerisation enhancement.

In addition to hIgG1 modifications, complement efficiency can also be modulated by selecting different isotypes. Human IgG2 and IgG4 are well characterised as CDC inactive isotypes [475, 476], and were also examined in the context of RTX μtp fusion constructs to determine if hexamerisation could overcome this lack of activity. There is clear evidence that fusion of the μtp C575S was not sufficient to induce an enhancement of in-solution hexamerisation or large increase in complement efficiency of hIgG2 (Figures 5.14, 5.17) or hIgG4 (Figures 5.16, 5.15). This weak complement cytotoxicity may result from a combination of weak on-target hexamerisation coupled to the inherently low C1q affinity and recruitment. Alternatively it could be considered that any increase is delivered by the on-target hexamerisation but that large effects in CDC are impaired by the low C1q affinity of these isotypes. Efforts to study receptor clustering or increase the C1q affinity of RTX hIgG2 μtp C575 may help to understand the mechanism further. An indication of how hexamerisation was able to drive the increased effector function of these isotypes was generated with the preformed μtp hexamers. Both hIgG2 and hIgG4 exhibited enhanced complement activity, albeit not as effectively as hIgG1 WT. This again indicated that a high avidity hexameric interaction for C1q can boost the activity of even low C1q affinity mAb formats.

The lack of on-target hexamerisation enhancement with the μtp C575S variants of these isotypes could suggest that the constant regions of the IgG isotypes dictate these Fc:Fc interactions. There is evidence that the CH3 domain of hIgG1 has residues that drive non-covalent Fc:Fc interaction

[197]. There are a number of differences in the amino acid sequences between hIgG1 and hIgG4 that impart different effector functionality, such as the amino acid at position 355 [423]. Therefore, it could be reasonable to assume that similar residue differences also dictate the Fc:Fc interactions underpinning hexamerisation. Work has been undertaken to exchange residues between hIgG1 and hIgG4 CH3 domains in an effort to dissect where differences in FcγR and C1q binding originates [401]. Further work at UCB has identified residues in the CH3 domains of hIgG1 and hIgG4 that are in-part responsible for the differences in the hexamerisation enhancement observed between Fc μtp C575S versions of these two isotypes. This difference in hexamerisation efficiency is also observed between non-Fc modified RTX hIgG μtp C575S constructs as hIgG1 or hIgG4 isotypes. Mutagenesis to switch residue 355 between hIgG1 and hIgG4 reverses the hexamerisation enhancement, giving hIgG4 higher levels of on-target hexamerisation (Figures 5.19, 5.20). The key residue at position 355 is located at the base of the Fc, in close proximity to the terminal lysine where the μtp is fused. There is also a charge switch between the two residues (Q and R). It could therefore be speculated that this residue interacts with or influences the μtp with an impact on the hexamerisation efficiency induced by the μtp C575S peptide. Although the levels of solution hexamerisation for hIgG4 μtp C575S/Q335R/W417G were comparable with the native hIgG1 μtp C575S construct, the overall CDC enhancement was still lower and comparable with RTX hIgG1 WT. This could be presumed to be a result of lower C1q affinity that is inherent with hIgG4. The augmented CDC activity is therefore likely driven by high avidity interaction between the Fc hexamer and C1q. In order to gain further understanding of this enhancement, glycan analysis could be performed. As previously shown, the μtp C575S glycan plays an important role in the hexamerisation enactment of μtp C575S constructs. It is possible that the enhancement observed with the hIgG4 μtp C575S/Q355R/W417G construct could be a result of increased glycan occupancy at the μtp glycan.

In addition to residues such as Q355 in the hIgG4 polypeptide sequence that have been implicated in low CDC activity, hIgG4 has a shorter hinge region than hIgG1 which has also been proposed to impart reduced flexibility and result in restricted complement activation [496–498]. In contrast to full-length hIgG4, hIgG4 Fc has been demonstrated to activate complement [499], suggesting that the isotype is capable of inducing complement activation but that it is restricted by other structural characteristics. One proposal has been that short hinge allows the Fab fragments to shield the C1q binding sites within the CH2, due to cis or trans binding between the CH1 and CH2 domains [500]. However, the current results would indicate this hypothesis is potentially flawed as full-length hIgG4 in either a hexamerisation enhanced (μtp C575S/Q355R/W417G) or preformed hexamer (μtp) format is capable of inducing efficient CDC activity. One such possibility is that the process of hexamerisation unlocks the C1q binding site through a conformational

change to a more open structure. Regardless, the data clearly demonstrate that, at least in part, the hexamerisation using μtp technology was able to provide CDC function to otherwise inactive isotypes.

It is important to recognise that all of these later mutations in the hIgG4 were introduced alongside an unplanned W417G mutation. Although missed in the original sequencing, this mutation was subsequently shown to be present in the following hIgG4 constructs: RTX hIgG4 μtp C575S/Q355R, ChiLob 7/4 μtp C575S, ChiLob 7/4 hIgG4 μtp C575S/Q355R. Sequence alignment indicates that this residue is conserved between hIgG1, 2, and 4, and structural analysis indicates it is also located at the base of the Fc in close proximity to the C-terminus. Furthermore, tryptophan has a large aromatic side-chain, whereas glycine has a small side-chain which may alter flexibility and hydrophobicity in the region and therefore could be functionally important in Fc mobility and potential Fc:Fc interactions. A literature search has not uncovered any function attributed to this residue in hIgG. In order to determine if this mutation could have any impact on the observed augmented activities further mutagenesis studies are required. This could include producing RTX hIgG4 μtp C575S/W417G, hIgG4 μtp C575S/Q355R, and hIgG4 μtp C575S/Q355R/W417G to be examined to assess any differences for in-solution hexamerisation, on-target hexamerisation, C1q binding, and CDC activity. If found that W417G promotes hexamerisation of hIgG4 μtp C575S constructs, this mutation could also be examined in the context of RTX hIgG1 μtp C575S for in-solution and on-target hexamerisation.

In summary, this chapter has shown that hIgG1 hexamers and on-target hexamers are impacted by C1q null mutations, albeit to a lesser extent than WT hIgG1, and still retain activity. It has also been shown that these constructs rely on glycosylation for CDC activity. Such technology is also able to provide an increase in CDC activity to non-functional isotypes (hIgG2/hIgG4) but is unable to convert them into reagents with activity greater than canonical hIgG1. However, it was shown that other mutations, both in the Fc and μtp C575S peptide can further enhance CDC with hIgG1 μtp C575S and convert the inactive hIgG4 μtp C575S into efficient complement activators. The utilisation of a CDC active hIgG4 could be therapeutically advantageous in instances when FcγR-mediated effectors are unwanted, but complement-mediated killing is beneficial. The impacts of the mutations studies here and use of alternative isotypes are summarised in Figure 5.21.

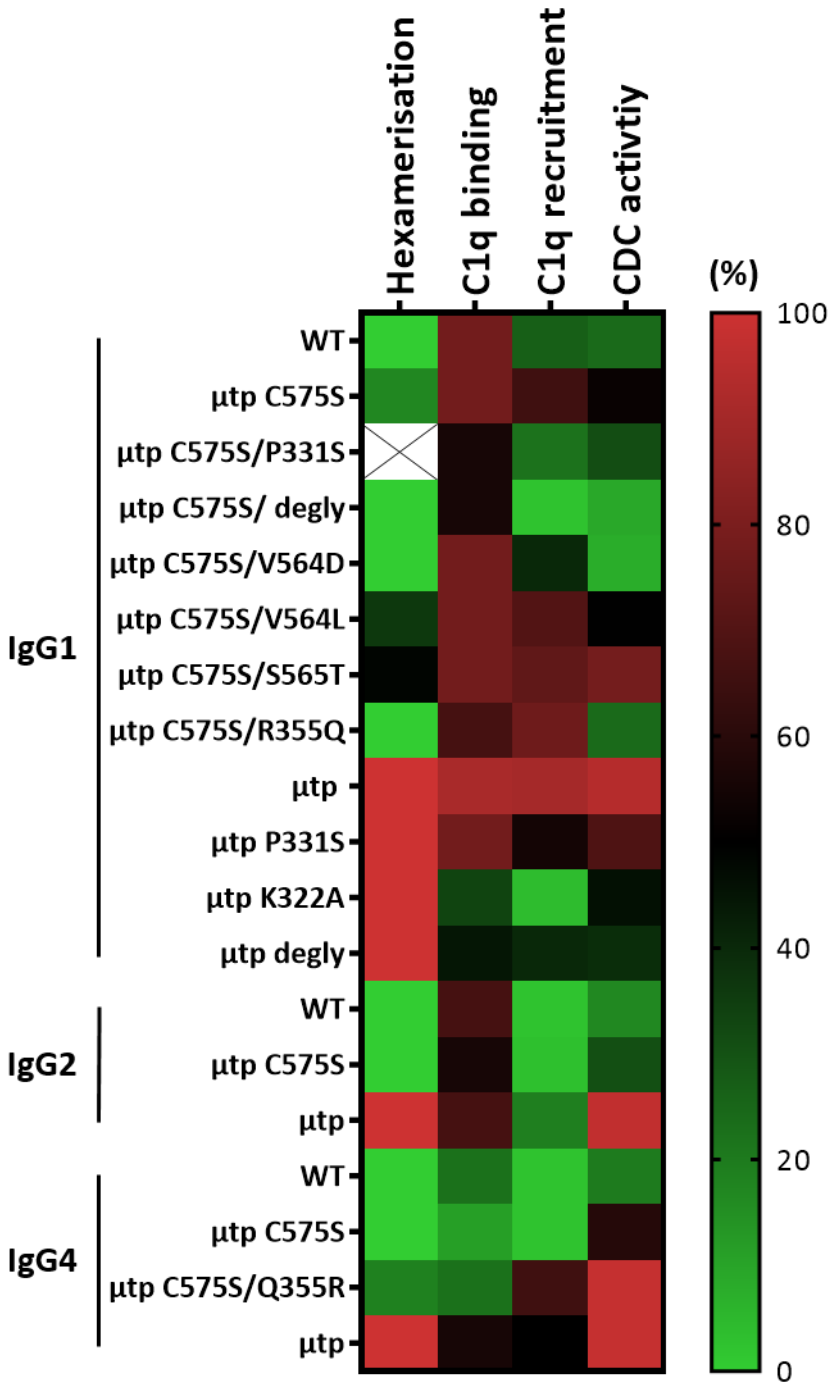

Figure 5.21: Summary of the *in vitro* complement activity induced by anti-CD20 μtp fusion mAb.
The solution hexamerisation efficiency and on-target hexamersiation efficiency of RTX hIgG1, 2, and 4 mAb expressed as a percentage (%) of maximal activity in each assay calculated using the mean. RTX hIgG1 CDC activity is against Raji cells as targets, RTX hIgG2 and 4 CDC activity is against Ramos cells as targets.

Chapter 6

Characterisation of hexamerisation-enhanced anti-CD40 antibodies

6.1 Chapter introduction

The advent of immunomodulatory antibodies to the arsenal of anti-cancer agents has so far demonstrated great promise. In particular, checkpoint blockers such as, ipilimumab (anti-CTLA-4) and nivolumab (anti-PD-1) have demonstrated impressive clinical responses. When combined with the conventional cytotoxic agent dacarbazine, patients treated with ipilimumab demonstrated an improved overall response rate (ORR) from 8.1 months to 19.3 months [285]. In a phase 3 study with ipilimumab, the 2-year overall survival rate was 24.2% although this response was driven by a small subset of patients [289]. Additionally, the fully human IgG4 anti-PD-1 mAb nivolumab has observed further increased survival rates in the treatment of solid tumours [287]. When used in combination with ipilimumab, the pair worked synergistically to provide even further therapeutic benefit [286, 288], resulting in 53% of patients exhibiting 4-year survival [501]. Although initial success has shown the huge potential of immunomodulatory mAb as anti-cancer therapeutics, not all patients respond and resistance and/or toxicity is frequently an issue. In addition, the mechanisms of response to these mAb is not well understood, and although these current results are promising, there is clearly room for improvement to increase the population of responsive individuals.

A possible alternative to the use of checkpoint blockers, is the use of immunostimulatory antibod-

ies, such as anti-CD40 mAb. CD40 is expressed primarily on APCs, whereby stimulation results in the licencing of APCs, such as DCs and B cells [291, 300, 301]. This can result in profound anti-tumour activity through expansion of tumour-specific CTLs and induction of a humoral response. Current clinical investigations using agonistic anti-CD40 mAb have only demonstrated limited therapeutic response [335–337], thought to be restricted either by a lack of receptor agonism [337] or by dose-limiting toxicities [338–341].

Current research has demonstrated the importance of receptor cross-linking for the agonistic activity of anti-CD40 mAb. For many antibodies this can be mediated by FcγRIIb [331, 332, 502]. One approach utilised to enhance the anti-tumour activity of anti-CD40 mAb has been to increase their affinity for FcγRIIb, exemplified by V11 or SELF mutations [352]. However, this approach is not the most desirable due to the requirement of high bioavailability of FcγRIIb for anti-tumour efficacy, and therefore in environments lacking this receptor these mAb will be ineffective. Furthermore, antibodies encompassing high affinity mutations for the inhibitory FcγR have the potential to bind FcγRIIb as a monomeric, non-target bound antibody, which could prevent receptor binding and subsequent agonism.

As previously mentioned, the natural ligand for CD40, CD40L, is a trimer that induces receptor trimerisation after binding [303]. The cross-linking provided by FcγRIIb in anti-CD40 mAb agonism has been proposed to aid in the receptor clustering required for stimulation. It is becoming evident that methods could be employed to produce FcγR-independent cross-linking mAb. The hIgG2 isotype has been shown to induce efficient CD40 agonism in the absence of FcγR cross-linking [90, 334]. Additionally, antibody engineering approaches can be employed. The use of the aforementioned E430G and E345K mutations to generate hexamerisation enhanced IgG has been used to enhance receptor clustering and subsequent activation, independent of FcγR cross-linking. This has been reported for mAb targeting the immunostimulatory receptor OX40 [379, 380].

Therefore it was proposed that the μtp C575S on-target hexamer and μtp hexamer technology may also be used to mediate increased CD40 agonism. This chapter focused on its application to the clinically-relevant anti-CD40 mAb, ChiLob 7/4. ChiLob 7/4 is a chimeric anti-CD40 antibody that has previously demonstrated agonistic activity *in vitro* and *in vivo* [503] and progressed to phase I clinical trials [504]. This anti-CD40 mAb was therefore examined as hIgG1, 2, and 4 isotypes in the presence of the μtp and μtp C575S peptides using a selection of *in vitro* and *in vivo* assays designed to observe CD40 activation.

6.2 Ability of anti-CD40 hexamerisation-enhanced IgG to drive CD40 signalling in a Jurkat NF-κB-GFP reporter cell line

As previously described in Chapter 3, hIgG1, 2, and 4 anti-CD40 (ChiLob 7.4) antibodies were designed, expressed, and purified in μtp hexamer and μtp C575S on-target hexamer formats (Appendix Tables A1, A2). As mentioned in Chapter 5, the RTX hIgG4 μtp C575S/Q355R construct had an unexpected W417G mutation. The W417G was originally embedded into the ChiLob 7/4 hIgG4 μtp C575S construct, that was mutated to produce ChiLob 7/4 hIgG4 μtp C575S/Q355R; leading in fact to a ChiLob 7/4 hIgG4 μtp C575S/Q355R/W417G protein. The latter construct was subsequently sub-cloned to encode the RTX V region producing RTX hIgG4 μtp C575S/Q355R/W417G.

Firstly, the agonistic potential of the mAb *in vitro* was examined using a Jurkat NF-κB-GFP reporter cell line transfected with hCD40. NF-κB activation results in GFP expression which can be analysed by flow cytometry (Figure 6.1,B). Following preliminary experiments assessing kinetics of activation, the cells were stimulated for 6 hours at concentrations between 10 - 0.00001 μg/ml with anti-CD40 mAb. Jurkat cells do not express FcγRs, therefore any observed agonism was independent of FcγR-mediated cross-linking, but instead attributed to the ability of the mAb to cluster the receptor.

In the context of hIgG1, the μtp hexamer displayed the highest GFP expression, with a peak response at 6,410 MFI, and higher when compared to the positive control, CP-870,893 (CP) hIgG2, which had a peak response of 4,531 MFI (Figure 6.1,C). Cells stimulated with either the WT or μtp C575S hIgG1 ChiLob 7/4 antibodies demonstrated comparable GFP expression, with peak responses around 500 MFI. The observed GFP expression was greatly reduced compared to the pre-formed μtp hexamer (12.8-fold lower) and CP hIgG2 (9-fold lower) (Figure 6.1,C). These results indicated that the on target hexamerisation enhancement (μtp C575S) does not enhance CD40 activation for hIgG1, but that preformed hexamers (μtp) do.

As expected, stimulation with hIgG2 WT induced robust GFP expression, with a peak response of 5,824 MFI at 0.01 μg/ml (Figure 6.1,C). The observed stimulation gave a bell-shaped curve, whereby the peak of the response was in the middle of the concentration range examined. Agonism with ChiLob 7/4 hIgG2 μtp C575S demonstrated comparable GFP expression when compared to its WT counterpart, and a peak response of 5,666 MFI also at 0.01 μg/ml (Figure 6.1,C). Similarly as with the hIgG1 mAb, the hIgG2 μtp hexamer exhibited the highest GFP expression, with a peak response of 7,987 MFI at 0.1 μg/ml (Figure 6.1,C). When compared to the CP hIgG2 positive control, it was observed that all three ChiLob 7/4 hIgG2 mAb exhibited higher CD40 agonism at lower concentrations (0.01-0.1 μg/ml) due to their bell-shaped curves.

White *et al* previously showed that ChiLob 7/4 hIgG4, like hIgG1, does not efficiently agonise CD40 *in vitro* [90]. The current results with the reporter assay were consistent with this finding showing that ChiLob 7/4 hIgG4 WT demonstrated no GFP expression, (Figure 6.1,C). However, cells stimulated with the hexamerisation enhanced hIgG4 μtp C575S/W417G demonstrated greatly increased GFP expression (peak of 3,361 MFI) compared to the WT, and comparable GFP stimulation to the positive control CP hIgG2 up until 0.1 μg/ml (Figure 6.1,C). Again, the μtp hexamer induced the highest level of GFP expression compared to all reagents examined, with a maximum peak MFI of 6,467 (1.4-fold greater than CP hIgG2) (Figure 6.1,C). Together, these results indicated that a preformed μtp hexamer was the optimum format to induce CD40 stimulation in Jurkat reporter cells. In the context of hIgG1 and hIgG2 isotypes there was no enhancement in CD40 agonism with the hexamerisation enhanced μtp C575S over their WT counterparts. However, the hexamerisation enhanced hIgG4 μtp C575S/W417G induced robust CD40 stimulation of the Jurkat reporter cell, thereby converting an agonistically-inactive mAb into a mAb capable of receptor agonism. The activity of these anti-CD40 mAb were next examined for their ability to elicit functional consequences of agonism including homotypic adhesion, phenotypic measures of activation, and proliferation, in the context of hCD40Tg mouse splenic B cells.

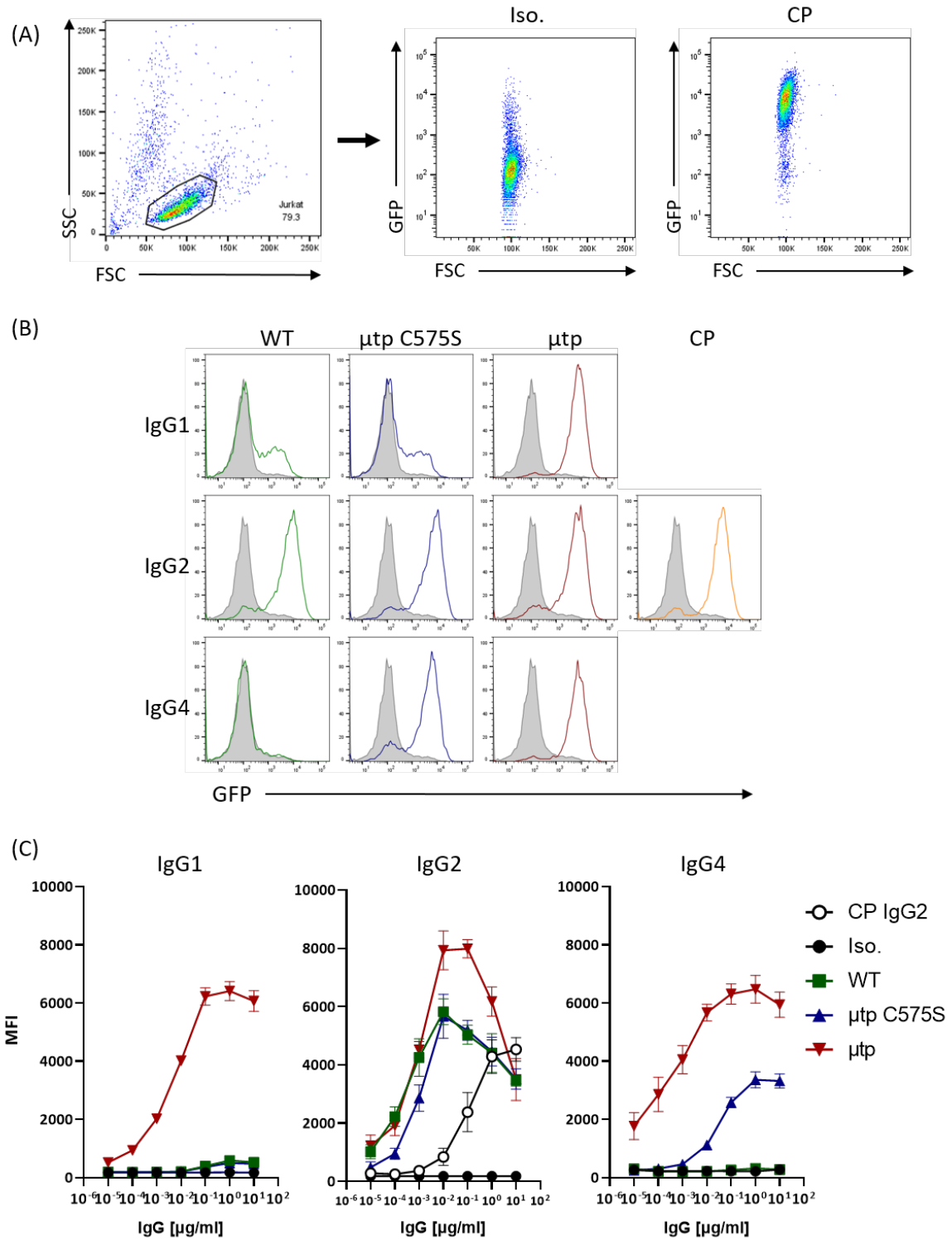

Figure 6.1: Effect of anti-CD40 hIgG μtp constructs on *in vitro* agonism of CD40 expressing Jurkat NF-κB-GFP reporter cells.

1 x 10^5 Jurkat NF-κB-GFP reporter cells transfected with the hCD40 gene were stimulated with RTX hIgG isotype controls or anti-CD40 mAb at various concentrations for 6 hours. Cells were analysed by flow cytometry for GFP expression which indicated CD40 activation (A) Flow cytometry gating strategy of live Jurkat cells and representative plots of isotype control (left) and CP hIgG2 (right) at 10 μg/ml demonstrating GFP fluorescence (B) Representative flow cytometry histograms showing GFP positivity of CD40 expressing Jurkat NF-κB-GFP cells with 10 μg/ml of isotype control (solid grey histogram) of anti-CD40 mAb (coloured overlay) (C) Results from a concentration range of mAb stimulated CD40 expressing Jurkat NF-κB-GFP cells. Graphs indicate results with hIgG1 (left), hIgG2 (middle), and hIgG4 (right) constructs. Data shows mean and SD from independent experiments; N=3.

6.3 Agonism of hCD40Tg B cells

6.3.1 Anti-CD40-mAb-induced homotypic adhesion

Homotypic adhesion of B cells was used as an early indication of cellular activation, reported previously with anti-CD40 mAb [90, 332]. In the current assay, B cells were purified from the splenocytes of hCD40Tg BL/6 mice and stimulated with anti-CD40 mAb for 48 hours. Homotypic adhesion was observed as clumps of cells (dark spots) by bright field microscopy at 4x magnification. The use of mouse B cells in this assay also means that there was murine FcγRIIb present, that would aid FcγR-mediated cross-linking.

Stimulation with ChiLob 7/4 hIgG1 WT revealed no homotypic adhesion of cells over the concentration range examined, but stimulation with hIgG1 μtp C575S led to homotypic adhesion being observed at the highest concentrations (>1 μg/ml). These results indicated that a modest but discernable enhancement in homotypic adhesion could be observed with the addition of the μtp C575S. More distinct cell clustering was observed with the ChiLob 7/4 hIgG1 μtp hexamers over the whole concentration range, compared to the control and WT hIgG1 (Figure 6.2).

Purified hCD40Tg mouse B cells were also stimulated with hIgG2 μtp mAb. Compared with the isotype control, all three formats (WT, μtp C575S, μtp) demonstrated cell clustering over the concentration range (Figure 6.3). The homotypic adhesion results for hIgG2 mAb did not indicate any obvious titration over the concentration range, and no obvious differences between formats. This suggested that ChiLob 7/4 hIgG2 was already highly active in this assay and no benefit could be added though hIgG2 on-target hexamerisation (μtp C575S) or hIgG2 hexamers (μtp).

Finally, the hCD40Tg B cells were incubated in the presence of hIgG4 mAb. It was apparent that ChiLob 7/4 hIgG4 WT was unable to induce B cell clustering. In the context of hIgG4 μtp C575S/W417G there was homotypic adhesion at the top concentrations (>1 μg/ml). As with the other isotypes, the homotypic adhesion observed with the μtp hexamer was potent over the whole concentration range, and still prominent at the lowest concentrations (Figure 6.4). This indicated that hIgG hexamers of all isotypes induced efficient homotypic adhesion and were active at very low concentrations .

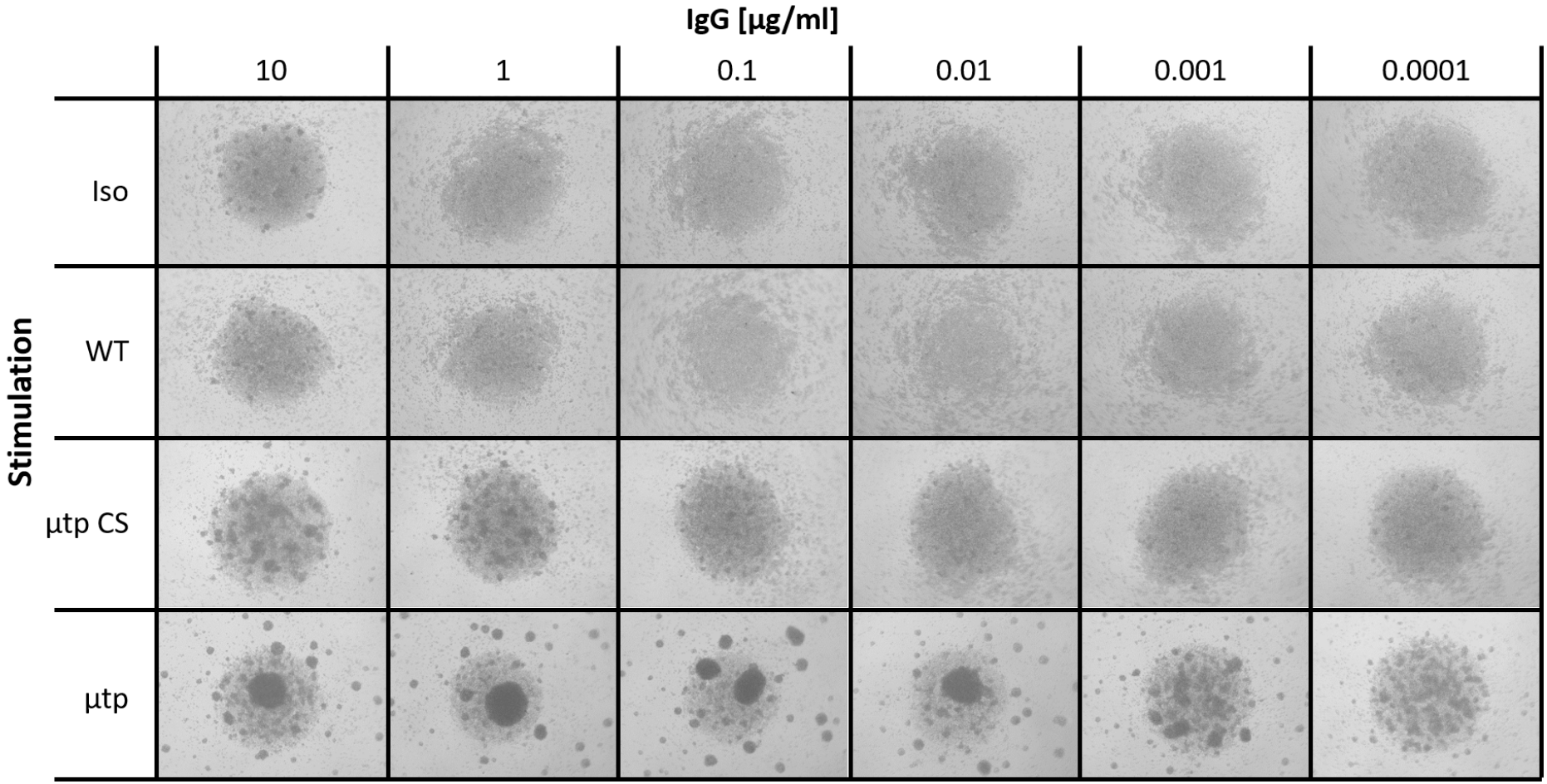

Figure 6.2: Effect of anti-CD40 hIgG1 hexamerisation on hCD40Tg mouse B cell homotypic adhesion.
1 x 10^5 purified mouse hCD40Tg B cells were incubated with hIgG1 anti-CD40 mAb formats (or RTX hIgG1 isotype control) for 48 hours over a concentration range. After 48 hours, cells were imaged at 4X magnification using bright field microscopy to assess B cell clustering induced by CD40 mAb stimulation. Dark spots on images signify homotypic adhesion of B cells.

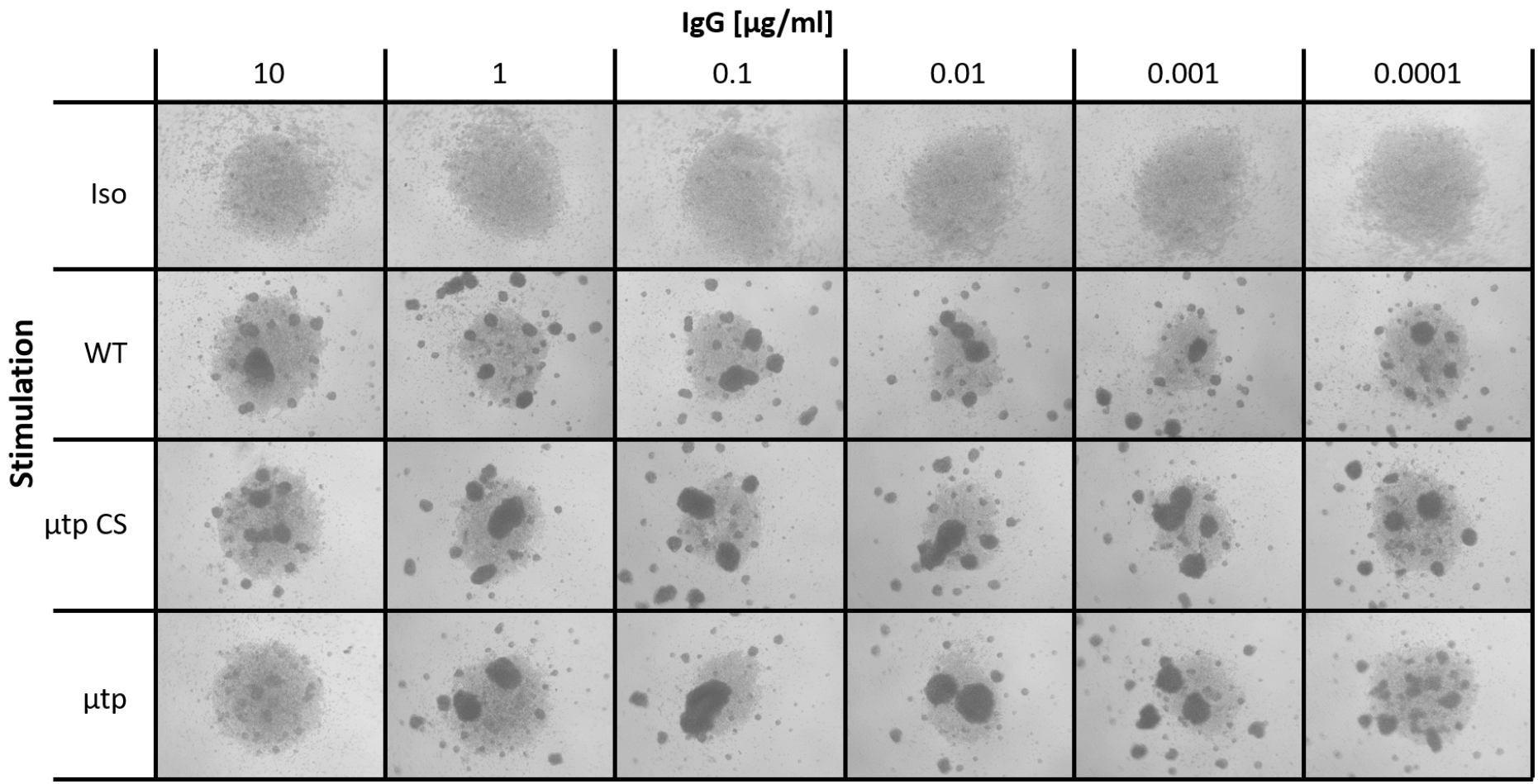

Figure 6.3: Effect of anti-CD40 hIgG2 hexamerisation on hCD40Tg mouse B cell homotypic adhesion.
1 x 10^5 purified mouse hCD40Tg B cells were incubated with hIgG2 anti-CD40 mAb formats (or RTX hIgG2 isotype control) for 48 hours over a concentration range. After 48 hours, cells were imaged at 4X magnification to assess B cell clustering induced by CD40 mAb stimulation. Dark spots on images signify homotypic adhesion of B cells.

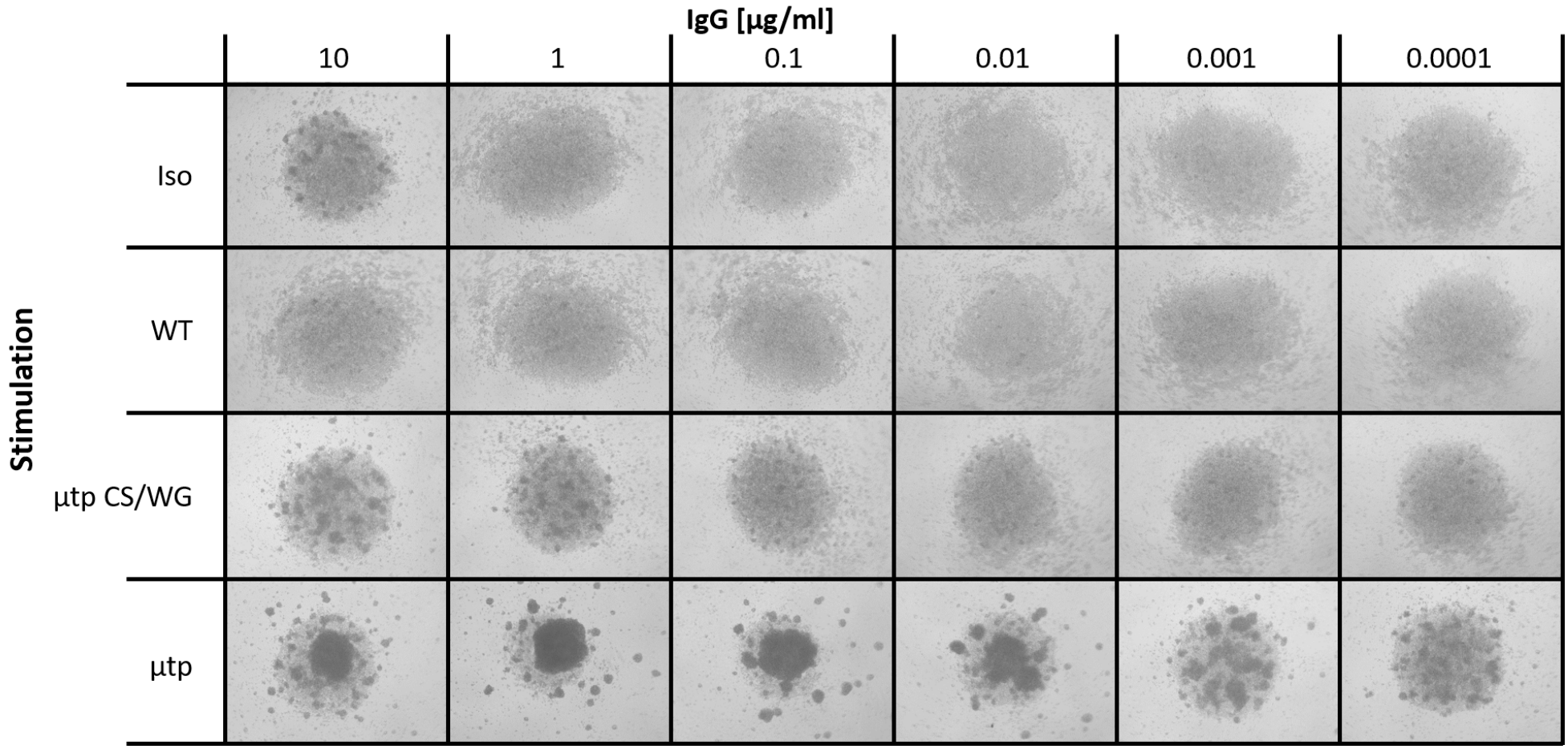

Figure 6.4: Effect of anti-CD40 hIgG4 hexamerisation on hCD40Tg mouse B cell homotypic adhesion.
1 x 10^5 purified mouse hCD40Tg B cells were incubated with hIgG4 anti-CD40 mAb formats (or RTX hIgG4 isotype control) for 48 hours over a concentration range. After 48 hours, cells were imaged at 4X magnification to assess B cell clustering induced by CD40 mAb stimulation. Dark spots on images signify homotypic adhesion of B cells.

6.3.2 Anti-CD40-induced B cell activation

B cell activation can also be measured by flow cytometry. Upregulation of CD23 has been historically used to evaluate the activation state of B cells stimulated with anti-CD40 mAb [90, 332, 334]. The purified B cells were stimulated with mAb for 48 hours prior to being assessed by flow cytometry for CD23 upregulation (Figure 6.5,A-B). Ancillary to ChiLob 7/4 hIgG1/2/4 μtp formats, CP hIgG2 was also examined as a positive control.

ChiLob 7/4 hIgG1 WT demonstrated little upregulation of CD23 over the isotype control molecule, with a peak response of 3,637 MFI at 10 μg/ml (Figure 6.5,C). A comparable result was observed with ChiLob 7/4 hIgG1 μtp C575S (peak response of 2,601 MFI at 10 μg/ml). Both were significantly lower than the CD23 levels evoked by CP hIgG2 (Figure 6.5,C). However, as a preformed hexamer, hIgG1 μtp promoted robust CD23 upregulation, exhibiting a response between 8,500 and 13,700 MFI that was sustained at low concentrations (Figure 6.5,C). At low concentrations (<0.01 μg/ml) the μtp hIgG1 hexamer exhibited higher activation than the CP hIgG2 positive control.

The hIgG2 ChiLob 7/4 mAb all produced similar activation responses, and the characteristic bell-shaped response curve (Figure 6.5,C). The MFI for all three reagents was comparable over the full concentration range, with an MFI range between 5,000 and 19,000 for all three mAb formats. As observed with hIgG1 μtp hexamer, at low concentrations the CD23 upregulation was higher than CP hIgG2 for WT, μtp, and μtp C575S constructs. These results are consistent with previous observations showing that hIgG2 hexamerisation does not enhance the CD40 agonistic activity of ChiLob 7/4 hIgG2.

The ChiLob 7/4 hIgG4 μtp C575S/W417G induced efficient stimulation of hCD40Tg B cells *in vitro* compared to its WT counterpart, with a peak MFI of 11,263 (Figure 6.5,C). The level of activation at 10 μg/ml was equivalent to that seen with the hIgG4 μtp hexamer, which induced potent CD23 upregulation, similar to hIgG1 and hIgG2 μtp constructs. The activity of the preformed μtp hexamer did not subside as the concentration was lowered, producing an MFI in the range of 11,605 - 17,545 across the concentration range. Again, at lower concentrations the μtp hexamer was more active than CP hIgG2 (Figure 6.5,C). These results suggested that incorporation of the μtp C575S/W417G or μtp could enhance the agonstic potential of the anti-CD40 ChiLob 7/4 hIgG4.

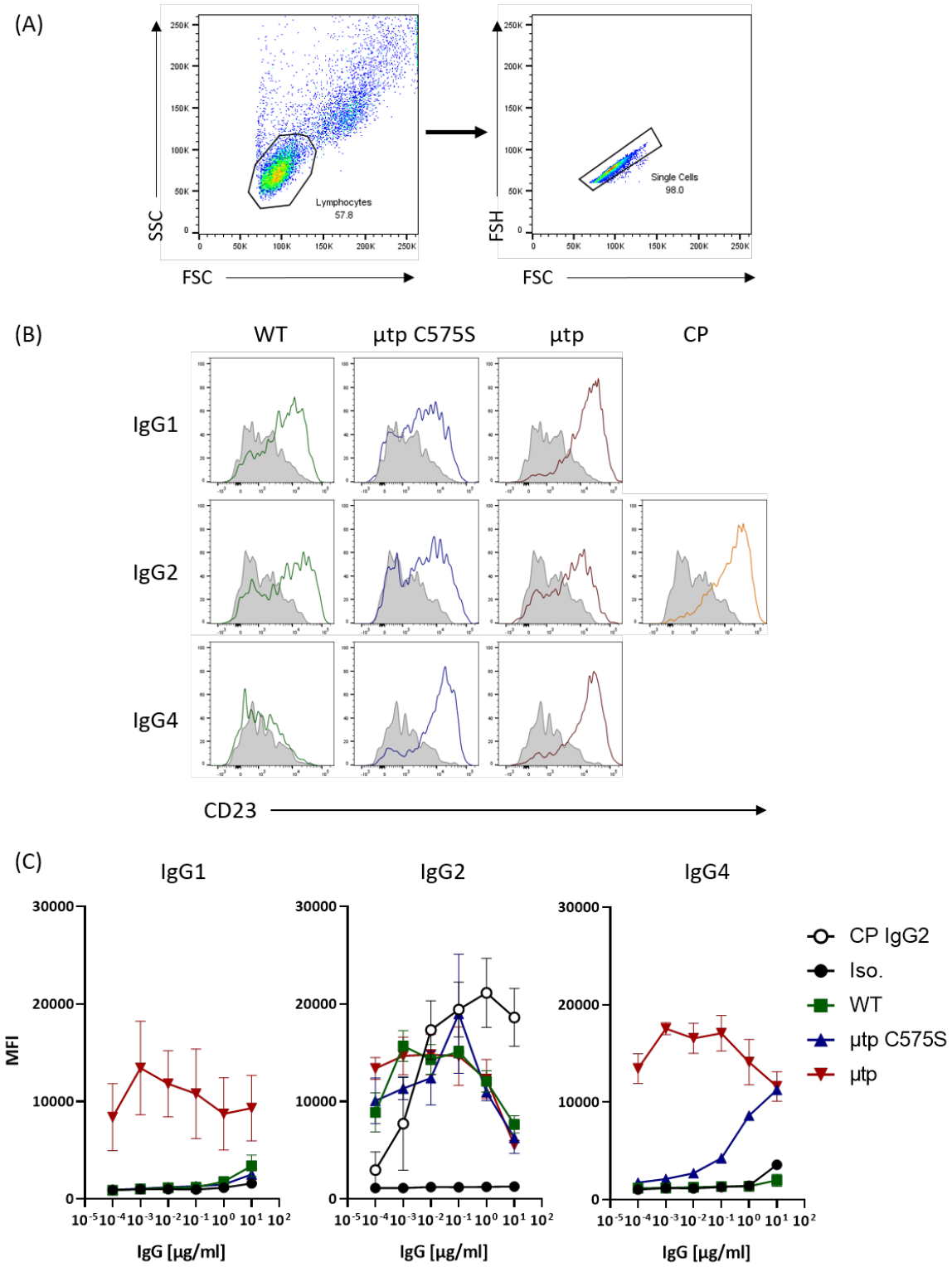

Figure 6.5: Effect of anti-CD40 hIgG hexamerisation on *in vitro* stimulation of hCD40Tg mouse B cells.
1 x 10^5 of purified mouse hCD40Tg B cells were incubated with hIgG anti-CD40 mAb formats (or RTX isotype controls) for 48 hours over a concentration range. After 48 hours cells were analysed by flow cytometry for mouse CD23 upregulation (A) Flow cytometry gating strategy for live hCD40Tg B cells (B) Representative flow cytometry histograms showing CD23 upregulation on hCD40Tg B cells stimulated with 10 μg/ml of isotype control (solid grey histogram) or anti-CD40 mAb (coloured overlay) (C) Concentration range of mAb stimulated hCD40Tg B cells against MFI of anti-CD23-PE fluorescence. Graphs indicate mAb of hIgG1 (left), hIgG2 (middle), and hIgG4 (right) constructs. Data shown is mean and SD from independent experiments; N=3.

6.3.3 Anti-CD40-induced B cell proliferation

One of the key functional assessments of B cells activation is proliferation. Therefore, proliferation was assessed for anti-CD40 stimulated hCD40Tg purified B cells by the uptake of tritiated (hydrogen-3 or ^{3}H) thymidine by actively proliferating cells. The ^{3}H thymidine was incorporated into new strands of chromosomal DNA during mitosis and measured by a scintillation β-counter that quantifies the radioactivity of DNA recovered from the cells. The level of radioactivity emitted was used to determine the relative level of of cell division, which was displayed as CPM. B cell proliferation was measured during days 4 - 5 in the current assay, where ^{3}H thymidine was added to cells on day 4 after stimulation and incubated for a further 18 hours.

The proliferation of ChiLob 7/4 hIgG1 stimulated hCD40Tg B cells followed a similar trend to the results observed for hIgG1-induced CD23 upregulation. The preformed hIgG1 μtp hexamer exhibited the highest level of proliferation (Figure 6.6). The level of measured proliferation was within the range of 7,965 - 13,809 CPM, compared with 896 - 10,310 CPM for CP hIgG2. Similar to the activation data, the hIgG1 WT and μtp C575S on-target hexamer exhibited comparably low levels of proliferation, comparable to the response seen with the isotype control (Figure 6.6). This was consistent with the activation data that suggested the hexamerisation enhanced ChiLob 7/4 hIgG1 μtp C575S was not able to agonise CD40 *in vitro*.

The ChiLob 7/4 hIgG2 μtp hexamer demonstrated the highest level of CD40-induced proliferation at the lowest concentrations, but was similar to WT and μtp C575S formats at the top concentration (3,863 - 6,337 CPM) (Figure 6.6). The ChiLob 7/4 hIgG2 WT and μtp C575S exhibited comparable levels of ^{3}H thymidine incorporation across the concentration range tested with CPM values between 3,100 - 8,200 (Figure 6.6). These results further reinforced the observation that addition of the μtp C575S to ChiLob 7/4 hIgG2 did not further augment the CD40 agonistic potential of the mAb.

The ChiLob 7/4 hIgG4 μtp C575S/W417G demonstrated an enhanced level of proliferation when compared to the hIgG4 WT, having a peak response of 4,481 CPM compared with 742 CPM at 10 μg/ml. Proliferation was higher still with the μtp hexamer (2.9-fold) and CP hIgG2 (2.3-fold) (Figure 6.6). The preformed hIgG4 hexamer (μtp) had the highest proliferation with a peak CPM of 13,198 (Figure 6.6). As previously mentioned, the hCD40Tg B cells express murine FcγRIIb which can act to cross-link mAb to provide efficient agonism of CD40 [332]. Therefore to establish the FcγR-independent agonistic activity of the various μtp constructs B cells from FcγR1234 KO/hCD40Tg mice were assessed in the next series of experiments.

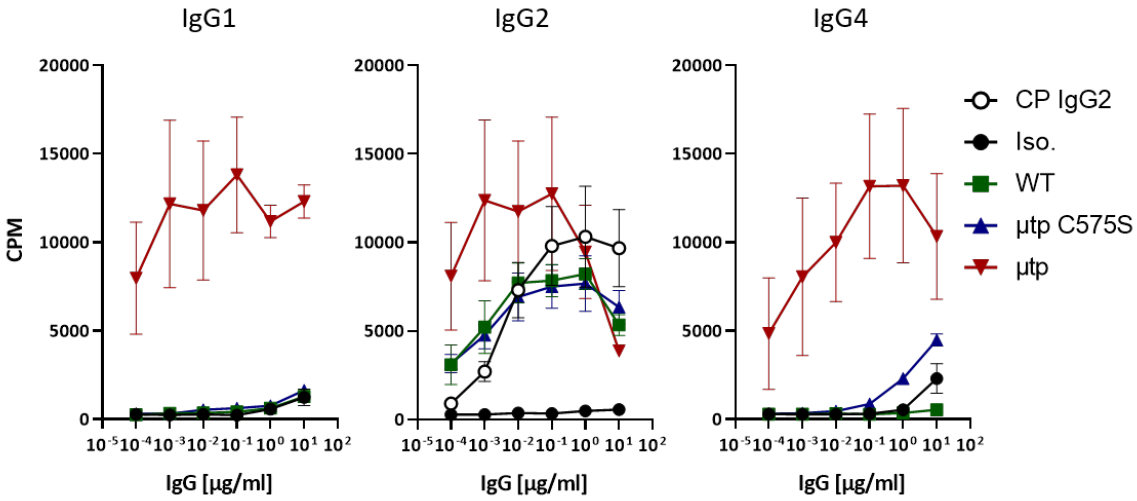

Figure 6.6: Effect of anti-CD40 hIgG hexamerisation on *in vitro* proliferation of hCD40Tg mouse B cells.
1 x 10^5 of purified mouse hCD40Tg B cells were incubated with anti-CD40 mAb constructs (or RTX isotype controls) over a concentration range. On Day 4, 1 μl of ^{3}H thymidine was added to each well, 18 hours later the cells were harvested and DNA analysed for ^{3}H thymidine incorporation, expressed as counts per minute (CPM). Graphs indicate mAb of hIgG1 (left), hIgG2 (middle), and hIgG4 (right) constructs. Data shows mean and SD from independent experiments; N=3.

6.4 Agonism of FcγR1234 KO/hCD40Tg B cells

6.4.1 Anti-CD40-mAb-induced homotypic adhesion

Firstly, the ability of the various mAb to elicit homotypic adhesion of FcγR1234 KO/hCD40Tg B cells was assessed. Consistent with previous results, only the hIgG1 μtp hexamer efficiently induced homotypic adhesion. Homotypic adhesion appeared to be most prominent between 10 - 0.01 μg/ml, below which the cell-cell interaction became less macroscopic, with smaller clusters (Figure 6.7). These data demonstrated that the homotypic adhesion induced with the ChiLob 7/4 hIgG1 μtp hexamer does not require FcγR cross-linking. Cells stimulated with hIgG1 WT and μtp C575S formats displayed no evidence of homotypic adhesion over the concentration range examined, comparable with the isotype control treated wells (Figure 6.7).

Analysis of FcγR1234 KO/hCD40Tg cells stimulated with ChiLob 7/4 hIgG2 WT, μtp C575S, and μtp formats suggested that all three constructs induced comparable levels of homotypic adhesion. Cell-cell clustering was obvious over the entire concentration range examined, with large B cell clusters observed and no sign of dissipation at the lowest concentration tested (Figure 6.8). These results indicated that the agonism observed with all hIgG2 mAb was independent of FcγR.

Results following stimulation with hIgG4 mAb also demonstrated FcγR-independent agonism in the context of ChiLob 7/4 hIgG4 μtp C575S/W417G and the hIgG4 μtp hexamer. There was clear and observable homotypic adhesion with the hIgG4 μtp C575S/W417G treated cells between 10

and 0.1 μg/ml, but at lower concentrations it was not evident. Homotypic adhesion was observed over all concentrations examined with the pre-formed hIgG4 μtp hexamer (Figure 6.9). Since B cell clustering was observed in the absence of FcγR, the next experiments focussed on the ability of μtp hexamers and μtp C575S on-target hexamers to elicit activation and proliferation of FcγR1234 KO/hCD40Tg B cells.

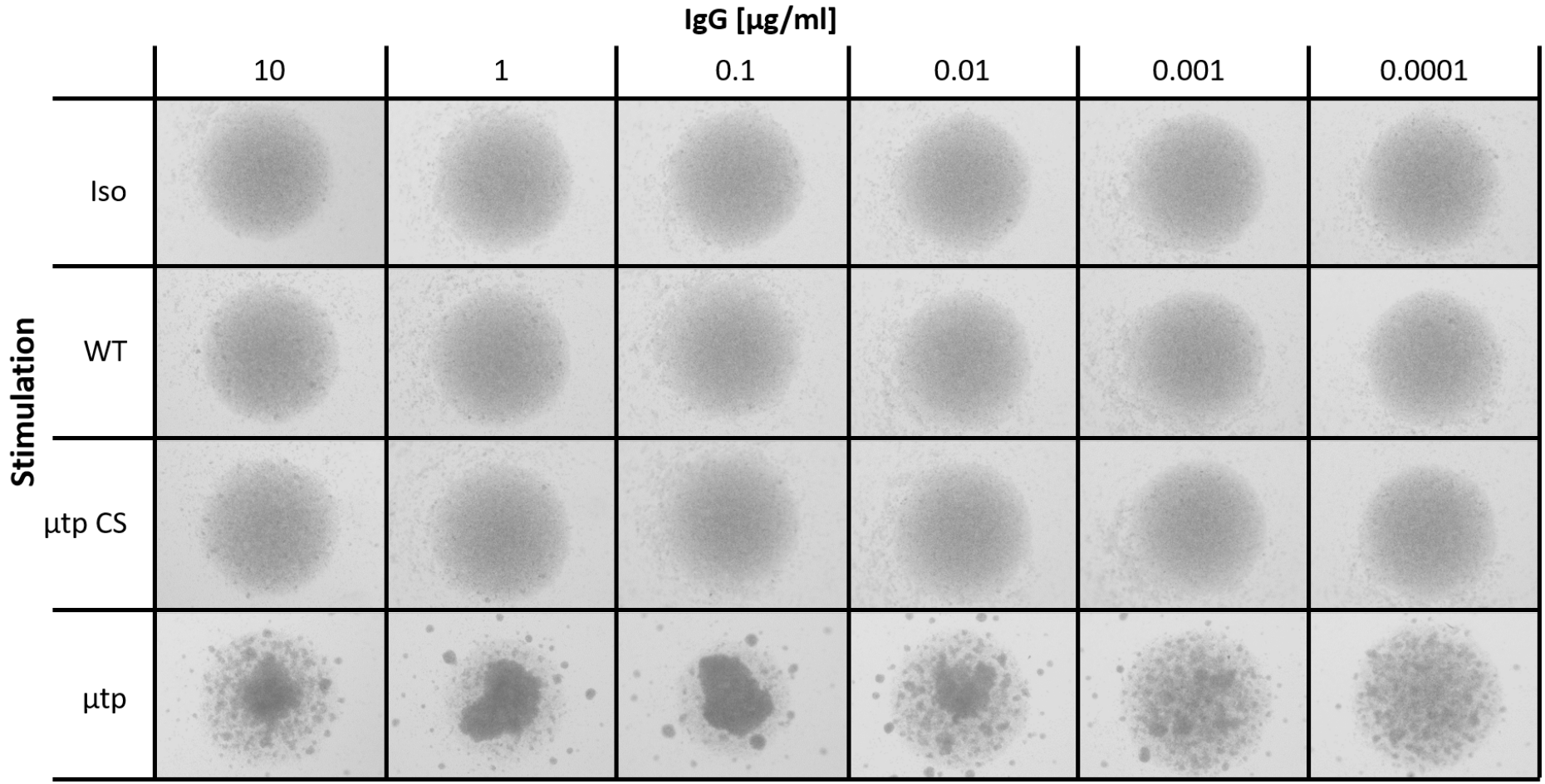

Figure 6.7: Effect of anti-CD40 hIgG1 hexamerisation on FcγR1234 KO/hCD40Tg mouse B cell homotypic adhesion.
1 x 10^5 purified mouse FcγR1234KO/hCD40Tg B cells were incubated with hIgG1 anti-CD40 mAb formats (or RTX hIgG1 isotype control) for 48 hours over a concentration range. After 48 hours cells were imaged at 4X magnification to assess B cell clustering induced by CD40 mAb stimulation. Dark spots on images signify homotypic adhesion of B cells.

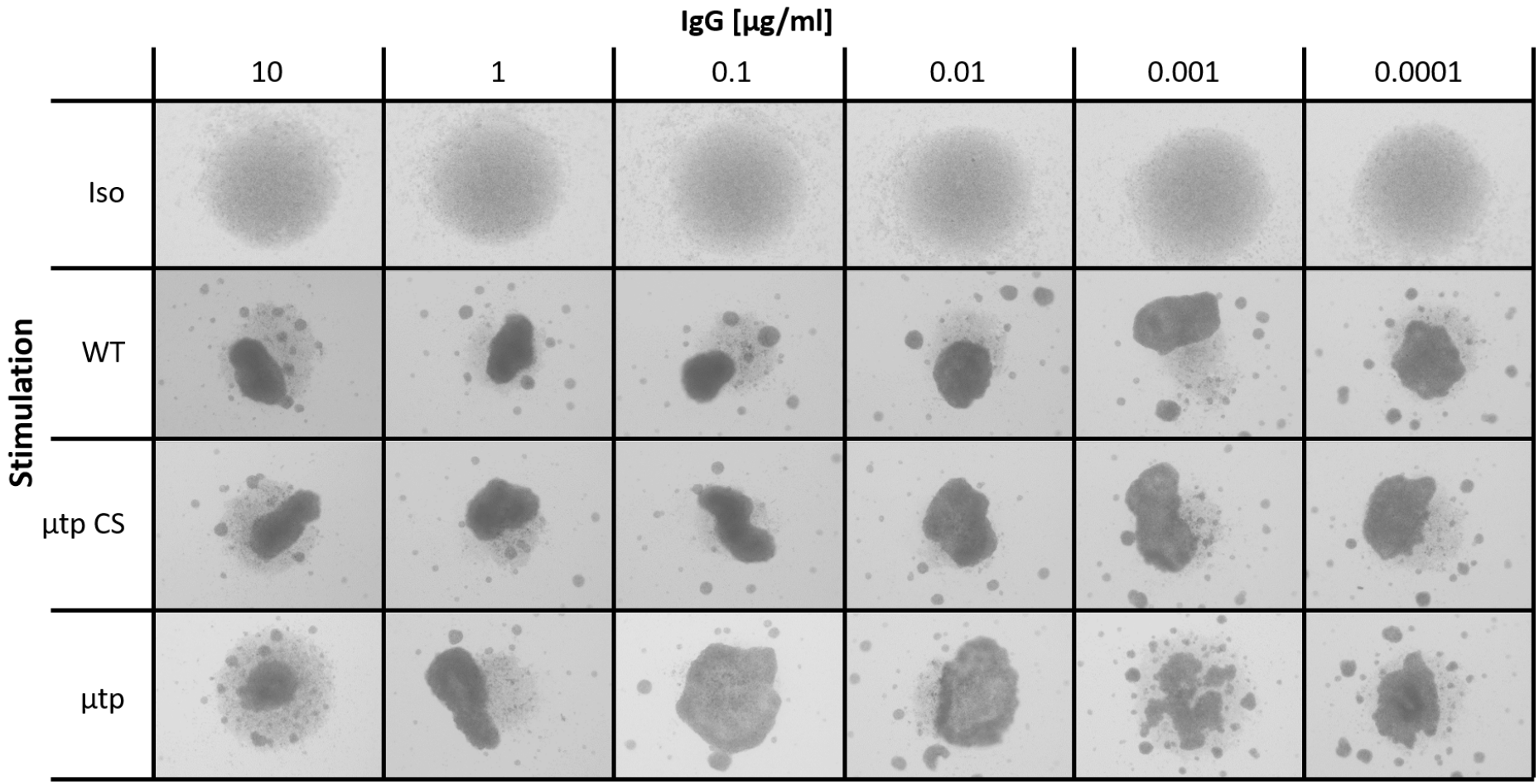

Figure 6.8: Effect of anti-CD40 hIgG2 hexamerisation on FcγR1234 KO/hCD40Tg mouse B cell homotypic adhesion.
1 x 10^5 purified mouse FcγR1234KO/hCD40Tg B cells were incubated with hIgG2 anti-CD40 mAb formats (or RTX hIgG2 isotype control) for 48 hours over a concentration range. After 48 hours cells were imaged at 4X magnification to assess B cell clustering induced by CD40 mAb stimulation. Dark spots on images signify homotypic adhesion of B cells.

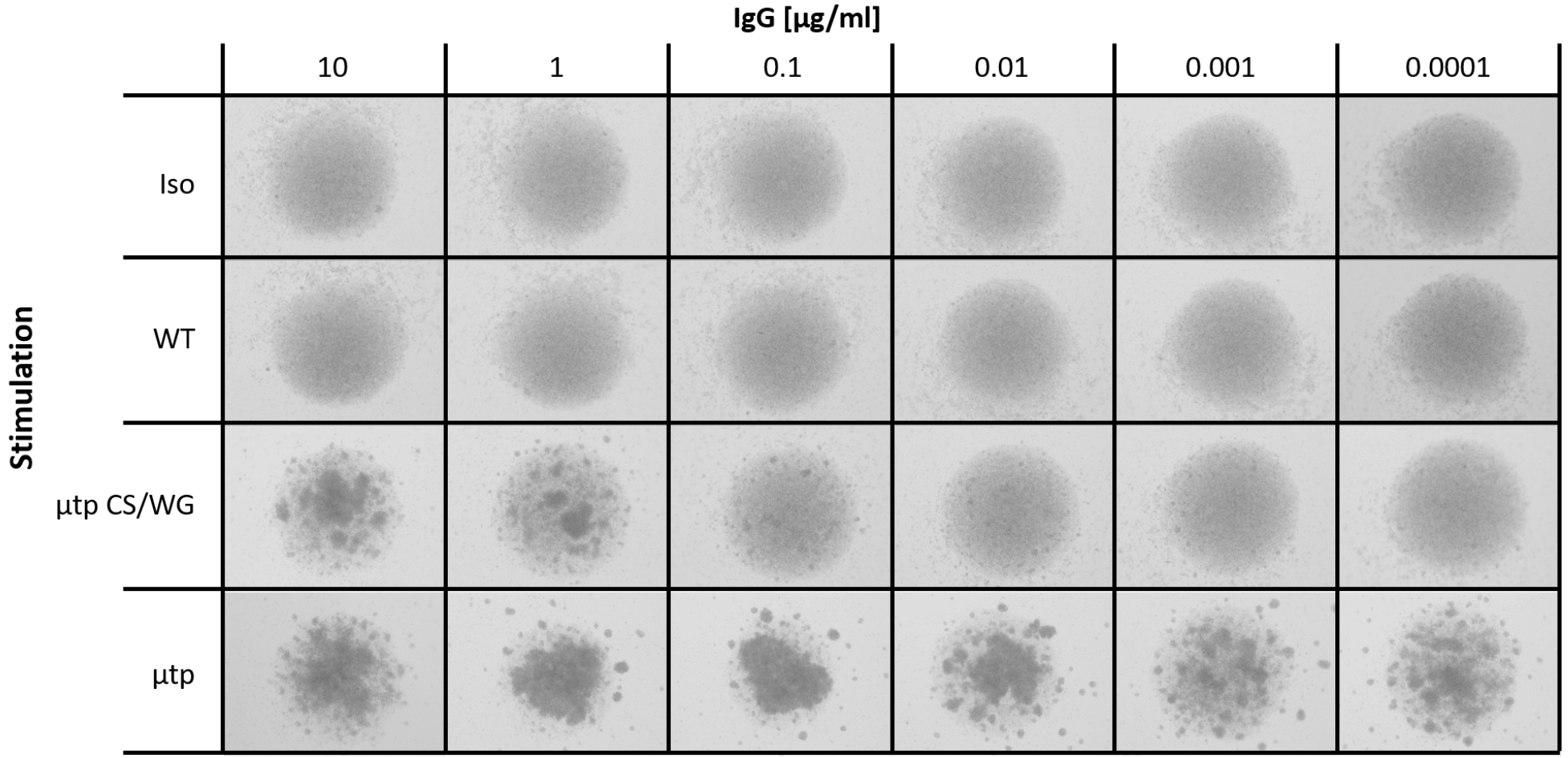

Figure 6.9: Effect of anti-CD40 hIgG4 hexamerisation on FcγR1234 KO/hCD40Tg mouse B cell homotypic adhesion.
1 x 10^5 purified mouse FcγR1234KO/hCD40Tg B cells were incubated with hIgG4 anti-CD40 mAb formats (or RTX hIgG4 isotype control) for 48 hours over a concentration range. After 48 hours cells were imaged at 4X magnification to assess B cell clustering induced by CD40 mAb stimulation. Dark spots on images signify homotypic adhesion ofed B cells.

6.4.2 Anti-CD40-mAb-induced B cell activation

The hIgG1 μtp hexamer exhibited higher levels of CD23 upregulation when compared with CP hIgG2, with a peak response of 6,588 MFI on FcγR1234 KO/hCD40Tg B cells. As previously observed with hCD40Tg B cells, the expression of CD23 upregulation did not alter over the concentration range tested (Figure 6.10). Notably, the peak level of CD23 upregulation was $\sim$50% lower than with hCD40Tg B cells (13,809 MFI vs 6,588 MFI). There was little CD23 upregulation observed with hIgG1 WT, with CD23 levels comparable to the isotype control, and a small but consistent increase with the hIgG1 μtp C575S treated cells at the top concentration (2,070 MFI). The upregulation of CD23 induced by CP hIgG2 was considerably lower than that seen with hCD40Tg B cells, with a peak response of 3,192 MFI using FcγR1234 KO/CD40Tg B cells compared to 21,000 MFI on hCD40Tg B cells.

As a hIgG2 isotype, all formats offered efficient CD23 upregulation across the entire concentration range. The CD40 stimulation was similar between WT, μtp C575S, and μtp formats with CD23 upregulation reported between $\sim$5,000 - $\sim$8,000 MFI, which was lower than the range observed with hCD40Tg B cells ($\sim$5,000 - $\sim$19,000 MFI). This was also lower than the response observed for CP hIgG2 stimulation (peak of 9,983 MFI) (Figure 6.10).

The ChiLob 7/4 hIgG4 μtp C575S/W417G demonstrated a clear activation enhancement over the hIgG4 WT. The CD23 upregulation of ChiLob 7/4 hIgG4 μtp C575S/W417G was comparable with CP hIgG2 at the top concentrations and had a peak response of 3,892 MFI at 10 μg/ml. This was considerably lower than seen with hCD40Tg B cells (peak response of $\sim$11,000 MFI). ChiLob 7/4 hIgG4 WT induced no CD23 upregulation, and was comparable with the isotype treated cells. The activation observed with hIgG4 μtp hexamer was seen at high levels over the entire concentration range ($\sim$3,700 - $\sim$5,000 MFI) and higher than CP hIgG2 over the concentration range used in the assay (Figure 6.10). Again it was considerably lower than the activation of hCD40Tg B cells ($\sim$11,500 - $\sim$17,500 peak MFI; Figure 6.5), indicating hIgG4 μtp constructs have some reliance on FcγRIIb for activation. Nonetheless, these results indicated that the CD23 upregulation previously observed with hCD40Tg B cells could be achieved independently of FcγR-mediated cross-linking in the case of hIgG1, hIgG2, and hIgG4 ChiLob 7/4 μtp hexamers, albeit to a lower extent with hIgG1 and hIgG4 isotypes. Moreover, the current results provided further evidence that the addition of μtp C575S or μtp does not significantly augment CD40 agonistic activity of hIgG2 mAb.

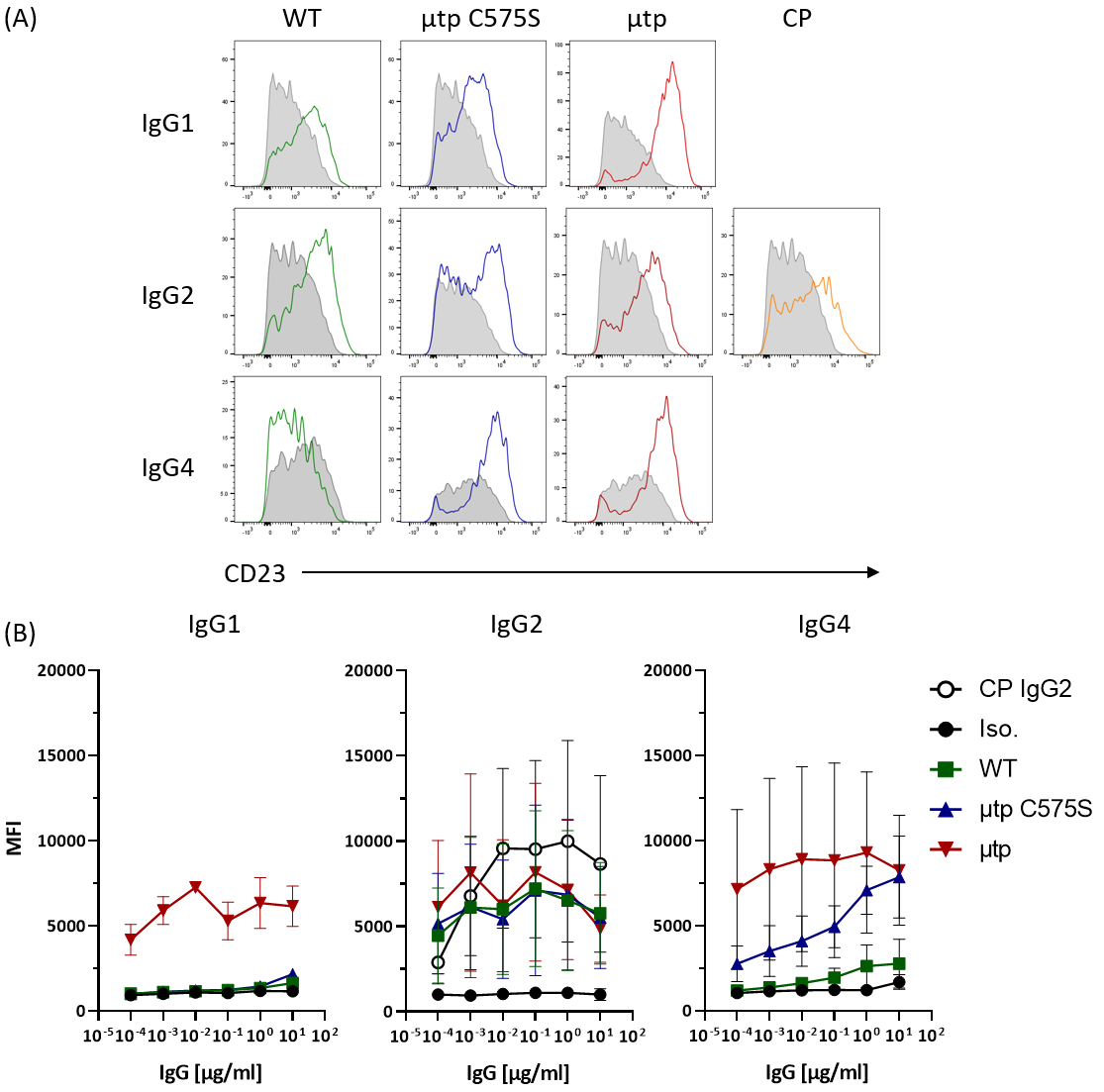

Figure 6.10: Effect of anti-CD40 hIgG hexamerisation on *in vitro* stimulation of FcγR1234 KO/hCD40Tg mouse B cells. 1 x 10^5 purified mouse FcγR1234 KO/hCD40Tg B cells were incubated with IgG anti-CD40 mAb formats (or RTX isotype controls) for 48 hours over a concentration range. After 48 hours cells were analysed by flow cytometry for mouse CD23 upregulation (A) Representative flow cytometry histograms showing CD23 upregulation on hCD40Tg B cells stimulated with 10 μg/ml of isotype control (grey histogram) or anti-CD40 mAb (coloured overlay) (B) Concentration range of mAb stimulated FcγR1234 KO/hCD40Tg B cells against MFI of anti-CD23-PE fluorescence. Graphs show mAb of hIgG1 (left), hIgG2 (middle), and hIgG4 (right) constructs. Data shows mean and SD from independent experiments; N=3.

6.4.3 Anti-CD40-mAb-induced B cell proliferation

Finally, the proliferation of FcγR1234 KO/CD40Tg B cells was examined after stimulation with ChiLob 7/4 constructs. Proliferation induced by CP hIgG2 was observed to be efficient with a peak response of 13,850 CPM, comparable with proliferation results of WT hCD40Tg B cells. The proliferation observed with the ChiLob 7/4 hIgG1 μtp hexamer was comparable to that of CP hIgG2, but was more active at the higher concentrations with a peak response of 18,363 CPM. There was also a dose-response observed which was not previously seen in the WT hCD40Tg B cells. In the absence of FcγR there was still a lack of efficient proliferation by monomeric ChiLob 7/4 hIgG1

WT and μtp C575S formats, with a peak response of 3,141 CPM and 5,781 CPM respectively at 10 μg/ml (Figure 6.11).

All hIgG2 constructs demonstrated comparable B cell proliferation, wherein hexamerisation enhanced or preformed hexamer formats did increase proliferation above the hIgG2 WT. In the context of FcγR1234 KO/hCD40Tg B cells all three formats induced a response between 1,600 - 3,400 CPM, significantly lower than the peak response of CP hIgG2 (13,850 CPM) and hIgG1/4 ChiLob 7/4 μtp hexamers (Figure 6.11). This was the opposite trend to that observed with CD23 upregulation.

Finally, analysis of hIgG4 mAb-induced proliferation of FcγR1234 KO/CD40Tg B cells indicated that ChiLob 7/4 hIgG4 μtp hexamers were still able to stimulate B cell proliferation, but to a lower extent than CP hIgG2 in the absence of FcγRs. Here, ChiLob 7/4 μtp produced a peak proliferation response of 6,328 CPM, 2-fold lower than that of CP hIgG2, and 2-fold lower than seen with WT hCD40Tg B cells. Stimulation with ChiLob 7/4 hIgG4 μtp C575S/W417G resulted in a peak CPM of 5,273 at 10 μg/ml, 4,400 CPM greater than ChiLob 7/4 hIgG4 WT. ChiLob 7/4 hIgG4 WT did not cause B cells to proliferate over the background level induced by the isotype control (Figure 6.11).

Overall, it was clear that ChiLob 7/4 hIgG4 μtp C575S/W417G demonstrated a clear agonistic enhancement over ChiLob 7/4 hIgG4 WT in both the presence and absence of FcγR. As previously demonstrated with anti-CD20 mAb, hIgG4 μtp C575S demonstrated enhanced solution hexamerisation and on-target hexamerisation (evidenced by improved C1q recruitment and complement-mediated lysis) in the context of Q355R (and W417G) mutations. Therefore, it was hypothesised that the same amino acid modification could be beneficial for agonistic CD40 mAb and was investigated next.

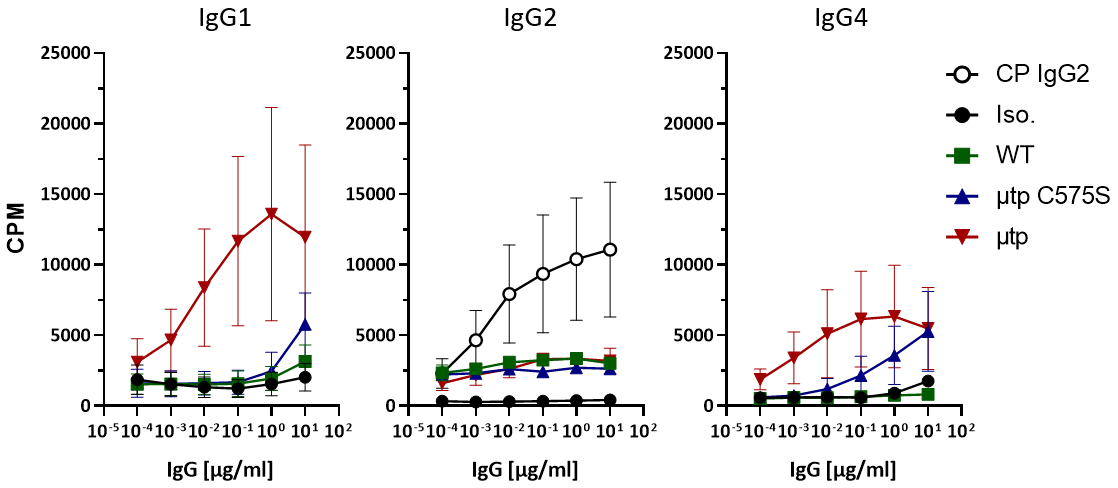

Figure 6.11: Effect of anti-CD40 hIgG hexamerisation on *in vitro* proliferation of FcγR1234 KO/hCD40Tg mouse B cells.
1 x 10^5 purified mouse FcγR1234 KO/hCD40Tg B cells were incubated with hIgG anti-CD40 mAb formats (or RTX isotype controls) over a concentration range. On Day 4 1 μl of ^{3}H thymidine was added to each well, 18 hours later the cells were harvested and DNA analysed for ^{3}H thymidine incorporation, expressed as counts per minute (CPM). Graphs indicate mAb of hIgG1 (left), hIgG2 (middle), and hIgG4 (right) constructs. Data shows mean and SD from independent experiments; N=3.

6.5 Enhancing IgG4 μtp C575S agonistic activity with molecular engineering

Accordingly, ChiLob 7/4 hIgG4 μtp C575S/W417G was modified to include the Q355R mutation. In addition, the reverse mutation R355Q was also introduced into hIgG1 (ChiLob 7/4 hIgG1 μtp C575S/R355Q). These constructs were expressed and purified as previously discussed, the yields and quality control of which are detailed in the Appendix Tables A1 and A2. Firstly, these antibodies were examined using the Jurkat NF-κB-GFP reporter cell line, whereby GFP expression was used to asses CD40 agonism. The results for hIgG1 stimulation followed a similar trend to the CDC lysis results observed in the Chapter 5 i.e. the R355Q mutation reduced the agonistic activity of ChiLob 7/4 hIgG1 μtp 1.6-fold compared to the ChiLob 7/4 hIgG1 μtp C575S (Figure 6.12). It can be presumed that this was a result of the decreased on-target hexamerisation that was demonstrated in Chapter 5. For ChiLob 7/4 hIgG4 μtp C575S mAb, both μtp C575S/W417G and μtp C575S/Q355R/W417G demonstrated a similar level of GFP expression when analysed by flow cytometry, with a peak GFP expression of around 3,200 MFI at 10 μg/ml (Figure 6.12). Interestingly, no enhancement in NF-κB induction was observed even though RTX hIgG4 μtp C575S/Q355R/W417G showed enhanced in-solution hexamerisation and on-target hexamerisation in Chapter 5.

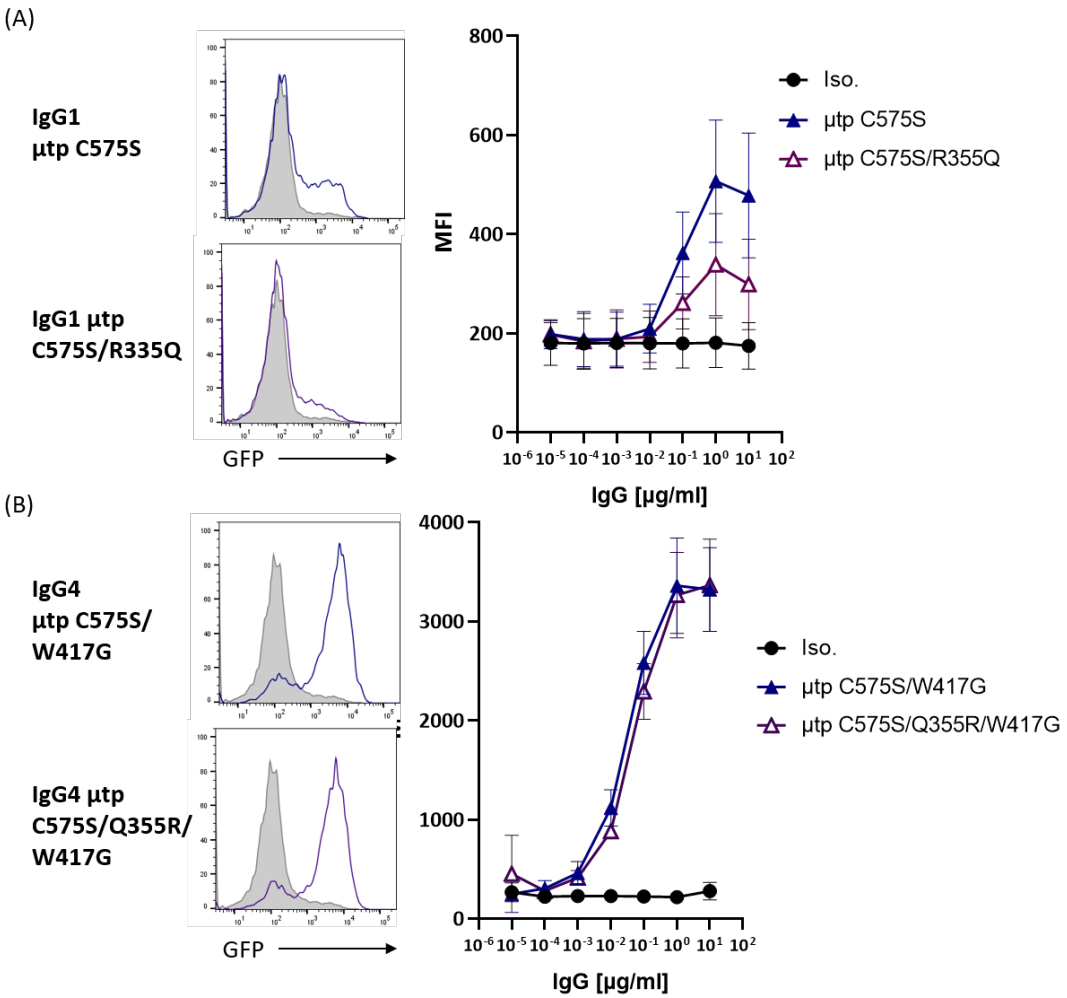

Figure 6.12: Effect of hIgG μtp C575S constructs on *in vitro* agonism of CD40 expressing Jurkat NF-κB-GFP reporter cells.
1 x 10^5 Jurkat F-κB-GFP reporter cells transfected with hCD40 gene were stimulated with anti-CD40 mAb (or RTX isotype controls) at various concentrations over 6 hours. Cells were analysed by flow cytometry and analysed for GFP expression which indicated CD40 activation. Figure is showing representative flow cytometry histograms showing GFP positivity of CD40 expressing Jurkat NF-κB-GFP cells with 10 μg/ml of isotype control (grey histogram) of anti-CD40 mAb (coloured overlay) (left) and MFI of GFP fluorescence over a concentration range of mAb (right) of stimulation by (A) hIgG1 R335Q µtp C575S and (B) hIgG4 Q335R µtp C575S. Data shows mean and SD from independent experiments; N=3.

Next, these residue 355 modified μtp C575S mAb were examined for B cell homotypic adhesion, activation and proliferation *in vitro* as previously performed. The results for ChiLob 7/4 hIgG1 μtp C575S demonstrated that upon introduction of the R355Q mutation there was a lower amount of homotypic adhesion at 10 μg/ml, and none at 1 μg/ml when compared to the ChiLob 7/4 hIgG4 μtp C575S/W417G (Figure 6.13). However, the opposite results were observed when hCD40Tg B cells were stimulated with hIgG4 antibodies. Introduction of Q355R into ChiLob 7/4 hIgG4 μtp C575S/W417G induced higher levels of observable B cell clustering at lower concentrations when compared to ChiLob 7/4 hIgG4 μtp C575S/W417G. Homotypic adhesion could be distinctly observed down to 0.1 μg/ml with ChiLob 7/4 hIgG4 μtp C575S/Q355R/W417G (Figure 6.14).

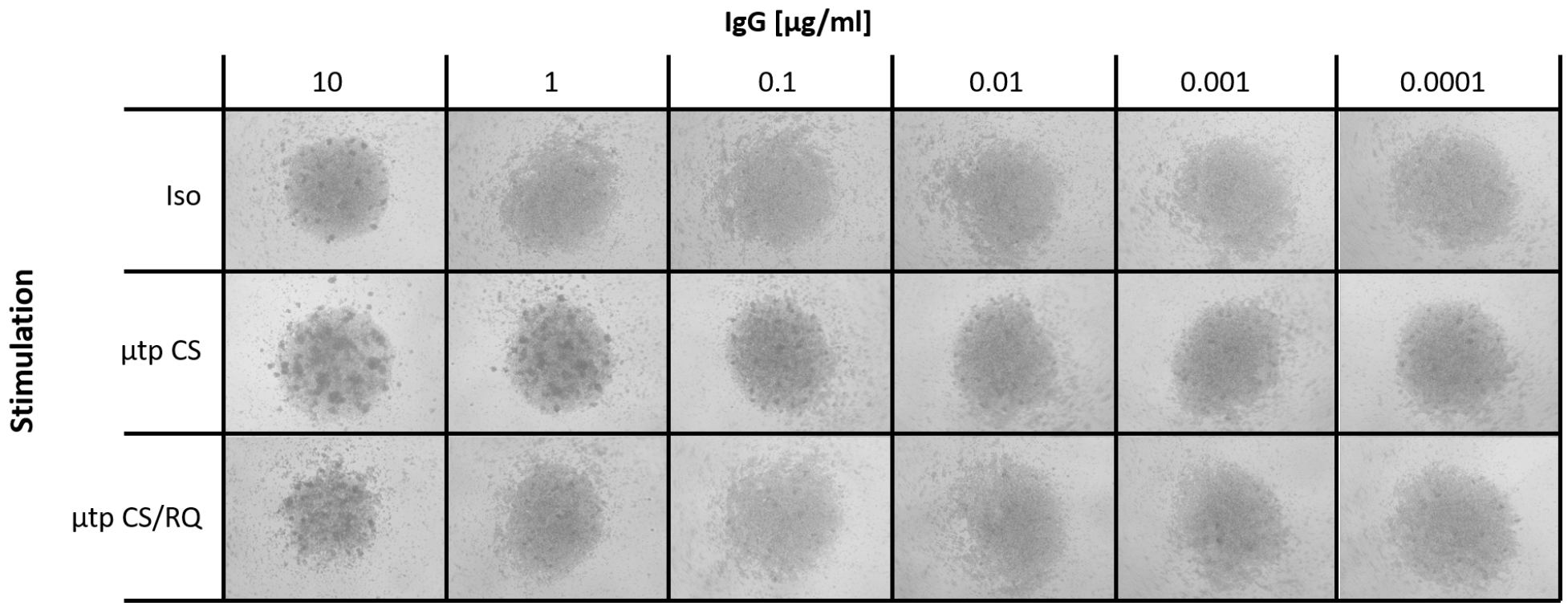

Figure 6.13: Effect anti-CD40 hIgG1 R355Q μtp C575S on hCD40Tg mouse B cell homotypic adhesion.
1 x 10^5 purified mouse hCD40Tg B cells were incubated with hIgG1 anti-CD40 mAb formats (or RTX hIgG1 isotype control) for 48 hours over a concentration range. After 48 hours cells were imaged at 4X magnification to assess B cell clustering induced by CD40 mAb stimulation. Dark spots on images signify homotypic adhesion of B cells.

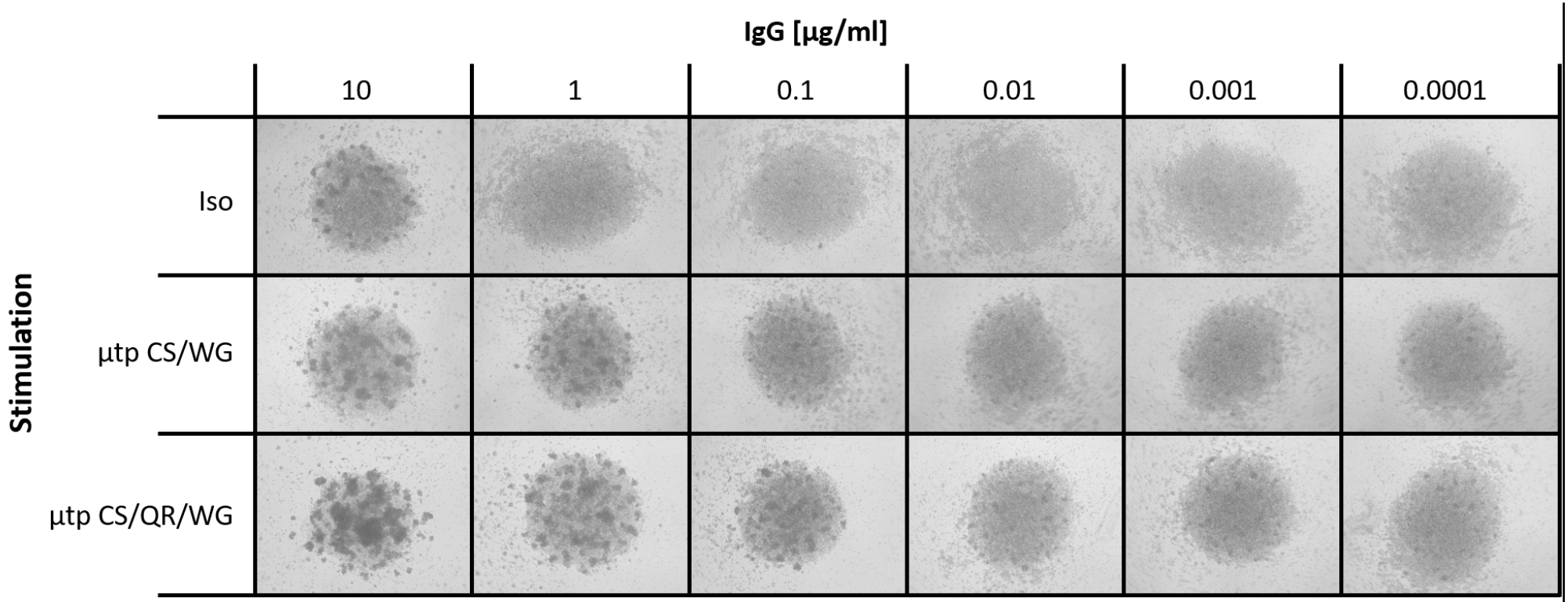

Figure 6.14: Effect anti-CD40 hIgG4 Q355R μtp C575S on hCD40Tg mouse B cell homotypic adhesion.
1 x 10^5 purified mouse hCD40Tg B cells were incubated with hIgG4 anti-CD40 mAb formats (or RTX hIgG4 isotype control) for 48 hours over a concentration range. After 48 hours cells were imaged at 4X magnification to assess B cell clustering induced by CD40 mAb stimulation. Dark spots on images signify homotypic adhesion of B cells.

Following analysis of CD40-induced B cell clustering, activation and proliferation of hCD40Tg B cells were examined. Similar to the results observed with the Jurkat reporter cell line, there was a slight reduction in CD23 expression upon the introduction of the R355Q mutation into the hIgG1 framework. The MFI was reduced from 2,601 with ChiLob 7/4 hIgG1 μtp C575S to 1,714 with ChiLob 7/4 hIgG1 μtp C575S/R355Q (Figure 6.15,A). The opposite result was observed in the proliferation results. The ChiLob 7/4 hIgG1 μtp C575S/R355Q increased proliferation when compared to ChiLob 7/4 hIgG1 μtp C575S, but only at 10 μg/ml. ChiLob 7/4 hIgG1 μtp C575S had a CPM of 1682 compared to 5639 for ChiLob 7/4 hIgG1 μtp C575S/R355Q (Figure 6.15,A).

For ChiLob 7/4 hIgG4 μtp C575S/Q355R/W417G there was no enhanced CD23 upregulation, similar to the results with the Jurkat reporter cell line. Both μtp C575S constructs exhibited a peak CD23 upregulation response of around 10,000 MFI at 10 μg/ml, indicating that the ChiLob 7/4 μtp C575S/Q355R/W417G construct did not induce higher levels of *in vitro* B cell activation than ChiLob 7/4 μtp C575S/W417G (Figure 6.15,B). Conversely, there was an observed increase in B cell proliferation with hIgG4 μtp C575S/Q355R/W417G on-target hexamers (8,463 CPM), compared to hIgG4 μtp C575S/W417G (4,481 CPM), however, this was only observed at 10 μg/ml (Figure 6.15,B).

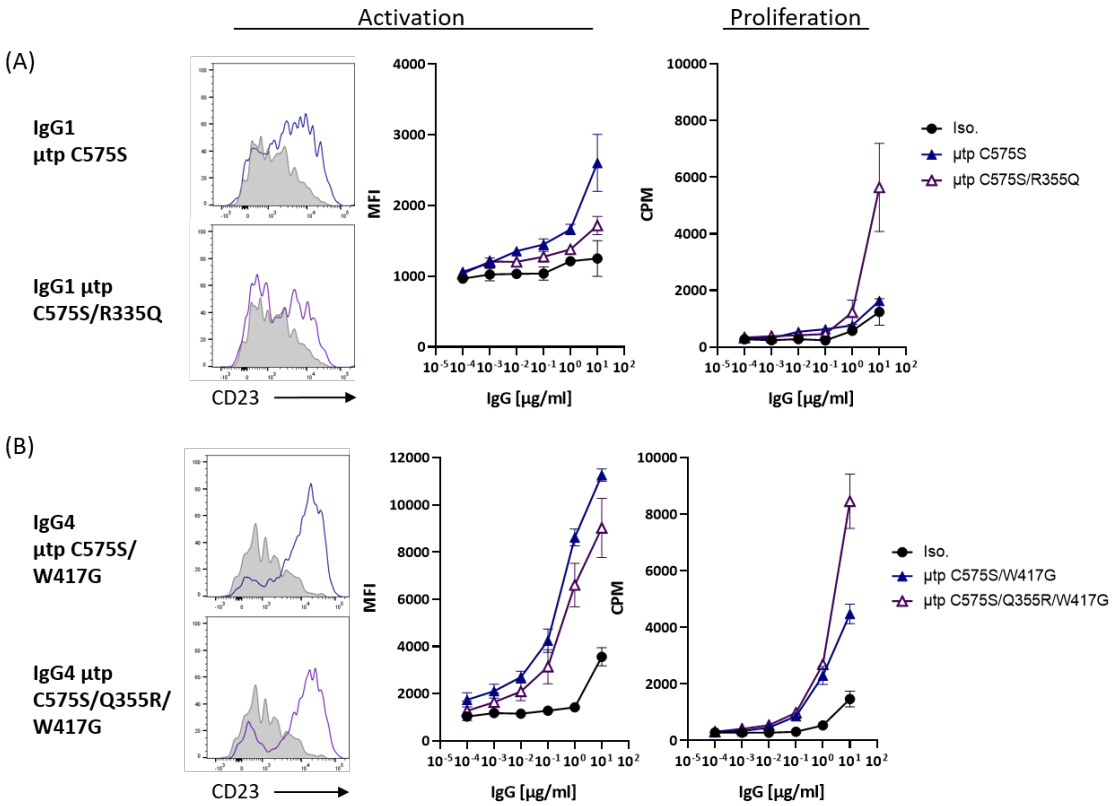

Figure 6.15: Effect of hIgG μtp C575S constructs on *in vitro* mouse CD40Tg B cell activation and proliferation.
1 x 10^5 purified mouse hCD40Tg B cells were incubated with hIgG anti-CD40 μtp C575S mAb (or RTX isotype controls). After 48 hours cells were analysed by flow cytometry for cell activation by assessing mouse CD23 upregulation or on days 4-5 ^{3}H thymidine incorporation by dividing cells was assessed for proliferation. Figure is showing representative flow cytometry histograms showing CD23 upregulation on hCD40Tg B cells stimulated with 10 μg/ml of isotype control (grey histogram) or anti-CD40 mAb (coloured overlay) (left), MFI of CD23-PE fluorescence over a concentration range of mAb (middle), and ^{3}H thymidine incorporation (CPM) (right) by (A) hIgG1 R335Q µtp C575S and (B) hIgG4 Q335R µtp C575S. Data shows mean and SD from independent experiments; N=3.

Next, FcγR1234 KO/CD40Tg B cells were stimulated with μtp C575S mAb to determine if the activities observed above were FcγR dependent. Firstly, B cell clustering was examined and no homotypic adhesion was visible with ChiLob 7/4 hIgG1 μtp C575S or the control treated wells. The ChiLob 7/4 hIgG1 μtp C575S/R355Q was capable of inducing homotypic adhesion, but only at the top concentration (Figure 6.16). The ChiLob 7/4 hIgG4 μtp C575S/Q355R/W417G construct demonstrated clear FcγR-independent homotypic adhesion. Distinct cell clustering was observed between 10 - 0.1 μg/ml for both ChiLob 7/4 hIgG4 μtp C575S constructs in the assay (Figure 6.17). There was no obvious enhancement observed with ChiLob 7/4 hIgG4 μtp C575S/Q355R/W417G over ChiLob 7/4 hIgG4 μtp C575S/W417G as seen with WT hCD40Tg mice.

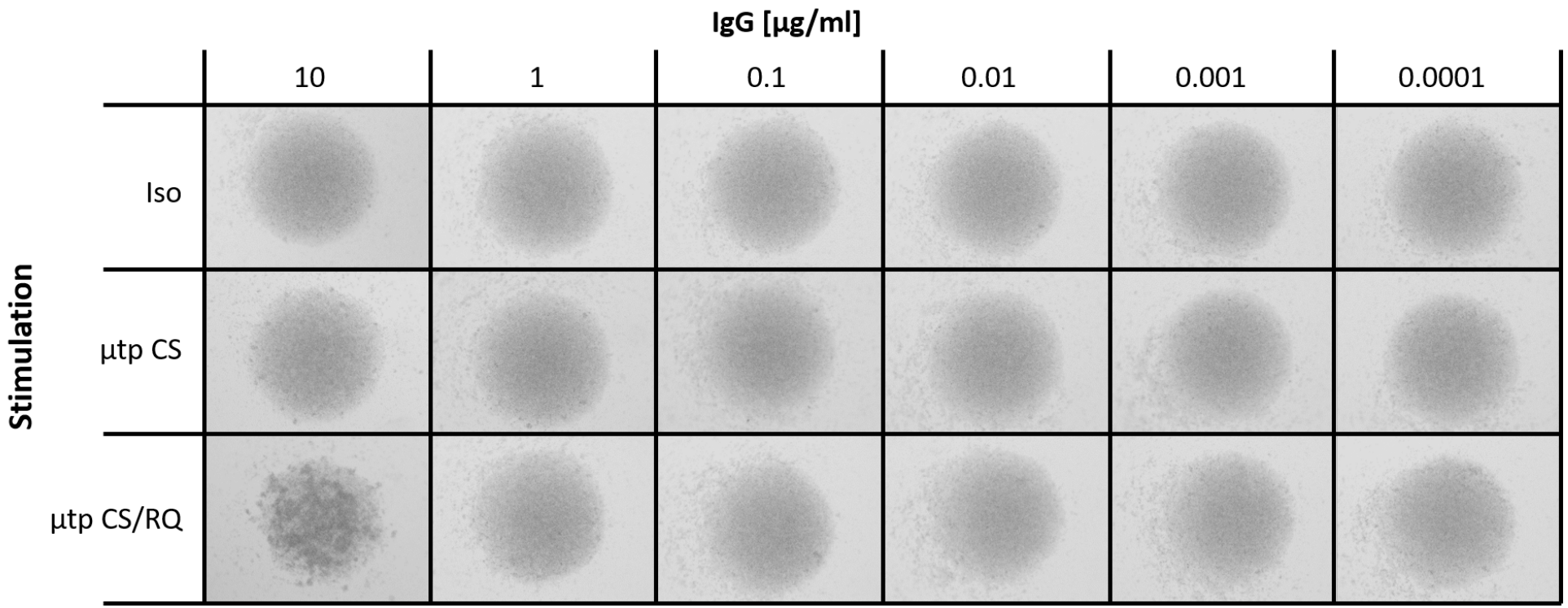

Figure 6.16: Effect of anti-CD40 hIgG1 μtp C575S/R355Q on FcγR1234 KO/hCD40Tg mouse B cell homotypic adhesion.
1 x 10^5 purified mouse FcγR1234 KO/hCD40Tg B cells were incubated with hIgG1 anti-CD40 mAb formats (or RTX hIgG1 isotype control) for 48 hours over a concentration range. After 48 hours cells were imaged at 4X magnification to assess B cell clustering induced by CD40 mAb stimulation. Dark spots on images signify homotypic adhesion of B cells.

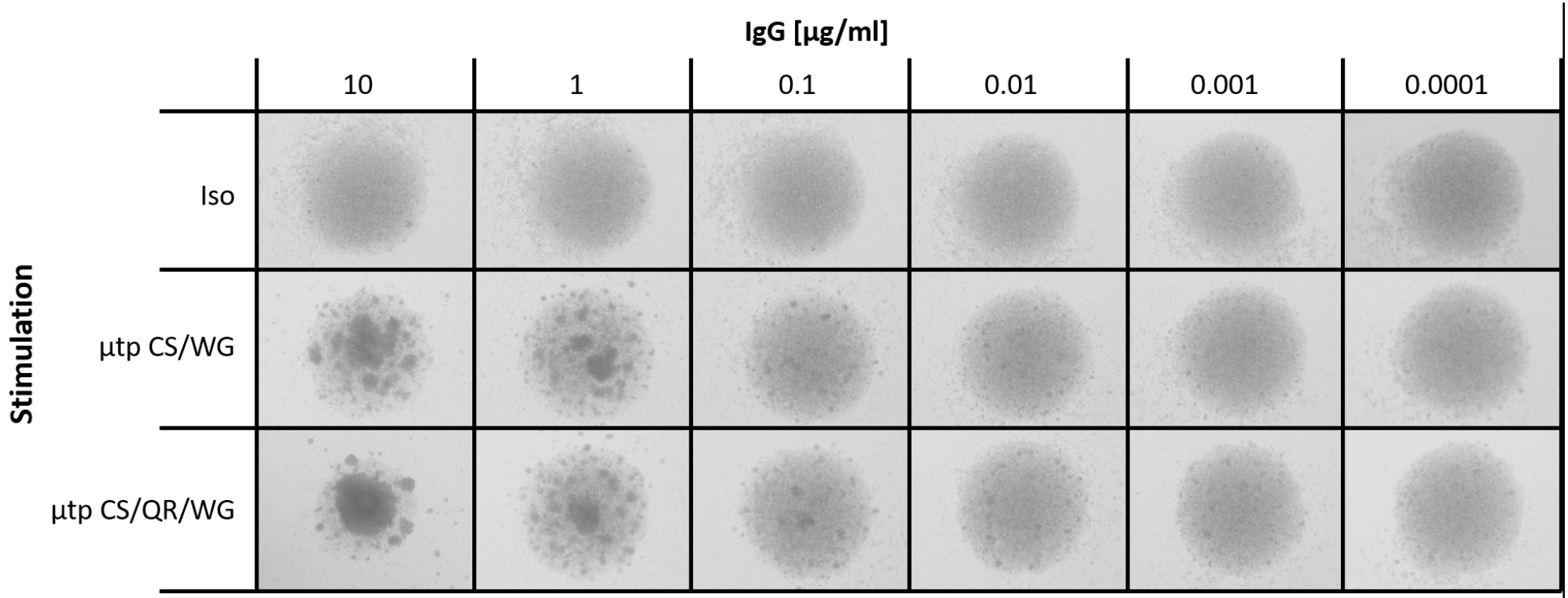

Figure 6.17: Effect of anti-CD40 hIgG4 μtp C575S/Q355R/W417G on FcγR1234 KO/hCD40Tg mouse B cell homotypic adhesion.
1 x 10^5 purified mouse FcγR1234 KO/hCD40Tg B cells were incubated with hIgG4 anti-CD40 mAb formats (or RTX hIgG4 isotype control) for 48 hours over a concentration range. After 48 hours cells were imaged at 4X magnification to assess B cell clustering induced by CD40 mAb stimulation. Dark spots on images signify homotypic adhesion of B cells.

When assessed for B cell activation, ChiLob 7/4 hIgG1 μtp C575S/R355Q induced lower levels of CD23 expression when compared with ChiLob 7/4 hIgG1 μtp C575S. However, the MFI for CD23 expression was low for both antibodies. A difference was only observed at 10 μg/ml with peak responses of 2,070 MFI for ChiLob hIgG1 7/4 μtp C575S compared with 1,583 MFI for ChiLob hIgG1 7/4 μtp C575S/R355Q (Figure 6.18,A). This reduction in activity was more visible in the analysis of proliferation whereby ChiLob 7/4 hIgG1 μtp C575S demonstrated enhanced B cell proliferation and a CPM of 5,781 at 10μg/ml, whereas the ChiLob hIgG1 7/4 μtp C575S/R355Q mAb induced no proliferation above the isotype control (Figure 6.18,A). ChiLob 7/4 hIgG4 μtp C575S/Q355R/W417G resulted in less CD23 upregulation compared to ChiLob 7/4 hIgG4 μtp C575S/W417G. The peak CD23 upregulation observed with these two mAb was at 10 μg/ml, and was 1.5-fold lower for ChiLob 7/4 hIgG4 μtp C575S/Q355R/W417G (Figure 6.18,B). However, the opposite effect was observed with respect to proliferation of these cells. The level of ^{3}H thymidine incorporation was enhanced when FcγR1234 KO/CD40Tg B cells were treated with ChiLob 7/4 hIgG4 μtp C575S/Q355R/W417G, which exhibited a peak CPM at 10 μg/ml of 10,491, 2-fold greater than ChiLob 7/4 hIgG4 μtp C575S/W417G (Figure 6.18,B). However, as seen with WT hCD40Tg B cells, this enhancement was only observed at the top concentration of 10 μg/ml.

Overall, the data demonstrated that the incorporation of the μtp C575S/W417G to ChiLob 7/4 hIgG4 is able to provide CD40 agonism to the previously inert ChiLob 7/4 hIgG4 WT, in an FcγR-independent manner. Mutation of Q355R in the hIgG4 Fc, which has previously been shown to enhance the in-solution hexamerisation and on-target hexamerisation activities, did not appear to have any benefit to the agonistic activity of ChiLob 7/4 hIgG4 μtp C575S/W417G in B cell assays *in vitro*. These mAb were subsequently examined for their ability to deliver CD40-mediated agonism *in vivo*.

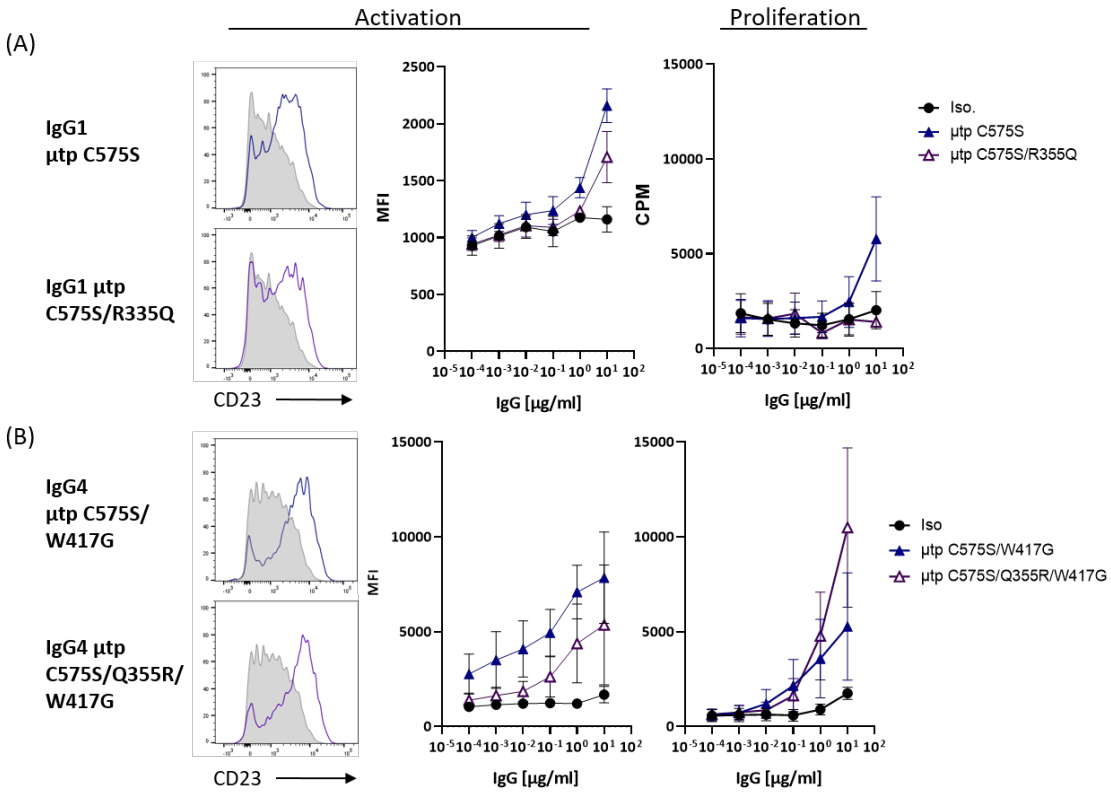

Figure 6.18: Effect of hIgG μtp C575S constructs on *in vitro* mouse FcγR1234 KO/hCD40Tg B cell activation and proliferation.
1 x 10^5 purified mouse FcγR1234 KO/hCD40Tg B-cells were incubated with hIgG anti-CD40 μtp C575S mAb (or RTX isotype controls). After 48 hours cells were analysed by flow cytometry for cell activation by mouse by assessing CD23 upregulation or on days 4-5 ^{3}H thymidine incorporation by dividing cells was assessed for proliferation. Figure is showing representative flow cytometry histograms showing CD23 upregulation on hCD40Tg B cells stimulated with 10 μg/ml of isotype control (grey histogram) or anti-CD40 mAb (coloured overlay) (left), MFI of CD23-PE fluorescence over a concentration range of mAb (middle), and ^{3}H thymidine incorporation (CPM) (right) by (A) hIgG1 R335Q µtp C575S and (B) hIgG4 Q335R µtp C575S. Data shows mean and SD from independent experiments; N=3.

6.6 Ability of anti-CD40 hexamerisation enhanced IgG to deliver immunostimualtion *in vivo*

6.6.1 OTI expansion in hCD40Tg mice

In vivo activity of the various mAb was assessed using an adoptive transfer model, whereby OTI splenocytes were transferred into hCD40Tg mice. The OTI CD8$^+$ cells express a transgenic TCR that binds the peptide SIINFEKL, derived from ovalbumin (OVA). Following adoptive transfer of OTI cells into hCD40Tg mice, the mice receive OVA, which is than processed and presented to OTI CD8$^+$ T cells to induce an OVA-specific expansion of these cells (Figure 6.19,A). Agonistic anti-CD40 mAb are then administered to enhance antigen presentation and activation of T cells by CD40 activated APCs, and hence provide an enhanced OVA-specific T cell response. This response is followed in the peripheral blood by collecting blood and staining for CD8 and SIINFEKL (using a PE labelled

SIINFEKL tetramer) and analysed by flow cytometry (Figure 6.19,B). CD8/SIINFEKL double positive T cell populations that can be monitored over time to follow the response induced by anti-CD40 mAb (Figure 6.19,C).

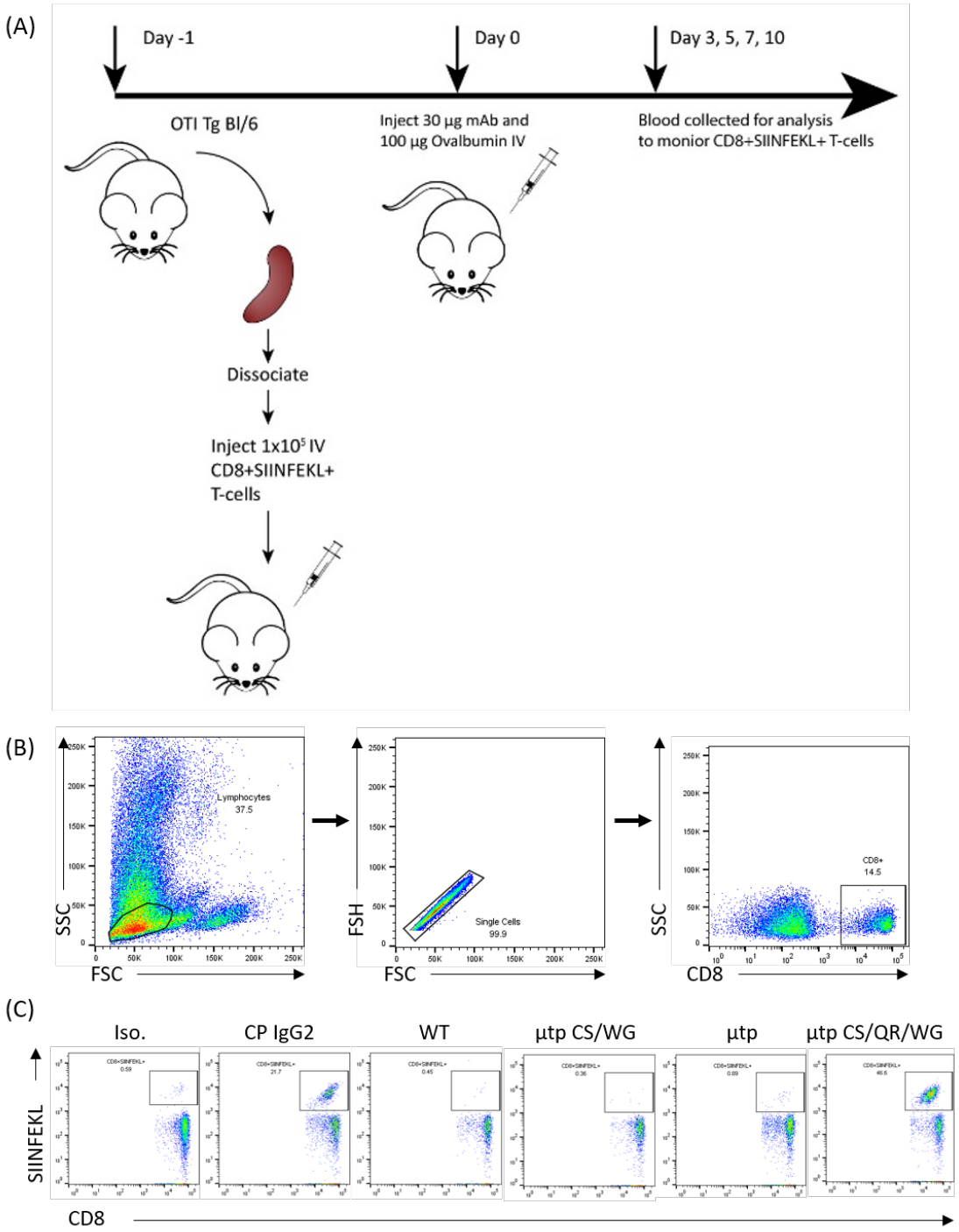

Figure 6.19: Effect of hIgG4 hexamerisation on *in vivo* OTI CD8$^+$ T cell expansion.
(A) Experimental design of *in vivo* OTI T cell expansion in hDC40Tg Bl/6 mice. OTI T cells are adoptively transferred into hCD40Tg Bl/6 mice and 1 day later treated with 100 μg OVA and 30 hIgG4 μg anti-CD40 mAb or RTX hIgG4 isotype control. Blood was taken to monitor CD8$^+$SIINFEKL$^+$ T cells in circulation (B) Flow cytometry gating strategy for CD8$^+$ T cells (C) Representative flow cytometry plots depicting CD8$^+$SIINFEKL$^+$ T cells at day 5.

ChiLob 7/4 hIgG4 mAb was administered at a dose of 30 μg per mouse ($\sim$1 mg/kg), chosen to negate the possibility of any unwanted toxicities if the mAb were highly agonistic *in vivo* (personal communication with Dr Ben Yu). At this dose there was no visual signs of toxicity (i.e. spiked fur, hunched posture) at the time of i.v. administration, or any drop in body weight after three days (Figure 6.20). The analysis of the weight did indicate that the mice treated with ChiLob 7/4 hIgG4 μtp C575S/W417G collectively had the lowest weight, whereas other treatment groups were more equally spread, although mice were of the same age. As a result, the experimental plan was continued and mice were bled by tail-tipping on days 3, 5, 7, and 10 to follow the kinetics of CD8/SIINFEKL T cell expansion.

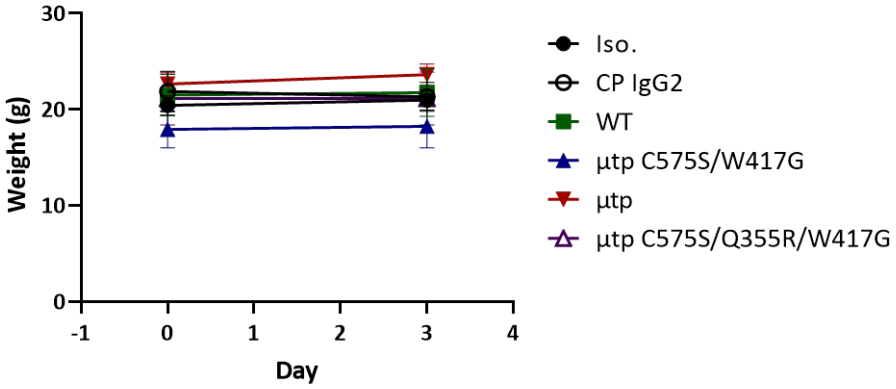

Figure 6.20: Weight measurement of hCD40Tg mice administered with hIgG4 μtp constructs.
hCD40Tg mice were adoptively transferred with OTI splenocytes and treated with 100 μg OVA and 30 hIgG4 μg anti-CD40 mAb or RTX hIgG4 isotype control. Body weight was monitored on the day of administration and at day 3 as a read-out for any possible toxicity. Data plotted is mean and SD from a single experiment; N=3-5 mice per group.

As before, CP hIgG2 was used as a positive control. Administration of CP hIgG2 led to an expansion of up to $\sim$20% CD8/SIINFEKL T cells in the overall $CD8^+$ T cell population. As expected, the ChiLob 7/4 hIgG4 WT induced no specific T cell expansion, consistent with the lack of agonistic activity observed *in vitro*. Interestingly, the hIgG4 μtp C575S/W417G on-target hexamer and μtp hexamer (which were active *in vitro*) demonstrated negligible activity *in vivo*, and had comparable percentage of CD8/SIINFEKL cells compared to the isotype control. The only ChiLob 7/4 hIgG4 antibody to display CD8/SIINFEKL T cell expansion was the hIgG4 μtp C575S/Q355R/W417G, which gave rise to a maximum peak expansion of $\sim$30% of total $CD8^+$ T cells (Figure 6.21). The peak of the response was observed at day 5 and by day 7 had subsided to 5% of total T cells with both CP hIgG2 and ChiLob 7/4 hIgG4 μtp C575S/Q355R/W417G, and the response was maintained at this level until day 10.

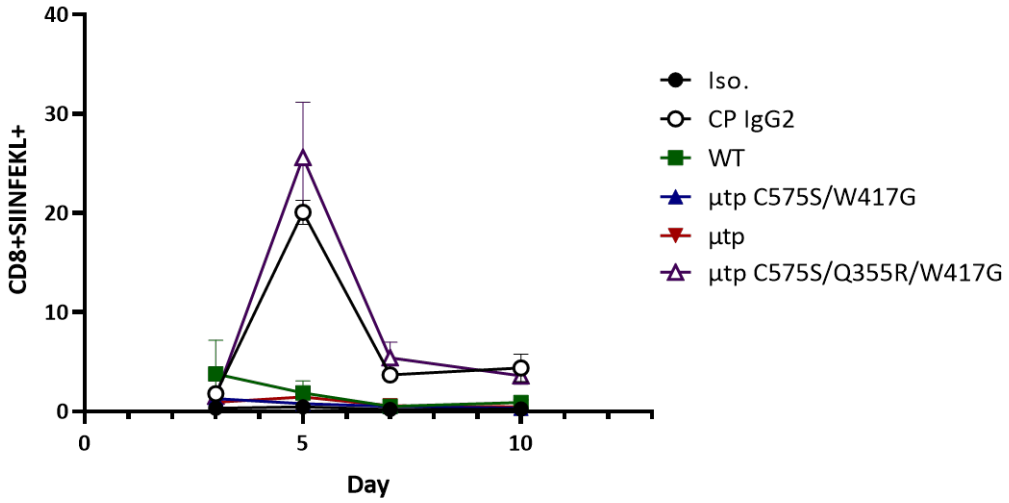

Figure 6.21: Effect of hIgG4 μtp hexamerisation on *in vivo* OTI CD8$^+$ T cell expansion in hCD40Tg mice.
hCD40Tg mice were adoptively transferred with 1x10^5 OTI T cells (non purified in splenocytes) and treated with 100 μg OVA and 30 μg hIgG4 anti-CD40 mAb or RTX hIgG4 isotype control 24 hours later. OTI T cell expansion in the circulation was monitored over time. Blood was collected by tail tipping and analysed by flow cytometry for the percentage of CD8$^+$SIINFEKL$^+$ T cells as a proportion of total T cells. Data plotted is mean and SEM from a single experiment; N=3-5 mice per group.

6.6.2 Augmentation of the humoral response in hCD40Tg mice

In addition to CD8$^+$ T cell expansion, the humoral response induced by CD40 stimulation was examined. As previously mentioned, further to increased APC cross-priming of T cells, CD40 also agonises B cells to produce an antibody response. Therefore, the concentration of anti-OVA antibody in the serum of the experimental animals detailed above was measured at day 12. The results follow a similar trend observed with the OTI T cell expansion. ChiLob 7/4 hIgG4 WT, μtp C575S/W417G, and μtp did not induce detectable levels of anti-OVA antibodies at day 12. However, CP hIgG2 and ChiLob 7/4 hIgG4 μtp C575S/Q355R/W417G, did induce a humoral response (Figure 6.22). On day 12 the CP hIgG2 treated mice had a mean concentration of 2.5 μg/ml. In animals treated with ChiLob 7/4 hIgG4 μtp C575S/Q355R/W417G the highest humoral response was seen with a mean of 6.8 μg/ml anti-OVA antibody measured. These results were produced in hCD40Tg mice with murine FcγR present. Therefore, the next experiment was performed in FcγR1234 KO/hCD40Tg mice to determine if these mAb were active in the absence of FcγRs.

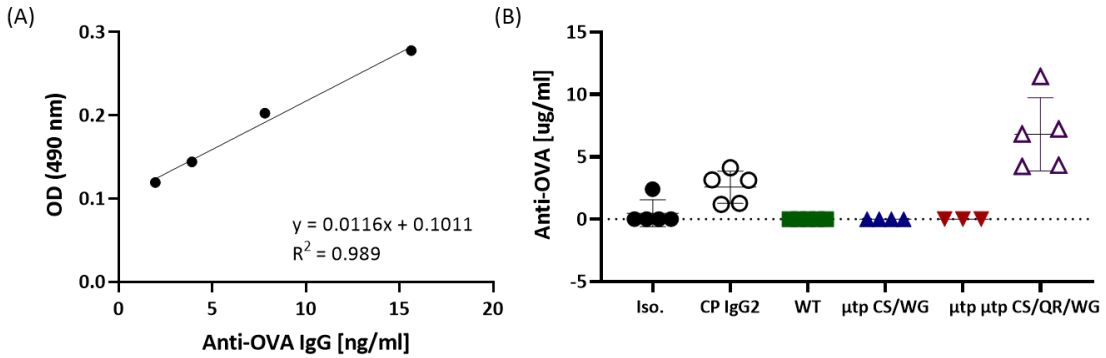

Figure 6.22: Effect of hIgG4 μtp mAb on *in vivo* stimulation of the humoral response in hCD40Tg mice.
The same mice indicated above in Figure 6.21 were also assessed for their anti-OVA antibody response in serum. Blood samples were taken on day 12 after administration of 100 μg OVA and 30 μg hIgG4 anti-CD40 mAb or RTX hIgG4 isotype control, and serum was collected by centrifugation of blood after clotting. Concentration of anti-OVA antibodies in mouse serum was determined by ELISA, using a standard curve of known anti-OVA IgG concentration (A) Standard curve of known anti-OVA IgG (B) Calculated concentration (μg/ml) of anti-OVA antibody present in serum samples. Data plotted is mean and SEM from a single experiment; N=3-5 mice per group.

6.6.3 OTI expansion in Fcγ1234 KO/hCD40Tg mice

Administration of OVA and anti-CD40 mAb in FcγR1234 KO/hCD40Tg mice harbouring adoptively transferred OTI splenocytes resulted in no adverse toxicities and no loss in body weight in any treatment group (Figure 6.23). Although no treatment group demonstrated a loss in weight, the groups did demonstrate a range of weights between $\sim$28 and $\sim$35 grams. Nontheless, this indicated that these mAb were safe to administer to this mouse strain at doses up to 30 μg/ml. As no toxicities were observed the experimental plan was continued and mice were bled by tail-tipping on days 4, 5, 7, 10, 12, and 28 to follow the kinetics of CD8/SIINFEKL T cell expansion.

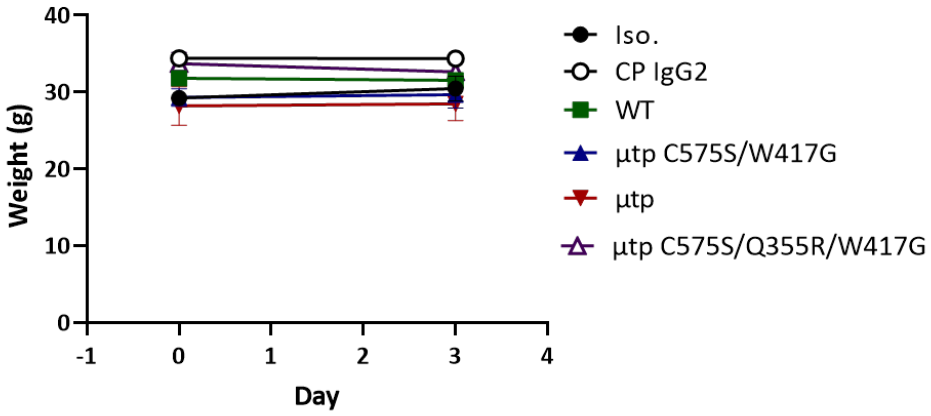

Figure 6.23: Weight measurement of FcγR1234 KO/hCD40Tg mice administered with hIgG4 μtp fusion mAb.
The body weight of FcγR1234 KO/hCD40Tg mice adoptively transferred with OTI splenocytes and treated with 100 μg OVA and 30 μg anti-CD40 mAb or RTX hIgG4 isotype control was monitored the day of administration and at day 3 as a read-out for any possible toxicity. Data plotted is mean and SD from a single experiment; N=3 mice per group.

CP induced a peak response of 6.9% at day 4 (Figure 6.24). The ChiLob 7/4 hIgG4 WT demonstrated no OTI T cell expansion. The ChiLob 7/4 hIgG4 μtp hexamer demonstrated activity, with

a peak of 14.7% OTI T cells seen on day 4. The hIgG4 μtp C575S/Q355R/W417G construct exhibited the highest level of CD8/SIINFEKL double positive T cells, and a peak response of 37.4% on day 4 (Figure 6.24). In these FcγR1234 KO/hCD40Tg mice the initial peak response was observed at day 4 and appeared to be decreasing by day 5 whereas the peak response in hCD40Tg mice was at day 5. However, the days of sampling were not identical and so this cannot be categorically determined. The other discrepancy between the experimental results in the two strains was that a second peak response was observed at day 10, in the absence of any further stimulation in FcγR1234 KO/CD40Tg mice. This was seen in animals treated with ChiLob 7/4 hIgG4 μtp C575S/Q355R/W417G and μtp hexamer to a comparable extent, although the mean response of the hIgG4 μtp hexamer was influenced by one animal experiencing an extremely large OTI T cell expansion of 81.5% (Figure 6.24). Following this second peak response, mice were bled 16 days later on day 28, by which time the OTI T cell response had subsided.

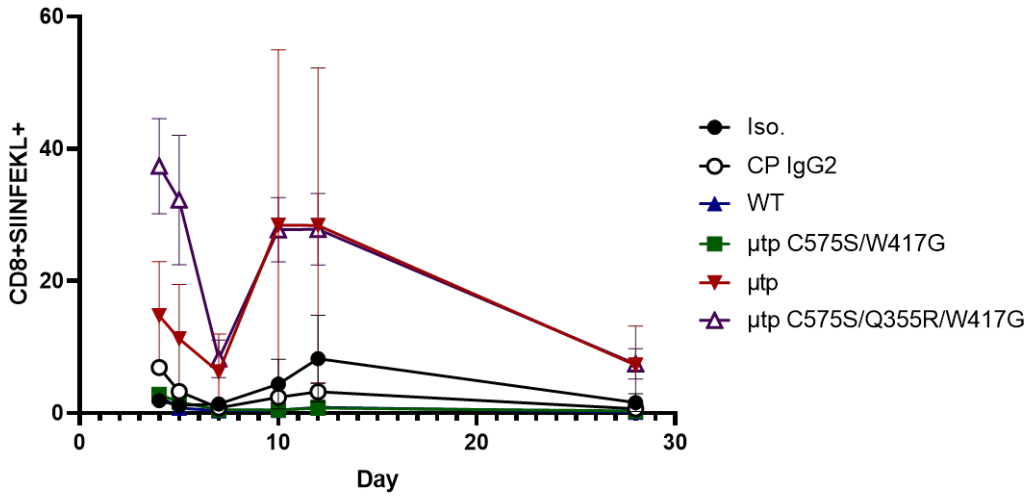

Figure 6.24: Effect of hIgG4 μtp mAb on *in vivo* OTI CD8$^+$ T cell expansion in FcγR1234 KO/hCD40Tg mice.
FcγR1234 KO/hCD40Tg mice were adoptively transferred with 1x10^5 OTI T cells (non purified in splenocytes) and treated with 100 μg OVA and 30 μg hIgG4 anti-CD40 mAb or RTX hIgG4 isotype control 24 hours later. OTI T cell expansion in the circulation was monitored over time. Blood was collected by tail tipping and analysed by flow cytometry for the percentage of CD8$^+$SIINFEKL$^+$ T cells as a proportion of total T cells. Data plotted is mean and SEM from a single experiment; n=3 mice per group.

6.6.4 Augmentation of the humoral response in FcγR1234 KO/hCD40Tg mice

Lastly, an anti-OVA ELISA was performed on the serum at day 12 to measure the level of antibody produced in response to OVA antigen and CD40 stimulation. CP hIgG2, ChiLob 7/4 hIgG4 WT, ChiLob 7/4 hIgG4 μtp C575S/W417G, and ChiLob 7/4 hIgG4 μtp did not induce any humoral response and no anti-OVA antibodies could be measured at day 12 (Figure 6.25). Similar to analysis in the hCD40Tg mice, the ChiLob 7/4 hIgG4 μtp C575S/Q355R/W417G did induce a humoral response and 6.1 μg/ml of anti-OVA antibody was detected by ELISA at this time-point (Figure 6.25).

These results indicated that of all the mAb tested in FcγR1234 KO/hCD40Tg mice only ChiLob 7/4 hIgG4 μtp C575S/Q355R/W417G was able to induce a humoral response.

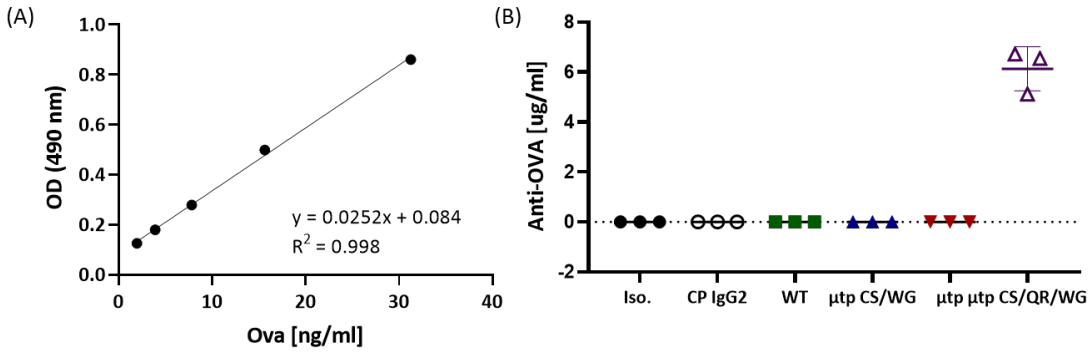

Figure 6.25: Effect of hIgG4 μtp mAb on *in vivo* stimulation of the humoral response in FcγR1234 KO/hCD40Tg mice. The same mice indicated above in Figure 6.24 were also assessed for their anti-OVA antibody response in serum. Blood samples were taken on day 12 after administration of 100 μg OVA and 30 μg hIgG4 anti-CD40 mAb or RTX hIgG4 isotype control, and serum was collected by centrifugation of blood after clotting. Concentration of anti-OVA antibodies in mouse serum was determined by ELISA, using a standard curve of known anti-OVA IgG concentration (A) Standard curve of known anti-OVA IgG (B) Calculated concentration (μg/ml) of anti-OVA antibody present in serum samples. Data plotted is mean and SEM from a single experiment; n=3 mice per group.

6.7 Chapter discussion

The previous chapters outlined the clear advantage of hIgG μtp hexamers and μtp C575S on-target hexamers in the recruitment and activation of the complement system. This chapter focussed on the application of μtp hexamers and μtp C575S on-target hexamers for the delivery of agonism; specifically for the anti-CD40 mAb, ChiLob 7/4. ChiLob 7/4 has demonstrated preclinical efficacy and progressed to early phase clinical trials, where its development has stalled due to a lack of observed clinical efficacy [504]. As previously described, CD40 is a member of the TNFR superfamily, activated by receptor clustering induced by its trimeric ligand, CD40L. Therefore, one obvious method of enhancing anti-CD40 mAbs, and potentially any anti-TNFR mAb, would be to utilise an antibody capable of clustering the receptor to artificially mimic the receptor trimerisation induced by CD40L. Herein, hIgG hexamers (μtp) and hexamerisation enhanced hIgG (μtp C575S) were formatted to target CD40 using the ChiLob7/4 V-region, in the context of hIgG1, 2, and 4 isotypes. The hypothesis was that hIgG μtp C575S and μtp hexamers would mediate enhanced receptor clustering, therefore enhancing agonism.

Previous studies demonstrated that ChiLob 7/4 hIgG1 does not induce *in vitro* agonistic activity in B cell homotypic adhesion, activation, and proliferation assays [90, 334, 505]. The only monomeric ChiLob 7/4 hIgG1 construct that have been previously demonstrated to induce CD40 activation were Fc-engineered with mutations that provide enhanced FcγRIIb-mediated cross-linking, such as SELF [505]. The engineering of ChiLob 7/4 hIgG1 to incorporate μtp C575S hex-

amerisation enhancement yielded no observable *in vitro* augmentation of anti-CD40 agonism in the various B cell assays, even in the presence of FcγR to provide cross-linking (Figures 6.1, 6.2, 6.5, 6.6, 6.7, 6.10, 6.11). This is in keeping with the weak agonistic activity of the parental ChiLob 7/4 antibody as a hIgG1 and indicated that hIgG1 hexamerisation enhanced (μtp C575S) mAb did not provide any beneficial anti-CD40 B cell activation. When produced as a pre-formed hexamer (μtp), hIgG1 could readily induce CD40 agonism *in vitro*, in the presence or absence FcγR-mediated cross-linking (Figures 6.1, 6.2, 6.5, 6.6, 6.7, 6.10, 6.11). However, CD23 upregulation was demonstrated to be lower in the context of FcγR1234 KO/hCD40Tg compared with hCD40Tg B cells, indicating some additional impact of FcγR cross-linking. Together these results indicate that TNFR can be activated by preformed hIgG1 μtp hexamers, independent of FcγR-mediated cross-linking. This was consistent with previous results demonstrating that a multimeric mouse IgG2a anti-CD40 antibody (but not its monomeric comparitors) can deliver therapeutic responses in FcγR-deficient mice [333]. Conversely, the results suggest that ChiLob 7/4 hIgG1 μtp C575S does not significantly agonise CD40 after target cell binding, despite demonstrating on-target hexamerisation abilities as RTX hIgG1 (Figures 4.2, 4.4, 4.5). The results described using ChiLob 7/4 hIgG1 mAb therefore suggest that the on-target hexamerisation provided by the μtp C575S peptide may not be enough to force sufficient receptor clustering that leads to effective CD40 signalling. This could also indicate that the ability to mediate receptor clustering through the μtp C575S addition is V gene specific and therefore epitope related, unable to cluster CD40 with ChiLob 7/4 but able to mediate agonistic activity for other mAb. This could be readily assessed by cloning other anti-CD40 mAb into the hIgG1 μtp C575S format. In addition, receptor clustering itself could be assessed using fluorescent microscopy, to see if hIgG1 μtp C575S does invoke increased clustering of CD40, but not activation.

The activation of CD40 had previously been demonstrated to be isotype dependent. Human IgG2 ChiLob 7/4 was the only isotype capable of robust CD40 stimulation, postulated to be due to the unique hinge region of hIgG2 [90]. The hinge of hIgG2 contains several cysteine residues that can shuffle their disulphide bond configuration resulting in multiple distinct isoforms and conformations. These isoforms have been termed A and B; wherein the A form is proposed to adopt a flexible structure and, the B form a more compact, rigid structure [88, 89, 506–508]. The B form of ChiLob 7/4 hIgG2 has been demonstrated to be more active, in an FcγR-independent manner. This is thought to be a result of its more compact conformation that allows for receptor clustering, or the lack of flexibility providing a more rigid lattice that favours downstream signalling [90]. This understanding of ChiLob 7/4 hIgG2 meant it was unsurprising that hIgG2 WT was highly active *in vitro*. However, there was no observable enhancement with either the on-target hIgG2 hexamer (μtp C575S) or pre-formed hexamer (μtp), in the presence (Figures 6.3, 6.5, 6.6) or ab-

sence (Figures 6.1, 6.8, 6.10, 6.11) of FcγR. Nonetheless, the agonism of FcγR1234 KO/hCD40Tg B cells was decreased compared to WT hCD40Tg B cells, indicating that FcγR cross-linking does augment CD40 agonism with hIgG2.

Previously, hIgG4 anti-CD40 mAb agonists had not been studied to the same extent as hIgG1 and hIgG2 isotypes, but in early studies ChiLob 7/4 hIgG4 had been shown not to induce *in vitro* CD40 stimulation [90]. Generally, the hIgG4 isotype is selected for its minimal FcγR interactions, with the aim of binding to its target antigen without strong immune effector mechanisms, such as ADCC or ADCP. This characteristic makes them attractive for immunomodulatory antibodies, specifically when the target antigen is on the surface of tumour-specific CTLs, such as in the case of the recently approved anti-PD1 antibodies, nivolumab and pembrolizumab. However, even though it is considered a non-functional isotype, hIgG4 is still able to bind FcγR as an immune complex [84] and activity can be influenced by FcγRIIb, as demonstrated for the anti-CD28 hIgG4 mAb TGN1412 [509]. It could be predicted that the current understanding of the requirement for cross-linking to induce sufficient activation may increase the development of hIgG4 therapeutics, due to them having comparable FcγRIIb affinity to other isotypes, but low affinity for activating FcγRs [84]. Consistent with previous results, ChiLob 7/4 hIgG4 WT had no agonistic activity in the *in vitro* or *in vivo* assays examined. As previously mentioned, the W417G mutation was unintentionally introduced into the ChiLob 7/4 hIgG4 μtp C575S construct. Interestingly, there was an agonistic enhancement observed with ChiLob 7/4 hIgG4 μtp C575S/W417G *in vitro* (Figures 6.1, 6.4, 6.5, 6.6, 6.9, 6.10, 6.11). The pre-formed ChiLob 7/4 hIgG4 μtp hexamer also exhibited potent *in vitro* agonistic activity (Figures 6.1, 6.4, 6.5, 6.6, 6.9, 6.10, 6.11), which demonstrated that hexamerisation clearly permits potent agonism in the context of hIgG4 mAb.

Taken together these results have demonstrated that preformed μtp hexamers were able to drive potent CD40 agonism in every isotype, thereby indicating that hexamerisation is driving CD40 agonism. However, only the hIgG4 μtp C575S construct enhanced CD40 agonism in the observed assays, which could be a result of the W417G mutation potentially inducing enhanced on-target hexamerisation. In Chapter 5 there was no observable in-solution or on-target hexamerisation enhancement with RTX hIgG4 μtp C575S, however, this construct did not contain the W417G mutation. For the current theory that on-target hexamerisation is driving hIgG μtp C575S agonism, these results may be indicative that W417G offers an additional hexamerisation enhancement. Due to not having evidence of the in-solution and on-target hexamerisation enhancement capabilities of the hIgG4 μtp C575S/W417G construct, it is not clear if the mechanism of action providing agonism is receptor clustering facilitated by on-target hexamerisation.

As previously shown, introduction of Q355R into hIgG4 μtp C575S/W417G gave a hexamerisa-

tion enhancement that could be utilised to enhance the CDC, and potentially agonistic activities of hIgG4 μtp C575S constructs. In the context of RTX hIgG4 μtp the C575S/Q355R/W417G mutant demonstrated efficient in-solution hexamerisation and on-target hexamerisation, indicated with enhanced C1q binding and CDC activity (Figures 5.19, 5.20). Despite this, the current results demonstrated that there was comparable CD40 agonistic activity between μtp C575S/W417G and μtp C575S/Q355R/W417G hIgG4 *in vitro* (Figure 6.12, 6.14, 6.15). Interestingly, mutagenesis of R355Q in the Fc of ChiLob 7/4 hIgG1 μtp C575S decreased the activation of NF-κB in the Jurkat reporter cell line (Figure 6.12), homotypic adhesion (Figure 6.13), and CD23 expression (Figure 6.15), suggesting that the lack of hexamerisation does hinder agonism. However, the levels of activation were already low with the hIgG1 μtp C575S constructs. There was also an observed increase in proliferation at 10 μg/ml with both hIgG1 R355Q and hIgG4 Q355R mAb which was observed in all three repeat experiments. These results were comparable in assays using FcγR1234 KO/hCD40Tg B cells (Figure 6.16, 6.17, 6.18), providing further evidence that hIgG4 μtp C575S mAb can induce augmented CD40 stimulation in the absence of cross-linking.

To fully resolve the impact of W417G further experiments are required, for example RTX hIgG4 μtp C575S/W417G, hIgG4 μtp C575S/Q355R, and hIgG4 μtp C575S/Q355R/W417G could be examined to assess any differences for in-solution hexamerisation, on-target hexamerisation, C1q binding, and CDC activity. Additionally, the different mutant combination for ChiLob 7/4 could also be assessed for NF-κB activation and in *in vitro* hCD40Tg B cell stimulation assays. These experiments should help to delineate the observed on-target hexamerisation and augmented agonism with the hIgG4 μtp C575S/Q355R/W417G constructs. Additionally, the observation that introduction of W417G may promote on-target hexamerisation of hIgG μtp C575S constructs suggests that the W417G mutation could also augment the agonism of ChiLob hIgG1 μtp C575S, which stimulated only low levels of agonism *in vitro* and was comparable to WT ChiLob hIgG1 in functional studies, and is something that should be considered for future studies. One further characteristic to note is the enhanced CDC activity of RTX hIgG4 μtp C575S/Q355R/W417G described in the previous chapter. The efficient induction of complement-mediated cell killing may have deleterious impacts to an agonistic antibody, such as target cell depletion, which should be considered. This impact could be negated by C1q null mutations or selective deglycosylation of the CH2 glycan site (i.e. with the use of the N297Q mutation). Assuming on-target hexamerisation is involved in hIgG4 μtp C575S agonism, the μtp glycan should be kept intact as it has been demonstrated in Chapter 5 to be important for the hexamerisation propensity.

Experimentation with the ChiLob 7/4 hIgG4 μtp fusion mAb *in vivo* indicated that these mAb are tolerated up to doses of $\sim$1 mg/kg. There were no observed adverse effects after administration, including physical symptoms or weight loss (Figure 6.20, 6.23). However, the measurement of

animal weights did highlight a range of weights between groups at the start of each experiment, and that the FcγR1234 KO/hCD40Tg mice were generally heavier. The FcγR1234 KO/hCD40Tg mice were older at the start of the experiment (between 4-5 months), whereas the hCD40Tg mice were younger (between 2-3 months). This may explain the differences in weights between experiments. Due to time restrictions of the remaining practical time at the end of the thesis the selection of mice used was not optimal, leading to differences between experiments and within experiments. Future investigation should be undertaken on age and weight matched animals where possible, to negate any variation these factors may cause.

It was clear that the augmented *in vitro* CD40 agonism of ChiLob 7/4 IgG4 μtp C575S/W417G was not translated to T cell expansion or antibody generation in the murine models examined (Figure 6.21). Additionally, hCD40Tg mice treated with ChiLob hIgG4 μtp hexamer did not demonstrate any *in vivo* activity in hCD40Tg mice either (Figure 6.21), even though there was greatly enhanced agonism *in vitro*. There was, however, OTI CD8$^+$ T cell expansion in FcγR1234 KO/hCD40Tg (Figure 6.24), indicating a potentially inhibitory role of murine FcγRs *in vivo*. It could be speculated that the high avidity interaction of hIgG hexamers for FcγRs cause FcγR:IgG hexamer internalisation and degradation, as was previously described for Fc μtp hexamers [399]. Therefore, the available circulating concentration of the mAb would be lower in hCD40Tg mice which would likely suppress CD40 agonism, as previous experience with the model shows that responses are dependent on the dose of anti-CD40 mAb administered (personal communication with Dr Ben Yu). This theory could be investigated in future work by analysing the half-life of hIgG4 hexamers in both mouse strains and monitoring the expression of FcγR after antibody administration. If half-life was shown to be the limiting factor then higher or multiple doses of the hIgG4 hexamers could be explored. It should be noted that the current dosing strategy for all the constructs was extremely conservative - based upon the activity of the most agonistic anti-CD40 mAb assessed in the group to date. Therefore, it may be that higher doses of some of these mAb may indeed lead to agonistic responses *in vivo*, such as with ChiLob 7/4 hIgG4 μtp C575S/W417G.

Interestingly, initial studies *in vivo* indicated that ChiLob 7/4 hIgG4 μtp C575S/Q355R/W417G induced increased OTI CD8$^+$ T cell expansion (Figure 6.21) and humoral immunity (Figure 6.22), indicative of CD40 agonism. More importantly, the ChiLob 7/4 μtp C575S/Q355R/W417G construct had FcγR-independent *in vivo* activity, as demonstrated with the use of an OTI adoptively transferred FcγR1234 KO/hCD40Tg mouse model (Figure 6.24). The benefit of inducing FcγR-independent agonism is that it removes the reliance for high bioavailability of local FcγR, which may be low in the case of some tumours or at sites of cell activation, rendering the mAb ineffective. Therefore, by not being dependent on FcγR-mediated cross-linking, such mAb may have applicability in the treatment of a larger range of tumours. However, it should be noted that OTI

T cells were adoptively transferred in the presence of B cells and other FcγR bearing cells present in splenocytes, which could impact the interpretation of the results due to low levels of FcγR expressing cells potentially providing mAb cross-linking. In order to negate this, OTI T cells could be purified and adoptively transferred in future experiments, or FcγR binding incompetent hIgG could be produced and investigated in the context of μtp C575S on-target hexamers. In order to discern the impact of the W417G mutation *in vivo*, further mutagenesis will be required to produce ChiLob 7/4 hIgG4 mAb with either μtp C575S, μtp C575S/W417G, μtp C575S/Q355R, or μtp C575S/Q355R/W417G mutations. As a result of the *in vivo* models being the only assay format where the activity between ChiLob 7/4 hIgG4 μtp C575S and ChiLob 7/4 hIgG4 μtp C575S/Q355R could be distinguished, the *in vivo* OTI adoptive transfer model will need to be utilised.

It has previously been postulated that hIgG4 adopts a more compact configuration compared to hIgG1 as a result of a shorter hinge with unstable disulphide bonds, and interactions between the CH1 and CH2 domains promoting the F(ab) arms folding back to lie parallel with the Fc (Figure 6.26,B) [500]. This structure may result in functionally monovalent molecules, binding to their antigen with only one F(ab) arm and the other F(ab) arm being distal from the membrane. This functional monovalency may permit efficient receptor clustering through on-target hexamerisation dictated by the μtp C575S peptide. Strasser *et al* have recently proposed that the assembly of on-target hexamers using hIgG1 E430G is mediated by one of two pathways, recruitment of IgG from solution or through lateral collision of antigen bound IgG. Human IgG1 binds readily through bivalent membrane attachment (Figure 6.26,A) which appeared to sterically suppress Fc:Fc interactions between colliding antigen-bound IgGs, diffusing across the membrane (lateral collision). The only way for bivalently bound hIgG1 to form on-target hexamers was shown to be through recruitment of hIgG1 from solution via Fc:Fc interactions which stimulated the release of one epitope, to form an antigen bound dimer. The hIgG1 dimer was then amenable to recruit additional hIgG1 molecules (Figure 6.26,C). Alternatively, membrane-bound monovalent hIgG1 (determined using a bispecific antibody) was able to assemble into hIgG1 hexamers through lateral Fc:Fc collisions (in the absence of solution hIgG1) more efficiently. In addition to the different mechanisms, there was different efficiencies of on-target hexamerisation induced, whereby hexamerisation of monovalent antibodies was more rapid (19 seconds for hIgG1 E430G) than bivalent antibodies (66.9 seconds with hIgG1 E430G) [198]. This current understanding of the hIgG4 conformation and the process of on-target hexamerisation gives rise to the theory that hIgG4 μtp C575S constructs could bind with a single F(ab) arm and recruit other antibody molecules to cluster CD40 and provide stimulation through the hexamerisation-enhancement provided by the μtp C575S interactions (Figure 6.26,D). This mechanism of on-target hexamerisation may not be as efficient for hIgG1 μtp C575S constructs due to potential bivalent interactions [198]. This may explain why

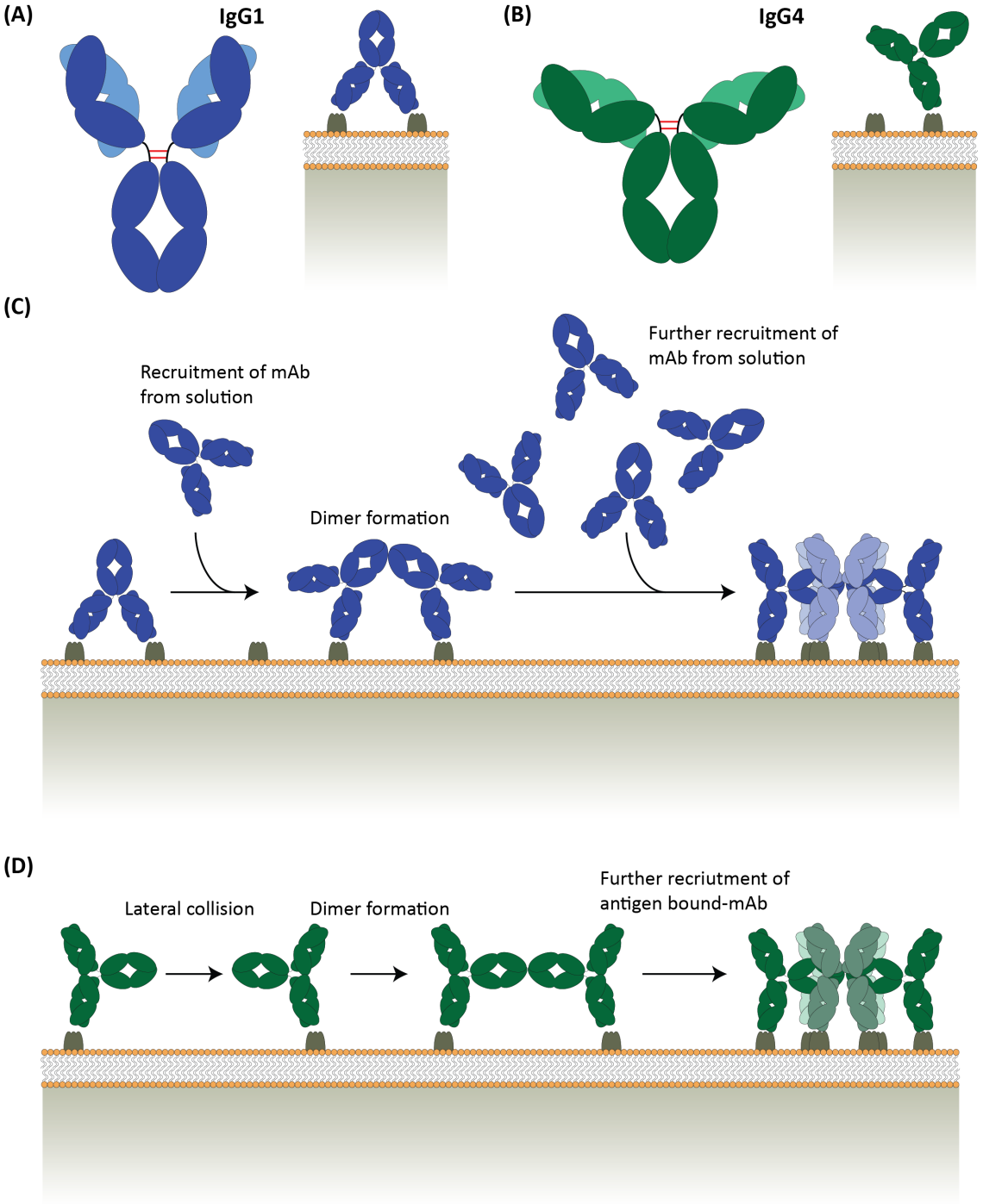

Figure 6.26: Potential on-target hexamerisation mechanisms of hIgG1 and hIgG4.
(A/B) Postulated conformational and binding differences between hIgG1 and hIgG4 (A) hIgG1 is proposed to adopt an open structure, with F(ab) arms extending away from the Fc (left), resulting in a more favourable bivalent binding orientation (right) (B) hIgG4 is proposed to adopts a more compact structure, with F(ab) arms bent backwards towards the CH2 domain (left), potentially resulting in monovlanet binding orientation (right) (C) Potential mechanism of hIgG1 on-target hexamerisation. hIgG1 molecules bind bivalaently at the cell surface and recruit additional hIgG1 molecules from solution (D) Potential mechanisms of IgG4 on-target hexamerisation. hIgG4 binds monovalently at the target cell surface and recruits additional antigen-bound hIgG4 molecules via lateral collision. B and C adapted from [198].

the ChiLob 7/4 hIgG4 μtp C575S constructs, but not the ChiLob 7/4 hIgG1 μtp C575S constructs engage CD40 for efficient activation. However, this is not consistent with the previous data in Chapter 4 showing efficient on-target hexamerisation of RTX hIgG1 μtp C575S (Figures 4.4, 4.5). Investigations into the monovalency of the current ChiLob 7/4 hIgG4 μtp C575S constructs may aid in understanding the agonism observed with hIgG4 μtp C575S constructs. This could be achieved by producing bispecific ChiLob 7/4 hIgG4 and hIgG1 μtp C575S constructs, where only one F(ab) is specific for CD40, and assessing their agonistic activities.

Overall, the results from this chapter indicated that the human IgG subclasses clearly have different properties that can be manipulated by addition of the μtp and μtp C575S technology in terms of immunostimulatory functionality, which are summarised in Figure 6.27. The differences in CD40 agonsim induced by hIgG1, 2, and 4 μtp C575S constructs observed here have not been fully characterised. As already mentioned, its application to multiple V regions targeting the different epitopes of CD40 should be explored. Similarly different TNFR could be explored. It is also important to fully evaluate each subclass and decide on the desired outcome, such as FcγR-dependency/-independency, to maximise therapeutic outcome in different contexts. Additionally, these hIgG4 μtp mAb will need to be examined using purified human immune cells to determine if this activity can be fully translated to human B cells expressing endogenous CD40. These studies will help determine the utility of this approach for the treatment of human malignancies. Human B, T, and dendritic cells can be purified and assessed for anti-CD40 stimulation in an array of assays previously described by White *et al* [90], and should be considered for future experiments.

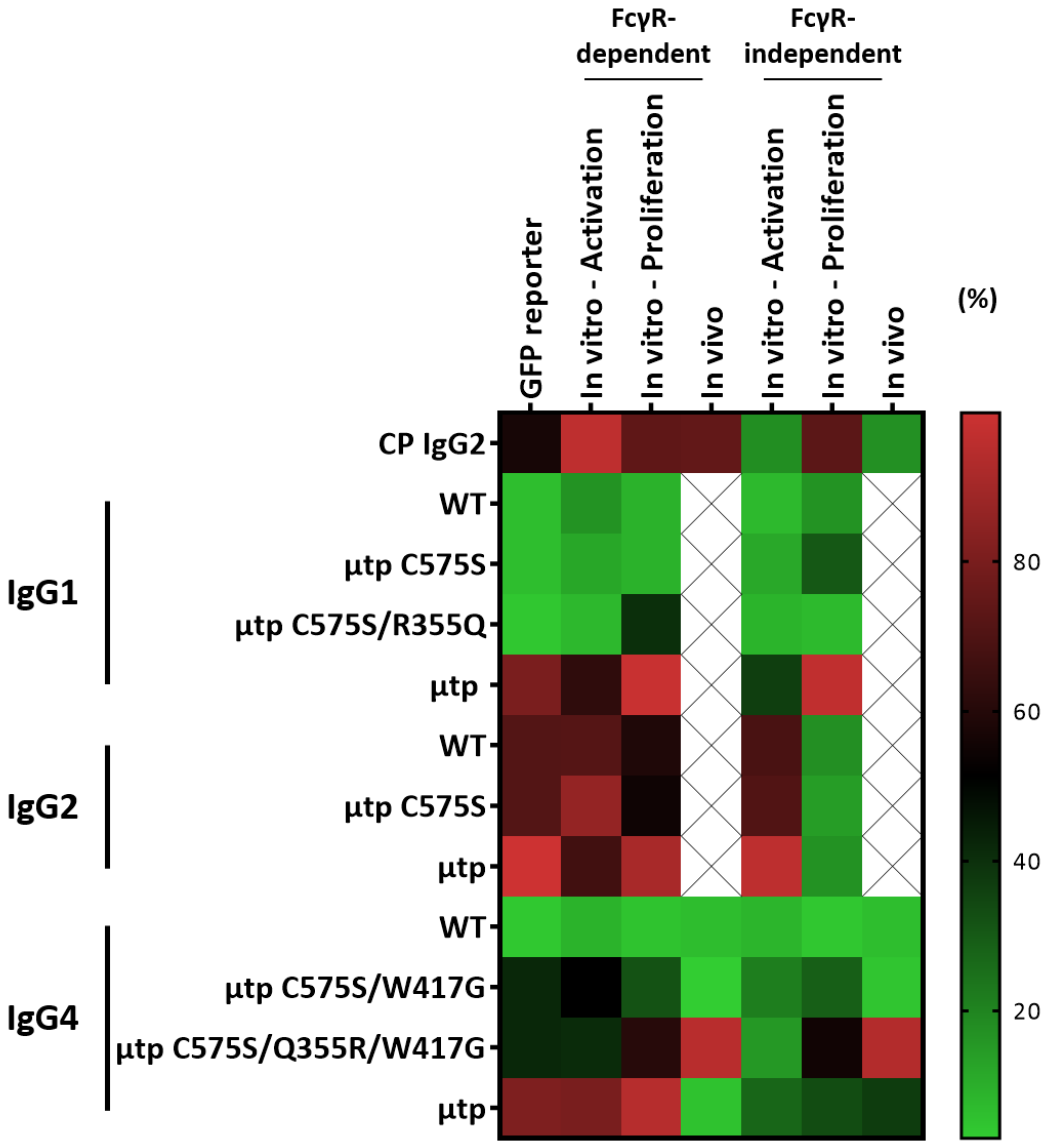

Figure 6.27: Summary of the *in vitro* and *in vivo* agonistic activity induced by anti-CD40 μtp fusion mAb.
The agonistic activity of ChiLob 7/4 hIgG1, 2, and 4 μtp mAb expressed as a percentage (%) of maximal activity in each assay calculated using the mean.

Chapter 7

General discussion

The concept of on-target IgG hexamers as direct targeting and immunostimulatory antibodies was first described in 2014. Diboldер *et al* characterised the E430G mutation, capable of enhanced on-target antigen clustering and CDC induction [197]. Such antibodies are monomeric in solution, similar to WT hIgG, but have a higher propensity to hexamerise after antigen binding via enhanced, non-covalent Fc:Fc interactions [198]. IgG on-target hexamers should therefore retain WT hIgG safety and pharmacokinetic profiles. Since this initial report, subsequent reports have characterised the E430G mutation and validated its utility for direct targeting antibodies against CD20 [271], EGFR [376], CD37 [377] and CD38 [271], in addition to stimulation of OX40 [379, 380] and DR5 [381] cell surface receptors. These subsequent studies have highlighted the potential for hIgG on-target hexamers as an approach to enhance current and future therapeutic mAb.

In this thesis, the naturally monomeric hIgG was combined with the tailpiece of the naturally multimeric hIgM (μtp; an 18-AA peptide located the C-terminus of hIgM heavy chain) (Figure 3.1) to enable the production of a hIgG molecule with the propensity to form covalent hexamers (Figure 3.4). This approach for producing hIgG hexamers was initially described in the 1990's, and was shown to produce hIgG complexes capable of high complement cytotoxicity [368, 369], which are consistent with the results observed in this thesis. The anti-CD20 hIgG1, 2, and 4 μtp hexamers demonstrated greatly enhanced CDC activity *in vitro* (Section 4.2). In addition, ChiLob 7/4 hIgG1 and 4 hexamers also demonstrated greatly enhanced CD40 agonism *in vitro*, compared to their WT counterparts (Section 6.2). Although, the preformed hIgG μtp hexamers have demonstrated significant augmentation of activity *in vitro*, these formats may not be optimal for future hIgG therapeutic antibodies as demonstrated in previous literature [399, 401] and this thesis. The observed lack of *in vivo* efficacy (Section 4.5) has been attributed to the considerably shorter half-life of hIgG hexamers compared to hIgG WT monomers (Figure 4.21). The hIgG hexamers have been

shown to bind with high avidity to human FcγRs which has the potential to lead to internalisation and degradation of the construct, as has previously been described with Fc μtp hexamers [399]. Therefore, hIgG hexamers are quickly removed from circulation, limiting their potential activity. In addition to the short half-life, it is also possible that systemic administration could result in unwanted pro-inflammatory responses, such as spontaneous complement (and possible FcγR) activation. Previous experiments have reported elevated levels of pro-inflammatory cytokines with fresh peripheral blood stimulated with hIgG1 Fc μtp hexamers [401]. Therefore, there is the possibility that hIgG hexamers could culminate in a cytokine storm comparable to that observed with TGN1412 [293].

An alternative solution, and a potentially preferential format, could therefore be hIgG on-target hexamers (as opposed to pre-formed hexamers discussed above). Herein, the development and characterisation of a novel engineering approach focussed on hIgG on-target hexamerisation was described. The driving force of the covalent antibody hexamerisation induced by the μtp is the penultimate cysteine residue in the peptide sequence. This amino acid permits disulphide bonds between adjacent μtp peptides resulting in stable multimers. Mutagenesis of this cysteine residue ablated stable hexamer formation resulting in hIgG μtp C575S monomers that could be expressed and purified following standard antibody purification techniques, without increased aggregation or loss in yield or quality (Sections 3.4, 3.5). More importantly, this format did not negatively impact the *in vivo* characteristics of the mAb, such as activity, clearance, or toxicity (Section 4.5).

Once the μtp C575S constructs had been successfully produced, the in-solution hexamerisation propensity was analysed. Analysis of the potential hexamerisation enhancement was performed by concentrating each mAb to 20 mg/ml, as a method to artificially force inter-antibody interactions. Here it was clear that the hIgG1 μtp C575S construct had increased hexamerisation propensity in solution (Figure 4.1). Further analysis demonstrated the hIgG1 μtp C575S construct demonstrated unaltered C1q binding compared with hIgG1 WT, whereas the preformed hIgG μtp hexamer had increased binding for C1q (Figure 4.2). However, following target cell opsonisation, hIgG1 μtp C575S demonstrated increased recruitment of C1q over WT hIgG1 (Figure 4.4), in-line with C1q recruitment of an hIgG μtp hexamer. The resulting C1q recruitment enhancement led to increased CDC activity of both hIgG1 μtp C575S and hIgG1 μtp (Figure 4.5). Taken together these results demonstrated that μtp C575S behaves akin to a monomer in solution, but comparable to a preformed μtp hexamer at the target cell surface. These characteristics are in-line with the previously described activity of the on-target hexamer hIgG1 E430G [271]. However, whereas the E430G mutation has been postulated to result in increased flexibility of the CH3:CH2 interface to enhance Fc:Fc interactions and promote on-target hexamerisation, the mechanism of μtp C575S driven hexamerisation was not fully resolved. The hypothesis was that the μtp C575S peptides

on adjacent hIgG μtp C575S molecules interact and stabilise as a hexamer after target binding, independent of enhanced Fc:Fc interactions. Future structural and modelling studies may help to uncover the interactions involved between hIgG1 μtp C575S molecules. This will help to elucidate whether the Fc's of adjacent antibodies are interacting or if the interaction is solely μtp:μtp mediated.

The hIgG1 μtp C575S was further demonstrated to have attained differential DCD activity, dependant on the type of anti-CD20 mAb (Figures 4.12, 4.13), and comparable FcγR-mediated effector functions to the hIgG1 WT (Figures 4.9, 4.11). The similarities in FcγR effector mechanisms has been postulated to be a result of unaltered binding to FcγR, as it remains a 1:1 stoichiometry, indicating FcγR are not preferentially stimulated by surface bound hIgG1 μtp hexamers. Assays examining the B cell depleting activities of hIgG1 μtp C575S on-target hexamers in fresh peripheral human blood and *in vivo* in hCD20Tg mice suggested that the complement enhancement observed did not achieve increased B cell depletion over hIgG1 WT. In fact, the hIgG1 μtp hexamers exhibited decreased B cell depletion (Sections 4.4, 4.5), suggesting that overactivation of complement may have negative implications. The only increase in B cell depletion observed was in the lymph nodes of animals treated with RTX hIgG1 μtp C575S (Figure 4.26). This may indicate that B cell depletion in the lymph nodes is more reliant on complement than FcγRs, and may represent an environment where hIgG1 μtp C575S constructs could be utilised to more effectively kill target cells than conventional hIgG1 mAb. This would be useful for haematological malignancies where the tumour cells migrate to lymph nodes and potentially evade depletion.

Analysis into the factors influencing enhanced CDC activity with the hIgG1 μtp hexamers revealed that similar amino acids in canonical hIgG1 involved in binding C1q were also important in the CDC activity of hIgG1 μtp constructs. Mutagenesis of P331S completely abolished C1q recruitment and CDC activity of RTX hIgG1 (Figure 5.1). The hIgG1 μtp hexamer mutated with either P331S or K322A exhibited significantly decreased C1q recruitment by 1.65-fold and 20.6 fold respectively. This resulted in a decrease in CDC activity, but not complete inhibition, with RTX hIgG1 μtp P331S demonstrating an EC50 of 3.75 μg/ml and RTX hIgG1 μtp K322A demonstrating an EC50 of 10μg/ml, compared with 0.31 μg/ml for native RTX hIgG1 μtp (Figure 5.2). Furthermore, treatment with PNGase F to deglycosylate RTX hIgG1 μtp did not render the construct completely ineffective at CDC activity, unlike for hIgG1 (Figure 5.6). Both of these modifications to hIgG1 are known to decrease the affinity for C1q, so these results indicated that hIgG1 hexamers could overcome the modifications previously thought to completely ablate complement-mediated lysis, whereby avidity for C1q (through hexamerisation) can overcome low affinity Fc binding. This indicates that hIgG hexamerisation is an important mechanism in the activation of the complement system and in order to completely abolish complement activity these Fc:Fc interactions driving

hexamerisation need to be restricted. Similarly, RTX hIgG1 μtp C575S/P331S demonstrated a decrease in C1q binding as measured by ELISA, but the antibody was still capable of recruiting C1q and inducing CDC, albeit to a lesser extent than the WT RTX hIgG1 μtp C575S (Figure 5.1). Deglycosylation of RTX hIgG1 μtp C575S also decreased C1q binding, but completely inhibited C1q recruitment and complement-lysis of target cells (Figure 5.5). Potentially more important was the observation that deglycosylation removed the propensity of the hIgG1 μtp C575S to hexamerise in solution (Figure 5.6), implying that the lack of on-target hexamerisation is preventing complement activity. Glycan analysis revealed that treatment with PNGase F cleaved the glycans from both the CH2 N297 and μtp N563 sites (Figure 5.3), which raises the question as to whether deglycosylation of the CH2 or μtp N-glycan, or both, was the driving factor in the loss of in-solution (and potentially covalent) hexamerisation and complement activity.

This was partly resolved with mutagenesis studies of the μtp peptide. Mutations were designed to alter the glycan occupancy of the μtp C575S N563 site, but leave the CH2 N297 glycan unaltered (Figures 5.7, 5.8). Characterisation of these mutants revealed that a decrease in glycan occupancy induced by the V564D mutation prevented in-solution hexamerisation (Figure 5.9) and CDC activity (Figure 5.10). Conversely, the increase in glycan occupancy observed with the S565T mutation enhanced the propensity to hexamerise in solution (Figure 5.9) and augmented complement-mediated lysis (Figure 5.10). Importantly both of these hIgG1 μtp C575S constructs had comparable C1q binding as determined by ELISA. Taken together, these results suggest that the glycan occupancy on the RTX hIgG1 μtp C575S regulates the hexamerisation enhcancement, which in turn is responsible for the level of C1q binding and CDC activity. Therefore, on-target hexamerisation is crucial for the enhanced complement activity of μtp C575S constructs and is likely driven or stabilised by glycan interactions between adjacent μtp peptides (Figure 7.1). It is also likely that Fc and μtp C575S both glycans play an important role in the overall complement activity; the Fc glycan being required for the initial C1q interaction, with the μtp glycan required for enhanced hexamerisation propensity. High occupancy at both glycan sites would appear to be optimal, as exemplified by the S565T mutant. Mutagenesis of either glycan site to remove the N-linked glycan and analysis of their in-solution and on-target propensity could help to confirm the role of each glycan. Future *in vivo* investigations using the very efficient RTX hIgG1 μtp C575S/S565T antibody could also be undertaken to determine if this approach could increase B cell depletion, both in the blood and lymph nodes. Alternatively, if CDC is a negative regulator of depletion, as described above with assessment in whole blood, then depletion may be expected to be lower. *In vivo* analysis will also permit the clearance rate and any potential toxicity to be examined. A further observation to note was that the trends between activity assays did not always align. For example, RTX hIgG1 μtp C575S/V564L demonstrated enhanced C1q recruitment

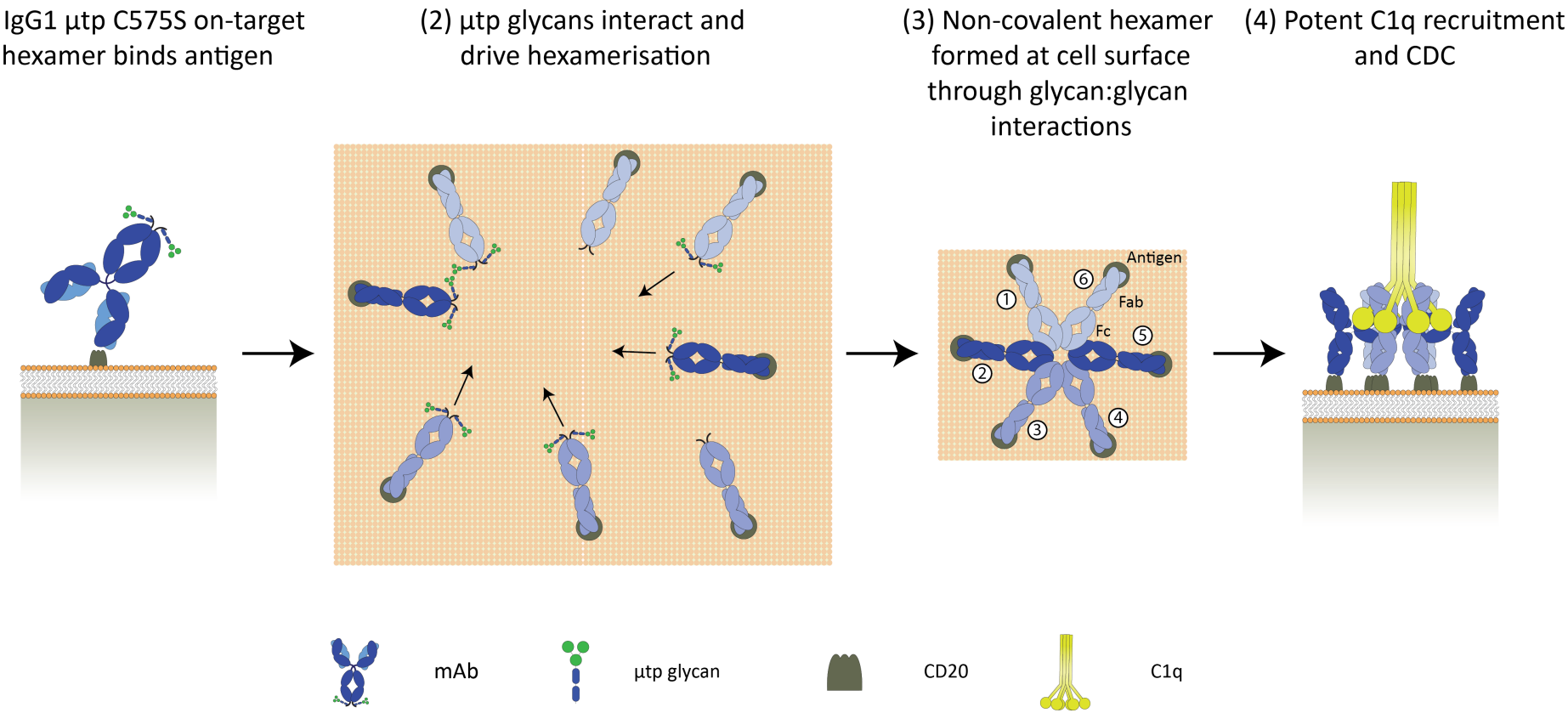

Figure 7.1: Proposed mechanism of glycan driven on-target hexamerisation of RTX hIgG1 μtp C575S constructs.
(1) hIgG1 μtp C575S mAb binds to CD20 as a monomer (2) μtp glycans drive hexamerisation through glycan:glycan interactions with adjacent antigen bound hIgG1 μtp C575S mAb, antibodies with no μtp glycan occupancy have little/none hexamerisation propensity and so do not interact (3) hIgG1 μtp C575S with N-linked glycans form non-covalent, on-target hexamers through glycan:glycan interactions and are stabilised (4) On-target hexamers can efficiently recruit C1q and elicit potent CDC activity.

but this did not translate into augmented CDC of target cells, whereas RTX hIgG1 μtp C575S/S565T exhibited both increased recruitment of C1q and complement-mediated cell death.

In addition to mutating residues and altering the glycosylation profile, the hIgG1 μtp anti-CD20 mAb constructs were isotype switched to hIgG2 and hIgG4. There was no in-solution hexamerisation with these isotypes in the μtp C575S formats at concentrations up to 20 mg/ml, indicating that this is a property of hIgG1. Initial characterisation of the hIgG1 μtp C575S in-solution hexamerisation was analysed at concentrations up to 70 mg/ml, which showed that the maximum hexamerisation possible with hIgG1 μtp C575S constructs was $\sim$40%. It is possible that further increasing the concentration of hIgG2 and hIgG4 μtp C575S may induce the interactions required for in-solution hexamers to form, but nonetheless suggests that their hexamerisation propensity is less efficient than hIgG1. The interaction forming IgG hexamers could also be less stable with the hIgG2 and hIgG4 μtp constructs, and in-solution hexamers may more readily dissociate due to potential dilution and stress of loading and migration through the UPLC column. However, due to the requirement for larger amounts of protein this was not feasible for the hIgG2 and hIgG4 μtp C575S constructs, but could be performed in future studies.

The hIgG2 and hIgG4 μtp constructs did however form hexamers in solution and displayed augmented CDC activity. The hIgG2 and hIgG4 μtp constructs demonstrated that hexamerisation of these isotypes could enhance their complement activities (Figures 5.15, 5.17). This suggests that high avidity interactions (mediated by hexamerisation) can still recruit C1q with these low affinity isotypes and provided a proof-of-concept that hIgG2 and hIgG4 hexamers could be utilised as complement inducing isotypes. However, this augmentation was not as clear with μtp C575S constructs (Figures 5.15, 5.17), and could indicate that the lack of on-target hexamerisation observed was a result of an inability to efficiently hexamerise in solution (Figures 5.14, 5.16) coupled to the inherently low C1q affinity [475, 476]. It is known that the CD20 antigen undergoes redistribution into lipid rafts after binding type I anti-CD20 antibodies, such as RTX [266, 268, 274]. It is possible that not all RTX hIgG isotypes induce CD20 clustering to the same extent, and as such hIgG2 and hIgG4 could be less effective in inducing CD20 reorganisation into lipid rafts, similar to the type II hIgG1 anti-CD20 mAb, BHH2. Inefficient CD20 clustering would result in lower levels of C1q recruitment and CDC observed with these isotpyes. Experiments involving modifying the hexamerisation propensity of hIgG1 μtp C575S (V564D) have demonstrated that by abrogating the hexamerisation propensity only, CDC activity can be inhibited. Therefore, together these data indicate that on-target hexamerisation is an important characteristic of CDC-inducing mAb. To support these conclusions, analysis of CD20 reorganisation into lipid rafts induced by hIgG2 and hIgG4 isotypes could be performed. Additionally, mutagenesis strategies that enhance the hexamerisation propensity of these isotypes, such as with S565T, could provide further enhancement

of the CDC activity of hIgG2 and hIgG4 μtp C575S constructs.

The majority (90%) of the hIgG1, 2, and 4 sequences are homologous to one another [80], therefore, it is the result of only a few amino acids that induce their overall pro- (hIgG1) or anti-inflammatory (hIgG2/4) properties. For example, it has been reported that residues in the CH2 of IgG4 are responsible for the lack of C1q binding, such as S331, and swapping this residue with the proline present in hIgG1 reverses this lack of C1q interaction. In this thesis, residues in the CH3 of hIgG4 were substituted with residues from hIgG1, as this is the reported interface in Fc:Fc interactions [271]. The IgG4 μtp C575S/Q355R construct demonstrated enhanced in-solution (Figure 5.19) and on-target hexamerisation (Figure 5.20). Conversely, the reverse mutations in RTX IgG1 μtp C575S/R355Q demonstrated an abrogation of in-solution hexamerisation (Figure 5.19) and a decrease of CDC (Figure 5.20). These results suggest that this residue is important in the hexamerisation propensity of hIgG1. However, the RTX hIgG4 μtp C575S/Q355R construct had an additional unintentional W417G mutation, later demonstrated to potentially be important for *in vivo* CD40 agonism. Unfortunately the presence of this additional mutation was only discovered towards the end of these studies and so the reliance on *in vitro* complement activity of W417G was not investigated here, and future mutagenesis studies to its importance are necessary.

In addition to *in vitro* characterisation, the hexamerisation enhanced hIgG2 and hIgG4 anti-CD20 mAb could be examined for target cell depleting efficacy *in vivo*. Due to their inability to efficiently engage FcγR-bearing cells to induce associated cell killing mechanisms, they could represent 'complement-only' antibodies and their efficacy in depleting B cells could be assessed. Further to the use of hexamerisation enhanced anti-CD20 antibodies, this technology could be examined in the context of additional, clinically relevant targets, such as Her2 and EGFR. This would provide evidence of the applicability of μtp C575S on-target hexamers for a range of targets being used in the treatment of a range of malignancies. In addition, it has been demonstrated that bacterial infections can be controlled by IgG via complement but not FcγR-mediated effector mechanisms [378, 470]. Therefore, hexamerisation-enhanced IgG are uniquely useful in this instance and could be used in combination with FcγR null isotypes to prevent engagement with FcγR to inhibit any competition with C1q recruitment.

Currently only hIgG1, 2, and 4 isotypes are used clinically [246] and therefore this thesis focussed on characterising these isotpyes in the context of μtp hexamers and μtp on-target hexamers. There are no hIgG3 based therapeutics, despite their highly potent CDC activity compared to the other hIgG isotypes [422]. The main reason development of hIgG3 therapeutics has not been as successful as the other isotypes is the relatively short serum half-life compared to the other hIgG isotypes [85]. The high clearance rate of hIgG3 is thought to be related to the lack of binding to

FcRn [86]. However, mutations to promote FcRn binding have been demonstrated to alleviate the short serum half-life of hIgG3 and provided comparable *in vivo* persistence to other hIgG isotypes [86]. Therefore, hIgG3 could be considered for future therapeutics and addition of the μtp C575S to hIgG3 assessed as a means to further augment target cell depletion and therapeutic efficacy.

As has been mentioned, the current spotlight of antibody therapeutics is on the development of immunomodulatory mAb. This has been intensified by recent clinical success which has led to the search for more effective, clinically relevant immunostimulatory antibodies. The results herein have indicated there was no enhancement in the agonism of CD40 observed with hIgG1 and hIgG2 ChiLob7/4 μtp C575S antibodies *in vitro* (Sections 6.2, 6.3, 6.4). The results for RTX hIgG1 and hIgG2 μtp C575S showed an enhancement in on-target hexamerisation, therefore it could be assumed that these isotypes should demonstrate increased CD40 agonism due to enhanced antigen clustering. However, the only hIgG μtp C575S constructs to demonstrate enhanced agonism were based on the hIgG4 framework. Furthermore, only the hIgG4 μtp C575S/Q355R/W417G was active in driving T cell expansion *in vivo* (Sections 6.5, 6.6). Of particular interest was the FcγR-independent nature of CD40 agonism previously described for ChiLob 7/4 hIgG2 WT mAb [90], which is a characteristic that is highly desirable in therapeutic antibodies. Importantly, these ChiLob 7/4 mAb did not demonstrate any sign of toxicities but were only administered at $\sim$1 mg/kg. Future studies will need to increase the dose and perform repeat dosing to understand the maximum tolerated dose of the antibodies and if any toxicities are associated with μtp C575S constructs.

Of the hIgG4 μtp C575S constructs only those containing Q355R/W417G were active in driving T cell expansion *in vivo* although all of them showed enhanced agonism *in vitro*. The difference between these *in vitro* and *in vivo* mechanisms of CD40 stimulation are currently unknown and require future investigation to understand the importance of Q355R and W417G *in vivo*. The in-solution and on-target hexamerisation of RTX hIgG4 μtp C575S/Q355R/W417G was enhanced compared to RTX hIgG4 μtp C575S, therefore this hexamerisation enhancement could be predicted to be involved in the augmentation of CD40 agonism with ChiLob 7/4 hIgG4 constructs. The low doses selected in the current studies may explain why there was no OTI cell expansion with mice treated with ChiLob 7/4 hIgG4 μtp C575S/W417G. Larger doses may induce OTI expansion and demonstrate that the *in vitro* agonism is transferable *in vivo*, simply indicating that ChiLob 7/4 hIgG4 μtp C575S/W417G is less potent than the ChiLob 7/4 hIgG4 μtp C575S/R355Q/W417G construct *in vivo*.

The augmented agonism with hIgG4 μtp C575S constructs over hIgG1 μtp C575S constructs was a surprising observation. The hIgG1 μtp C575S construct had previously been demonstrated to

possess enhanced hexamerisation propensity which was hypothesised to enable efficient CD40 clustering and subsequent activation, however, no enhancement was observed over the ChiLob 7/4 hIgG1 WT construct. Conversely, the hIgG4 μtp C575S/R355Q/W417G had demonstrated, both, an enhanced hexamerisation propensity and CD40 agonism over its WT counterpart, suggesting that on-target hexamerisation of hIgG4 resulted in efficient CD40 activation. Although the hIgG isotypes are highly homologous, there are known differences in the hinge region between hIgG1 and hIgG4 [80], resulting in differences in the structural conformation and disulphide bond configurations. This alters the flexibility and potentially the antigen binding modalities of each isotype. Due to such differences in the hinge, the antigen binding of hIgG4 has been postulated to be monovalent [500], whereas hIgG1 more readily binds bivalently [198]. One proposed hypothesis for the agonistic enhancement of hIgG4 μtp C575S over hIgG1 μtp C575S on-target hexamers was that hIgG4 constructs bind monovalently, which enhances the process of on-target hexamerisation by enabling efficient Fc:Fc interaction of antigen bound mAb. This hypothesis will need to be investigated further, such as with the use of bispecific hIgG4 antibodies that will only bind monovalently, or with the use of anti-idiotype antibodies to assess the presence of free F(ab) arms following antigen binding.

Overall, the results have clearly indicated that hIgG μtp hexamers are capable of inducing potent CD40 agonism of inactive hIgG isotypes, such as hIgG1 and hIgG4. This represents a potential technology that could be exploited to augment the agonism of previously inert TNFR agonists. However, as has been discussed the use of preformed hIgG μtp hexamers are not necessarily the ideal format for providing *in vivo* agonism. In addition to preformed μtp hexamers, the ChiLob 7/4 hIgG4 μtp C575S/Q355R/W417G on-target hexamer had augmented *in vivo* agonism compared to WT ChiLob 7/4 hIgG4, and provided a potential format that could be utilised to improve TNFR agonists *in vivo*. However, further investigations are required to provide evidence that this technology could be used as a cancer therapy and have wider target applicability, as this thesis has focussed on observing only T cell expansion using a single anti-CD40 mAb. The use of murine models involving haematological or solid tumours treated with these μtp C575S constructs will give an indication of whether these antibodies provide the activity required for tumour control.

Prior to further investigation into *in vivo* tumour models, the impact of the W417G mutant will need to be clarified. Due to time constraints, this thesis did not determine if this mutant is required, and what impact it had on the OTI expansion described here. In addition to the μtp C575S mutants characterised here, the S565T mutation could also be investigated in the context of the ChiLob7/4 hIgG4 μtp C575S construct as an alternative method to enhance the on-target hexamerisation and potentially CD40 agonism of ChiLob 7/4 hIgG4 *in vitro* and *in vivo*. This mutation has been shown to enhance the in-solution and on-target hexamerisation of hIgG1 μtp C575S, and so

could be hypothesised to be useful in the augmentation of CD40 agonism. However, S565T constructs have not been investigated *in vivo*, and so investigations are required to initially understand if these constructs are tolerated and have comparable clearance rates to WT hIgG1.

The current investigation into the application of μtp C575S peptides on anti-CD40 mAb was performed with the agonistic ChiLob 7/4 mAb, a previously characterised V-region with known agonistic activity. There are other characterised anti-CD40 mAb that have demonstrated no agonistic activity, except when in conditions of FcγR cross-linking [334]. In order to provide further evidence of the utility of μtp C575S agonistic mAb in the wider application of immunostimulatory antibodies it would be interesting to introduce V regions of these non-agonistic anti-CD40 antibodies into hIgG4 μtp C575S on-target hexamers and investigate their agonistic activity. In addition, there is also scope for the technology to be applied to other TNFR's that have been proposed as immunostimulatory targets, such as 4-1BB and OX40 [162]. This will provide evidence as to whether or not this augmentation is limited to CD40 targeting antibodies, and provide a proof-of-concept for this technology in future cancer treatments.

In summary, hIgG μtp C575S constructs have been characterised in a variety of *in vitro* and *in vivo* assays for anti-CD20 and anti-CD40 specificity. This study has demonstrated that the use of μtp C575S on-target hexamers can be applied to multiple cellular targets as a platform technology, demonstrating enhanced ability to induce CDC of CD20$^+$ cells and agonise CD40$^+$ cells, which has been suggested to be dependent on hIgG hexamerisation enhancement provided by the μtp C575S peptide (Figure 7.2). Interestingly, the augmentation in these two classes of therapeutic antibodies is reliant on different isotypes, i.e. hIgG1 is most potent for direct targeting antibodies, whereas hIgG4 demonstrated potent immunostimulatory activity. Ultimately, the aim would be to produce a robust technology whereby the μtp C575S peptide and its derivatives could be applied to current and future therapeutic antibodies to provided augmented therapeutic efficacies. Providing more potent treatment options may help to overcome the current lack of response and resistance observed in the treatment of many cancers.

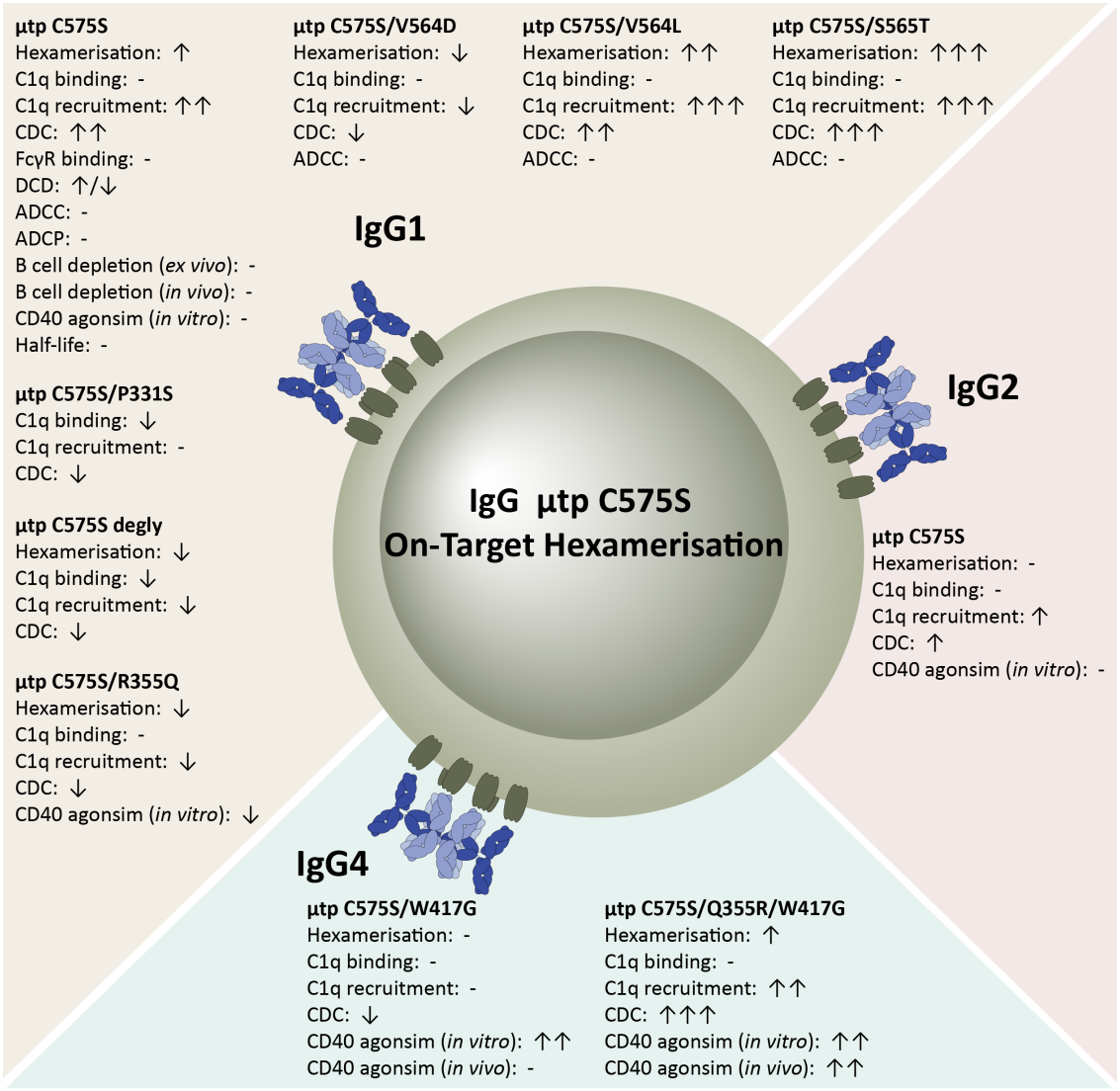

Figure 7.2: Summary of anti-CD20 and anti-CD40 μtp C575S antibodies efficacy *in vitro* and *in vivo*.
Activity of hIgG1, hIgG2, and hIgG4 anti-CD20 and anti-CD40 μtp C575S on-target hexamer antibodies in all assays examined *in vitro* and *in vivo*, as compared with their non-modified counterparts. ↑ indicates an increase in activity, ↓ indicates a decrease in activity, - indicates no observed difference.

Appendix

κ LC

RTVAAPSVFIFPPSDEQLKSGTASVVCLLNNFYPREAKVQWKVDNALQSGNSQESVTEQDSKDSTYSLSSTLTL
SKADYEKHKVYACEVTHQGLSSPVTKSFNRGEC

Figure A1: κ LC amino acid sequence.

(A) hIgG1 HC

ASTKGPSVFPLAPSSKSTSGGTAALGCLVKDYFPEPVTVSWNSGALTSGVHTFPAVLQSSGLYSLSSVVTVPSSS
LGTQTYICNVNHKPSNTKVDKKVEPKSCDKTHTCPPCPAPELLGGPSVFLFPPKPKDTLMISRTPEVTCVVVDV
SHEDPEVKFNWYVDGVEVHNAKTKPREEQYNSTYRVVSVLTVLHQDWLNGKEYKCKVSNKALPAPIEKTISK
AKGQPREPQVYTLPPSRDELTKNQVSLTCLVKGFYPSDIAVEWESNGQPENNYKTTPPVLDSDGSFFLYSKLTV
DKSRWQQGNVFSCSVMHEALHNHYTQKSLSLSPGK

(B) hIgG1 μtp C575S HC

ASTKGPSVFPLAPSSKSTSGGTAALGCLVKDYFPEPVTVSWNSGALTSGVHTFPAVLQSSGLYSLSSVVTVPSSS
LGTQTYICNVNHKPSNTKVDKKVEPKSCDKTHTCPPCPAPELLGGPSVFLFPPKPKDTLMISRTPEVTCVVVDV
SHEDPEVKFNWYVDGVEVHNAKTKPREEQYNSTYRVVSVLTVLHQDWLNGKEYKCKVSNKALPAPIEKTISK
AKGQPREPQVYTLPPSRDELTKNQVSLTCLVKGFYPSDIAVEWESNGQPENNYKTTPPVLDSDGSFFLYSKLTV
DKSRWQQGNVFSCSVMHEALHNHYTQKSLSLSPGKPTLYNVSLVMSDTAGTSY

(C) hIgG1 μtp HC

ASTKGPSVFPLAPSSKSTSGGTAALGCLVKDYFPEPVTVSWNSGALTSGVHTFPAVLQSSGLYSLSSVVTVPSSS
LGTQTYICNVNHKPSNTKVDKKVEPKSCDKTHTCPPCPAPELLGGPSVFLFPPKPKDTLMISRTPEVTCVVVDV
SHEDPEVKFNWYVDGVEVHNAKTKPREEQYNSTYRVVSVLTVLHQDWLNGKEYKCKVSNKALPAPIEKTISK
AKGQPREPQVYTLPPSRDELTKNQVSLTCLVKGFYPSDIAVEWESNGQPENNYKTTPPVLDSDGSFFLYSKLTV
DKSRWQQGNVFSCSVMHEALHNHYTQKSLSLSPGKPTLYNVSLVMSDTAGTCY

Figure A2: hIgG1 HC amino acid sequences.
Amino acid sequences of (A) hIgG1 HC (B) hIgG1 μtp C575S HC and (C) hIgG1 μtp HC

(A) hIgG2 HC

ASTKGPSVFPLAPCSRSTSESTAALGCLVKDYFPEPVTVSWNSGALTSGVHTFPAVLQSSGLYSLSSVVTVPSSN
FGTQTYTCNVDHKPSNTKVDKTVERKCCVECPPCPAPPVAGPSVFLFPPKPKDTLMISRTPEVTCVVVDVSH
EDPEVQFNWYVDGVEVHNAKTKPREEQFNSTFRVVSVLTVVHQDWLNGKEYKCKVSNKGLPAPIEKTISKT
KGQPREPQVYTLPPSREEMTKNQVSLTCLVKGFYPSDISVEWESNGQPENNYKTTPPMLDSDGSFFLYSKLT
VDKSRWQQGNVFSCSVMHEALHNHYTQKSLSLSPGK

(B) hIgG2 μtp C575S HC

ASTKGPSVFPLAPCSRSTSESTAALGCLVKDYFPEPVTVSWNSGALTSGVHTFPAVLQSSGLYSLSSVVTVPSSN
FGTQTYTCNVDHKPSNTKVDKTVERKCCVECPPCPAPPVAGPSVFLFPPKPKDTLMISRTPEVTCVVVDVSH
EDPEVQFNWYVDGVEVHNAKTKPREEQFNSTFRVVSVLTVVHQDWLNGKEYKCKVSNKGLPAPIEKTISKT
KGQPREPQVYTLPPSREEMTKNQVSLTCLVKGFYPSDISVEWESNGQPENNYKTTPPMLDSDGSFFLYSKLT
VDKSRWQQGNVFSCSVMHEALHNHYTQKSLSLSPGKPTLYNVSLVMSDTAGTSY

(C) hIgG2 μtp HC

ASTKGPSVFPLAPCSRSTSESTAALGCLVKDYFPEPVTVSWNSGALTSGVHTFPAVLQSSGLYSLSSVVTVPSSN
FGTQTYTCNVDHKPSNTKVDKTVERKCCVECPPCPAPPVAGPSVFLFPPKPKDTLMISRTPEVTCVVVDVSH
EDPEVQFNWYVDGVEVHNAKTKPREEQFNSTFRVVSVLTVVHQDWLNGKEYKCKVSNKGLPAPIEKTISKT
KGQPREPQVYTLPPSREEMTKNQVSLTCLVKGFYPSDISVEWESNGQPENNYKTTPPMLDSDGSFFLYSKLT
VDKSRWQQGNVFSCSVMHEALHNHYTQKSLSLSPGKPTLYNVSLVMSDTAGTCY

Figure A3: hIgG2 HC amino acid sequences.
Amino acid sequences of (A) hIgG2 HC (B) hIgG2 μtp C575S HC and (C) hIgG2 μtp HC

(A) hIgG4 HC

ASTKGPSVFPLAPCSRSTSESTAALGCLVKDYFPEPVTVSWNSGALTSGVHTFPAVLQSSGLYSLSSVVTVPSSS
LGTKTYTCNVDHKPSNTKVDKRVESKYGPPCPPCPAPEFLGGPSVFLFPPKPKDTLMISRTPEVTCVVVDVSQ
EDPEVQFNWYVDGVEVHNAKTKPREEQFNSTYRVVSVLTVLHQDWLNGKEYKCKVSNKGLPSSIEKTISKAK
GQPREPQVYTLPPSQEEMTKNQVSLTCLVKGFYPSDIAVEWESNGQPENNYKTTPPVLDSDGSFFLYSRLTVD
KSRWQEGNVFSCSVMHEALHNHYTQKSLSLSLGK

(B) hIgG4 μtp C575S HC

ASTKGPSVFPLAPCSRSTSESTAALGCLVKDYFPEPVTVSWNSGALTSGVHTFPAVLQSSGLYSLSSVVTVPSSS
LGTKTYTCNVDHKPSNTKVDKRVESKYGPPCPPCPAPEFLGGPSVFLFPPKPKDTLMISRTPEVTCVVVDVSQ
EDPEVQFNWYVDGVEVHNAKTKPREEQFNSTYRVVSVLTVLHQDWLNGKEYKCKVSNKGLPSSIEKTISKAK
GQPREPQVYTLPPSQEEMTKNQVSLTCLVKGFYPSDIAVEWESNGQPENNYKTTPPVLDSDGSFFLYSRLTVD
KSRWQEGNVFSCSVMHEALHNHYTQKSLSLSLGKPTLYNVSLVMSDTAGTSY

(C) hIgG4 μtp HC

ASTKGPSVFPLAPCSRSTSESTAALGCLVKDYFPEPVTVSWNSGALTSGVHTFPAVLQSSGLYSLSSVVTVPSSS
LGTKTYTCNVDHKPSNTKVDKRVESKYGPPCPPCPAPEFLGGPSVFLFPPKPKDTLMISRTPEVTCVVVDVSQ
EDPEVQFNWYVDGVEVHNAKTKPREEQFNSTYRVVSVLTVLHQDWLNGKEYKCKVSNKGLPSSIEKTISKAK
GQPREPQVYTLPPSQEEMTKNQVSLTCLVKGFYPSDIAVEWESNGQPENNYKTTPPVLDSDGSFFLYSRLTVD
KSRWQEGNVFSCSVMHEALHNHYTQKSLSLSLGKPTLYNVSLVMSDTAGTCY

Figure A4: hIgG4 HC amino acid sequences.
Amino acid sequences of (A) hIgG4 HC (B) hIgG4 μtp C575S HC and (C) hIgG4 μtp HC

Isotype	Format	Mutations	Titre (mg/L)	Volume (L)	Yield (mg)
RTX					
γ1	WT	-	360	0.45	163.9
γ1	WT	P331S	333	0.1	33.3
γ1	μtp	-	220	0.45	99.9
γ1	μtp	P331S	365	0.1	36.5
γ1	μtp	K322A	181	0.1	18.1
γ1	μtp	C575S	41.0	0.45	183.7
γ1	μtp	P331S/C575S	434	0.1	43.4
γ1	μtp	V564D/C575S	471	0.1	47.1
γ1	μtp	V564L/C575S	596	0.1	59.6
γ1	μtp	S565T/C575S	189	0.1	18.9
γ1	μtp	C575S/R355Q	799	0.1	79.9
γ2	WT	-	307	0.1	30.7
γ2	μtp	-	206	0.1	20.6
γ2	μtp	C575S	694	0.1	69.4
γ4	WT	-	741	0.1	74.1
γ4	μtp	-	530	0.1	53.0
γ4	μtp	C575S	437	0.1	43.7
γ4	μtp	C575S/Q355R/W417G	711	0.1	71.1
BHH2					
γ1	WT	-	326	0.45	147.1
γ1	μtp	-	60	0.45	30.8
γ1	μtp	C575S	380	0.45	172.3
Herceptin					
γ1	WT	-	123	0.45	55.5
γ1	μtp	-	220	0.45	97.2
γ1	μtp	C575S	280	0.45	125.1
ChiLOB7/4					
γ1	WT	-	98	0.1	9.8
γ1	μtp	-	250	0.1	25
γ1	μtp	C575S	395	0.1	39.5
γ1	μtp	C575S/R355Q	718	0.1	71.8
γ2	WT	-	218	0.1	21.8
γ2	μtp	-	238	0.1	23.8
γ2	μtp	C575S	185	0.1	18.5
γ4	WT	-	298	0.1	29.8
γ4	μtp	-	172	0.1	17.2
γ4	μtp	C575S/W417G	280	0.1	28.0
γ4	μtp	C575S/Q355R/W417G	446	0.1	44.6
21.4.1 (CP)					
γ2	WT	-	302	0.1	30.2
γ2	μtp	-	60	0.1	6.0
γ2	μtp	C575S	126	0.1	12.6
γ4	WT	-	163	0.1	16.3
γ4	μtp	-	132	0.1	13.2
γ4	μtp	C575S	68	0.1	6.8
1151					
γ1	WT	-	112	0.45	50.6
γ1	μtp	-	80	0.45	36.0
γ1	μtp	C575S	290	0.45	128.7

Table A1: Expressions yields from electroporation of IgG construct plasmids into CHO-SXE cells.
Aproximate yield from representative expression cultures of various constructs calculated by the protein G assay described in Figure 3.3. The elution profile was compared to an IgG standard to calculate titre (mg/L) of IgG present in the culture supernatant. Titre was used to estimate the total yield from the expression volume (Yield (mg) = Titre (mg/L) x Volume (L)).

Isotype	Format	Mutations	MW (kDa)*	Concentration (mg/ml)	Yield (mg)	Purity (%)	Eu/mg
RTX							
γ1	WT	-	145.00	5.2	145.6	100.0	0.35
γ1	WT	P331S	144.98	6.1	17.8	95.5	0.00
γ1	μtp	-	893.04	2.4	22.8	96.7	0.71
γ1	μtp	P331S	892.92	0.7	24.2	93.8	0.00
γ1	μtp	K322A	892.32	1.4	15.4	93.0	0.42
γ1	μtp	C575S	148.80	4.3	129.0	99.7	<1.00
γ1	μtp	P331S/C575S	148.78	2.3	6.8	97.6	1.50
γ1	μtp	V564D/C575S	148.84	3.9	11.8	96.3	0.14
γ1	μtp	V564L/C575S	148.83	6.5	32.5	100.0	0.81
γ1	μtp	S565T/C575S	148.83	2.5	12.5	95.2	0.97
γ1	μtp	C575S/R355Q	148.74	1.2	8.4	95.3	0.08
γ2	WT	-	144.59	0.7	2.8	98.7	0.14
γ2	μtp	-	890.52	0.2	0.6	97.3	0.79
γ2	μtp	C575S	148.39	0.3	1.4	95.8	0.33
γ4	WT	-	144.63	2.2	9.9	99.6	0.45
γ4	μtp	-	890.76	0.4	2.6	99.9	0.75
γ4	μtp	C575S	148.43	2.4	7.2	98.8	0.04
γ4	μtp	C575S/Q355R/W417G	148.49	1.4	9.1	98.7	0.07
BHH2							
γ1	WT	-	146.34	0.9	30.6	100.0	<0.5
γ1	μtp	-	900.96	3.8	38.0	97.4	0.56
γ1	μtp	C575S	150.12	4.3	120.4	100.0	0.21
Herceptin							
γ1	WT	-	145.34	3.5	58.0	99.4	0.29
γ1	μtp	-	895.08	0.9	8.0	97.6	<1.87
γ1	μtp	C575S	149.14	0.5	10.0	100.0	<2.00
ChiLOB7/4							
γ1	WT	-	146.33	0.9	1.4	97.8	0.38
γ1	μtp	-	900.96	1.6	4.5	100.0	0.02
γ1	μtp	C575S	150.13	1.6	14.6	100.0	1.26
γ1	μtp	C575S/R355Q	150.07	2.1	10.5	95.8	0.82
γ2	WT	-	145.92	1.8	5.4	97.7	2.10
γ2	μtp	-	898.50	1.0	2.9	100.0	0.03
γ2	μtp	C575S	149.75	3.0	12.5	100.0	0.24
γ4	WT	-	146.02	5.4	38.0	97.7	1.80
γ4	μtp	-	899.10	0.4	1.0	93.5	0.030
γ4	μtp	C575S/W417G	149.81	2.9	22.6	99.0	1.00
γ4	μtp	C575S/Q355R/W417G	149.88	1.0	5.0	98.2	0.58
21.4.1 (CP)							
γ2	WT	-	154.84	1.5	12.1	100.0	2.50
γ2	μtp	-	953.66	0.5	1.4	96.1	0.04
γ2	μtp	C575S	158.94	3.4	11.5	93.4	0.04
γ4	WT	-	155.24	1.9	15.8	97.0	0.40
γ4	μtp	-	954.26	1.4	3.3	100.0	0.13
γ4	μtp	C575S	159.04	1.1	9.4	100.0	0.50
1151							
γ1	WT	-	144.62	2.9	46.4	99.7	0.02
γ1	μtp	-	890.76	1.7	17.0	95.6	0.87
γ1	μtp	C575S	148.46	2.9	81.2	99.8	0.46

Table A2: Results of purifications from expression supernatants of IgG constructs.
The concentration of purified protein was calculated using a nanodrop. Final yield was calculated based on the volume of mAb. Purity was calculated by analytical SEC. Endotoxin levels (EU/mg) were calculated by LAL assay from Charles River. * = Expected MW

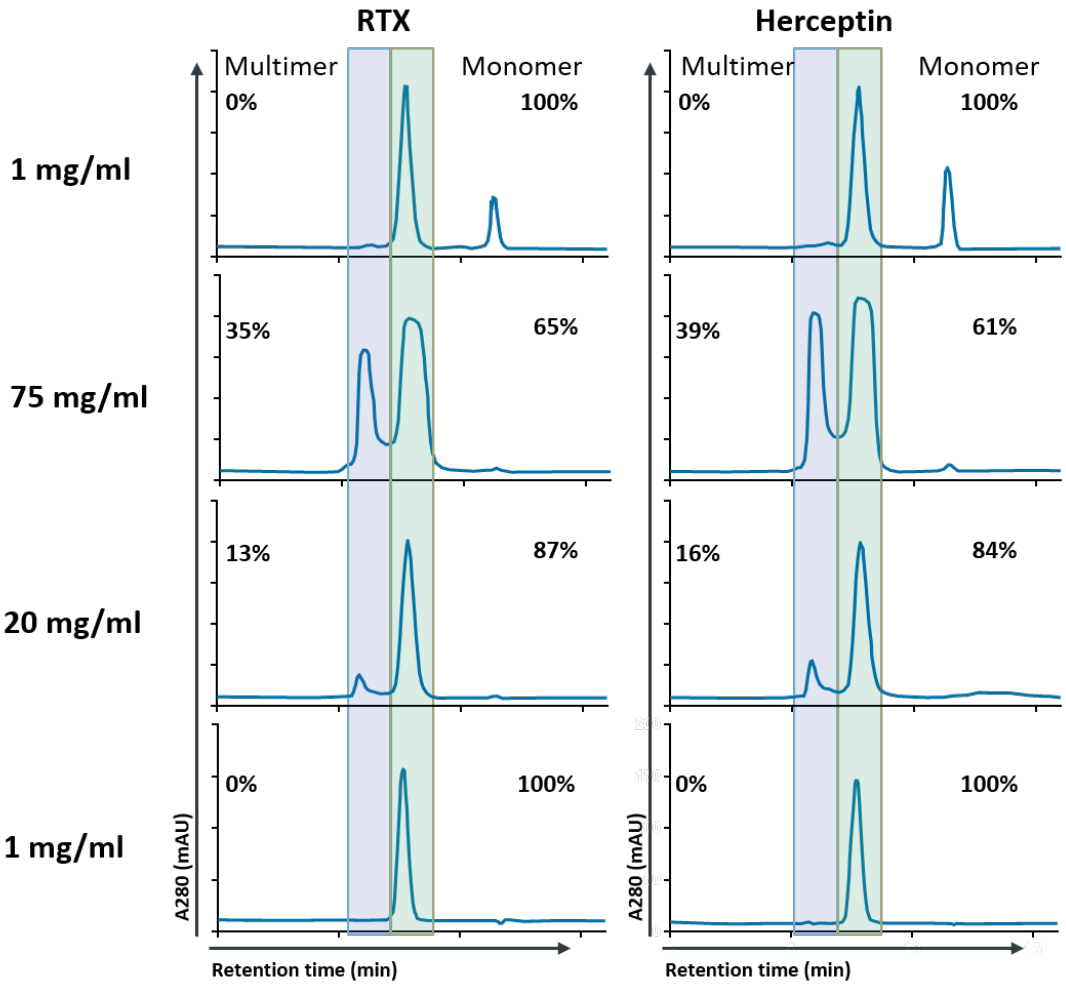

Figure A5: Hexamerisation propensity of RTX and Herceptin hIgG1 μtp C575S mutant construct at increasing concentrations in solution measured by SE-HPLC.
RTX and Herceptin hIgG1 μtp C575S constructs were concentrated to 75 mg/ml and diluted to 20 mg/ml and 1 mg/ml. 50 μg was was analysed by SE-HPLC to determine the percentage of monomeric and multimeric species. Representative SE-HPLC trace's of RTX hIgG1 μtp C575S (left) and Herceptin hIgG1 μtp C575S (right).

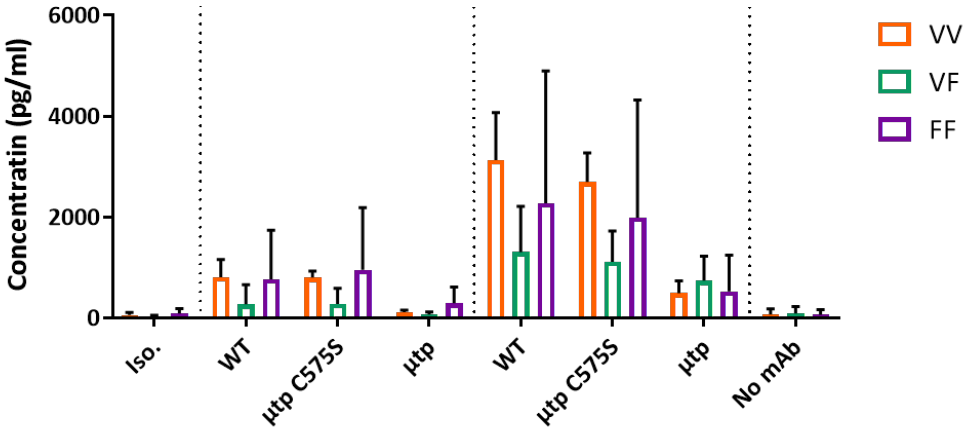

Figure A6: Effect of FcγRIIIa polymorphism Effect of FcγRIIIa polymorphism on whole blood B cell depletion of anti-CD20 hIgG1 µtp fusions.
Fresh peripheral whole blood was incubated with 1 µg/ml isotype control (1151 hIgG1) or anti-CD20 antibody for 24 hours. Plasma was collected by centrifugation and MSD plate used to calculate IFN-γ production (pg/ml). FcγRIIIa phenotypes indicated by colour – VV = red; VF = green; FF = blue. Data plotted showing mean and SD for individual donors treated with RTX antibodies and BHH2 antibodies (N=12).

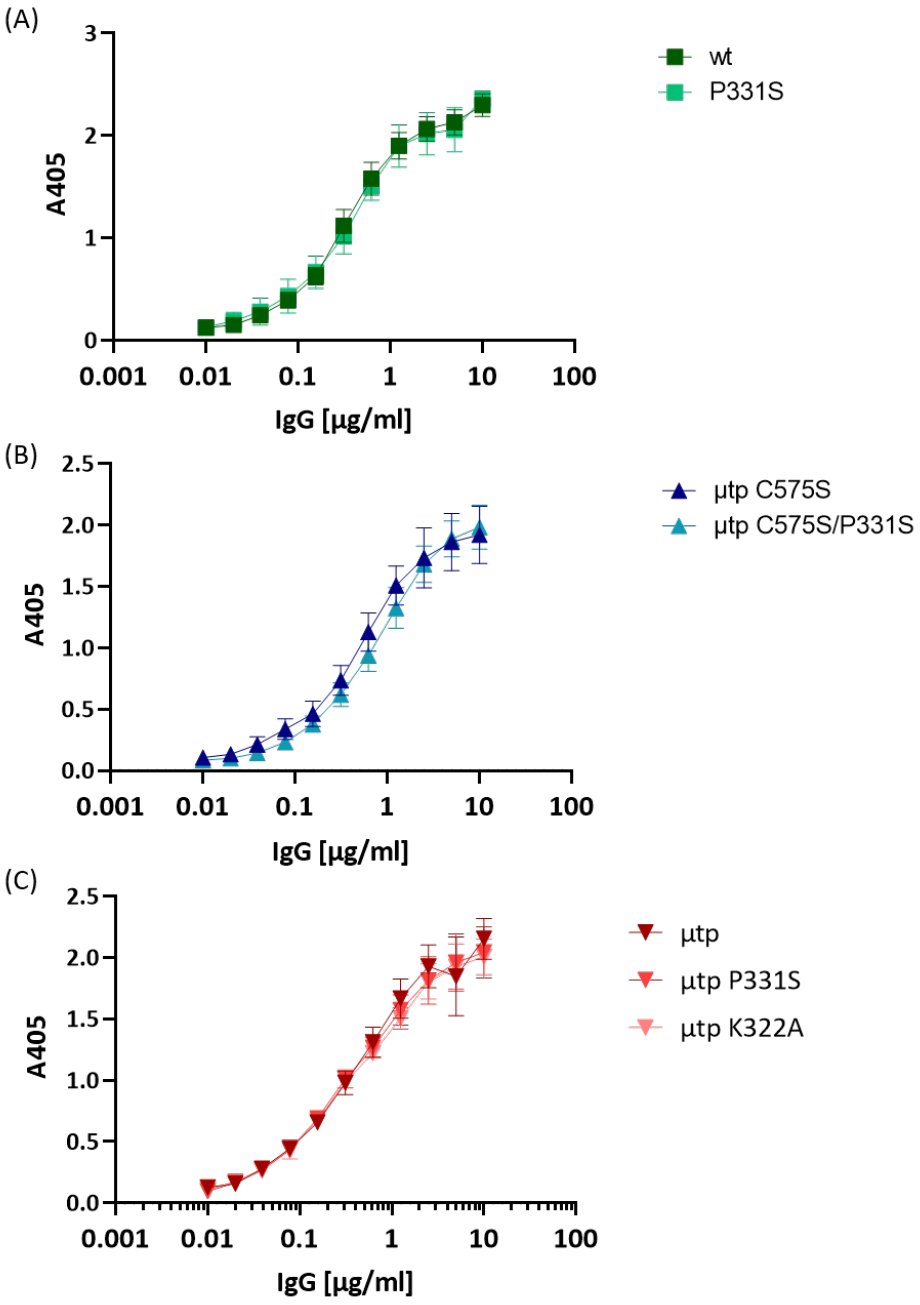

Figure A7: Levels of RTX μtp constructs bound to 96-well plates for side-by-side analysis of C1q binding in an ELISA. ELISA plates were coated with RTX hIgG1 at various concentrations and detected with an HRP-conjugated goat anti-human IgG to confirm similar levels of antibody was bound to the plate compared to the C1q binding plate. Graphs are showing (A) hIgG1 WT (B) hIgG1 μtp C575S and (C) hIgG1 μtp. Data plotted is mean and SEM of duplicate results from independent experiments (N=3).

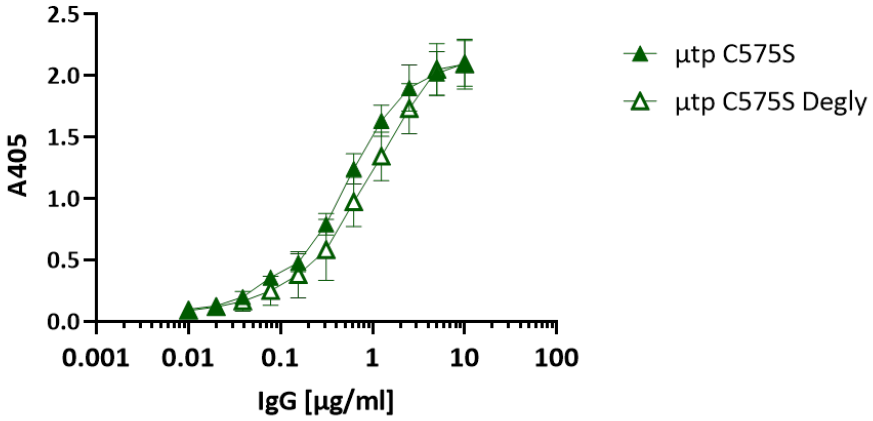

Figure A8: Levels of RTX μtp C575S bound to 96-well plates for side-by-side analysis of C1q binding in an ELISA.
ELISA plates were coated with RTX hIgG1 μtp C575S at various concentrations and detected with an HRP-conjugated goat anti-human IgG to confirm similar levels of antibody was bound to the plate compared to the C1q binding plate. Data plotted is mean and SEM of duplicate results from independent experiments (N=4).

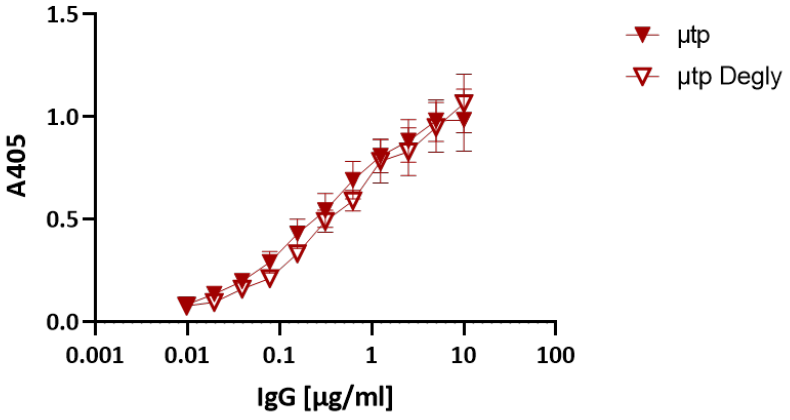

Figure A9: Levels of RTX μtp bound to 96-well plates for side-by-side analysis of C1q binding in an ELISA.
ELISA plates were coated with RTX hIgG1 μtp at various concentrations and detected with an HRP-conjugated goat anti-human IgG to confirm similar levels of antibody was bound to the plate compared to the C1q binding plate. Data plotted is mean and SEM of duplicate results from independent experiments (N=3).

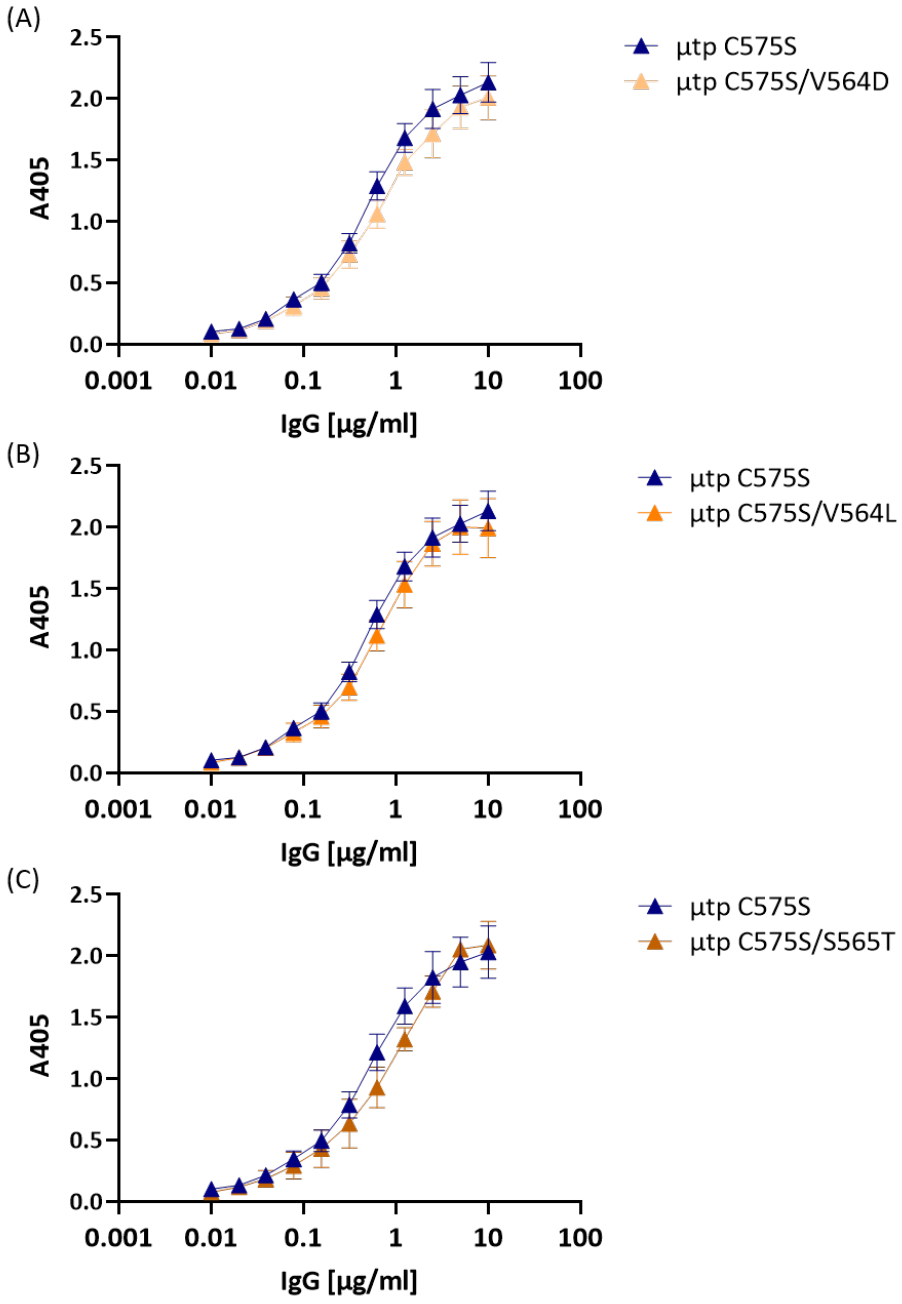

Figure A10: Levels of RTX hIgG1 μtp C575S constructs bound to 96-well plates for side-by-side analysis of C1q binding in an ELISA.

ELISA plates were coated with RTX hIgG1 μtp C575S constructs at various concentrations and detected with an HRP-conjugated goat anti-human IgG to confirm similar levels of antibody was bound to the plate compared to the C1q binding plate. Graphs are showing (A) hIgG1 μtp C575S/V564D (B) hIgG1 μtp C575S/V564L and (C) hIgG1 μtp C575S/S565T. Data plotted is mean and SEM of duplicate results from independent experiments (N=4).

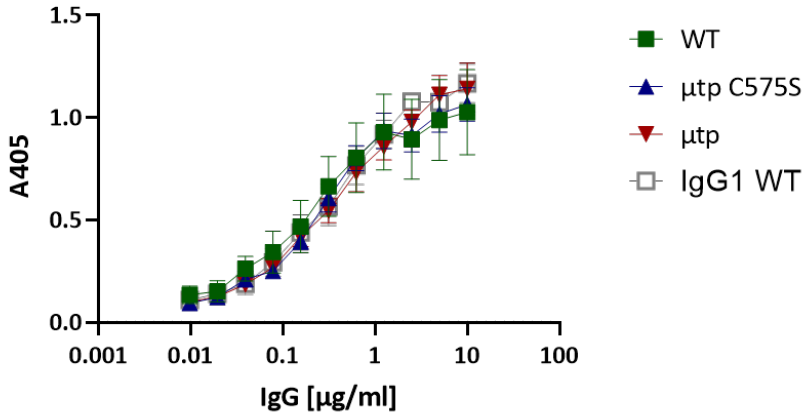

Figure A11: Levels of RTX hIgG2 μtp bound to 96-well plates for side-by-side analysis of C1q binding in an ELISA. ELISA plates were coated with RTX hIgG2 μtp at various concentrations and detected with an HRP-conjugated goat anti-human IgG to confirm similar levels of antibody was bound to the plate compared to the C1q binding plate. Data plotted is mean and SEM of duplicate results from independent experiments (N=6).

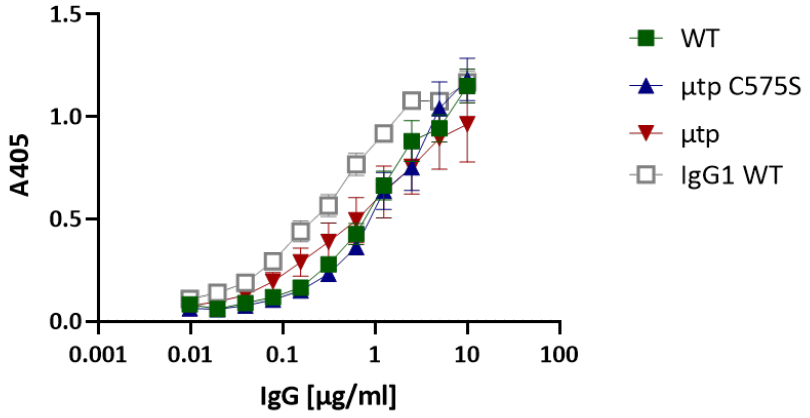

Figure A12: Levels of RTX hIgG2 μtp bound to 96-well plates for side-by-side analysis of C1q binding in an ELISA. ELISA plates were coated with RTX hIgG2 μtp at various concentrations and detected with an HRP-conjugated goat anti-human IgG to confirm similar levels of antibody was bound to the plate compared to the C1q binding plate. Data plotted is mean and SEM of duplicate results from independent experiments (N=6).

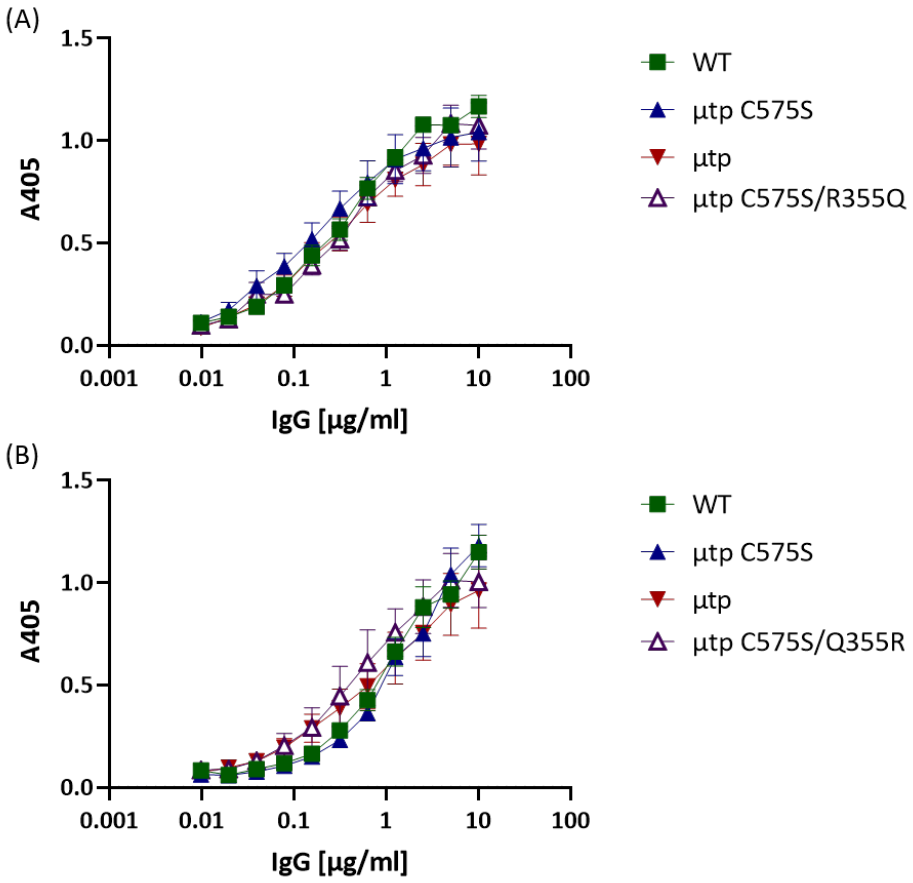

Figure A13: Levels of RTX hIgG μtp bound to 96-well plates for side-by-side analysis of C1q binding in an ELISA. ELISA plates were coated with RTX hIgG μtp at various concentrations and detected with an HRP-conjugated goat anti-human IgG to confirm similar levels of antibody was bound to the plate compared to the C1q binding plate. Graphs are showing (A) hIgG1 constructs and (B) hIgG4 constructs. Data plotted is mean and SEM of duplicate results from independent experiments (N=6).

References

1. Schenten, D. & Medzhitov, R. in *Advances in Immunology* 87–124 (2011).
2. Beutler, B. Innate immunity: an overview. *Molecular immunology* **40,** 845–59 (2004).
3. Janeway, C., Travers, P. & Walport, M. *Janeway's Immunobiology. Ninth Edition* (2018).
4. Kumar, H., Kawai, T. & Akira, S. Pathogen recognition by the innate immune system. *International Reviews of Immunology* **30,** 16–34 (2011).
5. Kawai, T. & Akira, S. The role of pattern-recognition receptors in innate immunity: Update on toll-like receptors. *Nature Immunology* **11,** 373–384 (2010).
6. Merle, N. S., Church, S. E., Fremeaux-Bacchi, V. & Roumenina, L. T. Complement System Part I – Molecular Mechanisms of Activation and Regulation. *Front Immunol* **6,** 262 (2015).
7. Amulic, B. *et al.* Neutrophil Function: From Mechanisms to Disease. *Annual Review of Immunology* **30,** 459–489 (2012).
8. Pruchniak, M. P., Arazna, M. & Demkow, U. Life of neutrophil: From stem cell to neutrophil extracellular trap. *Respiratory Physiology and Neurobiology* **187,** 68–73 (2013).
9. Jakubzick, C. V., Randolph, G. J. & Henson, P. M. Monocyte differentiation and antigen-presenting functions. *Nature Reviews Immunology* **17,** 349–362 (2017).
10. Auffray, C., Sieweke, M. H. & Geissmann, F. Blood Monocytes: Development, Heterogeneity, and Relationship with Dendritic Cells. *Annual Review of Immunology* **27,** 669–692 (2009).
11. Boltjes, A. & van Wijk, F. Human dendritic cell functional specialization in steady-state and inflammation. *Frontiers in Immunology* **5,** 131 (2014).
12. Joffre, O. P., Segura, E., Savina, A. & Amigorena, S. Cross-presentation by dendritic cells. *Nature Reviews Immunology* **12,** 557–569 (2012).
13. Roche, P. A. & Furuta, K. The ins and outs of MHC class II-mediated antigen processing and presentation. *Nature Reviews Immunology* **15,** 203–216 (2015).
14. Thielens, A., Vivier, E. & Romagné, F. NK cell MHC class I specific receptors (KIR): From biology to clinical intervention. *Current Opinion in Immunology* **24,** 239–245 (2012).
15. Saunders, P. M. *et al.* A bird's eye view of NK cell receptor interactions with their MHC class I ligands. *Immunological Reviews* **267,** 148–166 (2015).
16. Kärre, K., Ljunggren, H. G., Piontek, G. & Kiessling, R. Selective rejection of H-2-deficient lymphoma variants suggests alternative immune defence strategy. *Nature* **319,** 675–678 (1986).
17. Smyth, M. J. *et al.* Activation of NK cell cytotoxicity. eng. *Mol Immunol* **42,** 501–510 (2005).
18. Noris, M. & Remuzzi, G. Overview of complement activation and regulation. *Seminars in Nephrology* **33,** 479–492 (2013).
19. Chinen, J., Fleisher, T. A. & Shearer, W. T. in *Middleton's Allergy: Principles and Practice: Eighth Edition* 2 Suppl 2, 20–29 (2013).
20. Sprent, J. T and B memory cells. *Cell* **76,** 315–322 (1994).
21. Van Der Merwe, P. A. & Dushek, O. Mechanisms for T cell receptor triggering. *Nature Reviews Immunology* **11,** 47–55 (2011).

22. Weiss, A. & Littman, D. R. Signal transduction by lymphocyte antigen receptors. *Cell* **76,** 263–274 (1994).

23. Wagner, D. H. Re-shaping the T cell repertoire: TCR editing and TCR revision for good and for bad. *Clinical Immunology* **123,** 1–6 (2007).

24. Attaf, M., Legut, M., Cole, D. K. & Sewell, A. K. The T cell antigen receptor: The Swiss army knife of the immune system. *Clinical and Experimental Immunology* **181,** 1–18 (2015).

25. Starr, T. K., Jameson, S. C. & Hogquist, K. A. Positive and negative selection of T cells. *Annual review of immunology* **21,** 139–76 (2003).

26. Sebzda, E. *et al.* Selection of the T cell Repertoire. *Annual Review of Immunology* **17,** 829–874 (1999).

27. Malissen, B. & Bongrand, P. Early T Cell Activation: Integrating Biochemical, Structural, and Biophysical Cues. *Annual Review of Immunology* **33,** 539–561 (2015).

28. Van Panhuys, N. TCR signal strength alters T-DC activation and interaction times and directs the outcome of differentiation. *Frontiers in Immunology* **7** (2016).

29. Sanchez-Paulete, A. R. *et al.* Deciphering CD137 (4-1BB) signaling in T-cell costimulation for translation into successful cancer immunotherapy. *European Journal of Immunology* **46,** 513–522 (2016).

30. Willoughby, J., Griffiths, J., Tews, I. & Cragg, M. S. OX40: Structure and function – What questions remain? *Molecular Immunology* **83,** 13–22 (2017).

31. Chen, L. & Flies, D. B. Molecular mechanisms of T cell co-stimulation and co-inhibition. *Nature Reviews Immunology* **13,** 227–242 (2013).

32. Zhu, J., Yamane, H. & Paul, W. E. Differentiation of Effector CD4 T Cell Populations. *Annual Review of Immunology* **28,** 445–489 (2010).

33. Mittrücker, H. W., Visekruna, A. & Huber, M. Heterogeneity in the Differentiation and Function of CD8+ T Cells. *Archivum Immunologiae et Therapiae Experimentalis* **62,** 449–458 (2014).

34. Mougiakakos, D. in *Innate Immune Regulation and Cancer Immunotherapy* 147–173 (2010).

35. Chang, J. T., Wherry, E. J. & Goldrath, A. W. Molecular regulation of effector and memory T cell differentiation. *Nature Immunology* **15,** 1104–1115 (2014).

36. Dal Porto, J. M. *et al.* B cell antigen receptor signaling 101. *Molecular Immunology* **41,** 599–613 (2004).

37. Ghia, P., Ten Boekel, E., Rolink, A. G. & Melchers, F. B-cell development: A comparison between mouse and man. *Immunology Today* **19,** 480–485 (1998).

38. Pieper, K., Grimbacher, B. & Eibel, H. B-cell biology and development. *The Journal of allergy and clinical immunology* (2013).

39. Jung, D., Giallourakis, C., Mostoslavsky, R. & Alt, F. W. Mechanism and Control of V(D)J Recombination at the Immunoglobulin Heavy Chain Locus. *Annual Review of Immunology* **24,** 541–570 (2006).

40. Combriato, G. & Klobeck, H. Vλ and Jλ-Cλ gene segments of the human immunoglobulin λ light chain locus are separated by 14 kb and rearrange by a deletion mechanism. *European Journal of Immunology* **21,** 1513–1522 (1991).

41. Gatto, D. & Brink, R. The germinal center reaction. *Journal of Allergy and Clinical Immunology* **126,** 898–907 (2010).

42. Eibel, H. *et al.* B cell biology: An overview topical collection on basic and applied science. *Current Allergy and Asthma Reports* **14,** 434 (2014).

43. Muramatsu, M. *et al.* Class switch recombination and hypermutation require activation-induced cytidine deaminase (AID), a potential RNA editing enzyme. *Cell* **102,** 553–563 (2000).

44. Berek, C., Berger, A. & Apel, M. Maturation of the immune response in germinal centers. *Cell* **67,** 1121–1129 (1991).

45. Küppers, R., Zhao, M., Hansmann, M. L. & Rajewsky, K. Tracing B cell development in human germinal centres by molecular analysis of single cells picked from histological sections. *The EMBO journal* **12,** 4955–67 (1993).

46. Stavnezer, J., Guikema, J. E. & Schrader, C. E. Mechanism and Regulation of Class Switch Recombination. *Annual Review of Immunology* **26,** 261–292 (2008).

47. Weisel, F. & Shlomchik, M. Memory B Cells of Mice and Humans. *Annual Review of Immunology* **35,** 255–284 (2017).

48. Reynaud, C. A. & Weill, J. C. in *Encyclopedia of Immunobiology* 3, 195–199 (2016).

49. Nagasawa, T. Microenvironmental niches in the bone marrow required for B-cell development. *Nature Reviews Immunology* **6,** 107–116 (2006).

50. Kindt, T., Osborne, B. & Goldsby, R. *Kuby Immunology* 6th ed. (W. H. Freeman & Company, 2006).

51. Szmuness, W. *et al.* Hepatitis B vaccine: demonstration of efficacy in a controlled clinical trial in a high-risk population in the United States. *The New England journal of medicine* **303,** 833–841 (1980).

52. Irani, V. *et al.* Molecular properties of human IgG subclasses and their implications for designing therapeutic monoclonal antibodies against infectious diseases. *Molecular Immunology* **67,** 171–182 (2015).

53. Hauptrock, B. & Hess, G. Rituximab in the treatment of non-Hodgkin's lymphoma. *Biologics : targets & therapy* **2,** 619–33 (2008).

54. Mok, C. C. Rituximab for the treatment of rheumatoid arthritis: An update. *Drug Design, Development and Therapy* **8,** 87–100 (2013).

55. Porter, R. R. The hydrolysis of rabbit γ-globulin and antibodies with crystalline papain. *Biochemical Journal* **73,** 119–127 (1959).

56. Madsen, L. H. & Rodkey, L. S. A method for preparing IgG F(ab')2 fragments using small amounts of serum. *Journal of immunological methods* **9,** 355–61 (1976).

57. Kerr, M. A. The structure and function of human IgA. *Human cell official journal of Human Cell Research Society* **271,** 285–296 (1990).

58. Mestecky, J. *et al.* Site of J chain attachment of human polymeric IgA. *Proceedings of the National Academy of Sciences of the United States of America* **71,** 544–548 (1974).

59. Yoo, E. M. *et al.* Structural requirements for polymeric immunoglobulin assembly and association with J chain. *Journal of Biological Chemistry* **274,** 33771–33777 (1999).

60. Brandtzaeg, P. & Prydz, H. Direct evidence for an integrated function of J chain and secretory component in epithelial transport of immunoglobulins. *Nature* **311,** 71–73 (1984).

61. Mattu, T. S. *et al.* The glycosylation and structure of human serum IgA1, Fab, and Fc regions and the role of N-glycosylation on FcaR receptor interactions. *Journal of Biological Chemistry* **273,** 2260–2272 (1998).

62. Brezski, R. J. & Georgiou, G. Immunoglobulin isotype knowledge and application to Fc engineering. *Current opinion in immunology* **40,** 62–69 (2016).

63. Putnam, F. W. *et al.* Complete amino acid sequence of the Mu heavy chain of a human IgM immunoglobulin. *Science (New York, N.Y.)* **182,** 287–91 (1973).

64. Kehry, M. *et al.* Amino acid sequence of a mouse immunoglobulin μ chain. *Proceedings of the National Academy of Sciences of the United States of America* **76,** 2932–2936 (1979).

65. Chapman, A. & Kornfeld, R. Structure of the high mannose oligosaccharides of a human IgM myeloma protein. II. The minor oligosaccharides of high mannose glycopeptide. *J. Biol. Chem.* **254,** 824–828 (1979).

66. Chapman, A. & Kornfeld, R. Structure of the high mannose oligosaccharides of a human IgM myeloma Structure Myeloma of the High Protein of a Human IgM. *The Journal of biological chemistry* (1979).

67. Mestecky, J. & Schrohenloher, R. E. Site of attachment of J chain to human immunoglobulin M. *Nature* **249,** 650–2 (1974).

68. Wiersma, E. J. *et al.* Analysis of IgM structures involved in J chain incorporation. *Journal of Immunology* **158,** 1719–1726 (1997).

69. Davis, A. C., Roux, K. H., Pursey, J. & Shulman, M. J. Intermolecular disulfide bonding in IgM: effects of replacing cysteine residues in the mu heavy chain. *The EMBO journal* **8,** 2519–26 (1989).

70. Johansen, Braathen & Brandtzaeg. Role of J chain in secretory immunoglobulin formation. *Scandinavian Journal of Immunology* **52,** 240–248 (2000).

71. Geisberger, R., Crameri, R. & Achatz, G. Models of signal transduction through the B-cell antigen receptor. *Immunology* **110,** 401–410 (2003).

72. Gould, H. J. *et al.* The biology of IGE and the basis of allergic disease. *Annual review of immunology* **21,** 579–628 (2003).

73. Sutton, B. J. & Gould, H. J. The human IgE network. *Nature* **366,** 421–8 (1993).

74. Gounni, A. S. *et al.* High-affinity IgE receptor on eosinophils is involved in defence against parasites. *Nature* **367,** 183–6 (1994).

75. Chaturvedi, A., Siddiqui, Z., Bayiroglu, F. & Rao, K. V. S. A GPI-linked isoform of the IgD receptor regulates resting B cell activation. *Nature immunology* **3,** 951–957 (2002).

76. Sun, Z. *et al.* Semi-extended solution structure of human myeloma immunoglobulin D determined by constrained X-ray scattering. *Journal of Molecular Biology* **353,** 155–173 (2005).

77. Übelhart, R. *et al.* Responsiveness of B cells is regulated by the hinge region of IgD. *Nature immunology* **16,** 534–43 (2015).

78. Riesbeck, K. & Nordstrom, T. Structure and immunological action of the human pathogen Moraxella catarrhalis IgD-binding protein. *Critical reviews in immunology* **26,** 353–76 (2006).

79. Pan, Q. & Hammarström, L. Molecular basis of IgG subclass deficiency. *Immunological reviews* **178,** 99–110 (2000).

80. Vidarsson, G., Dekkers, G. & Rispens, T. IgG Subclasses and Allotypes: From Structure to Effector Functions. *Frontiers in Immunology* **5,** 520 (2014).

81. Israel, E. J. *et al.* Expression of the neonatal Fc receptor, FcRn, on human intestinal epithelial cells. *Immunology* **92,** 69–74 (1997).

82. Pincetic, A. *et al.* Type I and type II Fc receptors regulate innate and adaptive immunity. *Nature immunology* **15,** 707–16 (2014).

83. Temming, A. R. *et al.* Human DC-SIGN and CD23 do not interact with human IgG. *Scientific Reports* **9** (2019).

84. Bruhns, P. *et al.* Specificity and affinity of human Fcγ receptors and their polymorphic variants for human IgG subclasses. *Blood* **113,** 3716–3725 (2009).

85. Morell, A., Terry, W. D. & Waldmann, T. A. Metabolic properties of IgG subclasses in man. *Journal of Clinical Investigation* **49,** 673–680 (1970).

86. Stapleton, N. M. *et al.* Competition for FcRn-mediated transport gives rise to short half-life of human IgG3 and offers therapeutic potential. *Nature communications* **2,** 599 (2011).

87. Barrett, D. J. & Ayoub, E. M. IgG2 subclass restriction of antibody to pneumococcal polysaccharides. *Clinical and experimental immunology* **63,** 127–34 (1986).

88. Wypych, J. *et al.* Human IgG2 antibodies display disulfide-mediated structural isoforms. *Journal of Biological Chemistry* **283,** 16194–16205 (2008).

89. Dillon, T. M. *et al.* Structural and functional characterization of disulfide isoforms of the human IgG2 subclass. *Journal of Biological Chemistry* **283,** 16206–16215 (2008).

90. White, A. L. *et al.* Conformation of the human immunoglobulin G2 hinge imparts superagonistic properties to immunostimulatory anticancer antibodies. *Cancer cell* **27,** 138–48 (2015).

91. Aalberse, R. C., van der Gaag, R. & van Leeuwen, J. Serologic aspects of IgG4 antibodies. I. Prolonged immunization results in an IgG4-restricted response. *Journal of immunology (Baltimore, Md. : 1950)* **130,** 722–726 (1983).

92. van der Neut Kolfschoten, M. *et al.* Anti-inflammatory activity of human IgG4 antibodies by dynamic Fab arm exchange. *Science (New York, N.Y.)* **317,** 1554–7 (2007).

93. Labrijn, A. F. *et al.* Species-Specific Determinants in the IgG CH3 Domain Enable Fab-Arm Exchange by Affecting the Noncovalent CH3-CH3 Interaction Strength. *Journal of immunology (Baltimore, Md. : 1950)* **187,** 3238–3246 (2011).

94. Rispens, T. *et al.* Dynamics of inter-heavy chain interactions in human immunoglobulin G (IgG) subclasses studied by kinetic fab arm exchange. *Journal of Biological Chemistry* **289,** 6098–6109 (2014).

95. Schuurman, J., Perdok, G. J., Gorter, A. D. & Aalberse, R. C. The inter-heavy chain disulfide bonds of IgG4 are in equilibrium with intra-chain disulfide bonds. *Molecular Immunology* **38,** 1–8 (2001).

96. Darnell, J. *et al. Molecular Cell Biology* 4th ed. (W. H. Freeman, 2000).

97. Rothman, J. E. & Lodish, H. F. Synchronised transmembrane insertion and glycosylation of a nascent membrane protein. *Nature* **269,** 775–780 (1977).

98. Chen, W., Helenius, J., Braakman, I. & Helenius, A. Cotranslational folding and calnexin binding during glycoprotein synthesis. *Proceedings of the National Academy of Sciences of the United States of America* **92,** 6229–33 (1995).

99. Bieberich, E. Synthesis, Processing, and Function of N-glycans in N-glycoproteins. *Advances in neurobiology* **9,** 47–70 (2014).

100. Arnold, J. N. *et al.* The impact of glycosylation on the biological function and structure of human immunoglobulins. *Annual review of immunology* **25,** 21–50 (2007).

101. Van de Bovenkamp, F. S., Hafkenscheid, L., Rispens, T. & Rombouts, Y. The Emerging Importance of IgG Fab Glycosylation in Immunity. *Journal of immunology (Baltimore, Md. : 1950)* **196,** 1435–41 (2016).

102. Mimura, Y. *et al.* The influence of glycosylation on the thermal stability and effector function expression of human IgG1-Fc: Properties of a series of truncated glycoforms. *Molecular Immunology* **37,** 697–706 (2001).

103. Nimmerjahn, F. & Ravetch, J. V. Fcgamma receptors as regulators of immune responses. *Nature Reviews Immunology* **8,** 34–47 (2008).

104. Van den Herik-Oudijk, I. E., Capel, P. J., van der Bruggen, T. & Van de Winkel, J. G. Identification of signaling motifs within human Fc gamma RIIa and Fc gamma RIIb isoforms. *Blood* **85,** 2202–11 (1995).

105. Wirthmueller, U., Kurosaki, T., Murakami, M. S. & Ravetch, J. V. Signal transduction by Fc gamma RIII (CD16) is mediated through the gamma chain. *The Journal of experimental medicine* **175,** 1381–90 (1992).

106. Van Vugt, M. J. *et al.* FcR gamma-chain is essential for both surface expression and function of human Fc gamma RI (CD64) in vivo. *Blood* **87,** 3593–9 (1996).

107. Scallon, B. J. *et al.* A human immunoglobulin G receptor exists in both polypeptide-anchored and phosphatidylinositol-glycan-anchored forms. *Proceedings of the National Academy of Sciences of the United States of America* **86,** 5079–83 (1989).

108. Simmons, D. & Seed, B. The Fcgamma receptor of natural killer cells is a phospholipid-linked membrane protein. *Nature* **336,** 568–570 (1988).

109. Nimmerjahn, F. & Ravetch, J. V. Divergent immunoglobulin g subclass activity through selective Fc receptor binding. *Science (New York, N.Y.)* **310,** 1510–2 (2005).

110. Nimmerjahn, F., Gordan, S. & Lux, A. Fcgamma R dependent mechanisms of cytotoxic, agonistic, and neutralizing antibody activities. *Trends in Immunology* **36,** 325–336 (2015).

111. Yuasa, T. *et al.* Deletion of fcgamma receptor IIB renders H-2(b) mice susceptible to collagen-induced arthritis. *The Journal of experimental medicine* **189,** 187–94 (1999).

112. Bruhns, P. & Jönsson, F. Mouse and human FcR effector functions. *Immunological Reviews* **268,** 25–51 (2015).

113. Kiyoshi, M. *et al.* Structural basis for binding of human IgG1 to its high-affinity human receptor FcγRI. *Nature Communications* **6,** 6866 (2015).

114. Lu, J. & Sun, P. D. Structural mechanism of high affinity FcγRI recognition of immunoglobulin G. *Immunological Reviews* **268,** 192–200 (2015).

115. Van der Poel, C. E., Spaapen, R. M., van de Winkel, J. G. J. & Leusen, J. H. W. Functional Characteristics of the High Affinity IgG Receptor, Fc RI. *The Journal of Immunology* **186,** 2699–2704 (2011).

116. Mancardi, D. A. *et al.* The high-affinity human IgG receptor FcγRI (CD64) promotes IgG-mediated inflammation, anaphylaxis, and antitumor immunotherapy. *Blood* **121,** 1563–1573 (2013).

117. Van Der Poel, C. E. *et al.* Cytokine-induced immune complex binding to the high-affinity IgG receptor, FcγRI, in the presence of monomeric IgG. *Blood* **116,** 5327–5333 (2010).

118. Clark, M. R. *et al.* Molecular basis for a polymorphism involving Fc receptor II on human monocytes. *Journal of immunology (Baltimore, Md. : 1950)* **143,** 1731–4 (1989).

119. Warmerdam, P. A. *et al.* A single amino acid in the second Ig-like domain of the human Fc gamma receptor II is critical for human IgG2 binding. *Journal of immunology (Baltimore, Md. : 1950)* **147,** 1338–43 (1991).

120. Powell, M. S. *et al.* Alteration of the FcγRIIa Dimer Interface Affects Receptor Signaling but Not Ligand Binding. *The Journal of Immunology* **176,** 7489–7494 (2006).

121. Richards, J. O. *et al.* Optimization of antibody binding to FcgammaRIIa enhances macrophage phagocytosis of tumor cells. *Molecular Cancer Therapeutics* **7,** 2517–2527 (2008).

122. Phillips, N. E. & Parker, D. C. Fc-dependent inhibition of mouse B cell activation by whole anti-mu antibodies. *J Immunol* **130,** 602–606 (1983).

123. Qin, D. *et al.* Fcγ Receptor IIB on Follicular Dendritic Cells Regulates the B Cell Recall Response. *The Journal of Immunology* **164,** 6268–6275 (2000).

124. Van der Heijden, J. *et al.* Phenotypic Variation in IgG Receptors by Nonclassical FCGR2C Alleles. *The Journal of Immunology* **188,** 1318–1324 (2012).

125. Metes, D. *et al.* Expression of functional CD32 molecules on human NK cells is determined by an allelic polymorphism of the FcgammaRIIC gene. *Blood* **91,** 2369–80 (1998).

126. Breunis, W. B. *et al.* Copy number variation at the FCGR locus includes FCGR3A, FCGR2C and FCGR3B but not FCGR2A and FCGR2B. *Human Mutation* **30,** E640–E650 (2009).

127. Su, K. *et al.* Genomic organization of classical human low-affinity Fcgamma receptor genes. *Genes and immunity* **3 Suppl 1,** S51–6 (2002).

128. Ernst, L. K., Metes, D., Herberman, R. B. & Morel, P. A. Allelic polymorphisms in the FcγRIIC gene can influence its function on normal human natural killer cells. *Journal of Molecular Medicine* **80,** 248–257 (2002).

129. Ravetch, J. V. & Perussia, B. Alternative membrane forms of Fc gamma RIII(CD16) on human natural killer cells and neutrophils. Cell type-specific expression of two genes that differ in single nucleotide substitutions. *The Journal of experimental medicine* **170,** 481–97 (1989).

130. Koene, H. R. *et al.* Fc gammaRIIIa-158V/F polymorphism influences the binding of IgG by natural killer cell Fc gammaRIIIa, independently of the Fc gammaRIIIa-48L/R/H phenotype. *Blood* **90,** 1109–14 (1997).

131. Cartron, G. *et al.* Therapeutic activity of humanized anti-CD20 monoclonal antibody and polymorphism in IgG Fc receptor FcgammaRIIIa gene. *Blood* **99,** 754–758 (2002).

132. Teeling, J. L. *et al.* Characterization of new human CD20 monoclonal antibodies with potent cytolytic activity against non-Hodgkin lymphomas. *Blood* **104,** 1793–1800 (2004).

133. Park, J. G., Isaacs, R. E., Chien, P. & Schreiber, A. D. In the absence of other Fc receptors, FcγRIIIA transmits a phagocytic signal that requires the cytoplasmic domain of its γ subunit. *Journal of Clinical Investigation* **92,** 1967–1973 (1993).

134. Golay, J., Leidi, M., Palumbo, G. A. & Introna, M. Human Macrophages Phagocytose Rituximab Opsonised Leukemic Cells Via CD16, CD32 and CD64 but Do Not Mediate ADCC. *Blood* **108,** 2507–2507 (2006).

135. Meknache, N. *et al.* Human basophils express the glycosylphosphatidylinositol-anchored low-affinity IgG receptor FcgammaRIIIB (CD16B). *Journal of immunology (Baltimore, Md. : 1950)* **182,** 2542–50 (2009).

136. Zhu, X. *et al.* Intracellular expression of Fc gamma RIII (CD16) and its mobilization by chemoattractants in human eosinophils. *Journal of immunology (Baltimore, Md. : 1950)* **161,** 2574–2579 (1998).

137. Ory, P. A. *et al.* Sequences of complementary DNAs that encode the NA1 and NA2 forms of Fc receptor III on human neutrophils. *Journal of Clinical Investigation* **84,** 1688–1691 (1989).

138. Salmon, J. E., Edberg, J. C. & Kimberly, R. P. Fc gamma receptor III on human neutrophils. Allelic variants have functionally distinct capacities. *Journal of Clinical Investigation* **85,** 1287–1295 (1990).

139. Golay, J. *et al.* Glycoengineered CD20 antibody obinutuzumab activates neutrophils and mediates phagocytosis through CD16B more efficiently than rituximab. *Blood* **122,** 3482–3491 (2013).

140. Stöckl, J. *et al.* Granulocyte activation via a binding site near the C-terminal region of complement receptor type 3 alpha-chain (CD11b) potentially involved in intramembrane complex formation with glycosylphosphatidylinositol-anchored Fc gamma RIIIB (CD16) molecules. *Journal of immunology (Baltimore, Md. : 1950)* **154,** 5452–63 (1995).

141. Yang, H. *et al.* Neutrophil CD16b crosslinking induces lipid raft-mediated activation of SHP-2 and affects cytokine expression and retarded neutrophil apoptosis. *Experimental Cell Research* **362,** 121–131 (2018).

142. Tsuboi, N., Asano, K., Lauterbach, M. & Mayadas, T. N. Human Neutrophil Fcγ Receptors Initiate and Play Specialized Nonredundant Roles in Antibody-Mediated Inflammatory Diseases. *Immunity* **28,** 833–846 (2008).

143. Treffers, L. W. *et al.* FcγRIIIb restricts antibody-dependent destruction of cancer cells by human neutrophils. *Frontiers in Immunology* **10** (2019).

144. Simister, N. E. & Rees, A. R. Isolation and characterization of an Fc receptor from neonatal rat small intestine. *European Journal of Immunology* **15,** 733–738 (1985).

145. Zhu, X. *et al.* MHC class I-related neonatal Fc receptor for IgG is functionally expressed in monocytes, intestinal macrophages, and dendritic cells. *Journal of immunology (Baltimore, Md. : 1950)* **166,** 3266–76 (2001).

146. Vidarsson, G. *et al.* FcRn: An IgG receptor on phagocytes with a novel role in phagocytosis. *Blood* **108,** 3573–3579 (2006).

147. Simister, N. E. & Mostov, K. E. An Fc receptor structurally related to MHC class I antigens. *Nature* **337,** 184–187 (1989).

148. Kim, J. K. *et al.* Mapping the site on human IgG for binding of the MHC class I-related receptor, FcRn. *European journal of immunology* **29,** 2819–25 (1999).

149. Sigounas, G., Harindranath, N., Donadel, G. & Notkins, A. L. Half-life of polyreactive antibodies. *Journal of Clinical Immunology* **14,** 134–140 (1994).

150. Firan, M. *et al.* The MHC class I-related receptor, FcRn, plays an essential role in the maternofetal transfer of gamma-globulin in humans. *International immunology* **13,** 993–1002 (2001).

151. Lencer, W. I. & Blumberg, R. S. A passionate kiss, then run: exocytosis and recycling of IgG by FcRn. *Trends in Cell Biology* **15,** 5–9 (2005).

152. Israel, E. J. *et al.* Increased clearance of IgG in mice that lack beta 2-microglobulin: possible protective role of FcRn. *Immunology* **89,** 573–578 (1996).

153. Yoshida, M. *et al.* Human neonatal Fc receptor mediates transport of IgG into luminal secretions for delivery of antigens to mucosal dendritic cells. *Immunity* **20,** 769–783 (2004).

154. Caaveiro, J. M. M., Kiyoshi, M. & Tsumoto, K. Structural analysis of Fc/FcγR complexes: a blueprint for antibody design. *Immunological Reviews* **268,** 201–221 (2015).

155. Titus, J. A. *et al.* Human K/natural killer cells targeted with hetero-cross-linked antibodies specifically lyse tumor cells in vitro and prevent tumor growth in vivo. *J Immunol* **139,** 3153–3158 (1987).

156. Anderson, C. *et al.* Phagocytosis mediated by three distinct Fc gamma receptor classes on human leukocytes. *The Journal of experimental medicine* **171,** 1333–45 (1990).

157. Ciardiello, F. & Tortora, G. A novel approach in the treatment of cancer: Targeting the epidermal growth factor receptor. *Clinical Cancer Research* **7,** 2958–2970 (2001).

158. Mukherji, S. Bevacizumab (Avastin). *American Journal of Neuroradiology* **31,** 235–236 (2010).

159. Takeda, K. *et al.* Targeting death-inducing receptors in cancer therapy. *Oncogene* **26,** 3745–3757 (2007).

160. Alduaij, W. *et al.* Novel type II anti-CD20 monoclonal antibody (GA101) evokes homotypic adhesion and actin-dependent, lysosome-mediated cell death in B-cell malignancies. *Blood* **117,** 4519–29 (2011).

161. Janas, E. *et al.* Rituxan (anti-CD20 antibody)-induced translocation of CD20 into lipid rafts is crucial for calcium influx and apoptosis. *Clinical and Experimental Immunology* **139,** 439–446 (2005).

162. Moran, A. E., Kovacsovics-Bankowski, M. & Weinberg, A. D. The TNFRs OX40, 4-1BB, and CD40 as targets for cancer immunotherapy. *Current Opinion in Immunology* **25,** 230–237 (2013).

163. Dall'Ozzo, S. *et al.* Rituximab-Dependent Cytotoxicity by Natural Killer Cells: Influence of FCGR3A Polymorphism on the Concentration-Effect Relationship. *Cancer Research* **64,** 4664–4669 (2004).

164. Lefebvre, M.-L., Krause, S. W., Salcedo, M. & Nardin, A. Ex Vivo-activated Human Macrophages Kill Chronic Lymphocytic Leukemia Cells in the Presence of Rituximab: Mechanism of Antibody-dependent Cellular Cytotoxicity and Impact of Human Serum. *Journal of immunotherapy* **29,** 388–397 (2006).

165. Van der Kolk, L. E. *et al.* Analysis of CD20-dependent cellular cytotoxicity by G-CSF-stimulated neutrophils. *Leukemia* **16,** 693–699 (2002).

166. Trapani, J. A. & Smyth, M. J. Functional significance of the perforin/granzyme cell death pathway. *Nature reviews. Immunology* **2,** 735–47 (2002).

167. Dale, D. C., Boxer, L. & Conrad Liles, W. The phagocytes: Neutrophils and monocytes. *Blood* **112,** 935–945 (2008).

168. Jones, D. H., Nusbacher, J. & Anderson, C. L. Fc receptor-mediated binding and endocytosis by human mononuclear phagocytes: Monomeric IgG is not endocytosed by U937 cells and monocytes. *Journal of Cell Biology* **100,** 558–564 (1985).

169. Flannagan, R. S., Jaumouillé, V. & Grinstein, S. The cell biology of phagocytosis. *Annual review of pathology* **7,** 61–98 (2012).

170. Scott, C. C. *et al.* Phosphatidylinositol-4, 5-bisphosphate hydrolysis directs actin remodeling during phagocytosis. *Journal of Cell Biology* **169,** 139–149 (2005).

171. Desjardins, M., Huber, L. A., Parton, R. G. & Griffiths, G. Biogenesis of phagolysosomes proceeds through a sequential series of interactions with the endocytic apparatus. *Journal of Cell Biology* **124,** 677–688 (1994).

172. Aktan, F. iNOS-mediated nitric oxide production and its regulation. *Life Sciences* **75,** 639–653 (2004).

173. Lam, G. Y., Huang, J. & Brumell, J. H. The many roles of NOX2 NADPH oxidase-derived ROS in immunity. *Seminars in Immunopathology* **32,** 415–430 (2010).

174. Lukacs, G. L., Rotstein, O. D. & Grinstein, S. Determinants of the phagosomal pH in macrophages: In situ assessment of vacuolar H+-ATPase activity, counterion conductance, and H+ ”leak”. *Journal of Biological Chemistry* **266,** 24540–24548 (1991).

175. Murray, P. J. & Wynn, T. A. Protective and pathogenic functions of macrophage subsets. *Nature Reviews Immunology* **11,** 723–737 (2011).

176. Martinez, F. O. & Gordon, S. The M1 and M2 paradigm of macrophage activation: time for reassessment. *F1000prime reports* **6,** 13 (2014).

177. Mantovani, A. *et al.* The chemokine system in diverse forms of macrophage activation and polarization. *Trends in Immunology* **25,** 677–686 (2004).

178. Chitu, V. & Stanley, E. R. Colony-stimulating factor-1 in immunity and inflammation. *Current Opinion in Immunology* **18,** 39–48 (2006).

179. Mantovani, A. *et al.* The chemokine system in cancer biology and therapy. *Cytokine & Growth Factor Reviews* **21,** 27–39 (2010).

180. Kessenbrock, K., Plaks, V. & Werb, Z. Matrix Metalloproteinases: Regulators of the Tumor Microenvironment. *Cell* **141,** 52–67 (2010).

181. Lin, E. Y. *et al.* Macrophages regulate the angiogenic switch in a mouse model of breast cancer. *Cancer Research* **66,** 11238–11246 (2006).

182. Woo, S.-R., Corrales, L. & Gajewski, T. F. Innate Immune Recognition of Cancer. *Annual Review of Immunology* **33,** 150126111626001 (2014).

183. Kishore, U. & Reid, K. B. C1q: Structure, function, and receptors. *Immunopharmacology* **49,** 159–170 (2000).

184. Van Schaarenburg, R. A. *et al.* The production and secretion of complement component C1q by human mast cells. *Molecular Immunology* **78,** 164–170 (2016).

185. Kishore, U. *et al.* Structural and functional anatomy of the globular domain of complement protein C1q. *Immunology Letters* **95,** 113–128 (2004).

186. Bredt, W., Wellek, B., Brunner, H. & Loos, M. Interactions between Mycoplasma pneumoniae and the first component of complement. *Infection and Immunity* **15,** 7–12 (1977).

187. Santoro, F., Ouaissi, M. A., Pestel, J. & Capron, A. Interaction between Schistosoma mansoni and the complement system: binding of C1q to schistosomula. *Journal of immunology* (1980).

188. Albertí, S. *et al.* Interaction between complement subcomponent C1q and the Klebsiella pneumoniae porin OmpK36. *Infection and Immunity* **64,** 4719–4725 (1996).

189. Korb, L. C. & Ahearn, J. M. C1q binds directly and specifically to surface blebs of apoptotic human keratinocytes: complement deficiency and systemic lupus erythematosus revisited. *Journal of immunology (Baltimore, Md. : 1950)* **158,** 4525–8 (1997).

190. Tacnet-Delorme, P., Chevallier, S. & Arlaud, G. J. β-Amyloid Fibrils Activate the C1 Complex of Complement Under Physiological Conditions: Evidence for a Binding Site for Aβ on the C1q Globular Regions. *The Journal of Immunology* **167,** 6374–6381 (2001).

191. Kojouharova, M. S. *et al.* Mutational analyses of the recombinant globular regions of human C1q A, B, and C chains suggest an essential role for arginine and histidine residues in the C1q-IgG interaction. *Journal of immunology (Baltimore, Md. : 1950)* **172,** 4351–8 (2004).

192. Burton, D. R. *et al.* The C1q receptor site on immunoglobulin G. *Nature* **288,** 338–344 (1980).

193. Marqués, G. *et al.* Arginine residues of the globular regions of human C1q involved in the interaction with immunoglobulin G. *The Journal of biological chemistry* **268,** 10393–402 (1993).

194. Roumenina, L. T. *et al.* Role of Ca 2+ in the electrostatic stability and the functional activity of the globular domain of human C1q. *Biochemistry* **44,** 14097–14109 (2005).

195. Sledge, C. R. & Bing, D. H. Binding properties of the human complement protein Clq. *The Journal of biological chemistry* **248,** 2818–23 (1973).

196. Hughes-Jones, N. & Gardner, B. Reaction between the isolated globular sub-units of the complement component Clq and IgG-complexes. *Molecular Immunology* **16,** 697–701 (1979).

197. Diebolder, C. A. *et al.* Complement Is Activated by IgG Hexamers Assembled at the Cell Surface. *Science (New York, N.Y.)* **343,** 1260–1263 (2014).

198. Strasser, J. *et al.* Unraveling the Macromolecular Pathways of IgG Oligomerization and Complement Activation on Antigenic Surfaces. *Nano Letters* (2019).

199. Ugurlar, D. *et al.* Structures of C1-IgG1 provide insights into how danger pattern recognition activates complement. *Science* **359,** 794–797 (2018).

200. Czajkowsky, D. M. & Shao, Z. The human IgM pentamer is a mushroom-shaped molecule with a flexural bias. *Proceedings of the National Academy of Sciences* **106,** 14960–14965 (2009).

201. Hiramoto, E. *et al.* The IgM pentamer is an asymmetric pentagon with an open groove that binds the AIM protein. *Science Advances* **4,** eaau1199 (2018).

202. Arlaud, G. J. *et al.* Structural biology of the C1 complex of complement unveils the mechanisms of its activation and proteolytic activity. *Molecular Immunology* **39,** 383–394 (2002).

203. Law, S. K. The covalent binding reaction of C3 and C4. *Annals of the New York Academy of Sciences* **421,** 246–58 (1983).

204. Nagasawa, S. & Stroud, R. M. Cleavage of C2 by C1s into the antigenically distinct fragments C2a and C2b: demonstration of binding of C2b to C4b. *Proceedings of the National Academy of Sciences of the United States of America* **74,** 2998–3001 (1977).

205. Ricklin, D., Hajishengallis, G., Yang, K. & Lambris, J. D. Complement: a key system for immune surveillance and homeostasis. *Nature immunology* **11,** 785–97 (2010).

206. Ehlenberger, A. G. The role of membrane receptors for C3b and C3d in phagocytosis. *Journal of Experimental Medicine* **145,** 357–371 (1977).

207. Merle, N. S., Church, S. E., Fremeaux-Bacchi, V. & Roumenina, L. T. Complement system part I - molecular mechanisms of activation and regulation. *Frontiers in Immunology* **6,** 262 (2015).

208. Kim, Y. U. *et al.* Covalent binding of C3b to C4b within the classical complement pathway C5 convertase: Determination of amino acid residues involved in ester linkage formation. *Journal of Biological Chemistry* **267,** 4171–4176 (1992).

209. Vogt, W., Schmidt, G., Von Buttlar, B. & Dieminger, L. A new function of the activated third component of complement: binding to C5, an essential step for C5 activation. *Immunology* **34,** 29–40 (1978).

210. Guo, R.-F. & Ward, P. A. Role of C5a in Inflammatory Responses. *Annual Review of Immunology* **23,** 821–852 (2005).

211. Klos, A. *et al.* The role of the anaphylatoxins in health and disease. *Molecular Immunology* **46,** 2753–2766 (2009).

212. Peng, Q., Li, K., Sacks, S. H. & Zhou, W. The role of anaphylatoxins C3a and C5a in regulating innate and adaptive immune responses. *Inflammation & allergy drug targets* **8,** 236–246 (2009).

213. Cooper, N. R. & Müller-Eberhard, H. J. The reaction mechanism of human C5 in immune hemolysis. *The Journal of experimental medicine* **132,** 775–93 (1970).

214. Podack, E. R., Tschoop, J. & Müller-Eberhard, H. J. Molecular organization of C9 within the membrane attack complex of complement. Induction of circular C9 polymerization by the C5b-8 assembly. *The Journal of experimental medicine* **156,** 268–82 (1982).

215. Lindorfer, M. A. *et al.* Real-time analysis of the detailed sequence of cellular events in mAb-mediated complement-dependent cytotoxicity of B-cell lines and of chronic lymphocytic leukemia B-cells. *Molecular immunology* **70,** 13–23 (2015).

216. Tschopp, J. Ultrastructure of the membrane attack complex of complement. Heterogeneity of the complex caused by different degree of C9 polymerization. *Journal of Biological Chemistry* **259,** 7857–7863 (1984).

217. Roos, A. *et al.* Functional characterization of the lectin pathway of complement in human serum. *Molecular Immunology* **39,** 655–668 (2003).

218. Ikeda, K. *et al.* Serum lectin with known structure activates complement through the classical pathway. *Journal of Biological Chemistry* **262,** 7451–7454 (1987).

219. Weis, W. I., Drickamer, K. & Hendrickson, W. A. Structure of a C-type mannose-binding protein complexed with an oligosaccharide. *Nature* **360,** 127–134 (1992).

220. Yongqing, T. *et al.* Mannose-binding lectin serine proteases and associated proteins of the lectin pathway of complement: Two genes, five proteins and many functions? *Biochimica et Biophysica Acta - Proteins and Proteomics* **1824,** 253–262 (2012).

221. Matsushita, M. & Fujita, T. Cleavage of the third component of complement (C3) by mannose-binding protein-associated serine protease (MASP) with subsequent complement activation. *Immunobiology* **194,** 443–48 (1995).

222. Pangburn, M. K., Schreiber, R. D. & Müller-Eberhard, H. J. Formation of the initial C3 convertase of the alternative complement pathway. Acquisition of C3b-like activities by spontaneous hydrolysis of the putative thioester in native C3. *The Journal of experimental medicine* **154,** 856–67 (1981).

223. Pangburn, M. K. & Müller-Eberhard, H. J. Relation of putative thioester bond in C3 to activation of the alternative pathway and the binding of C3b to biological targets of complement. *The Journal of experimental medicine* **152,** 1102–14 (1980).

224. Fearon, D. T., Austen, K. F. & Ruddy, S. Formation of a hemolytically active cellular intermediate by the interaction between properdin factors B and D and the activated third component of complement. *The Journal of experimental medicine* **138,** 1305–13 (1973).

225. Kinoshita, T. *et al.* C5 convertase of the alternative complement pathway: covalent linkage between two C3b molecules within the trimolecular complex enzyme. *The Journal of Immunology* **141,** 3895–3901 (1988).

226. Nicholson-Weller, A. & Wang, C. E. Structure and function of decay accelerating factor CD55. *The Journal of laboratory and clinical medicine* **123,** 485–491 (1994).

227. Fujita, T. *et al.* The mechanism of action of decay-accelerating factor (DAF). DAF inhibits the assembly of C3 convertases by dissociating C2a and Bb. *The Journal of experimental medicine* **166,** 1221–8 (1987).

228. Meri, S. *et al.* Human protectin (CD59), an 18,000-20,000 MW complement lysis restricting factor, inhibits C5b-8 catalysed insertion of C9 into lipid bilayers. *Immunology* **71,** 1–9 (1990).

229. Farkas, I. *et al.* CD59 blocks not only the insertion of C9 into MAC but inhibits ion channel formation by homologous C5b-8 as well as C5b-9. *The Journal of Physiology* **539,** 537–545 (2002).

230. Köhler, G. & Milstein, C. Continuous cultures of fused cells secreting antibody of predefined specificity. *Nature* **256,** 495–497 (1975).

231. Barnstable, C. J. *et al.* Production of monoclonal antibodies to group A erythrocytes, HLA and other human cell surface antigens-new tools for genetic analysis. *Cell* **14,** 9–20 (1978).

232. Partridge, L. J. in *Biomembrane Protocols* 65–86 (Springer New York, New Jersey, 1994).

233. Norman, D. J. *et al.* A Randomized Clinical Trial of Induction Therapy with OKT3 in Kidney Transplantation. *Transplantation* **55,** 44–50 (1993).

234. Mayes, J. T. *et al.* Reexposure to OKT3 in renal allograft recipients. *Transplantation* **45,** 349–53 (1988).

235. Taylor, L. D. *et al.* A transgenic mouse that expresses a diversity of human sequence heavy and light chain immunoglobulins. *Nucleic Acids Research* **20,** 6287–6295 (1992).

236. Lee, E.-C. *et al.* Complete humanization of the mouse immunoglobulin loci enables efficient therapeutic antibody discovery. *Nature biotechnology* **32,** 356–63 (2014).

237. Chan, C. E. Z., Lim, A. P. C., MacAry, P. a. & Hanson, B. J. The role of phage display in therapeutic antibody discovery. *International immunology* **26,** 649–57 (2014).

238. Clackson, T., Hoogenboom, H. R., Griffiths, A. D. & Winter, G. Making antibody fragments using phage display libraries. *Nature* **352,** 624–8 (1991).

239. Breitling, F. *et al.* A surface expression vector for antibody screening. *Gene* **104,** 147–53 (1991).

240. Thie, H. *et al.* Affinity maturation by phage display. *Methods in Molecular Biology (Clifton, N.J.)* **525,** 309–22, xv (2009).

241. Lu, D. *et al.* Tailoring in vitro selection for a picomolar affinity human antibody directed against vascular endothelial growth factor receptor 2 for enhanced neutralizing activity. *The Journal of biological chemistry* **278,** 43496–507 (2003).

242. Kunert, R. & Reinhart, D. Advances in recombinant antibody manufacturing. *Applied Microbiology and Biotechnology* **100,** 3451–3461 (2016).

243. Butler, M. & Spearman, M. The choice of mammalian cell host and possibilities for glycosylation engineering. *Current Opinion in Biotechnology* **30,** 107–112 (2014).

244. Jayapal, K., Wlaschin, K., Hu, W. & Yap, G. Recombinant protein therapeutics from CHO cells-20 years and counting. *Chemical Engineering Progress* **103,** 40–47 (2007).

245. Dumont, J. *et al.* Human cell lines for biopharmaceutical manufacturing: history, status, and future perspectives. *Critical reviews in biotechnology* **1,** 1–13 (2015).

246. Reichert, J. M. *Approved Antibodies - www.antibodysociety.org/resources/approved-antibodies/* 2019.

247. *Monoclonal Antibody Therapeutics Market - Insights - www.coherentmarketinsights.com/market-insight/monoclonal-antibody-therapeutics-market-2403* 2019.

248. Collins, C. *et al.* Differential activation of human and guinea pig complement by pentameric and hexameric IgM. *European journal of immunology* **32,** 1802–10 (2002).

249. Marks, L. The birth pangs of monoclonal antibody therapeutics. *mAbs* **4,** 403–412 (2012).

250. Slamon, D. J. *et al.* Use of Chemotherapy plus a Monoclonal Antibody against HER2 for Metastatic Breast Cancer That Overexpresses HER2. *New England Journal of Medicine* **344,** 783–792 (2001).

251. Johnstone, R. W., Frew, A. J. & Smyth, M. J. The TRAIL apoptotic pathway in cancer onset, progression and therapy. *Nature Reviews Cancer* **8,** 782–798 (2008).

252. Tedder, T. F. & Engel, P. CD20: a regulator of cell-cycle progression of B lymphocytes. *Immunology Today* **15,** 450–454 (1994).

253. Beers, S. A. *et al.* Antigenic modulation limits the efficacy of anti-CD20 antibodies: Implications for antibody selection. *Blood* **115,** 5191–5201 (2010).

254. Cragg, M. S., Walshe, C. A., Ivanov, A. O. & Glennie, M. J. in *B Cell Trophic Factors and B Cell Antagonism in Autoimmune Disease* 140–174 (2004).

255. Beck, A. *et al.* Characterization of therapeutic antibodies and related products. eng. *Anal Chem* **85,** 715–736 (2013).

256. Tedder, T. F., Streuli, M., Schlossman, S. F. & Saito, H. Isolation and structure of a cDNA encoding the B1 (CD20) cell-surface antigen of human B lymphocytes (lymphocyte differentiation antigen/gene expression/in vitro translation). *Immunology* **85,** 208–212 (1988).

257. Polyak, M. J., Tailor, S. H. & Deans, J. P. Identification of a cytoplasmic region of CD20 required for its redistribution to a detergent-insoluble membrane compartment. *Journal of immunology (Baltimore, Md. : 1950)* **161,** 3242–3248 (1998).

258. Bubien, J. K. *et al.* Transfection of the CD20 cell surface molecule into ectopic cell types generates a Ca2+ conductance found constitutively in B lymphocytes. *Journal of Cell Biology* **121,** 1121–1132 (1993).

259. Polyak, M. J., Li, H., Shariat, N. & Deans, J. P. CD20 homo-oligomers physically associate with the B cell antigen receptor: Dissociation upon receptor engagement and recruitment of phosphoproteins and calmodulin-binding proteins. *Journal of Biological Chemistry* **283,** 18545–18552 (2008).

260. Petrie, R. J. & Deans, J. P. Colocalization of the B cell receptor and CD20 followed by activation-dependent dissociation in distinct lipid rafts. *Journal of immunology (Baltimore, Md. : 1950)* **169,** 2886–91 (2002).

261. O'Keefe, T. L., Williams, G. T., Davies, S. L. & Neuberger, M. S. Mice carrying a CD20 gene disruption. *Immunogenetics* **48,** 125–132 (1998).

262. Uchida, J. *et al.* The Innate Mononuclear Phagocyte Network Depletes B Lymphocytes through Fc Receptor–dependent Mechanisms during Anti-CD20 Antibody Immunotherapy. *Journal of Experimental Medicine* **199** (2004).

263. Kuijpers, T. W. *et al.* CD20 deficiency in humans results in impaired T cell-independent antibody responses. *Journal of Clinical Investigation* **120,** 214–222 (2010).

264. Morsy, D. E. D. *et al.* Reduced T-Dependent Humoral Immunity in CD20-Deficient Mice. *The Journal of Immunology* **191,** 3112–3118 (2013).

265. DiLillo, D. J. *et al.* Maintenance of long-lived plasma cells and serological memory despite mature and memory B cell depletion during CD20 immunotherapy in mice. *Journal of immunology (Baltimore, Md. : 1950)* **180,** 361–371 (2008).

266. Deans, J. P., Robbins, S. M., Polyak, M. J. & Savage, J. A. Rapid Redistribution of CD20 to a Low Density Detergent-insoluble Membrane Compartment. *Journal of Biological Chemistry* **273,** 344–348 (1998).

267. Niederfellner, G. *et al.* Epitope characterization and crystal structure of GA101 provide insights into the molecular basis for type I/II distinction of CD20 antibodies. *Blood* **118,** 358–367 (2011).

268. Cragg, M. S. *et al.* Complement-mediated lysis by anti-CD20 mAb correlates with segregation into lipid rafts. *Blood* **101,** 1045–1052 (2003).

269. Du, J., Yang, H., Guo, Y. & Ding, J. Structure of the Fab fragment of therapeutic antibody Ofatumumab provides insights into the recognition mechanism with CD20. *Molecular Immunology* **46,** 2419–2423 (2009).

270. Oldham, R. J., Cleary, K. L. S. & Cragg, M. S. CD20 and Its Antibodies: Past, Present, and Future. *Forum on Immunopathological Diseases and Therapeutics* **5,** 7–23 (2014).

271. De Jong, R. N. *et al.* A Novel Platform for the Potentiation of Therapeutic Antibodies Based on Antigen-Dependent Formation of IgG Hexamers at the Cell Surface. *PLoS biology* **14,** e1002344 (2016).

272. Lim, S. H. *et al.* Fc gamma receptor IIb on target B cells promotes rituximab internalization and reduces clinical efficacy. *Blood* **118,** 2530–2540 (2011).

273. Vaughan, A. T. *et al.* Inhibitory FcγRIIb (CD32b) becomes activated by therapeutic mAb in both cis and trans and drives internalization according to antibody specificity. *Blood* **123,** 669–677 (2014).

274. Chan, H. T. C. *et al.* CD20-induced lymphoma cell death is independent of both caspases and its redistribution into triton X-100 insoluble membrane rafts. *Cancer research* **63,** 5480–9 (2003).

275. Ivanov, A. *et al.* Monoclonal antibodies directed to CD20 and HLA-DR can elicit homotypic adhesion followed by lysosome-mediated cell death in human lymphoma and leukemia cells. *The Journal of clinical investigation* **119,** 2143–59 (2009).

276. Sopp, J. & Cragg, M. S. Deleting malignant B cells with second-generation Anti-CD20 antibodies. *Journal of Clinical Oncology* **36,** 2323–2325 (2018).

277. Reff, M. E. *et al.* Depletion of B cells in vivo by a chimeric mouse human monoclonal antibody to CD20. *Blood* **83,** 435–445 (1994).

278. Casak, S. J. *et al.* U.S. Food and drug administration approval: rituximab in combination with fludarabine and cyclophosphamide for the treatment of patients with chronic lymphocytic leukemia. *The oncologist* **16,** 97–104 (2011).

279. Teeling, J. L. *et al.* The biological activity of human CD20 monoclonal antibodies is linked to unique epitopes on CD20. *Journal of immunology (Baltimore, Md. : 1950)* **177,** 362–71 (2006).

280. Cameron, F. & McCormack, P. L. Obinutuzumab: First global approval. *Drugs* **74,** 147–154 (2014).

281. Mössner, E. *et al.* Increasing the efficacy of CD20 antibody therapy through the engineering of a new type II anti-CD20 antibody with enhanced direct and immune effector cell-mediated B-cell cytotoxicity. en. *Blood* **115,** 4393–402 (2010).

282. Herter, S. *et al.* Glycoengineering of therapeutic antibodies enhances monocyte/macrophage-mediated phagocytosis and cytotoxicity. *Journal of Immunology* **192,** 2252–2260 (2014).

283. Tipton, T. R. W. *et al.* Antigenic modulation limits the effector cell mechanisms employed by type I anti-CD20 monoclonal antibodies. *Blood* **125,** 1901–1909 (2015).

284. Pardoll, D. M. The blockade of immune checkpoints in cancer immunotherapy. *Nature Reviews. Cancer* **12,** 252–64 (2012).

285. Robert, C. *et al.* Ipilimumab plus Dacarbazine for Previously Untreated Metastatic Melanoma. *New England Journal of Medicine* **364,** 2517–2526 (2011).

286. Wolchok, J. D. *et al.* Nivolumab plus Ipilimumab in advanced melanoma. *New England Journal of Medicine* **369,** 122–133 (2013).

287. Topalian, S. L. *et al.* Survival, durable tumor remission, and long-term safety in patients with advanced melanoma receiving nivolumab. *Journal of Clinical Oncology* **32,** 1020–1030 (2014).

288. Sznol, M. *et al.* Survival, response duration, and activity by BRAF mutation (MT) status of nivolumab (NIVO, anti-PD-1, BMS-936558, ONO-4538) and ipilimumab (IPI) concurrent therapy in advanced melanoma (MEL). *Journal of Clinical Oncology* **32,** LBA9003–LBA9003 (2017).

289. Hodi, F. S. *et al.* Improved Survival with Ipilimumab in Patients with Metastatic Melanoma. *New England Journal of Medicine* **363,** 711–723 (2010).

290. Cameron, F., Whiteside, G. & Perry, C. Ipilimumab. *Drugs* **71,** 1093–1104 (2011).

291. Melero, I. *et al.* Immunostimulatory monoclonal antibodies for cancer therapy. *Nature Reviews Cancer* **7,** 95–106 (2007).

292. Lee, C. S., Cragg, M., Glennie, M. & Johnson, P. Novel antibodies targeting immune regulatory checkpoints for cancer therapy. *British Journal of Clinical Pharmacology* **76,** 233–247 (2013).

293. Suntharalingam, G. *et al.* Cytokine Storm in a Phase 1 Trial of the Anti-CD28 Monoclonal Antibody TGN1412. *New England Journal of Medicine* **355,** 1018–1028 (2006).

294. Van Kooten, G. & Banchereau, J. CD40-CD40 ligand. *Journal of Leukocyte Biology* **67,** 2–17 (2000).

295. Paulie, S. *et al.* A p50 surface antigen restricted to human urinary bladder carcinomas and B lymphocytes. *Cancer immunology, immunotherapy : CII* **20,** 23–8 (1985).

296. Smith, C. A., Farrah, T. & Goodwin, R. G. The TNF receptor superfamily of cellular and viral proteins: Activation, costimulation, and death. *Cell* **76,** 959–962 (1994).

297. Fesik, S. W. Insights into programmed cell through structural biology. *Cell* **103,** 273–282 (2000).

298. Idriss, H. T. & Naismith, J. H. TNFα and the TNF receptor superfamily: Structure-function relationship(s). *Microscopy Research and Technique* **50,** 184–195 (2000).

299. Armitage, R. J. *et al.* Molecular and biological characterization of a murine ligand for CD40. *Nature* **357,** 80–82 (1992).

300. Grewal, I. S. & Flavell, R. A. CD40 and CD154 on Cell-Mediated Immunity. *Annual Review of Immunology* **16,** 111–135 (2002).

301. Eliopoulos, A. G. & Young, L. S. The role of the CD40 pathway in the pathogenesis and treatment of cancer. *Current Opinion in Pharmacology* **4,** 360–367 (2004).

302. Remer, M. *et al.* in *Current Topics in Microbiology and Immunology* 165–207 (2017).

303. Bishop, G. A. *et al.* TRAF proteins in CD40 signaling. *Advances in Experimental Medicine and Biology* **597,** 131–151 (2007).

304. Matsuzawa, A. *et al.* Essential cytoplasmic translocation of a cytokine receptor-assembled signaling complex. *Science* **321,** 663–668 (2008).

305. Dadgostar, H. *et al.* Cooperation of multiple signaling pathways in CD40-regulated gene expression in B lymphocytes. *Proceedings of the National Academy of Sciences* **99,** 1497–1502 (2002).

306. Gallagher, E. *et al.* Kinase MEKK1 is required for CD40-dependent activation of the kinases Jnk and p38, germinal center formation, B cell proliferation and antibody production. *Nature Immunology* **8,** 57–63 (2007).

307. Vonderheide, R. H. & Glennie, M. J. Agonistic CD40 antibodies and cancer therapy. *Clinical Cancer Research* **19,** 1035–1043 (2013).

308. Taraban, V. Y., Rowley, T. F. & Al-Shamkhani, A. Cutting Edge: A Critical Role for CD70 in CD8 T Cell Priming by CD40-Licensed APCs. *The Journal of Immunology* **173,** 6542–6546 (2004).

309. Taraban, V. Y., Rowley, T. F., Tough, D. F. & Al-Shamkhani, A. Requirement for CD70 in CD4 + Th Cell-Dependent and Innate Receptor-Mediated CD8 + T Cell Priming. *The Journal of Immunology* **177,** 2969–2975 (2006).

310. Feau, S. *et al.* The CD4+ T-cell help signal is transmitted from APC to CD8 + T-cells via CD27-CD70 interactions. *Nature Communications* **3** (2012).

311. Tesselaar, K. *et al.* Expression of the Murine CD27 Ligand CD70 In Vitro and In Vivo. *The Journal of Immunology* **170,** 33–40 (2003).

312. Quezada, S. A., Jarvinen, L. Z., Lind, E. F. & Noelle, R. J. CD40/CD154 Interactions at the Interface of Tolerance and Immunity. *Annual Review of Immunology* **22,** 307–328 (2004).

313. Noelle, R. J. *et al.* A 39-kDa protein on activated helper T cells binds CD40 and transduces the signal for cognate activation of B cells. *Proceedings of the National Academy of Sciences* **89,** 6550–6554 (1992).

314. Tsubata, T., Wu, J. & Honjo, T. B-cell apoptosis induced by antigen receptor crosslinking is blocked by a T-cell signal through CD40. *Nature* **364,** 645–648 (1993).

315. Klaus, S. J., Berberich, I., Shu, G. & Clark, E. A. Cd40 and its ligand in the regulation of humoral immunity. *Seminars in Immunology* **6,** 279–286 (1994).

316. Bensinger, W. *et al.* A phase 1 study of lucatumumab, a fully human anti-CD40 antagonist monoclonal antibody administered intravenously to patients with relapsed or refractory multiple myeloma. *British Journal of Haematology* **159,** 58–66 (2012).

317. Todryk, S. M. *et al.* CD40 ligation for immunotherapy of solid tumours. *Journal of Immunological Methods* **248,** 139–147 (2001).

318. Van Mierlo, G. J. D. *et al.* CD40 stimulation leads to effective therapy of CD40- tumors through induction of strong systemic cytotoxic T lymphocyte immunity. *Proceedings of the National Academy of Sciences* **99,** 5561–5566 (2002).

319. Ridge, J. P., Di Rosa, F. & Matzinger, P. A conditioned dendritic cell can be a temporal bridge between a CD4 + T-helper and a T-killer cell. *Nature* **393,** 474–478 (1998).

320. Schoenberger, S. P. *et al.* T-cell help for cytotoxic T lymphocytes is mediated by CD40–CD40L interactions. *Nature* **393,** 480–483 (1998).

321. Bennett, S. R. *et al.* Help for cytotoxic-T-cell responses is mediated by CD4O signalling. *Nature* **393,** 478–480 (1998).

322. French, R. R., Chan, H. T. C., Tutt, A. L. & Glennie, M. J. CD40 antibody evokes a cytotoxic T-cell response that eradicates lymphoma and bypasses T-cell help. *Nature Medicine* **5,** 548–553 (1999).

323. Nowak, A. K., Robinson, B. W. S. & Lake, R. A. Synergy between chemotherapy and immunotherapy in the treatment of established murine solid tumors. *Cancer research* **63,** 4490–6 (2003).

324. Tutt, A. L. *et al.* T Cell Immunity to Lymphoma Following Treatment with Anti-CD40 Monoclonal Antibody. *The Journal of Immunology* **168,** 2720–2728 (2002).

325. Beatty, G. L. *et al.* CD40 agonists alter tumor stroma and show efficacy against pancreatic carcinoma in mice and humans. *Science* **331,** 1612–1616 (2011).

326. Long, K. B. *et al.* IFNγ and CCL2 cooperate to redirect tumor-infiltrating monocytes to degrade fibrosis and enhance chemotherapy efficacy in pancreatic carcinoma. *Cancer Discovery* **6,** 400–413 (2016).

327. Griffith, T. S. *et al.* Monocyte-mediated Tumoricidal Activity via the Tumor Necrosis Factor–related Cytokine, TRAIL. *The Journal of Experimental Medicine* **189,** 1343–1354 (1999).

328. Klimp, A. H., de Vries, E. G. E., Scherphof, G. L. & Daemen, T. A potential role of macrophage activation in the treatment of cancer. *Critical reviews in oncology/hematology* **44,** 143–61 (2002).

329. Lum, H. D. In vivo CD40 ligation can induce T cell-independent antitumor effects that involve macrophages. *Journal of Leukocyte Biology* **79,** 1181–1192 (2006).

330. Jackaman, C., Cornwall, S., Graham, P. T. & Nelson, D. J. CD40-activated B cells contribute to mesothelioma tumor regression. *Immunology and Cell Biology* **89,** 255–267 (2011).

331. Li, F. & Ravetch, J. V. Inhibitory Fcγ receptor engagement drives adjuvant and anti-tumor activities of agonistic CD40 antibodies. *Science* **333,** 1030–1034 (2011).

332. White, A. L. *et al.* Interaction with FcγRIIB Is Critical for the Agonistic Activity of Anti-CD40 Monoclonal Antibody. *The Journal of Immunology* **187,** 1754–1763 (2011).

333. White, A. L. *et al.* Fcγ Receptor Dependency of Agonistic CD40 Antibody in Lymphoma Therapy Can Be Overcome through Antibody Multimerization. *The Journal of Immunology* **193,** 1828–1835 (2014).

334. Yu, X. *et al.* Complex Interplay between Epitope Specificity and Isotype Dictates the Biological Activity of Anti-human CD40 Antibodies. *Cancer Cell* **33,** 664–675.e4 (2018).

335. Vonderheide, R. H. *et al.* Clinical activity and immune modulation in cancer patients treated with CP-870,893, a novel CD40 agonist monoclonal antibody. *Journal of Clinical Oncology* **25,** 876–883 (2007).

336. Rüter, J. *et al.* Immune modulation with weekly dosing of an agonist CD40 antibody in a phase I study of patients with advanced solid tumors. *Cancer Biology and Therapy* **10,** 983–993 (2010).

337. Johnson, P. W. *et al.* A Cancer Research UK phase I study evaluating safety, tolerability, and biological effects of chimeric anti-CD40 monoclonal antibody (MAb), Chi Lob 7/4. *Journal of Clinical Oncology* **28,** 2507–2507 (2017).

338. Tong, A. W. & Stone, M. J. Prospects for CD40-directed experimental therapy of human cancer. *Cancer Gene Therapy* **10,** 1–13 (2003).

339. Chiodoni, C. *et al.* Triggering CD40 on endothelial cells contributes to tumor growth. *The Journal of Experimental Medicine* **203,** 2441–2450 (2006).

340. Galy, A. H. & Spits, H. CD40 is functionally expressed on human thymic epithelial cells. *Journal of immunology (Baltimore, Md. : 1950)* **149,** 775–82 (1992).

341. Yellin, M. J. Functional interactions of T cells with endothelial cells: the role of CD40L-CD40-mediated signals. *Journal of Experimental Medicine* **182,** 1857–1864 (1995).

342. Vitale, L. A. *et al.* Development of CDX-1140, an agonist CD40 antibody for cancer immunotherapy. *Cancer Immunology, Immunotherapy* **68,** 233–245 (2019).

343. Sanborn, R. *et al.* Preliminary results from a first-in-human phase 1 study of the CD40 agonist monoclonal antibody (mAb) CDX-1140. *Society for Immunotherpy of Cancer* (2018).

344. Shields, R. L. *et al.* High resolution mapping of the binding site on human IgG1 for Fc gamma RI, Fc gamma RII, Fc gamma RIII, and FcRn and design of IgG1 variants with improved binding to the Fc gamma R. eng. *J Biol Chem* **276,** 6591–6604 (2001).

345. Holliger, P. & Hudson, P. J. Engineered antibody fragments and the rise of single domains. *Nature biotechnology* **23,** 1126–1136 (2005).

346. Shields, R. L. *et al.* Lack of fucose on human IgG1 N-linked oligosaccharide improves binding to human Fc gamma RIII and antibody-dependent cellular toxicity. *Journal of Biological Chemistry* **277,** 26733–26740 (2002).

347. Dall'Acqua, W. F. *et al.* Modulation of the effector functions of a human IgG1 through engineering of its hinge region. eng. *J Immunol* **177,** 1129–1138 (2006).

348. Lazar, G. A. *et al.* Engineered antibody Fc variants with enhanced effector function. *Proceedings of the National Academy of Sciences of the United States of America* **103,** 4005–4010 (2006).

349. Idusogie, E. E. *et al.* Engineered antibodies with increased activity to recruit complement. *Journal of immunology (Baltimore, Md. : 1950)* **166,** 2571–2575 (2001).

350. Mimoto, F. *et al.* Novel asymmetrically engineered antibody Fc variant with superior FcγR binding affinity and specificity compared with afucosylated Fc variant. *mAbs* **5,** 229–236 (2013).

351. Chu, S. Y. *et al.* Inhibition of B cell receptor-mediated activation of primary human B cells by coengagement of CD19 and FcγRIIb with Fc-engineered antibodies. *Molecular Immunology* **45,** 3926–3933 (2008).

352. Dahan, R. *et al.* Therapeutic Activity of Agonistic, Human Anti-CD40 Monoclonal Antibodies Requires Selective FcγR Engagement. *Cancer Cell* **29,** 820–831 (2016).

353. Kaneko, Y., Nimmerjahn, F. & Ravetch, J. V. Anti-inflammatory activity of immunoglobulin G resulting from Fc sialylation. *Science* **313,** 670–3 (2006).

354. Walker, M. R., Lund, J., Thompson, K. M. & Jefferis, R. Aglycosylation of human IgG1 and IgG3 monoclonal antibodies can eliminate recognition by human cells expressing Fc gamma RI and/or Fc gamma RII receptors. *The Biochemical journal* **259,** 347–53 (1989).

355. Jefferis, R., Lund, J. & Pound, J. D. IgG-Fc-mediated effector functions: Molecular definition of interaction sites for effector ligands and the role of glycosylation. *Immunological Reviews* **163,** 59–76 (1998).

356. Yamane-Ohnuki, N. *et al.* Establishment of FUT8 knockout Chinese hamster ovary cells: An ideal host cell line for producing completely defucosylated antibodies with enhanced antibody-dependent cellular cytotoxicity. *Biotechnology and Bioengineering* **87,** 614–622 (2004).

357. Kinder, M. *et al.* An Fc engineering approach that modulates antibody-dependent cytokine release without altering cell-killing functions. *mAbs* **7,** 494–504 (2015).

358. Sutterwala, F. S., Noel, G. J., Salgame, P. & Mosser, D. M. Reversal of proinflammatory responses by ligating the macrophage Fcgamma receptor type I. *The Journal of experimental medicine* **188,** 217–22 (1998).

359. Pander, J. *et al.* Activation of tumor-promoting type 2 macrophages by EGFR-targeting antibody cetuximab. *Clinical Cancer Research* **17,** 5668–5673 (2011).

360. Brekke, O. H. *et al.* Human IgG isotype-specific amino acid residues affecting complement-mediated cell lysis and phagocytosis. *European Journal of Immunology* **24,** 2542–2547 (1994).

361. Natsume, A. *et al.* Engineered antibodies of IgG1/IgG3 mixed isotype with enhanced cytotoxic activities. *Cancer Research* **68,** 3863–3872 (2008).

362. Kelton, W. *et al.* IgGA: A "cross-isotype" engineered human Fc antibody domain that displays both IgG-like and IgA-like effector functions. *Chemistry and Biology* **21,** 1603–1609 (2014).

363. Van Egmond, M. *et al.* Enhancement of polymorphonuclear cell-mediated tumor cell killing on simultaneous engagement of fcgammaRI (CD64) and fcalphaRI (CD89). *Cancer research* **61,** 4055–4060 (2001).

364. Weisbart, R. H., Kacena, A., Schuh, A. & Golde, D. W. GM-CSF induces human neutrophil IgA-mediated phagocytosis by an IgA Fc receptor activation mechanism. *Nature* **332,** 647–8 (1988).

365. Boross, P. *et al.* IgA EGFR antibodies mediate tumour killing in vivo. *EMBO Molecular Medicine* **5,** 1213–1226 (2013).

366. Russell, M. W., Reinholdt, J. & Kilian, M. Anti-inflammatory activity of human IgA antibodies and their Fab?? fragments: Inhibition of IgG-mediated complement activation. *European Journal of Immunology* **19,** 2243–2249 (1989).

367. Russell, M. W. & Mansa, B. Complement-fixing properties of human IgA antibodies. Alternative pathway complement activation by plastic-bound, but not specific antigen-bound, IgA. *Scandinavian journal of immunology* **30,** 175–83 (1989).

368. Smith, R. I. F. & Morrison, S. L. Recombinant Polymeric IgG: An Approach to Engineering More Potent Antibodies. *Bio/Technology* **12,** 683–688 (1994).

369. Smith, R. I., Coloma, M. J. & Morrison, S. L. Addition of a mu-tailpiece to IgG results in polymeric antibodies with enhanced effector functions including complement-mediated cytolysis by IgG4. *Journal of immunology (Baltimore, Md. : 1950)* **154,** 2226–36 (1995).

370. Brown, J. C. & Koshland, M. E. Activation of antibody Fc function by antigen-induced conformational changes. *Proceedings of the National Academy of Sciences of the United States of America* **72,** 5111–5 (1975).

371. Brown, J. C. & Koshland, M. E. Evidence for a long-range conformational change induced by antigen binding to IgM antibody. *Proceedings of the National Academy of Sciences of the United States of America* **74,** 5682–6 (1977).

372. Burton, D. R. Antibody: the flexible adaptor molecule. *Trends in Biochemical Sciences* **15,** 64–69 (1990).

373. Kuznetsov, Y. G., Day, J., Newman, R. & McPherson, A. Chimeric human-simian anti-CD4 antibodies form crystalline high symmetry particles. *Journal of Structural Biology* **131,** 108–115 (2000).

374. Saphire, E. O. *et al.* Crystallization and preliminary structure determination of an intact human immunoglobulin, b12: An antibody that broadly neutralizes primary isolates of HIV-1. *Acta Crystallographica Section D: Biological Crystallography* **57,** 168–171 (2001).

375. Wang, G. *et al.* Molecular Basis of Assembly and Activation of Complement Component C1 in Complex with Immunoglobulin G1 and Antigen. *Molecular Cell* (2016).

376. Tammen, A. *et al.* Monoclonal Antibodies against Epidermal Growth Factor Receptor Acquire an Ability To Kill Tumor Cells through Complement Activation by Mutations That Selectively Facilitate the Hexamerization of IgG on Opsonized Cells. *The Journal of Immunology,* 1601268 (2017).

377. Oostindie, S. C. *et al.* CD20 and CD37 antibodies synergize to activate complement by Fc-mediated clustering. *Haematologica,* haematol.2018.207266 (2019).

378. Gulati, S. *et al.* Complement alone drives efficacy of a chimeric antigonococcal monoclonal antibody. *PLOS Biology* **17,** e3000323 (2019).

379. Zhang, D., Goldberg, M. V. & Chiu, M. L. Fc engineering approaches to enhance the agonism and effector functions of an anti-OX40 antibody. *Journal of Biological Chemistry,* jbc.M116.757773 (2016).

380. Zhang, D. *et al.* Functional optimization of agonistic antibodies to OX40 receptor with novel Fc mutations to promote antibody multimerization. *mAbs* **9,** 1129–1142 (2017).

381. Horst, H. J. V. D. *et al.* Potent Ex Vivo Anti-Tumor Activity in Relapsed Refractory Multiple Myeloma Using Novel DR5-Specific Antibodies with Enhanced Capacity to Form Hexamers upon Target Binding. *Blood* **05,** 1–5 (2019).

382. Gelfand, E. W. Intravenous Immune Globulin in Autoimmune and Inflammatory Diseases. *New England Journal of Medicine* **367,** 2015–2025 (2012).

383. Katz-Agranov, N., Khattri, S. & Zandman-Goddard, G. The role of intravenous immunoglobulins in the treatment of rheumatoid arthritis. *Autoimmunity Reviews* **14,** 651–658 (2015).

384. Von dem Borne, A. E. *et al.* Autoimmune Thrombocytopenia: Detection of Platelet Autoantibodies with the Suspension Immunofluorescence Test. *British Journal of Haematology* **45,** 319–327 (1980).

385. Tjon, A. S., Van Gent, R., Geijtenbeek, T. B. & Kwekkeboom, J. Differences in anti-inflammatory actions of intravenous immunoglobulin between mice and men: More than meets the eye. *Frontiers in Immunology* **6,** 197 (2015).

386. Fehr, J., Hofmann, V. & Rappeler, U. Transient Reversal of Thrombocytopenia in Idiopathic Thrombocytopenic Purpura by High-Dose Intravenous Gamma Globulin. *New England Journal of Medicine* **306,** 1254–1258 (1982).

387. Basta, M., Fries, L. F. & Frank, M. M. High doses of intravenous Ig inhibit in vitro uptake of C4 fragments onto sensitized erythrocytes. *Blood* **77,** 376–380 (1991).

388. Hansen, R. J. & Balthasar, J. P. Intravenous immunoglobulin mediates an increase in antiplatelet antibody clearance via the FcRn receptor. *Thrombosis and haemostasis* **88,** 898–9 (2002).

389. Debré, M. *et al.* Infusion of Fc gamma fragments for treatment of children with acute immune thrombocytopenic purpura. *Lancet (London, England)* (1993).

390. Kimberly, R. P. *et al.* Modulation of mononuclear phagocyte function by intravenous γ-globulin. *Journal of Immunology* **132,** 745–750 (1984).

391. Tankersley, D. L. Dimer formation in immunoglobulin preparations and speculations on the mechanism of action of intravenous immune globulin in autoimmune diseases. *Immunological reviews* **139,** 159–72 (1994).

392. Bleeker, W. K. *et al.* Vasoactive side effects of intravenous immunoglobulin preparations in a rat model and their treatment with recombinant platelet-activating factor acetylhydrolase. *Blood* **95,** 1856–61 (2000).

393. Bolli, R. *et al.* l-Proline reduces IgG dimer content and enhances the stability of intravenous immunoglobulin (IVIG) solutions. *Biologicals* **38,** 150–157 (2010).

394. Jain, A. *et al.* Fully recombinant IgG2a Fc multimers (stradomers) effectively treat collagen-induced arthritis and prevent idiopathic thrombocytopenic purpura in mice. *Arthritis Research and Therapy* **14,** R192 (2012).

395. Czajkowsky, D. M. *et al.* Developing the IVIG biomimetic, hexa-Fc, for drug and vaccine applications. en. *Scientific reports* **5,** 9526 (2015).

396. Ortiz, D. F. *et al.* Elucidating the interplay between IgG-Fc valency and FcγR activation for the design of immune complex inhibitors. *Science Translational Medicine* **8** (2016).

397. Zhou, H. *et al.* A fully recombinant human IgG1 Fc multimer (GL-2045) inhibits complement-mediated cytotoxicity and induces iC3b. *Blood Advances* **1,** 504–515 (2017).

398. Sun, H. *et al.* Recombinant human IgG1 based Fc multimers, with limited FcR binding capacity, can effectively inhibit complement-mediated disease. *Journal of Autoimmunity* **84,** 97–108 (2017).

399. Qureshi, O. S. *et al.* Multivalent Fcγ-receptor engagement by a hexameric Fc-fusion protein triggers Fcγ-receptor internalisation and modulation of Fcγ-receptor functions. *Scientific Reports* **7,** 17049 (2017).

400. Spirig, R. *et al.* rIgG1 Fc Hexamer Inhibits Antibody-Mediated Autoimmune Disease via Effects on Complement and FcγRs. *The Journal of Immunology* **200,** 2542–2553 (2018).

401. Rowley, T. F. *et al.* Engineered hexavalent Fc proteins with enhanced Fc-gamma receptor avidity provide insights into immune-complex interactions. *Communications Biology* **1,** 146 (2018).

402. Cain, K. *et al.* A CHO cell line engineered to express XBP1 and ERO1-L?? has increased levels of transient protein expression. *Biotechnology Progress* **29,** 697–706 (2013).

403. Krop, I. *et al.* Self-renewal of B-1 lymphocytes is dependent on CD19. *European Journal of Immunology* **26,** 238–242 (1996).

404. Coffman, R. L. Surface antigen expression and immunoglobulin gene rearrangement during mouse pre-B cell development. *Immunological reviews* **69,** 5–23 (1982).

405. McGuire, A. T. *et al.* Specifically modified Env immunogens activate B-cell precursors of broadly neutralizing HIV-1 antibodies in transgenic mice. *Nature Communications* **7,** 10618 (2016).

406. Medyouf, H. *et al.* Acute T-cell leukemias remain dependent on Notch signaling despite PTEN and INK4A/ARF loss. *Blood* **115,** 1175–1184 (2010).

407. Loken, M. R., Brosnan, J. M., Bach, B. A. & Ault, K. A. Establishing optimal lymphocyte gates for immunophenotyping by flow cytometry. *Cytometry* **11,** 453–459 (1990).

408. Favaloro, E. J. *et al.* Endothelial cells and normal circulating haemopoietic cells share a number of surface antigens. *Thrombosis and Haemostasis* **61,** 217–224 (1989).

409. Lanier, L. L., Allison, J. P. & Phillips, J. H. Correlation of cell surface antigen expression on human thymocytes by multi-color flow cytometric analysis: implications for differentiation. *Journal of immunology (Baltimore, Md. : 1950)* **137,** 2501–7 (1986).

410. Dahal, L. N. *et al.* STING activation reverses lymphoma-mediated resistance to antibody immunotherapy. *Cancer Research* **77,** 3619–3631 (2017).

411. Tutt, A. L. *et al.* Development and Characterization of Monoclonal Antibodies Specific for Mouse and Human Fc Receptors. *The Journal of Immunology* **195,** 5503–5516 (2015).

412. Burbano, C. *et al.* Potential involvement of platelet-derived microparticles and microparticles forming immune complexes during monocyte activation in patients with systemic lupus erythematosus. *Frontiers in Immunology* **9,** 322 (2018).

413. Ahuja, A. *et al.* Depletion of B Cells in Murine Lupus: Efficacy and Resistance. *The Journal of Immunology* **179,** 3351–3361 (2007).

414. Erickson, L. D. *et al.* Short-circuiting long-lived humoral immunity by the heightened engagement of CD40. *Journal of Clinical Investigation* **109,** 613–620 (2002).

415. Hogquist, K. A. *et al.* T cell receptor antagonist peptides induce positive selection. *Cell* **76,** 17–27 (1994).

416. Rother, R. P. *et al.* Discovery and development of the complement inhibitor eculizumab for the treatment of paroxysmal nocturnal hemoglobinuria. *Nature biotechnology* **25,** 1256–64 (2007).

417. Kinder, M. *et al.* Engineered protease-resistant antibodies with selectable cell-killing functions. *The Journal of biological chemistry* **288,** 30843–54 (2013).

418. O'Kennedy, R., Murphy, C. & Devine, T. Technology advancements in antibody purification. *Antibody Technology Journal* **Volume 6,** 17–32 (2016).

419. Higel, F., Seidl, A., Sorgel, F. & Friess, W. N-glycosylation heterogeneity and the influence on structure, function and pharmacokinetics of monoclonal antibodies and Fc fusion proteins. *European Journal of Pharmaceutics and Biopharmaceutics* **100,** 94–100 (2016).

420. Angal, S. *et al.* A single amino acid substitution abolishes the heterogeneity of chimeric mouse/human (IgG4) antibody. *Molecular immunology* **30,** 105–8 (1993).

421. Idusogie, E. E. *et al.* Mapping of the C1q binding site on rituxan, a chimeric antibody with a human IgG1 Fc. *Journal of immunology (Baltimore, Md. : 1950)* **164,** 4178–4184 (2000).

422. Tao, M. H., Smith, R. I. & Morrison, S. L. Structural features of human immunoglobulin G that determine isotype-specific differences in complement activation. *The Journal of experimental medicine* **178,** 661–7 (1993).

423. Xu, Y., Oomen, R. & Klein, M. H. Residue at position 331 in the IgG1 and IgG4 CH2 domains contributes to their differential ability to bind and activate complement. *The Journal of biological chemistry* **269,** 3469–74 (1994).

424. Moh, E. S. X., Lin, C. H., Thaysen-Andersen, M. & Packer, N. H. Site-Specific N-Glycosylation of Recombinant Pentameric and Hexameric Human IgM. *Journal of the American Society for Mass Spectrometry* **27,** 1143–1155 (2016).

425. Kornfeld, R. & Kornfeld, S. Assembly of Asparagine-Linked Oligosaccharides. *Annual Review of Biochemistry* **54,** 631–664 (1985).

426. Bornemann, K. D. *et al.* Roles of heavy and light chains in IgM polymerization. *Proceedings of the National Academy of Sciences* **92,** 4912–4916 (1995).

427. Brewer, J. W., Randall, T. D., Parkhouse, R. M. E. & Corley, R. B. Mechanism and subcellular localization of secretory IgM polymer assembly. *Journal of Biological Chemistry* **269,** 17338–17348 (1994).

428. Brenckle, R. & Kornfeld, R. Structure of the oligosaccharides of mouse immunoglobulin M secreted by the MOPC 104E plasmacytoma. *Archives of Biochemistry and Biophysics* **201,** 160–173 (1980).

429. Cals, M.-M. *et al.* IgM polymerization inhibits the Golgi-mediated processing of the μ-chain carboxy-terminal glycans. *Molecular Immunology* **33,** 15–24 (1996).

430. Loos, A. *et al.* Expression and glycoengineering of functionally active heteromultimeric IgM in plants. *Proceedings of the National Academy of Sciences* **111,** 6263–6268 (2014).

431. Pabst, M. *et al.* A Microarray-Matrix-assisted Laser Desorption/Ionization-Mass Spectrometry Approach for Site-specific Protein N-glycosylation Analysis, as Demonstrated for Human Serum Immunoglobulin M (IgM). *Molecular & Cellular Proteomics* **14,** 1645–1656 (2015).

432. Gawlitzek, M., Estacio, M., Fürch, T. & Kiss, R. Identification of cell culture conditions to control N-glycosylation site-occupancy of recombinant glycoproteins expressed in CHO cells. *Biotechnology and Bioengineering* **103,** 1164–1175 (2009).

433. Akhouri, R. R. *et al.* Architecture of Human IgM in Complex with P. falciparum Erythrocyte Membrane Protein 1. *Cell Reports* **14,** 723–736 (2016).

434. Sahin, E. & Roberts, C. J. Size-exclusion chromatography with multi-angle light scattering for elucidating protein aggregation mechanisms. *Methods in Molecular Biology* **899,** 403–423 (2012).

435. Davis, T. A. *et al.* Rituximab anti-CD20 monoclonal antibody therapy in non-Hodgkin's lymphoma: Safety and efficacy of re-treatment. *Journal of Clinical Oncology* **18,** 3135–3143 (2000).

436. Rezvani, A. R. & Maloney, D. G. *Rituximab resistance* 2011.

437. Nose, M. & Wigzell, H. Biological significance of carbohydrate chains on monoclonal antibodies. *Proc Natl Acad Sci U S A* **80,** 6632–6636 (1983).

438. Peschke, B. *et al.* Fc-galactosylation of human immunoglobulin gamma isotypes improves C1q binding and enhances complement-dependent cytotoxicity. *Frontiers in Immunology* **8** (2017).

439. Goede, V. *et al.* Obinutuzumab plus chlorambucil in patients with CLL and coexisting conditions. *The New England journal of medicine* **370,** 1101–10 (2014).

440. Hussain, K. *et al.* Impact of human FcγR gene polymorphisms on IgG-triggered cytokine release: Critical importance of cell assay format. *Frontiers in Immunology* **10** (2019).

441. Van den Bremer, E. T. J. *et al.* Human IgG is produced in a pro-form that requires clipping of C-terminal lysines for maximal complement activation. en. *mAbs* **7,** 672–80 (2015).

442. Müller, C. A. *et al.* Serum levels of procarboxypeptidase B and its activation peptide in patients with acute pancreatitis and non-pancreatic diseases. *Gut* **51,** 229–35 (2002).

443. Sondermann, P., Huber, R., Oosthulzen, V. & Jacob, U. The 3.2-Å crystal structure of the human IgG1 Fc fragment-FcγRIII complex. *Nature* **406,** 267–273 (2000).

444. Radaev, S. *et al.* The Structure of a Human Type III Fcγ Receptor in Complex with Fc. *Journal of Biological Chemistry* **276,** 16469–16477 (2001).

445. Ramsland, P. A. *et al.* Structural Basis for FcγRIIa Recognition of Human IgG and Formation of Inflammatory Signaling Complexes. *The Journal of Immunology* **187,** 3208–3217 (2011).

446. De Goeij, B. E. & Lambert, J. M. New developments for antibody-drug conjugate-based therapeutic approaches. *Current Opinion in Immunology* **40,** 14–23 (2016).

447. Chowdhury, F. *et al.* Development of immunomonitoring of antibody□dependent cellular cytotoxicity against neuroblastoma cells using whole blood. *Cancer immunology, immunotherapy : CII* **63,** 559–69 (2014).

448. Gelderman, K. A., Tomlinson, S., Ross, G. D. & Gorter, A. Complement function in mAb-mediated cancer immunotherapy. *Trends in Immunology* **25,** 158–164 (2004).

449. Wang, S. Y., Racila, E., Taylor, R. P. & Weiner, G. J. NK-cell activation and antibody-dependent cellular cytotoxicity induced by rituximab-coated target cells is inhibited by the C3b component of complement. *Blood* **111,** 1456–1463 (2008).

450. Wang, S. Y. *et al.* Depletion of the C3 component of complement enhances the ability of rituximab-coated target cells to activate human NK cells and improves the efficacy of monoclonal antibody therapy in an in vivo model. *Blood* **114,** 5322–5330 (2009).

451. Trinchieri, G., Santoli, D. & Knowles, B. Tumour cell lines induce interferon in human lymphocytes. *Nature* **270,** 611–613 (1977).

452. Trinchieri, G., Santoli, D. & Koprowski, H. Spontaneous cell-mediated cytotoxicity in humans: role of interferon and immunoglobulins. *Journal of immunology (Baltimore, Md. : 1950)* **120,** 1849–55 (1978).

453. Bryceson, Y. T., March, M. E., Ljunggren, H. G. & Long, E. O. Synergy among receptors on resting NK cells for the activation of natural cytotoxicity and cytokine secretion. *Blood* **107,** 159–166 (2006).

454. Anegón, I., Cuturi, M. C., Trinchieri, G. & Perussia, B. Interaction of Fc receptor (CD16) ligands induces transcription of interleukin 2 receptor (CD25) and lymphokine genes and expression of their products in human natural killer cells. *The Journal of experimental medicine* **167,** 452–72 (1988).

455. Wu, J. *et al.* A novel polymorphism of FcgammaRIIIa (CD16) alters receptor function and predisposes to autoimmune disease. *Journal of Clinical Investigation* **100,** 1059–1070 (1997).

456. Weng, W. K. & Levy, R. Two immunoglobulin G fragment C receptor polymorphisms independently predict response to rituximab in patients with follicular lymphoma. *Journal of Clinical Oncology* **21,** 3940–3947 (2003).

457. Mellor, J. D. *et al.* A critical review of the role of Fc gamma receptor polymorphisms in the response to monoclonal antibodies in cancer. *Journal of hematology & oncology* **6,** 1 (2013).

458. Datta-Mannan, A. *et al.* Monoclonal Antibody Clearance. *Journal of Biological Chemistry* **282,** 1709–1717 (2007).

459. Johansson, A. G. *et al.* Liver cell uptake and degradation of soluble immunoglobulin G immune complexes in vivo and in vitro in rats. *Hepatology* **24,** 169–175 (1996).

460. Løvdal, T., Andersen, E., Brech, A. & Berg, T. Fc receptor mediated endocytosis of small soluble immunoglobulin G immune complexes in Kupffer and endothelial cells from rat liver. *Journal of cell science* **113 (Pt 1,** 3255–66 (2000).

461. Mannik, M. Pathophysiology of circulating immune complexes. *Arthritis & Rheumatism* **25,** 783–787 (1982).

462. Lee, S. J. *et al.* Mannose receptor-mediated regulation of serum glycoprotein homeostasis. *Science* **295,** 1898–1901 (2002).

463. Goetze, A. M. *et al.* High-mannose glycans on the Fc region of therapeutic IgG antibodies increase serum clearance in humans. *Glycobiology* **21,** 949–959 (2011).

464. Linehan, S. A., Martínez-Pomares, L., Stahl, P. D. & Gordon, S. Mannose receptor and its putative ligands in normal murine lymphoid and nonlymphoid organs: In situ expression of mannose receptor by selected macrophages, endothelial cells, perivascular microglia, and mesangial cells, but not dendritic cells. *Journal of Experimental Medicine* **189,** 1961–1972 (1999).

465. Kogelberg, H. *et al.* Clearance mechanism of a mannosylated antibody - Enzyme fusion protein used in experimental cancer therapy. *Glycobiology* **17,** 36–45 (2007).

466. Yang, J. *et al.* Impact of Glycation on Antibody Clearance. *AAPS Journal* **17,** 237–244 (2015).

467. Overdijk, M. B. *et al.* Crosstalk between Human IgG Isotypes and Murine Effector Cells. *The Journal of Immunology* **189,** 3430–3438 (2012).

468. Beers, S. A. *et al.* Type II (tositumomab) anti-CD20 monoclonal antibody out performs type I (rituximab-like) reagents in B-cell depletion regardless of complement activation. *Blood* **112,** 4170–4177 (2008).

469. Matthews, K. W., Mueller-Ortiz, S. L. & Wetsel, R. A. Carboxypeptidase N: A pleiotropic regulator of inflammation. *Molecular Immunology* **40,** 785–793 (2004).

470. Oyong, D. A. *et al.* Induction and kinetics of complement-fixing antibodies against Plasmodium vivax MSP3α and relationship with IgG subclasses and IgM. *The Journal of Infectious Diseases* (2019).

471. Hezareh, M. *et al.* Effector Function Activities of a Panel of Mutants of a Broadly Neutralizing Antibody against Human Immunodeficiency Virus Type 1. *Journal of Virology* **75,** 12161–12168 (2001).

472. Tao, M. H. & Morrison, S. L. Studies of aglycosylated chimeric mouse-human IgG. Role of carbohydrate in the structure and effector functions mediated by the human IgG constant region. eng. *J Immunol* **143,** 2595–2601 (1989).

473. Mimura, Y. *et al.* The influence of glycosylation on the thermal stability and effector function expression of human IgG1-Fc: properties of a series of truncated glycoforms. *Molecular immunology* **37,** 697–706 (2000).

474. Krapp, S. *et al.* Structural Analysis of Human IgG-Fc Glycoforms Reveals a Correlation Between Glycosylation and Structural Integrity. *Journal of Molecular Biology* **325,** 979–989 (2003).

475. Salfeld, J. G. Isotype selection in antibody engineering. *Nature Biotechnology* **25,** 1369–1372 (2007).

476. Könitzer, J. D., Sieron, A., Wacker, A. & Enenkel, B. Reformatting rituximab into human IgG2 and IgG4 isotypes dramatically improves apoptosis induction in vitro. *PLoS ONE* **10** (2015).

477. Beers, S. A., Glennie, M. J. & White, A. L. Influence of immunoglobulin isotype on therapeutic antibody function. *Blood* **127,** 1097–1101 (2016).

478. Sigma-Aldrich. *N-Linked Glycan Stratagies*

479. Shakin-Eshleman, S. H., Spitalnik, S. L. & Kasturi, L. The amino acid at the X position of an Asn-X-Ser sequon is an important determinant of N-linked core-glycosylation efficiency. *Journal of Biological Chemistry* **271,** 6363–6366 (1996).

480. Huang, Y. W. *et al.* Residues Comprising the Enhanced Aromatic Sequon Influence Protein N-Glycosylation Efficiency. *Journal of the American Chemical Society* **139,** 12947–12955 (2017).

481. Huang, Y. *et al.* Characterization of novel endo-β-N-acetylglucosaminidases from Sphingobacterium species, Beauveria bassiana and Cordyceps militaris that specifically hydrolyze fucose-containing oligosaccharides and human IgG. *Scientific Reports* **8** (2018).

482. Norris, G. E., Stillman, T. J., Anderson, B. F. & Baker, E. N. The three-dimensional structure of PNGase F, a glycosylasparaginase from Flavobacterium meningosepticum. *Structure (London, England : 1993)* **2,** 1049–59 (1994).

483. Fuster, M. M. & Esko, J. D. The sweet and sour of cancer: Glycans as novel therapeutic targets. *Nature Reviews Cancer* **5,** 526–542 (2005).

484. Hanson, S. R. *et al.* The core trisaccharide of an N-linked glycoprotein intrinsically accelerates folding and enhances stability. *Proceedings of the National Academy of Sciences* **106,** 3131–3136 (2009).

485. Häuselmann, I. & Borsig, L. Altered Tumor-Cell Glycosylation Promotes Metastasis. *Frontiers in Oncology* **4,** 28 (2014).

486. Moyle, W. R. *et al.* Models of glycoprotein hormone receptor interaction. *Endocrine* **26,** 189–205 (2005).

487. Takahashi, M. *et al.* N-glycan of ErbB family plays a crucial role in dimer formation and tumor promotion. *Biochimica et Biophysica Acta - General Subjects* **1780,** 520–524 (2008).

488. Liu, Y.-C. *et al.* Sialylation and fucosylation of epidermal growth factor receptor suppress its dimerization and activation in lung cancer cells. *Proceedings of the National Academy of Sciences* **108,** 11332–11337 (2011).

489. Jefferis, R. Isotype and glycoform selection for antibody therapeutics. *Archives of Biochemistry and Biophysics* **526,** 159–166 (2012).

490. Gavel, Y. & Heijne, G. V. Sequence differences between glycosylated and non-glycosylated asn-x-thr/ser acceptor sites: Implications for protein engineering. *Protein Engineering, Design and Selection* **3,** 433–442 (1990).

491. Helenius, A. & Aebi, M. Roles of N-Linked Glycans in the Endoplasmic Reticulum. *Annual Review of Biochemistry* **73,** 1019–1049 (2004).

492. Schwarz, F. & Aebi, M. Mechanisms and principles of N-linked protein glycosylation. *Current Opinion in Structural Biology* **21,** 576–582 (2011).

493. Petrescu, S. M. *et al.* Tyrosinase and glycoprotein folding: Roles of chaperones that recognize glycans. *Biochemistry* **39,** 5229–5237 (2000).

494. Wormald, M. R. *et al.* Conformational studies of oligosaccharides and glycopeptides: Complementarity of NMR, X-ray crystallography, and molecular modelling. *Chemical Reviews* **102,** 371–386 (2002).

495. Xu, C. & Ng, D. T. Glycosylation-directed quality control of protein folding. *Nature Reviews Molecular Cell Biology* **16,** 742–752 (2015).

496. Gregory, L. *et al.* The solution conformations of the subclasses of human IgG deduced from sedimentation and small angle X-ray scattering studies. *Molecular Immunology* **24,** 821–829 (1987).

497. Phillips, M. L., Mi-Hua, T., Morrison, S. L. & Schumaker, V. N. Human/mouse chimeric monoclonal antibodies with human IgG1, IgG2, IgG3 and IgG4 constant domains: Electron microscopic and hydrodynamic characterization. *Molecular Immunology* **31,** 1201–1210 (1994).

498. Horgan, C., Brown, K. & Pincus, S. H. Studies on antigen binding by intact and hinge-deleted chimeric antibodies. *The Journal of Immunology* **150,** 5400–5407 (1993).

499. Isenman, D. E., Dorrington, K. J. & Painter, R. H. The structure and function of immunoglobulin domains. II. The importance of interchain disulfide bonds and the possible role of molecular flexibility in the interaction between immunoglobulin G and complement. *Journal of immunology (Baltimore, Md. : 1950)* **114,** 1726–9 (1975).

500. Aalberse, R. C. & Schuurman, J. IgG4 breaking the rules. *Immunology* **105,** 9–19 (2002).

501. Hodi, F. S. *et al.* Nivolumab plus ipilimumab or nivolumab alone versus ipilimumab alone in advanced melanoma (CheckMate 067): 4-year outcomes of a multicentre, randomised, phase 3 trial. *The Lancet Oncology* **19,** 1480–1492 (2018).

502. Richman, L. P. & Vonderheide, R. H. Role of crosslinking for agonistic CD40 monoclonal antibodies as immune therapy of cancer. *Cancer immunology research* **2,** 19–26 (2014).

503. Geldart, T. R. *et al.* Cancer immunotherapy with a chimeric anti-CD40 monoclonal antibody: Evidence of preclinical efficacy. *Journal of Clinical Oncology* **22,** 2577–2577 (2017).

504. Johnson, P. *et al.* Clinical and biological effects of an agonist anti-CD40 antibody a cancer research UK phase I study. *Clinical Cancer Research* **21,** 1321–1328 (2015).

505. White, A. L. *et al.* FcγRIIB controls the potency of agonistic anti-TNFR mAbs. *Cancer Immunology, Immunotherapy* **62,** 941–948 (2013).

506. Liu, Y. D. *et al.* Human IgG2 antibody disulfide rearrangement in vivo. *Journal of Biological Chemistry* **283,** 29266–29272 (2008).

507. Martinez, T. *et al.* Disulfide connectivity of human immunoglobulin G2 structural isoforms. *Biochemistry* **47,** 7496–7508 (2008).

508. Allen, M. J. *et al.* Interchain disulfide bonding in human IgG2 antibodies probed by site-directed mutagenesis. *Biochemistry* **48,** 3755–3766 (2009).

509. Hussain, K. *et al.* Upregulation of FγRIIb on monocytes is necessary to promote the super-agonist activity of TGN1412. *Blood* **125,** 102–110 (2015).